This is to certify that the

dissertation entitled

SEISMOLOGICAL STUDIES IN NORTHEASTERN RUSSIA

presented by

Kevin G. Mackey

has been accepted towards fulfillment
of the requirements for

Phd. degree in Geological Sciences

Kazuya Fujita
Major professor

Date December 10, 1997

SEISMOLOGICAL STUDIES IN NORTHEAST RUSSIA

By

Kevin G. Mackey

A DISSERTATION

Submitted to
Michigan State University
in partial fulfillment of the requirements
for the degree of

DOCTOR OF PHILOSOPHY

Department of Geological Sciences

1999

ABSTRACT

SEISMOLOGICAL STUDIES IN NORTHEASTERN RUSSIA

By

Kevin G. Mackey

A seismicity catalog and associated list of seismic phases for larger events has been compiled for northeast Russia using published and unpublished data from the regional networks operating in eastern Russia (primarily Magadan, Yakutsk, and Amur), the western Alaska network, and international data files. The catalog contains over 40,000 events and over 110,000 arrival times. The resultant catalog is contaminated by industrial explosions, particularly in the Amur and central Magadan districts. The level of contamination is analyzed using the temporal distribution of events as anthropogenic events occur primarily during local day. Dramatic differences are observed between daytime and nighttime seismicity for the Amur district. Removal of anthropogenic sources allows easier identification of active faults. A seismicity trend was found to extend westward from the Seward peninsula to northern Kamchatka, which is interpreted to define the northern boundary of a proposed Bering plate. Clockwise rotation of this plate about an Euler pole in northeast Chukotka is suggested to be driven by terrane accretion is southern Alaska and coupling with the Pacific plate.

A preliminary crustal velocity model is developed by obtaining best fit travel time curves over 3 x 5 degree regions. The velocities obtained are generally in agreement with inferred tectonic regimes with high velocities in Precambrian platforms, low velocities in

active rifts, and average velocities in Mesozoic terrane assembledges. The velocity model is then used to relocate larger regional events. Relocated events are used to develop a preliminary regional upper mantle tomographic model of northeast Russia.

ACKNOWLEDGMENTS

First, I would like to thank my advisor, Kaz Fujita, for all the guidance, support, and help over the past 6 years while I worked on this project. I would also like to thank the members of my guidance committee: Bill Cambray, Dave Hyndman, Larry Ruff, and Tom Vogel.

Many ideas resulted from helpful conversations with other scientists both in Russia and the US, including David Stone, Paul Layer, Dan McNamara, Guy Tytgat, Marina Odinyets, Boris Sedoff, Art Grantz, Doug Christensen, Simon Klemperer, Thomas Hearn, and Jeff Amato.

In the process of assembling the database of northeastern Russia, there have been many people who have assisted in the acquisition or entry of data. For data acquisition, I would like to thank Boris Koz'min, Larissa Gounbina, Valery Imaev, Valentin Kovalev, Andrey Savchenko, Sasha Larionov, Natasha Koz'mina, Evgeni Gordeev, and the station operators in Stekolnyi and Seimchan for Russian regional network data, Charlotte Rowe, Guy Tytgat, and Roger Hansen for Western Alaska network data, and Bob Engdahl for ISC data. For data entry, I would like to thank Boris Koz'min, Larissa Gounbina, Nastia Antropova, Trent Faust, Rob McCaleb, Alexandra Dejong, Alan McNamara, Paula Figura, Melissa McLean, and Steve Riegel.

This project would not have been possible without the help of many individuals. Many thanks go the all the people who provided logistical support while in the field. In Magadan, this includes the Gounbin family (Larissa, Dima, Tanya, and Keesa), the Kovalev family (Valentin and Zena), Andrey Savchenko, and all the people of the Magadan EMSD

(Thanks for all the agates!), and Lerun Izmailov and Pavell Minyouk of NEISRI. In Yakutsk, I thank the Koz'min family (Boris, Gala, Natasha, Zhenya (Irkutsk), and Baba Tanya), the Imaev family (Valery, Luda, and Timor), Len Parfenov, Zena Kornilova, Pavell Izbekov, and Vilodia Oxman. I would also like to thank Svetlana and Olga in Ust'Nera, Anna and Albina in Talaya, the Matrosova Gold Mine, and Gala in Batagai. In Alaska, I thank David Stone, Paul Layer, Roger Hansen, Ann Trent, Diane and Cliff Gray, and Dena and David Vought. In California many thanks to Sharron Morrison.

Last but not least, I would like to thank my wife, Michelle, for all the years of love, encouragement, support, and understanding while I have worked on this dissertation, especially with all the nights at the lab until 5 am and summers when I ran off to Siberia. I would also like to thank my parents for their love, encouragement, and support since I started graduate school.

Support for this project was provided by, the National Science Foundation Office of Polar Programs grants 92-24193, 94-24139, and 98-06130, Incorporated Research Institutions for Seismology Joint Seismic Progran and Global Seismic Network Program, the Defense Threat Reduction Agency contract DTRA01-98-C-0168, and Michigan State University. Their support is gratefully acknowledged

TABLE OF CONTENTS

LIST OF TABLES

LIST OF FIGURES

INTRODUCTION

OVERVIEW OF STUDY

From a tectonic standpoint, Northeastern Russia (Figure I-1; Figure I-2) is one of the least studied large continental regions in the world. This was due to its geographic remoteness and the lack of accessibility, both to the region as well as to Soviet studies concerning it. Since the collapse of the Soviet Union, access to the region's scientists and their data has become possible, allowing the first comprehensive studies to be undertaken. This dissertation focuses on the seismicity distribution, velocity structure, and tectonic boundaries in the region.

A database of all known seismicity for the region, as well as the associated phase arrival times, was first assembled. Chapter one, "The Northeastern Russia Seismicity Database," outlines the sources and data acquired, and discusses the intricacies and inconsistencies involved in building a useful database. The assembly of this database would not have been possible without a direct knowledge of the operational procedures used in the region, as they explain many of the little quirks and oddities discovered in the data.

One of the problems encountered in the seismicity database was that of explosion contamination, discussed in chapter two, "Explosion Contamination in the Northeast Russia Seismicity Catalog." Some regions in northeastern Russia show high levels of seismic activity, but with most of the reported events being of anthropogenic origin. This can easily result in erroneous interpretation of plate boundaries, active faults, seismic hazards, etc. On the other hand, known explosions are helpful for developing better travel time curves, which can be used to improve epicenter locations and investigate crustal structure.

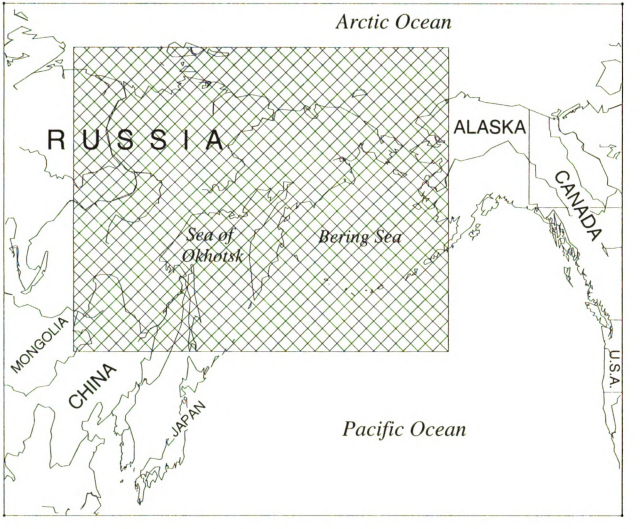

Figure I-1. Location of the northeastern Russia study area.

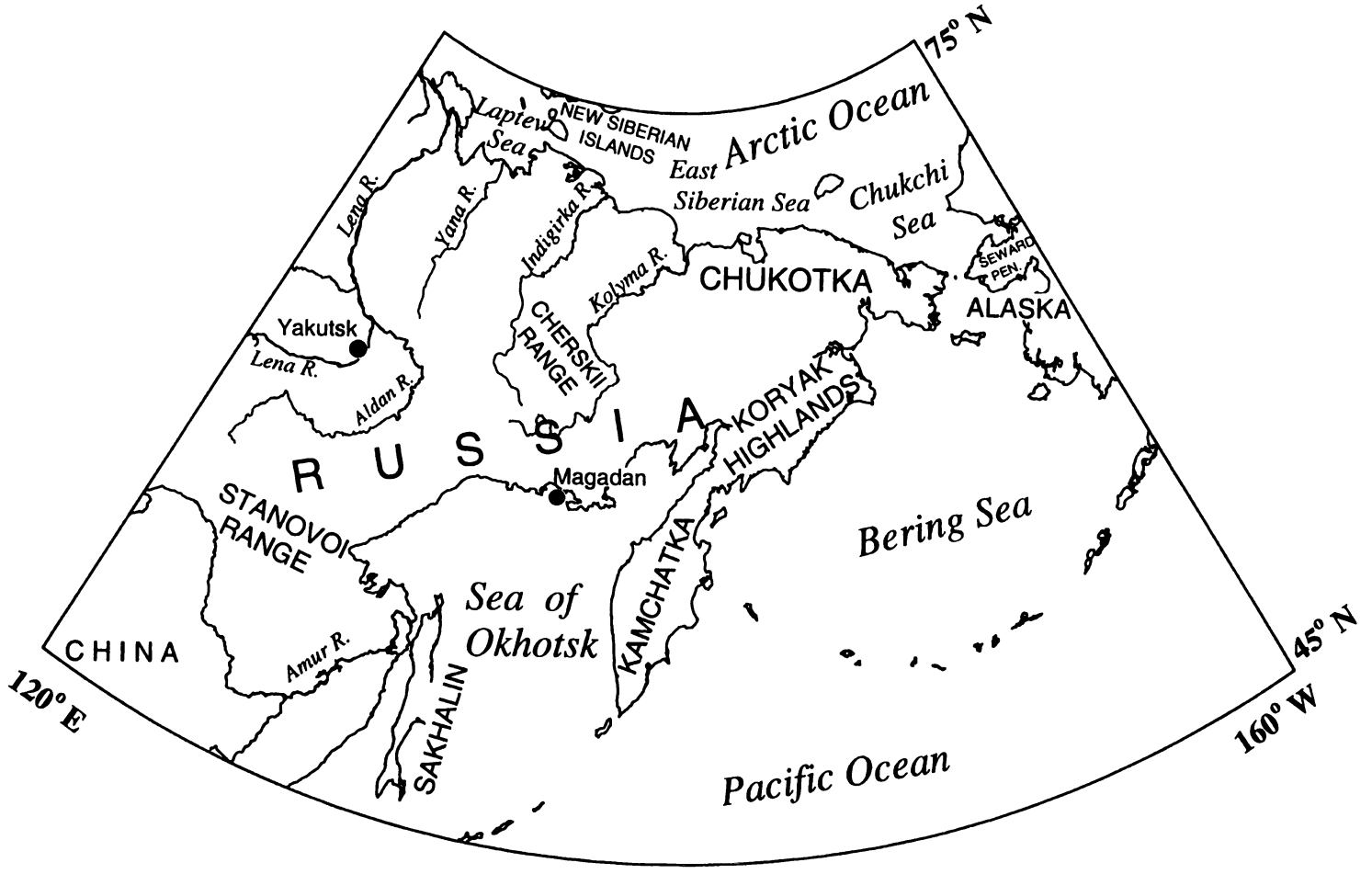

Figure I-2. Index map of the study area in northeast Russia.

Chapter three, "Relocations of Northeast Russia Earthquakes," develops regional crustal travel time curves specifically calibrated to small regions. The calibrated travel time curves are used to relocate the larger events throughout the region. The travel time curves presently in use by the Russian networks were, in some cases, developed from a specific refraction study which may have been conducted several thousand kilometers from the region where epicenters are being located.

In chapter four, "Upper Mantle Tomography of Northeastern Russia," the epicenter relocations and associated phase data are used in an attempted tomographic study of upper mantle velocities. The study area is an important region to image as the transition from an extensional regime to a transpressional boundary between the North American and Eurasian plates occurs within the region. This transition is not well understood, thus improved knowledge of the regions' velocities may be illustrative of the processes at work.

The assembled seismicity data can then be used to better evaluate the region as a whole, rather than as isolated regions. This was extremely important in developing an understanding of the tectonics in the Bering Strait region, as discussed in chapter five, "Seismicity of the Bering Strait Region: Evidence for a Bering Sea Plate." Here, an understanding of tectonic processes across the Bering Strait was essential to developing a regional framework in which the previously enigmatic tectonics of central Alaska can be understood.

A BRIEF OVERVIEW OF THE TECTONIC REGIME AND GEOLOGIC HISTORY

The tectonics of Northeast Russia result from complex plate interactions between the North American (NA), Eurasian (EU), and Pacific (PA) plates and a number of microplates between them (Figure I-3), such as Okhotsk (OK), Amur (AM), and Bering (BE) that have been previously studied using teleseismic earthquakes (e.g., Chapman and Solomon, 1976; Koz'min, 1984; Fujita et al., 1990a,b; Imaev et al., 1990; Riegel et al., 1993; Seno et al., 1996; Fujita et al., 1997, Mackey et al., 1997). The majority of the seismicity occurs along the Chersky Seismic Belt (CSB) on the North America - Eurasia - Okhotsk boundary and the Stanovoi Seismic Zone (SSZ) on the Eurasia - Amur boundary. Most of the larger teleseisms in the area have had focal mechanisms generated either by routine moment tensor determinations, first motions, and/or by waveform analysis (Chapman and Solomon, 1976; Koz'min, 1984; McMullen, 1985; Cook et al., 1986; Cook, 1988; Olson, 1990; Fujita et al., 1990a,b; Riegel et al., 1993; Riegel, 1994).

These studies indicate that the North American and Eurasian plates are presently converging in northeast Russia, resulting in the southward extrusion of the Okhotsk Block (Figure I-3; Riegel et al., 1993; see also Seno et al., 1996). The northern portion of the study area includes the Laptev Sea rift system. The Laptev Sea rift system is the extension of the Arctic Mid-Ocean Ridge onto the Siberian continental shelf, expressed as a system of grabens (Kim, 1986; Fujita et al., 1990a; Drachev, 1998). Within the Laptev Sea rift system, Kim (1986) suggests the Omoloi graben is the presently active zone of extension. Drachev (1998) indicates extensional features throughout the southern portions of the Laptev Sea.

To the south of the Siberian platform is the Stanovoi seismic zone, along which left-lateral motion is taking place between the Amur and Eurasian plates. This motion is thought

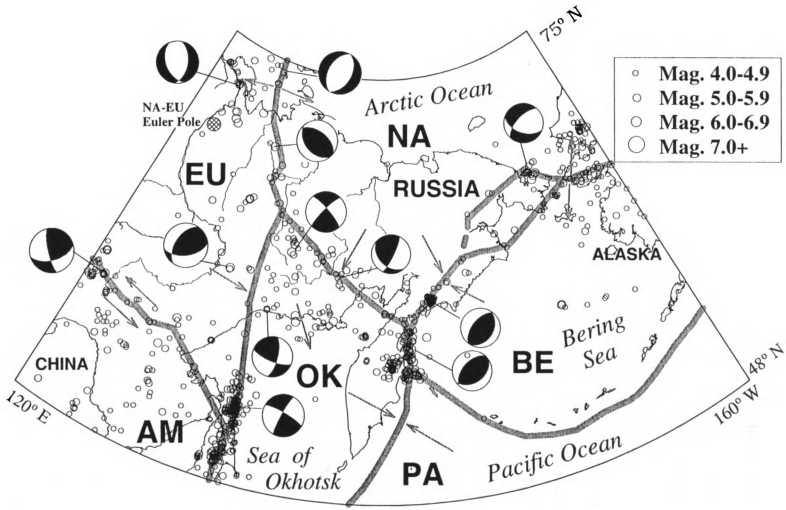

Figure I-3. Plate tectonic map of northeast Russia with teleseismic earthquakes, representative focal mechanisms, and relative plate motions. Plates are North American (NA), Eurasian (EU), Amur (AM), Okhotsk (OK), Pacific (PA), and Bering (BE).

to be due to far-field effects of the India-Eurasia collision, which results in the eastward extrusion of the Amur plate relative to the Eurasian plate (Tapponnier et al., 1982; Peltzer and Tapponnier, 1988). The Bering block, encompassing the Bering Sea, is driven by subduction of the Pacific Plate and extrusion of southwestern Alaska causing a clockwise rotation relative to the North American plate (Mackey et al., 1997; see Chapter 5).

The western portion of the study area contains the eastern portions of the Siberian platform. The Siberian platform generally consists of Precambrian basement overlain by a few kilometers of flat lying Riphean, Cambrian, and Jurassic sedimentary materials (Parfenov, 1991). The southern edge of the Siberian platform is separated from exotic terranes to the south by the Hauterivian to Aptian (131-110 Ma) Mongol-Okhotsk Suture (Nokleberg et al., 1998). Bounding the eastern edge of the Siberian platform is the Verkhoyansk range, which is a fold-and-thrust belt of Mesozoic age associated with the terrane accretion in the central portion of the study area occurring during that time period (Nokleberg et al., 1998). The central portion of the study area is composed of a series of exotic terranes and associated island arcs which accreted in the Mesozoic forming the Kolyma-Omolon Superterrane and Kolyma Structural Loop (Figure I-4; e.g., Parfenov, 1991; Zonenshain et al., 1990; Nokleberg et al., 1994). The central part of the study area, in the Chersky Range, participated in an extensional episode in the Pliocene which resulted in the formation of the Moma rift system (Grachev, 1973; Fujita et al., 1990a). Within the past 0.5 m.y., the pole of rotation for the NA-EU plates (Figure I-2) is suggested to have moved north and extensional activity along the Moma rift ceased (Cook et al., 1986). In Chukotka, in the north-eastern portion of the study area is the South Anyui Suture, which probably represents the closure of the South Anyui Ocean coincident with the opening of the Canada Basin at

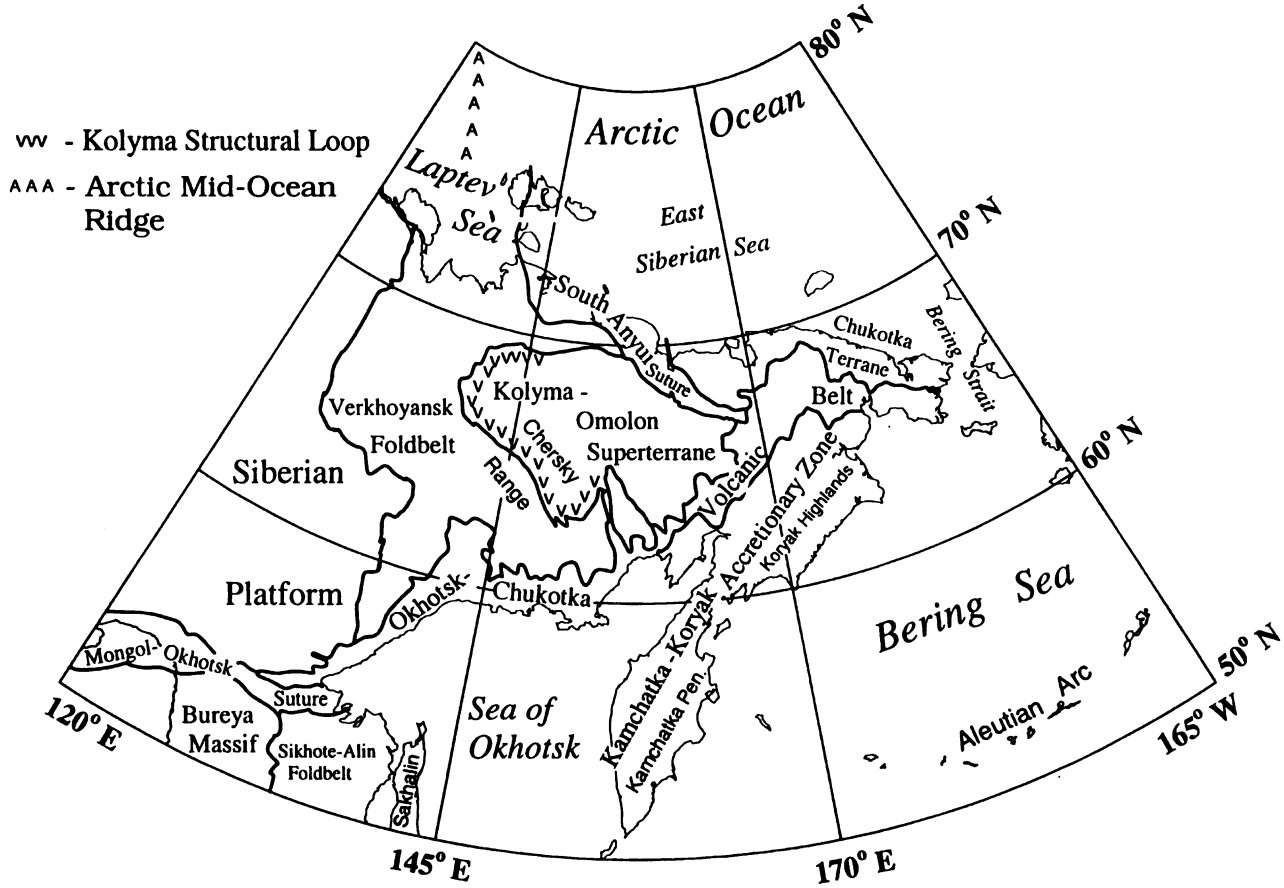

Figure I-4. Geologic index map of northeast Russia

about 120 Ma (Nokleberg et al., 1998). Beyond the South Anyui Suture lies the Chukotka Terrane, the Bering Strait and the terranes of Arctic Alaska. Superimposed over the southern edge of the Mesozoic accretionary terranes is the Okhotsk-Chukotka Volcanic Belt, dated at 67-89 Ma (Fujita et al., 1997). Southeast of the Okhotsk-Chukotka Volcanic Belt is the Kamchatka-Koryak Accretionary Zone consisting of a number of Cenozoic accreted terranes, which form the Kamchatka Peninsula and the Koryak highlands (Stavsky et al., 1990; Cook, 1988). Presently, the Pacific plate is subducting along the Aleutian Arc and the eastern edge of the Kamchatka peninsula.

REFERENCES

Cook, D.B., 1988, *Seismology and tectonics of the North American plate in the Arctic: northeast Siberia and Alaska*: Ph.D. Dissertation, Michigan State University, East Lansing, xi + 250 pp.

Cook, D.B., Fujita, K., and McMullen, C.A., 1986, Present-day plate interactions in northeast Asia: North American, Eurasian and Okhotsk plates: *Journal of Geodynamics*, v. 6, p. 33-51.

Chapman, M.E., and Solomon, S.C., 1976, North American - Eurasian plate boundary in Northeast Asia: *Journal of Geophysical Research*, v. 81, p. 921-930.

Drachev, S., Savostin, L.A., Groshev, V.G., and Bruni, I.E., 1998, Structure and geology of the continental shelf of the Laptev Sea, Eastern Russian Arctic: Tectonophysics, v. 298(4), p. 357-393.

Fujita, K., Stone, D.B., Layer, P.W., Parfenov, L. M., and Koz'min, B.M., 1997, Cooperative program helps decipher tectonis of northeastern Russia: *Transactions of the American Geophysical Union (Eos)*, v. 78, p. 245, 252-253.

Fujita, K., Cambray, F.W., and Velbel, M.A., 1990a, Tectonics of the Laptev Sea and Moma rift systems, northeastern USSR: *Marine Geology*, v. 98, p. 95-118.

Fujita, K., Cook, D.B., Hasegawa, H., Forsyth, D., and Wetmiller, R., 1990b, Seismicity and focal mechanisms of the Arctic region and the North American plate boundary in Asia, *in* Grantz, A., Johnson, L., and Sweeney, J. F., eds., *The Arctic Ocean Region; The Geology of North Americ*a v. L: The Geological Society of America, Boulder, p. 79-100.

Grachev, A.F., 1973, Moma continental rift (Northeast USSR): *Geofizicheskie Metody Razvedki v Arktike*, v. 8, p. 56-75 (in Russian).

Imaev, V.S., Imaeva, L.P., and Koz'min, B.M., 1990, *Active Faults and Seismotectonics of Northeast Yakutia*: Yakut Science Center, Yakutsk, 138 pp. (in Russian).

Kim, B.I., 1986, Structural continuation of the rift valley of Gakkel' ridge on the Laptev shelf, *in* Egiazarov, B. K., and Kazmin, Y. B., eds., *Struktura i Istoriya Razvitiya Severnogo Lodovitogo Okeana Sevmorgeologiya*: NIIGA, Leningrad, p. 133-139 (in Russian).

Koz'min, B.M., 1984, *Seismic belts of Yakutia and the focal mechanisms of their earthquakes*: Moskva, Nauka, 125 pp. (in Russian).

Mackey, K.G., Fujita, K., Gunbina, L.V., Kovalev, V.N., Imaev, V.S., Koz'min, B.M., and Imaeva, L.P., 1997, Seismicity of the Bering Strait region: evidence for a Bering block: *Geology*, v. 25, p. 979-982.

McMullen, C.A., 1985, *Seismicity and tectonics of the northeastern Sea of Okhotsk*: M.S. Thesis, Michigan State University, East Lansing, vi + 107 pp.

Nokleberg, W.J., Parfenov, L.M., Monger, J.W.H., Norton, I.O., Khanchuk, A.I., Stone, D.B., Scholl, D.W., and Fujita, K., 1998, *Phanerozoic tectonic evolution of the circum-north Pacific*: U. S. Geological Survey Open-File Report 98-754, 125 pp.

Nokleberg, W.J., Parfenov, L.M., Monger, J.W.H., Baranov, B.V., Byalobzhesky, S.G., Bunbtzen, T.K., Feeney, T.D., Fujita, K., Gordey, S.P., Grantz, A., Khanchuk, A.I., Natal'in, B.A., Natapov, L.M., Norton, I.O., Patton, W.W., Jr., Plafker, G., Scholl, D.W., Sokolov, S.D., Sosunov, G.M., Stone, D.B., Tabor, R.W., Tsukanov, N.V., Vallier, T.L., Wakita, K., 1994, *Circum-North Pacific tectonostratigraphic terrane map*: U. S. Geological Survey Open-File Report 94-714, 221 pp., 5 plates.

Olson, D.R., 1990, *The Eurasian - North American plate boundary through the area of the Laptev Sea*: M.S. Thesis, Michigan State University, East Lansing, viii + 65 pp.

Parfenov, L. M., 1991, Tectonics of the Verkhoyansk-Kolyma Mesozoides in the context of plate tectonics: *Tectonophysics*, v. 199, p. 319-342.

Peltzer, G., and Tapponnier, P., 1988, Formation and Evolution of Strike-Slip Faults, Rifts, and Basins During the India-Asia Collision: An Experimental Approach: *Journal of Geophysical Research*, v. 93, p. 15,085-15,117.

Riegel, S.A., 1994, *Seismotectonics of northeast Russia and the Okhotsk plate*: M.S. Thesis, Michigan State University, East Lansing, ix + 70 pp.

Riegel, S.A., Fujita, K., Koz'min, B.M., Imaev, V.S., and Cook, D.B., 1993, Extrusion tectonics of the Okhotsk plate, northeast Asia: *Geophysical Research Letters*, v. 20, p. 607-610.

Seno, T., Sakurai, T., and Stein, S., 1996, Can the Okhotsk plate be discriminated from the North American plate?: *Journal of Geophysical Research*, v. 101, p. 11305-11315.

Stavsky, A.P., Chekhovitch, V.D., Kononov, M.V., and Zonenshain, L.P., 1990, Plate tectonics and palinspastic reconstructions of the Anadyr-Koryak region, northeast USSR: *Tectonics*, v. 9(1), pp.81-101.

Tapponnier, P., Peltzer, G., Le Dain, A.Y., Armijo, R., and Cobbold, P., 1982, Propagating extrusion tectonics is Asia: new insights from simple experiments with plasticine: *Geology*, v. 10, p. 611-616.

Zonenshain, L.P., Kuz'min, M.I., and Natapov, L.M., 1990, Geology of the USSR: A plate tectonic synthesis: *American Geophysical Union, Geodynamics Series*, v. 21, 242 pp.

CHAPTER 1

The Northeastern Russia Seismicity Database

INTRODUCTION

Prior to the beginning of this study, there was no comprehensive database covering continental seismicity in northeastern Russia. In the past 30 years several regional networks including Yakutsk, Magadan, and others, in Russia and the Western Alaska network in the US, have operated in the study area. Unfortunately, data were not exchanged between them resulting in incomplete data sets being used for epicenter locations, resulting in artificial discontinuities at network boundaries (Figure 1-1). To better understand the neotectonic setting of northeastern Russia, it is necessary to combine as much data as possible from all sources. The combined data can be re-evaluated to improve travel time curves, hypocenter parameters, and tectonic models; better understand seismicity levels, determine regions of anthropogenic sources, etc.

There are two major sections to the developed database: a complete as possible catalog of hypocenters for northeast Russia and western Alaska, and a database of arrival times from combining data of all sources and networks. Supplemental information includes industrial explosions and seismic station parameters. In assembly of the database, several published and unpublished sources were used. A section which discusses each of the seismic networks considered, covering data problems, some network procedures, and data sources for each network is also included. A combined alphabetized list of seismic stations and parameters can be found in Appendix A.

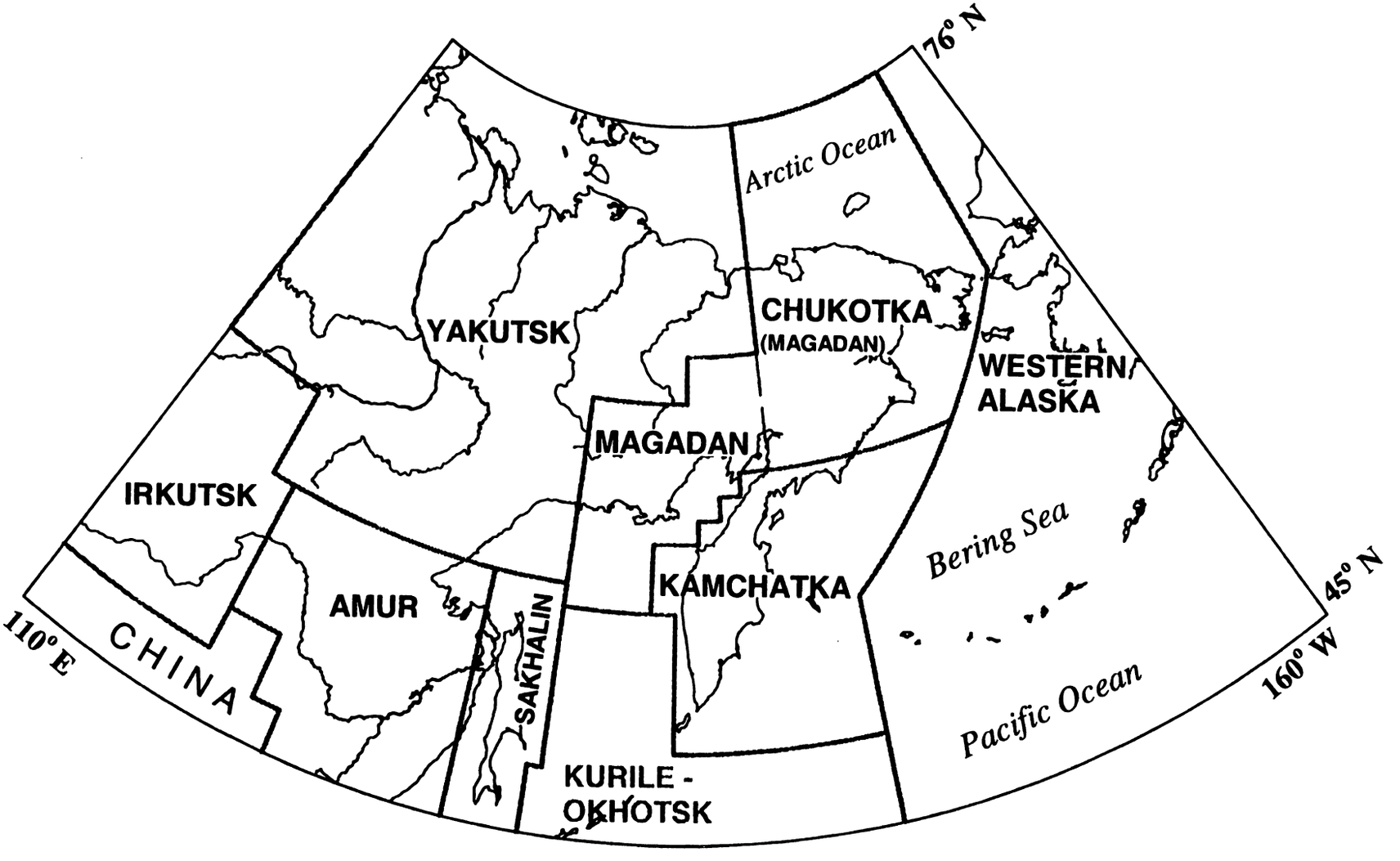

Figure 1-1. Seismic network boundaries in northeastern Russia.

This study has compiled a list of approximately 40,000 individual earthquakes identified throughout the region (Figure 1-2). Most of the events in the database occur between 1968 and 1998. Yearly plots of the seismicity can be found in Appendix B. Epicenters listed in Russian sources are usually precise to 0.1 or 0.01 degree. In regions where many events located to 0.1 degree are reported, lineations with 0.1 degree separation are visible in epicenter plots. For over 8,500 events (Figure 1-3), phase data have been acquired and entered into a computerized database of over 110,000 arrival times. Phase data were available in unpublished sources for a few events outside the designated study area which results in a few events shown on Figure 1-3 that are not depicted on Figure 1-2. Given the amount of data and number of sources used, it must be noted that the discussions on data sources in different networks are only generalizations and there are always some odd epicenters or arrival times acquired elsewhere. It is also impossible to discuss every discrepancy between data sources, although all the major ones are covered. Historic events and data recorded teleseismically for the entire study area are taken from standard sources such as the International Seismological Summary (ISS), International Seismological Centre Bulletin (ISC), United States Geological Survey (NEIC), etc., and are also not discussed with regard to specific regional networks. In addition, and database containing the approximate locations and origin times of about 10,000 mine blasts covering the Magadan region was compiled.

It is standard practice among Russian seismic networks to only report magnitudes for events of about M_b = 4.0 and larger. However, all events, both small and large, have sizes reported as a K-class value, which is based on the logarithm (base 10) of work released in

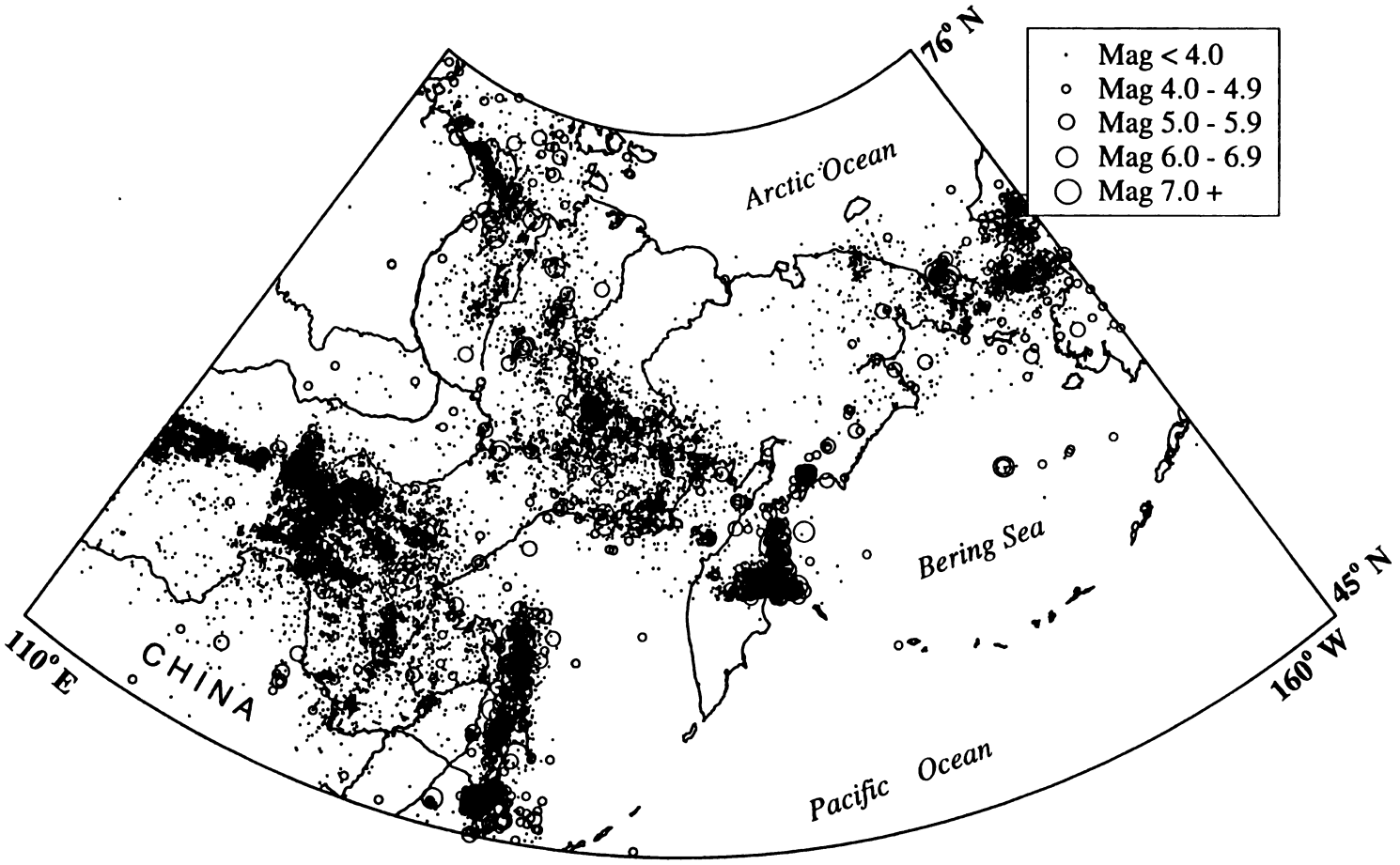

Figure 1-2. Plot of seismicity catalog compiled for northeastern Russia. Seismicity related to subduction of the Pacific plate under Kamchatka, the Kurile Islands, and the Aleutian Islands are omitted.

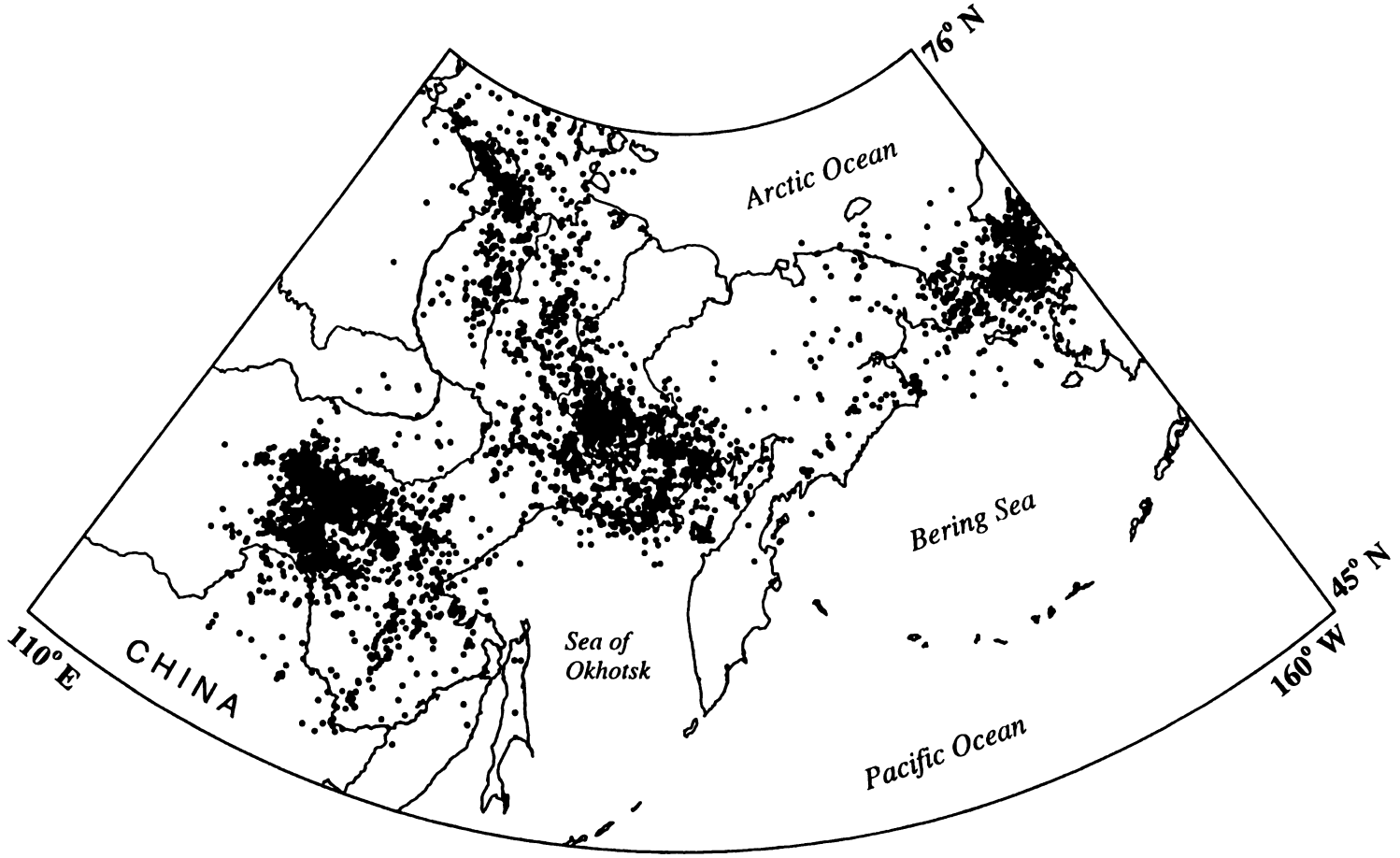

Figure 1-3. Events in the seismicity catalog for which phase data has been acquired.

Ergs. For determining K-class, the maximum ground motion amplitude A_{max} is determined using

$$A_{\max} = \frac{A_p + A_s}{T} \qquad (1\text{-}1)$$

where A_p and A_s are the respective maximum amplitudes of the P and S arrivals (in microns), and T is the period (in seconds) of the wave. If no amplitude is available for the P phase, only the S is used. Then, using S-P time difference or distance, the K-class value is read off a nomogram calibrated for each particular region (Solonenko, 1974; Pustovitenko and Kul'chitskii, 1974: Gounbina, pers. comm.). A sample nomogram for the Magadan region is given in Figure 1-4. Unfortunately, the nomograms calibrated for different regions or networks vary significantly, resulting in inconsistent size determinations between networks. For example an earthquake having a magnitude of 3.5 may be reported to have a K-class of 9.0 in one network, and a K-class of 10.5 from a neighboring network. To better understand the sizes of earthquakes reported in the compiled seismicity catalog, linear regressions were calculated relating K-class to magnitude for each network. Magnitudes used are ISC reported M_b values for magnitudes up to 5.5. Events larger than magnitude 5.5 use ISC or NEIC reported M_s values as body wave magnitude begins to saturate (Lay and Wallace, 1995).

Network boundaries shown throughout the study are taken from the *Materialy po Seismichnosti Sibiri* and *Zemletryseniya v SSSR* bulletins, which are discussed below. For some networks, there are one or two seismic stations that fall outside the official boundaries

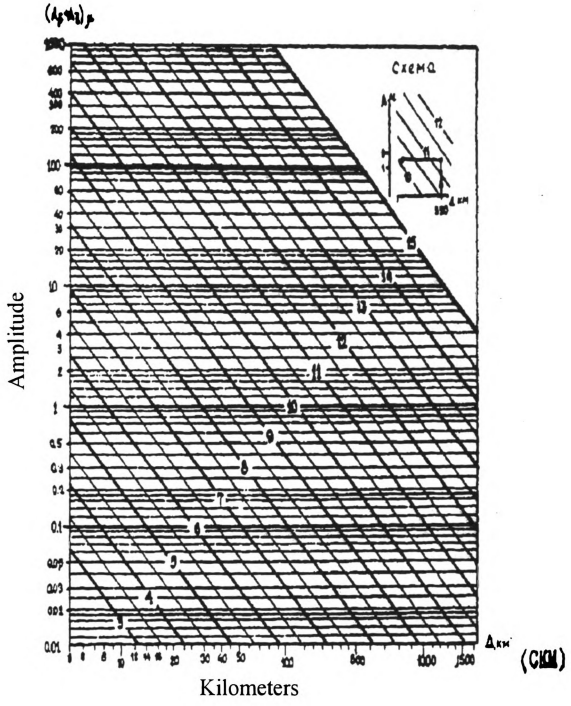

Figure 1-4. Nomogram for determining K-class values of earthquakes in the Magadan region using a SKM seismometer. Horizontal axis is distance in km, while vertical axis is the amplitude of ground motion (maximum P wave amplitude plus maximum S wave amplitude) in microns. The K-class value is read off the diagonal lines.

of the network. On maps of individual netwoks, seismic stations visible but belonging to a different network are labeled in gray.

Seismic station codes and coordinates have been compiled for stations that have operated in northeast Russia. Most seismic station codes for Russian regional stations are internal to this study and do not necessarily correspond to international designations. Accuracy of station coordinates may vary considerably. Seismic station parameters (name, coordinates, elevation, and open and close dates of operation) were compiled primarily by K. Fujita (pers. comm.). Most station coordinates were obtained from Russian published sources or directly from the seismic station networks. Russian publications usually give station coordinates to 0.01°, but sometimes to only 0.1°. Some stations were simply located in the appropriate town on the map and coordinates read. For stations in small towns, this is usually accurate to better than 0.02°. Other stations were visited by the author and GPS coordinates obtained. Quality levels (column 'Qu' on seismic station tables) for seismic stations are as follows:

G - Location determined with GPS (accuracy to within 100 m).
1 - Coordinates from Russian sources checked on Russian Military or TPC topographic maps and looks reasonable. Stations in small towns may also be assigned this quality level (accuracy to within 2 km).
2 - Some questions on exact location and/or two or more competing locations possible (accuracy may exceed 10 km).
3 - Location guessed or estimated; could be significantly in error.

Note that quality levels have not been assigned to all stations. Some stations are known to have been moved slightly but new coordinates are not known; in this case the coordinates are shown in brackets.

DATA SOURCES

Zemletryseniya v SSSR (1963-1991; Earthquakes of the USSR; hereafter *Zemlet*) and *Zemletryseniya Severnoi Evrazii* (1992; Earthquakes of Northern Eurasia; also referred to as *Zemlet*). This publication contains a yearly bulletin listing event parameters for the larger earthquakes which occurred within each regional network. In general, only events of K-class 8.5 and larger are listed, although this has varied from year to year and from network to network. In addition, the cutoff was often raised for large aftershock sequences. *Zemlet* is published in Moscow and has historically been available in the U.S.

Materialy po Seismichnosti Sibiri (1970-1990; Materials on the Seismicity of Siberia; hereafter *Materialy*). This is a bi-monthly publication produced in Irkutsk containing both epicenter lists and phase data for each of the seismic networks in Siberia that investigate seismicity of continental regions (Irkutsk, Magadan, Yakutsk, Amur (1979-1990), and Altai). The epicenter list provided here is generally complete, although isolated events listed in the *Far East Bulletin* and in the unpublished data seem to be missing. The largest fraction of the assembled epicenter list comes from this bulletin. This bulletin also contains phase data and arrival times for events equal to or larger than a K-class of 9.5 occurring within a network. *Materialy* issues were published with a low print run of 50 or 75 per issue, with distribution generally restricted to the seismic networks in Siberia.

Seismologicheskii Bulleten - Dalnie Vostok (Intermittent years; Seismological Bulletin - Far East; hereafter *Far East Bulletin*). This quarterly bulletin published in Yuzhno Sakhalinsk is similar in format to *Materialy*, and contains both epicenter lists and phase data.

The *Far East Bulletin* covers the Magadan (listed as separate networks of the "Far East" and "Chukotka"), Amur, Sakhalin, Kamchatka, and Kurile networks. The epicenter list provided here is generally complete for Magadan and Amur, although isolated events found in the unpublished data are missing. For the Kamchatka network, only events of K-class larger than 9.0 are listed. Coverage of phase data varies from network to network. For both portions of the Magadan network as well as the Kamchatka network, phase data for all earthquakes listed are included. For the Amur network, phase data is listed only for events of K-class 8.5 and larger. Phase data from the Sakhalin network are included for shallow events larger than K-class 7.6. The *Far East Bulletin* was also published with a low print run of approximately 60 copies per issue. Complete sets of the *Far East Bulletin* were obtained for 1980-1983 and 1985-1988, and partial sets for 1972-1979 and 1984.

Unpublished Magadan Network Bulletin (1977-1998). Data from 1977 through 1990 were acquired as photocopies, while 1991 through 1998 were computerized files. The epicenter lists and phase data for located events is identical in content and format to that found in the *Far East Bulletin*, although the unpublished bulletins contain much additional material on explosions and unlocated events. The unpublished bulletins are well organized into sections as follows:

-Epicenters of the Far East

-Phase data and arrival times for located earthquakes of the Far East

-Phase data and arrival times for small, unlocatable events of the Far East

-Epicenters of Chukotka

-Phase data and arrival times for located earthquakes of Chukotka

-Phase data and arrival times for small, unlocatable events of Chukotka

-Industrial explosions of the Far East

-Industrial explosions of Chukotka

-Phase data and arrival times for events that occurred within the neighboring Yakutsk network (no epicenter given)

-For 1991, there is a small supplement of arrival times for events which occurred in Alaska

Unpublished Yakutsk Network Draft Material (Intermittent years). Unpublished data from the Yakutsk network was acquired in varying degrees of completeness. The material includes epicenters and phase arrival times from all earthquakes within the Yakutsk network. Also included are epicenters and phase arrival times for some events that occurred in the Magadan, Sakhalin, Amur, and Irkutsk networks. Explosions with associated arrival times are also given but not always located. Most of the Yakutsk data was acquired as photocopies, although some data was entered into the computerized database in Yakutsk. Data entered in Yakutsk does not contain explosions or other supplemental information. Format of the Yakutsk data is generally rough, being handwritten with pencil in script Russian, and not quite in chronological order. For some years of the Yakutsk draft material, a supplement of unpublished Irkutsk network data is included. This supplement contains Irkutsk determined hypocenter parameters and phase data for events that occurred within the Yakutsk network boundaries but were well recorded by Irkutsk stations.

Unpublished Kamchatka Seismicity Catalog. An epicenter catalog was obtained from Petropavlovsk listing all seismicity in the Kamchatka network from 1962 - 1996. The catalog contains over 55,000 located earthquakes. Only events north of 56° were incorporated into the database developed here.

Western Alaska Network Data Tape. The epicenter catalog from the Western Alaska network was taken from Biswas et al. (1983). The complete computerized phase and arrival time listings were downloaded from archive tapes at the Geophysical Institute, University of Alaska, Fairbanks.

Seismograms. Supplemental arrival times were hand picked by Mackey, Fujita, Riegel, Gounbina, and Koz'min from seismograms in Yakutsk and Magadan, as well as develocorder film in Alaska by Mackey.

Other. Miscellaneous data were acquired from various other publications. Earthquake data for 1920-1999 were obtained from the International Seismological Centre, the International Seismological Summary, the U.S. Geological Survey Preliminary Determination of Epicenters (PDE) and Earthquake Data Report (EDR), Alaska Earthquake Information Center (AEIC), Kondorskaya and Shebalin (1982), Andreev (1967), Kovachev et al. (1995), Avetisov (1996), and Starovoit et al. (1995). Additional information on explosions was obtained from Godzikovskaya (1995). Data of the *SSR Catalog* were obtained from the USGS CD-ROM hypocenter database. The *SSR Catalog* is based on data from *Zemlet* and Kondorskaya and Shebalin (1982).

SEISMIC NETWORKS AND DATABASE ASSEMBLY

Yakutsk Regional Network

The first station opened in Yakutsk in 1958, with the Yakutsk network being established in 1960's to monitor regional seismicity. The Yakutsk network initially worked closely with the Magadan EMSD in the collection and analysis of data. In 1982, the cooperative relationship with Magadan EMSD deteriorated and each network began operating independently with little exchange of data. The Yakutsk network has operated a large number of permanent seismic stations in the region, with the maximum number in the late 1980's and early 1990's (Table 1-1). Beginning in 1993, economic problems stemming from the collapse of the Soviet Union resulted in drastic cutbacks by the network and the closure of several stations. In 1993 and 1995, Global Seismograph Network (GSN) stations were opened by IRIS in Yakutsk and Tiksi respectively. The station in Ust'Nera was moved in 1992, and converted to 24 bit digital acquisition in the June of 1999 (Appendix C). There have been many short-term deployments of seismic stations in the Yakutsk network since the mid 1960's (Table 1-1). In addition, four temporary stations were deployed in 1971 for aftershock studies of the magnitude 7.0 Artyk earthquake, and five stations were deployed in 1989 for aftershock studies of the magnitude 6.6 South Yakutia earthquake (Table 1-2).

All earthquake locations determined by the Yakutsk network are done by the historical arcs on map method. For location purposes, the Yakutsk network is broken into northern (Figure 1-5) and southern regions (Figure 1-6). The northern region locates earthquakes on a 1:5,000,000 scale map, and includes stations north of 60° N, while the

Table 1-1. Seismic stations operated by the Yakutsk network.

English Code	Russ. Code	Station Name	Lat.	Long.	Elev. (m)	Date Open	Date Closed	Qu
		Aku	56.46	120.91	700	--.68	--.68	1
AMMS		Ammonl'naya	64.55	143.18	540	--.61	--.62	1
AYKS	АР	Artyk	64.18	145.13	700	—.88		1
BTGS	БТГ	Batagai	67.653	134.630	127	--.75		1
		Bazovskii	56.53	123.42	1080	--.70	--.70	1
CGD	ЧГД	Chagda	58.75	130.60	185	--.68		1
CES	ЧРС	Cherskii	68.75	161.33	10	--.79	--.88	1
		Chil'chi	56.06	122.33	500	--.70	--.70	1
CL1S	ЧЛМ	Chul'man-1	56.85	124.90	650	--.62	--.86	1
CLNS	ЧЛМ	Chul'man-2	56.84	124.90	760	--.86		1
DUYS	ДН	Dunai	73.92	124.49	5	11.89		1
		Dyrynmakit	56.60	121.13	460	--.67	--.67	1
		Imangra-1	56.75	121.24	395	07.67	08.67	1
IMNS	ИМГ	Imangra-2	56.62	120.71	540	--.75	--.79	1
UL2S	КМН	Kamenistyi	65.41	144.83	670	--.88	--.88	1
KHG	ХНД	Khandyga	62.65	135.56	125	--.69	--.94	1
KHNS	ХН	Khani	57.04	121.01	390	--.67 --.75?	--.67 --.76?	1
KHY	ХТС	Khatystyr	55.71	121.57	475	--.68 --.75	--.68 --.82?	1
		Kurul'ta	56.90	121.11	495	--.68	--.68	1
		Kyubyme	63.38	140.95	950	--.74	--.74	2
KYUS	КСР	Kyusyur	70.68	127.37	20	--.85	08.89	1
		Lapri	55.69	124.91	640	--.72	--.73	1
MKUS	МОМА	Moma-Khonuu	66.47	143.22	192	--.83		1

Table 1-1 (cont'd).

		Nagornyi	55.95	124.92	840	--.69	--.69	1
	НГР	Nagornyi Sta	55.92	124.97	920	--.77	--.77	1
NAYS	НБ	Naiba	70.85	130.73	5	--.85		1
NYGS	НРГ	Neryungri	56.68	124.66	760	--.77 --.80	--.78 --.82	1
NZDS	НЖД	Nezhdaninsk	62.50	139.06	603	--.80		1
SAYS	СД	Saidy	68.70	134.45	88	--.80		1
SSYS	ССР	Sasyr	65.16	147.08	580	--.86		1
		Slyuda	56.33	124.12	1080	--.73	--.73	2
SOTS	СТБ	Stolb	72.40	126.82	10	--.85		1
		Sutam	55.96	127.59	700	--.69	--.69	1
TBKS	ТБЛ ТБ	Tabalakh	67.54	136.52	200	--.80		1
TMLS	ТМЛ ТМР	Taimylyr	72.61	121.92	60	--.86		1
		TasYuryakh-1	56.64	121.33	395	02.67	03.67	1
		TasYuryakh-2	56.62	121.41	415	07.67	08.67	1
TLIS	ТНК	Tenkeli	70.18	140.78	110	--.84	--.93	1
TIK	ТКС	Tiksi	71.632	128.863	38	3.56	--.93	1
TIXI		Tiksi-GSN	71.64	128.87	30	--.95		1
		Tokarikan	56.10	126.42	800	--.72	--.73	3
TUG1		Tungurcha-1	57.33	121.48	440	--.70	--.70	1
TUG	ТНГ	Tungurcha-2	57.27	121.48	315	--.78		1
UL1S	ТЕБ	Tyubelyakh	65.37	143.15	380	--.88	--.88	3
UNR1	У-НР	Ust' Nera-1	64.566	143.230	485	--.62	--.92	1
UNR	У-Н	Ust' Nera-2	64.565	143.242	485	--.92		G
USZ	У-Н	Ust' Nyukzha	56.56	121.59	415	--.64		1

Table 1-1 (cont'd).

UURS	УРК	Ust' Urkima	56.31	123.16	540	--.81		1
YAK1		Yakutsk-1	62.015	129.722	90	10.57	--.62	1
YAK	ЯК	Yakutsk-2	62.030	129.677	91	--.62		1
YUBS	ЮБЛ ЮБТ	Yubileniya	70.74	136.10	10	--.86	--.93	1
ZYRS	ЗРН	Zyryanka	65.72	149.82	120	--.82	--.90	1

Table 1-2. Temporary seismic stations from the Yakutsk region. The 1989 South Yakutia and the 1971 Artyk deployments were aftershock studies.

English Code	Russ. Code	Station Name	Lat.	Long.	Elev. (m)	Date Open	Date Closed	Qu
1989 South Yakutia Deployment								
ACHS	АМД	Amedichi	57.03	122.85	930	05.89	08.89	1
CKHS	ЧКЧ	Chokchoi	57.65	121.72	240	--.89	--.89	1
KBKS	КБК КБТ	Kabaktan	56.68	122.42	1010	05.89	08.89	1
SYLS	СЛХ	Syllakh	57.12	121.86	600	--.89	--.89	1
YRGS	ЯРГ	Yaruga	57.49	123.07	780	--.89	--.89	2
1971 Artyk Deployment								
AYKS	АР	Artyk	64.18	145.13	700	06.71	--.71	1
AY1S		Kobdi	64.20	145.51	800	06.71	--.71	1
AY2S	ОЗР	Ozernaya	63.75	146.11	875	06.71	--.71	2
AY3S		Tungusskii	64.20	146.38	1080	--.71	--.71	1

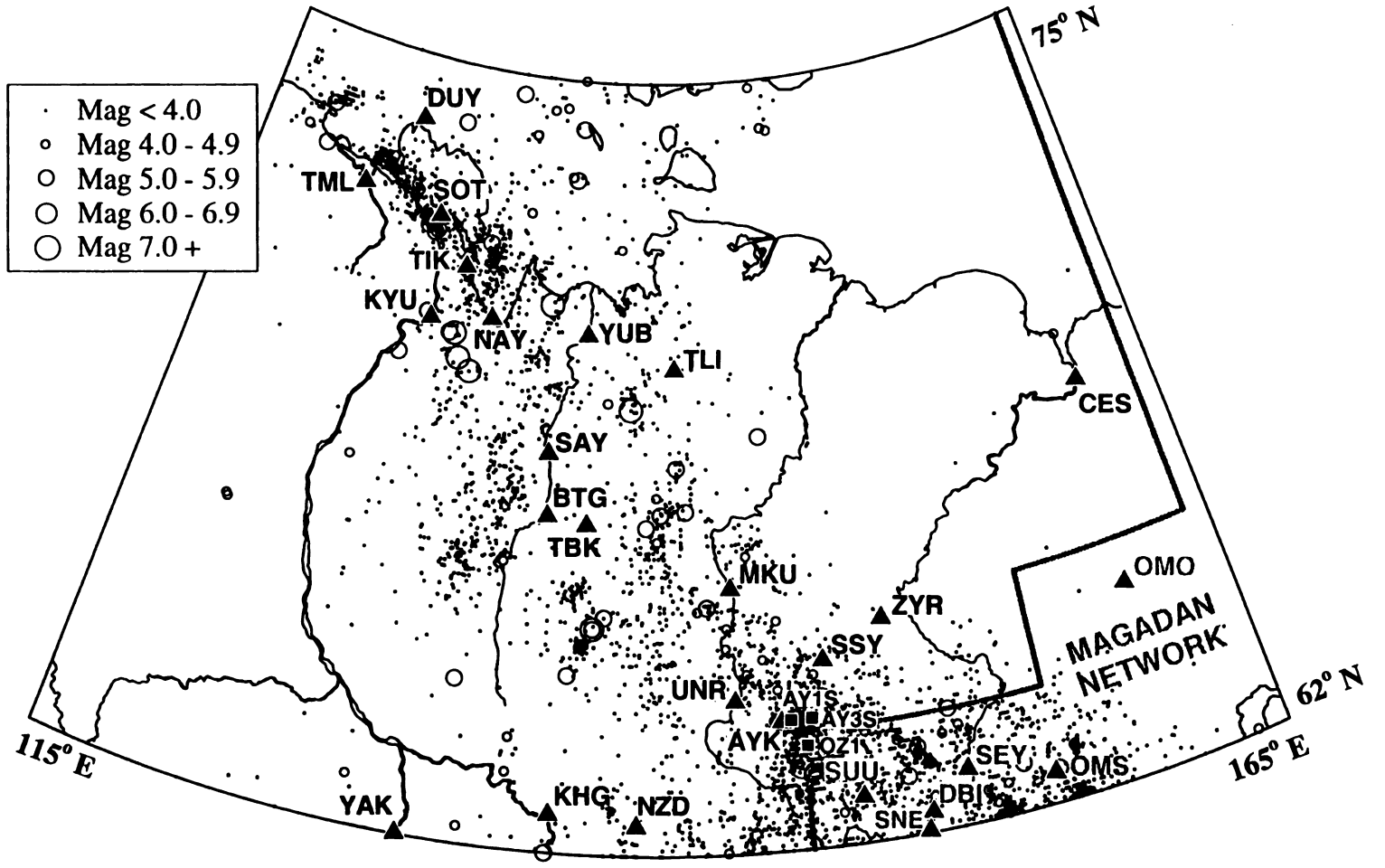

Figure 1-5. Seismicity and seismic stations of the northern Yakutsk network. Temporary seismic stations deployed after the 1971 Aryk earthquake are shown as squares.

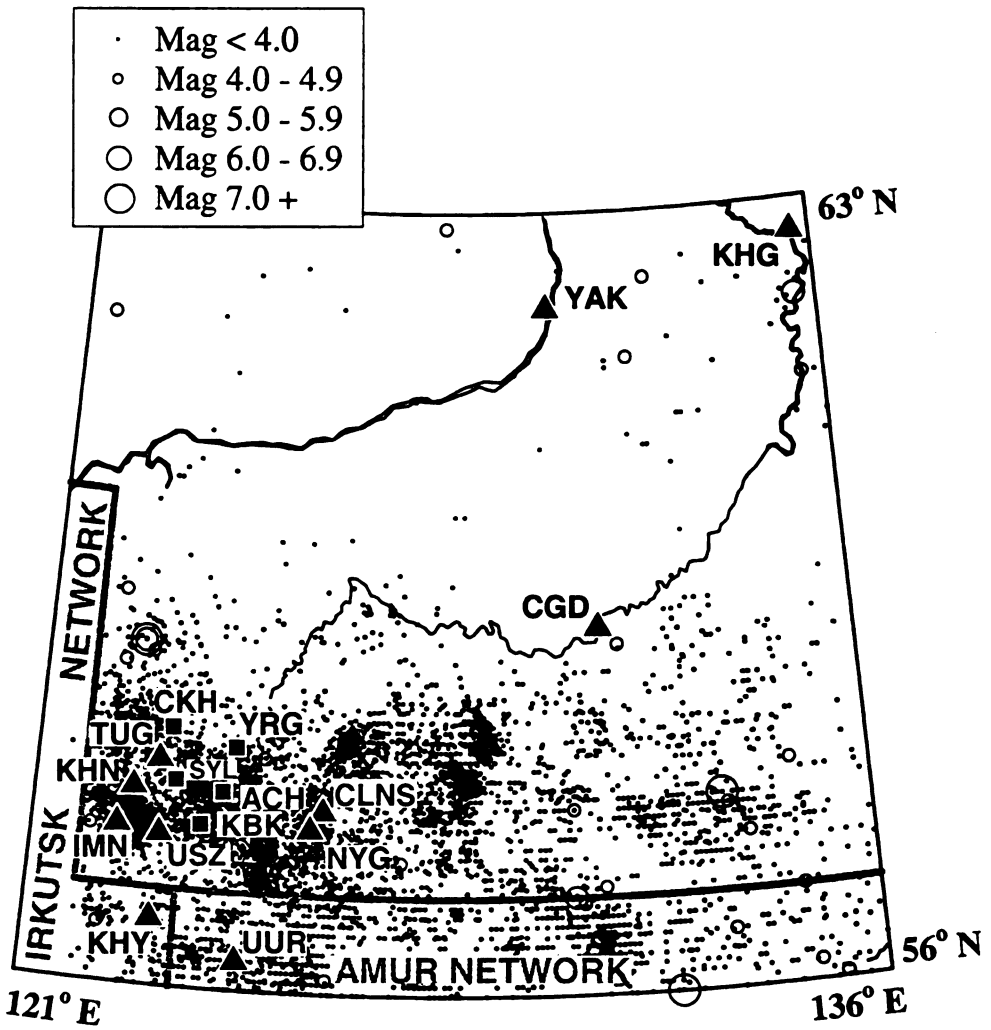

Figure 1-6. Seismicity and seismic stations of the southern Yakutsk network. Temporary seismic stations deployed after the 1989 south Yakutia earthquake are depicted as squares.

southern region includes stations south of 63° N. Stations at Yakutsk, Khandyga, and Nezhdandinsk are included in both regions. Sometimes, for the Lena River Delta and Laptev Sea regions, a 1:2,400,000 scale map is used. In many cases, data are acquired for stations which are physically off the map used in determining locations. Data from such stations are omitted from the location process; only those stations within the bounds of the map on which the arcs are drawn are used. Thus, data from the northern region are not used when locating earthquakes from the southern region, as the northern stations do not fit on the map, and vice versa. Epicentral distances are determined by Sg-Pg time differences for each station. Many earthquakes have phase arrival times from only three or four stations, and only one P arrival (usually Pg). In this case, the one available Sg-Pg time is used to define the origin time and other distances are determined using the Sg - Origin time difference from remaining stations. Locations in the northern region use a Pg velocity of 6.1 km/sec. Sg velocities used are 3.5 km/sec or 3.6 km/sec, whichever works best for the particular earthquake. Generally, 3.5 km/sec works best in the Laptev Sea and Lena River Delta region around Tiksi. In the southern region, Pg velocities used are 6.0 km/sec or 6.1 km/sec, whichever is best for the particular earthquake. The Sg velocity used is 3.6 km/sec, except for the Aldan shield, where 3.7 km/sec works best (Koz'min, pers. comm.).

There were much data acquired by stations in the Magadan, Amur, and Irkutsk networks which were not exchanged with the Yakutsk network, and subsequently not included in any of the published bulletins. Historically, the Yakutsk network had access to data from the Magadan stations of Susuman, Seimchan, Kulu, and Debin (See Magadan Network below), and occasionally others. However, overall, the unpublished Magadan network bulletin added a significant amount of phase and arrival time data for events in the

Yakutsk network. Of stations in the Amur region, generally only Kirovskii was used by the Yakutsk network. In comparison of Kirovskii arrivals reported in the Yakutsk unpublished bulletin with those in published sources, there are some differences in reported phases and arrival times. The discrepancy is suspected to be a result of Yakutsk receiving the preliminary Kirovskii station bulletin with times and phases determined by the station operator. The phases and times of arrivals in published sources of the Amur data (*Materialy*, and *Far East Bulletin*) represent the final interpretation, which would have presumably been done in conjunction with other records by the Amur network. When possible, what is believed to be the final interpretation for Kirovskii phases and arrival times is used in the database. Unfortunately, there were no additional unpublished data from the Amur regional network available for Yakutsk region events beyond that which was already contained in the Yakutsk bulletin. Additional data most certainly does exist in the Amur network. For earthquakes in the Yakutsk region that are located by the Irkutsk network from Irkutsk stations, a printout of the hypocenter, phases, and arrival times is supplied to Yakutsk. From this printout, Yakutsk normally uses only the data from Tupik (TUP), Srednyi Kalar (SRK), and Chara (CRS) in their locations. Other stations will not fit on the map used in the locations, thus are not used. For the database assembled here, all the available Irkutsk data were included.

There are some problems with data supplied to global databases, such as ISC, for events occurring in the Yakutsk region. Data reported for stations in Yakutsk network (UNR, YAK, TIK, USZ, UUR, and CLN) are preliminary time picks by station operators and often have high residuals. This can result from poor time picks, or a secondary Pg phase being reported as a first arriving Pn phase. In these cases the phase and time from the

unpublished data are used in the database assembled here, as they are not derived from preliminary seismogram analysis.

For this database, hypocenter parameters were primarily taken from *Zemlet* and *Materialy* (1963-1990) and unpublished draft material (1991-1996). Phase data and arrival times for events larger than K-class of 9.5 were taken from *Materialy* (1970-1990). Phase data and arrival times for smaller events are from unpublished Yakutsk network bulletins (1982-1990). Unpublished data from the 1971 Artyk and 1989 South Yakutia aftershock studies are also included in the database. All data since 1990 are from unpublished network bulletins. For several events along the boundary with the Magadan network, supplemental arrival times were read from Magadan network seismograms.

In comparing data from the three primary sources of *Materialy, Zemlet*, and the unpublished network bulletin, no major variations were found. The unpublished draft material contains hypocenters which sometimes differ with those found in *Materialy* and *Zemlet*. The reason for this is not entirely clear. The seismicity catalog in *Zemlet* is identical to that in *Materialy*, except it does not list events smaller than K-class 7.5. For all years, events with statistically poor locations listed in *Materialy* and *Zemlet* have origin times rounded to the nearest second and coordinates to nearest 0.1 degree. For these events, the unpublished draft material gives origin time to 0.1 second and coordinates to 0.01 degree. In many cases, the hypocenter parameters were originally entered into the database using *Materialy* or *Zemlet*, and retain the less precise coordinates.

A linear regression relating K-class for the Yakutsk network to ISC magnitude is shown in Figure 1-7. The relationship determined is

$$K = 2.05 + 2.15\ (M) \qquad (1\text{-}2)$$

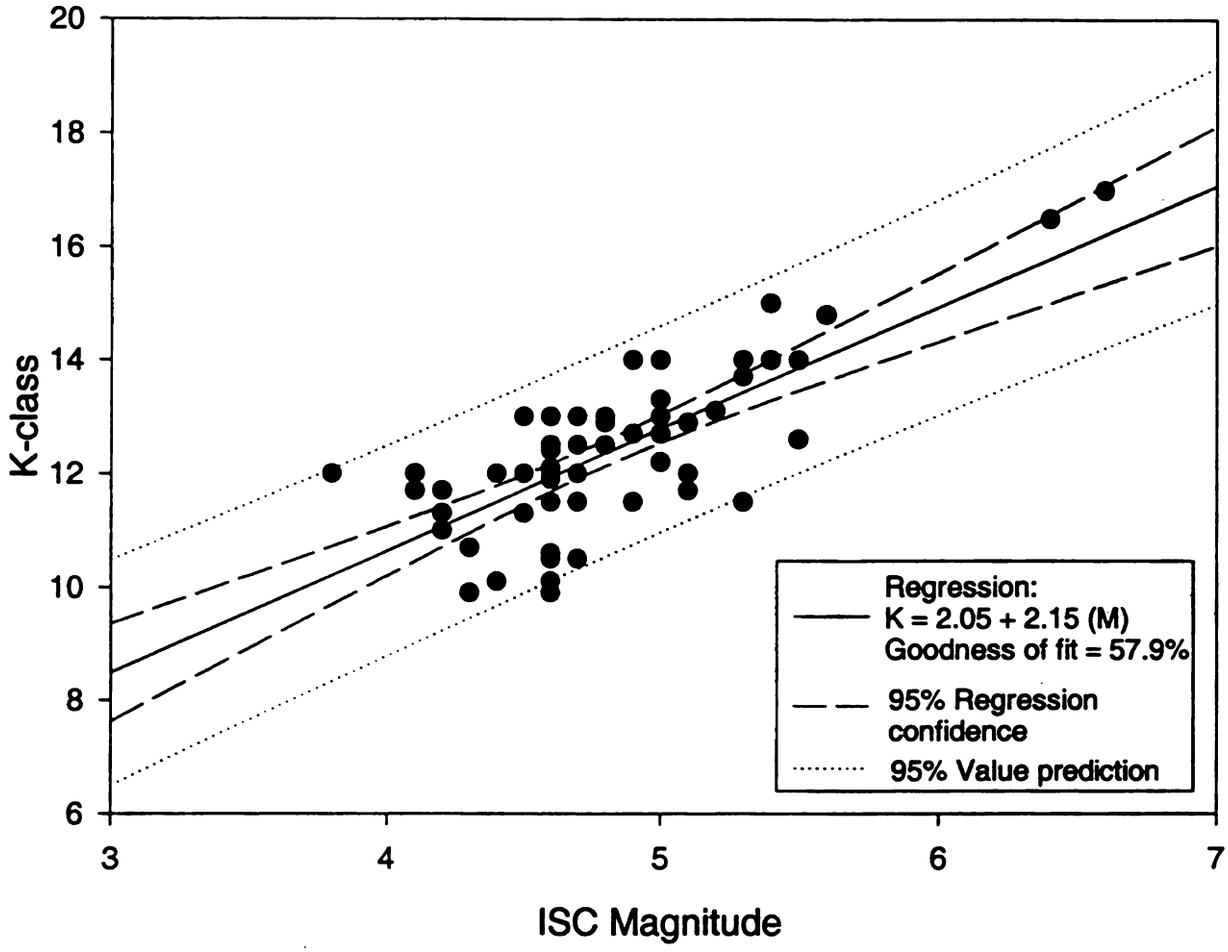

Figure 1-7. Relationship between K-class and ISC reported magnitude in the Yakutsk network.

where K is K-class and M is magnitude. In general, it was found that events occurring in the Laptev Sea tend to have a lower K-class value than continental events for a given magnitude. There are two possible reasons for this. First, many of the Yakutsk epicenters are further south than the ISC locations. This may put the events erroneously close to the Yakutsk stations, which for a given amplitude will tend to lower the K-class value assigned. Second, most of the raypaths from Laptev Sea events to Yakutsk network seismic stations travel down the axis of the Laptev Sea rift. This may result in preferentially greater attenuation of signals at Yakutsk stations relative to teleseismic stations used to calculate magnitude.

Temporary stations in the Lena River Delta, Laptev Sea, and New Siberian Islands

The Laptev Sea region has had several temporary stations or networks deployed. The All-Union Research Institute of Ocean Geology (VNIIOkeanologiya) operated one to three stations per summer in the New Siberian Islands from 1972 through 1976 (Figure 1-8; Table 1-3; Avetisov, 1983, 1996). Three stations were operated just west of the Lena River Delta from July to September, 1975 (Table 1-3; Avetisov, 1983, 1996). Several local networks of stations were also deployed during the summers in and around the Lena River Delta between 1984 and 1988 (Figure 1-9; Avetisov, 1996). With a few exceptions, the events located in studies by Avetisov were not located by the Yakutsk regional network.

In July and August, 1989, the P. P. Shirshov Institute of Oceanology deployed a small five station array of ocean bottom seismometers (OBS) in two locations within Buorkhaya Bay, in the Laptev Sea (Figure 1-10; Table 1-3; Kovachev et al., 1995). A total of 26 events were located from the two OBS deployments, two of which were also located by the Yakutsk regional network.

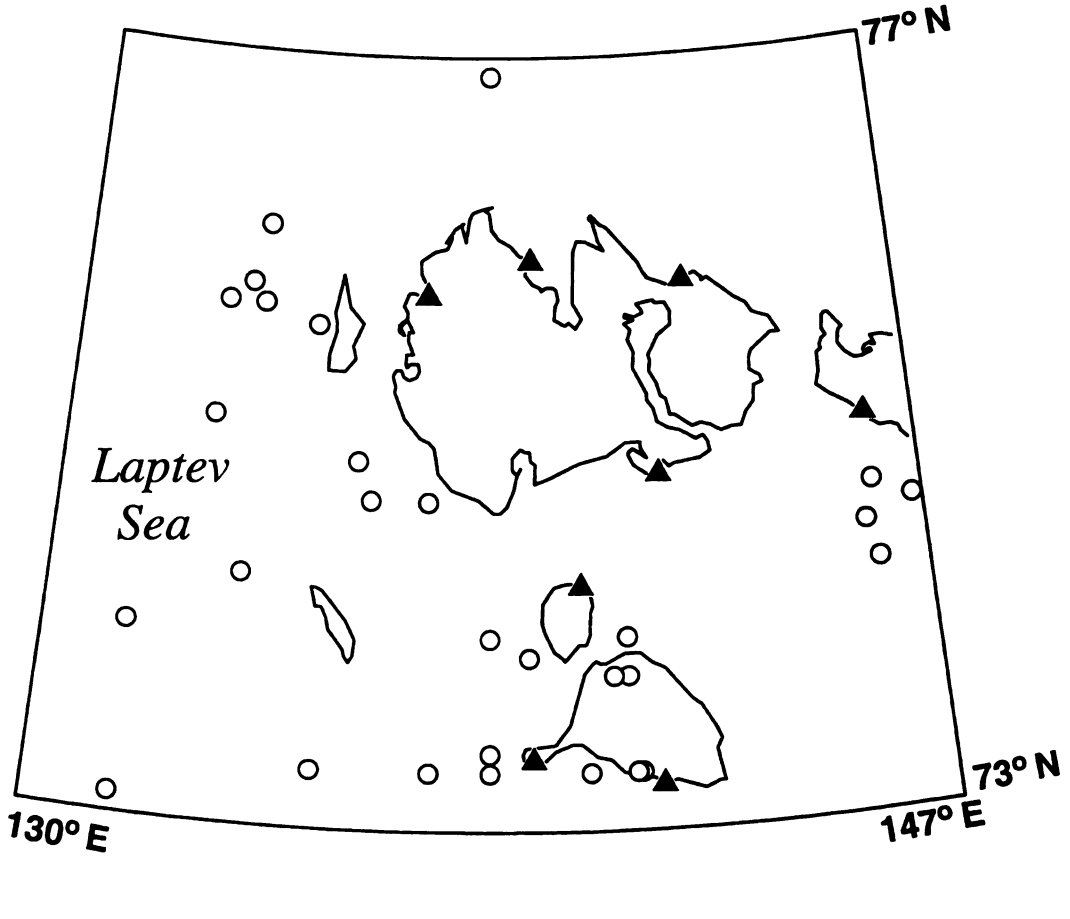

Figure 1-8. Summer seismic station deployments in the New Siberian Islands region from Avetisov (1996). Stations shown as triangles and located events as circles.

Table 1-3. Temporary stations in the New Siberian Islands, west of the Lena River Delta (Avetisov, 1983; Avetisov, 1996) and the Laptev Sea (Kovachev et al., 1996).

English Code	Russ. Code	Station Name	Lat.	Long.	Elev. (m)	Date Open	Date Closed	Qu
New Siberian Islands Stations								
		Kotelnyi	75.760	137.600		8.72	9.72	-
		Kigilyakh	73.367	139.867		6.73	9.73	-
		Dimnoe	73.233	142.400		3.74	4.74	-
		Zemlya Bunge	74.8330	142.583		4.75	6.75	-
		Novaya Sibir	75.0500	147.000		4.75	6.75	-
		Mys Khvoinova	74.2670	140.883		4.76	6.76	-
		Mys Nerpichii	75.8330	143.333		4.76	6.76	-
		Mys Diring-Ayan	75.9500	139.917		5.76	6.76	-
Stations west of the Lena River Delta - All dates are 1975								
		Udzha	71.25	117.17		08/27	09/19	-
		Kalgannakh	71.83	114.33		07/21	08/10	-
		Chochurdakh	72.83	116.25		08/13	09/26	-
Laptev Sea Ocean Bottom Seismometer Deployment 1 - All dates are 1989								
	# 1		71.75	131.40	-18	07/28	08/9	-
	# 2		71.85	131.22	-20	07/28	08/9	-
	# 3		71.90	130.42	-17	07/29	08/9	-
	# 4		71.77	130.82	-17	07/29	08/9	-
	# 5		71.62	130.78	-16	07/29	08/9	-

Table 1-3 (Cont'd)

Laptev Sea Ocean Bottom Seismometer Deployment 2 - All dates are 1989								
	# 1		72.283	131.30	-18	08/10	08/22	-
	# 2		72.45	130.35	-10	08/10	08/22	-
	# 3		72.466	131.20	-19	08/10	08/22	-
	# 4		72.616	130.60	-16	08/10	08/22	-
	# 5		72.267	130.65	-13	08/10	08/22	-

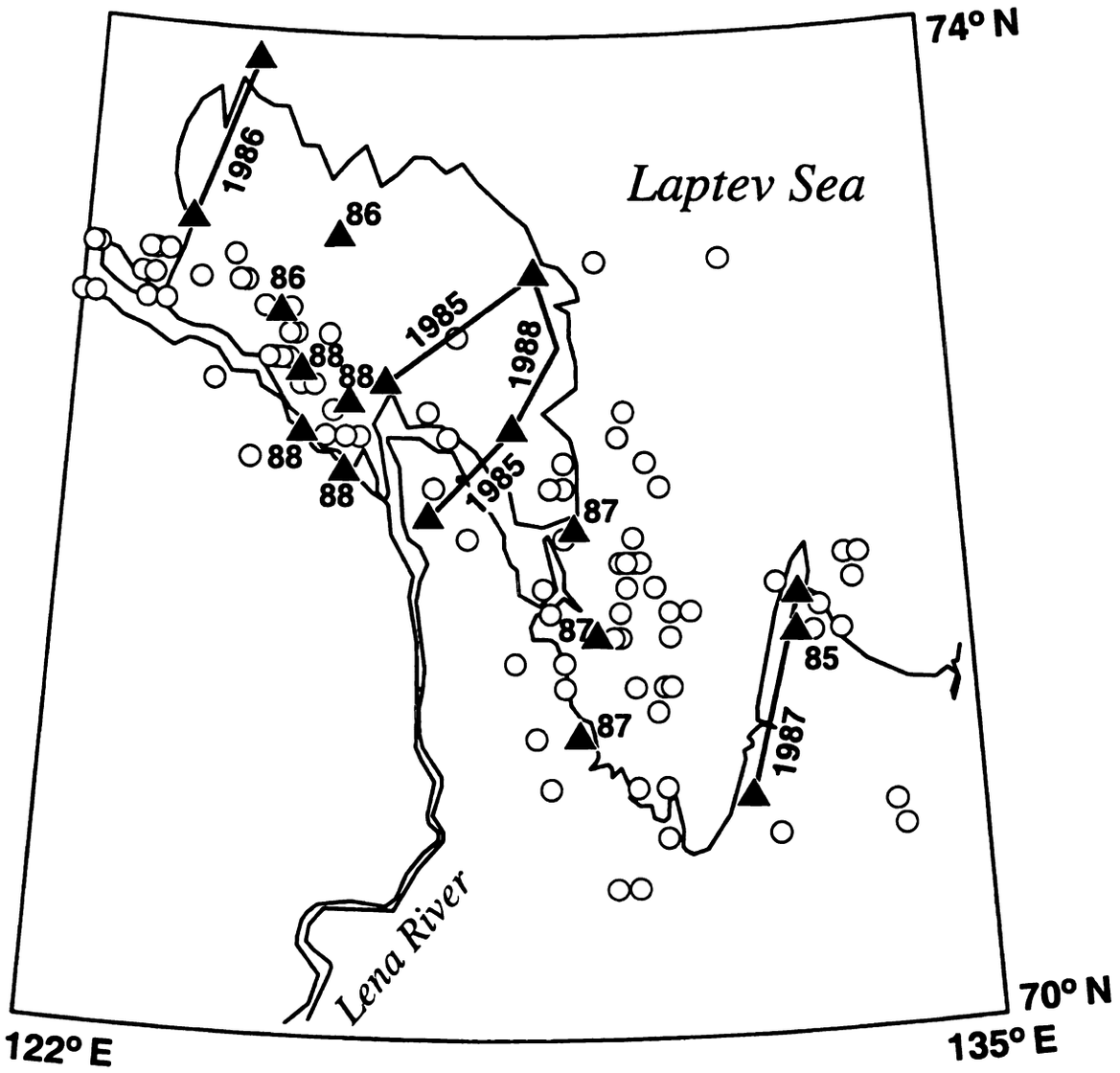

Figure 1-9. Summer seismic station deployments in the Lena River Delta region from Avetisov (1996). Stations shown as triangles and located events as circles. Stations deployed for refration profiles shown as lines. Numbers indicate years of operation.

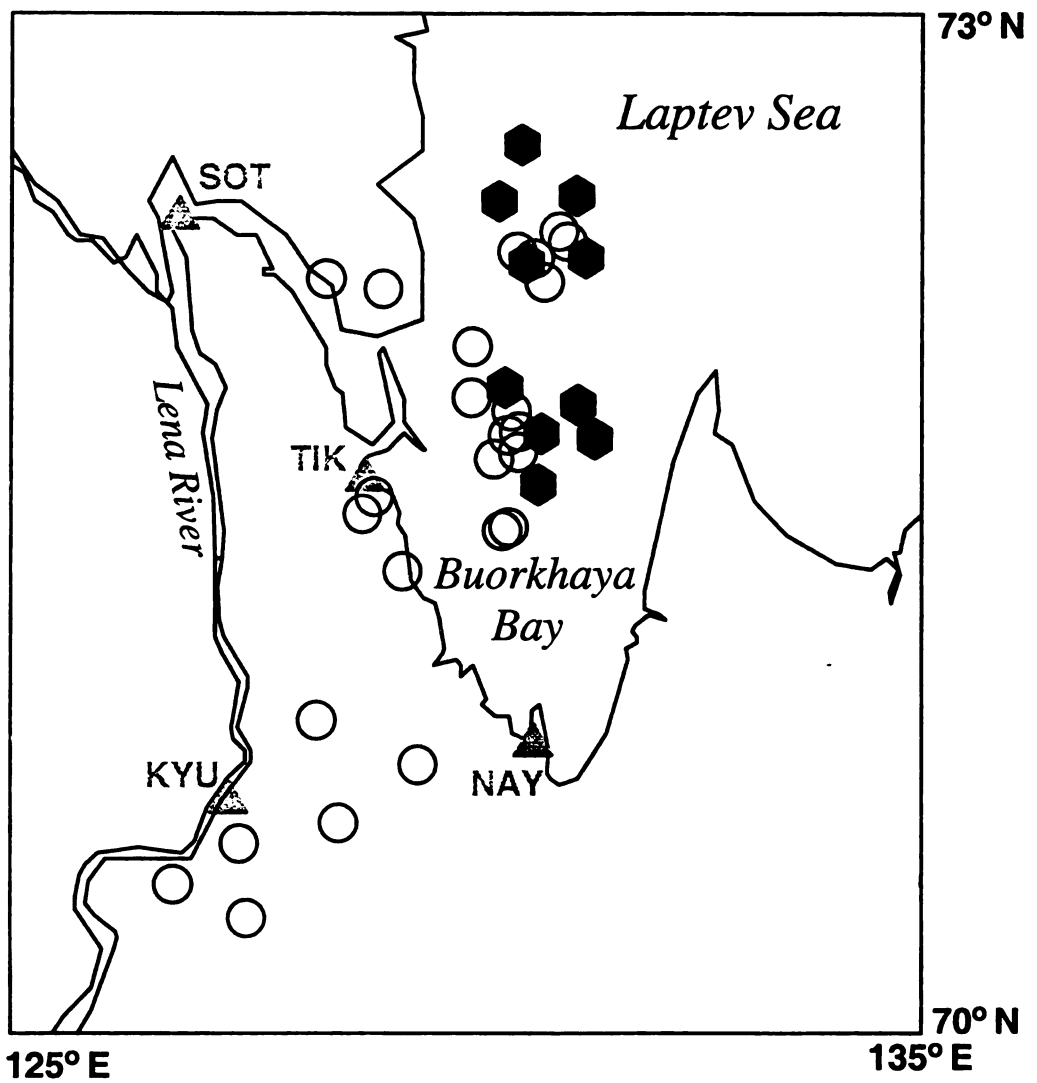

Figure 1-10. The 1989 summer deployments of ocean bottom seismometers shown as hexagons and located seismicity shown as circles. Events and stations from Kovachev et al. (1995). Yakutsk network stations in gray for reference.

The temporary OBS, New Siberian Islands, and the Lena River Delta seismic stations were operated independently from the Yakutsk network stations. Events located and listed in Kovachev et al. (1995) and Avetisov (1996) are included in the database. Phase data were not available.

Magadan Regional Network

The first station opened in the region was Magadan in 1952. In the late 1960's following the deployment of the northeast Russia test network, installation of permanent seismic stations began. These stations were operated in conjunction with stations in the Yakutsk network. The Magadan Experimental Methodological Seismological Division (EMSD) network was established as a separate entity in December, 1979 to monitor regional seismicity. The Magadan EMSD initially worked closely with the network in Yakutsk in the collection and analysis of data. In 1982, the cooperative relationship with Yakutsk deteriorated and each network began operating independently with little exchange of data. The reason for this is not clear. The Magadan EMSD has operated a total of 15 permanent seismic stations in the region, excluding those in the Chukotka network, which were also operated by the Magadan EMSD (Figure 1-11; Table 1-4). All stations in the Magadan region operate at least one complete three component set of instruments. Horizontal instruments deployed in the Magadan region are oriented with respect to local magnetic north, not geographic north (Savchenko, pers. comm.). The largest number of stations were active in the late 1980's and early 1990's. Three temporary stations, Obo, Orotukan, and Yagodnoya were operated in 1977. A few arrival times are also reported for a station Obo

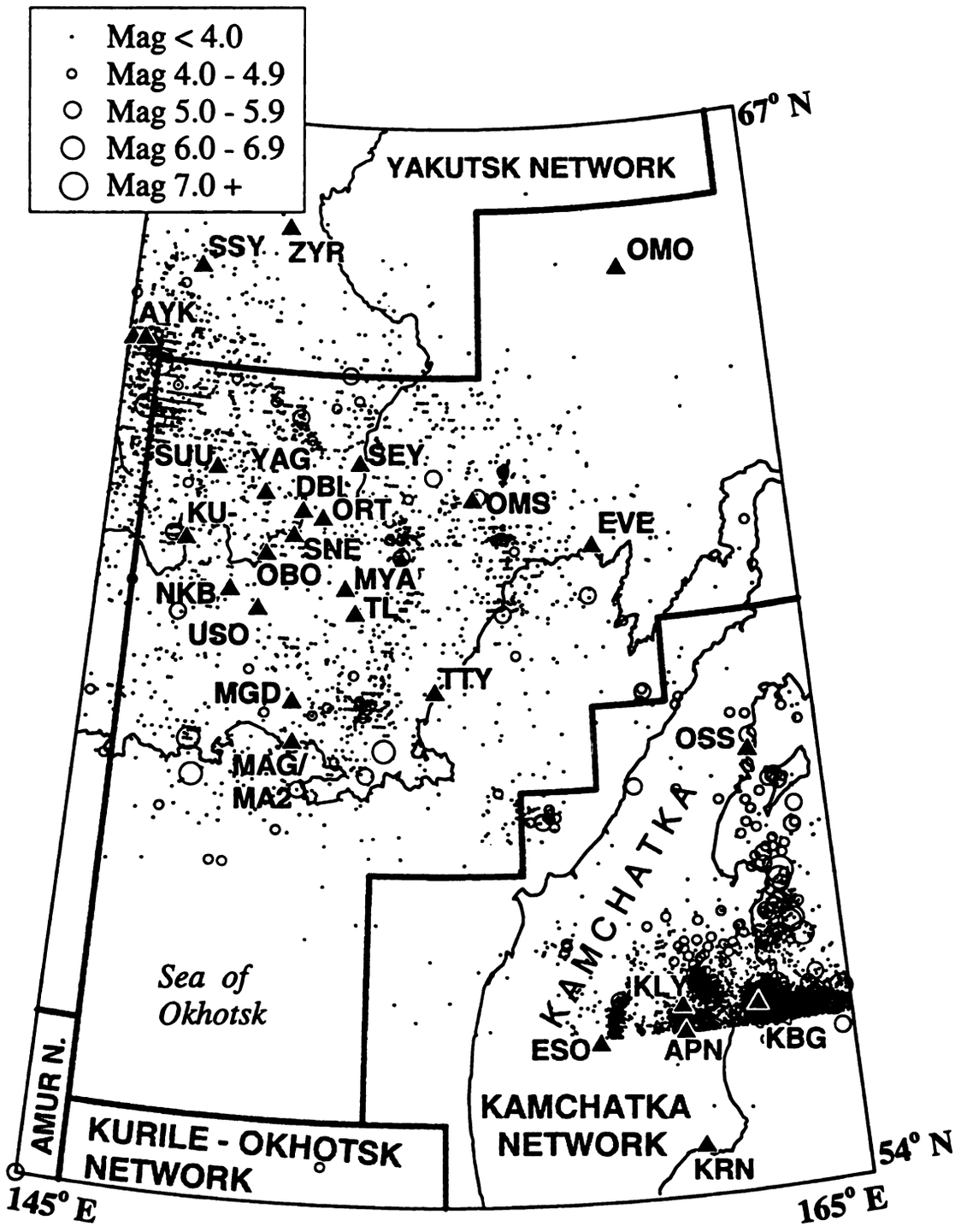

Figure 1-11. Seismicity and seismic stations of the Magadan network.

Table 1-4. Seismic stations operated in the Magadan region. All stations were operated by the Magadan EMSD.

English Code	Russ. Code	Station Name	Lat.	Long.	Elev. (m)	Date Open	Date Closed	Qu
DBI	ДБН	Debin	62.339	150.751	332	--.74	--.92	G
EVES	ЭВН	Evensk	61.92	159.23	22	--.80	7.93	1
KU-S	КЛ КЛУ	Kulu	61.889	147.431	655	1.80	10.92	G
MAG	МГД	Magadan	59.560	150.805	78	1.52	1.92	1
MA2	MA2	Magadan-GSN	59.575	150.768	339	9.93		1
MYAS	МКТ	Myakit	61.407	152.093	670	--.83	--.88	G
NKBS	НЛБ	Nel'koba	61.34 61.338	148.81 148.813	531	9.83 6.97	6.97 9.99	1 G
OBO		Obo	61.80	149.77	440	--.77	—.77	1
OMCH	ОМЧ	Omchak	61.67	147.87	820	9.99		1
OMOS	ОМЛ	Omolon	65.23	160.54	260	6.82	7.93	1
OMS	ОМС	Omuskchan	62.52	155.77	527	12.67		1
ORT		Orotukan	62.26	151.34	470	--.77	--.77	1
SEY	СМЧ	Seimchan	62.93	152.38	211	4.69		1
SNES	СНГ	Sinegor'e	62.09	150.52	400	--.76	--.88	1
MGD	MA1 МГД-1 СТК	Stekol'nyi	60.046 (60.046)	150.730 (150.730)	221	3.71 –.94	–.94	1 1
SUUS	СМН ССМ	Susuman	62.78 (62.78) 62.779	148.15 (148.15) 148.163	640	8.69 --.95 --.98	--.95 --.98	1 1 G
TTYS	ТХТ	Takhtoyamsk	60.20	154.68	11	9.87		1
TL-S TLAS	ТЛА ТЛ	Talaya	61.134	152.398	730	1.89		G
USO	У-ОМ	Ust' Omchug	61.13	149.63	580	--.68	--.83	1
YAG		Yagodnoe	62.53	149.62	480	--.77	--.77	1

in 1981. Beginning in 1992, economic problems stemming from the collapse of the Soviet Union resulted in drastic cutbacks by the network and the closure of several stations.

By the mid 1990's, the Magadan network was reduced to operational stations only in Susuman, Omsukchan, Seimchan, Magadan, and Stekolnyi. Two other stations, Talaya and Nelkoba, were mothballed. The economic situation for the network was sufficiently bad that vegetables were sold out of the stations to keep them open (Savchenko, pers. comm.). Today, seven stations remain open, with Magadan (MA2) being a GSN station and Seimchan (SEY) being a Geoscope station. Equipment problems in Seimchan have resulted in a significant amount (years) of downtime for the Geoscope station. In the summer of 1999, stations in Nelkoba, Seimchan, Susuman, and Talaya were converted from photo paper to PC based 24 bit resolution digital recording in conjunction with M.S.U. (Appendix C). The station in Seimchan uses the existing Streckeisen seismometer installed by Geoscope. In late September 1999, the town of Nelkoba was abandoned, and the station was moved to Omchak, approximately 70 km to the northwest of Nelkoba.

Several stations of the Magadan regional network were also moved slightly in the mid to late 1990's. In 1994, Stekolnyi was moved approximately 0.6 km north from its original location. Nelkoba was moved approximately 150 m north in the summer of 1997. Susuman was moved twice. First, in 1995 the station was moved 100 - 200 m, but the location remained near the center of town. In the fall of 1998, the station was moved approximately 1 km to the east to the meteorological station outside of town. For these stations, codes or coordinates were not changed or updated in any of the available data sources, published or unpublished.

There have been three methods of determining earthquake locations in the Magadan network, each using Sg minus Pg times. Prior to 1982, locations were computed primarily by hand, and occasionally using a "Besmas 6" electronic calculating machine. In 1982, they began using computers for locations, which were compared to arc on map epicenters. The computer determined epicenters were often "adjusted" to better agree with a paper location if there was a discrepancy between the two. The adjustment procedure was dropped in the early 1990's, when the network switched to computer only hypocenter calculations. In the location procedure, the travel time curves used were derived from the 1959 Magadan-Ust'Srednikan DSS (Deep Seismic Sounding; refraction) profile (Ansimov et al., 1967; Davydova et al., 1968). The model for calculation of the travel time curves uses a three layer crust (Figure 1-12). The uppermost layer is 6.0 km thick and has a P velocity of 5.3 km/s. The velocity at the base of layer one is 6.0 km/s, which is used for the Pg velocity. The second layer extends from 6.0 km to a depth of 20.0 km and has a P velocity of 5.8 km/s. A refraction surface at the base of the second layer has a P velocity of 6.7 km/s and is used as the Conrad discontinuity for P*. The third crustal layer lies between 20 and 35 km depth and has a P velocity of 6.1 km/s. The base of layer three is the Moho, with a Pn velocity of 8.1 km/s. Table 1-5 lists the travel times used in the Magadan network for Pg, Sg, P*, S*, Pn, and Sn phases. These travel times are derived from this model and are calibrated for a hypocenter depth of 5.0 km. The travel times are also plotted in Figure 1-13. The crustal model used here is counterintuitive from a geologic standpoint, as high velocity planes are sandwiched between thick low velocity layers (Figure 1-12). Vertical velocity profiles with thin high velocity zones between much thicker low velocity layers is typical of those determined from DSS profiles in the former Soviet Union (Gal'perin, 1974). Slopes of travel

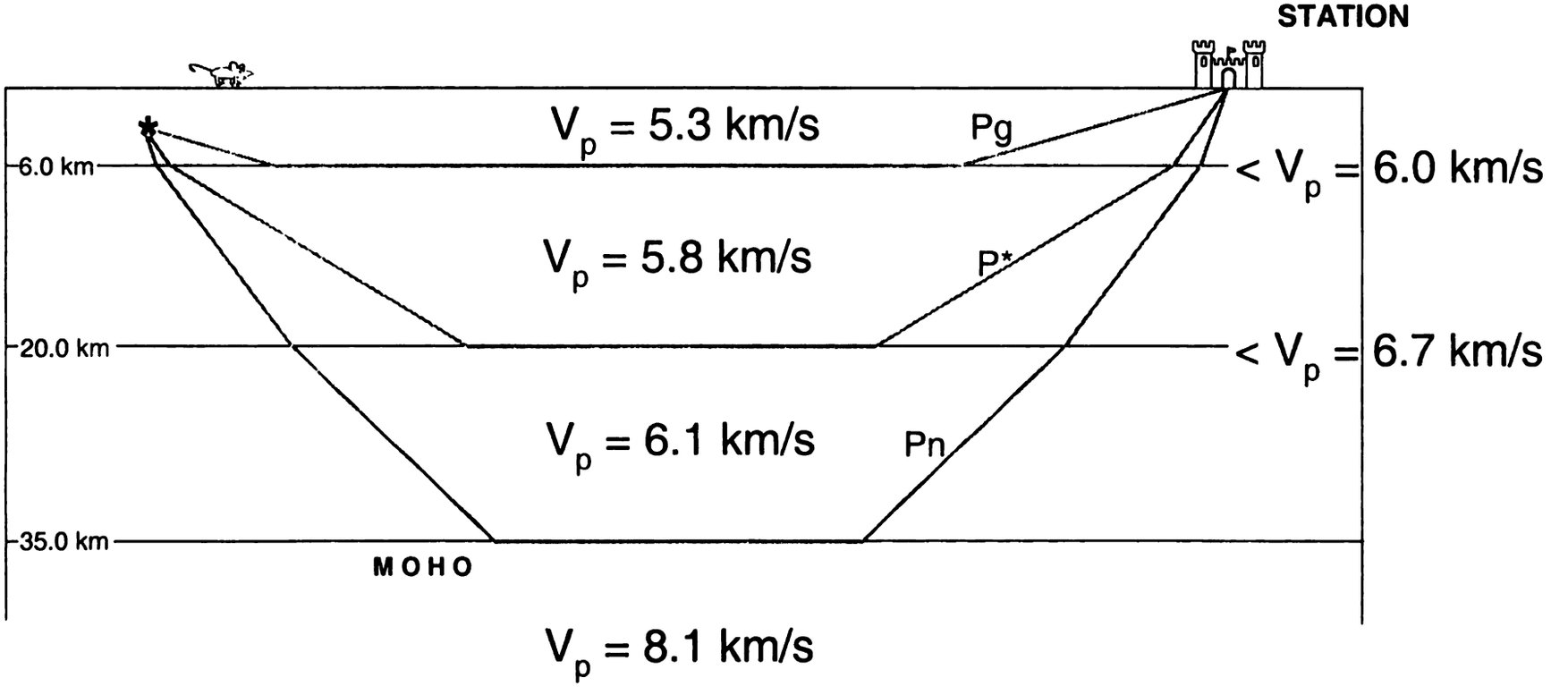

Figure 1-12. Crustal velocity profile used for locating earthquakes in the Magadan region. Assumed raypaths for a 3 km deep event (asterisk) are shown.

Table 1-5. Travel time curve used for locating earthquakes in the Magadan network. This table depicts travel times for a hypocentral depth of 5 km.

km	Pg (s)	Sg (s)	P* (s)	S* (s)	Pn (s)	Sn (s)
0.0	0.7	1.3	4.3	7.5	8.7	15.1
10.0	2.4	4.2	5.8	10.1	9.9	17.3
20.0	4.1	7.1	7.3	12.7	11.2	19.4
30.0	5.7	10.0	8.8	15.3	12.4	21.6
40.0	7.4	12.9	10.3	17.9	13.6	23.7
50.0	9.1	15.8	11.8	20.5	14.9	25.9
60.0	10.7	18.7	13.3	23.1	16.1	28.0
70.0	12.4	21.6	14.8	25.7	17.3	30.2
80.0	14.1	24.5	16.3	28.3	18.6	32.3
90.0	15.7	27.4	17.7	30.9	19.8	34.5
100.	17.4	30.3	19.2	33.5	21.0	36.6
110.	19.1	33.2	20.7	36.1	22.3	38.8
120.	20.7	36.1	22.2	38.7	23.5	40.9
130.	22.4	39.0	23.7	41.3	24.7	43.1
140.	24.1	41.9	25.2	43.9	26.	45.2
150.	25.7	44.8	26.7	46.5	27.2	47.3
160.	27.4	47.7	28.2	49.1	28.4	49.5
170.	29.1	50.6	29.7	51.7	29.7	51.6
180.	30.7	53.5	31.2	54.2	30.9	53.8
190.	32.4	56.4	32.7	56.8	32.1	55.9
200.	34.1	59.3	34.2	59.4	33.4	58.1
210.	35.7	62.2	35.7	62.0	34.6	60.2
220.	37.4	65.1	37.1	64.6	35.9	62.4
230.	39.1	68.0	38.6	67.2	37.1	64.5
240.	40.7	70.9	40.1	69.8	38.3	66.7
250.	42.4	73.8	41.6	72.4	39.6	68.8
260.	44.1	76.7	43.1	75.0	40.8	71.0
270.	45.7	79.6	44.6	77.6	42.0	73.1
280.	47.4	82.5	46.1	80.2	43.3	75.3
290.	49.1	85.4	47.6	82.8	44.5	77.4
300.	50.7	88.3	49.1	85.4	45.7	79.6
320.	54.1	94.1	52.1	90.6	48.2	83.9
340.	57.4	99.9	55.1	95.8	50.7	88.2
360.	60.7	105.7	58.0	101.0	53.1	92.5
370.	62.4	108.6	59.5	103.6	54.4	94.6
380.	64.1	111.5	61.0	106.2	55.6	96.8
400.	67.4	117.3	64.0	111.4	58.1	101.1
420.	70.7	123.1	67.0	116.6	60.5	105.3
440.	74.1	128.9	70.0	121.8	63.0	109.6
460.	77.4	134.7	73.0	127.0	65.5	113.9
480.	80.7	140.5	76.0	132.2	68.0	118.2
500.	84.1	146.3	78.9	137.4	70.4	122.5
520.	87.4	152.1	81.9	142.5	72.9	126.8
540.	90.7	157.9	84.9	147.7	75.4	131.1
560.	94.1	163.7	87.9	152.9	77.8	135.4
580.	97.4	169.5	90.9	158.1	80.3	139.7
600.	100.7	175.3	93.9	163.3	82.8	144.0
650.	109.1	189.8	101.3	176.3	88.9	154.8
700.	117.4	204.3	108.8	189.3	95.1	165.5
750.	125.7	218.8	116.3	202.3	101.3	176.2
800.	134.1	233.3	123.7	215.3	107.5	187.0
850.	142.4	247.8	131.2	228.2	113.6	197.7
900.	150.7	262.3	138.6	241.2	119.8	208.5
950.	159.1	276.8	146.1	254.2	126.0	219.2
990.	165.7	288.4	152.1	264.6	130.9	227.8

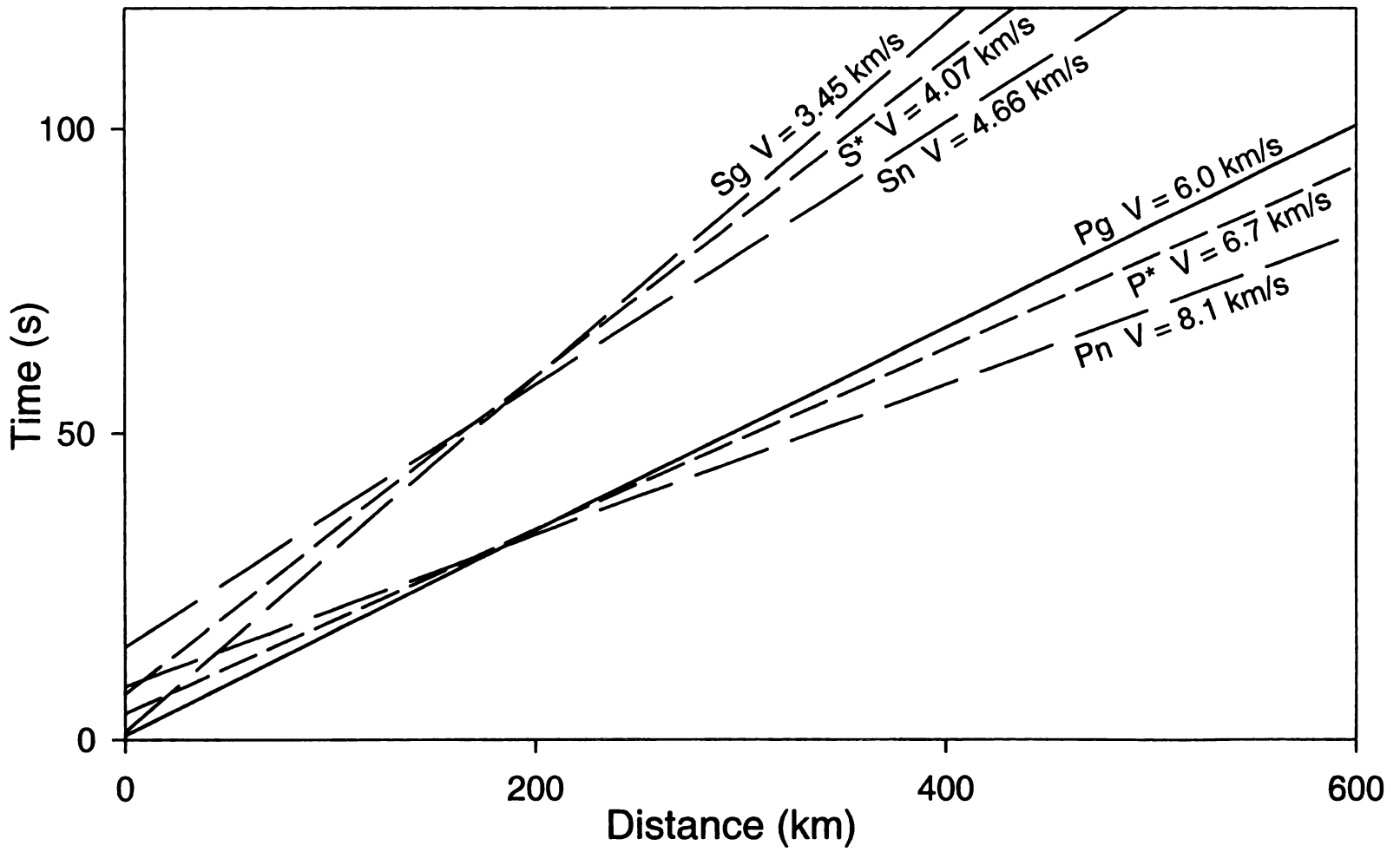

Figure 1-13. Travel time curves used for earthquake locations in the Magadan network. These curves are calibrated for a hypocentral depth of 5 km.

time curves depicted in Figure 1-13 reflect only the thin high velocity planes. It is unclear how the initial time offset of the seismic phases at a distance of 0.0 km is determined. The time offset at 0.0 km is not calculated using the layer velocities in the model applied to a vertical path. At 0.0 km distance, there should be no arriving P* or Pn phases but only reflections from the boundaries. Reflections on the travel time curve refractions branching off asymptotically, not merely be extensions of the refraction travel time curve as depicted.

In the computer locations, the depth is usually constrained if the first depth estimate is greater than 30 km. In the published bulletins with Magadan network data, if no depth is listed, it is assumed to be 5 or 6 km. In the location procedure, no station corrections are used and station elevation is not considered (Gounbina, pers. comm.).

The unpublished Yakutsk bulletin provided a significant amount of additional data for earthquakes in the Magadan Region. This supplemental data is not included in any of the published bulletins containing Magadan network data, as it was not exchanged with the Magadan EMSD. Historically, the Magadan network only had access to data from the Yakutsk network station in Ust'Nera. However, the reported phases and arrival times for Ust'Nera listed in the Yakutsk unpublished bulletin were often slightly different (within 2.0 sec.) than the data reported to Magadan. The discrepancy is a result of Magadan receiving the preliminary Ust'Nera station bulletin with times and phases determined by the Ust'Nera station operator. The phases and times of arrivals in the unpublished Yakutsk data represent the final interpretation, which is done in conjunction with other records by one interpreter at the network headquarters in Yakutsk. The final interpretation for Ust'Nera phases and arrival times is used in the database.

There are some similar problems with data supplied to global databases, such as ISC, for events occurring in the Magadan region. Often preliminary time picks are reported for stations in the Magadan network (MGD, MAG, and SEY) with high residuals. This is often a result of a secondary Pg phase being reported as a first arriving Pn phase. In these cases the phase and time from the unpublished data is used, as they are not derived from preliminary seismogram analysis.

For data, hypocenter parameters were primarily taken from *Zemlet* and *Materialy* (1963-1990) and unpublished network bulletins (1991-1998). Phase data and arrival times for events larger than K-class of 9.5 were taken from *Materialy* (1970-1990). Phase data and arrival time for smaller events are from the *Far East Bulletin* (1972 and 1974) and unpublished Magadan network bulletins (1977-1990). All data since 1990 is from unpublished network bulletins. For several events along the boundary with the Yakutsk network supplemental arrival times were read from Yakutsk seismograms.

In comparison of data from the four primary sources, *Materialy, Zemlet, Far East Bulletin*, and the unpublished network bulletin, there are some variations found. From 1972 - 1982, the unpublished network bulletin and the *Far East Bulletin* contain identical origin times and hypocenters, which are sometimes different than those found in *Materialy* and *Zemlet*. This may be a result of events being relocated by those who produce the *Materialy* bulletin. The seismicity catalog in *Zemlet* is identical to that in *Materialy*, except for not listing events smaller than a K-class of 8.5. Since 1983, all four sources contain identical event parameters. For all years, events with statistically poor locations listed in *Materialy* and *Zemlet* have origin times rounded to nearest second and coordinates to the nearest 0.1

degree. For these events, the unpublished network bulletin and *Far East Bulletin* give origin time to 0.1 second and coordinates to 0.01 degree.

A linear regression relating K-class for the Magadan network to ISC magnitude is shown in Figure 1-14. The relationship determined is

$$K = 2.84 + 2.03\ (M) \qquad (1\text{-}3)$$

where K is K-class and M is magnitude. This is somewhat different than the relationship

$$K = 4.3 + 1.8\ (M) \qquad (1\text{-}4)$$

which is cited by Andreev et al. (1967), which does not fit the data (Figure 1-14).

Data of Station Iul'tin (ILT) and the Magadan EMSD Chukotka Network

Small events occurring in the Chukotka region were undetected until 1966, when seismic station Iul'tin (ILT; Figure 1-15; Table 1-6) opened in Chukotka. ILT was operated by the Institute of Physics of the Earth from 1966 until mid-1995. Chukotka epicenters reported in Kondorskaya and Shebalin (1982; NCSE) from 1966 to 1974 and *Zemlet* (1966-1982) are single station locations from ILT. These single station locations determine epicentral distances from S-P time differences and obtain azimuth from the polarization of the first arrival on both horizontal components (Lazareva, 1975). This has led to some difficulties for interpretation of the data. First, there is a clear unnatural looking linear trend of epicenters to the north and south of the station (Figure 1-15), indicating possible poor locations. Second, analysis of the epicenter cluster to the northwest of ILT has shown that they are explosions misidentified as tectonic events (Figure 1-15; See Chapter 2). These events are listed as explosions in the compiled seismicity catalog. Analysis of some of these

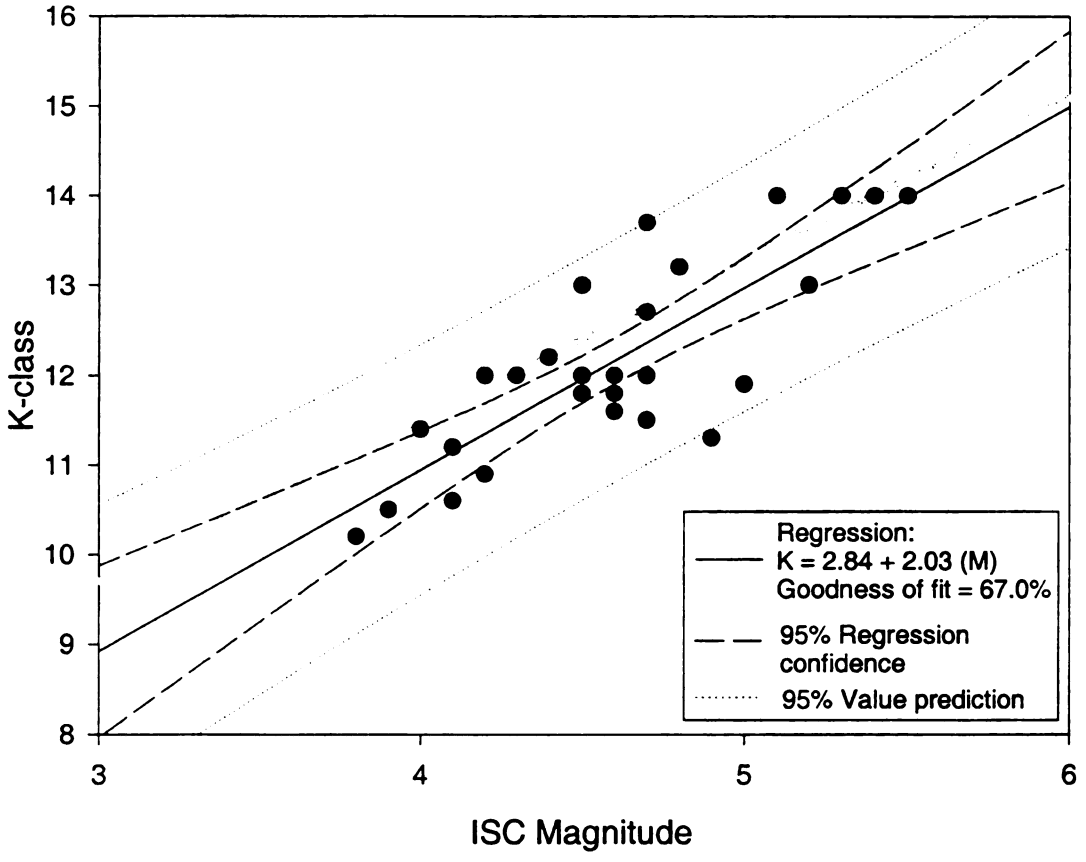

Figure 1-14. Relationship between K-class and ISC reported magnitude in the Magadan network. The heavy gray line depicts the K-M relationship cited by Avdreev et al. (1967) for the Magadan region.

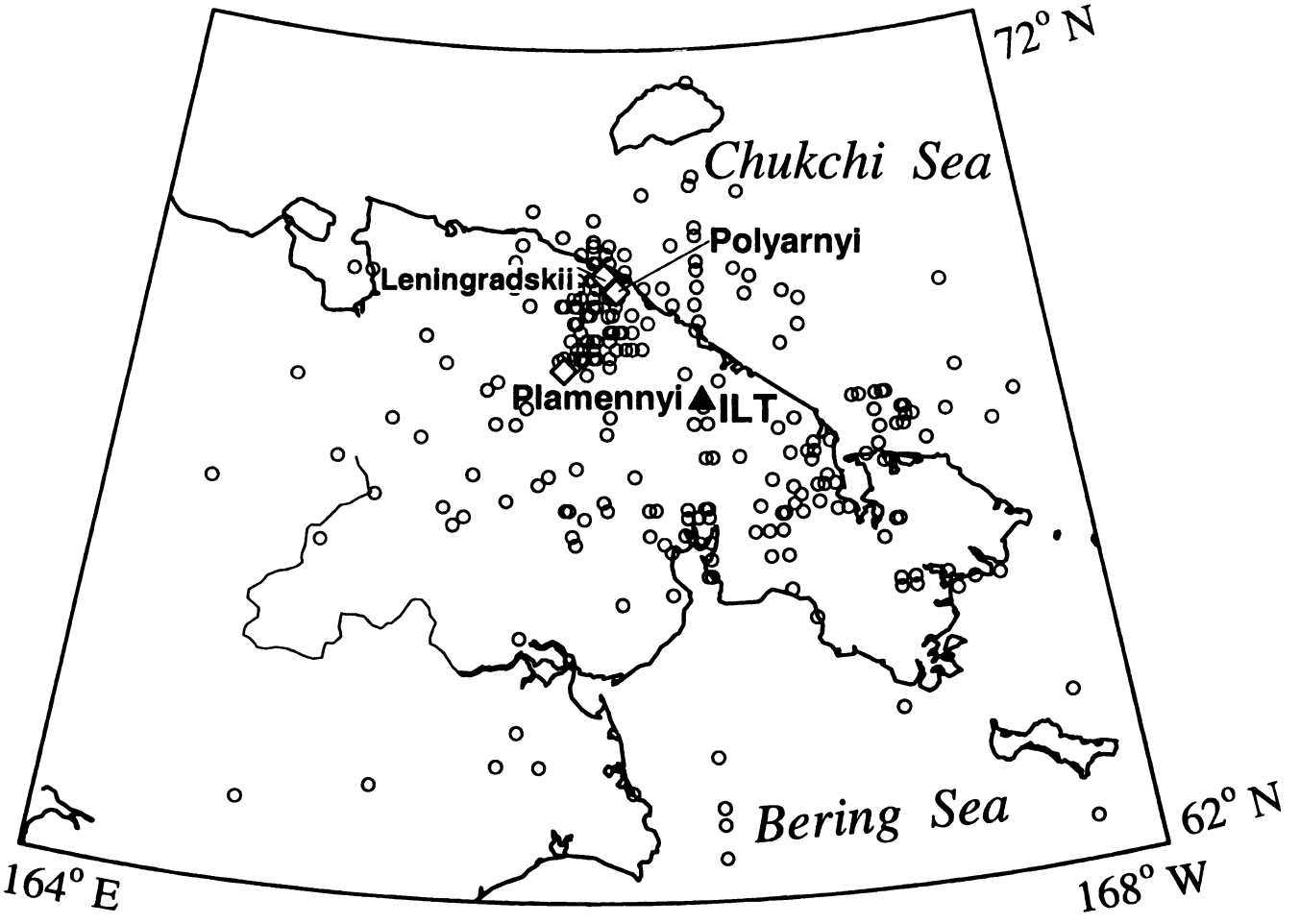

Figure 1-15. Seismicity located by station Iul'tin (ILT) from 1966-1982. The large cluster of seismicity to the northwest of Iul'tin is most likely explosion contamination (See chapter 2). Major mine locations are also shown.

Table 1-6. Permanent seismic stations to operate in Chukotka. All but station Iul'tin were operated by the Magadan EMSD. Station Uelen was abandoned shortly after opening because noise prevented the return of any useful data.

English Code	Russian Code	Station Name	Lat.	Long.	Elev. (m)	Date Open	Date Closed	Qu
ANSS	АНД	Anadyr-1	64.77	177.57	40	11.80	1.89	3
ANYS	АНД	Anadyr	64.734	177.496	55	4.89 9.96	7.93	1
BILS	БЛБ БЛН	Bilibino	68.059	166.449	283	8.81	4.92	1
BILL	BILL	Bilibino GSN	68.065	166.452	299	8.95.		1
EGVS	ЭГВ	Egvekinot	66.323	179.127W	18	–.90	–.94	1
ILT	ИЛТ	Iul'tin	67.87	178.74 W	235	3.66	7.93	1
MKI	МАЙ	Maiskii	68.97	173.71	261	8.82	6.94	1
MKVS MKN	МРК	Markovo	64.68	170.41	25	10 .86	4.92	1
PVD	ПРВ	Provideniya	64.424	173.226W	25	9.80	12 .93	G
		Uelen	66.16	169.84 W	5	--.81	–.82	1

epicenters are of reasonable quality given the difficulties of single station locations (Table 1-7; See the Western Alaska network section later in this chapter).

The Chukotka regional network contained six seismic stations which were operated from 1981 to 1993 by the Magadan Experimental Methodological Seismological Division (MEMSD; Figure 1-16: Table 1-6). However, the Chukotka network only operated as an experimental network in 1981 and 1982 and phase data were not compiled. Data were recorded using a galvanometer and photographic paper. A seventh station, located at Uelen (Figure 1-16), operated intermittently for about three months in 1981 but was abandoned due to extreme noise. The station at Uelen also operated with somewhat different instruments (Artamonov and Mishina, 1984). Fifteen epicenters located in Chukotka have been identified as possible explosions from the mining around Polyarnyi, Leningradskii, and Plamennyi (Godzikovskaya, 1995; see Chapter 2). These events are flagged in the database as possible explosions.

Focal parameters from the Chukotka network were determined using the same procedures and seismic velocities as described below for the Magadan network. Arrival times from station ILT supplemented data from the Chukotka network in analysis and were included in the Russian phase bulletins. Unfortunately, in 1993, all seismic stations in Chukotka were closed because of financial constraints, although Anadyr (ANYS) was reopened in 1996 with assistance from the Chukotka regional government. In 1995, a new GSN station was opened in Bilibino by IRIS.

Hypocenteral parameters were primarily taken from *Zemlet* (1966-1982) and *Materialy* (1983-1990). Occasionally, the *Zemlet* and *Materialy* bulletins disagree on whether longitude is east or west. When compared with the unpublished network bulletin

Table 1-7. Comparison of origin times and epicenters for earthquakes located by ILT, the Western Alaska network (WAK), and those relocated in this study.

Date	ILT Time and Epicenter	WAK Time and Epicenter	Relocation Time and Epicenter
April 06, 1981	23 33 39. 67.1 N 174.0 W	23 34 06.5 66.310 N 169.871 W	23 33 48.4 67.37 N 172.48 W
April 06, 1981	23 45 36. 67.1 N 174.0 W	23 46 23.9 64.089 N 168.019 W	23 45 45.0 67.40 N 172.55 W
April 07, 1981	07 08 29. 67.1 N 174.0 W	07 09 50.6 65.943 N 168.642 W	07 08 37.61 66.68 N 174.15 W
April 07, 1981	07 14 52. 67.1 N 174.0 E	Data Acquired But No Epicenter Calculated	07 16 03.0 66.65 N 174.08 W
January 16, 1982	12 35 15.6 64.0 N 169.5 W	12 35 08.0 64.774N 171.405 W	12 35 09.9 64.80 N 170.84 W

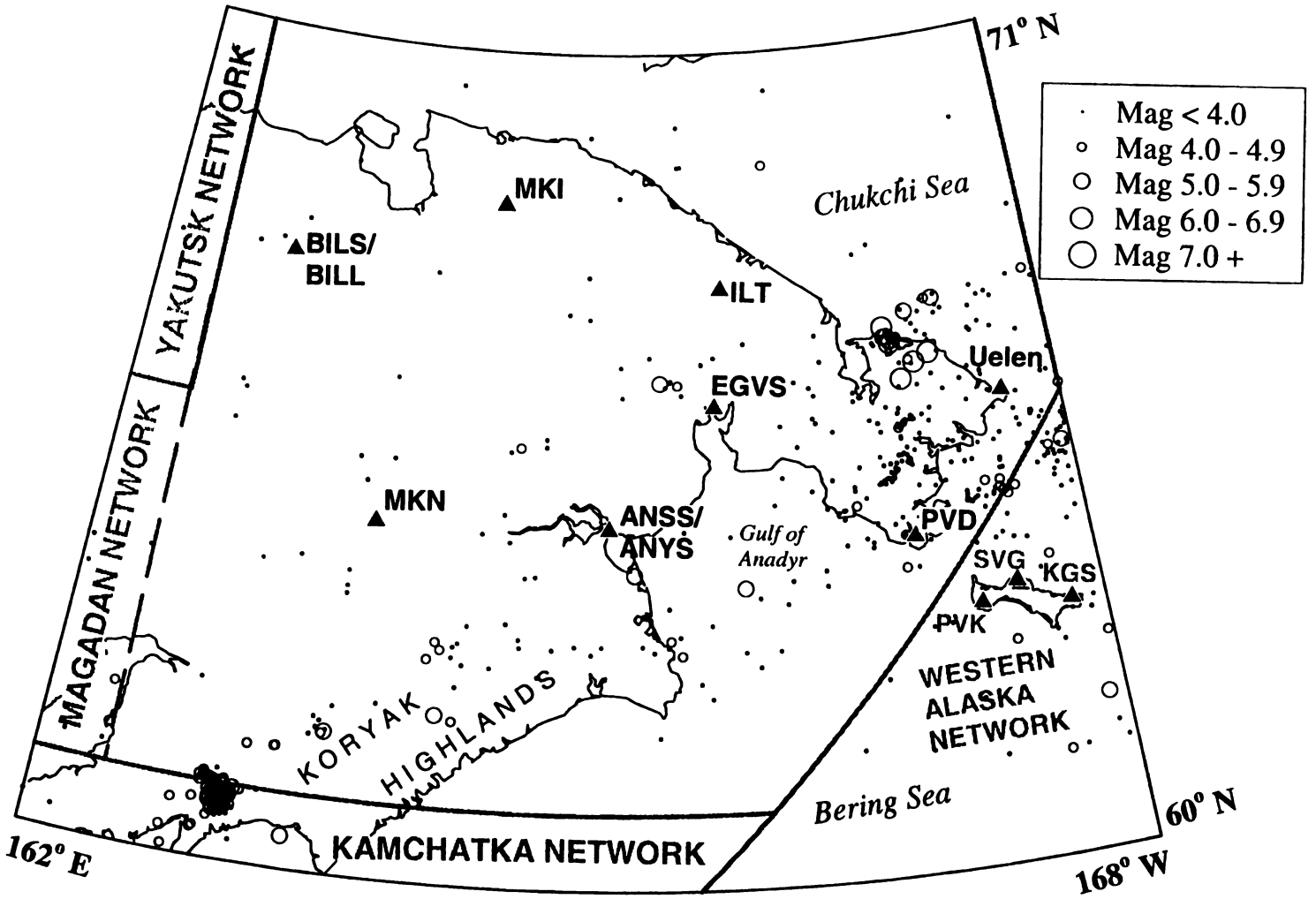

Figure 1-16. Seismicity and seismic stations of the Chukotka network.

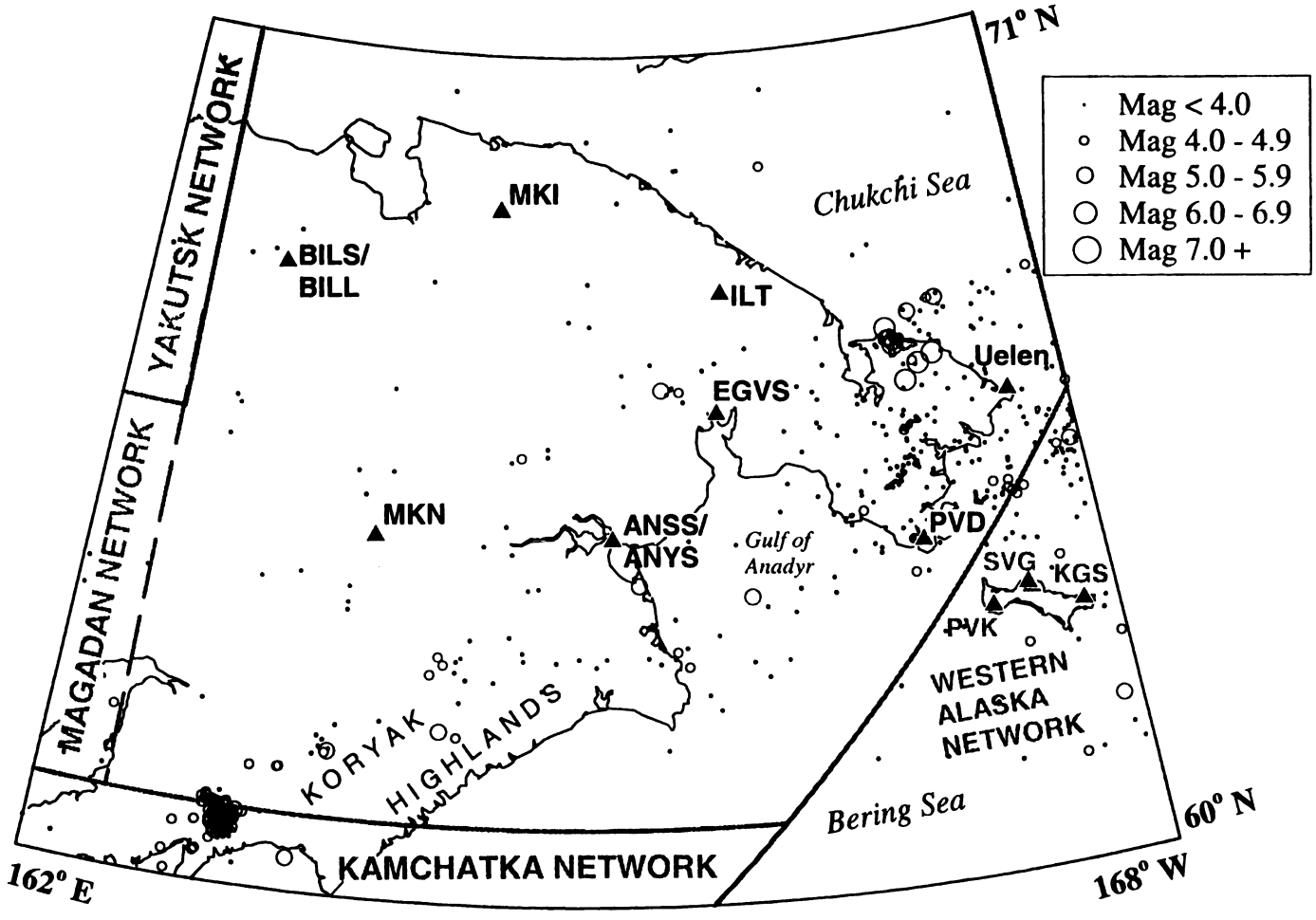

Figure 1-16. Seismicity and seismic stations of the Chukotka network.

and a close look at the arrival times, *Zemlet* is usually found to be incorrect. *Materialy* (1983-1990) contains phase data and arrival times only for events larger than K-class of 9.5. The unpublished Magadan network bulletins (1983-1990) contain phase data for all events. All data since 1990 is from unpublished network bulletins. For approximately 50 events, phase data and arrival times from the Chukotka network were supplemented with data from Alaskan stations (primarily Anvil Mountain; AVN). In comparison of data from the four primary sources which contain Chukotka data, *Materialy, Zemlet, Far East Bulletin*, and the unpublished network bulletin, all are found to report the original hypocenter parameters determined by the Magadan network. The only exception being events with statistically poor epicenters. For these events, the unpublished network bulletin and *Far East Bulletin* give hypocenter parameters to 0.1 second for origin time and 0.01 degree for coordinates. Origin time is rounded to nearest second and coordinates to nearest 0.1 degree in *Materialy* and *Zemlet*.

A linear regression relating K-class to ISC magnitude for the Chukotka region is shown in Figure 1-17. The relationship determined is

$$K = 8.02 + 1.00\ (M) \qquad (1\text{-}5)$$

where K is K-class and M is magnitude. This relationship is anomalous when compared to other regions discussed below. However, the poor fit to the data should be noted. Kondorskaya and Shebalin (1982) citing Rautian (1960) report a relationship of

$$K = 6.5 + 1.5\ (M) \qquad (1\text{-}6)$$

between K-class and magnitude for Chukotka, which was also considered anomalous (Figure 1-18). Addition of magnitudes from the Western Alaska network and K-class determinations from station ILT for events located by both (Table 1-7) yield

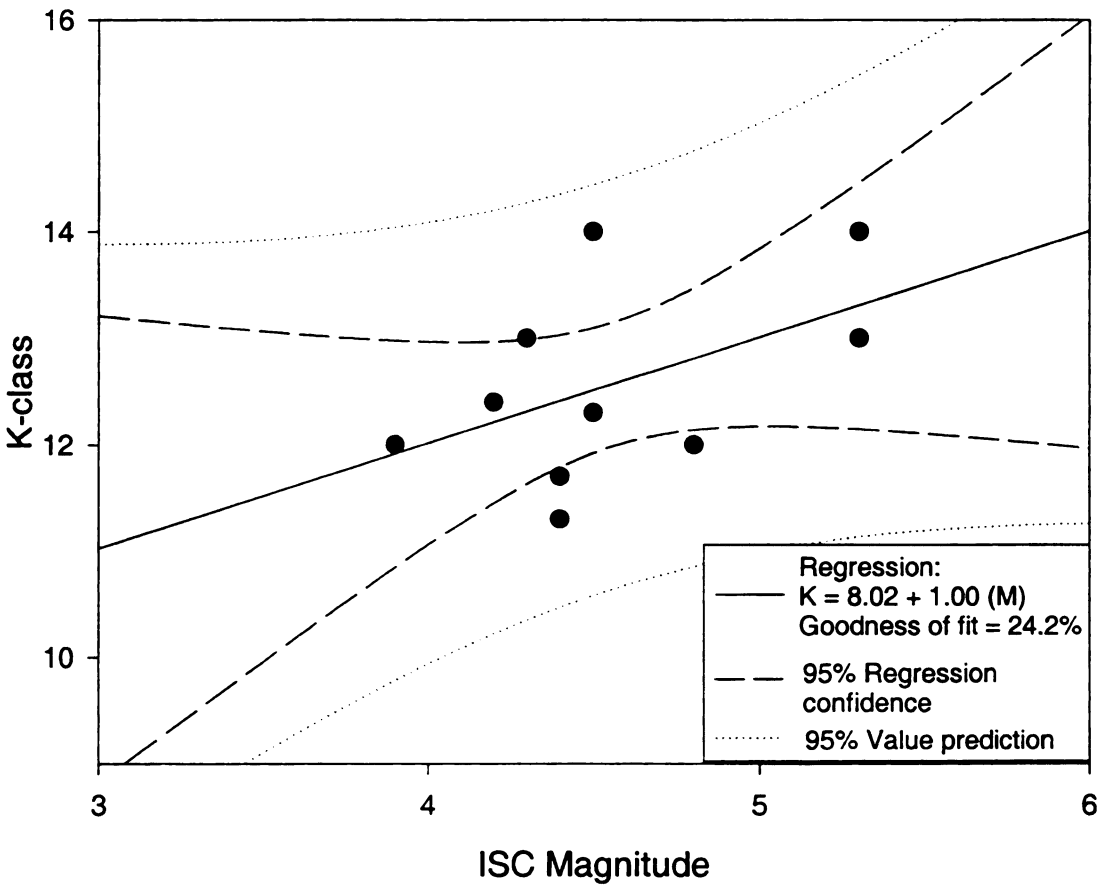

Figure 1-17. Relationship between K-class and ISC reported magnitude in the Chukotka network.

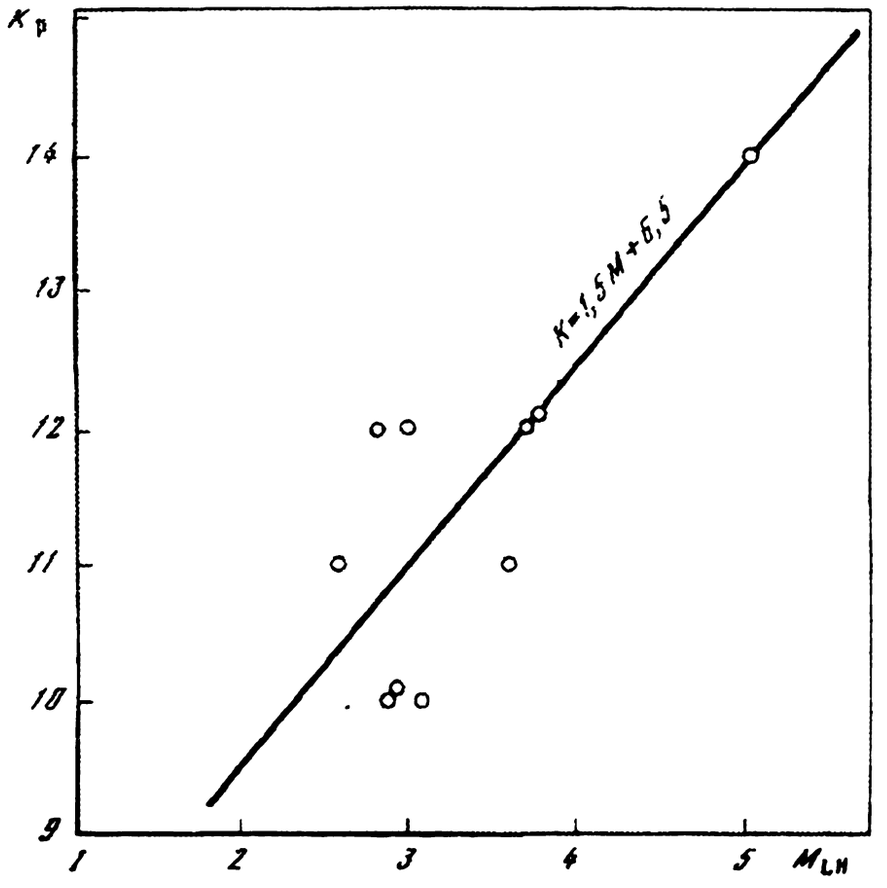

Figure 1-18. Relationship between local magnitude and K-class as reported by Kondorskaya and Shebalin (1982).

$$K = 7.35 + 1.13\ (M) \qquad (1\text{-}7)$$

(Figure 1-19). However, the poor locations by the Western Alaska network result in an underestimation of magnitude for all but the January 16, 1982 event, as the epicenters were assumed to be too close to the stations. Use of only the January 16, 1982 event in the regression yields

$$K = 4.58 + 1.73\ (M) \qquad (1\text{-}8)$$

which is probably the best determination possible given the available data set (Figure 1-20). This relationship is closer to the regressions determined for other regions discussed below. Overall, the difficulty in determining a relationship between K - class and magnitude for Chukotka may be a result of poor data.

Northeast Russia Test Network

In the mid 1960's (1962 - 1967) a number of experimental seismic stations were established throughout northeast Russia to determine background seismicity levels to aid in developing permanent seismic networks (Mishin, 1967; Table 1-8). The distribution of seismicity located using this "test network" (Figure 1-21) was instrumental in site selection for future seismic stations, particularly in the Magadan region and Chukotka. Most of the temporary stations were deployed between six months and one year. Because only a few stations were deployed at any given time, the test network did not locate a large number of events. Hypocenters obtained from the test network are from Andreev (1967) and are included in the database. Arrival times and phase data for the recorded events are not available.

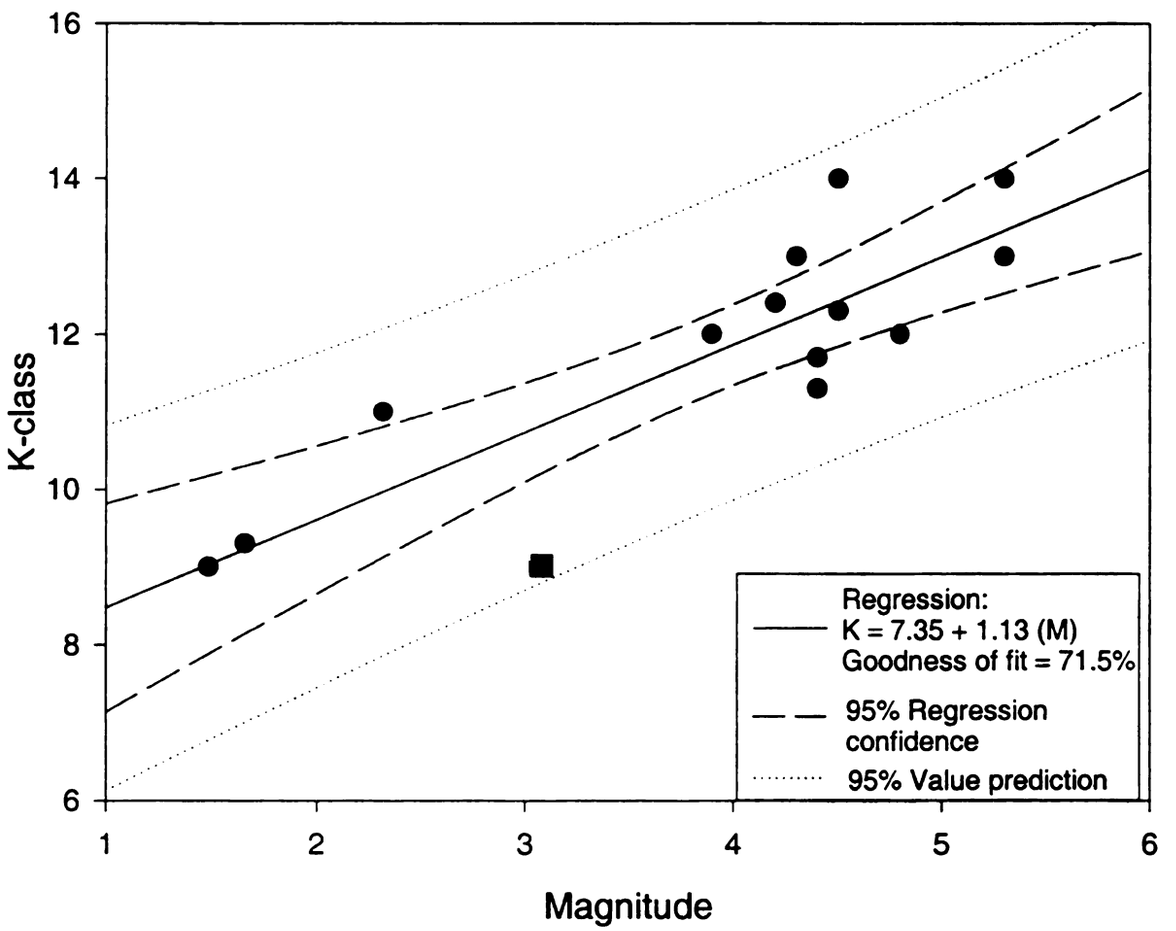

Figure 1-19. Relationship between K-class and magnitude in the Chukotka network. Magnitudes greater than 3.5 are from the ISC catalog, while those less than 3.5 are from the western Alaska network. The January 16, 1982 event is depicted as a square. ISC magnitudes are M_b, while those from the Western Alaska network are M_l.

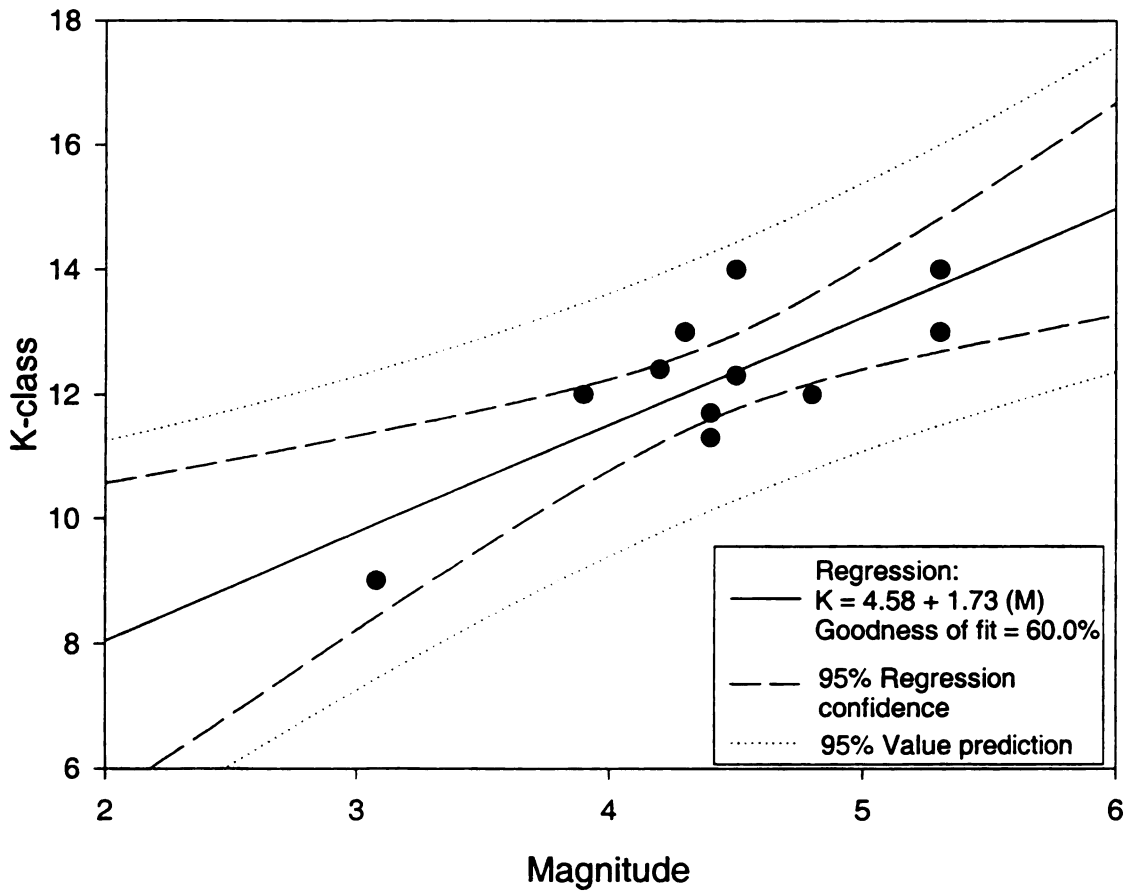

Figure 1-20. Relationship between K-class and magnitude in the Chukotka network. Magnitudes greater than 3.5 are from the ISC catalog, while the remaining magnitude 3.1 event is from the Western Alaska network.

Table 1-8. Seismic stations and station parameters from the temporary network established in northeast Russia in the mid 1960's. Parameters from Mishin (1967).

English Code	Russ. Code	Station Name	Lat.	Long.	Elev. (m)	Date Open	Date Closed	Qu.
AMG	АМГ	Amguema	67.05	178.88W	150	11.65	4.66	2
ANC	АНС	Anyuisk	68.34	161.56	10	6.64	3.65	1
BLG	БЛГ	Balygychan	63.91	154.09	139	7.63	6.64	1
BL1	БЛБ	Bilibino-1	68.04	166.44	260	8.64	1.65	1
GRM	ГРМ	Garmanda	62.18	159.08	140	12.66	5.67	1
ILR	ИЛР	Ilirnei	67.26	167.96	350	10.64	10.65	1
LMT	ЛМТ	Lamutskoe	65.54	168.85	178	4.65	10.65	1
SMT	ШМТ	Mys Shmidta	68.88	179.38W	5	4.65	1.66	1
NK1	НЛБ	Nel'koba	61.34	148.81	531	6.63	1.64	1
OL1	ОМЛ	Omolon-1	65.25	160.52	260	12.63	1.65	1
OS1	ОМС	Omsukchan	62.52	155.77	527	1.63	1.64	1
VRN	ВРН	O. Vrangelya	70.94	179.62W	10	2.66	4.66	3
PVK	ПВК	Pevek	69.70	170.27	20	5.65	11.65	1
PV1	ПРВ	Provideniya-1	64.45	173.18W	20	1.65	6.66	2
S-K	С-К	Srednekolymsk	67.46	158.71	30	4.64	12.64	1
STK	СТК	Stekol'nyi	60.046	150.730	221	7.64	5.66	1
U-B	У-Б	Ust' Belaya	65.51	173.28	20	11.66	5.67	1
SRD	СРД	Ust' Srednikan	62.44	152.32	580	12.62	11.63	1
VNK	ВНК	Vankarem	67.84	175.85W	10	3.66	6.66	1
ZY1	ЗРН	Zyryanka-1	65.74	150.89	37	1.64	10.64	1

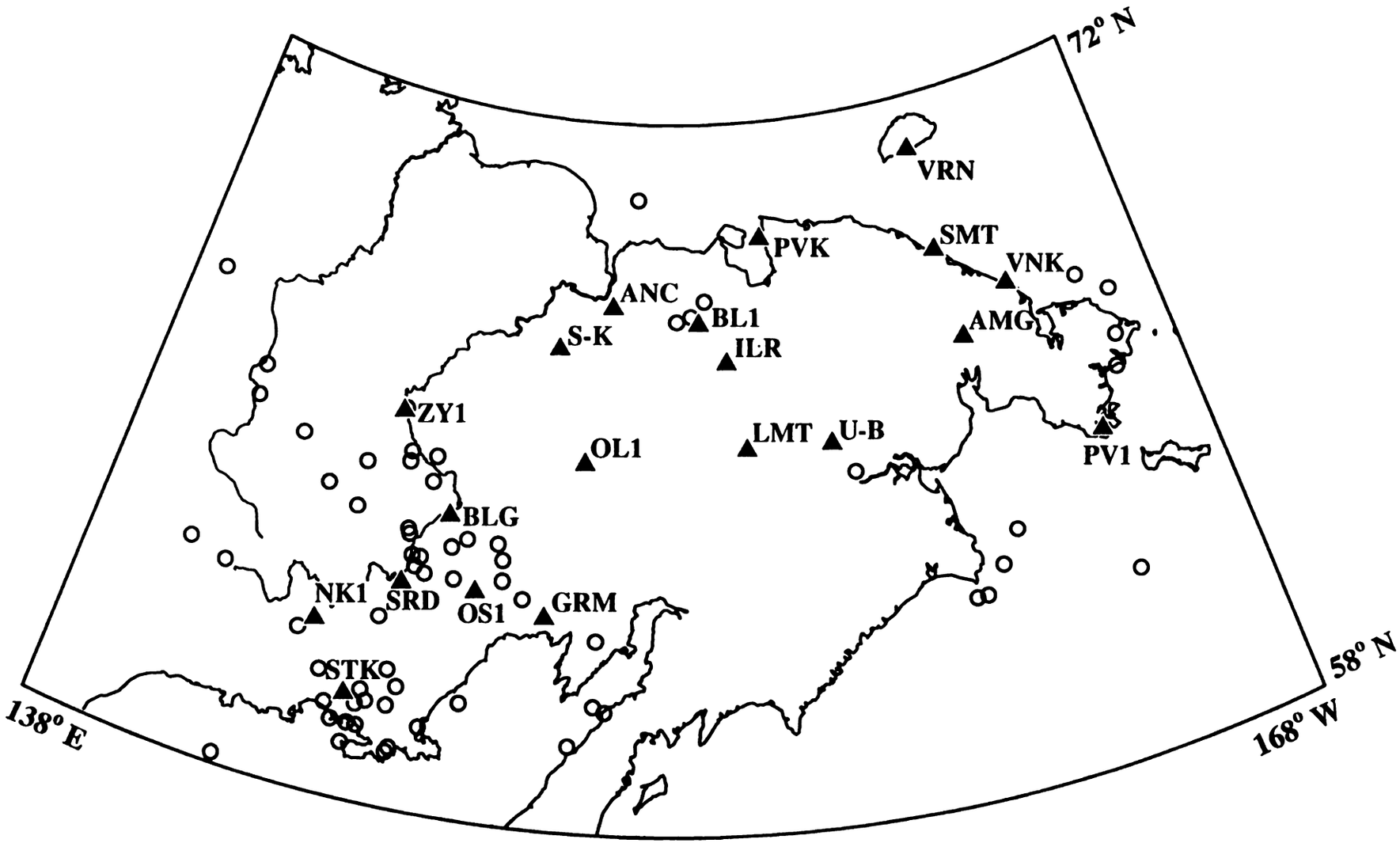

Figure 1-21. Seismicity and seismic stations of the northeast Russia temporary network (1962-1967).

Western Alaska Network

The Western Alaska Network was operated from January 1977 through June 1982 (closed for 1980), in the region of the Seward Peninsula, Alaska (Figure 1-22). The network contained 20 field seismic stations, and two permanent stations, Anvil Mountain (AVN) and Granite Mountain (GMA; Table 1-9), which were recorded on develocorder film in Nome, Alaska (Biswas et al., 1980, 1983). Granite Mountain was closed in April of 1978. A total of 1,010 earthquakes were located by the network, indicating high levels of microseismicity (Biswas et al., 1983). The largest earthquake located by the network was a M_L 5.2 near Kotzebue (station KTA). Most events located are in the southern half of the Seward Peninsula and in the Kotzebue Sound region, with a lesser number in the Bering Strait and Chukotka. Focal parameters were determined using first arrival P times and S-P time differences. From July 1982 until 1998, the only seismic station operating in western Alaska was AVN (Figure 1-22). In 1998, a new seismic station was opened at Tin City, on the western tip of the Seward Peninsula.

For database assembly, an attempt was made to supplement western Alaska data from 1981 and 1982 with arrival times from the Chukotka network, which was being set up at the time. Although seismograms for more than 100 events were investigated, only a few useful arrival times were acquired, with most events showing only weak emergent arrivals. This is a result of the Chukotka stations being poorly optimized for good recording (amplification, noise, etc.).

A few events located by the Western Alaska network were also located by the IPE station at Iul'tin (ILT). Comparison of the epicenter locations indicates that the differences in locations are consistently greater than 100 km and in one case approaches several hundred

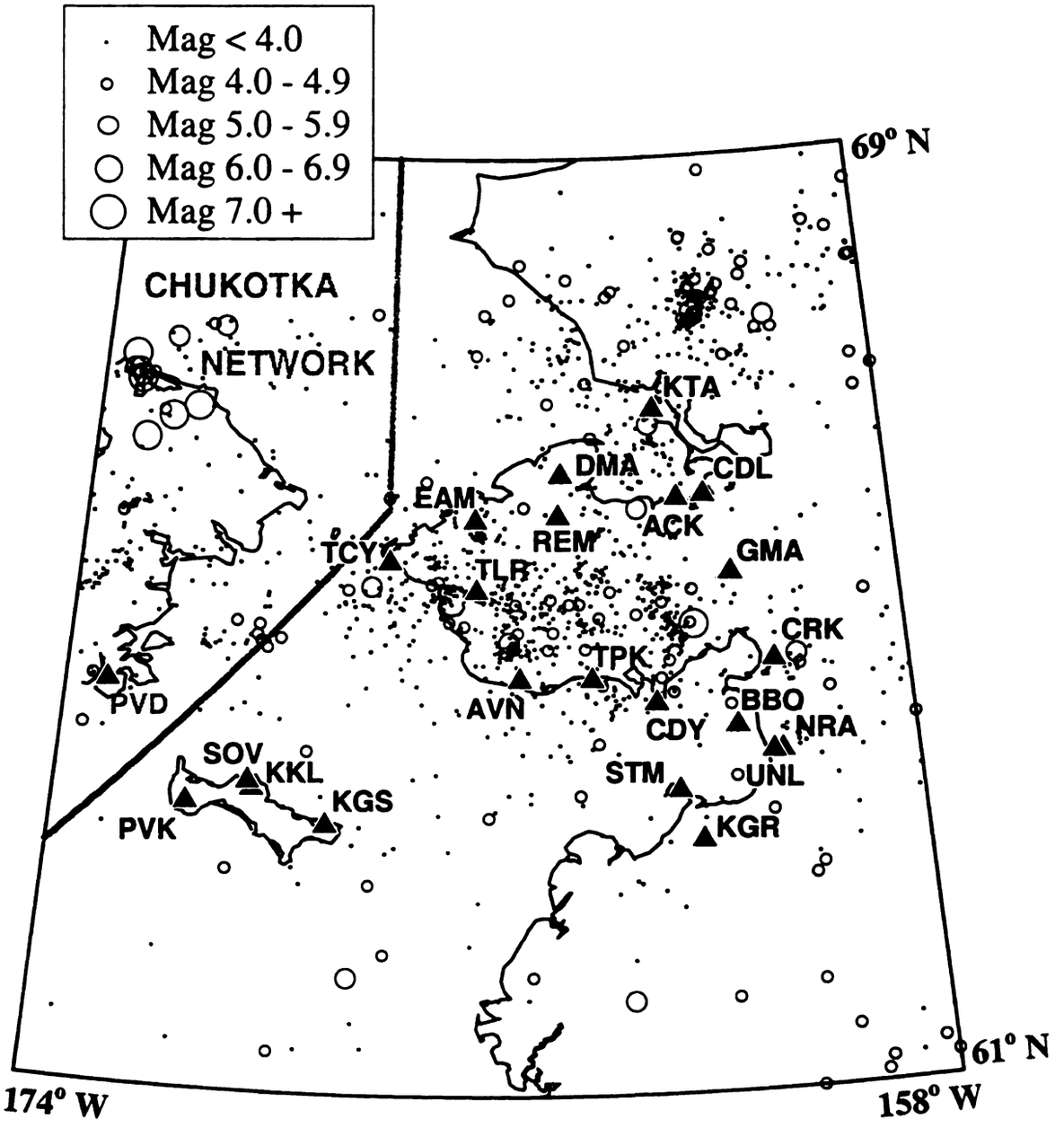

Figure 1-22. Seismicity and seismic stations of the western Alaska network.

Table 1-9. Seismic stations and station parameters of the Western Alaska network. Parameters from Biswas et al. (1980), and Biswas et al. (1983).

Station Name	Code	Latitude	Longitude	Elevation (m)	Satellite Delay (Sec)	Site Geologic Formations
Alder Creek	ACK	66.083	162.195	377		Permafrost Metamorphic
Anvil Mt.	AVN	64.56	165.37	323		Metamorphic
Besboro Is.	BBO	64.12	161.30	244		Volcanic
Cape Darby	CDY	64.34	162.79	335		Volcanic
Candle Creek	CDL	66.1	161.66	75	0.54?	Siliceous Metasedimentary
Christmas Creek	CRK	64.67	160.53	680		Sedimentary
Devil Mt.	DMA	66.30	164.52	238	0.54	Volcanic
Ear Mt.	EAM	65.92	166.24	701	0.54	Igneous
Granite Mt.	GMA	65.43	161.23	858		Volcanic
Kogog River	KGR	63.16	162.05	320		Volcanic
Kanguksam Mt.	KGS	63.30	168.99	488	0.54	Volcanic
Kookooligit Mt.	KKL	63.59	170.37	655	0.54	Volcanic
Kotzebue	KTA	66.84	162.59	24	0.54	Permafrost Sedimentary
North River	NRA	63.89	160.51	107	0.54?	Metamorphic
Poovook	PVK	63.44	171.55	411	0.54	Volcanic
Remote	REM	65.95	164.58	358	0.54?	Basalt
Savoonga	SOV	63.65	170.45	198	0.54	Volcanic
Stuart Is.	STM	63.59	162.43	140		Volcanic
Tin City	TCY	65.56	167.95	72	0.54	Igneous
Teller	TLR	65.32	166.21	122	0.54	Metamorphic
Topkok Pt.	TPK	64.55	163.99	122		Volcanic
Unalakleet	UNL	63.89	160.67	122		Volcanic

kilometers. Because epicenters determined from the Western Alaska network data were determined using several stations, the assumption would be that locations from the Western Alaska network are probably better than the single station locations calculated from ILT data alone. This assumption is shown to be false when the arrival times from the Western Alaska network are used in relocating the events. Relocated events fall closer to the single station ILT locations than the Western Alaska network locations (Table 1-7). Origin times from the relocations are also closer and more consistent with ILT origin times. The relocations use original network picked Pn arrivals supplemented with secondary Pg and Sg arrivals picked from the original develocorder film seismograms. Output from the relocations is given in Appendix D. Several things may have contributed to poor epicenter determinations in the Western Alaska network. First, only the first arriving P and S phases were picked. For close events, the first arrivals were not differentiated as to crustal phases (Pg and Sg) or mantle refraction phases (Pn and Sn). This ignores the second arriving, but useful, Pg and Sg phases. Second, many of the arrivals picked as first arriving P or S are actually mispicked later arriving Pg or Sg phases. The mispicked phases were not identified in the location process and sometimes result in large errors when using a small number of recording stations. Third, many earthquakes have origin times that are later than the first arrival. This could be a result of bad time picks or a problem with the location procedure used. It appears that when determining locations, all events were run through the location algorithm and the resulting focal parameters were used without attention to individual events or regard to whether the solutions were reasonable. The preceding discussion calls into question the overall quality of the Western Alaska network locations.

Kamchatka Peninsula Network

Klyuchi was the first seismic station to open on the Kamchatka peninsula in 1948, followed by Petropavlovsk in 1951. Most other stations in the network opened in the early 1960's and later (Figure 1-23; Table 1-10). Seismic station histories and parameters given here are less well researched than for the Magadan network because of their lesser impact on the study area.. Because of subduction of the Pacific plate under the Kamchatka peninsula, this network monitors the most seismically active region in northeast Russia, as well as activity on many of the peninsula's active volcanoes. The Kamchatka network also records seismic activity to the north of the subduction zone into the southern portion of the Koryak Highlands. As this study is interested primarily in non-subduction related crustal events, only earthquakes in the region north of 56° N (the northern edge of the Pacific subduction zone) are included.

Approximately 5,000 hypocenter locations for the Kamchatka network north of 56° N were taken from the unpublished Kamchatka seismicity catalog for 1962 to 1996. For the Kamchatka network, *Zemlet* generally lists only events having a K-class greater than 8.5, although this does vary for some years. Earthquake locations were computed by hand up until 1978, when location procedures were computerized (Gordeev, pers. comm.). Along the boundary with the Magadan network in the Koryak Highlands and in Shelikhov Bay, many events were independently located by each network. There seems to have been essentially no exchange of phase data for anything but the largest teleseismically recorded events in these regions. Given a choice, the Magadan network hypocenter is usually preferred over that from the Kamchatka network because the Magadan network generally had better azimuthal station coverage.

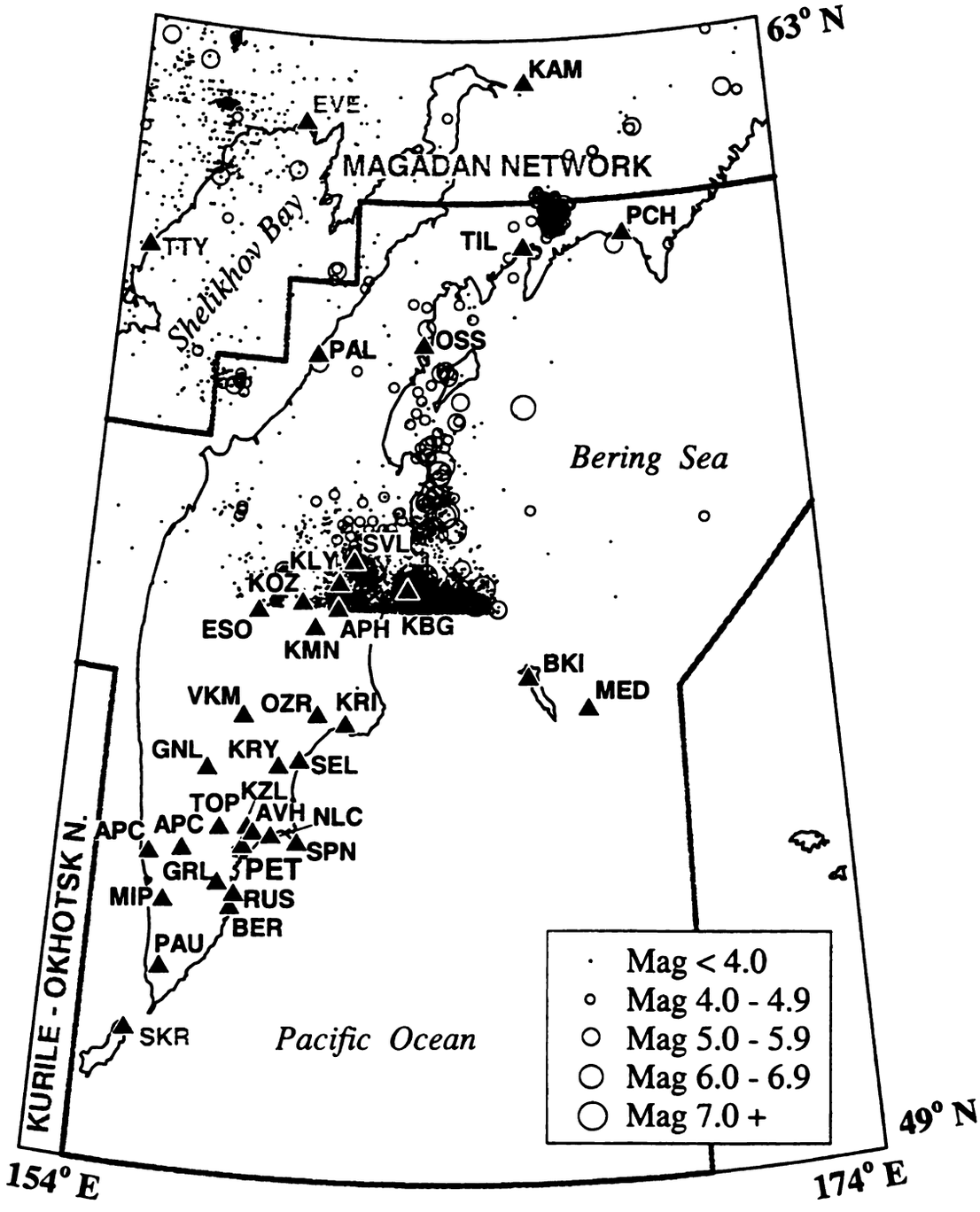

Figure 1-23. Seismicity and seismic stations of the Kamchatka network. Only seismicity north of 56° north are included. A few stations associated with volcano monitoring are omitted for clarity.

Table 1-10. Seismic stations and station parameters of the Kamchatka network.

English Code	Russ. Code	Station Name	Lat.	Long.	Elev. (m)	Date Open	Date Closed	Qu
APC		Apacha	52.925	157.131		2.90		1
APN	АПХ	Apakhonchich	56.00	160.84	700	–.64	–.80	1
AVH	АВЧ	Avacha - old	53.07	158.5		–.63	10.76	-
AVH	АВЧ	Avacha - new	53.265	158.738	900	7.76		1
BER	БРЗ	Berezovaya	52.27	158.433		–.81	–.94	1
BKI	БРН БРГ	Bering (Nikol'skoe)	55.195	165.99	40	–.62		1
BGC		Bogachevka	54.850	160.900		–.64	–.65	1
BLC			53.193	158.800		–.76		1
CIR			56.127	160.725	1600	10/98		1
ESO	ЭСС	Esso	55.925	158.700	490	–.65		1
GNL	ГНЛ	Ganali	53.942	157.620	1200	1.88		1
GRL	ГРЛ	Gorely	52.552	158.080	1250	7.80		1
INS		Institut Vulkanologii	53.066	158.605	175	11.81		1
KMN		Kamenistaya	55.76	160.240	1100	10.90		1
KAM		Kamenskoe	62.456	166.210		–.94		1
KBT			56.208	162.819	200	10.97		1
KII	КАР КРМ	Karymski - old	54.030	159.480	790	7.74	–.86	1
KRY		Karymski -new	54.036	159.449	900	9.89		1
KLY	КЛЧ	Klyuchi	56.313	160.852	80	–.48 2.89		1
		Kolokol'chik				–.67	–.67	-
KRT		Korito	55.966	160.222	1000	10.97		1
KRK	КРК	Koryak	53.292	158.636	1050	7.75		1
KZL	КЗЛ	Kozelskaya	53.201	158.894	950	–.76	–.84	1

Table 1-10 (cont'd).

KOZ	КЗР	Kozyrevsk	56.058	159.872	40	–.61	9.89	1
KZY		Kozyr	56.070	159.900	450	11.89		1
KPL			56.592	161.296	1700	--.86	–.90	1
KRS		Krestovskii	56.214	160.558	1200	7.87		1
KRI	КРН	Kronoki	54.596	161.134	5	8.66		1
KBG	КБГ КБ КРБ	Krutoberegovo	56.255	162.705	10	–.68		1
LGN			56.083	160.690	2500	9.99		1
MED	МДН	Mednyi	54.786	167.556		–.73	–.75	1
MIP		Mal. Ipelka	52.276	156.758	370	8.97		1
MLK	МЛК	Milkovo	54.700	158.630	155	–.62 10.89	–.63 –.93	1
NLC	НЛЧ	Nalychevo	53.171	159.345	5	–.67 3.69 3.84	–.67 12.69	- - 1
OSS	ОСС	Ossora	59.25	163.065	10	–.73		1
OZR	ОЗР	Ozero	54.692	160.392		10.66	–.77?	1
PCH		Pakhach	60.558	169.125		–.92	–.94	1
PAL		Palana	59.093	159.963		–.94	–.96	1
PAU	ПЖТ	Pauzhetka	51.467	156.810	110	11.61		1
PET	ПТР	Petropavlovsk	53.024	158.650	150	–.51		1
PDK	ПДК	Podkova	56.140	160.780	800	–.83?		1
RUS	РУС	Russkaya	52.432	158.507	75	12.87		1
SDL		Sedlovina	53.278	158.884	1235	9.91		1
SEL	СМЛ	Semlyachik	54.12	159.98		11.61	7.74	1
SMA			53.263	158.801	1235	2.91		1
SPN	ШРН	Shipunski	53.107	160.011	170	4.85		1
SRD			56.317	159.717	800	1.92		1
SVL	ШВЛ	Tsiveluch	56.583	161.225	900	10.80		1

Table 1-10 (cont'd).

TIL		Tilichiki	60.433	166.075		–.94	–.96	1
TOP	ТОП ТПЛ	Topolovo	53.230	158.041	155	11.61	–.93	1
UGL			53.209	158.824	1140	8.92		1
UBL		Ust' Bolsheretsk	52.842	156.308	20	11.61	–.64	1
VDP	ВДР	Vodopadnii	55.770	160.220	1060	–.77	–.91	1
VKM		Verkhene Kamchatsk	54.627	158.473	170	10.66	–.71	1
ZLN			56.018	160.804	1100	8.88		1

In comparing events listed both in *Zemlet* and the unpublished Kamchatka catalog, it is found that many events prior to 1968 and after 1983 sometimes list different hypocenter parameters for the same event. Events since 1983 have been relocated by the Kamchatka network to improve the uniformity of the locations and remove errors, which results in the differences between the catalogs for those years (Gordeev, pers. comm.). Events prior to 1968 may also have been relocated at some time in the past, resulting in a similar situation. The velocity structure used for the Kamchatka network locations is taken from Kuzin (1973) and Kuzin et al. (1974). A linear regression relating K-class for the Kamchatka network to ISC magnitude was found to be

$$K = 3.74 + 1.61\ (M) \qquad (1\text{-}9)$$

where K is K-class and M is magnitude. The regression and data are shown in Figure 1-24. Phase data for Kamchatka network events are not included in the database.

Amur Regional Network

The Amur network monitors seismicity between the Eurasian plate and the Amur Plate. The Sakhalin network monitors seismicity along the boundary between the Amur plate and Okhotsk block. Unfortunately, this study has not worked directly with the the Amur network, thus first hand knowledge of operational procedures and unpublished data were not available. As reported in the *Far East Bulletin*, earthquakes are located graphically. Velocities used by the Amur network for locating earthquakes are based on average velocities for the Irkutsk region, assuming a crustal thickness of 40 km. Velocities used are:

Pg = 6.15 km/s	Sg = 3.55 km/s
Pn = 7.9 km/s	Sn = 4.4 km/s

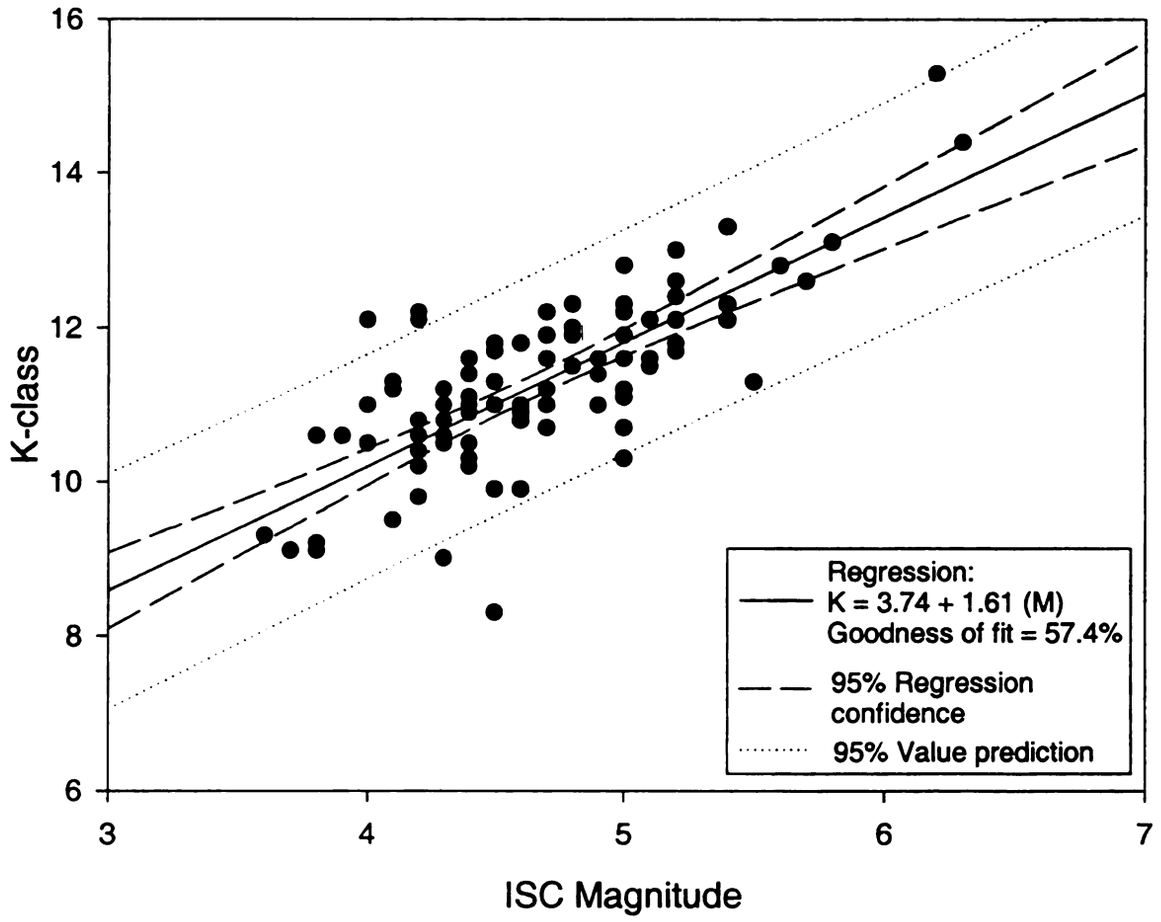

Figure 1-24. Relationship between K-class and ISC reported magnitude in the Kamchatka network.

Permanent seismic stations in the Amur network region first opened in the early 1970's (Table 1-11; Figure 1-25). Seismicity data from the Amur network comes primarily from the *SSR catalog* and the *Far East Bulletin* for events prior to 1979. Since 1979, event parameters are taken from the *SSR catalog, Materialy, Zemlet*, and the *Far East Bulletin*. Since 1982, many additional events, not found in other sources, which occured in the Amur region are available in the unpublished Yakutsk network bulletin. As with other networks, statistically poor events have origin times rounded to the nearest second and epicenters rounded to 0.1 degree when listed in the *SSR catalog, Zemlet* or *Materialy*. In the Amur region, *SSR catalog* reports event parameters the same as *Zemlet*, except K-class is converted to magnitude according to the relation

$$K = 3.99 + 1.80(M) \qquad (1\text{-}10)$$

where K is K-class and M is magnitude. This has essentially the same slope, but a slightly lower K-class axis intercept than the relationship between reported K-class and ISC magnitude (Figure 1-26) which was determined in this study to be

$$K = 4.69 + 1.83\ (M) \qquad (1\text{-}11)$$

Phase data from the Amur region is taken from the *Far East Bulletin* (1972, 1974, 1985-1988), *Materialy* (1979-1990), and unpublished Yakutsk network bulletins (1982-1995). Some phase data from the Sakhalin, Yakutsk, and Irkutsk network stations are given in the published bulletins of Amur region events. The unpublished Yakutsk network bulletins also add a significant amount of phase data to that available in published sources for the Amur region. Hypocenters calculated by the Yakutsk network often differ greatly from those determined by the Amur network, which are found in published sources. Upon

Table 1-11. Seismic stations and station parameters for the Amur network.

English Code	Russ. Code	Station Name	Lat.	Long.	Elev. (m)	Date Open	Date Closed	Qu
BMKS	БМН	Bomnak	54.705	128.847	325	3.74		1
EKI	ЕКМ	Ekimchan	53.067	132.945	485	11.79		1
GRZ GRT	ГРТ	Gornotaezhnoe	43.70	132.15	220	7.90		3
GRD GRV	ГРВ	Gornovodnoe	43.70	134.733	270	7.88		1
GNY	ГРН	Gornyi	50.762	136.455	500	12.78		2
KNN KNG	ХНГ	Khingansk	49.122	131.192	520	7.80	4.84	1
KIRS	КРС	Kirovskii	54.428	126.983	440	4.74		1
KLDS	КЛД	Kul'dur	49.205	131.642	425	--.--	--.--	1
LZR	ЛЗР	Lazarev	52.2	141.493	120	12.80		2
NKL	НКЛ	Nikolaevsk-Amur	53.142	140.783	25	9.70		1
RMNS	РМН	Romny	50.855	129.4	210	10.78	--.87	2
TEI	ТРН	Ternei	45.067	136.6	30	7.82		2
VLA	ВЛД	Vladivostok	43.12	131.893	75	--.29 --.34	--.31	-
YASS	ЯСН	Yasnyi	53.29	127.983	310	1.75		1
ZEA	ЗЕЯ	Zeya	53.755	127.293	270	6.76		1
ZMN	ЗМН	Zimniki	45.475	134.258	150	7.88		2
UNYS	УНЮ	Unknown						

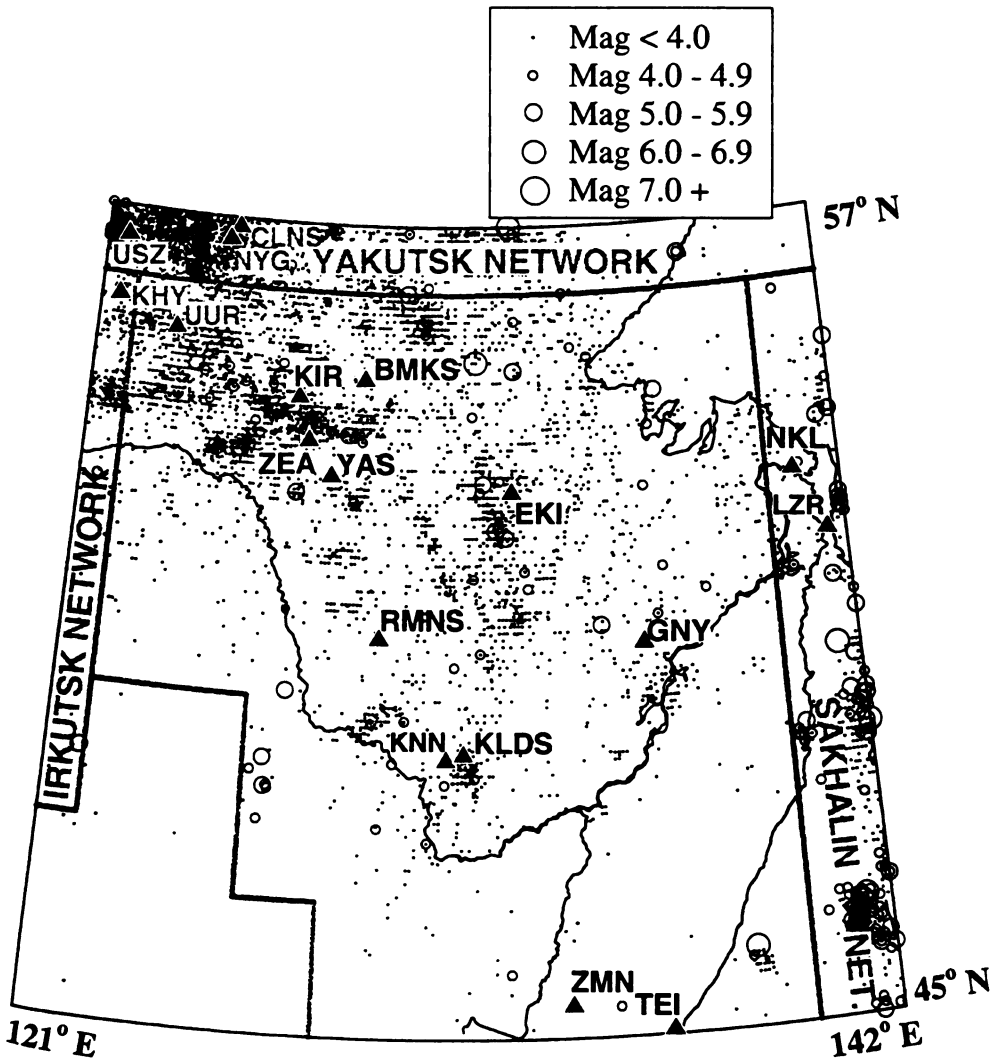

Figure 1-25. Seismicity and seismic stations of the Amur network.

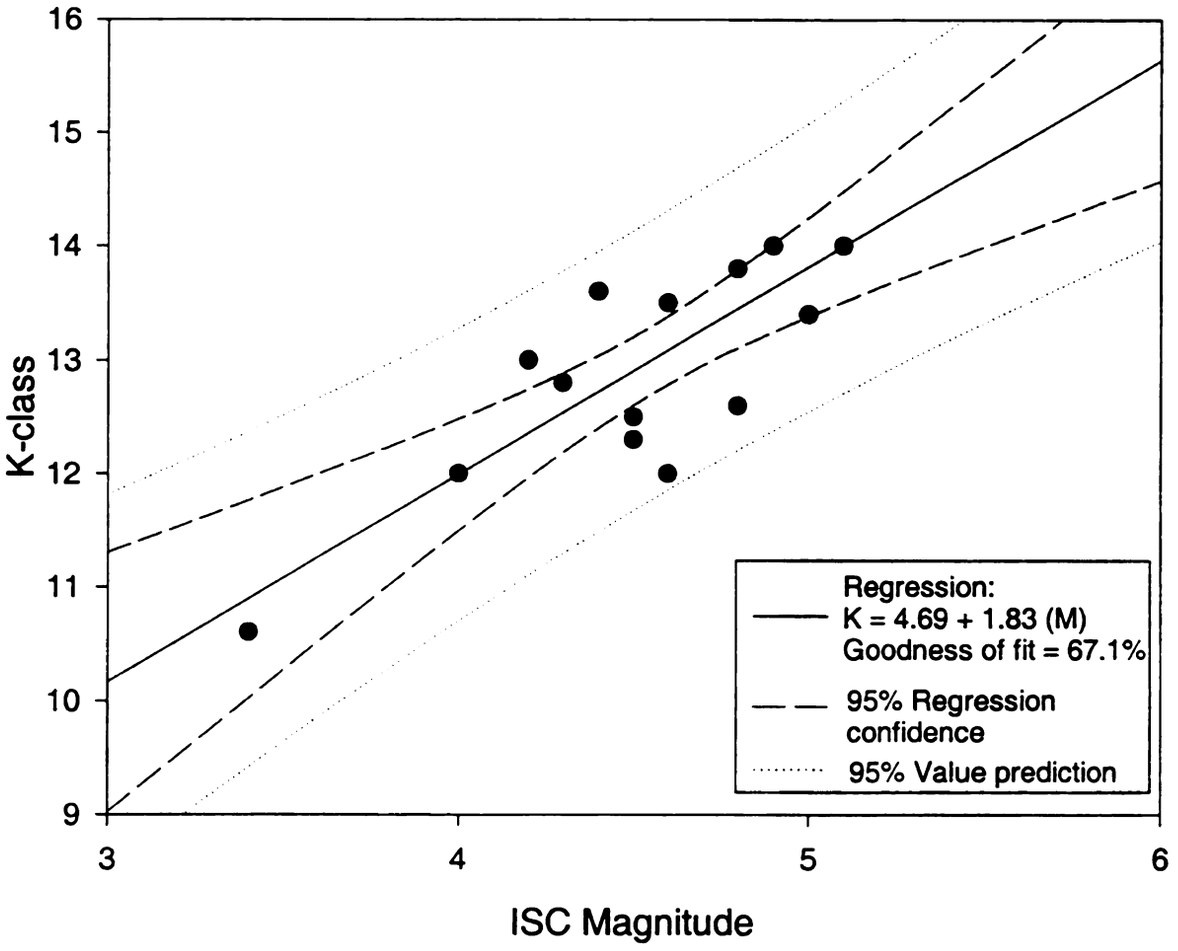

Figure 1-26. Relationship between K-class and ISC reported magnitude in the Amur network.

relocation of the events with the combined data set, parameters consistently match better with the Amur network locations.

Sakhalin Island Network

Seismic stations were first established on Sakhalin Island in the early part of the century by the Imperial Japanese government. These stations were closed in 1945 when Sakhalin was occupied by the Soviet Union following the end of World War II. Russian network stations were first deployed in the late 1960's, which led to the establishment of the Sakhalin network headquartered in Yuzhno Sakhalinsk (Table 1-12; Figure 1-27). The Sakhalin network monitors seismicity along the boundary between the Amur plate and Okhotsk block. Seismicity for Sakhalin was obtained from *Zemlet*, the *Far East Bulletin*, and the *SSR catalog*. The *Far East Bulletin* contains many smaller events not found in the other catalogs. Deep focus events under southern Sakhalin Island due to subduction of the Pacific plate are not included in the database.

Unfortunately, this study has not worked directly with the Sakhalin Island network, thus first hand knowledge of operational procedures and unpublished data were generally not available. As reported in the *Far East Bulletin*, earthquakes are located graphically with circles on maps. The crustal model used for calculation of travel time curves uses a two layer crust over the Moho. Total crustal thickness is 33 km, with the Conrad discontinuity at a depth of 15 km. Velocities are reportedly taken from Jeffreys (assumed Jeffreys and Bullen, 1940, based on context). Velocities used are:

Pg = 5.6 km/s	Sg = 3.3 km/s
P* = 6.4 km/s	S* = 3.9 km/s
Pn = 7.75 km/s	Sn = 4.42 km/s

Table 1-12. Seismic stations and station parameters for the Sakhalin Island network.

English Code	Russ. Code	Station Name	Lat.	Long.	Elev. (m)	Date Open	Date Closed	Qu
		Bykov	47.317	142.567	40	6.68	10.68	-
ESU		Esutoru (Uglegorsk)	49.083	142.033	100	12.39	--.45	-
		Firsovo	47.65	142.567	20	8.79	11.79	-
		Gornozavodsk	46.567	141.85	50	12.71	6.72	-
		Korsakov				--.51	1.52	-
		Kotikovo	49.133	144.25	10	7.69	9.70	-
		Lesogorsk	49.442	142.2	40	7.69	10.69	-
		Lopatino	46.6	141.825	40	4.69	10.69	-
		Moneron	46.258	141.25	40	9.71	5.72	-
		Nizhnii Armudan	50.817	142.533	150	9.66	4.69	-
	НКЛ	Nogliki	51.817	143.15	25	10.64	12.64	-
						--.88		-
NVV	НВР	Nyvrovo	54.317	142.617	5	11.81		-
		Ogon'ki	46.775	142.383	70	6.68	9.68	-
OKH	OXA	Okha	53.55	142.933	24	12.58	--.65	-
		Okha (New)				--.65		-
OOT		Ootomari (Korsakov)	46.65	142.767	36	--.09	--.45	-
OTI		Otiai (Bykov?)	47.325	142.783	20	2.34	--.45	-
		Ozhidaevo	47.033	142.392	220	--.76	--.77	-
		Pravda	46.942	142.008	40	9.71	11.71	-
		Shebunino	46.433	141.858	40	9.71	11.71	-
SKK		Shikka (Shikuka) (Poronaisk)	49.233	143.117	2	--.28	--.45	-
		Sovetskaya Gavan	48.967	140.283	50	6.69	11.70	-

Table 1-12 (con't).

		Tikhmenevo	49.2	142.9	150	6.69	10.69	-
		Toyohara (Yuzhno)				--.43	--.45	-
TYV TMSS	TMC	Tymovskoe	50.85	142.65	100	4.69		-
UGL	УГЛ	Uglegorsk	49.083	142.083	20	-.51		-
		Utesnoe	46.6	143.075	20	7.73	9.79	-
		Vzmor'e	48.85	142.517	20	7.82	12.82	-
		Yablochnyi	47.167	142.067	20	6.68	9.68	-
YSS1		Yuzhno Sakhalinsk (Novo Aleks-androvsk)	47.02	142.717	40	10.47	--.57	-
YSS	ЮСХ	Yuzhno Sakhalinsk	46.958	142.762	100	--.57		1

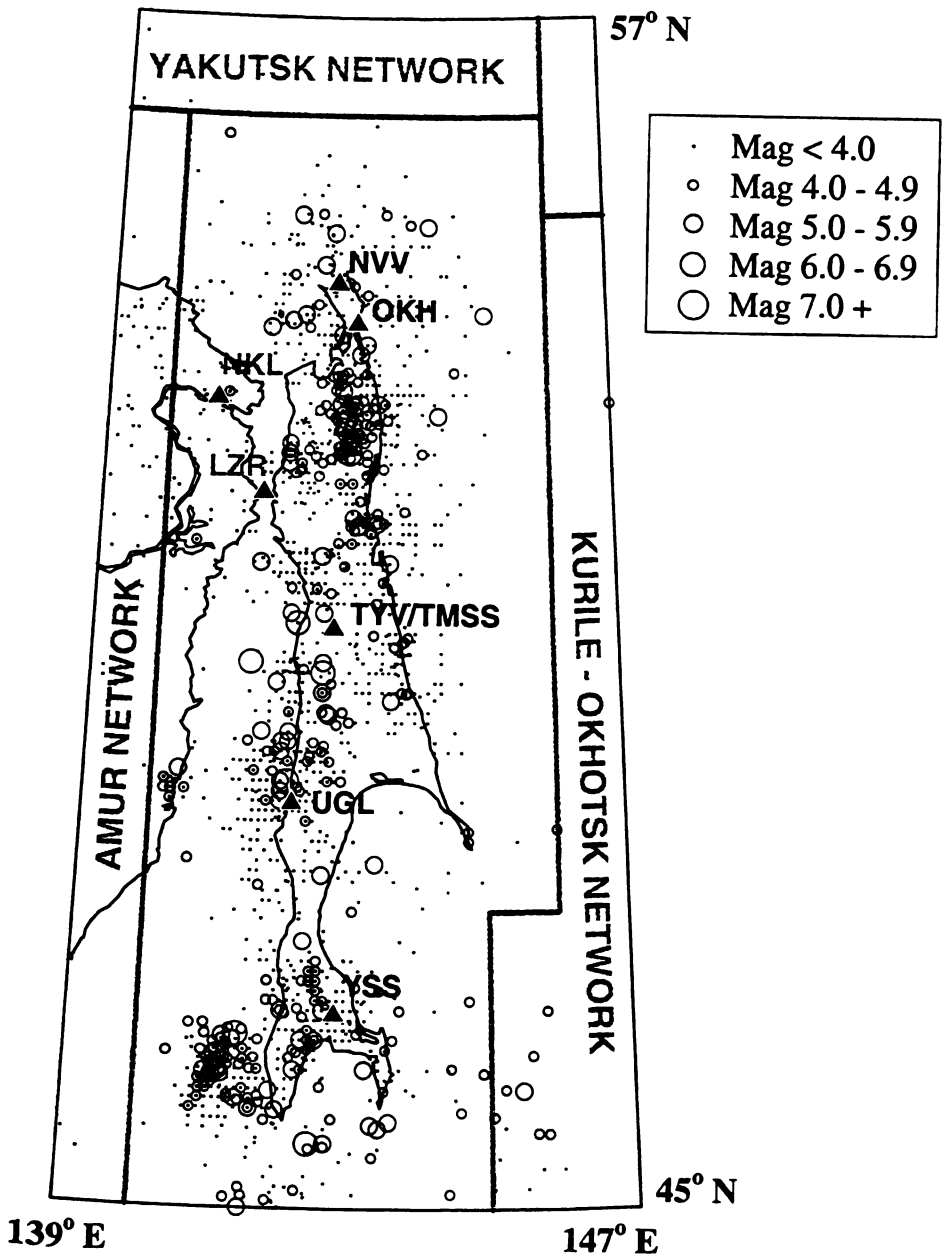

Figure 1-27. Seismicity and seismic stations of the Sakhalin network.

A linear regression relating K-class for the Sakhalin network to ISC magnitude was found to be

$$K = 3.84 + 1.31\ (M) \qquad (1\text{-}12)$$

where K is K-class and M is magnitude. The regression and data are shown in Figure 1-28. Phase data, although available in the *Far East Bulletin*, was not entered into the database of this study. Earthquakes located by the Sakhalin network use data from the Amur network, and generally have a large number of P* and S* phases reported, indicating that Sakhalin Island may have a well developed Conrad discontinuity.

Irkutsk Regional Network

Seismic stations in the Irkutsk region were first established in the 1950's, with the exception of Irkutsk, which opened in 1901 (Table 1-13; Figure 1-29). The Irkutsk network monitors seismicity between the the Eurasian and Amur plates, and includes the Baikal rift. The formal study area includes only a small portion of the Irkutsk network (south of 56° N between 120° and 122° E) and all seismicity was compiled for this area only. Epicenter data for the portion of the Irkutsk network of interest is taken from *Materialy*. Seismicity for the remaining portion of the Irkutsk network as listed in *Materialy* between 1970 and June, 1972 are included. Phase data for the Irkutsk network events are not included in the database. The relationship between K-class and ISC magnitude was not determined for the Irkutsk network.

CONCLUSION

The final compiled seismicity map with plate boundaries, network boundaries, and seismic stations is shown in Figure 1-30. Plate boundaries shown are primarily determined

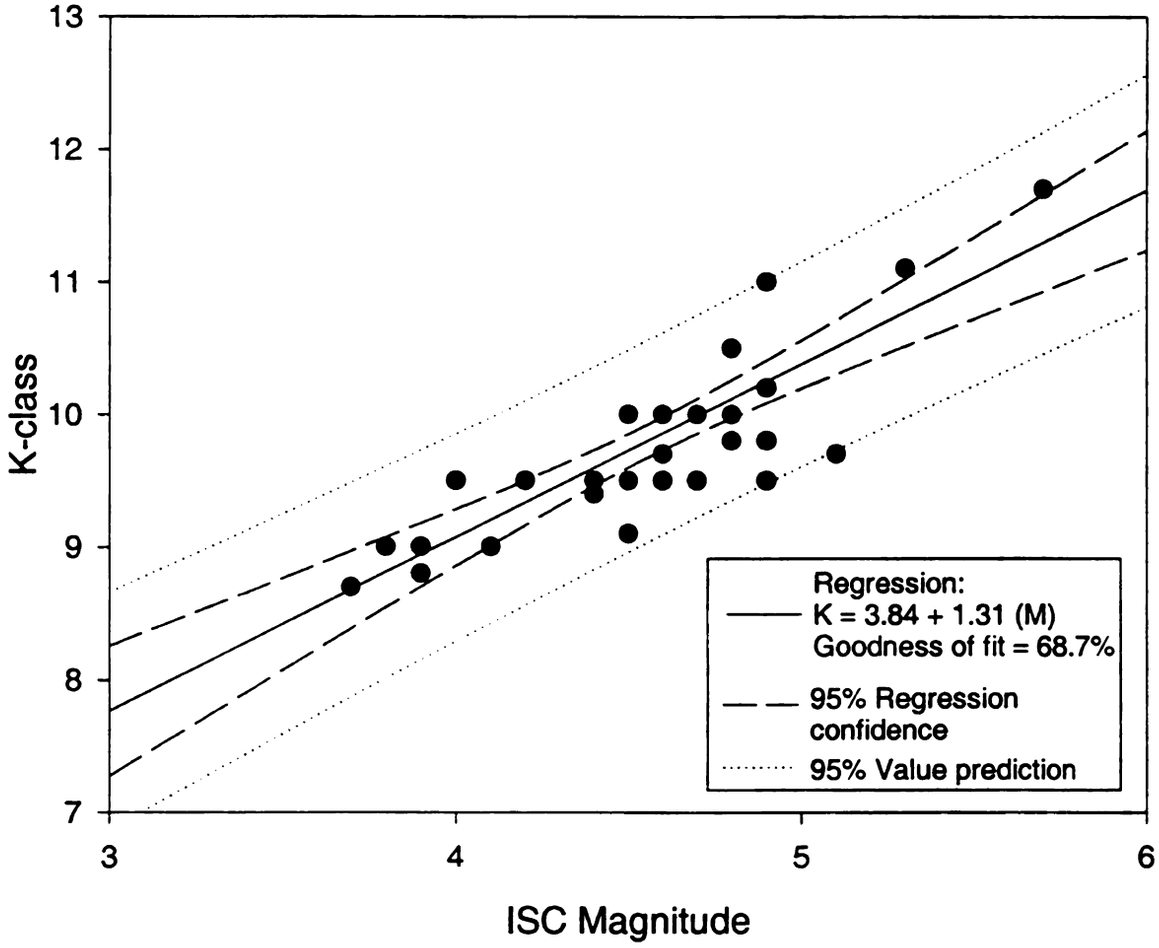

Figure 1-28. Relationship between K-class and ISC reported magnitude in the Sakhalin network.

Table 1-13. Seismic stations and station parameters for the Irkutsk network.

English Code	Russ. Code	Station Name	Lat.	Long.	Elev. (m)	Date Open	Date Closed	Qu
ALL	АЛ	Alla	54.688	110.82	550	10.63	5.70	1
ALY		Alygdzher	53.633	98.216	920	1.66	1.67	1
AGK		Angarakan	56.348	113.67	1430	11.76	8.81	1
ARS	АРШ	Arshan	51.908	102.433	840	–.58		1
BAU		Babushkin	51.717	105.867	470	6.66	9.66	1
BKK		Baikal'sk	51.522	104.133	460	1.64	2.66	1
BGZ	БРГ	Barguzin	53.617	109.633	475	9.61	5.70	1
BRUS		Barluk	54.533	101.717	525	11.60		1
BOD	БДБ	Bodaibo	57.807	114.03	245	11.60		1
BDN	БОД БДН	Bodon	53.713	110.1	540	11.69	--.83	1
CRS	ЧР	Chara	56.9	118.267	710	11.61		1
CIT	ЧТ	Chita	52.033	113.55	790	6.70		1
DAS		Davsha	54.538	109.503	460	1.64	6.65	1
DOV		Dovochan	56.462	117.533	1094	7.62	9.63	1
EMG		Emegachi	56.567	118.158	960	9.62	4.63	1
GOO	ГСН	Gusinoozersk	51.283	106.517	600	11.71	2.72	1
IKN		Irkana	55.867	111.253	480	1.64	3.66	1
IRK	ИРК	Irkutsk	52.272	104.31	467	12.01		1
KAB	КБ	Kabansk	52.05	106.658	465	1.51		1
KRMS		Karam	55.133	107.583	600	1.66	3.66	1
KAIS	ХМ	Khaim	52.602	108.085	480	10.69	5.70	1
KPC	КПЧ	Khapcheranga	49.707	112.392	950	12.68		1
KVO	КВК	Kovokta	56.133	113.05	1180	--.81		1
KTB		Krestovaya	52.665	106.395	560	7.71	9.71	1

Table 1-13 (Con't).

KMO	KMP	Kumora	55.883	111.208	475	9.66		1
KBK		Kurbulik	53.708	109.038	460	1.64	9.65	1
KYA	KXT	Kyakhta	50.35	106.45	760	3.52	5.70	1
LRB		Lurbun	56.63	117.883	780	8.62 5.67	9.63 9.68	1
MOY	МНД	Mondy	51.673	100.993	1300	–.58		1
MUO		Murino	51.475	104.408	470	8.66	9.66	1
MRU		Maritui	51.783	104.217	520	–.08	–.18	1
NMG		Naminga	56.60	118.517	1380	5.67	4.69	1
NMG1		Naminga-1	56.70	118.583	1160	–.63	–.63	1
NLY	НЛТ	Nelyaty	56.492	115.7	470	1.61		1
NSR	НСТ	Nesterikha	53.647	109.708	480	7.70	9.70	1
NKO		Nikola	51.893	104.827	460	7.71	9.71	1
NIZ	Н-А	Nizhne Angarsk	55.766	109.55	487	10.61		1
OIM		Oimur	53.333	106.833	460	10.59	–.60	1
OLK		Ol'khon	53.20	107.342	490	7.69	9.69	1
ONR	ОНГ	Onguren	53.233	107.592	500	–.88		2
ORA	ОРН	Oran	55.933	113.667	705	9.79		1
ORL	ОРЛ	Orlik	52.517	99.827	1365	2.67		1
OZE	ОЗН	Ozernaya	56.295	113.983	620	9.78		1
PLK		Polovinka	51.798	104.35	470	8.66	9.66	1
SOV		Savino	52.543	102.15	720	9.68	8.69	1
SVBS	С-Б	Severo Baikalsk	55.64	109.35	505	–.78	–.89	1
SVK	С-М	Severo Muisk	56.183	113.533	850	11.76		2
SHMS		Shamanka	53.125	105.6	700	8.59	2.63	1

Table 1-13 (Con't).

SRTS		Shara-Tagot	53.005	106.717	500	10.59	–.60	1
SMKS		Shimki	51.675	102.012	765	11.66	11.67	1
SOL	СЛЦ	Solontsovaya	54.17	108.35	458	–.79	–.87	1
SRK	КЛР	Srednii Kalar	55.86	117.38	716	--.61		1
SDK		Srednii Sakutan	56.898	118.095	750	2.63	10.63	1
SUVS	СУВ	Suvo	63.655	110.008	1000	--.84		1
SYB		Syul'ban	56.605	117.222	1000	6.62	9.63	1
TLY	ТАЛ	Talaya	51.681	103.644	579	11.82		1
TKH	ТХ	Tokhoi	51.361	106.608	640	11.71	4.73	1
TNL	ТНЛ	Tonnel'nyi	56.283	113.35	820	11.76		1
ZIP	ЦРК	Tsipikan	54.917	113.35	1110	--.75	2.86	1
TUP	ТПК	Tupik	54.425	119.933	630	11.61		1
TRNS		Turan	51.633	101.666	870	12.66	11.68	1
TNKS	ТНК	Turikan	56.383	113.108	695	8.81		1
TYD	ТНД	Tynda	55.133	123.717	610	7.70	1.72	2
TRG	ТРГ	Tyrgan	52.758	106.342	600	1.60		1
UKT	УКТ	Uakit	55.495	113.62	1140	12.62	--.75	2
UDK		Udokan	56.75	118.305	810	4.67	4.69	1
UKC	УЛК	Ulyukchikan	53.87	109.598	490	7.70	9.70	1
ULNS	ОЛЯ	Ulyunkhan	54.867	111.07	560	7.89		2
YOA	УН	Uoyan	56.13	111.77	520	--.79		1
ZAK	ЗКМ	Zakamensk	50.383	103.292	1125	12.60		1
ZAP		Zapadnyi	56.613	118.433	1600	4.67	8.67	1
ZARS		Zarech'e	52.550	107.15	460	7.59 7.69	–.60 9.69	1
ZRY		Zarya	57.24	118.917	655	10.59	9.68	2
ZGL		Zhigalovo	54.808	105.15	625	12.67	2.67	1
ZRV	ЖРВ	Zhuravlikha	53.517	109.375	475	7.70	9.70	1

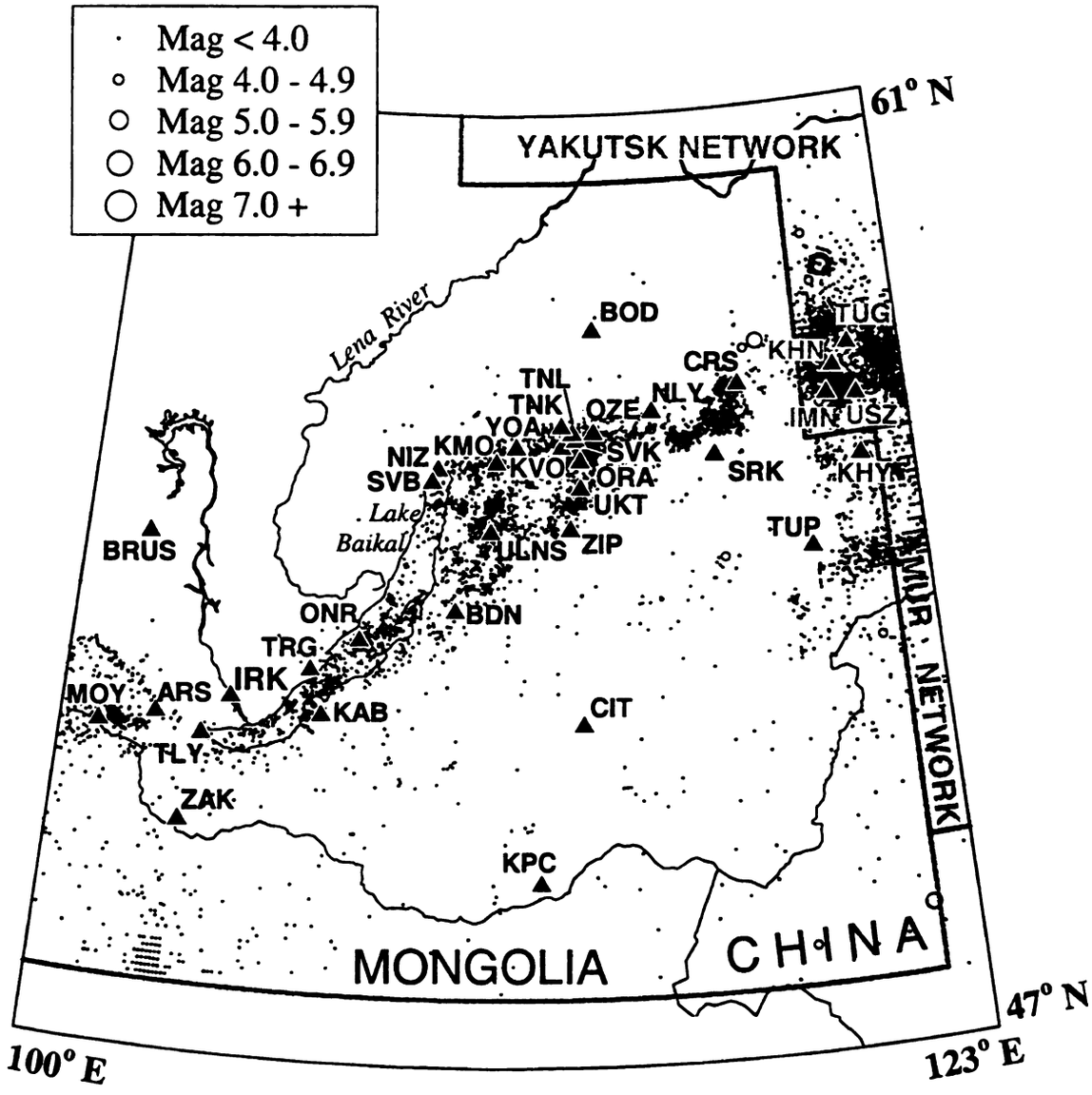

Figure 1-29. Seismicity and seismic stations of the Irkutsk network. Seismicity shown is primarily from 1970 and 1971.

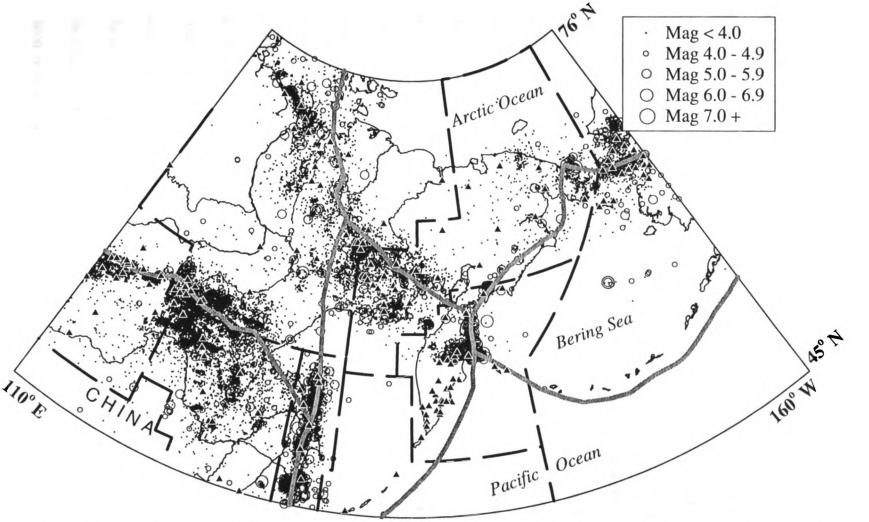

Figure 1-30. Plot of seismicity catalog compiled for northeastern Russia. Plate boundaries are depicted as gray lines, network boundaries as dashed lines, and seismic stations as triangles.

by connecting the largest events. However, in reality, the distribution of microseismicity indicates diffuse plate boundaries, probably having motion partitioned on many individual faults in a complex system, which is consistent with continental deformation (England and Jackson, 1989). Within the individual plate boundaries, there are many localized trends and clusters in the seismicity distribution which have never been studied in detail. However, several of these clusters and trends, particularly in the Amur region, are a result of anthropogenic sources (see Chapter 2). In general, the plate boundaries tend to follow the pre-existing large scale structural trends in northeast Russia, which probably represent structurally weaker, and thus easier to deform, regions. The boundary between the Amur and Eurasian plates trends along the Mongol-Okhotsk suture, which follows the southern edge of the Siberian Platform (Figure I-4). The boundaries along the North American-Eurasian plates and the North American-Okhotsk plates parallels the western edge of the Mesozoic Kolyma-Omolon Superterrane (Figure I-4). The Bering-North American plate boundary appears less diffuse, particularly through the Koryak Highlands, where it parallels the boundaries between some of the Cenozoic accreted terranes. This boundary is discussed extensively in Chapter 5. Finally, the proposed boundary between the Eurasian plate and the Okhotsk plate is somewhat problematic. There have been relatively few teleseismic events defining the location of the boundary and there is an almost complete lack of located microseismicity in the region. This may, however, be entirely an artifact of the distribution of the regional seismic networks. Note on Figure 1-30 that this region is near the intersection of the Magadan, Yakutsk, Amur, Sakhalin, and Kurile-Okhotsk networks. Furthermore, the division between the northern and southern portions of the Yakutsk networks is in this region. There is microseismicity trending into the region from each of the Magadan,

Yakutsk, and Sakhalin networks. Given the distances to individual network stations and the lack of data exchange between neighboring networks, small events occurring in this region are most likely below the detection or location threshold for any individual network. Only the Sakhalin network has close stations, but even here there has never been the three stations necessary for determining event locations. Since data were not exchanged between networks, the region appears aseismic.

Overall, seismicity levels in northeast Russia are much higher than is generally recognized in the literature. Unfortunately, economic conditions in Russia at the present time have resulted in the closure of many, if not most, of the regions seismic stations. This illustrates the importance of compiling the historic data, as further economic collapse in Russia could result in the permanent loss of the original data, at worst. At best, it would take the installation of several tens of permanent digital stations and a minimum of two decades to duplicate the database using modern acquisition methods.

REFERENCES

Andreev, T.A., Kravets, I.F., and Mishin, S.V., 1967, On the seismic activity of the Northeast: *Trudy SVKNII*, Magadan, v. 30, p. 159-166 (in Russian).

Ansimov, E.M., Sedov, B.M., and Shvarts, D.B., 1967, Seismic exploration in the northeast USSR, *in* Fotiadi, E.E., ed., *Geologicheskie Rezul'taty Geofizicheskikh Issledovanii v Sibiri i na Del'nem Vostoke*: Novosibirsk, Nauka, p. 438-442 (in Russian).

Artamonov, V.V., and Mishina, L.V., 1984, Recording possibilities of the network of seismic stations in the Northeast USSR, *in* Izmailov, L. I., and Lin'kova, T. I., eds., *Seismic processes in the Northeast USSR*: SVKNII, Magadan, p. 99-115 (in Russian).

Avitesov, G.P., 1983, Seismological data on the deep structure of the New Siberian Islands and adjacent sea areas: *International Geology Review*, v. 25, p. 651-660.

Avetisov, G.P., 1996, *Seismically active zones of the Arctic*: Saint Petersburg, VNII Okeangeologiya, 185 pp. (in Russian).

Biswas, N.N., Gedney, L., and Agnew, J., 1980, Seismicity of western Alaska: *Bulletin of the Seismological Society of America*, V. 70, p. 873-883.

Biswas, N.N., Pujol, J., Tytgat, G., and Dean, K., 1983, *Synthesis of seismicity studies for western Alaska*, Final report, contract NA81-RAC00112: Fairbanks, Alaska, University of Alaska Geophysical Institute, 74 pp.

Davydova, N.I., Shvarts, Ya.B., and Yaroshevskaya, G.A., 1968, Wave patterns in deep seismic sounding along Magadan-Kolyma profile, *in* Deep Seismic Soundings of the Earth's Crust in the USSR: *International Geology Review* - Book Section, v. 10, p. 93-102.

England, P., and Jackson, J., 1989, Active deformation of the continents: *Annual Reviews of Earth and Planetary Science Letters*, v. 17, p. 197-226.

Gal'perin, E.I., 1974, *Vertical seismic profiling*: Special publication No. 12, Society of exploration geophysicists, Tulsa, 270 pp.

Godzikovskaya, A.A., 1995, *Local explosions and earthquakes*: Rossiskoe Aksionernoe Obshchestvo Evergy and Electrification "EES Rossii," Moscow, p. 55-56 (In Russian).

Kondorskaya, N.V., and Shebalin, N.V., eds., 1982, *New catalog of strong earthquakes in the U.S.S.R. from ancient times through 1977*: World Data Center A for Solid Earth Geophysics, Report SE-31, xi+608 pp.

Kovachev, S.A., Kuzin, I.P., and Soloviev, S.L., 1995, Short-term study of microseismicity in the Guba Buorkhaya, Laptev Sea, using ocean bottom seismographs: *Physics of the Solid Earth*, english translation, v. 30 (7/8), p. 647-658.

Kuzin, I.P., 1973, Velocity of the P and S-waves in upper mantle in Kamchatka: *Izvestia, AN SSSR, Physics of the Earth*, N3, p. 3-16.

Kuzin, I.P., 1974, *Subduction zone and upper mantle structure in East Kamchatka*: Moscow, Nauka, 132 pp.

Lazareva, A.P., 1975, Earthquakes of the Arctic in 1970 and 1971, *in* Gorbunova, I. V., Kondorskaya, N. V., and Shebalin, N. V., eds., *Earthquakes of the USSR in 1971*: Nauka, Moscow, p. 145-149 (in Russian).

Lay, T., and Wallace, T.C., 1995, *Modern global seismology*: Academic Press, San Diego, 521 pp + xii.

Materialy po Seismichnost' Sibiri, 1970-1990: Academy of Sciences of the USSR, Siberian Branch, Irkutsk (bi-monthly, in Russian).

Mishin, S.V., 1967, *Experimental instrumental seismological investigations in the northeast USSR*: Laboratory of Regional Geodynamics, NEISRI, Magadan, 165 pp. (In Russian).

Pustovitenko, B.G., and Kul'chitskii, B.E., 1974, About energy estimates of earthquakes in the Crimea-Black Sea region, *in* Kondorskaya, N.V., Nersesov, I.L., Gorbunova, I.V., Rautian, T.G., and Korchagina, T.G., eds., *Magnitude and Energy Classification of Earthquakes,* v. 2,: IPE AS USSR, Moscow, p. 113-124 (In Russian).

Seismologicheskii Bulleten' - Dal'nego Vostok, 1972-1988: Academy of Science of the USSR, Far Eastern Branch, Yuzhno Sakhalinsk (in Russian).

Solonenko, 1974, Evergy classification of earthquakes of Prebaikalia, *in* Kondorskaya, N.V., Nersesov, I.L., Gorbunova, I.V., Rautian, T.G., and Korchagina, T.G., eds., *Magnitude and Energy Classification of Earthquakes*, v. 2,: IPE AS USSR, Moscow, p. 174-179 (In Russian).

Zemletryaseniya v SSSR, 1961-1989: Nauka, Moscow (annual, in Russian).

Zemletryaseniya v SSSR, 1990-1991: Russian Academy of Science, Moscow (annual, in Russian).

Zemletryaseniya Severnoi Evrazii, 1992: Geoinformmark, Moscow (in Russian).

CHAPTER 2

Explosion Contamination in the Northeast Russia Seismicity Catalog

INTRODUCTION

The newly compiled seismicity catalog for Eastern Russia (see Chapter 1) allows us to re-examine the regional seismicity of northeastern Russia to determine the level of explosion contamination and obtain a better idea of the level of natural seismicity in the region. In this part of Russia explosions occur in tin, coal, and gold (both underground and placer) mines, as well as in the construction of roads, railways, and dams. Many of the active mining regions are geographically associated with the seismically active regions, which can result in misidentification of mine blasts as natural earthquakes. In addition, contamination of the seismicity catalog with explosions results in an erroneous perception of natural seismicity and seismic risk assessment.

This chapter investigates and identifies the regions of explosion contamination in the study area through temporal analysis of origin times. Both time of year and time of day are considered. While analysis of waveform data for all reported earthquakes would be desirable, it would require an unrealistic re-examination of several hundred thousand analog seismograms. A qualitative estimate of the level of explosion contamination, however, can be obtained by examining the size, spatial, and temporal characteristics of earthquakes located by the regional networks.

DATA SOURCES

The origin times of earthquakes used here come from the compiled seismicity database for northeastern Russia described in Chapter 1. Information on known explosion locations comes from the unpublished Magadan and Yakutsk network bulletins. The unpublished Magadan bulletin lists a separate compilation of explosions by either region (nearest town) or mine, but specific coordinates are omitted in either case (Figure 2-1; Table 2-1). Many specific mines or regions have hundreds of explosions identified. The unpublished Yakutsk bulletin lists explosion locations and origin times determined with S - P time differences (Figure 2-1). Unfortunately, an explosion specific listing is not seperated from the rest of the data. The location procedure is the same as used for earthquakes (Chapter 1). For explosions which are not locatable, the region of the explosion is given along with the approximate origin time. In some cases, explosions identified by mine or region in the Magadan bulletin are located by the Yakutsk network and coordinates are given. A small number of located explosions in the Amur region are given in Godzikovskaya (1995; Figure 2-1) for the time period 1990-1991. Mine locations from throughout the study region were taken from 1:200,000 scale Russian military topographic maps, as well as 1:500,000 TPC and 1:1,000,000 ONC U.S. air navigation charts.

PREVIOUS WORK

Early attempts at explosion filtering from the late 1960's through mid 1970's in the Magadan region simply removed all events within a particular radius of some mining regions (Riegel, 1994; Kovalev, pers. comm.). Of course, this also removes the wanted tectonic

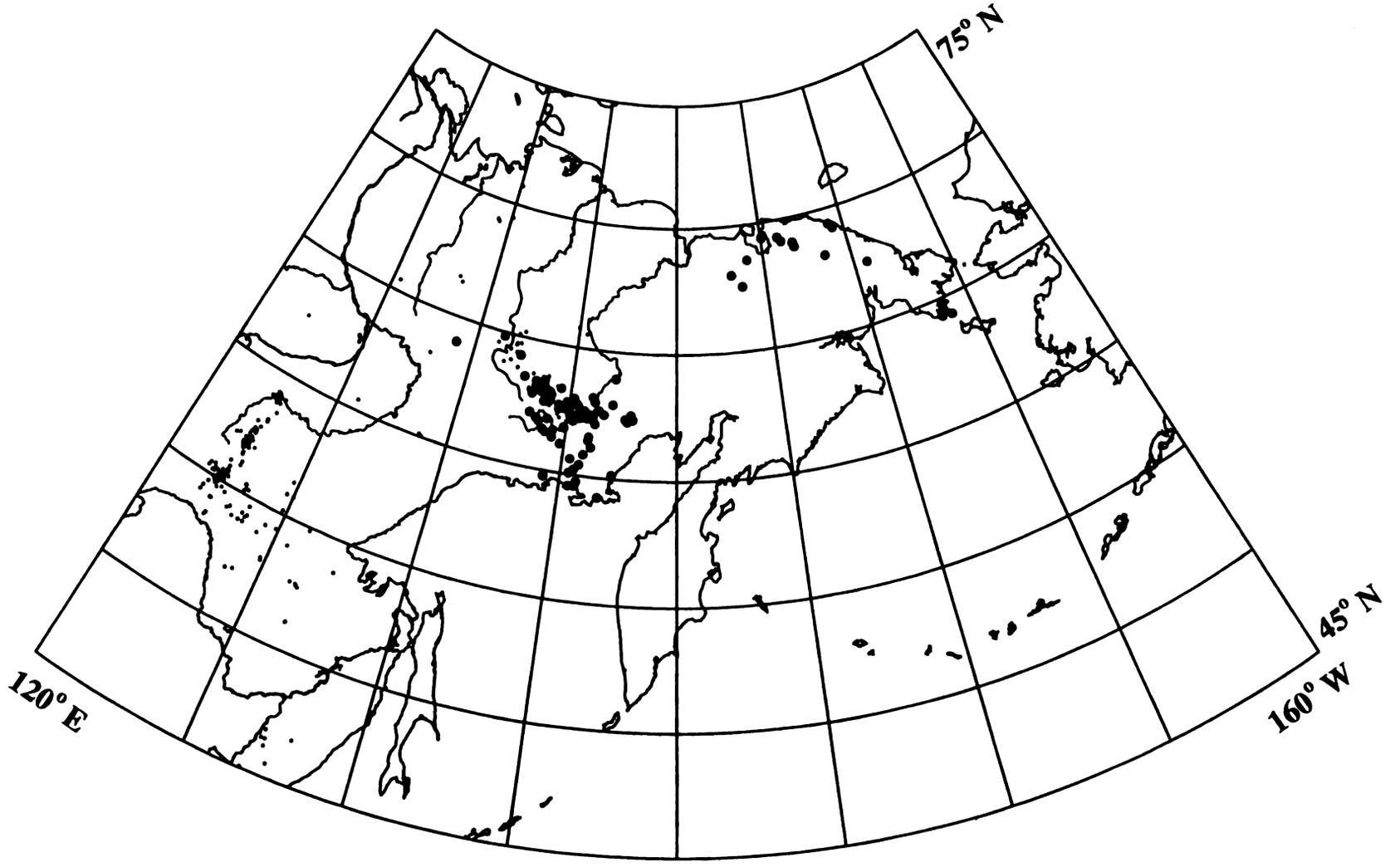

Figure 2-1. Explosion sources in northeast Russia listed in Russian bulletins. Small dots are individual located explosions, and large dots are towns or mines with multiple explosions.

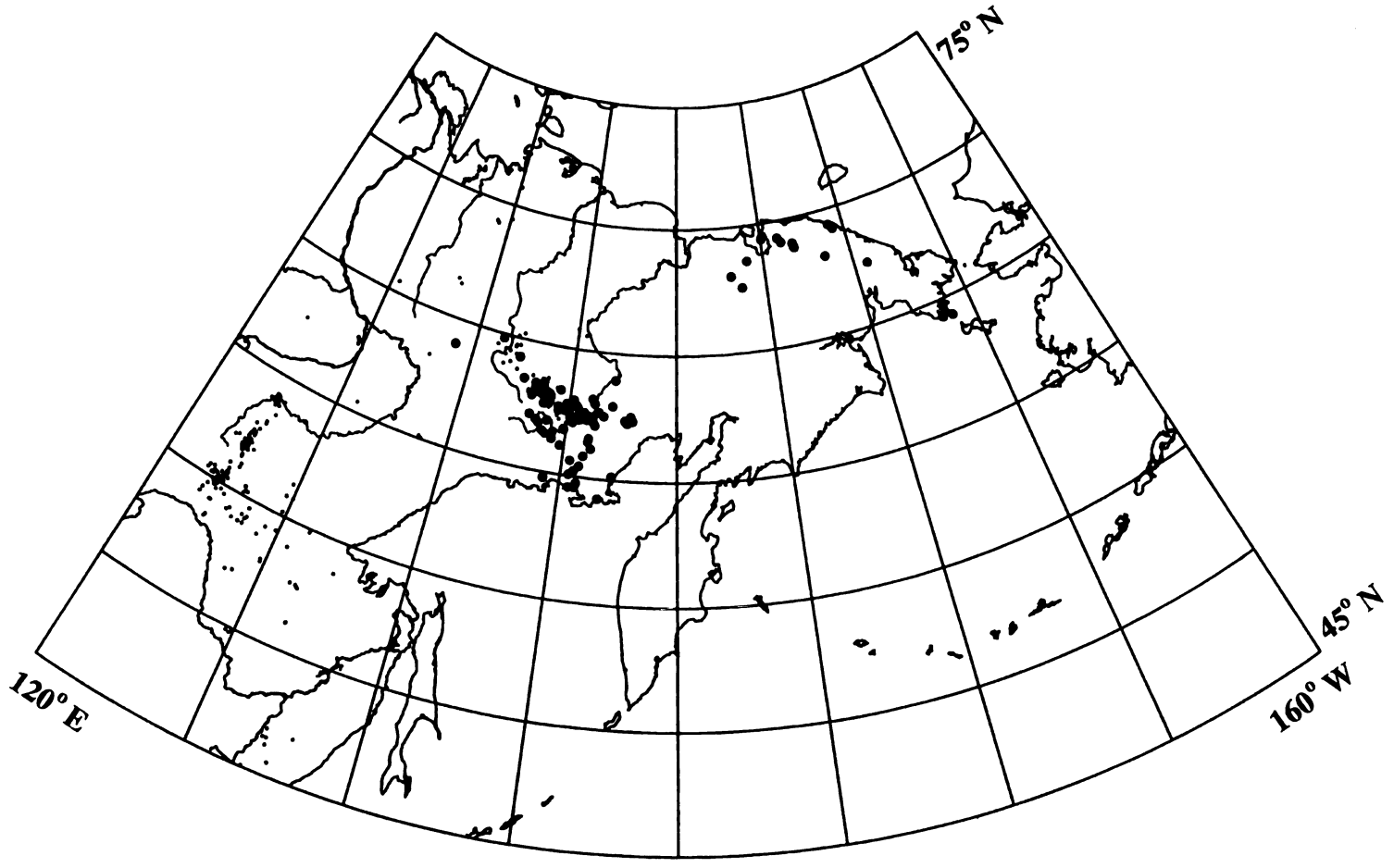

Figure 2-1. Explosion sources in northeast Russia listed in Russian bulletins. Small dots are individual located explosions, and large dots are towns or mines with multiple explosions.

Table 2-1. Town and mine locations from which explosions are reported in the unpublished Magadan bulletins.

Town/mine	Long.	Lat.
Adigalakha	146.40	62.91
Aliskerova	167.30	67.53
Anadyr	177.496	64.734
Arkagala	146.93	63.15
At-Uryakh	150.10	62.65
Atki	151.79	60.83
Avrora	150.05	62.50
Baranikhi	168.12	68.57
Belechan	148.16	62.88
Belovo		
Biestrie		
Bilibino	166.15	68.02
Binda		
Boligichan	154.11	63.93
Bolshevik	147.59	62.68
Burkandya	147.43	63.32
Burkhala	149.00	62.66
Buyunda	152.81	62.61
Chaplino	-172.16	64.25
Chelbanya	148.07	62.70
	147.22	63.38
Debin	150.75	62.34
Delyankir	145.40	63.49
Detrina		
Dukat	155.26	62.36
Durkhali		
Duskanya	148.84	61.62
Dzhelgaly	149.08	62.49
Elgin	150.69	62.79
	151.75	62.90
Frolich		
Galimogo	155.97	62.35
Gastello	147.85	61.60
Geologicheskii	152.37	62.20
Gorkogo		
Gvardiyets	147.14	62.00
Iul'tin	-178.56	67.43
Juletta		
Kadikchana	147.05	63.09
Kamenki		
Karamkena	151.10	60.21
Kedrovia		
Khatingnakh	148.15	62.03
Klepki	151.41	59.75
Kolyma		
Komsomolskii	172.42	69.11
Krasnoarmeiskii	172.02	69.30
Kulinskom		
Kulu	147.43	61.89
Larukovaya	151.80	62.25
Lazo	152.13	63.12
Leningradskii	178.33	69.35
Lunnogo	154.05	62.90
Madayan	150.70	60.60
Magadan	150.81	59.56
Maiskii	173.70	68.975
Maldyk	148.23	63.00
Moi-Urustra		
Molodezhnia	149.04	63.30
Myakit	152.09	61.41
Myaundzhi	147.19	63.05
Neksikan	147.67	62.67
Nelkoba	148.81	61.34
Nevskogo	155.48	62.25
Obinokogo		
Obo	149.77	61.80
Odinokyi		
Oktybrna	142.66	64.83
Ola	151.30	59.58
Omsukchan	155.77	62.52
Orotukan	151.34	62.26
Pervomaiskia	147.61	62.95
Pevek	170.19	69.41
Plamennyi	177.10	68.17
Pobera	144.59	64.27
Polevogo		
Polyarnyi	178.72	69.17
Promezhytochnie	178.83	68.80
Provideniya	-173.11	64.30
Pyatiletki	150.96	62.37
Rabochia		
Raskovoe	146.50	62.15
Rechnoe		
Ribnogo	150.19	62.32
Salkalykh		
Seimchan	152.38	62.93
Sherokee	148.05	63.10
Shturmovoe	149.77	62.82
Sinegoria	150.52	62.09
Spornogo	151.05	62.22
Srednekanskom	152.57	62.07
Srednii	153.35	59.21
Stan-Ut		
Stekolnyi	150.73	60.05
Strelki	152.13	61.54
Susuman	148.15	62.78
Svetlya	138.14	64.04
Takhtoyamsk	154.40	60.12
Talaya	152.39	61.13
Talona	148.60	59.79
Tangara		
Taskan	150.38	62.99
Tenkinskom		
Transportnyi	148.18	61.49
Udarnik	147.90	63.14
Ust'khakchan	146.57	63.41
Ust'omchuga	149.63	61.13
Ust'srednikan	152.34	62.43
Ust'taskan	150.84	62.72
Ust'ugol		
Ust'utinogo	151.47	62.55
Valkyneya	170.12	69.35
Verkhne-Buyunda	153.30	62.47
Vetrennee	149.81	61.77
Yablonego	151.51	60.42
Yagodnaya	149.62	62.53
Yasnee		

events, and results in peculiar rings of seismicity. Beginning in the late 1970's, seismic station operators attempted to discriminate close events (up to 50 - 70 km) based on waveform characteristics and information from the mining companies. Unfortunately, not all mining companies provided information on their blasting activities for various reasons (Kovalev, pers. comm.).

Previous work on identifying explosion contamination in the seismicity catalog was undertaken by Godzikovskaya (1995). Godzikovskaya (1995) identified several regions of explosion contamination, particularly in the Zeya basin region of Amur, near the Kolyma and Ust' Srednekan dams on the Kolyma River, and the Polyarnyi mining district in Chukotka. However, many regions and trends of contamination were not identified because of an incomplete seismicity catalog. Odinyets (1996) identified the problem of explosion contamination in the Kolyma region. In this case, it was determined that a large fraction of earthquakes reported in the central Kolyma region are actually explosions. Industrial explosions locatable by the regional networks generally have magnitudes of about 1.5 - 3.0 (converted from Russian K-class) and occur during local day (Godzikovskaya, 1995; Odinyets, 1996). Placer deposit explosions are also concentrated during the late winter and early spring, when frozen ground is broken up for the summer processing season.

DISCUSSION

Although the regional networks operating in northeastern Russia have attempted to discriminate between industrial explosions and earthquakes, all seismicity catalogs containing events of less than magnitude 3.5 from the region remain contaminated with explosions.

Examination of temporal biases in the seismicity can indicate potential regions of explosion contamination (Agnew, 1990), as blasting generally occurs during the day. However, unlike standard mining practice in the United States, blasting in northeast Russia is not confined to a specific time of the day, such as noon, but instead may occur at any time during the workday. A small but not statistically significant number of explosions are also known to occur during the "nighttime" hours in many locations throughout the study area (Godzikovskaya, 1995). In Figure 2-2, the study area is divided into cells in which the percentages of "daytime" earthquakes are calculated. Cells containing fewer than ten events were not considered to be statistically significant, thus were not analyzed. As there are five time zones spanning the region, the 12 hour local period of "daytime" is shifted accordingly. Dark gray areas represent regions where seismicity is more or less balanced between night and day, and light gray areas are those in which seismicity is concentrated during local night. There are several areas of "nighttime" biased seismicity, most of which are in seismically less active regions and away from network seismic stations. Bias of seismicity to local night is not unexpected since almost all regional seismic stations in the study area are located in buildings in populated areas, and thus have lower cultural noise levels during the night. The general concept can be illustrated by analyzing the temporal distribution of a large number of known earthquakes. Figure 2-3 shows the temporal distribution of the aftershock sequence of the 1989 South Yakutia earthquake. Note the bias towards larger numbers of "nighttime" events. Of 3,492 events from the aftershock sequence, 1,677 events occurred during "daytime" hours, and 1,815 events occurred during the night. This corresponds to a day/night ratio of 0.924 (a day/night ratio of 1.000 would indicate no bias). The bias may not be as great for these events as for regions away from the network due to the close proximity of

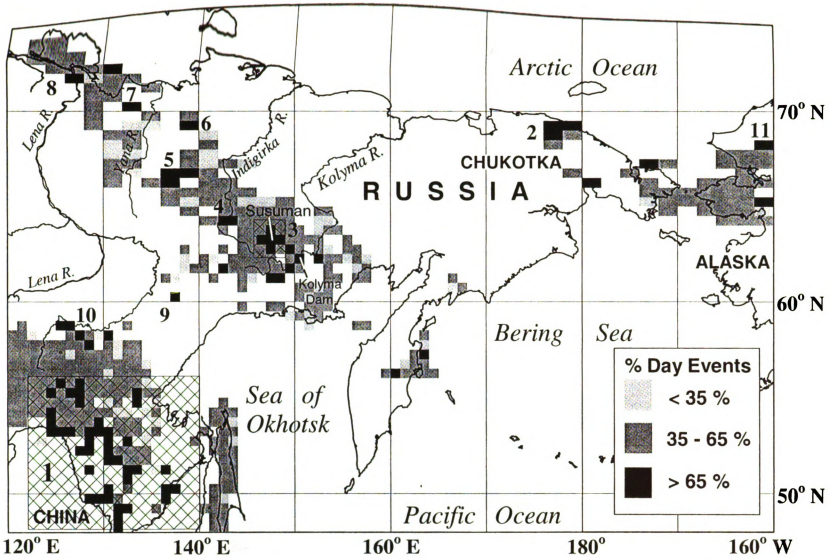

Figure 2-2. Percentage of seismicity occurring during local "daytime." Numbered regions are discussed in the text.

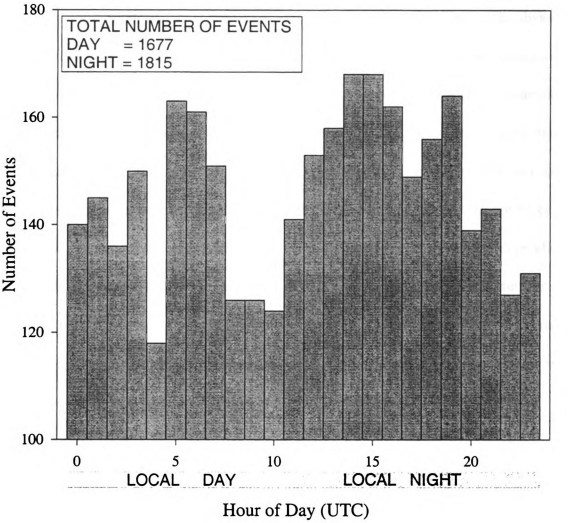

Figure 2-3. Histogram of event origin times from aftershocks of the 1989 South Yakutia earthquake. Note a slight bias towards "nighttime" events.

several seismic stations. Black areas on Figure 2-2 represent regions where more than 65% of the seismicity occurs during local day. Many of the regions with predominantly "daytime" events are associated with discrete clusters or trends of seismicity, most of which can be associated with mining or construction related blasting. Several clusters of reported seismicity in the Amur region have more than 90% of the events occurring during local day. A few cells with predominantly "daytime" seismicity do not correlate with obvious identifiable explosion sources. These locations are probably a result of random statistics of small numbers as these cells generally are close to the 10 event cutoff. We have examined several regions of "daytime" bias which can be positively related to explosion contamination. As a cautionary note, it should be mentioned that some events occurring at night may also be explosions. Russian law requires that explosives loaded into boreholes can not be kept overnight, but must be detonated. This may result in some "nighttime" blasting, depending on the work schedule of the particular mine. This is supported by a limited number of "nighttime" blasts listed in the unpublished network bulletins. The numbers of "nighttime" blasts are small when compared to those occurring in the "daytime". Numbers for the regions listed below correspond to numbered locations on Figure 2-2.

1. Amur District

The clearest region of explosion contamination is the Amur District. When plotting "daytime" and "nighttime" epicenters separately (Figures 2-4 and 2-5 respectively), we see some distinct differences. There are several large clusters of "daytime" seismicity that correlate geographically with specific mining regions. For these regions, we also identify contamination level changes with season. Figures 2-6 through 2-18 show the number of events that occur during

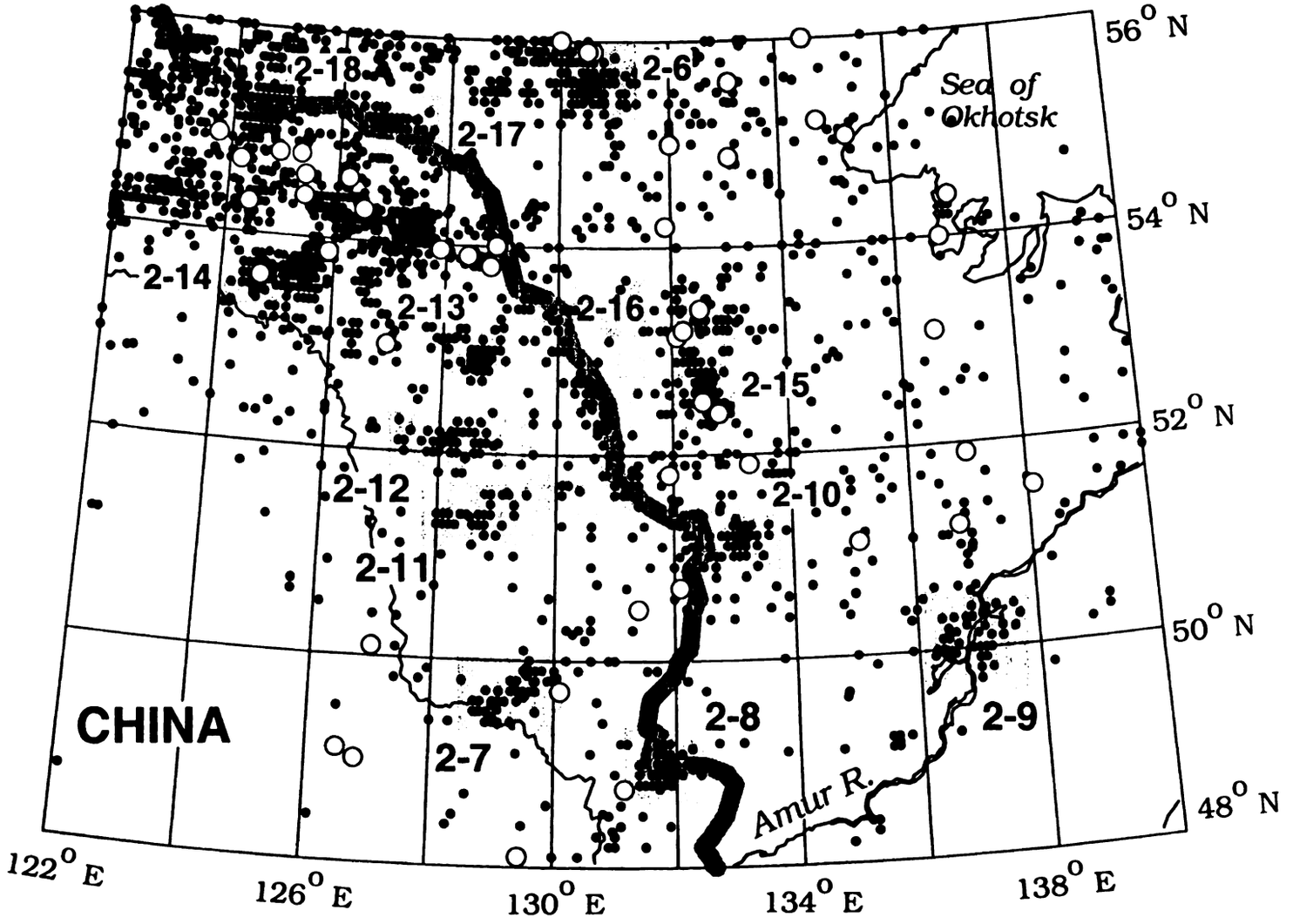

Figure 2-4. "Daytime" seismicity of the Amur region. Temporal statistics of the clusters of epicenters in gray boxes are shown in figures of corresponding numbers. The Baikal-Amur railway is indicated with the heavy gray line. Teleseismically recorded events of magnitude greater than 4.0 are depicted with large open circles.

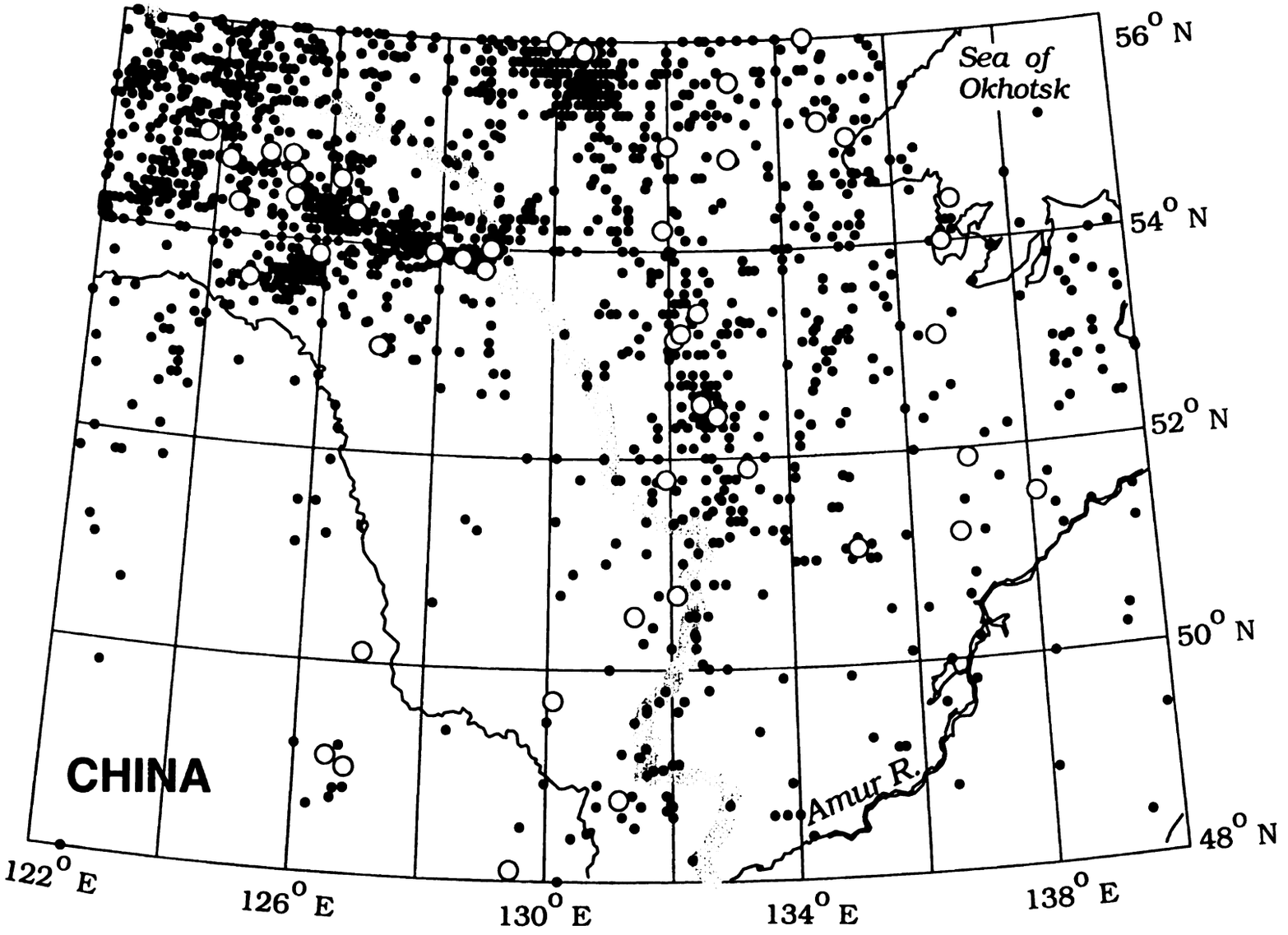

Figure 2-5. "Nighttime" seismicity of the Amur region.

specific hours of specific months of the year. Figure 2-6 analyzes a reported cluster of seismicity in the northern part of Figure 2-4. The seismicity in this region is believed to be tectonic, as the region is unpopulated, and there is no known mining or development in the area. The analysis of this region can therefore be used as a baseline to which other analyses can be compared. The area analyzed contains 399 located earthquakes, with 189 having occurred during local "daytime" and 205 during local night. This corresponds to a day/night ratio of 0.922, which is essentially the same as that found for the 1989 aftershock sequence discussed above. The numbers of summer and winter events occurring in this region are also similar.

In southern Amur, analysis of reported seismicity around the Raychikhinsk coal mining region shows activity only during winter months and daylight hours (Figure 2-7). This is somewhat different from the nearby Khingansk mining region, where events occur throughout the year instead of being restricted to winter months (Figure 2-8). Figure 2-9 corresponds to mining or quarries in the region around Komsomolsk' na Amur. On average, origin times of events in the Raychikhinsk, Khingansk, and Komsomolsk' na Amur center around 05 hours UTC, which corresponds to 1 pm local time. Mining also occurrs about 5 km to the north of Chegdomyn, which accounts for the high level of "daytime" seismicity in the region (Figure 2-10). However, here origin times average slightly earlier at around 04 hours UTC, or 12 noon local time, and there is a shift towards summer months. It is unknown what is being mined here. Temporal analysis of the reported seismicity in the region of Svobodniy (Figure 2-11) is also consistent with sources of anthropogenic origin. However, the existence of mining in this region is unclear from the available maps. Events here may also show a slight bias toward summer months and slightly later origin times averaging 07 hours UTC, or 3 pm local time. To the north of Svobodniy are mining regions near Shimanovsk (Figure 2-12) and Oktyabrskiy (Figure 2-13).

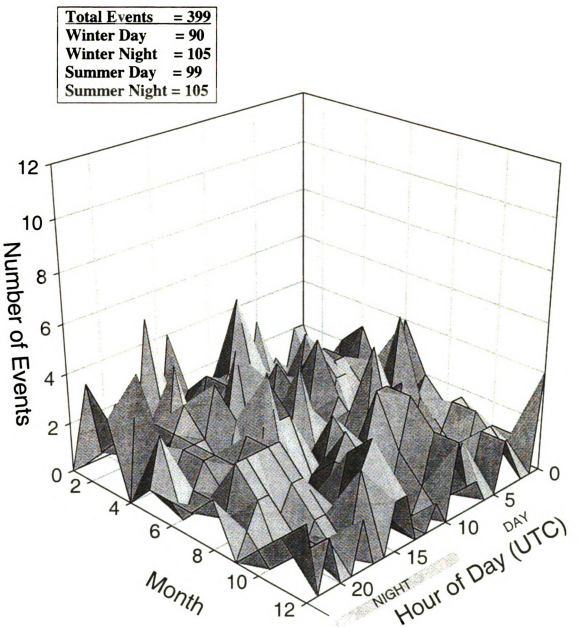

Figure 2-6. Temporal variation of probable tectonic earthquakes.

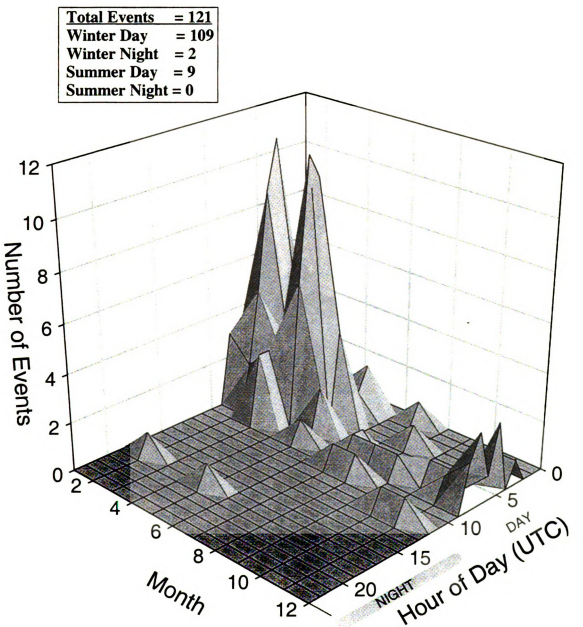

Figure 2-7. Temporal variation of reported seismicity in the Raychikhinsk mining region.

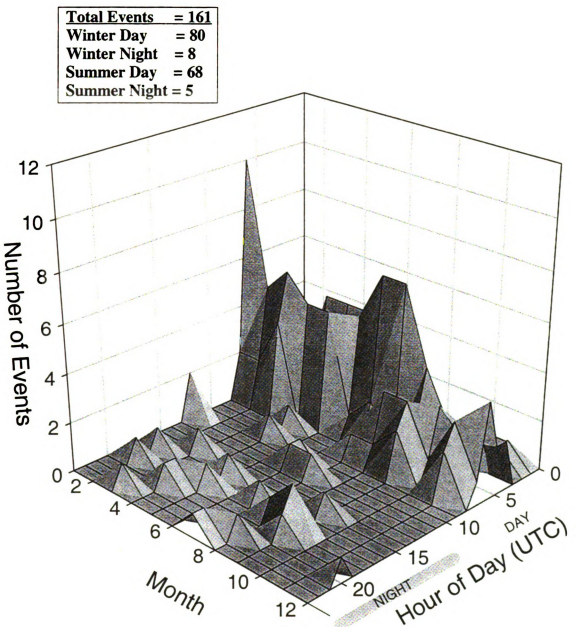

Figure 2-8. Temporal variation of reported seismicity in the Khingansk mining region.

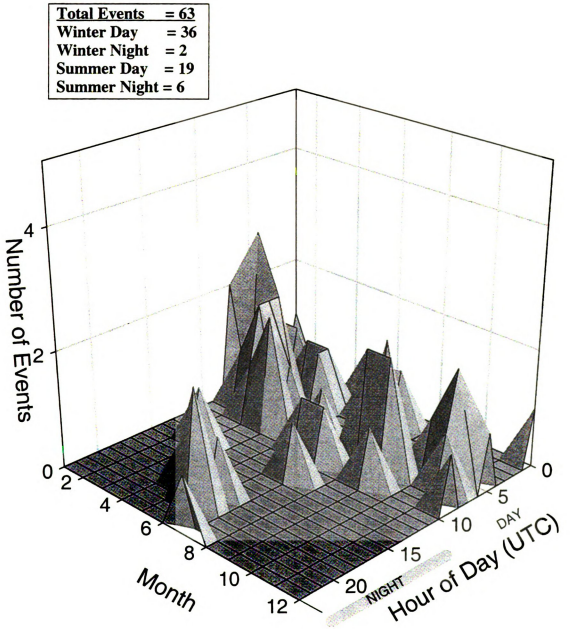

Figure 2-9. Temporal variation of reported seismicity in the Komsomolsk' na Amur mining region.

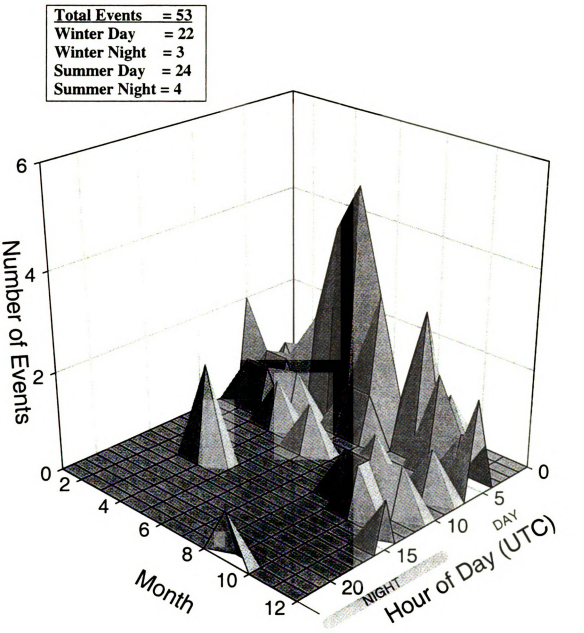

Figure 2-10. Temporal variation of reported seismicity in the Chegdomyn mining region.

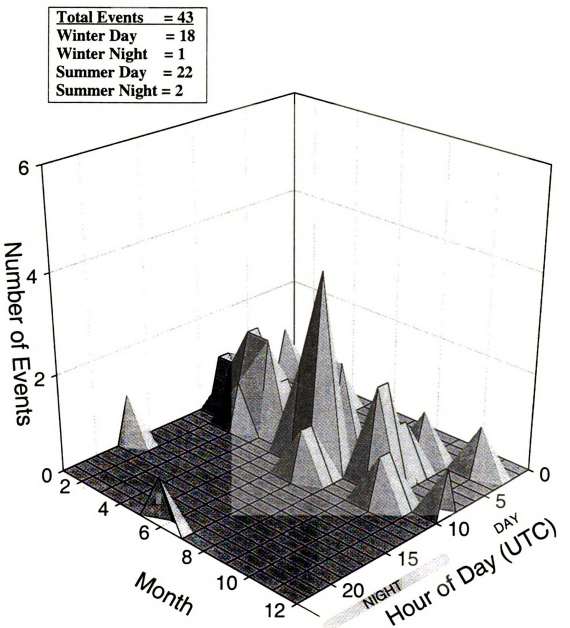

Figure 2-11. Temporal variation of reported seismicity in the Svobodniy region.

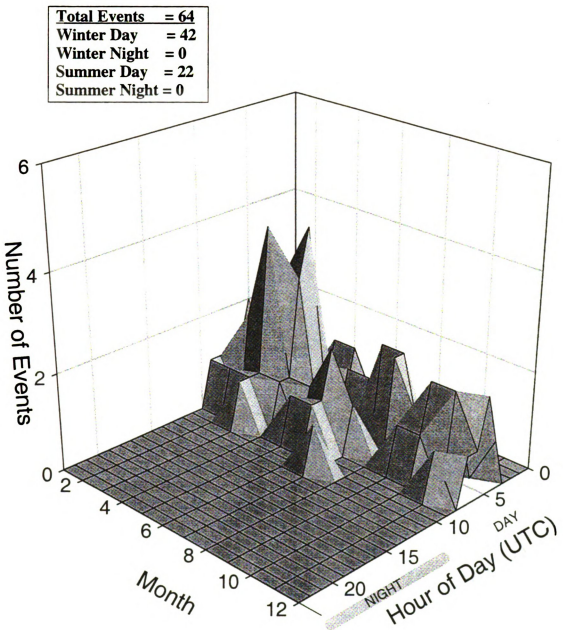

Figure 2-12. Temporal variation of reported seismicity in the Shimanovsk mining region.

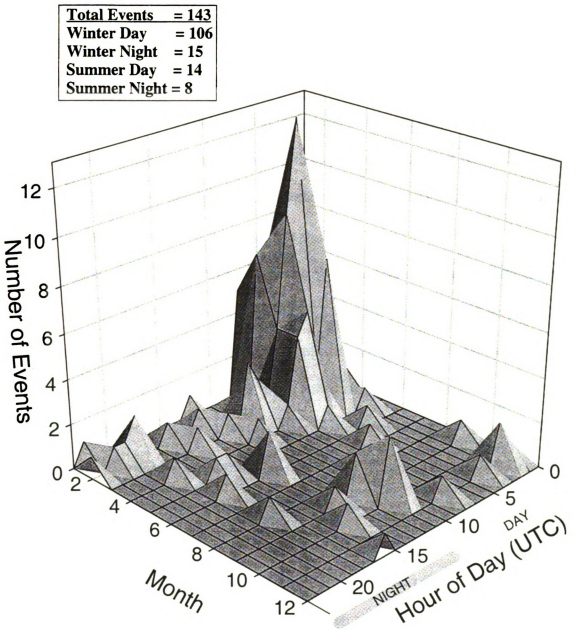

Figure 2-13. Temporal variation of reported seismicity in the Oktyabrskiy placer mining region.

Mining near Shimanovsk occurs approximately 40 km to the northeast of the town, along the west bank of the Zeya river. Events located in this region occur exclusively during daylight hours, but with a slight bias towards mid winter. For Oktyabrskiy, extensive placer mining has occurred in the vicinity of the town, primarily to the north, southeast, and along the Gar' River valley to the south. Analysis of origin times for the Oktyabrskiy mining region indicate that almost all blasting occurs during the winter "daytime". Each of the reported seismicity regions analyzed in Figures 2-6 through 2-13 appear as isolated or partially isolated discrete clusters or trends of events. Based on the strong biases of origin times, it is believed that essentially all reported earthquakes in these clusters are of anthropogenic origin due to mining.

To the northwest of Oktybrskiy is a seismicity cluster near the town of Taldan (Figure 2-14). Prior to 1981, a small number of earthquakes occurred in this region with no bias in origin times, indicating this cluster probably contains some natural seismicity. Beginning in 1981, the numbers of events rose drastically, and a strong "daytime" bias was introduced into the origin times. Although this is strongly suggestive of the commencement of mining operations, no mines are indicated on the available maps, which are dated 1986. Godzikovskaya (1995) reports two explosions as having occurred within the bounds of this cluster. The low level of natural seismicity appears also to have continued, with a magnitude 5.0 event occurring during the night of January 31, 1985. Explosion contamination due to dam construction in the Zeya basin region to the east (approximately 54° N x 127° E) has been noted and is discussed at length by Godzikovskaya (1995). Temporal analysis of the region around Ekimchan is also consistent with a mix of tectonic events and explosions (Figure 2-15). There are a total of 283 events in this region, with 92 occurring during the "nighttime". If we assume the number of "daytime" tectonic events is 92% of the "nighttime" level (85 events; percentage based on the temporal variation of

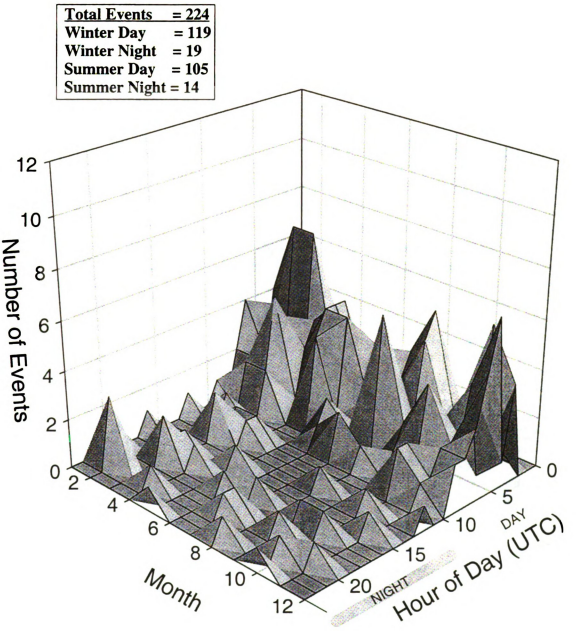

Figure 2-14. Temporal variation of reported seismicity in the Taldan region.

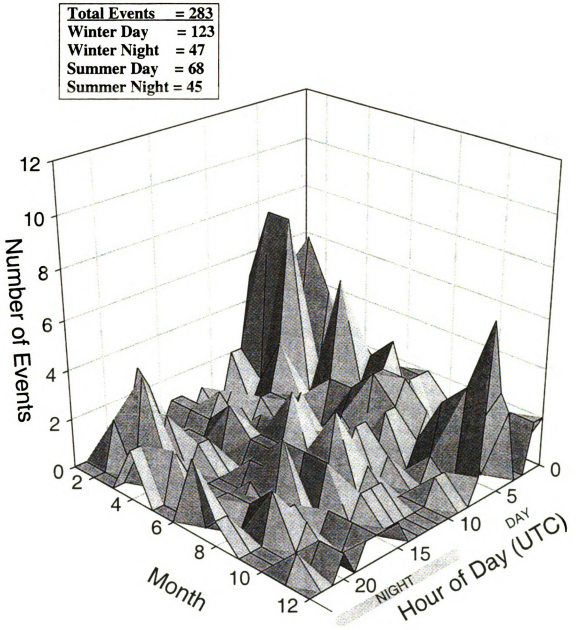

Figure 2-15. Temporal variation of reported seismicity in the Ekimchan mining region.

tectonic events discussed above), then the total number of tectonic events in this region is about 177. Therefore, the number of explosions is 106, representing a 37 % contamination of the database.

In the north-central portion of Figure 2-4, there is a northwest-southeast trend of predominantly "daytime" seismicity extending several hundred kilometers. The temporal distribution of these events is shown in Figures 2-16 for the central segment and 2-17 for the northern segment. This trend correlates with the route of the Baikal-Amur Mainline railroad (BAM). Explosions associated with its construction in the 1980's are listed as earthquakes in the seismicity catalogs. Note also that most events are located to the west of the track in the central portion, and to the north of the track in the northern portion, indicating systematic errors in the location procedure.

The region covered by Figure 2-18 is somewhat more problematic. This region probably does has tectonic earthquakes, as there are a reasonable number of "nighttime" events, but there is a clear bias towards "daytime" events. Here, there seem to be two possible explanations. A branch of the railway extends south from the town of Tynda. Construction along this segment of the railway may account for the "daytime" events. However, the Tynda region events are biased more towards early winter than those along the mainline railway, which tend more towards summer (Figures 2-16 and 2-17). This may suggest a mining origin as opposed to railroad construction, but maps do not show any apparent mining activities.

Overall, as explosion contamination appears to be primarily confined to daylight hours, "nighttime" seismicity should better reflect the natural tectonic distribution of earthquakes (Figure 2-5). If one compares "daytime" and "nighttime" seismicity, a different, more northerly trend appears in the plotted "nighttime" earthquake epicenters. This probably delineates an active

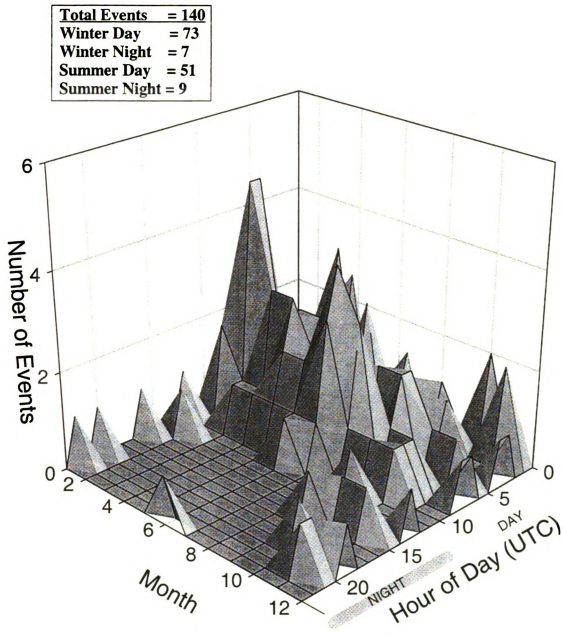

Figure 2-16. Temporal variation of reported seismicity along the central segment of the Baikal-Amur railway.

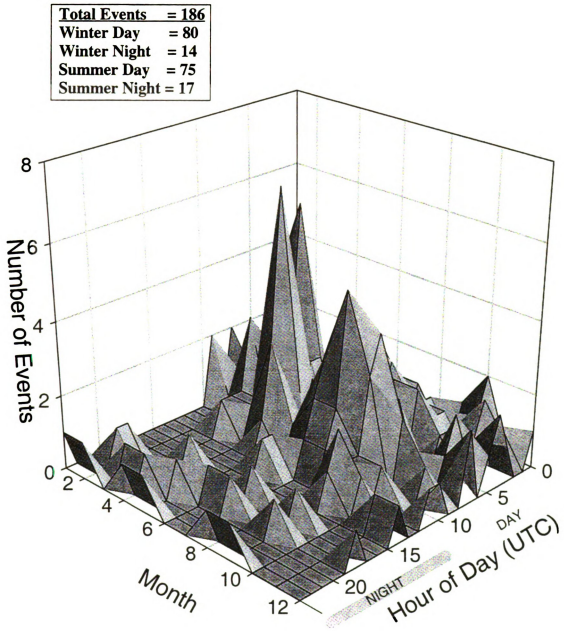

Figure 2-17. Temporal variation of reported seismicity along the northern segment of the Baikal-Amur railway.

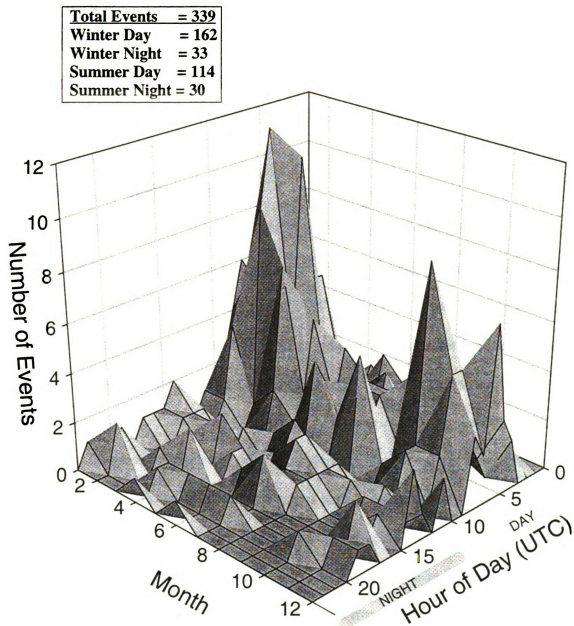

Figure 2-18. Temporal variation of reported seismicity in the Tynda region.

tectonic feature that was previously obscured by clusters and trends of explosions. When observing locations of the larger teleseismically located events, it is found that they fall almost entirely within the regions where seismicity occurs at night. Clusters and trends of primarily "daytime" occurring events have very few earthquakes of magnitude 4 or larger. In summary, for the Amur region it is clear that any future studies of seismicity or neotectonics must consider the extent of explosion contamination in the seismicity catalog.

2. Polyarnyi-Leningradsky-Plamennyi

Polyarnyi and Leningradsky are placer gold deposits located along the coast of the Chukchi Sea in Chukotka. Plamennyi was a mercury deposit about 100 km south of Polyarnyi which was mined from 1967 to 1972 (Pilyasov, 1993). From 1966 to 1982, most of the events located in this area were single station locations obtained by the three-component seismic station at Iul'tin (ILT; Figure 2-19). A clear bias towards winter and "daytime" is evident for the cluster of events in the mining region (Figure 2-20). The ILT data analyzed here also contains 15 events located by the Magadan Chukotka network in the 1980's which are also consistent with explosions both in origin time and location. Several of the located events near the Plamennyi mine occured after the 1972 close date of the mine. There are two possible explanations for this. First, the location accuracy of the ILT epicenters is on the order of 50 or 100 km, thus events from Polyarnyi or Leningradsky may be mislocated to the south. Second, the unpublished Magadan bulletin contains explosions as having originated at Plamennyi, suggesting on-going exploration work or a limited resumption of mining activities. Comparison of origin times of ILT located events with the more recent known explosions from the same mining region yields a nearly identical

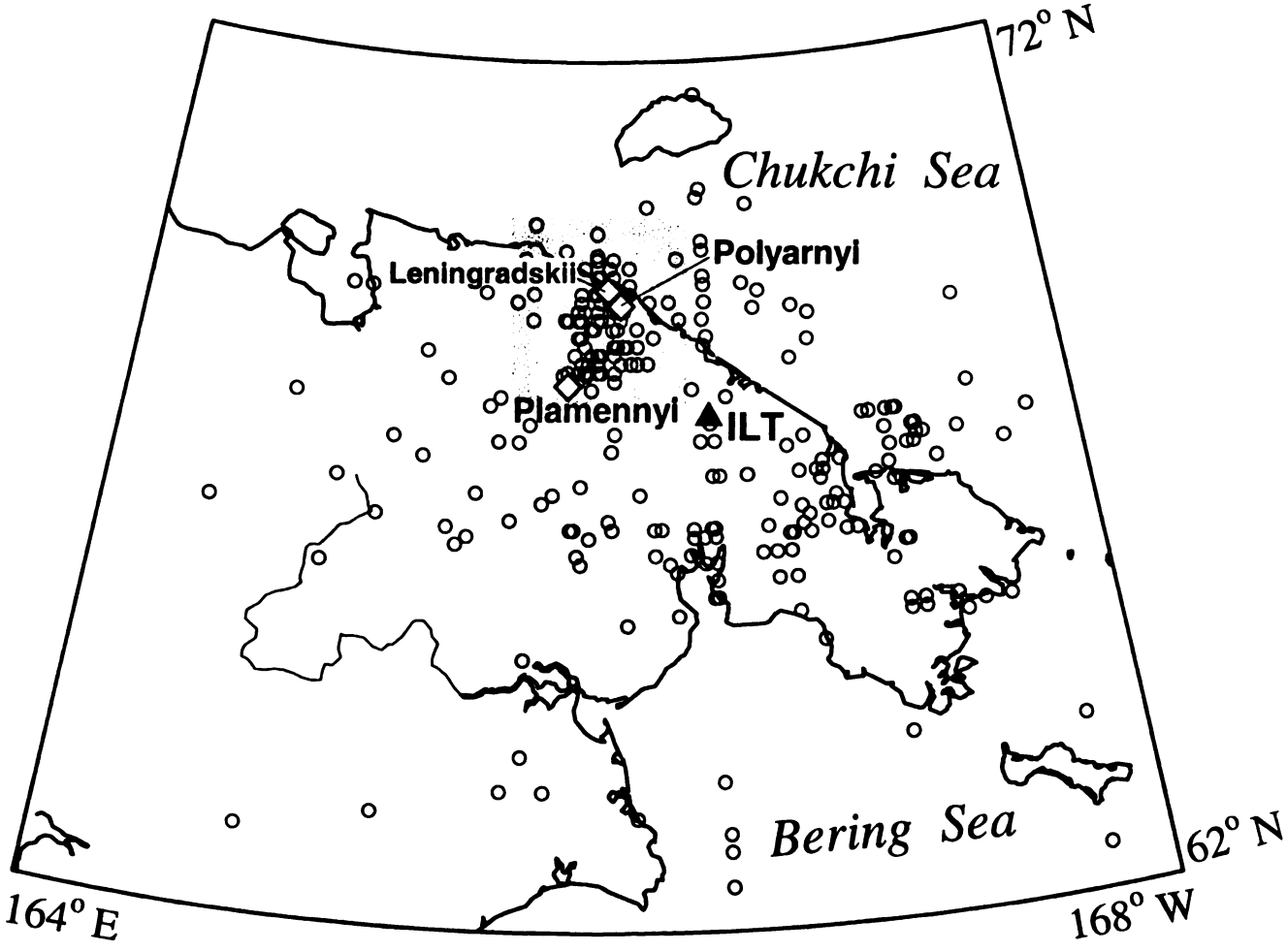

Figure 2-19. Iul'tin (ILT) seismicity with mine locations. Shaded area indicates region used in temporal analysis of event origin times.

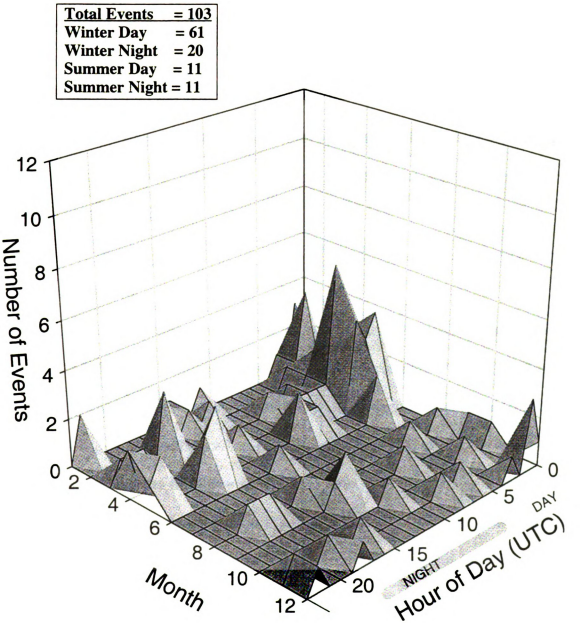

Figure 2-20. Temporal variation of reported seismicity in the Polyarnyi, Leningradsky, and Plamennyi mining region.

temporal distribution, with blasting primarily in the daylight hours of late winter and spring (Figure 2-21). Note also the low level of "nighttime" blasts. The complete lack of teleseismically recorded events around Polyarnyi-Leningradsky-Plamennyi as compared to the region a few hundred kilometers to the southeast is also consistent with explosions (Figure 1-26). Previous authors have attempted to use the explosions reported in tectonic models (Lander, 1996) and assessment of seismic risk (V. Kovalev, pers. comm.), both of which illustrate the magnitude of the contamination problem in the region. Other earthquakes located by ILT (Figure 2-19) do not show any temporal bias, thus probably generally represent tectonic events..

3. Kolyma Gold Belt

A cross of predominantly "daytime" seismicity lies along the Kolyma gold mining belt (Figure 2-2). Tectonically, this region is extremely complex in that it is located just south of the Ulakhan Fault system (Figure 2-22) along which motion occurs between the Okhotsk block and the North American plate (Imaev et al., 1994), thus statistical separation of anthropogenic sources from tectonic events is more difficult. Mining in this region is primarily placer gold but also includes coal and other minerals. "Daytime" and "nighttime" seismicity are shown in Figures 2-22 and 2-23 respectively. Temporal analysis of the large cluster of events in the area northwest of the town of Susuman indicates a bias towards local day and winter/spring (Figure 2-24). This bias is consistent with the distribution of known explosions from the Magadan Seismic Bulletin for the Susuman region (Figure 2-25). Based on the Day/Night seismicity plots in Figures 2-22 and 2-23, the eastern half of the seismicity cluster is entirely explosions, while the western half probably contains some tectonic events.

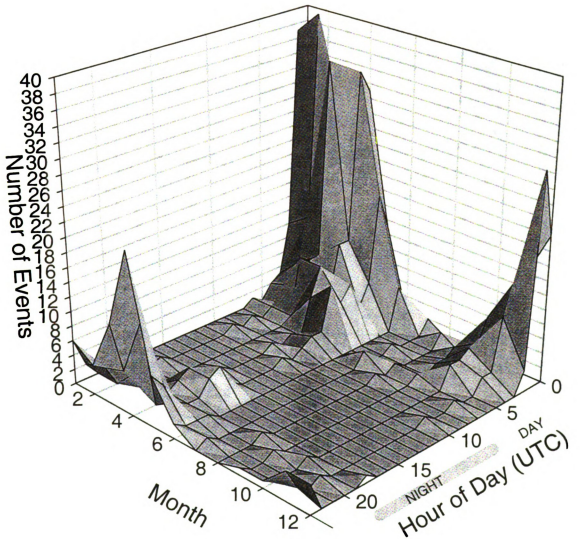

Figure 2-21. Temporal variation of explosions from the Polyarnyi, Leningradsky, and Plamennyi mining regions.

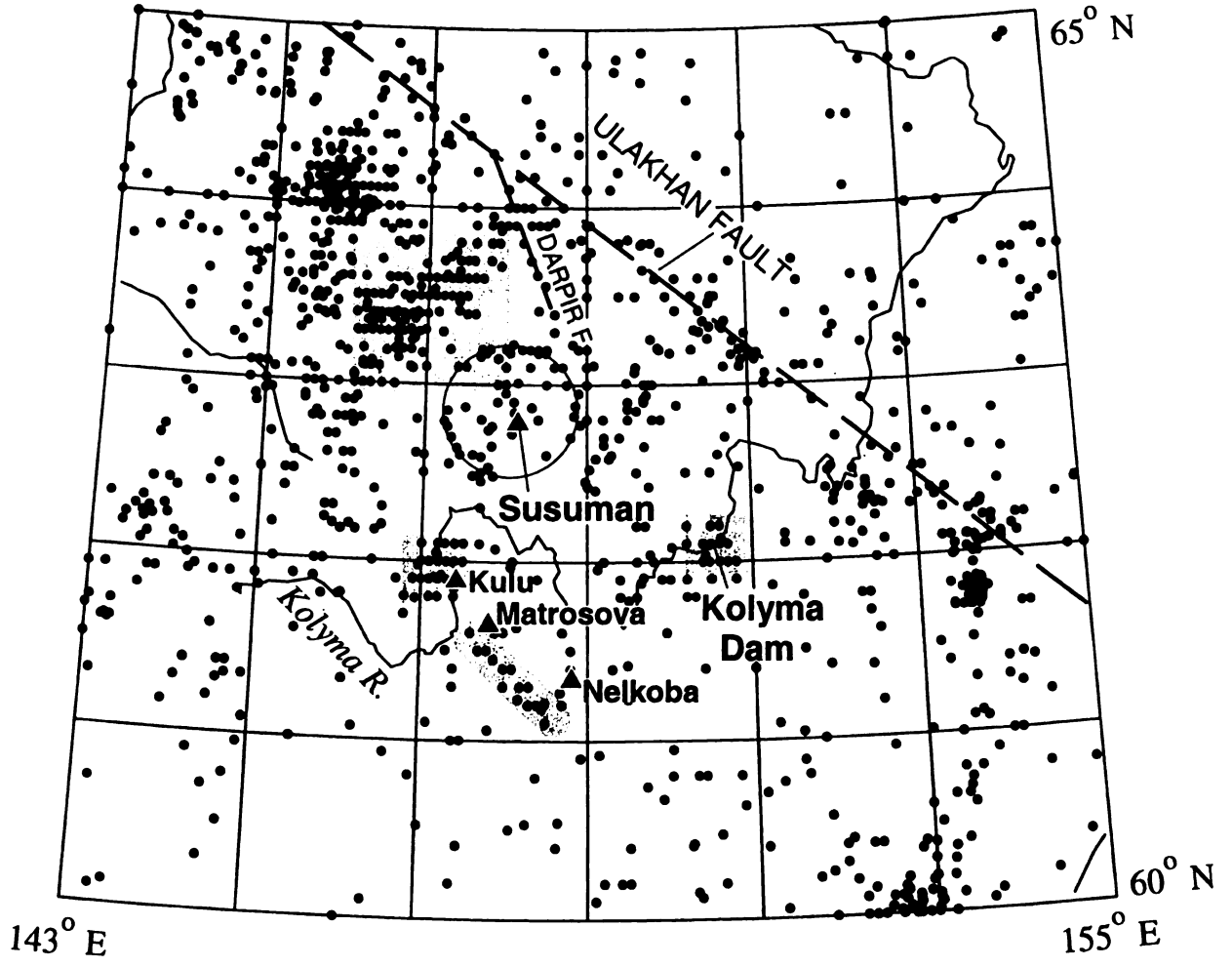

Figure 2-22. "Daytime" seismicity of the Kolyma gold belt. Shaded areas indicate regions used in temporal analysis of event origin times and other regions of explosion contamination. Note ring of seismicity around Susuman.

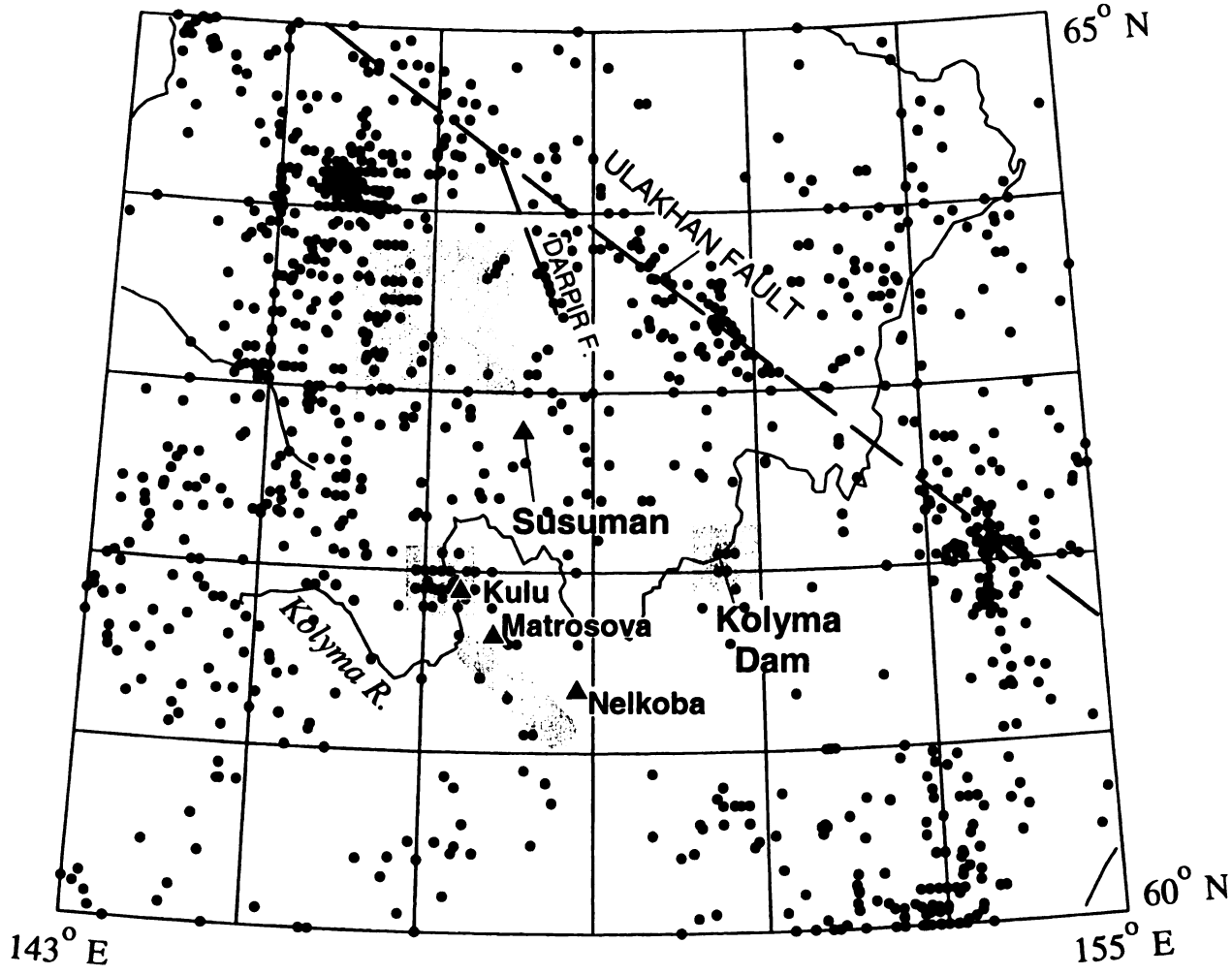

Figure 2-23. "Nighttime" seismicity of the Kolyma gold belt. Compare shaded regions to Figure 2-22.

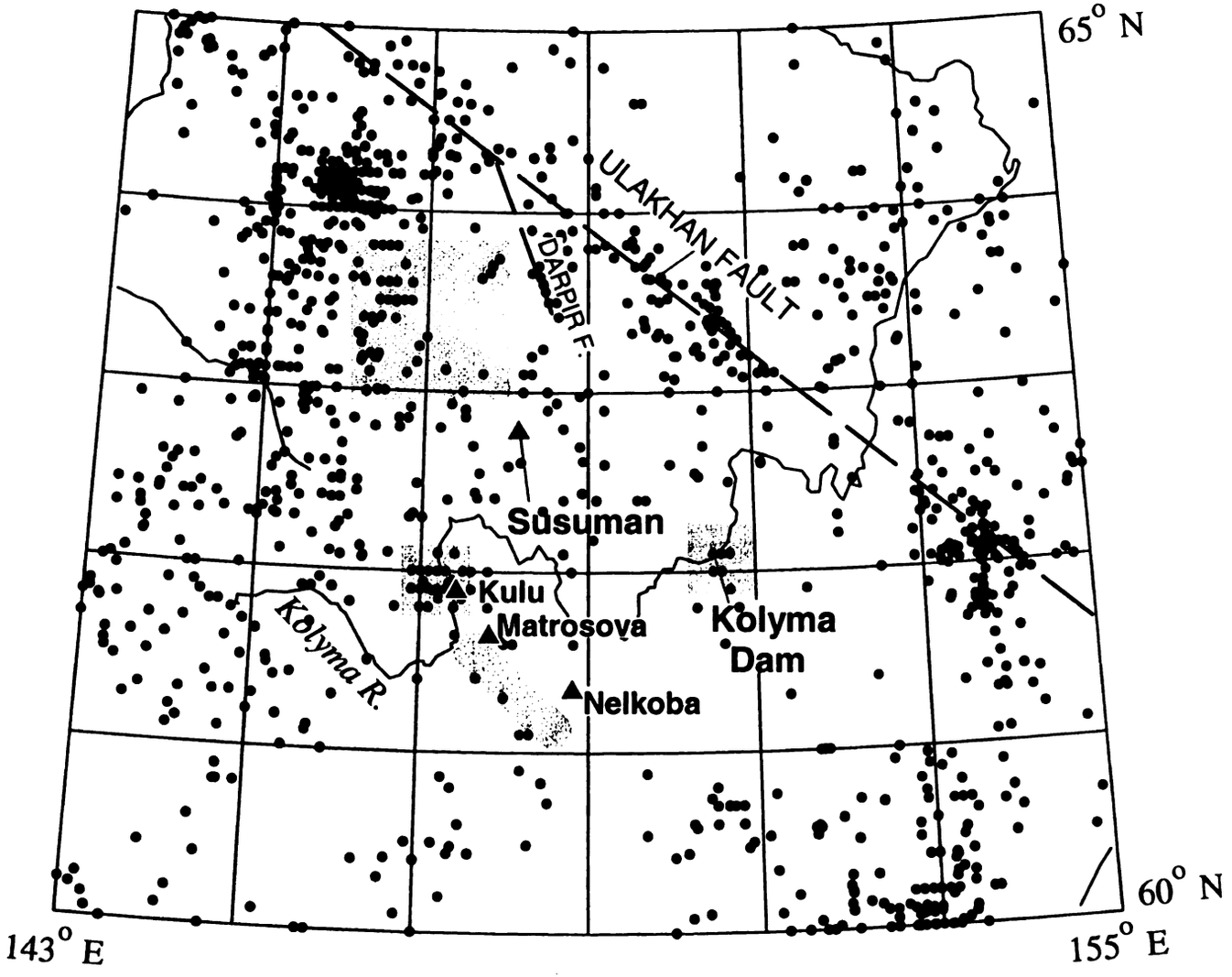

Figure 2-23. "Nighttime" seismicity of the Kolyma gold belt. Compare shaded regions to Figure 2-22.

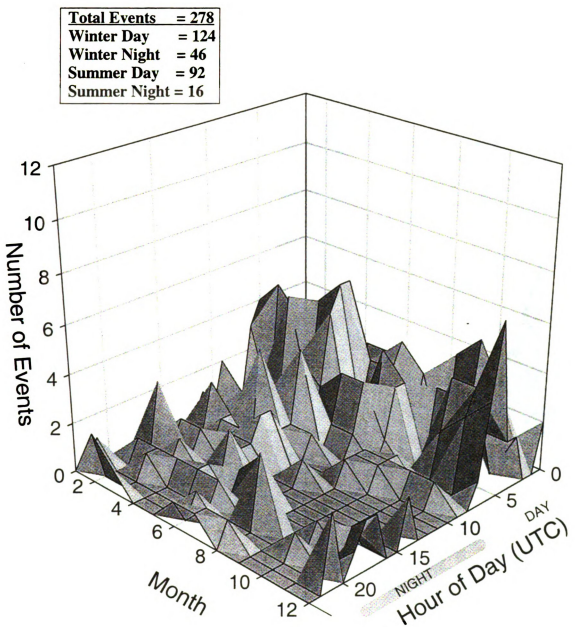

Figure 2-24. Temporal variation of reported seismicity in the region northwest of Susuman.

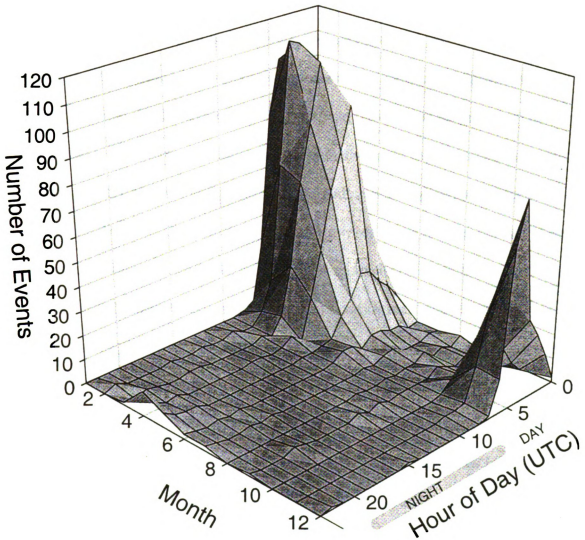

Figure 2-25. Temporal variation of explosions in the Susuman region.

Note also the increased numbers of "daytime" events within a 100 kilometer radius of Susuman, which is also probably a result of mining.

About 200 kilometers southeast of Susuman is the Kolyma hydroelectric station and dam. Blasting during construction of this dam resulted in contamination of the earthquake catalog (Godzikovskaya, 1995). Temporal analysis of explosions in the Kolyma dam region is shown in Figure 2-26. There are also highly elevated levels of "daytime" seismicity for approximately 100 km upriver from the dam, and a diffuse cluster of primarily "daytime" events approximately 120 km to the east. The cluster to the east is in the vicinity of the Ust' Srednikan dam project, where Godzikovskaya (1995) also notes explosion contamination.

One puzzling cluster of seismicity is associated with the region around the town of Kulu (Figures 2-22 and 2-23). This cluster is biased towards winter months, but only slightly towards daylight hours (Figure 2-27). However, this seismicity cluster is from events which occurred in the 1970's and 1980, with a few events occurring each year. In 1980, when the seismic station at Kulu opened, the earthquakes essentially stopped, with only a few events located since (See yearly plots in Appendix B). This would be consistent with explosions, as the local operator could distinguish the events as explosions and they would be removed from the catalog. For comparison, temporal analysis of known explosions from the Kulu region are shown (Figure 2-28). Explosions in the Kulu region are probably a result of mineral exploration studies. On site inspection of the Kulu region showed no evidence of mining. The closest mining noted was at Matrosova, about 40 km to the south (Figure 2-22). From Matrosova, there is a small lineation of "daytime" events extending about 70 km to the southeast (Figure 2-22). This trend parallels an extensive placer mining operation extending

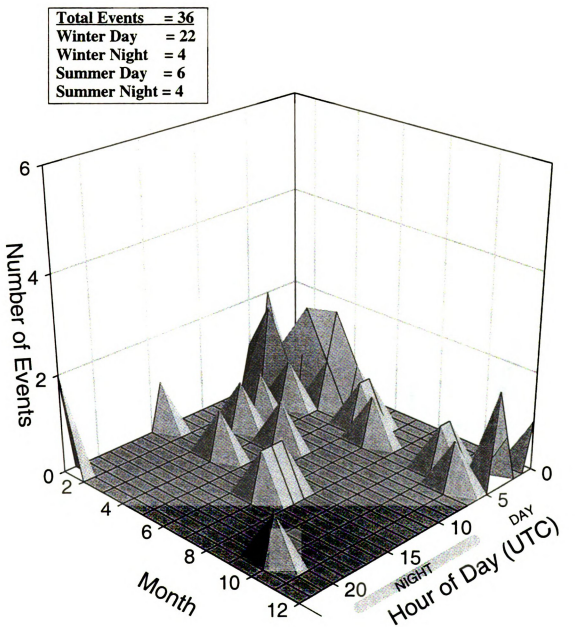

Figure 2-26. Temporal variation of seismicity from the region of the Kolyma dam.

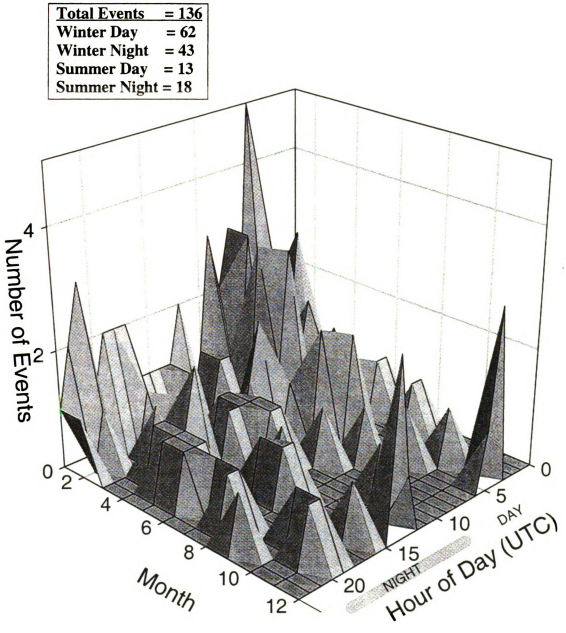

Figure 2-27. Temporal variation of reported seismicity in the Kulu region.

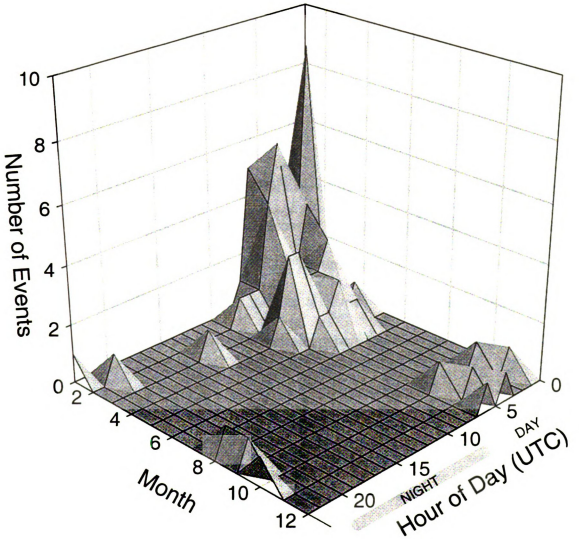

Figure 2-28. Temporal variation of explosions in the Kulu region.

from Matrosova to Nelkoba, which follows the main highway through the region. This may indicate a location bias for events in this region.

Explosion contamination of the seismicity catalog has clearly affected analysis of seismic hazards in the region. Vazhenin et al. (1997), citing T. A. Andreev, shows increased seismic hazards in the regions north of Susuman, around Kulu and the trend extending south, and near the Kolyma hyodoelectric station, all of which are a result of explosion contamination.

4. Ust' Nera

Placer gold deposits around Ust' Nera are on the northwest extension of the Kolyma gold belt. As indicated on Figure 2-2, seismicity reported in the vicinity of Ust' Nera is temporally biased towards "daytime", with 10 "daytime" events, versus 2 "nighttime" events, although statistics of small numbers may be a factor. The region immediately to the southeast of Ust' Nera is very active tectonically, where events of up to magnitude 7 have occurred.

5. Lazo

Lazo is a gold placer deposit between the Adycha and Nel'gese Rivers at 66.5° N, 137.0° E (Figure 2-2). "Daytime" and "nighttime" seismicity of Lazo and northern Yakutia are shown in Figures 2-29 and 2-30 respectively. The reported cluster of seismicity near Lazo is almost entirely confined to the "daytime" in the early part of the year, thus it is believed they are almost exclusively explosions (Figure 2-31). A similar looking cluster of seismicity about 100 km south of Lazo was also analyzed for temporal variation (Figure 2-

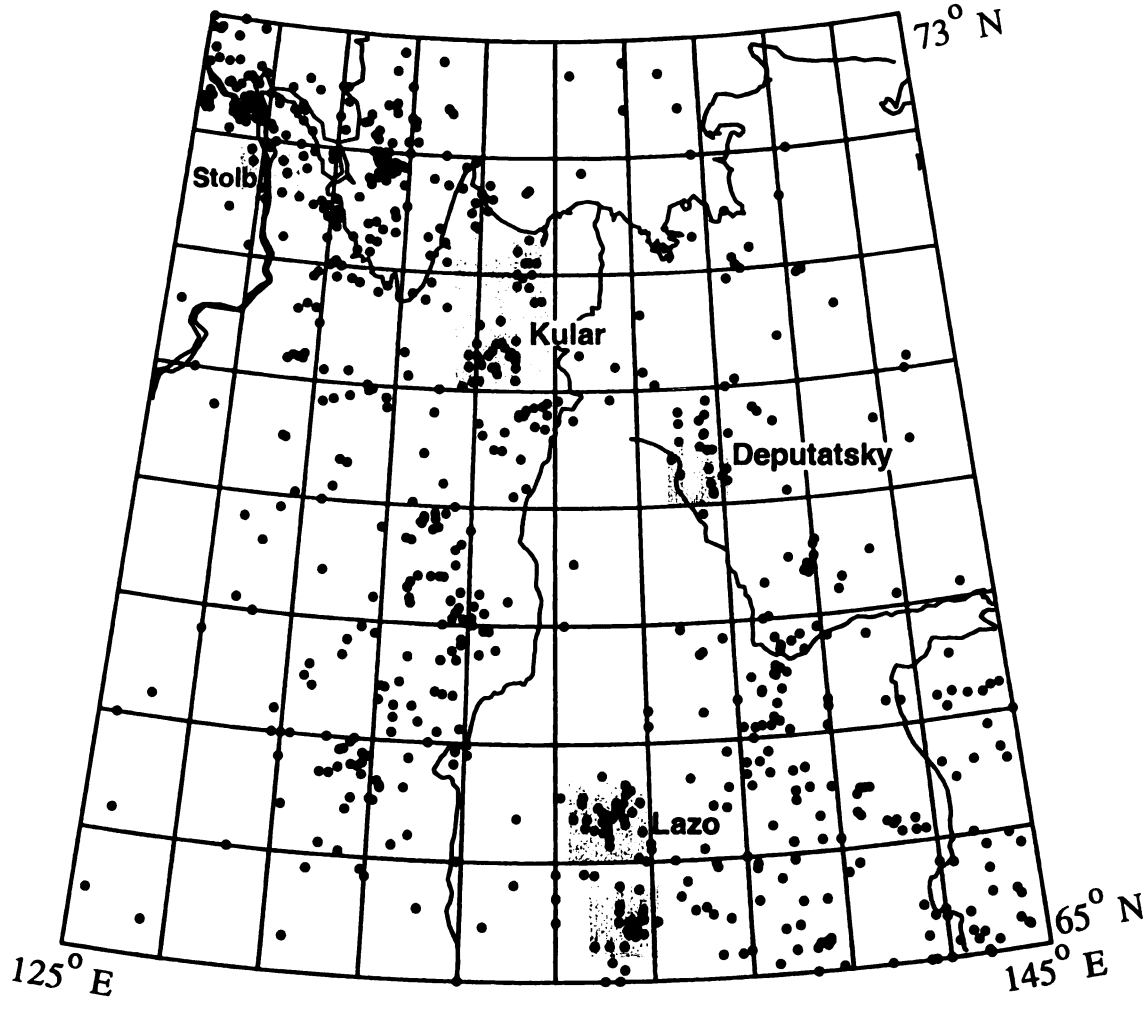

Figure 2-29. "Daytime" seismicity of northern Yakutia. Shaded areas indicate regions used in temporal analysis of event origin times.

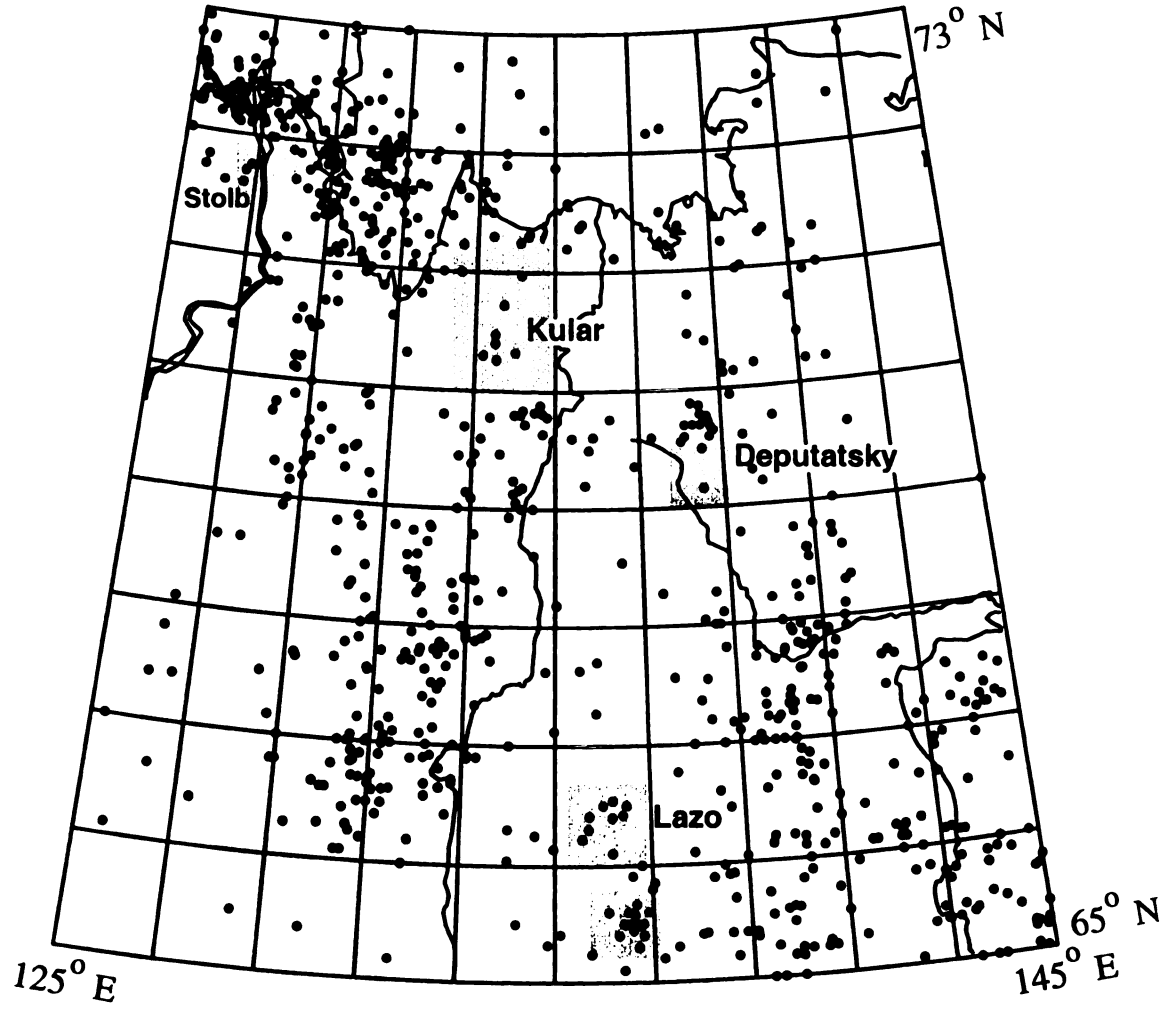

Figure 2-30. "Nighttime" seismicity of northern Yakutia. Shaded areas indicate regions used in temporal analysis of event origin times.

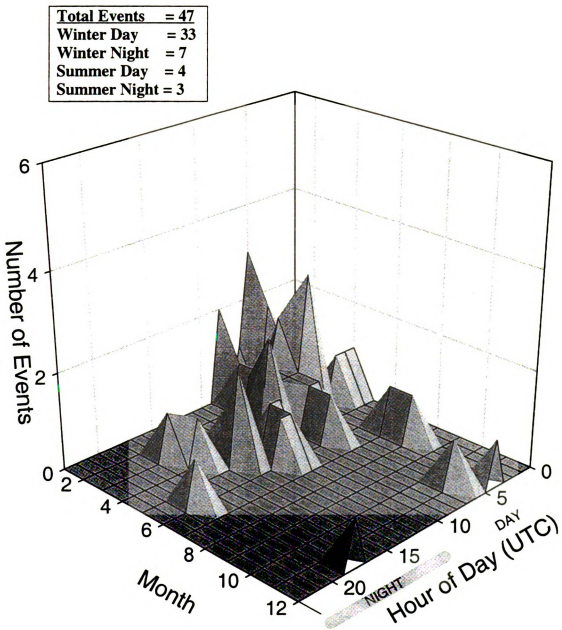

Figure 2-31. Temporal variation of reported seismicity in the Lazo mining region.

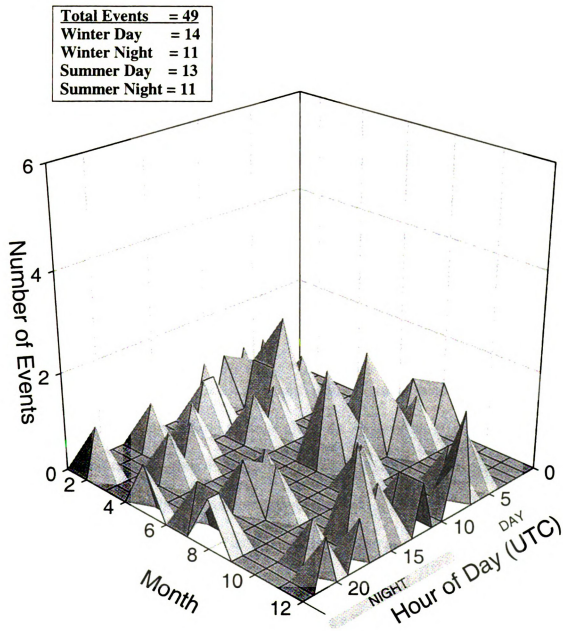

Figure 2-32. Temporal variation of reported seismicity in the cluster of epicenters south of the Lazo mining region.

32). This cluster of seismicity was suggested to be of mining origin (V. Imaev, pers. comm.), though the temporal variation is more consistent with tectonic activity.

6. Deputatsky

The Deputatsky tin mining region is completely biased to winter events, with 13 events reported during winter day and 2 events during winter night (Figure 2-33). There are no events reported in the summer months, which is a good indicator of an anthropogenic origin. However, caution must be taken as the number of events is small. Temporal analysis of an additional small cluster of seismicity immediately to the north is more consistent with tectonic events.

7. Kular

The region around Kular and to the north is an extensive placer gold mining region. Coal has also been mined southeast of Kular along the banks of the Yana River. The coal mining operations closed in the past few years but in the mid-1990's gold mining operations began south of Severnyi, about 25 km southeast of Kular (V. Imaev, pers. comm.). Reported seismicity in the Kular region forms an elongated north-south trend (Figure 2-29), which shows an excellent correlation with explosion locations (Figure 2-1). Temporal analysis of reported seismicity in the Kular region shows a strong bias to winter "daytime", which is consistent with explosion contamination from mining (Figure 2-34).

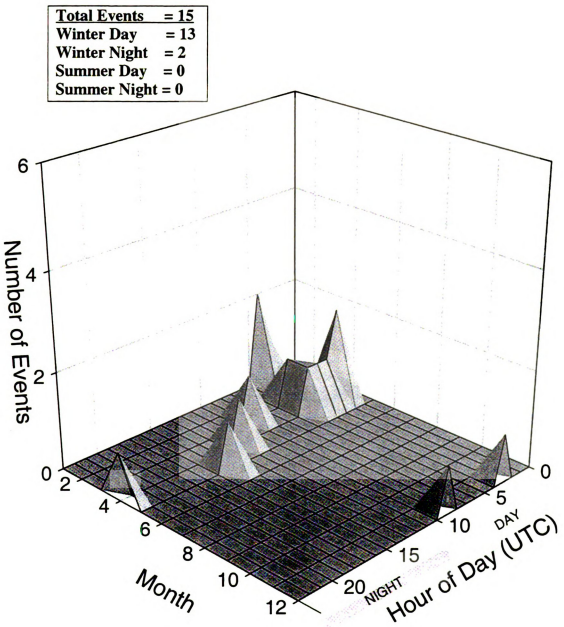

Figure 2-33. Temporal variation of reported seismicity in the Deputatsky mining region.

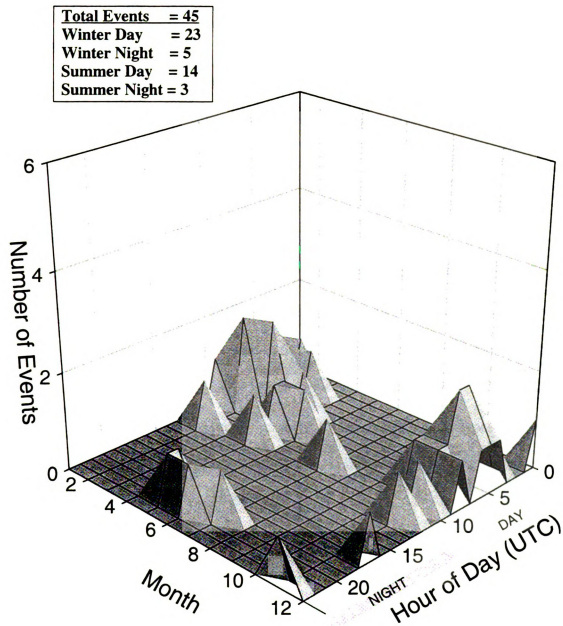

Figure 2-34. Temporal variation of reported seismicity in the Kular mining region.

8. Stolb

Reported seismicity in the Stolb region is probably contaminated by "daytime" explosions. From 1988 to present, the geological survey in Moscow has been conducting explosions in this region along the Lena River looking for placer deposits of diamonds (V. Imaev, pers. comm.). Although there are only 12 events that fall within this region, 9 occur during daylight hours, and 8 occur between 1989 and 1994, which is consistent with the exploration work (Figure 2-35).

9. Yugorenok

Yugorenok is a mining region along the Yudoma and Allakh-Yun rivers (V. Imaev, pers. comm.), which is geographically coincident with a discrete cluster of earthquake epicenters. Of the 25 earthquakes located in the vicinity, 20 occur during winter "daytime" hours (Figure 2-36). In addition, there are no large events associated with this cluster of seismicity. Two other small seismicity clusters to the north are both associated with teleseismic events and do not show any strong temporal biases in their origin times, which suggests tectonic origins.

10. South Yakutia

South Yakutia is similar to the Kolyma gold belt in that there are tectonic events occurring in the vicinity of mining regions. Several cells in this area show strong "daytime" biases, each of which is associated with mining. Figures 2-37 and 2-38 plot the "daytime" and "nighttime" seismicity of southern Yakutia. Three regions are of note in south Yakutia. Aldan is a mining region with extensive deposits of gold and phlogopite mica (Shabad,

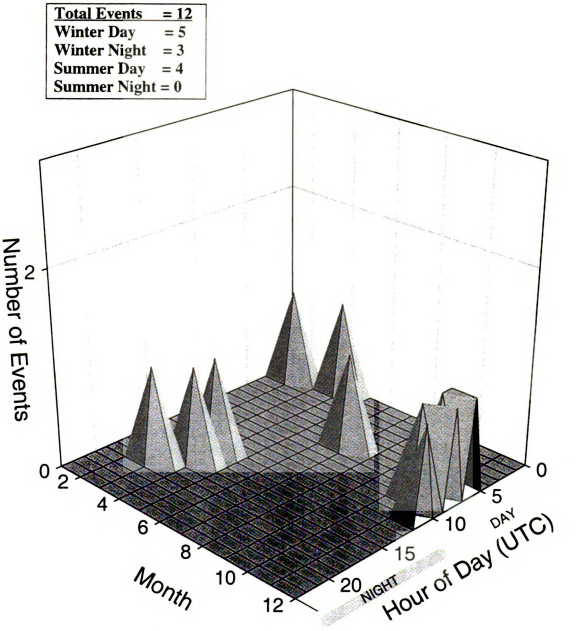

Figure 2-35. Temporal variation of reported seismicity in the Stolb region.

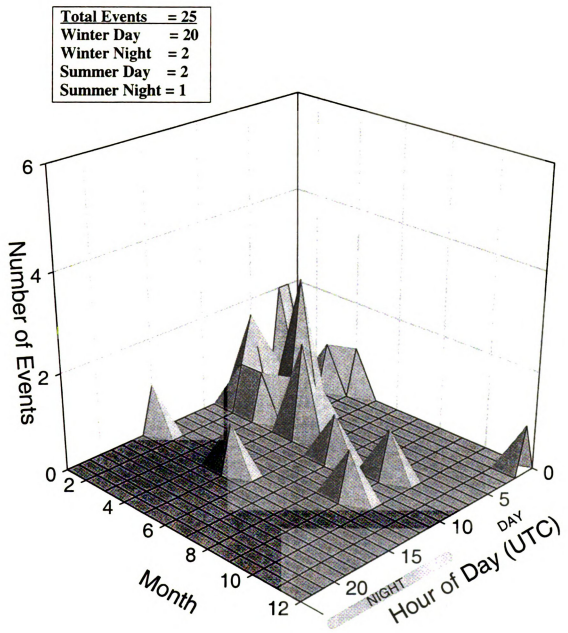

Figure 2-36. Temporal variation of reported seismicity in the Yugorenok nining region.

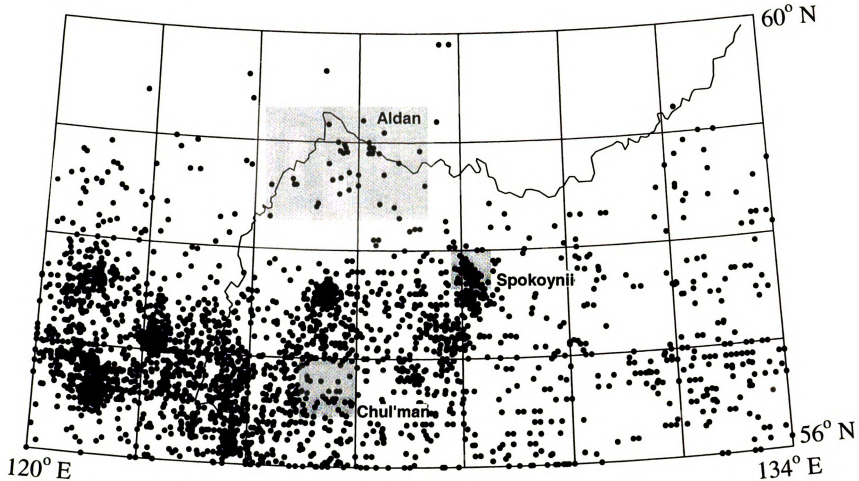

Figure 2-37. "Daytime" seismicity of southern Yakutia. Shaded areas indicate regions used in temporal analysis of event origin times.

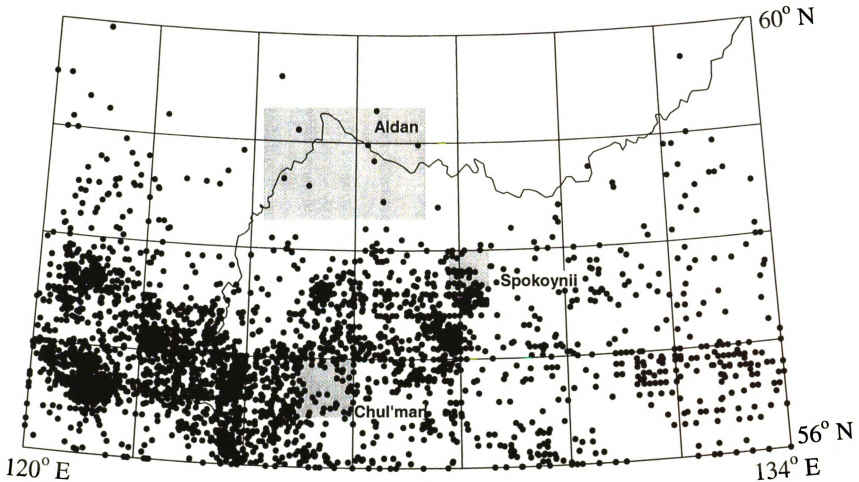

Figure 2-38. "Nighttime" seismicity of southern Yakutia. Shaded areas indicate regions used in temporal analysis of event origin times.

1969). The region is associated with a diffuse cluster of predominantly "daytime" seismicity (Figure 2-39). Although the seismicity occurs throughout the year, its concentration during daylight hours is more consistent with an anthropogenic source than tectonic. Explosions from the Aldan mining region are located and listed in the unpublished Yakutsk bulletin (Figure 2-1).

Approximately 200 km south of the Aldan mining region is an extensive coal mining region near Chul'man. The Chul'man mining region produces many explosions (Figure 2-1), some of which are located by the Yakutsk network and listed in the unpublished data. The seismic station at Chul'man seems able to identify and filter the explosions. A plot of the temporal distribution of reported earthquakes (Figure 2-40) shows a bias towards "nighttime" events similar to that found for the tectonic event test area and the 1989 South Yakutia earthquake aftershock sequence (Figures 2-3 and 2-6).

To the northeast of Chul'man is a dense cluster of seismicity near the settlement of Spokoyny (Figure 2-37). Temporal analysis of the cluster shows a strong bias towards winter "daytime" events, which would be consistent with placer mining (Figure 2-41). Soviet military 1:200,000 scale topographic maps (dated 1986) show extensive mine workings in the region, but list all settlements as uninhabited. This is inconsistent, as the events located here occur from the 1970's through the mid 1990's. The published literature makes no mention of any mining activity in this region, nor does the unpublished Yakutsk network bulletin locate anything identified as an explosion in the region. Overall, the nature of activity at this location remains unclear, but is suspect.

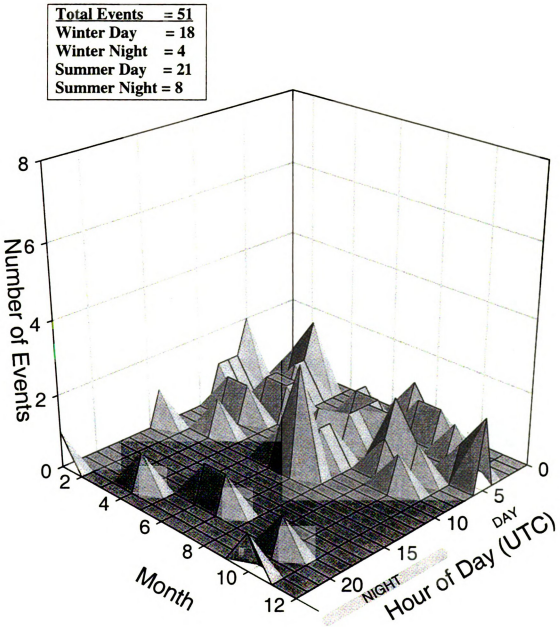

Figure 2-39. Temporal variation of reported seismicity in the Aldan mining region.

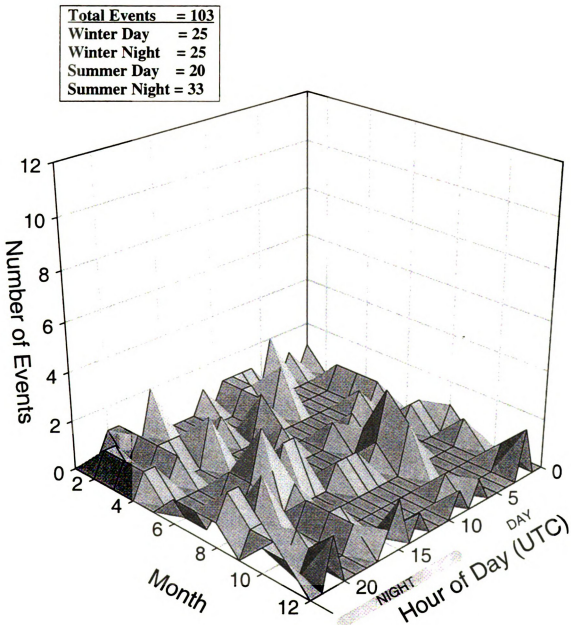

Figure 2-40. Temporal variation of reported seismicity in the Chulman mining region.

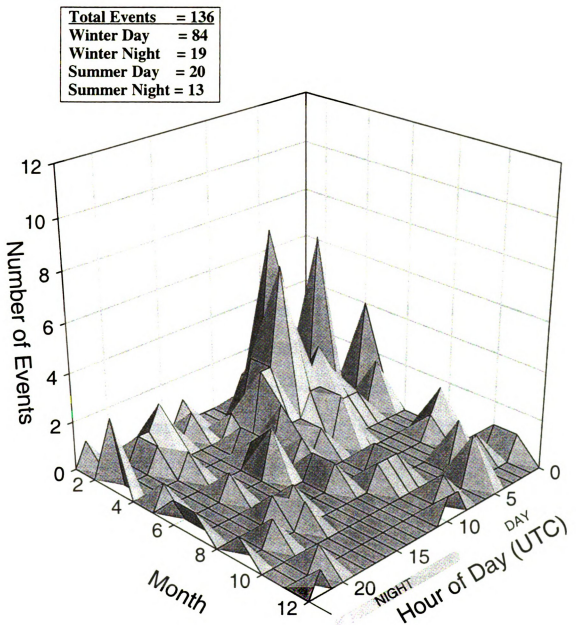

Figure 2-41. Temporal variation of reported seismicity in the Spokoynii mining region.

11. Red Dog

In compiling the continental seismicity database for northeast Russia, epicenters from the Western Alaska Network in the region of the Seward Peninsula, Alaska were included. In the northern portion of Alaska on Figure 2-2, there is one cell associated with seismicity predominantly in the summer and fall (Figure 2-42). This coincides with the location of the Red Dog mine in the western Brooks range. Exploration work prior to the opening of the mine was taking place when the Western Alaska Network was in operation, which probably recorded and located a limited number of blasts (D. Thurston, pers. comm).

INTERPRETATIVE RESULTS

Identification of the explosions and their removal from the northeast Russia seismicity catalog is essential in studying and understanding the tectonics and associated natural seismicity of the region. This is particularly evident in the Amur region. Active faults mapped in the Amur region are summarized in Figura et al. (1996). Mapped active faults are plotted with both day and night seismicity in Figures 2-43 and 2-44 respectively. Several things become evident regarding active seismicity along the mapped faults. Faults mapped in the southern portion of the Amur region (Bureya, Khingan, Tanlu, and smaller unnamed) appear to have some correlation with reported "daytime" seismicity, suggesting they are active. However, the correlation is actually with the mining contamination; little correlation exists between "nighttime" microseismicity and mapped faults. The southern termination of the Khingan fault appears to have some correlation with "nighttime" seismicity, although the seismicity here may be a continuation of the north-south trend roughly paralleling the 132° E longitude (Figure 2-44). The Bureya fault shows correlation

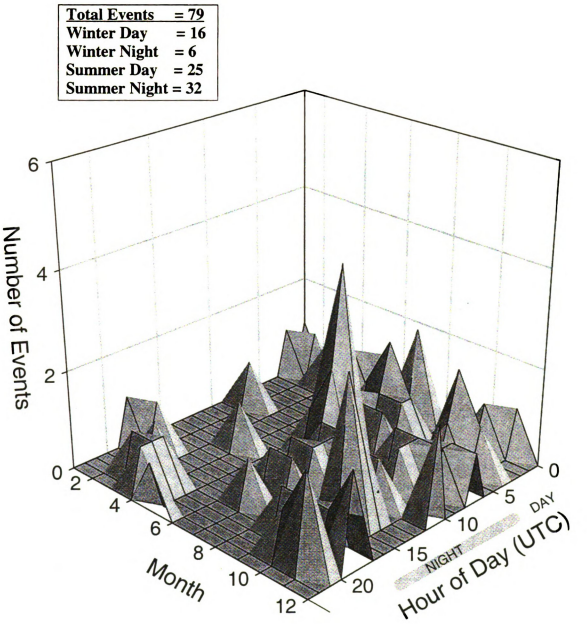

Figure 2-42. Temporal variation of reported seismicity in the Red Dog mining region.

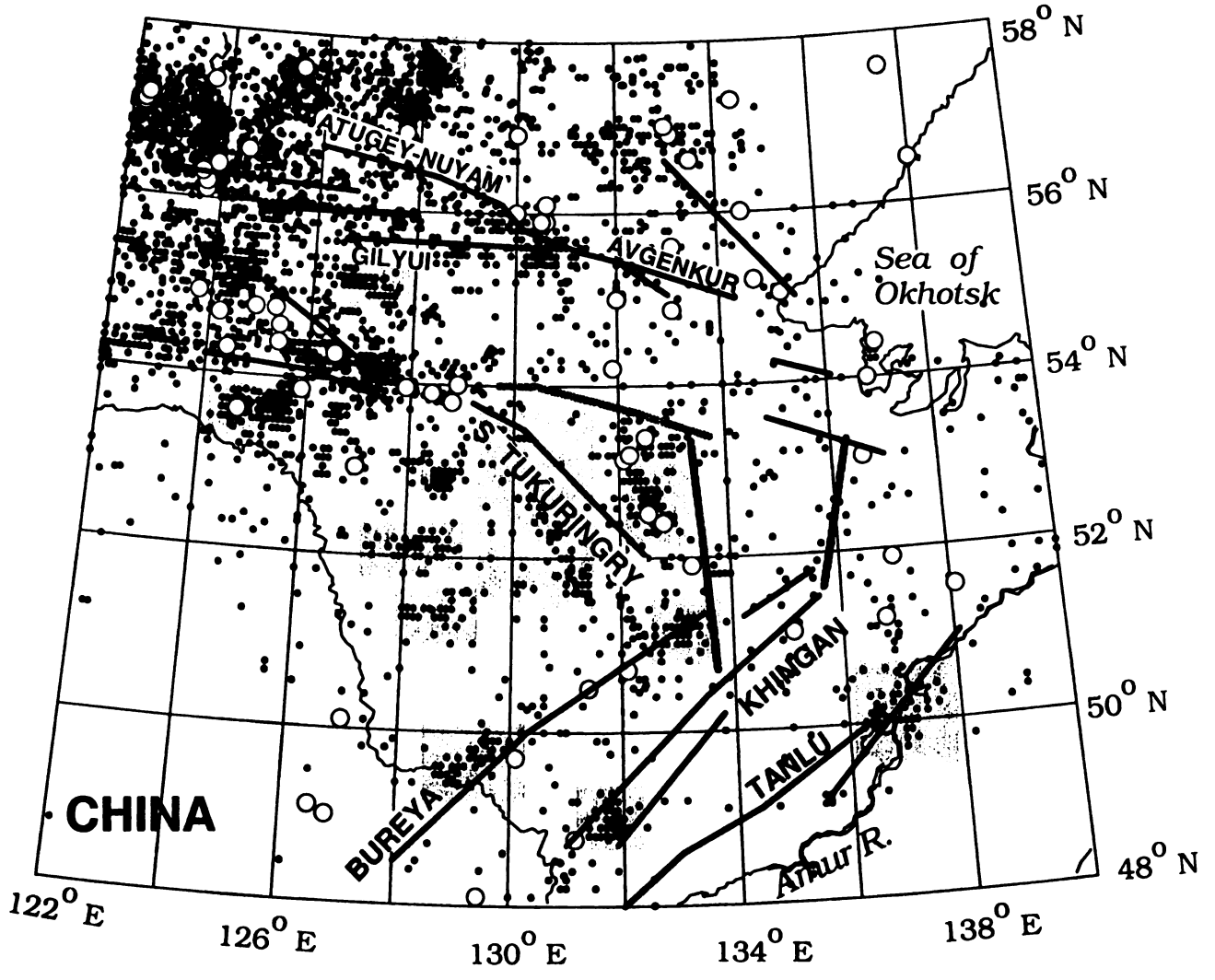

Figure 2-43. Daytime and teleseismic seismicity of the Amur region with mapped faults. Black lines indicate strike-slip faults and dark gray lines, thrust faults. Gray indicates regions of explosion contamination.

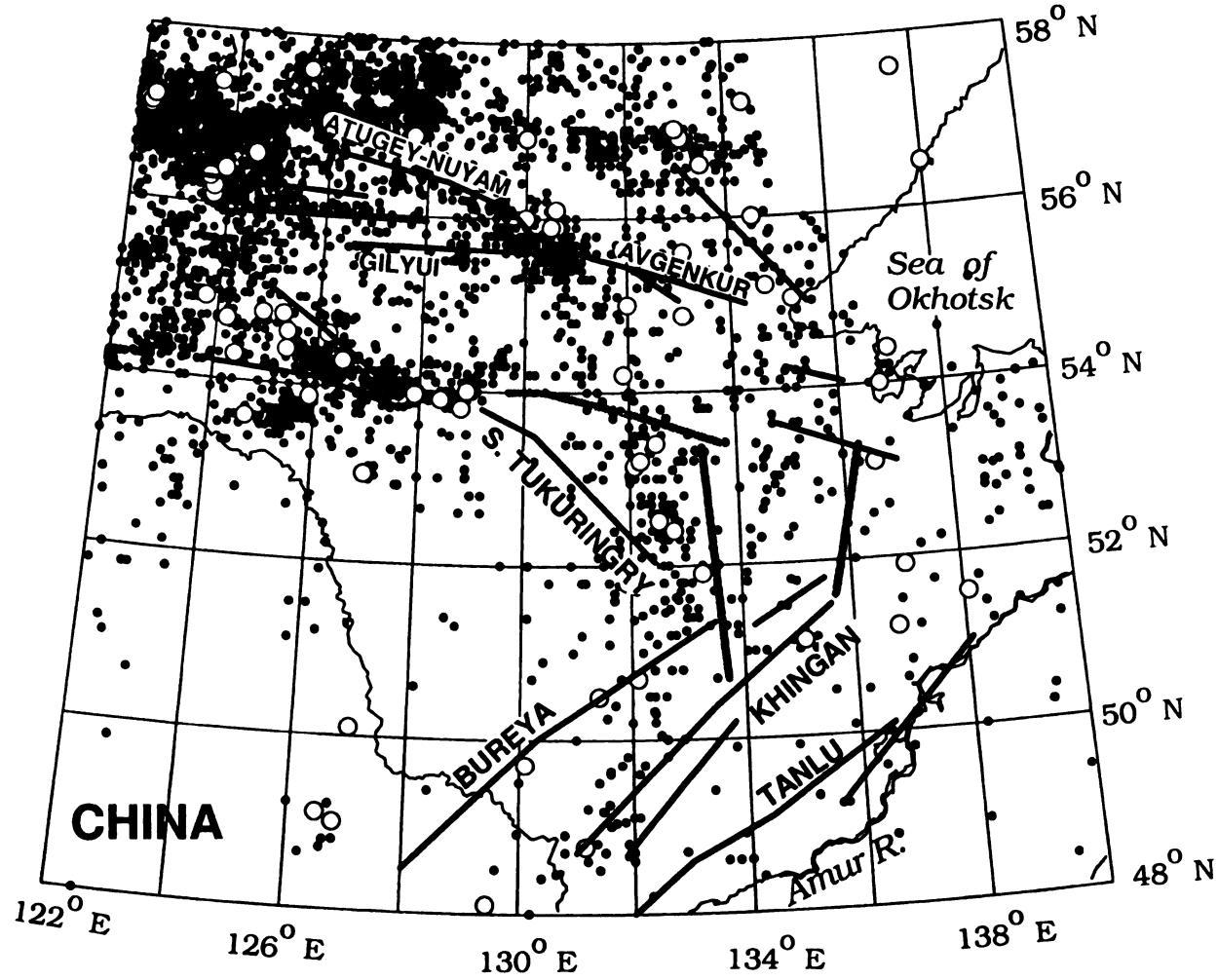

Figure 2-44. Nighttime and teleseismic seismicity of the Amur region with mapped faults. Black lines represent strike-slip faults and dark gray lines, thrust faults.

with three magnitude 4 events. The two eastern events may correlate with the N-S trend, while the western event could be a large explosion associated with the nearby mining. This western event was a "daytime" occurring magnitude 4.1 event, but is listed as such only in *Zemlet*, with no entry in the ISC Bulletin. In the central part of the Amur region, the South Tukuringry fault, as mapped, also shows no correlation with seismicity. However, an extension of the northern portion of the fault is co-linear with a well defined trend in the "nighttime" seismicity. Overall, mapped faults in the southern portion of the Amur region do not correlate with tectonic microseismicity and thus may not be active.

Faults mapped in the northern Amur region and southern Yakutia generally correlate with "nighttime" seismicity, consistent with tectonic activity. Clear seismicity trends are associated with the Atugey-Nuyam fault, various unnamed faults, and the intersection between the Atugey-Nuyam, Gilyui, and Avgenkur faults. Many of the faults mapped in this region show clear lineations on topographic maps and meteor satellite images. Given the distribution of seismicity in the region, it is clear that many additional active faults exist; lineaments associated with some of them are visible on Figure 2-45.

Focal mechanisms from the Amur region are found in Koz'min (1984), Parfenov et al. (1987), and the *Materialy* and *Zemlet* catalogs (Figure 2-45; Table 2-2). Focal mechanisms in the northern part of the Amur region are generally consistent with a left-lateral transpressional boundary. Focal mechanisms in the central Amur region are concentrated along the north-south seismicity trend between 132 and 133 degrees east. These mechanisms are predominantly northeast - southwest thrusting events, although individual mechanisms vary somewhat. In some cases, the orientations of the planes can be adjusted as they are constrained with little data. The north - south seismicity trend may therefore

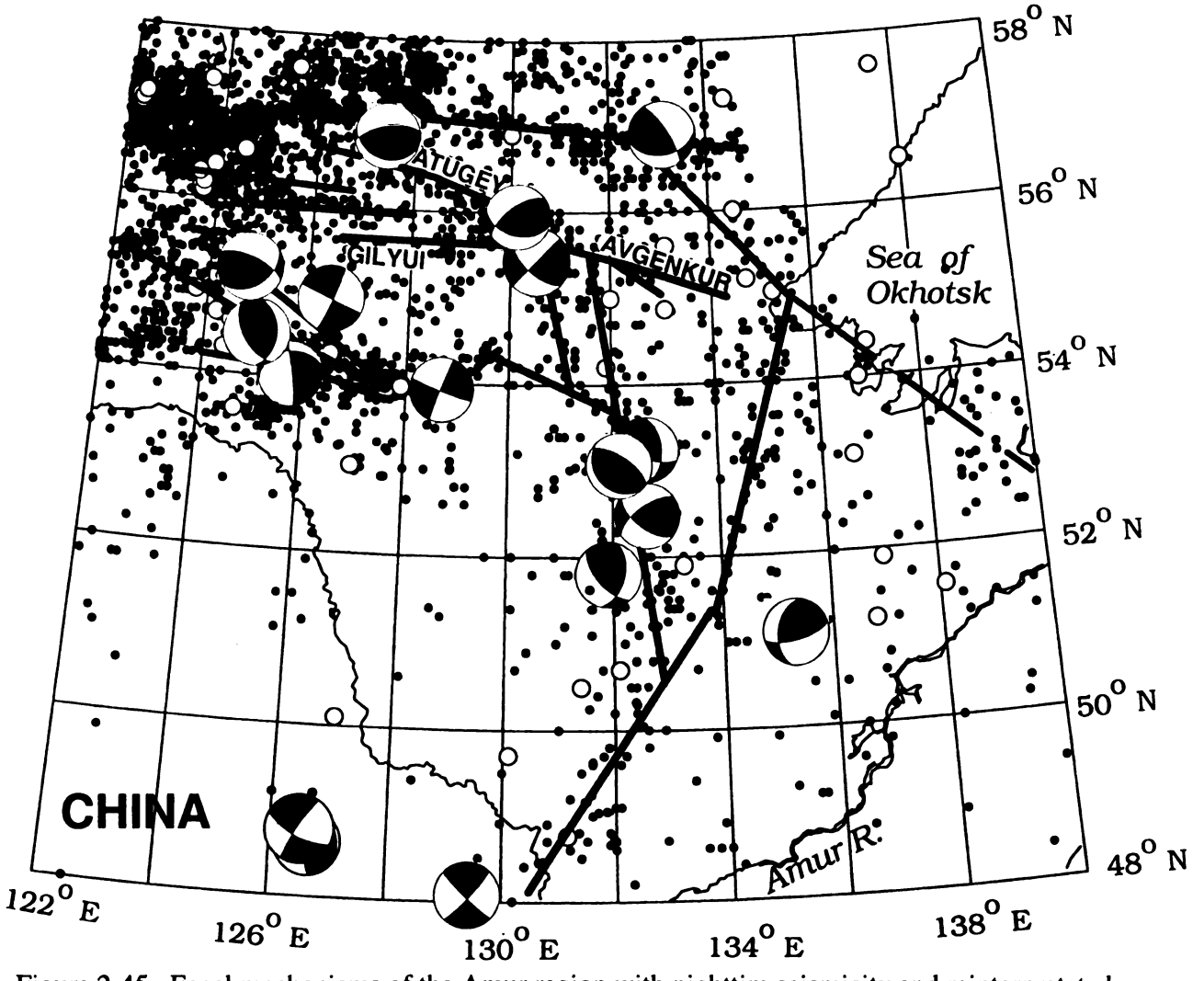

Figure 2-45. Focal mechanisms of the Amur region with nighttim seismicity and reinterpreteted faults based on seismicity trends.

Table 2-2. Focal mechanisms of the Amur region. Planes are given as Strike - Dip - Rake. References are: KOZ - Koz'min (1984), PAR - Parfenov et al. (1987), CHU - Chung et al. (1995), PDE - USGS Preliminary Determination of Epicenters, ZEM - *Zemlet*, and MAT - *Materialy*.

DATE	ORIGIN	LAT	LONG	MAG	PLANE1			PLANE2			REF
78 08 21	10 15 54.4	55.22	124.80	.	292	63	-	065	36	-	KOZ
89 07 23	12 01 30.0	54.50	125.05	4.7	006	32	118	154	62	74	ZEM
73 11 02	07 31 32.9	54.04	125.75	4.9	354	79	- -	248	35	- -	KOZ
86 08 15	20 20 34.4	48.93	126.45	5.2	116	63	- 12	212	79	-153	PDE
72 06 13	10 45 03.2	54.91	126.46	4.9	026	80	-	296	89	-	KOZ
86 02 28	17 07 24.4	48.64	126.66	4.9	179	84	97	309	9	41	ZEM
72 08 09	20 51 51.8	56.84	127.41	4.7	116	30	122	260	65	63	KOZ
77 08 16	13 56 59.8	53.93	128.7	4.2	022	90	-	112	86	-	PAR
79 04 27	19 38 18.	55.94	130.17	4.6	234	63	59	106	41	134	KOZ
77 11 01	03 54 26.	55.41	130.52	4.5	225	90	152	135	62	180	KOZ
63 06 21	13 44 20.	47.91	130.61	5.3	134	85	8	043	82	174	CHU
82 03 10	20 33 .	51.80	131.90	.	015	48	137	138	60	52	ZEM
75 06 29	12 24 43.3	53.07	132.11	4.8	304	66	-	134	24	-	KOZ
87 03 05	20 39 22.7	52.48	132.64	4.9	127	58	148	235	64	36	MAT
83 07 30	15 42 12.	53.24	132.64	4.9	107	68	44	357	50	150	ZEM
71 04 09	11 02 49.	56.9	133.1	4.4	327	76	128	075	39	22	KOZ
70 08 29	14 59 23.9	51.08	135.30	5.4	072	70	-	188	40	-	KOZ

represent a thrust boundary, and the main active tectonic feature in southern and central Amur. There are also a few mechanisms in China near southern Amur. One of these strike-slip mechanisms falls near the extension of the north-south trend through Amur, indicating right-lateral motion.

The north-south trend mapped here may be the active extension of the right-lateral Tanlu fault in eastern China. From eastern China, the mapped active segment of Tanlu fault crosses the Russian border near 48° N x 131° E (Huang et al., 1996), correlating almost exactly with the trend visible in the Amur region. The traditional location of the Tanlu fault in Russia is usually further to the east, along the Amur River valley, which is not supported by the seismicity evidence (Figures 2-43 and 2-44). It is suggested here that the right-lateral Tanlu fault of eastern China has an active extension into the Amur region of Russia. In the Amur region, the strike of the fault gradually changes from northeast-southwest in the south to slightly northwest-southeast further north. As the strike of the fault changes, motion changes from right-lateral strike-slip to northeast-southwest directed thrusting, which is consistent with focal mechanisms for the region (Figure 2-45).

CONCLUSION

Based on a very simplistic temporal analysis, it is evident that the seismicity catalog of northeast Siberia is heavily contaminated with industrial explosions. Overall, it appears that the majority of contamination in the seismicity catalog results from "daytime" mine blasts. As a first step in removing contamination, a map of only "nighttime" events (Figure 2-46) provides a better idea of the level and distribution of natural background

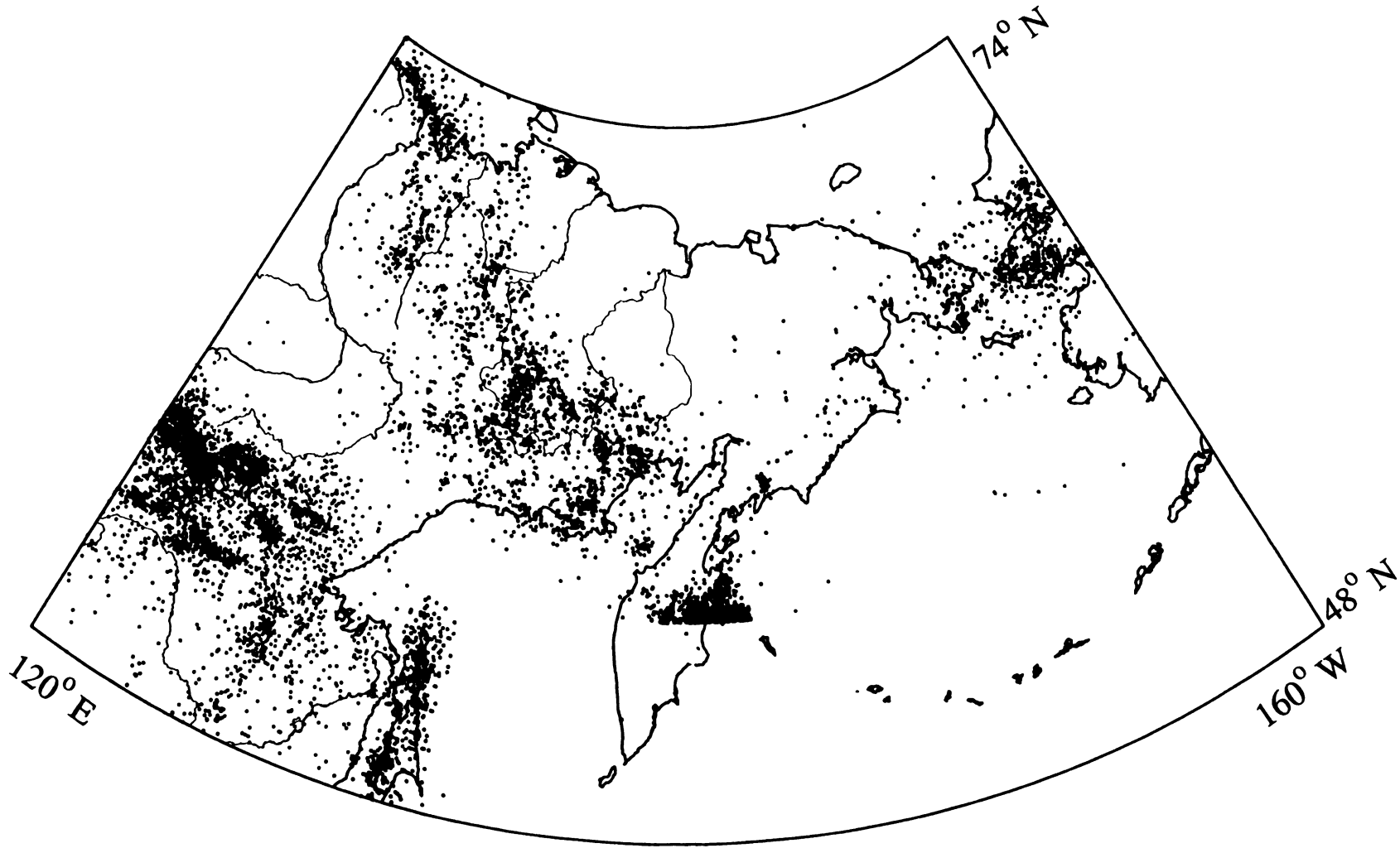

Figure 2-46. "Nighttime" seismicity of northeastern Russia.

microseismicity in the region. In northeastern Russia, "nighttime" seismicity plots are better for identification of active tectonics and faulting.

REFERENCES

Agnew, D.C., 1990, The use of time-of-day seismicity maps for earthquake/explosion discrimination by local networks, with an application to the seismicity of San Diego county, *Bulletin of the Seismological Society of America,* v. 80, p. 747-750.

Chung, W.-Y, Wei, B.-Z, and Brantley, B.J., 1995, Faulting mechanisms of the Liyang, China, earthquakes of 1974 and 1979 from regional and teleseismic waveforms - evidence of tectonic inversion under a fault-bounded basin: *Bulletin of the Seismological Society of America*, v. 85, p. 560-570.

Godzikovskaya, A.A., 1995, *Local explosions and earthquakes*: Rossiskoe Aksionernoe Obshchestvo Energy and Electrification "EES Rossii", Moscow, p. 55-66 (In Russian).

Figura, P., Faust, T., Fujita, K., and Koz'min, B.M., 1996, Seismotectonics of the Amur Region, Eastern Russia.: *Transactions, American Geophysical Union (EOS)*, 1996 Fall Meeting, v. 77, # 46, Supplement, p. 521.

Huang, W., Gao, W., and Ding, G., 1996, Neogene volcanism and Holocene earthquakes in the Tanlu fault zone, eastern China: *Tectonophysics*, v. 260, p. 259-270.

Imaev, V.S., Imaeva, L.P., Koz'min, B.M., and Fudzhita, K, 1994, Active faults and modern geodynamics of the Yakutia seismic belts: *Geotektonika*, p. 59-71 (in Russian).

Lander, A.V., Bukchin, B.G., Droznin, D.V., and Kiryushin, A.V., 1996, The tectonic environment and source parameters of the Khailino, Koryakia earthquake of March 8, 1991: Does a Beringia plate exist?: *Computational Seismology and Geodynamics*, v. 3, p. 80-96.

Koz'min, B.M., 1984, *Seismic belts of Yakutia and the focal mechanisms of their earthquakes*: Moskva, Nauka, 126 p. (in Russian).

Materialy po Seismichnost' Sibiri, 1970-1990: Academy of Sciences of the USSR, Siberian Branch, Irkutsk (bi-monthly, in Russian).

Odinets, M.G., 1996, The problem of polluting the earthquake catalog with industrial blasts in northeastern Russia, *in* Lin'kova, T. I., and Bobrobnikov, V. A., eds., *Geophysical Models of Geologic Processes in Northeast Russia*: NEISRI, Magadan, p. 90-99 (in Russian).

Parfenov, L.M., Koz'min, B.M., Imaev, V.S., and Savostin, L.A., 1987, The tectonic character of the Olekma-Stanovoy seismic zone: *Geotectonics*, 21 (6), p. 560-572.

Pilyasov, A. N., 1993, Regularities in the mining-industrial mastery of northeast Russia: *Kolyma*, 1993 (8), p. 5-12 (in Russian).

Riegel, S.A., 1994, *Seismotectonics of northeast Russia and the Okhotsk plate*: M.S. Thesis, Michigan State University, East Lansing, ix + 70 pp.

Shabad, T., 1969, *Basic industrial resources of the USSR*: Columbia University Press, New York, 393 pp.

Vazhenin, B.P., Mishin, S.V., Sharafudinova, L.V., 1997, Earthquakes in the Magadan Region: NEISRI, Magadan, 44 pp.

Zemletryaseniya v SSSR, for 1963-1989: Nauka, Moscow (annual, in Russian).

Zemletryaseniya v SSSR, for 1990-1991: Russian Academy of Sciences, Moscow (annual, in Russian).

Zemletryaseniya Severnoi Evrazii, 1992: Geoinformmark, Moscow (in Russian).

CHAPTER 3

Relocations of Northeast Russia Earthquakes

INTRODUCTION

The quality of hypocenter locations is of utmost importance when earthquake data are used in seismicity distribution studies as well as in developing better velocity or tomographic models. Of course, high quality locations depend on using the correct travel time curves in the location procedure. The existing database contains several thousand events that have been located by several seismic networks, each employing different location methodology, travel time curves, and phase data. Hypocenter determinations throughout the study area can be improved by using a single methodology, calibrated travel time curves, and combined phase data from adjoining networks. Location procedures used in individual networks are discussed in Chapter 1. In this chapter, the larger events in the study area will be relocated in conjunction with developing best-fit crustal travel time curves.

PREVIOUS WORK

In effort to gain a better understanding of the Russian computed locations, travel time curves based on the original epicenter and origin times are plotted. Figures 3-1 through 3-4 show travel time curves for Pn, Pg, Sn, and Sg phases respectively. Note significant scatter as well as trends of misassociated phases. The misassociated phases are most evident on Figure 3-3 where many Sg arrivals are cataloged as Sn arrivals. On the Sg travel time curve (Figure 3-4) there are parallel trends of arrivals. These are a result of the minute of the arrival times either recorded or typed incorrectly, as they delineate multiples of 60 second

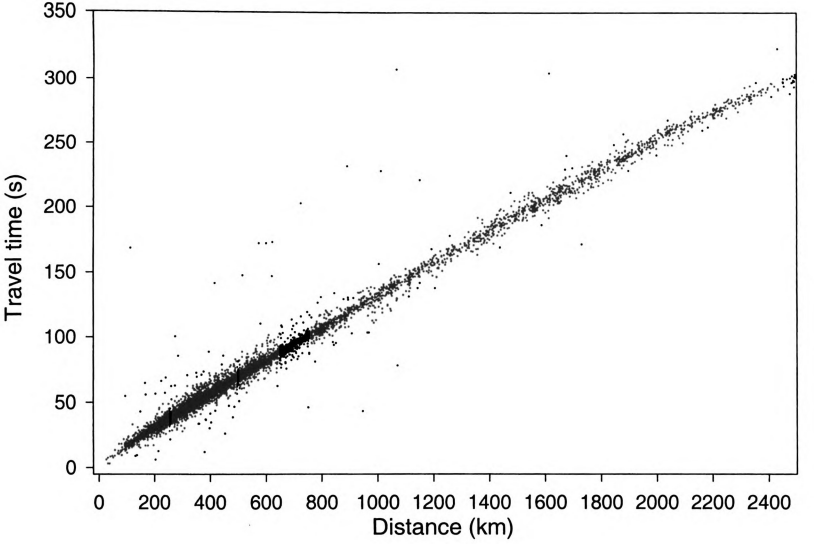

Figure 3-1. Pn phase arrival travel time curve for northeastern Russia. Russian reported hypocenters and origin times were used. The plot contains 9,342 arrivals. Data shown is only from northeastern Russia stations.

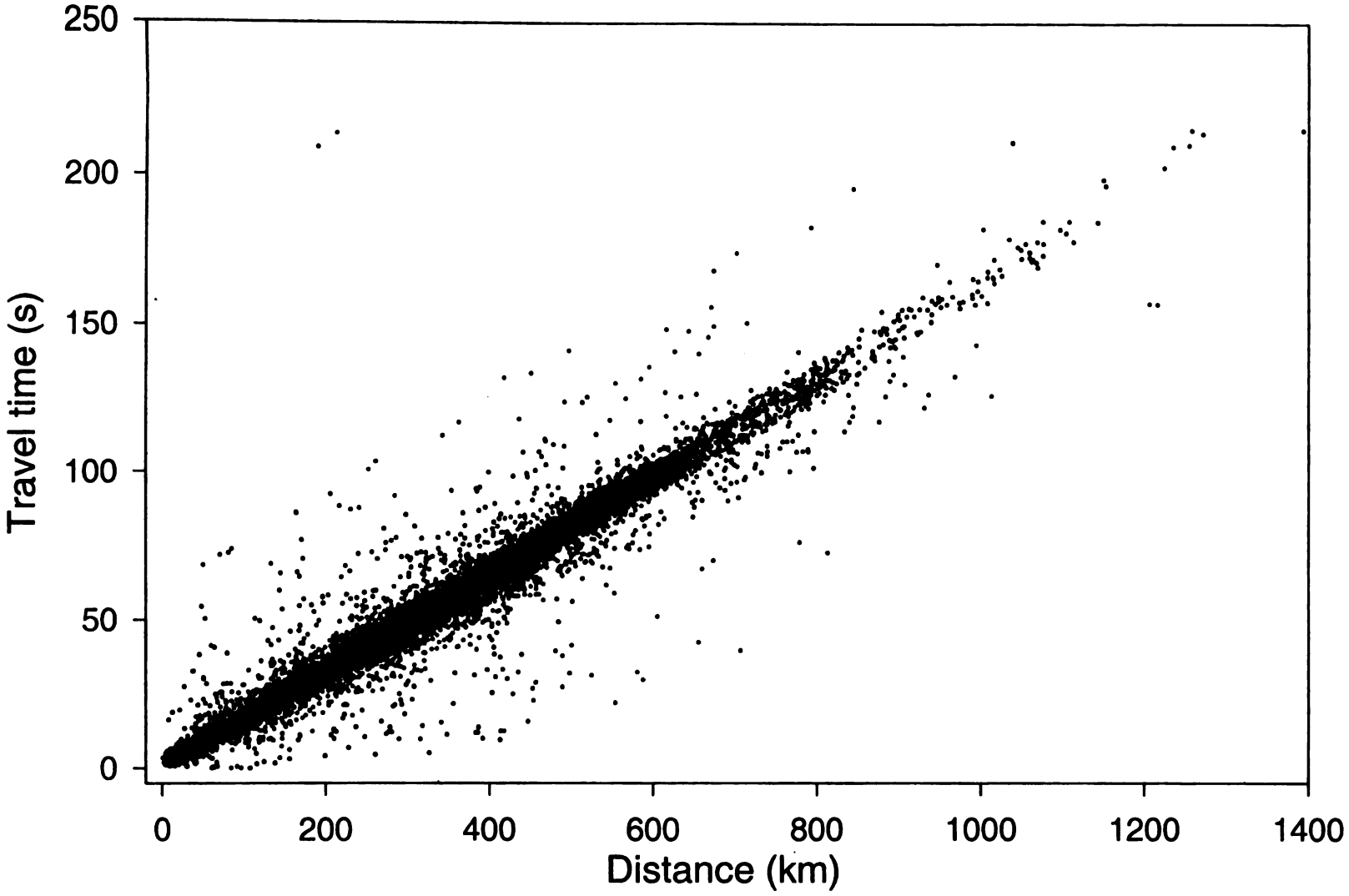

Figure 3-2. Pg phase arrival travel time curve for northeastern Russia. Russian reported hypocenters and origin times were used. The plot contains 35,257 arrivals.

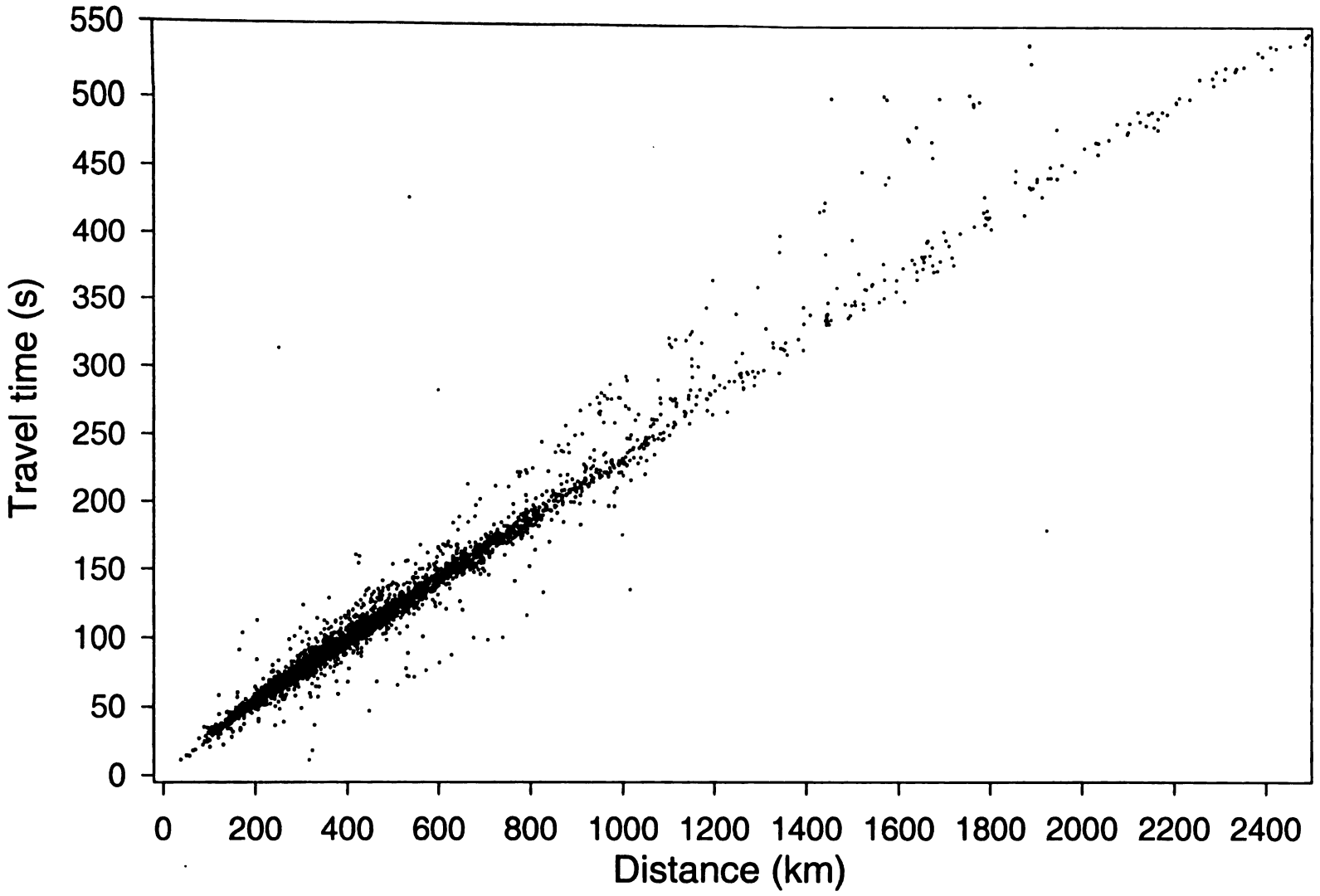

Figure 3-3. Sn phase arrival travel time curve for northeastern Russia. Russian reported hypocenters and origin times were used. The plot contains 4,873 arrivals. Data shown is only from northeastern Russia stations.

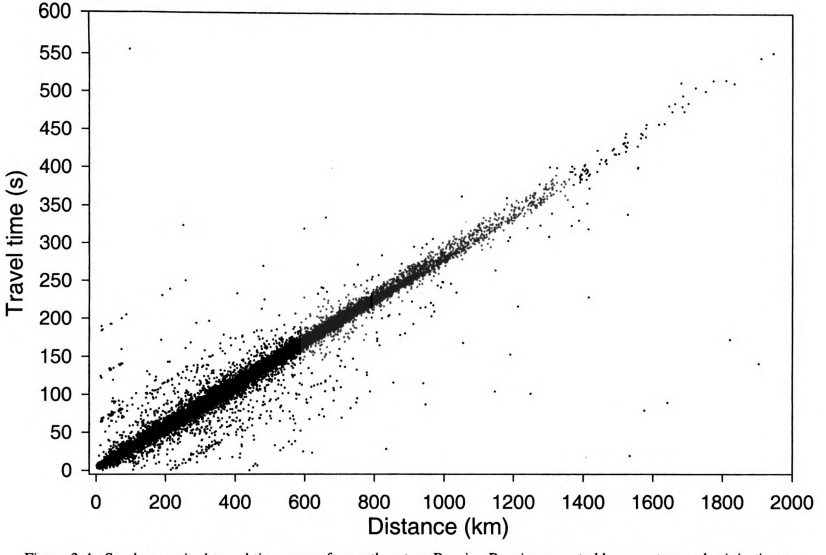

Figure 3-4. Sg phase arrival travel time curve for northeastern Russia. Russian reported hypocenters and origin times were used. The plot contains 68,811 arrivals.

offsets from the main Sg trend. Similar trends are visible to a lesser extent on the Pg and Sn travel time curves (Figures 3-2 and 3-3). A composite reduced travel time curve is shown in Figure 3-5.

The only previous study attempting a systematic relocation of events in the study area looked at a set of 75 events in the southern Magadan and northern Yakutsk networks (Mackey, 1996; Mackey et al., 1998). In this study, events were located using only the Pg phase, assuming a crustal velocity of 6.00 km/s. High residual arrivals were omitted from the location routine and several misassociated phases were corrected. Travel time data were then inverted to solve for the best fitting Pg and Pn velocities and new origin times for the events. Although the primary focus of this study was to determine crustal thickness based on seismic velocities and Pg/Pn crossover points, the regional best-fit P wave velocities were also determined (5.992 km/s crust, and 7.961 km/s upper mantle). This crustal velocity is less than the 6.1 km/s crustal P velocity used for the original Russian locations in the region (Figure 3-2). The relocations and inversion of the data resulted in a significant reduction in data scatter on the travel time curves (Figures 3-6 through 3-8).

DISCUSSION

Relocations computed here are intended to build on relocation work presented in Mackey (1996), and Mackey et al. (1998). The basic location routine is a least squares best fit routine called 'HYP2DT,' originally from Caltech. Originally, this program used only one travel time curve, thus hypocenter parameters could be computed using only one phase. The routine was modified for this study to accept multiple phases, specifically Pg, Pn, and Sg. Sn arrivals are not used as the data are very noisy.

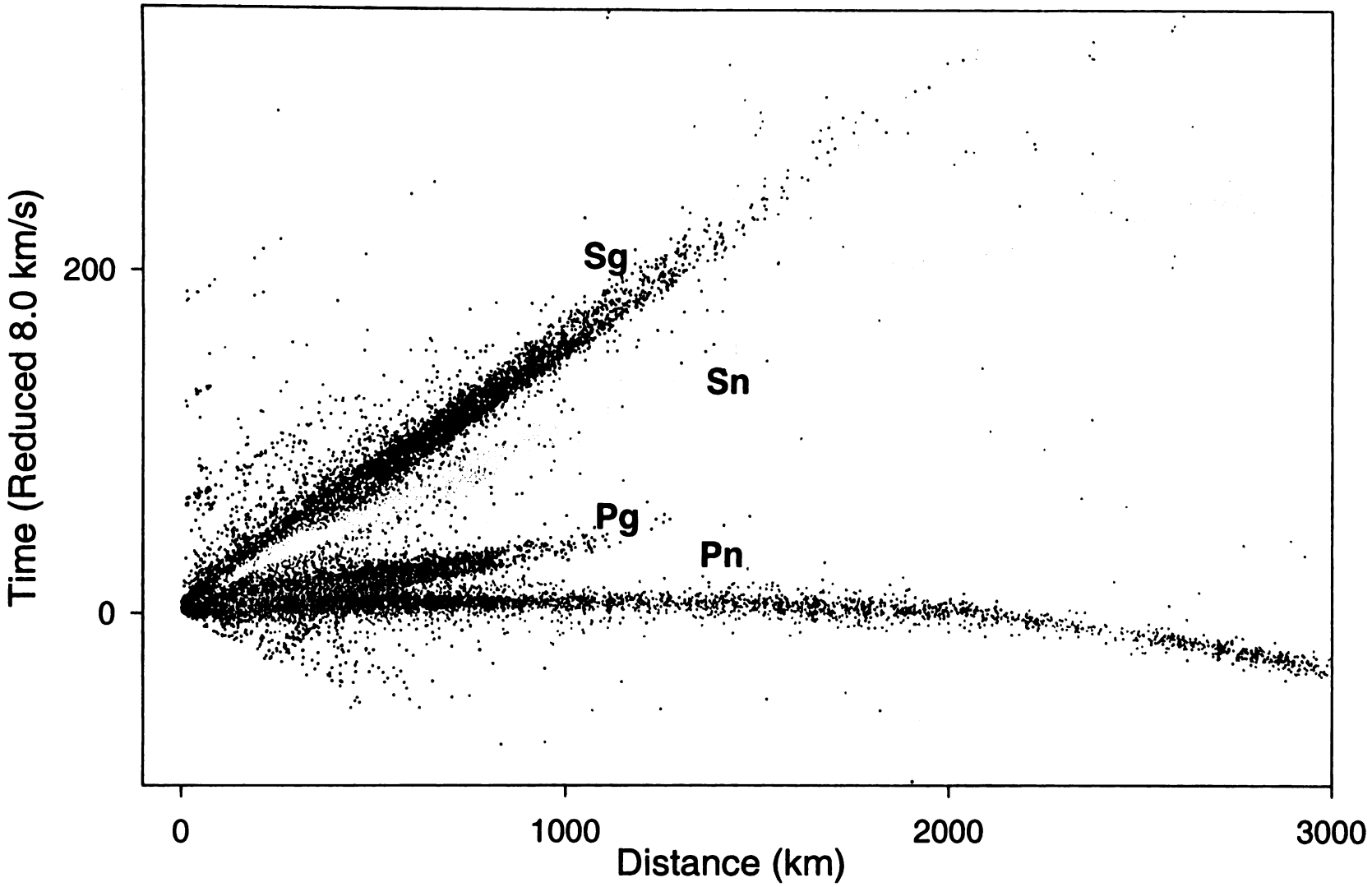

Figure 3-5. Composite reduced travel time curve for northeastern Russia. Only data from northeastern Russia stations are shown.

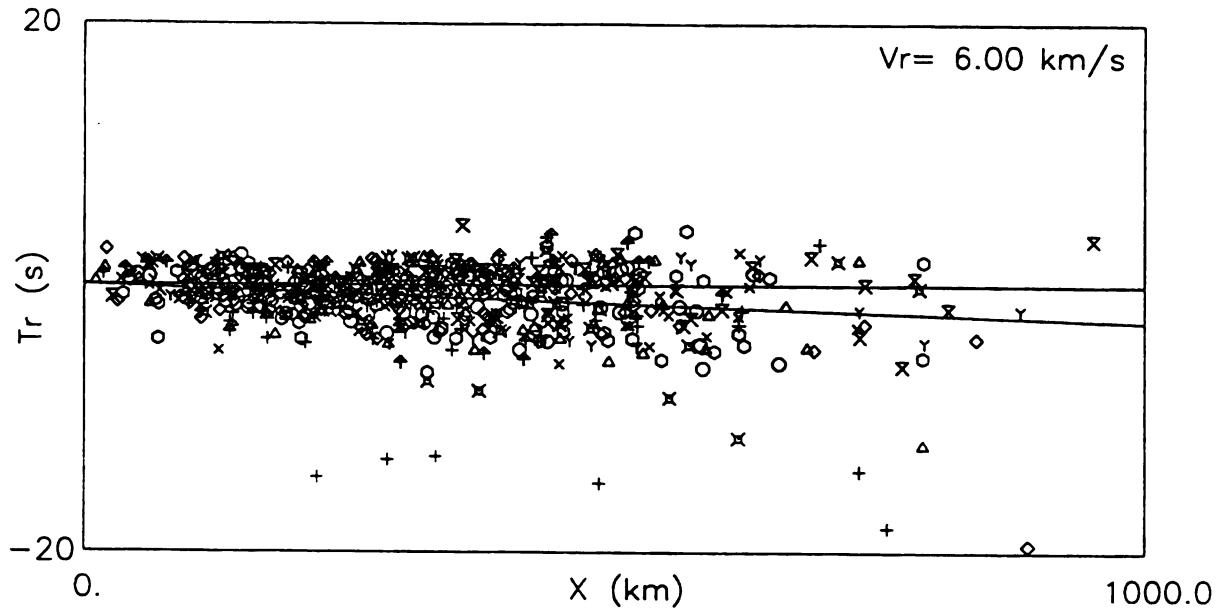

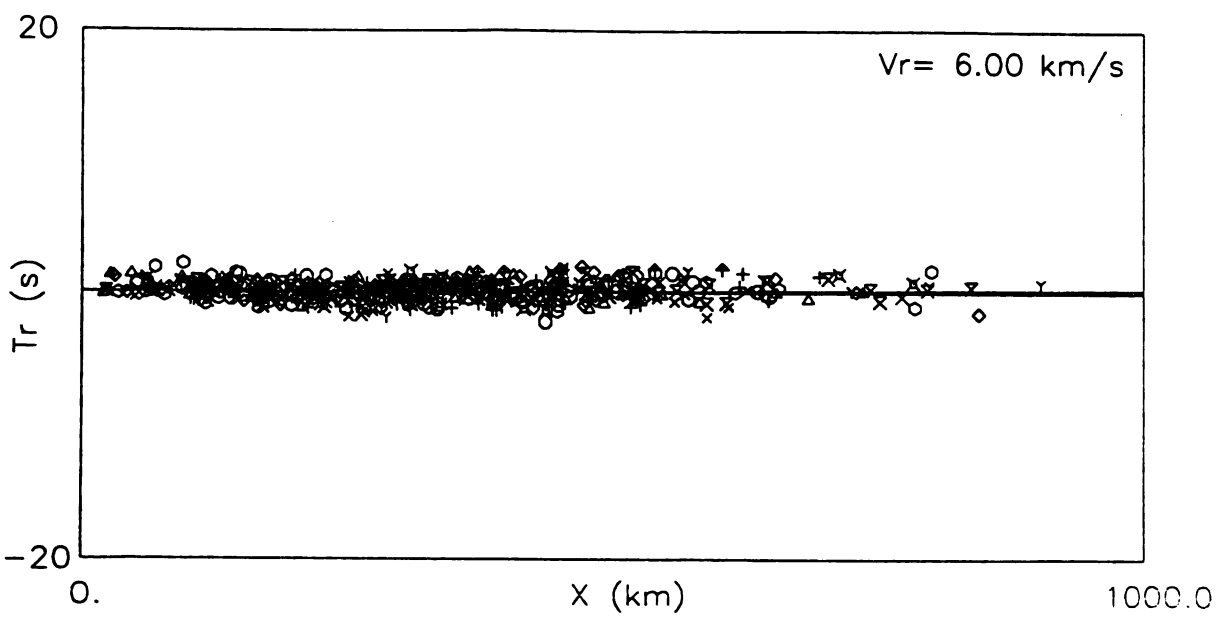

Figure 3-6. Pg reduced travel time curves for 75 events used in Mackey (1996) and Mackey et al. (1998). Upper curve uses original Russian determined hypocenter parameters and reflects a velocity of 6.1 km/s. Lower curve plots the same data after all events were relocated and inverted for velocity and origin time. Reduction velocity is 6.0 km/s. Figure from Mackey (1996).

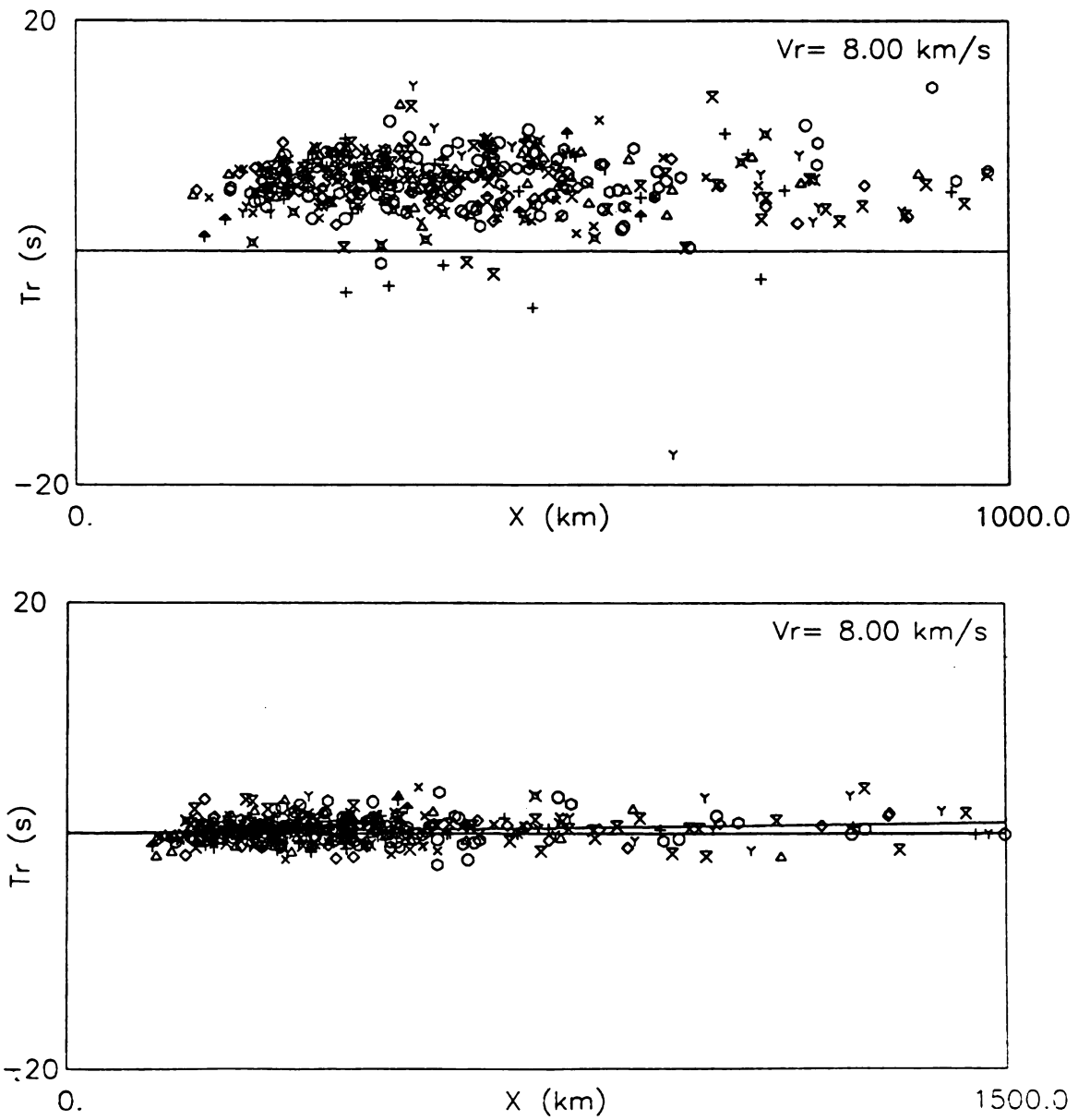

Figure 3-7. Pn reduced travel time curves for 75 events used in Mackey (1996) and Mackey et al. (1998). Upper curve uses original Russian determined hypocenter parameters. Lower curve plots the same data after all events were relocated and inverted for velocity. Reduction velocity is 8.0 km/s. Figure from Mackey (1996).

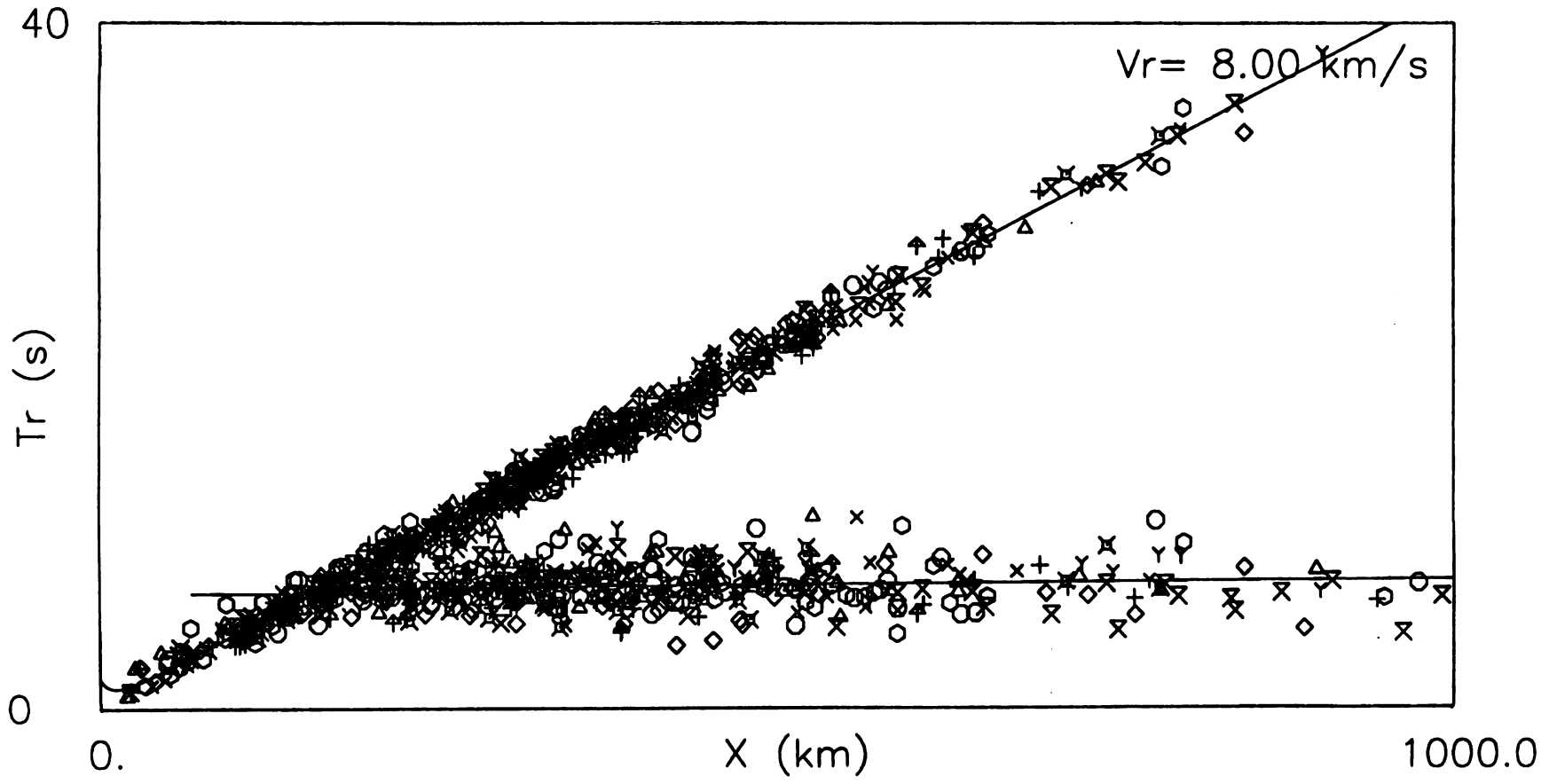

Figure 3-8. Reduced composite travel time curve from 75 events used in Mackey (1996) and Mackey et al. (1998). All data plotted use the Pg phase relocated epicenter and origin times determined from inversion of the data after high residual arrivals were removed. The Pg-Pn crossover point is consistent with a regional crustal thickness of 37 km. Pg velocity plotted is 5.99 km/s and Pn velocity is 7.96 km/s. Reduction velocity is 8.0 km/s. Figure from Mackey (1996).

Throughout the study area, many geologic and tectonic environments exist, which combined with the physical vastness of the region makes it likely that no single velocity or travel time curve will reflect actual seismic velocities for any particular phase. In order to overcome this problem, the study area was broken into cells, and the best fitting velocities were determined by minimizing the sum of event RMS residuals through trial of multiple travel time curves. Cell sizes are generally 3° north-south by 5° east-west, although this was adjusted in areas with sparse activity in order to increase the number of useable events (Figure 3-9). For any given block, only events containing Pn phase arrivals (generally 2 or more) were used. This selects only the larger events, which contain more arrivals and have better azimuthal coverage of receiving stations.

Travel time curves for Pg and Sg phases were calculated assuming a flat-earth-straight-ray approach. This is reasonable because Pg and Sg phases are confined to the crust, thus the distance traveled between epicenter and station is equivalent to the surface distance. For hypocenters at depth, the travel path is assumed to be the hypotenuse of the triangle made by the depth and the surface distance. Event depths are restricted to a maximum of 33 km, as all events are assumed crustal in nature. Events for which depth tends above the surface are restricted to 0 km.

In order to determine the best crustal velocities for locating events within a given cell, the selected events are first located with crustal velocities 'guessed' for the region. The velocities used in the guess were generally the best fit velocities from an adjacent cell. The resulting output is analyzed for high residual arrivals, generally those greater than 3.5 seconds. High residuals are generally a result of either typographical errors, misassociated phases, or bad time picks. Typographical errors and misassociated phases are corrected if

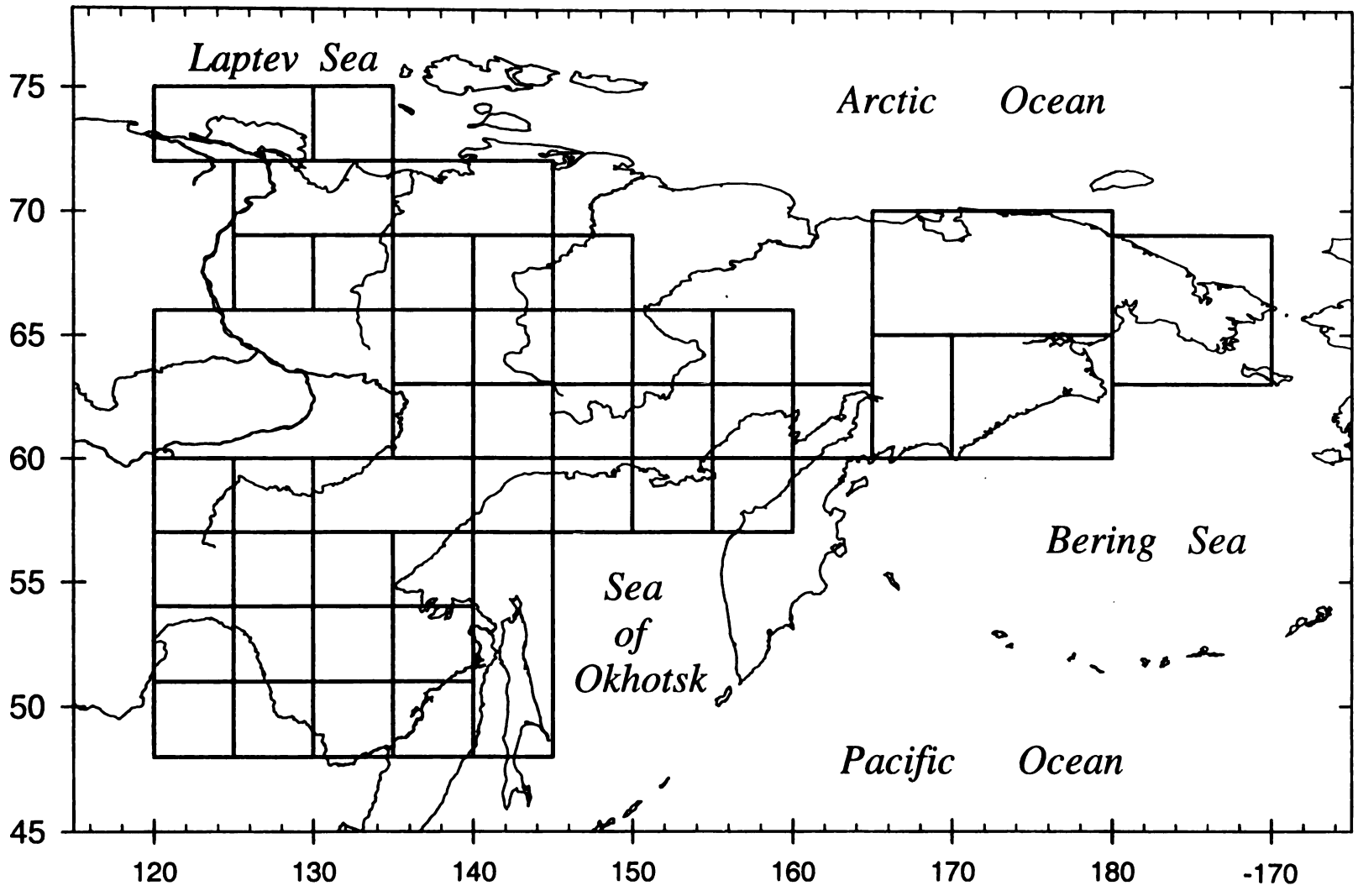

Figure 3-9. Grid of individual regions where calibrated crustal velocities were determined.

possible, while bad time picks are flagged to be omitted from use in further locations. Unstable events having many high residual arrivals such that it was impossible to get a reasonably good location and events with four or fewer recording stations are omitted from further analysis. Overall, less than 5% of the originally selected events were omitted due to stability problems.

In order to determine the better fitting travel time curve to use for Pn arrivals in the location procedure, the Jeffreys-Bullen (JB; Jeffreys and Bullen, 1970) P wave travel time curve was compared to the IASPEI 91 (I-91) curve by Kennett (1991). Results for test regions in the Amur, northern Yakutia, Magadan, and Chukotka regions indicate that the JB table does a better job of fitting the Pn arrivals in the region. The Pg and Sg velocities used in each comparison were the same. Overall, when comparing RMS residuals for events located using the two travel time curves, approximately 80% of the events have a lower RMS residual when the JB table is used as opposed to the I-91 table. Therefore, the JB table was used in all relocations computed in this study. This is reasonable as the JB table was constructed at a time when continental observations determined the data set, as opposed to the I-91 table which incorporates more oceanic data.

Following removal of large residual time picks and correction of misassociated phases, the remaining selected events for a given block are located multiple times using different crustal velocities. Crustal velocities tested for each block range from 5.875 km/sec to 6.350 km/sec in 0.025 km/sec increments for Pg, and 3.470 km/sec to 3.650 km/sec in 0.020 km/sec increments for Sg. In this manner, the crustal velocities which best fit the events in the cell are found. The newly found best fitting velocity for each cell is then used to relocate the events a second time. After locating with the new velocity, any additional

high residual arrivals are omitted or corrected. Arrivals with residuals over 3.0 seconds were removed. Arrivals with lower residuals were occasionally removed if the station was very close to the epicenter, or if a single residual had a value several times larger than all others for a particular event and 'stood out'. If any arrivals were removed or had phase associations changed, the events in the cell were again subjected to a search for the best fit crustal velocities. Three-dimensional plots of a cell's cumulative residuals for varying Pg and Sg velocities are useful to illustrate how the residuals change with differing velocities. Figures 3-10 and 3-11 illustrate how the residuals change for specific cells in the Magadan and south Yakutia regions respectively. Note the absolute minimum in each plot is different, which shows lower velocities are better in the Magadan cell, while higher velocities work better in the south Yakutia cell. Final crustal velocities for each cell are shown on Figures 3-12 and 3-13, and are given in Table 3-1. A total of 1311 earthquakes were relocated (Appendix E) in 45 geographic cells. Crustal velocities in northern Yakutia are somewhat problematic, with adjacent cells alternating between high and low velocities. This region is re-evaluated with a slightly different method discussed below.

In this study, the Pn phase controls the depth determination of the hypocenter, while the crustal phases better constrain the origin time and coordinates. This is a result of the geometry of the raypaths. The crustal phases are not sensitive to depth because a change in depth has a negligible effect on the raypath length for distant stations. For example, a change in depth from 0 to 10 km results in an increase of the raypath length of 0.5 km for a station 100 km distant. This corresponds to a difference in Pg travel time of less than 0.1 second, which is less than timing or picking errors. Because few earthquakes in this study have more than one station within 100 km of the epicenter, the crustal phases exert little influence in

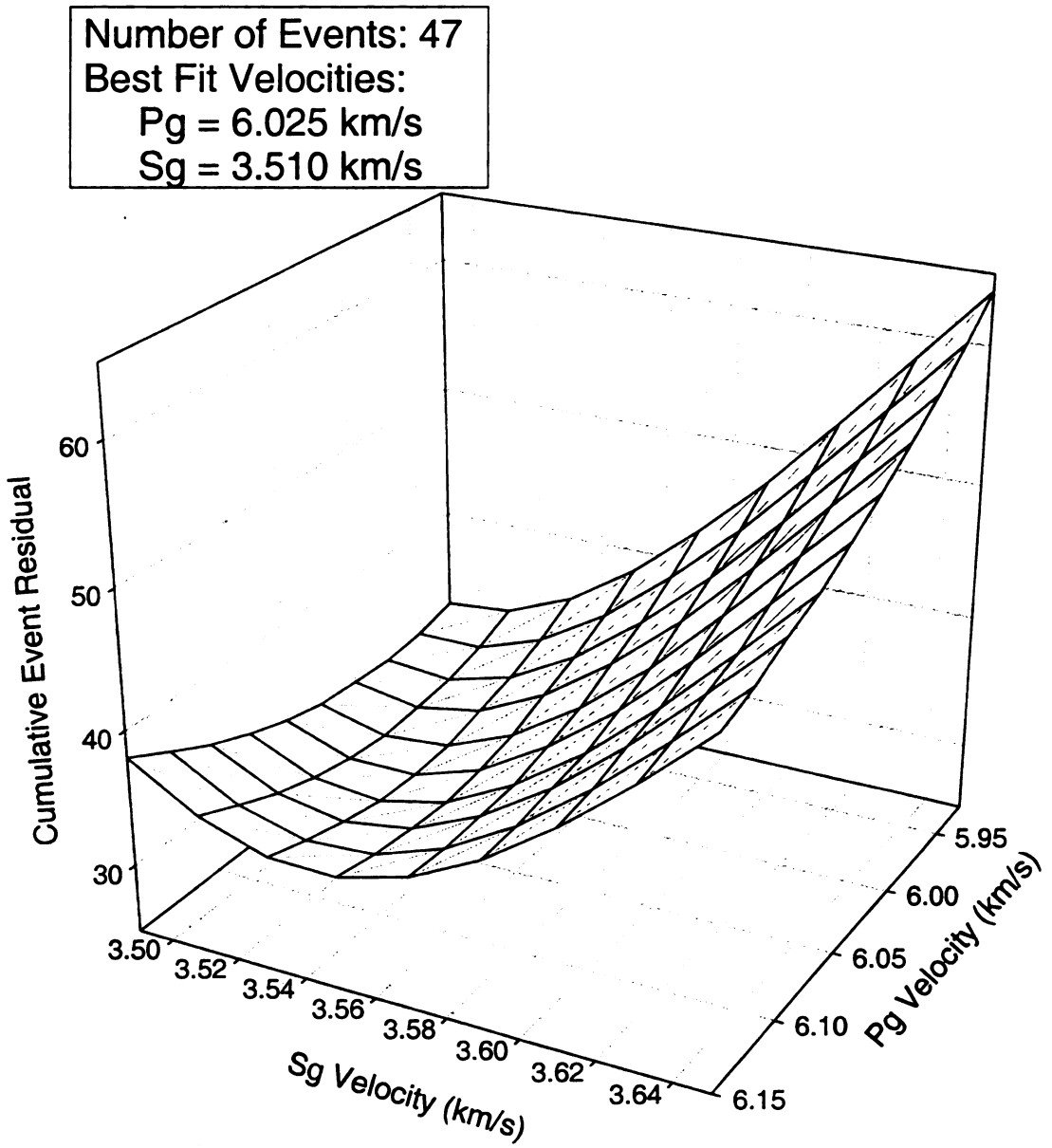

Figure 3-10. Pg-Sg velocity residual graph for the region 60 - 63° N x 145 - 150° E.

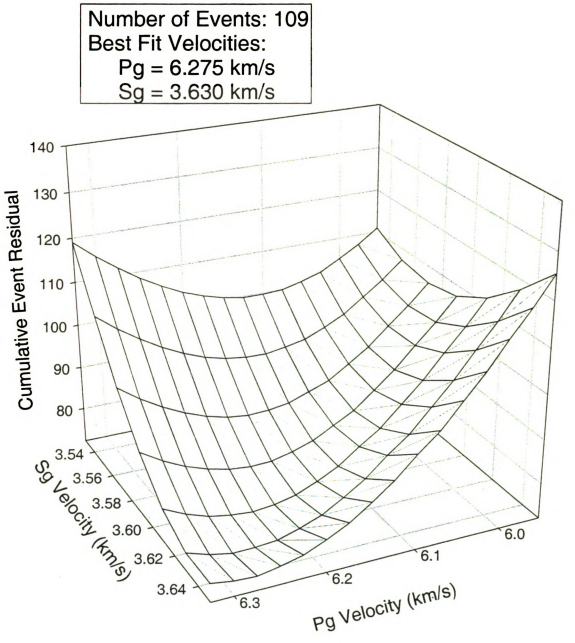

Figure 3-11. Pg-Sg velocity residual graph for the region 54 - 57° N x 125 - 130° E.

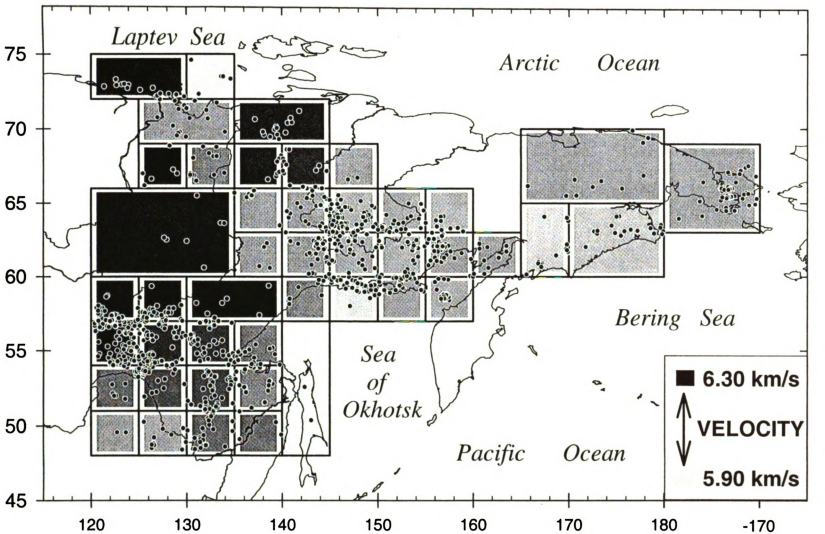

Figure 3-12. Grid of calibrated Pg velocities. Original epicenters shown for reference.

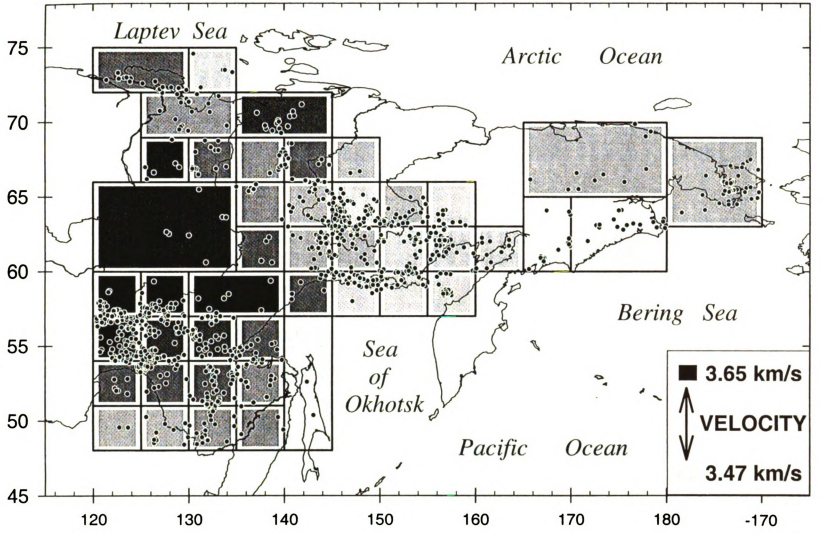

Figure 3-13. Grid of calibrated Sg velocities. Original epicenters shown for reference.

Table 3-1. Best fit velocities and number of events per geographic region.

Region		Best Velocities	km / sec	Number of events
48-51N	120-125E	Pg=6.040	Sg=3.530	2
48-51N	125-130E	Pg=6.025	Sg=3.530	12
48-51N	130-135E	Pg=6.100	Sg=3.550	28
48-51N	135-140E	Pg=6.100	Sg=3.550	4
48-57N	140-145E	Pg=5.875	Sg=3.470	2
51-54N	120-125E	Pg=6.100	Sg=3.570	14
51-54N	125-130E	Pg=6.125	Sg=3.570	32
51-54N	130-135E	Pg=6.125	Sg=3.570	47
51-54N	135-140E	Pg=6.075	Sg=3.550	20
54-57N	120-125E	Pg=6.275	Sg=3.630	109
54-57N	125-130E	Pg=6.175	Sg=3.590	69
54-57N	130-135E	Pg=6.150	Sg=3.590	40
54-57N	135-140E	Pg=6.100	Sg=3.570	19
57-60N	120-125E	Pg=6.275	Sg=3.630	149
57-60N	125-130E	Pg=6.300	Sg=3.650	44
57-60N	130-140E	Pg=6.275	Sg=3.630	9
57-60N	140-145E	Pg=6.075	Sg=3.570	7
57-60N	145-150E	Pg=5.950	Sg=3.510	42
57-60N	150-155E	Pg=6.040	Sg=3.510	33
57-60N	155-160E	Pg=6.025	Sg=3.510	35
60-63N	135-140E	Pg=6.050	Sg=3.570	4
60-63N	140-145E	Pg=6.050	Sg=3.530	35
60-63N	145-150E	Pg=6.025	Sg=3.530	47
60-63N	150-155E	Pg=6.025	Sg=3.510	47
60-63N	155-160E	Pg=6.06	Sg=3.51	63
60-63N	160-165E	Pg=6.05	Sg=3.51	11
60-65N	165-170E	Pg=5.975	Sg=3.470	19
60-65N	170-180E	Pg=6.000	Sg=3.470	19
60-66N	120-135E	Pg=6.225	Sg=3.610	7
63-66N	135-140E	Pg=6.050	Sg=3.550	11
63-66N	140-145E	Pg=6.050	Sg=3.530	31
63-66N	145-150E	Pg=6.025	Sg=3.510	103
63-66N	150-155E	Pg=6.025	Sg=3.530	29
63-66N	155-160E	Pg=6.025	Sg=3.510	10
63-69N	180-160W	Pg=6.050	Sg=3.530	48
65-69N	165-180E	Pg=6.060	Sg=3.530	11
66-69N	125-130E	Pg=6.275	Sg=3.610	6
66-69N	130-135E	Pg=6.075	Sg=3.570	14
66-69N	135-140E	Pg=6.200	Sg=3.550	8
66-69N	140-145E	Pg=6.175	Sg=3.570	17
66-69N	145-150E	Pg=6.040	Sg=3.53	2
69-72N	125-135E	Pg=6.050	Sg=3.550	18
69-72N	135-145E	Pg=6.200	Sg=3.590	14
72-75N	120-130E	Pg=6.225	Sg=3.570	15
72-75N	130-135E	Pg=5.900	Sg=3.510	5

determining the depth of the earthquakes. On the other hand, the same shift in depth reduces the path length of the Pn phase a couple of kilometers, as well as allowing the Pn phase a longer time in the higher velocity upper mantle, and shorter time in the lower velocity crust, all of which reduce the travel time. Overall, variations in depth of an earthquake from the surface to 33 km can change the Pn travel time about 3 seconds, thus depth determinations are primarily a result of Pn phase travel times.

A problem can arise with both hypocenter parameters and origin time if the actual seismic velocity along the Moho is different than in the travel time curve used in the location procedure. An incorrect Pn velocity can affect the origin time and coordinates (particularly depth) in a drastic manner if the azimuth window of recording stations is small. With a small azimuth window of recording stations, a shift in origin times as well as distance from stations to epicenter can easily accommodate incorrect crustal velocities. In the process of locating earthquakes in the northern Yakutia region, such a problem was suspected of developing. Note from Figures 3-12 to 3-13 and Table 3-1 that velocities determined in adjacent cells in northern Yakutia vary drastically, with no smooth gradient throughout the region. It was thought that a drastically incorrect Moho velocity was causing sufficiently large shifts in origin times, or locations of events, such that the best fitting crustal velocities were erratic. Unfortunately, exclusion of Pn arrivals from the location procedure removes the primary depth constraint for hypocenter parameters. This led to the development of an alternate method of depth determination without using the Pn phase in the location procedure (Appendix F). It was found, however, that omitting all Pn arrivals from the location procedure and solving for best fitting crustal velocities resulted in essentially the same best fit crustal velocities in northern Yakutia, with the erratic velocity shifts in adjoining cells

remaining. As a result of this, the alternate method of depth determination was not used in the final analysis. The method does illustrate the dependence of depth on Pn arrivals when the crust is assumed to be one layer with one velocity for crustal Pg and Sg arrivals.

The final analysis of hypocenter locations for Yakutia north of 66° was done using a 5° x 3° moving window, shifting the window in 1° increments. For each cell, the best fitting crustal velocities were determined by trial of multiple Pg and Sg velocities as discussed above. This resulted in a similar velocity structure as determined earlier, but with greatly smoothed velocity shifts (Figures 3-14 and 3-15). The overall pattern of Pg velocities is similar to that of the Sg velocities.

RESULTS

Crustal velocities determined in the location process correlate well with the regional tectonic provinces. Generally the highest velocities (Pg velocities ranging from 6.225 to 6.300 km/s and Sg from 3.61 to 3.65 km/s) occur in the western portion of the study region, which is associated with the Siberian platform. Elevated crustal velocities in the Siberian platform are consistent with seismic studies conducted by Suvorov et al. (1999), where Pg velocities were generally found to range from 6.2 - 6.3 km/s. South of the Siberian platform, velocities decrease across the Mongol - Okhotsk suture (Figure I-4). This velocity decrease is consistent with with the results of Suvorov and Kornilova (1985). Velocities also drop sharply in the Verkhoyansk foldbelt, along the eastern edge of the Siberian platform. From the Verkhoyansk foldbelt and east through the Mesozoic terrane assemblages (Kolyma - Omolon superterrane) to the Bering Strait, crustal velocities are consistently in the 6.00 - 6.05 km/s range, and Sg velocities in the 3.51 - 3.55 km/s range, with only a few cells

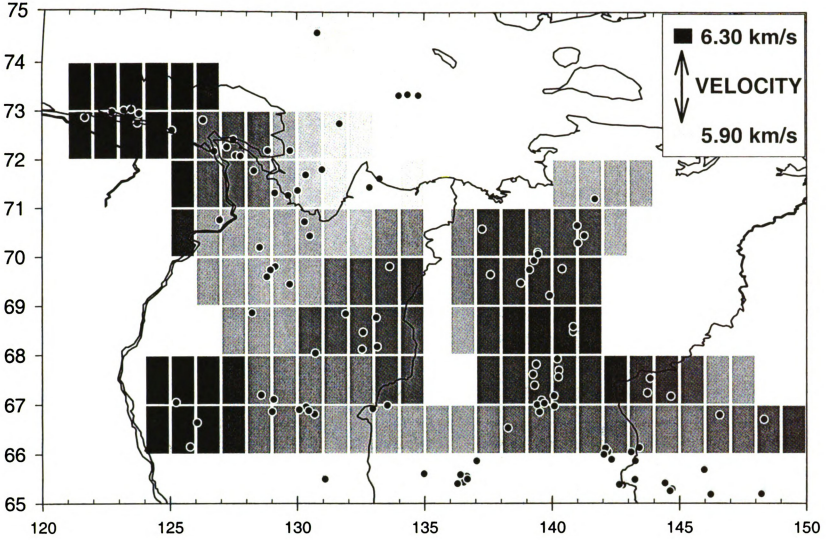

Figure 3-14. Pg velocities for northern Yakutia determined by using a moving window.

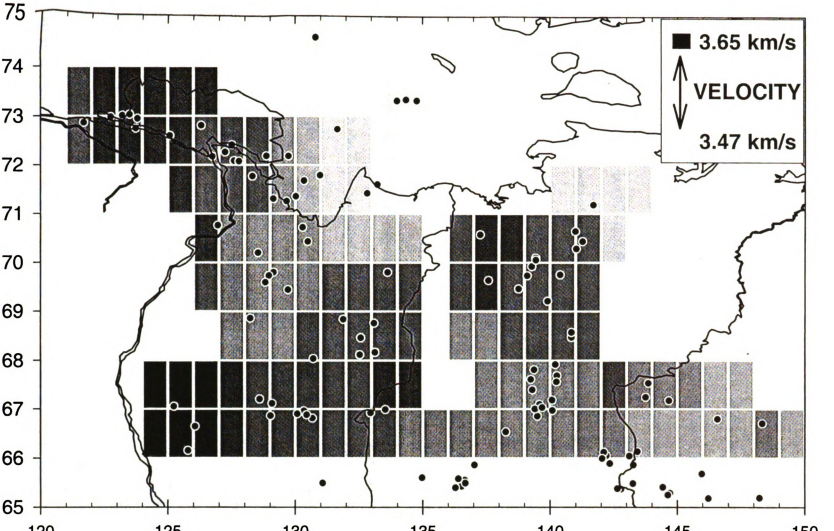

Figure 3-15. Sg velocities for northern Yakutia determined by using a moving window.

deviating slightly. The final analysis for velocities in northern Yakutia indicate that the highest velocities are associated with the Siberian platform along the western edge of the region. The lowest velocities occur in the Laptev Sea and correspond to active rifting along the extension of the Arctic Mid-Ocean Ridge. The velocity shifts in northern Yakutia are probably a result of rapidly changing velocity gradients associated with presently active rifting adjacent to the Siberian platform and other older tectonic structures. The low velocity region in the Laptev Sea extends into the continent, where it generally follows the strike of the grabens outlined in Fujita et al. (1990). Crustal velocities determined for Sakhalin are greatly reduced, although this determination was done with only 2 events, and is thus not statistically reliable.

The newly determined velocities in each cell were used in the final relocation of events. Plots comparing original and relocated epicenters show clear improvement of relative locations. In the Amur region, there is clear improvement on a seismicity trend extending through the Zeya basin and clear tightening of seismicity clusters throughout the region (Figure 3-16). It is expected that an improvement in event locations will result in better defined lineations in the seismicity as earthquakes occur on faults, which are planar. It is also expected that clusters of events would concentrate into smaller areas for point sources, such as aftershock sequences. Relocated epicenters in the Magadan region show a tightening of several clusters of seismicity and a slightly improved lineation of events along the trace of the Ulakhan fault (Figure 3-17). The cluster near 62° N x 157° E is due to an aftershock sequence following an event on February 11, 1987. Clusters of seismicity in the eastern portion of Chukotka are reduced to much smaller lineations (Figure 3-18). It is difficult to judge whether epicenters in the Koryak Highlands are improved as there are not

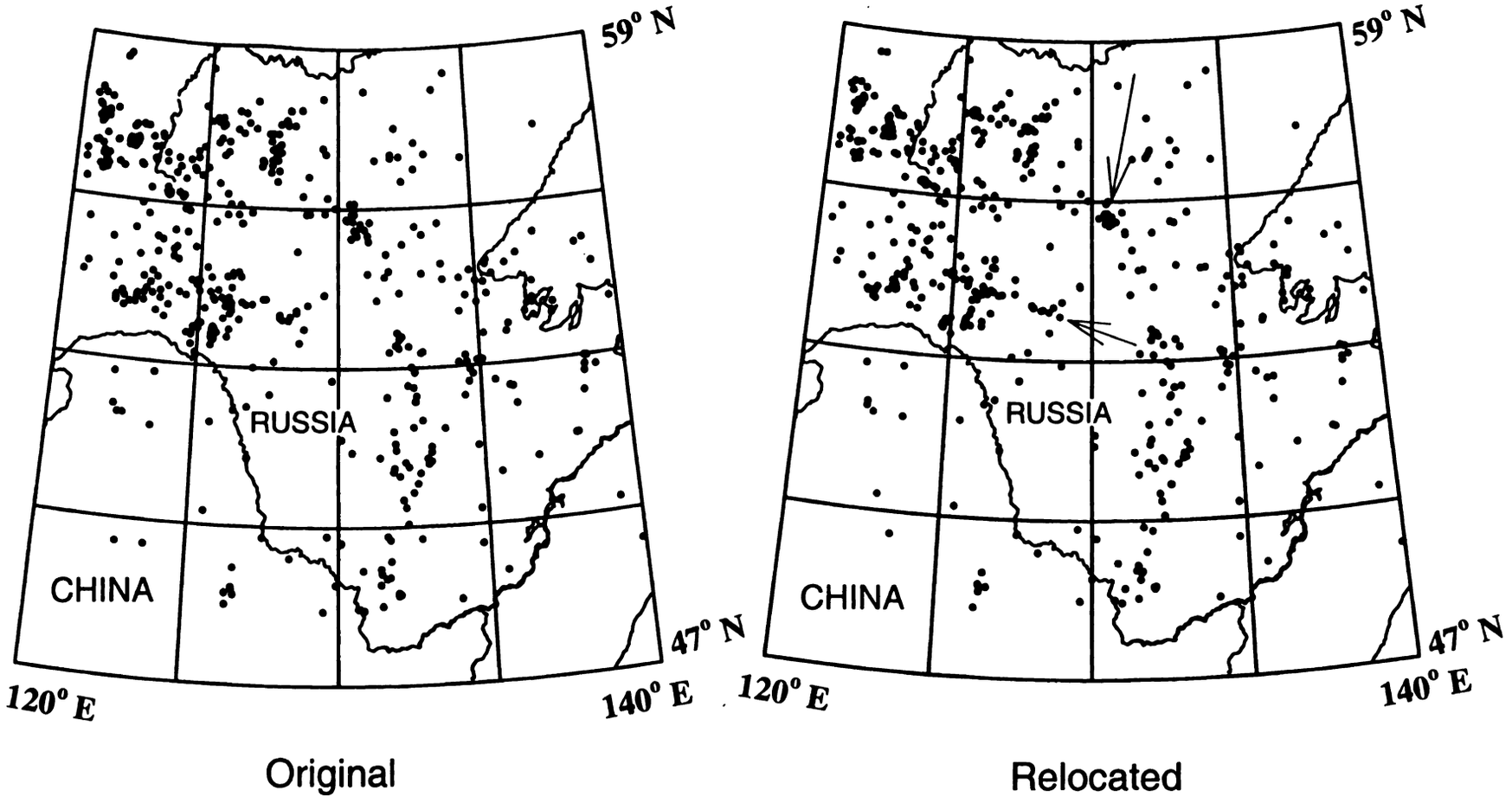

Figure 3-16. Original vs. relocated epicenters for the Amur region. Arrows indicate locations of improved definition of some seismicity clusters and trends.

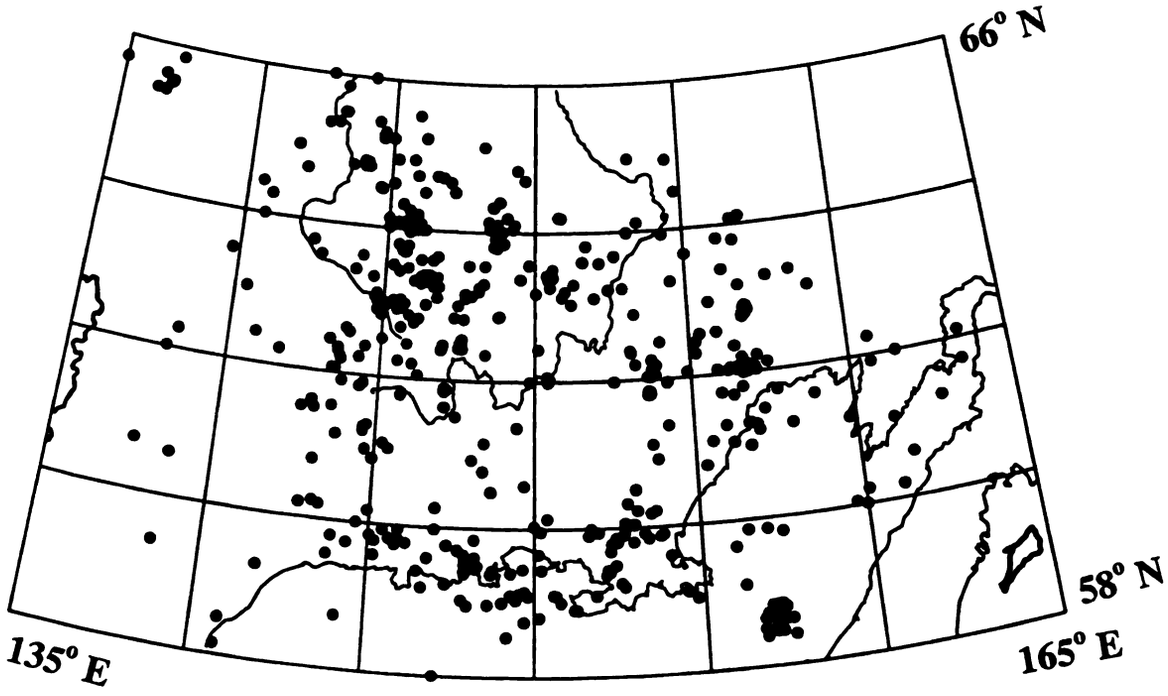

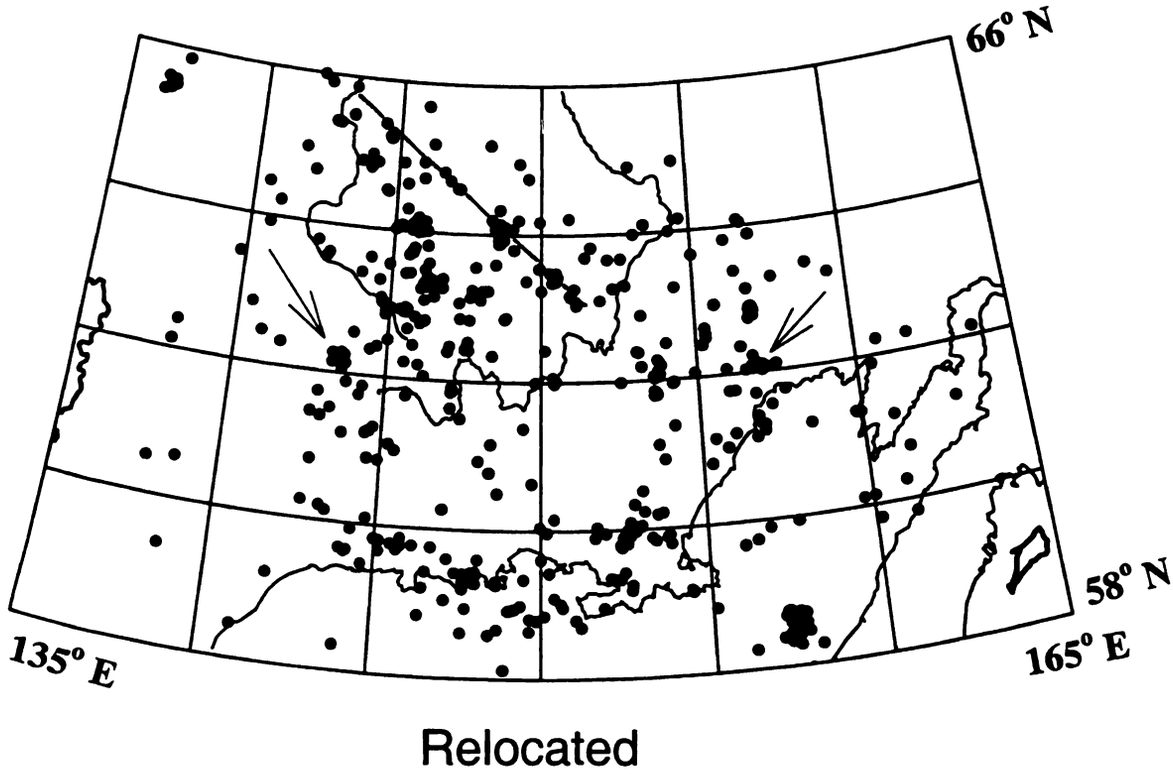

Figure 3-17. Original vs. relocated epicenters for the Magadan region. Ulakhan fault shown by gray line. Note improvement in relative locations of clusters indicated with arrows, as well as many other smaller clusters.

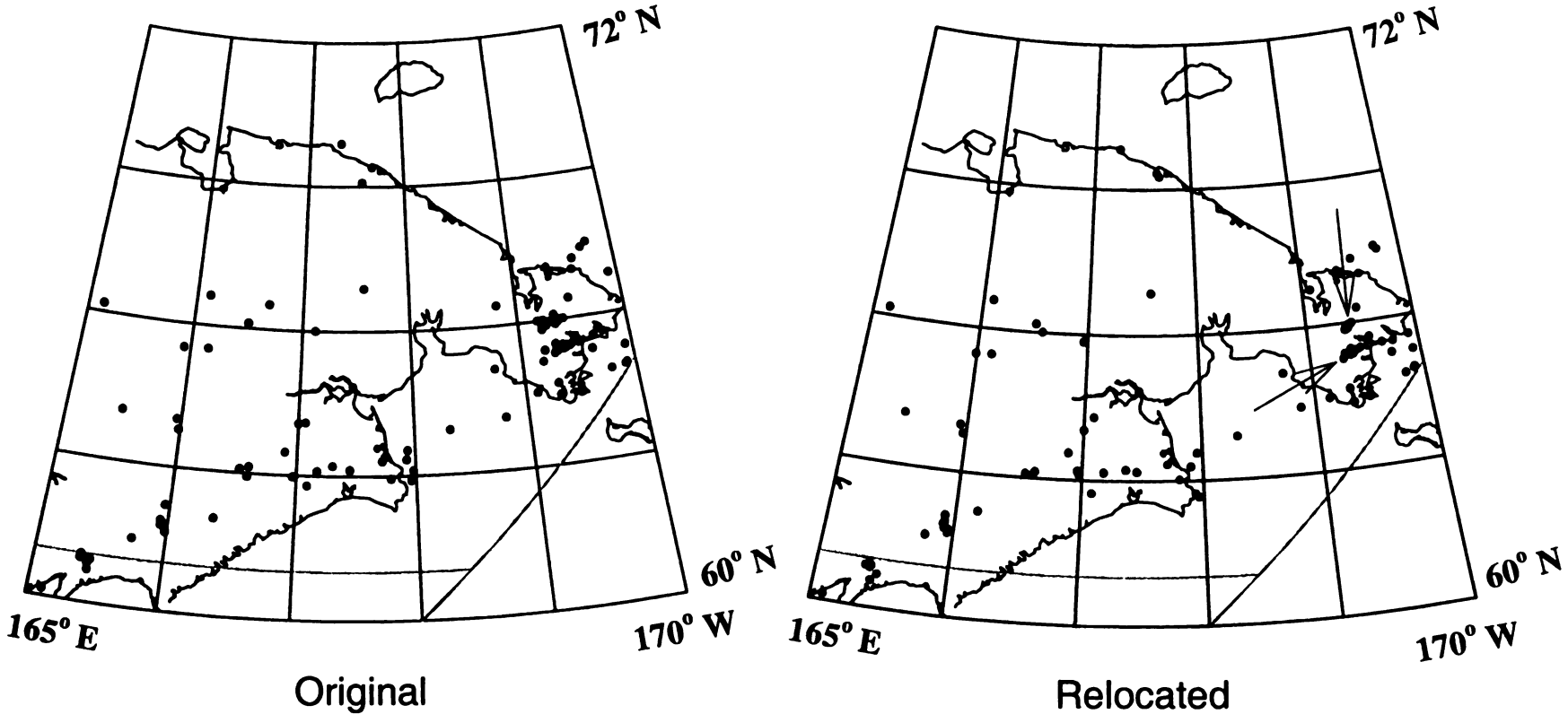

Figure 3-18. Original vs. relocated epicenters for Chukotka. Arrows indicate improved lineations. Network boundaries shown in gray.

enough events, particularly if seismicity here is partitioned on several faults. Original and relocated epicenters for northern Yakutia are plotted in Figure 3-19. Although epicenters clearly moved in the relocation process, the lack of clear clusters and trends makes it difficult to evaluate any improvement in relative locations.

Overall, depths determined in the location process are reasonable. A histogram of event depths shows a clear peak centered around 10 km (Figure 3-20). There are also peaks for depths of 0 and 33 km, which were the confining limits for the depth determinations. As depths determined in this study are primarily dependent on Pn arrivals, any variation in Moho depth will affect event depth. A thickened crust will increase the travel path for the Pn phase. Because the path is longer, it will take longer for the Pn phase to reach the station, giving it a positive residual relative to the assumed thinner crust model. To reduce the residual, the Pn path length must be lengthened in the thinner crust model, which will move the event to a shallower depth. Of course, this may trade off with Moho velocity. Thicker crust may have higher Moho velocities which will result in a earlier Pn arrival, thus offsetting the shallow event depth. Likewise, a thinner crust and lower velocity Moho would have the opposite effects. It is difficult to account for either of these variables without significant prior knowledge of Moho depth and velocity. To further improve hypocenters, it would also be necessary to develop corresponding travel time corrections for all stations and all possible source locations.

Travel time curves resulting from the relocated events show a distinct improvement. A composite travel time curve derived from all relocated events (Figure 3-21) shows a decrease in level of scatter when compared to those derived from the original Russian locations (Figure 3-5). Figure 3-21 is a composite travel time curve for relocations computed

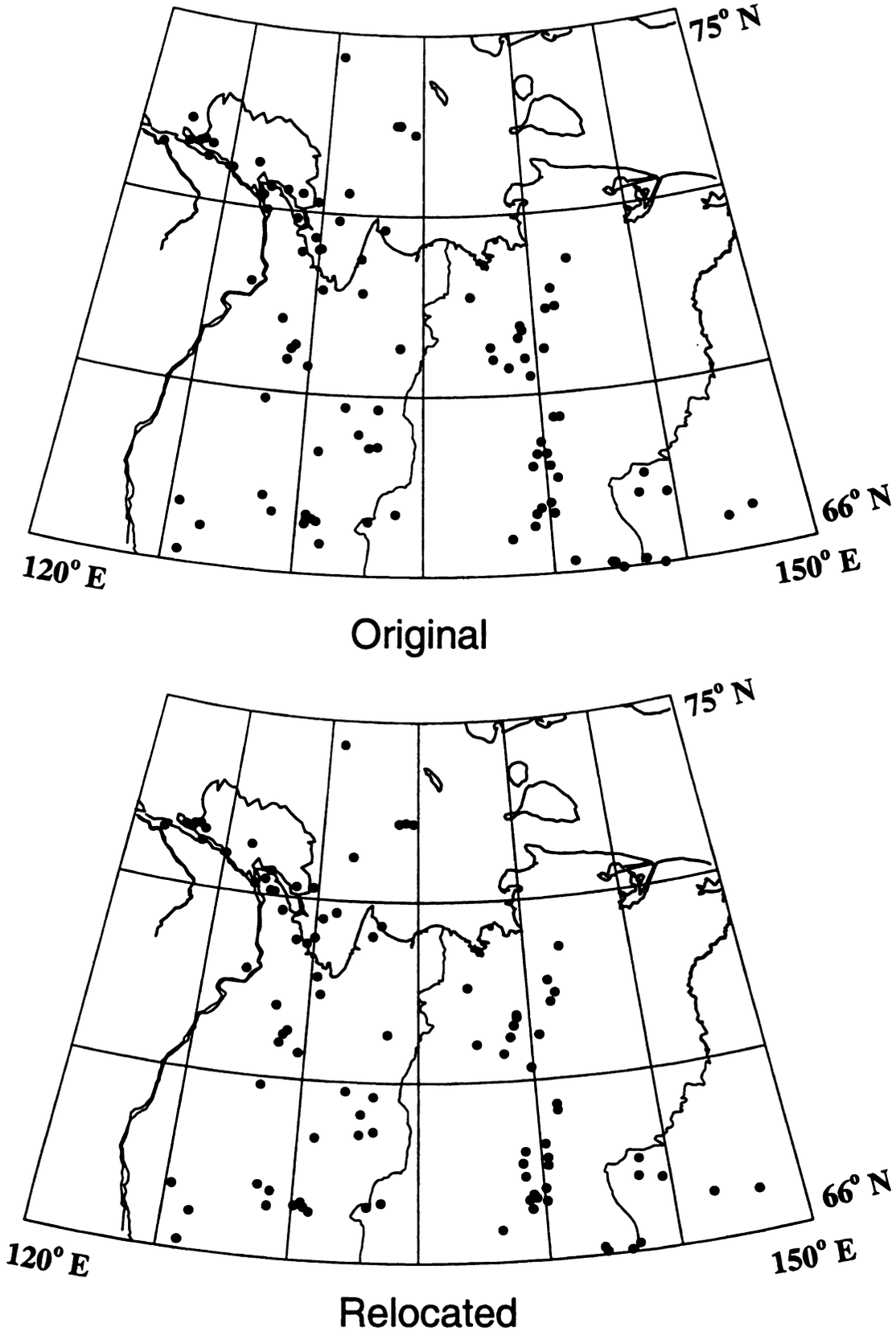

Figure 3-19. Original vs. relocated epicenters for northern Yakutia.

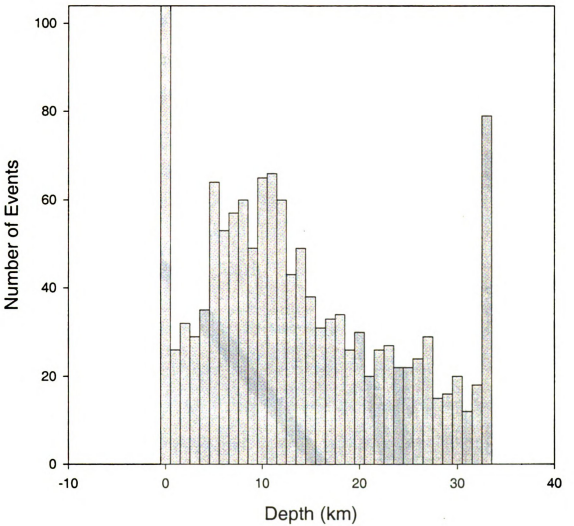

Figure 3-20. Histogram of relocated event depths. Most event depths are around 10 km.

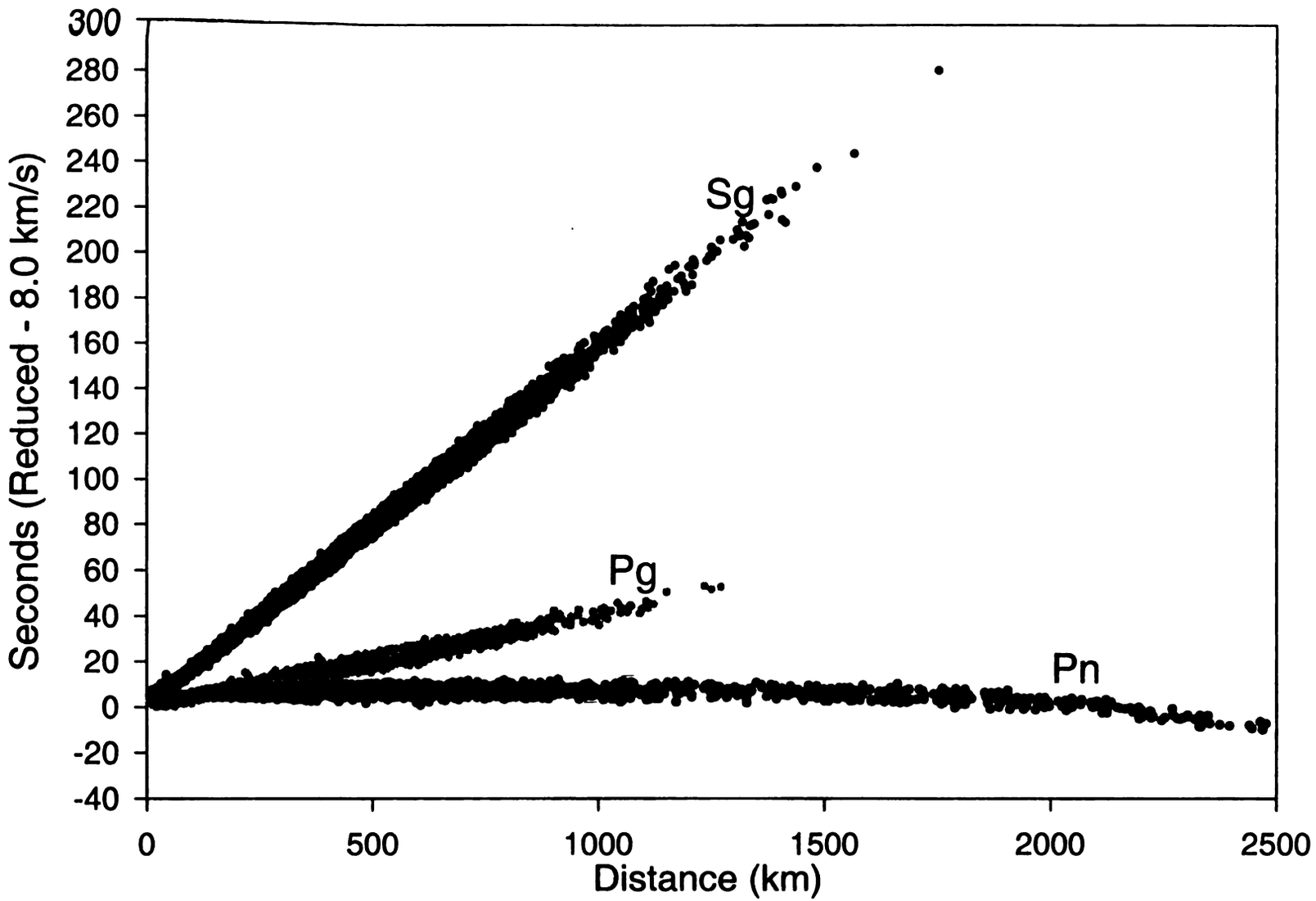

Figure 3-21. Composite regional reduced travel time curve for northeast Russia using hypocenter parameters from relocations. Sn data are omitted.

in all cells. Because each cell used distinct calibrated crustal velocities, the composite travel time curve is somewhat smeared, as it reflects all velocities used in the relocation process. Sn data are omitted, as they were not used in the relocation process. Travel time curves from individual cells better show the improvement obtained. Figures 3-22 and 3-23 compare travel time curves for individual cells in the Magadan and south Yakutia regions respectively. In each case, the level of scatter is reduced for all phases using the relocations, consistent with improved hypocenter parameters. The cells shown here are the same cells for which the 3-D velocity residual graphs are shown (Figures 3-10 and 3-11). Travel time curves from different cells can also be compared. Figure 3-24 compares travel time curves for the Magadan and South Yakutia cells, where the higher crustal velocities in the south Yakutia cell are evident.

FUTURE WORK

Without question, hypocenter parameters have been improved in this study, and the general knowledge of the regional crustal velocity structure has been expanded. However, there is still room for improvement of the hypocenter locations. This is particularly true in regions such as northern Yakutia, where there are large horizontal velocity gradients. In general, hypocenters located in regions of high velocity gradients will shift towards the higher velocity region, and there will be a bias in all the locations in that region. The best way to overcome this problem is to develop correction surfaces for each station that would account for the residuals introduced from differing velocities in all directions and at all distances (see Bondáir et al., 1998). Correction surfaces can be developed for both crustal and mantle phases.

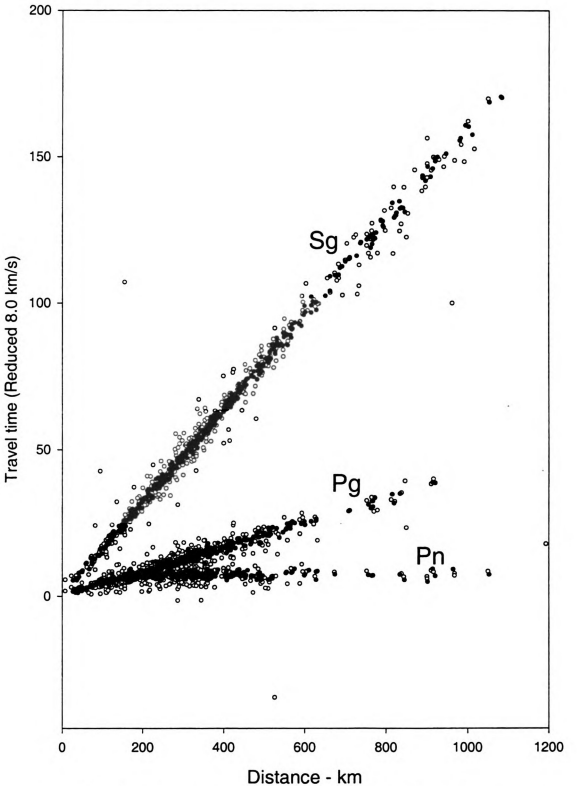

Figure 3-22. Travel time curve for the region 60-63°N x 145-150°E comparing original (open circles) with relocated event parameters (closed circles). Note the significant reduction in scatter of data points. Sn data are omitted.

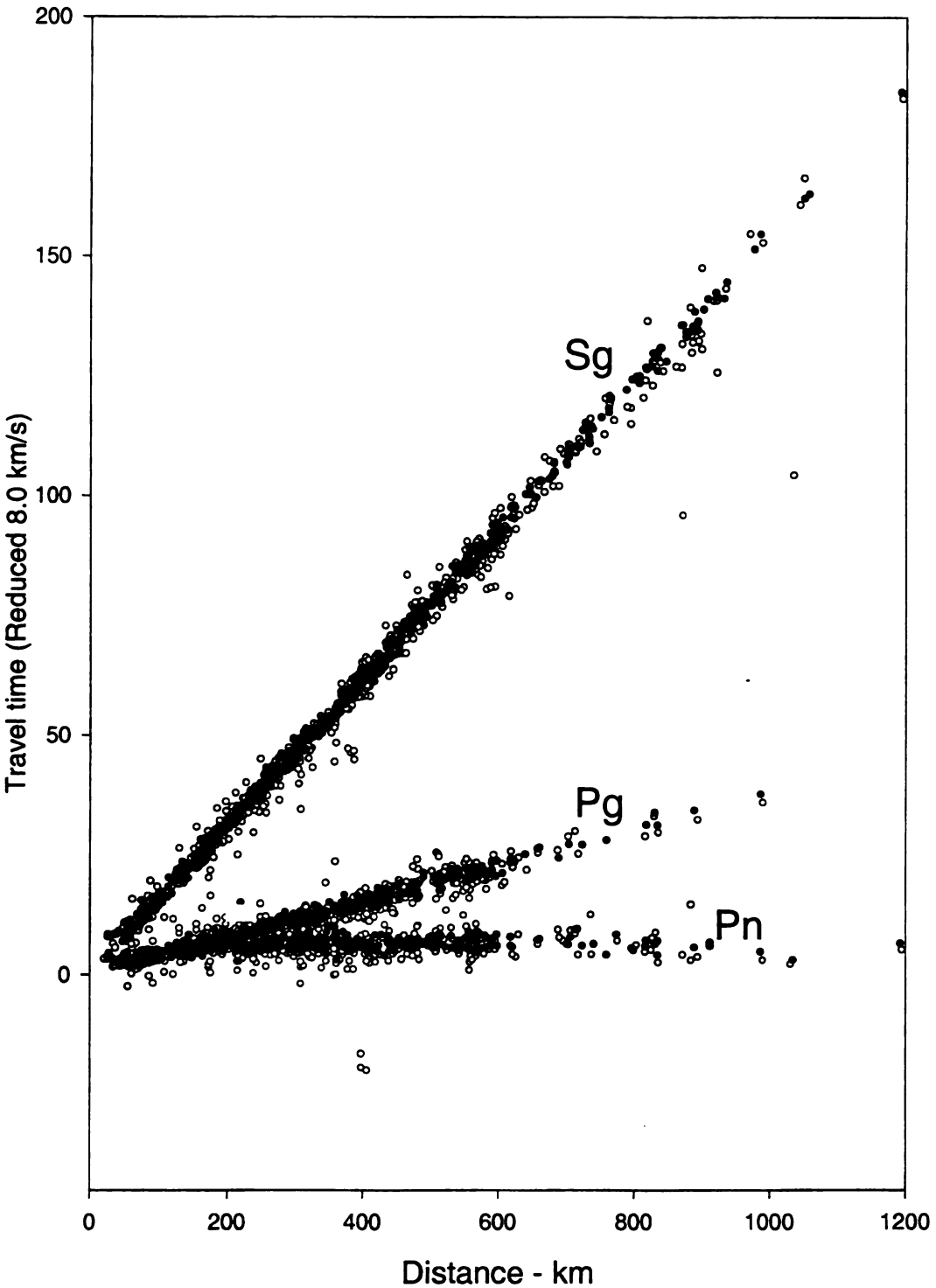

Figure 3-23. Travel time curve for the region 54-57°N x 125-130°E comparing original (open circles) with relocated event parameters (closed circles). Note the significant reduction in scatter of data points. Sn data are omitted.

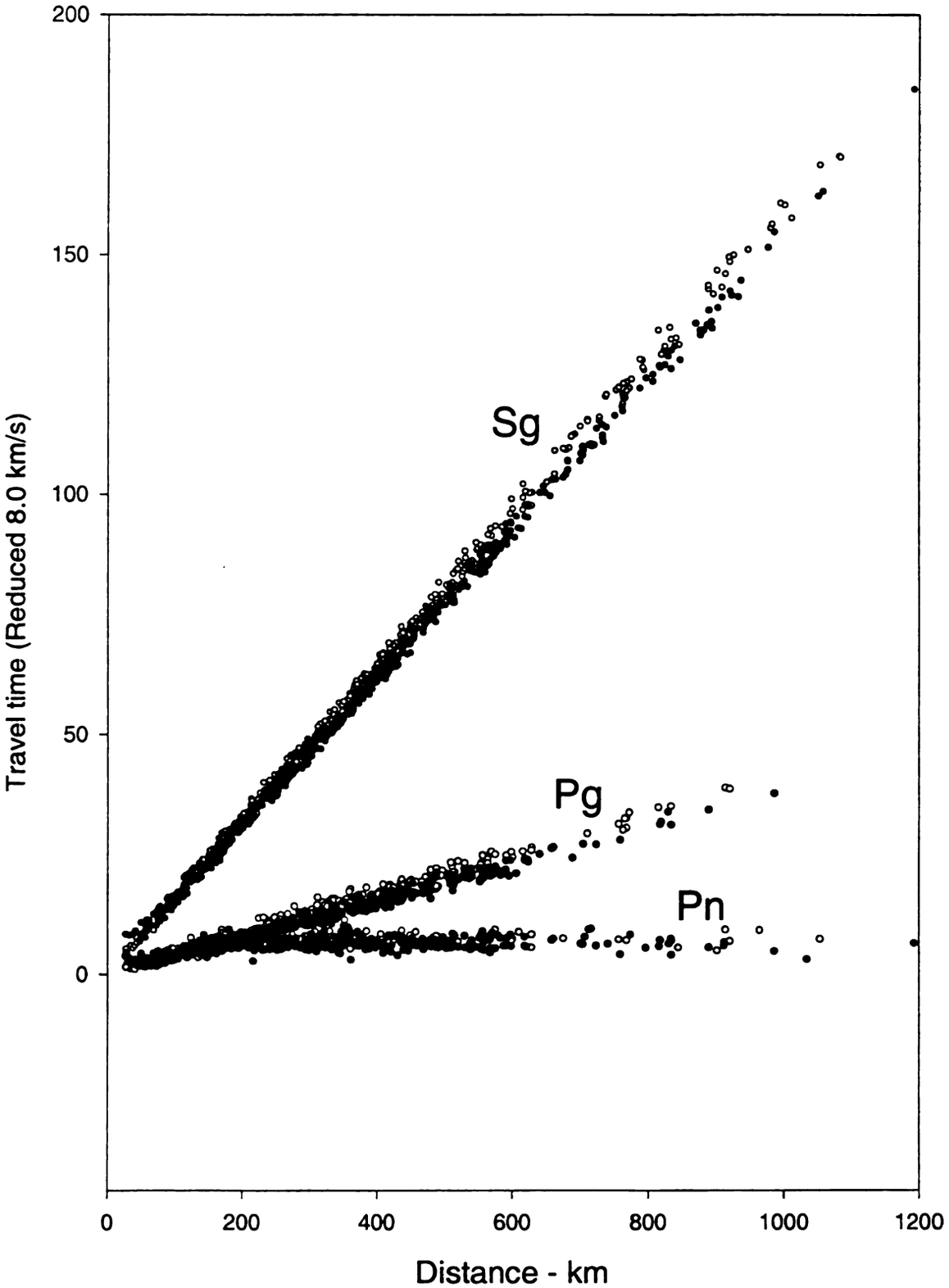

Figure 3-24. Travel time curve comparing the regions 60-63°N x 15-150°E (solid; Magadan) and 54-57° N x 125-130° E (open; south Yakutia). Note increased velocities for relocated events in south Yakutia. Sn data are omitted.

CONCLUSIONS

The earthquake relocation process used here has improved the quality of hypocenter locations over the original Russian determinations, as well as developed regionally calibrated, best-fit crustal velocity models. Regional crustal velocities determined are consistent with the known geologic and tectonic setting, with higher velocities associated with the Precambrian Siberian platform, and lower velocities associated with the Mesozoic terrane assembledges. Improvements in epicenter locations have clarified several seismicity clusters and fault lineations in northeast Russia.

REFERENCES

Bondáir, I., Yang, X., Wang, J., Bahavar, M., Israelsson, H., and McLaughlin, K., 1998, Tuning and calibration activities at the PIDC: *20th Annual seismic research symposium on monitoring a comprehensive test ban treaty (CTBT), proceedings*, p. 1-10.

Fujita, K., Cambray, F.W., and Velbel, M.A., 1990, Tectonics of the Laptev Sea and Moma rift systems, northeast USSR: *Marine Geology*, v. 93, p. 95-118.

Jeffreys, H., and Bullen, K.E., 1970, *Seismological Tables*: Office of the British Association, London, 50 pp.

Kennett, B.N.L., 1991, *IASPEI 1991 Seismological Talbes*: Research School of Earth Sciences, Australian National University, Canberra, 167 pp.

Mackey, K.G., 1996, *Crustal thickness of Northeast Russia*: M.S. Thesis, Michigan State University, ix + 102 pp.

Mackey, K.G., Fujita, K., and Ruff, L.J., 1998, Crustal thickness of northeast Russia: *Tectonophysics*, v. 284, p. 283-297.

Suvorov, V.D., and Kornilova, Z.A., 1985, Deep structure of the Aldan shield according to near earthquake data: *Soviet Geology and Geophysics*, v. 26 (2), p. 79-84.

Suvorov, V.D., Parasotka, B.S., and Chernyi, S.D., 1999, Deep seismic sounding studies in Yakutia: *Izvestia, Physics of the Solid Earth*, v. 35 (7-8), p. 612-629.

CHAPTER 4

Tomography of Northeastern Russia

INTRODUCTION

This chapter attempts to develop upper mantle Pn tomography models for northeastern Russia and associate velocity variations with the regional geology. Data used in the tomography are the Pn arrivals of the events relocated in Chapter 3. Of particular interest for tomographic study is the Laptev Sea and northern Yakutia region, where the boundary between the North American plate and Eurasian plate changes from extension to compression (Cook et al., 1986).

PREVIOUS WORK

The shallow velocity structure of northeastern Russia is essentially unstudied by tomographic methods. The only previous attempt of Pn wave tomography was done by Wallace and Tinker (1998). This study investigated the portion of Siberia between 70° E and 180° E using events recorded at 11 digital broadband stations installed in the 1990's (primarily IRIS stations). This study obtained 237 arrivals from 43 earthquakes in and around Siberia. Given the geographic size of the area and the small number of raypaths, conclusive results were not obtained.

METHODOLOGY

Tomography Code

The tomography used an expanded form of the time term method developed by Hearn (1984). The tomography code used was written by D. McNamara for investigating Pn tomography in the Tibetan Plateau (McNamara, 1995).

It is assumed that Pn is a head wave that propagates along the Moho. The Pn phase is therefore modeled as three segments: a segment in the upper mantle, one down going crustal segment below the event, and one up going crustal segment below the recording station (Figure 4-1). The travel time t can then be expressed by the time term equation

$$t = a + b + Ds \tag{4-1}$$

where D is the horizontal distance from the event and the station, s is slowness of the Moho, and a and b are the respective static time delays for the event and station (Hearn et al., 1991). The event and station delays (a or b) can be expressed as

$$delay = \int (s_c^2 - s^2)^{1/2} dz \tag{4-2}$$

where s_c is the crustal slowness profile as a function of depth (Hearn et al., 1991). For the tomographic study, the area of investigation is gridded into cells. A modified time term equation can then be used to estimate the slowness in each cell. The travel time for any individual raypath then becomes the sum of the crustal static delays plus the slowness of each cell multiplied by the path length traveled in each cell

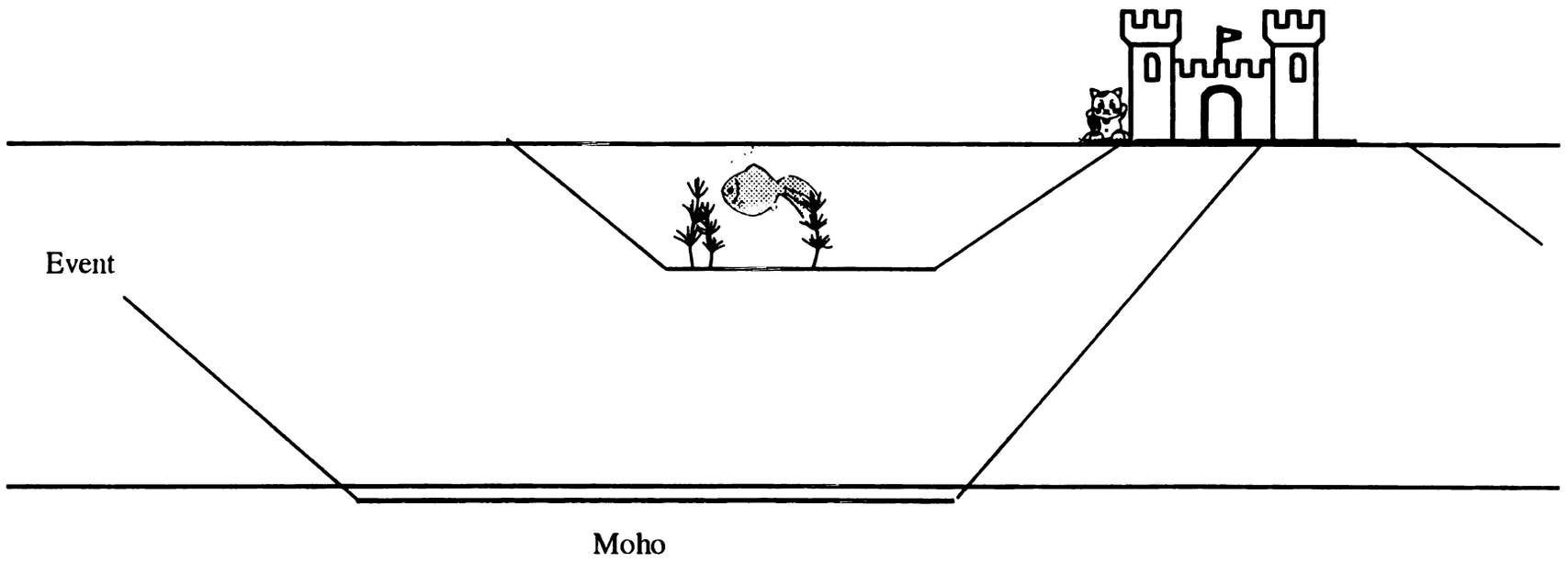

Figure 4-1. Pn is assumed to be a head wave propagating along the Moho. Static corrections are calculated for the event (downgoing leg) and the receiver (upgoing leg). The big moat around the station holds fish and lizards that are disturbed by the earthquakes.

$$t = a + b + \sum d_i s_i \qquad (4\text{-}3)$$

where d_i and s_i are the distance the ray travels and slowness in cell i, respectively. The sum is over all cells in which the ray travels (Hearn et al., 1991).

In this tomography code, assumptions are made regarding average crustal thickness, average crustal velocity and average Moho velocity. From these assumptions, the static corrections (mean Pn residual) associated with each event are determined, and new residuals are calculated. The event delays calculated are dependent on crustal thickness and velocity variations, as well as errors in hypocenter depth and origin time. The individual effects of these parameters will trade off with one another, thus the actual event statics cannot be interpreted in a meaningful way (Hearn et al., 1991).

Static corrections for receiving stations are next determined using the mean residuals for each station and new residuals are again calculated. Static corrections for the stations are primarily dependent on crustal velocity and crustal thickness. Crustal thickness can affect station statics the most (about 1 second per 10 km change in crustal thickness; Hearn et al., 1991), thus they can be interpreted as such. The affect of crustal thickness to station static delays is similar in concept to the alternate method of determining hypocenter depths in Appendix E.

Finally, using (4-3), cell slownesses are estimated from the weighted mean of the apparent slowness of all rays passing through each cell. The weighting for slowness in a given cell is the product of the rays traversing the cell, adjusted for the fraction of each rays total length that is included within the cell. In each iteration, the full residual remaining after the static corrections is applied to the Moho leg of the travel path. To remove any cells

with extreme slowness values due to poorly sampled cells, the model is smoothed between each iteration by averaging each cell with its eight neighbors. This is, in effect, the only dampening that occurs in the process. Once the new model is determined, an updated average Moho velocity for the entire study region is calculated. New residuals are again calculated based on the updated average Moho velocity and the process beginning with event static corrections is repeated until the data converge. Iterations are usually stopped when the change in RMS residuals from one iteration to the next becomes less than 1 % (McNamara et al., 1997).

Data Selection

Pn data selected for use must exclude misassociated Pg arrivals, and deeper penetrating P arrivals. There were several specific criteria used in the selection of useable Pn arrivals.

1. The Pg/Pn crossover distances in northeast Russia generally range between 100 to 150 km, thus misassociation of phases can be a serious problem (Pg arrivals reported as Pn) at close distances. Therefore, only Pn arrivals from a distance greater than 150 km are used. For distances between 150 and 350 km, Pn arrivals are excluded unless the Pg phase for the particular station and event is also reported. This should, in most cases, eliminate the misassociation problem. Pg arrivals are generally not misidentified as Pn at distances significantly beyond the crossover point (> 350 km). The minimum distance was changed in some model trials.
2. For distances greater than 350 km and up to 1,500 km, all reported Pn arrivals were selected. The maximum distance varied between 1,100 and 1,500 km for different

models calculated. Beyond 1500 km, the rays begin to penetrate deeper material and apparent velocities increase, thus are not suitable for Pn tomography. The maximum distance was changed in some model trials.

3. Pn arrivals with too high or too low apparent velocities were excluded to remove data outliers. The cutoff velocities varied from model to model.

4. Events with fewer than 2 Pn arrivals passing criteria one through three above are also excluded from the usable data as it is not reasonable to calculate event static corrections when there is only one recorded Pn phase. This was adjusted to three or four Pn arrivals in some models.

DISCUSSION

Initial models

The initial tomographic model developed used primarily the original Russian computed hypocenters and origin times. Some teleseismically recorded events for which Russian determinations are unavailable or of poor quality used hypocenter and origin time determinations from the ISC bulletin or the USGS Earthquake Data Report (EDR). The number of teleseismic events is small relative to regional events. Data used included only Russian stations reported in either the local bulletins, the ISC bulletin, or the EDR.

Pn arrivals with selection criteria one through three above are shown in the travel time curve in Figure 4-2. From the original database of Russian determined event parameters, a total of 6,437 Pn arrivals from 116 stations were selected from 1,624 events. The distance range for accepted arrivals was 150 - 1500 km. Arrivals with apparent

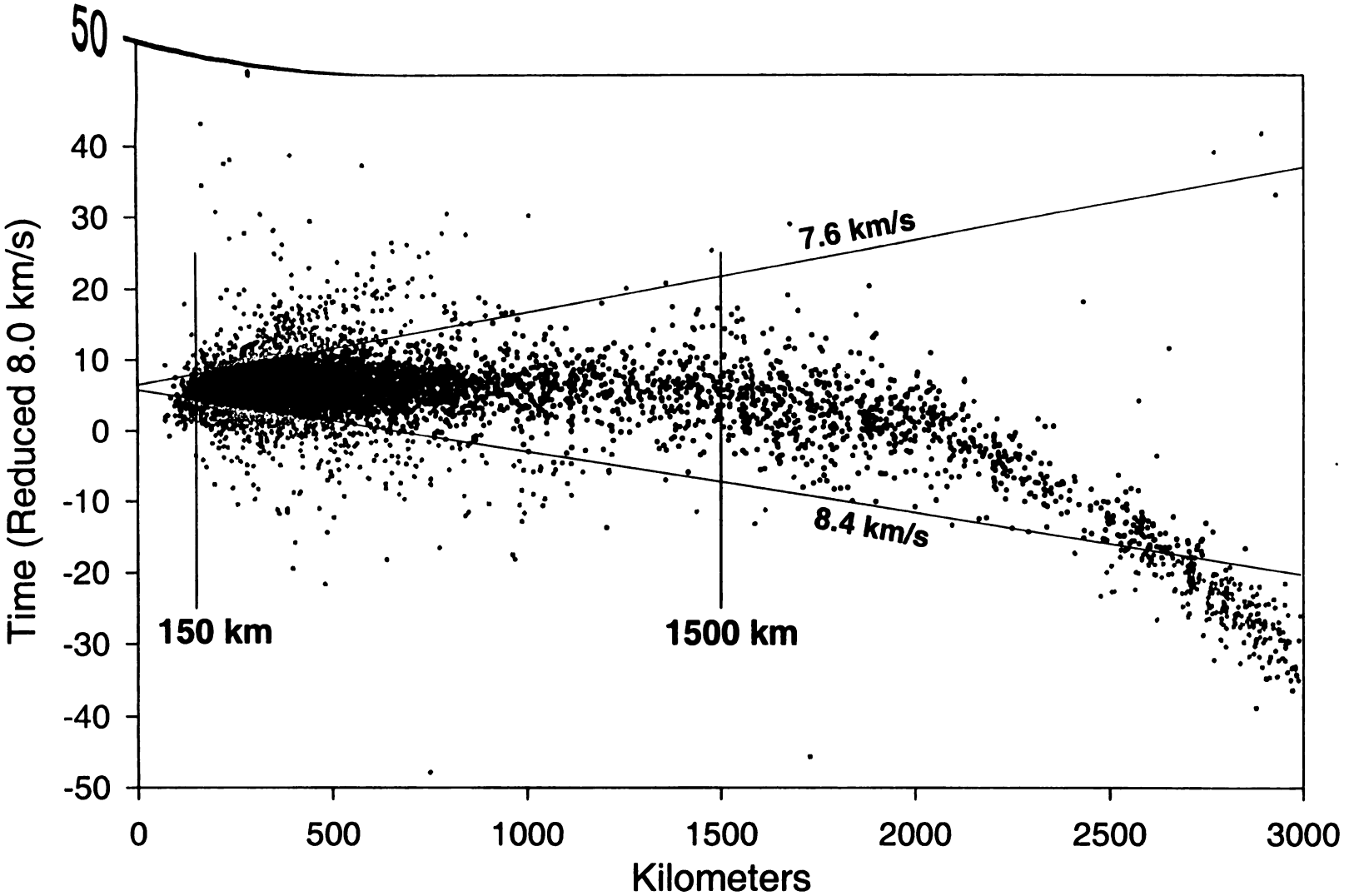

Figure 4-2. Pn arrivals based on original Russian hypocenters. Gray points fall outside the 7.4 km/s and 8.6 km/s velocity criteria and are not used. Vertical lines denote the accepted distance range of values used.

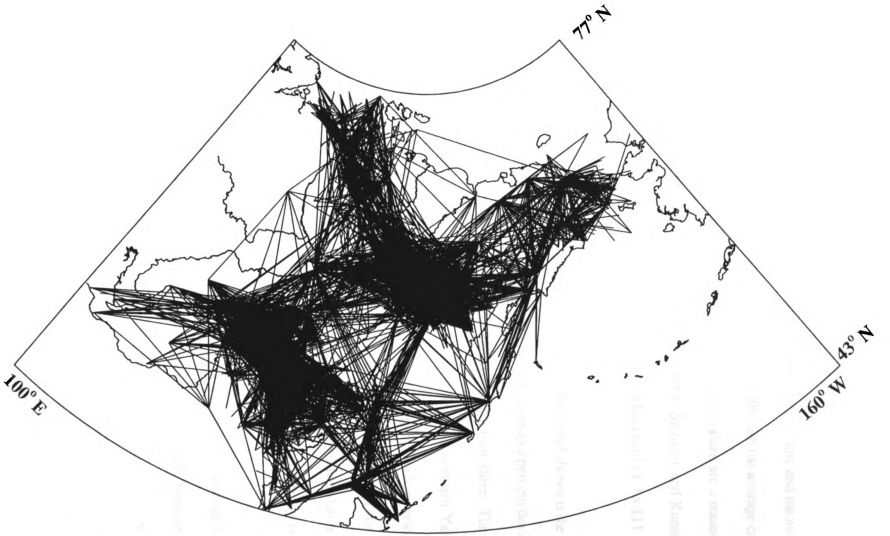

Figure 4-3. Raypath coverage for the preliminary tomography model using Russian hypocenters.

velocities greater than 8.6 km/s or less than 7.4 km/s were also excluded. The resulting raypath coverage from the selected arrivals is shown in Figure 4-3.

The average crustal thickness for the area was assumed to be 37 km, and the average Moho velocity 8.0 km/s (Mackey, 1996; Mackey et al., 1998). Although the average crustal thickness and Moho velocity are known to vary considerably, these values are a reasonable estimate for average values (Mackey, 1996; Mackey et al., 1998; Suvorov and Kornilova, 1985; Suvorov and Kornilova, 1986). Northeast Russia was gridded into 111.2 x 111.2 km square cells for the tomography.

The velocity model calculated is shown in Figure 4-4. The model shown is the third iteration computed. Contours on the model map velocity perturbations as a percent deviation from 8.02 km/s, which is the average Moho velocity calculated on iteration three. The most prominent feature is a large low velocity zone in the Laptev Sea and northern Yakutia, coincident with the Laptev Sea Rift. To the south and west of the Laptev Sea Rift, velocities increase on the Siberian Craton. Velocities decrease south of the Siberian Craton along the Eurasia - Amur plate boundary. The highest velocities are found in the Magadan region. Although the model calculated seems consistent with the tectonic setting, there are several potentially serious problems.

First, the RMS residual error for the model decreases only two iterations before beginning to increase (Figure 4-5). The model shown in Figure 4-4 is the third iteration, with the minimum RMS residual error. This indicates that the model does not converge readily. In addition, the overall decrease of the RMS residual error is from 0.957 to 0.901 seconds, or 5.9 %. This is significantly less than the average travel time residual reduction from 1.26

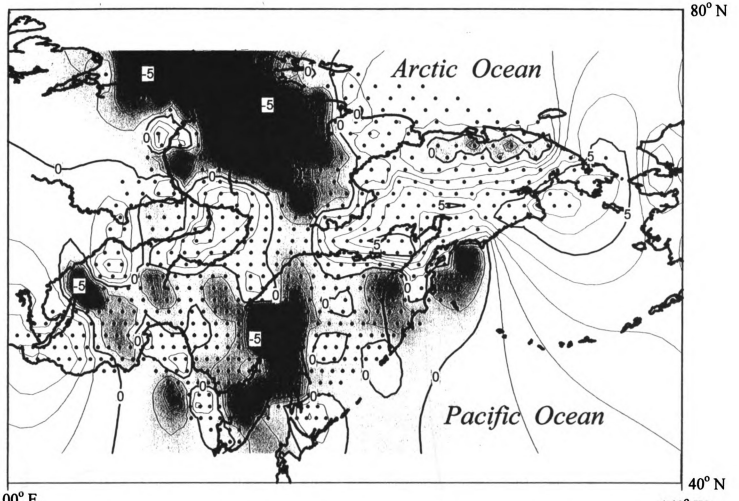

Figure 4-4. Pn tomography of northeastern Russia using Russian determined hypocenters. Contours of velocity perturbations are in percent deviation from 8.0 km/s. Points represent cell locations where perturbations were calculated. Rythmic appearance of contours in northern Yakutia are an artifact of the automated contouring.

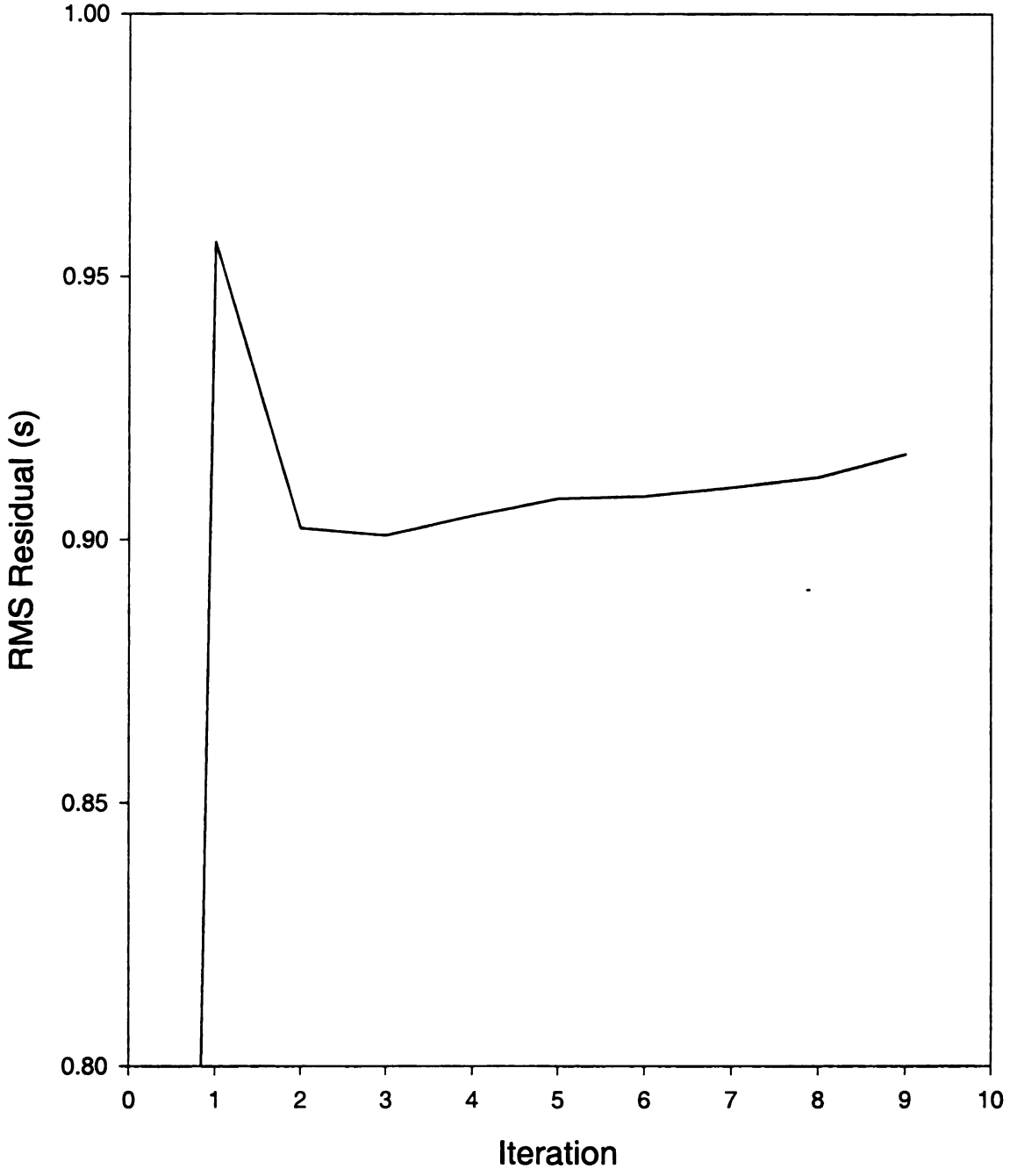

Figure 4-5. RMS residual vs. Iteration for tomography based on data from original Russian hypocenters. The minimum residual is on iteration 3.

to 0.55 seconds in 8 iterations for the study of the Tibetan Plateau (McNamara et al., 1997), which used the same code.

Second, as evident on Figure 4-6, a shift from higher velocities in the Magadan network to lower velocities in the Yakutsk correlates well with the network boundary. Different event location procedures used in the two networks probably introduces biases in hypocenter parameters that are being resolved by the tomography. In this region, the tomography may be mapping the seismic network boundary, and not perturbations in the velocity of the Moho.

Third, station static corrections are unreasonable, with static corrections ranging from minus 15 seconds to plus 12 seconds (Figure 4-7). This is an order of magnitude greater than that found in the Tibetan Plateau by McNamara et al. (1997). Although stations with the largest corrections are those with few arrivals, other stations supplying large amounts of data still show unreasonable static corrections. For example, Batagai, one of the Yakutsk network's best stations, has an unreasonable static offset of 6.7 seconds. The distribution of static corrections does show consistent polarities in the statics. In general, the Yakutsk network stations generally have negative static corrections, while the Magadan and Kamchatka networks consistently have positive station static corrections.

Models using relocations

Regional Model

The next study investigated Pn velocity of northeast Russia using 1,311 relocated events and their arrival times calculated in Chapter 3. For initial parameters, the average crustal thickness for the area was again assumed to be 37 km, and average Moho velocity is

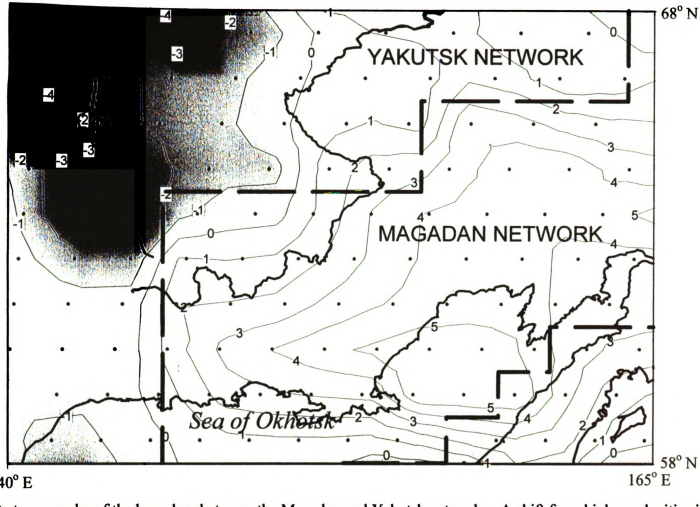

Figure 4-6. Pn tomography of the boundary between the Magadan and Yakutsk networks. A shift from higher velocities in the Magadan network to lower velocities in the Yakutsk network correlates with the network boundary. Different location procedures between networks may result in the tomography mapping the network boundaries and not real Moho velocity. Contours of velocity perturbations are in percent deviation from 8.0 km/s. Points represent cell locations where perturbations were calculated.

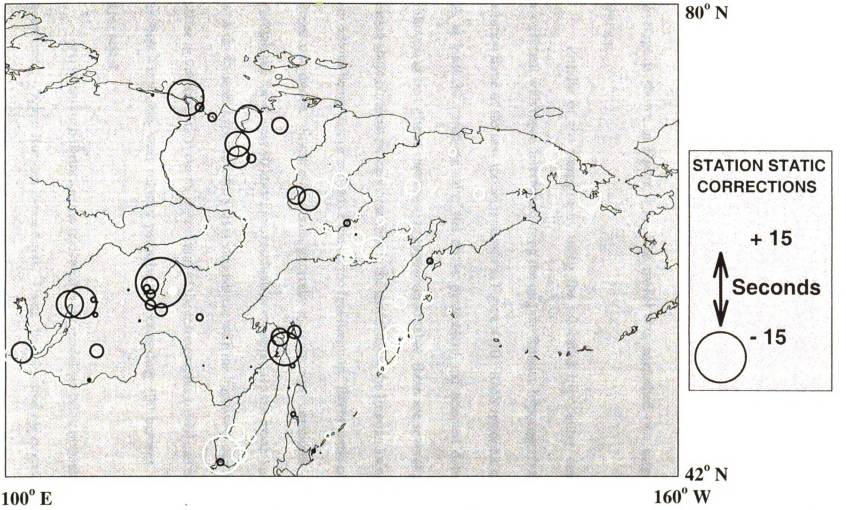

Figure 4-7. Station static corrections for tomography using original Russian hypocenters. Static corrections range from minus 15 seconds to plus 12 seconds.

8.0 km/s (Mackey, 1996; Mackey et al., 1998). Grid spacing was again 111.2 x 111.2 km square cells for the tomography. Data selected for use in the tomography have apparent velocities between 7.4 km/s and 8.6 km/s, and fall in the distance range between 150 and 1500 km (Figure 4-8). Removal of data outside these parameters results in the number of useable events being reduced to 1,066 having a total of 5,146 useable arrivals. Raypath coverage is shown in Figure 4-9. The model was smoothed two times between each iteration.

Results of the tomography using the relocated hypocenter determinations are inconsistent with those determined using the original Russian hypocenters discussed above. Iteration three of the new model is shown in Figure 4-10. RMS residuals drop consistently for at least 30 iterations using the above parameters and selected data (Figure 4-11). Although at first glance these results appear reasonable, there are several problems. First, station static corrections are worse than in the model using the Russian locations, with some corrections being tens of seconds even on the first iteration. Event static corrections are of similar magnitude. Static corrections generally increase with iterations. Although RMS residuals fall for at least 30 iterations, residuals never approach the lower values found when using the Russian hypocenters. This is inconsistent with the improved locations and reduced scatter in the travel time curve. Inspection of the tomographic model calculated on the 30th iteration show cells with velocity perturbations exceeding 100 percent, which is clearly nonsensical.

Perturbation polarities in the relocated event model are often opposite of those in the model using original Russian hypocenters. Using the relocated hypocenters, the Siberian Craton shows reduced velocities, while northern Yakutia shows higher velocities. Both

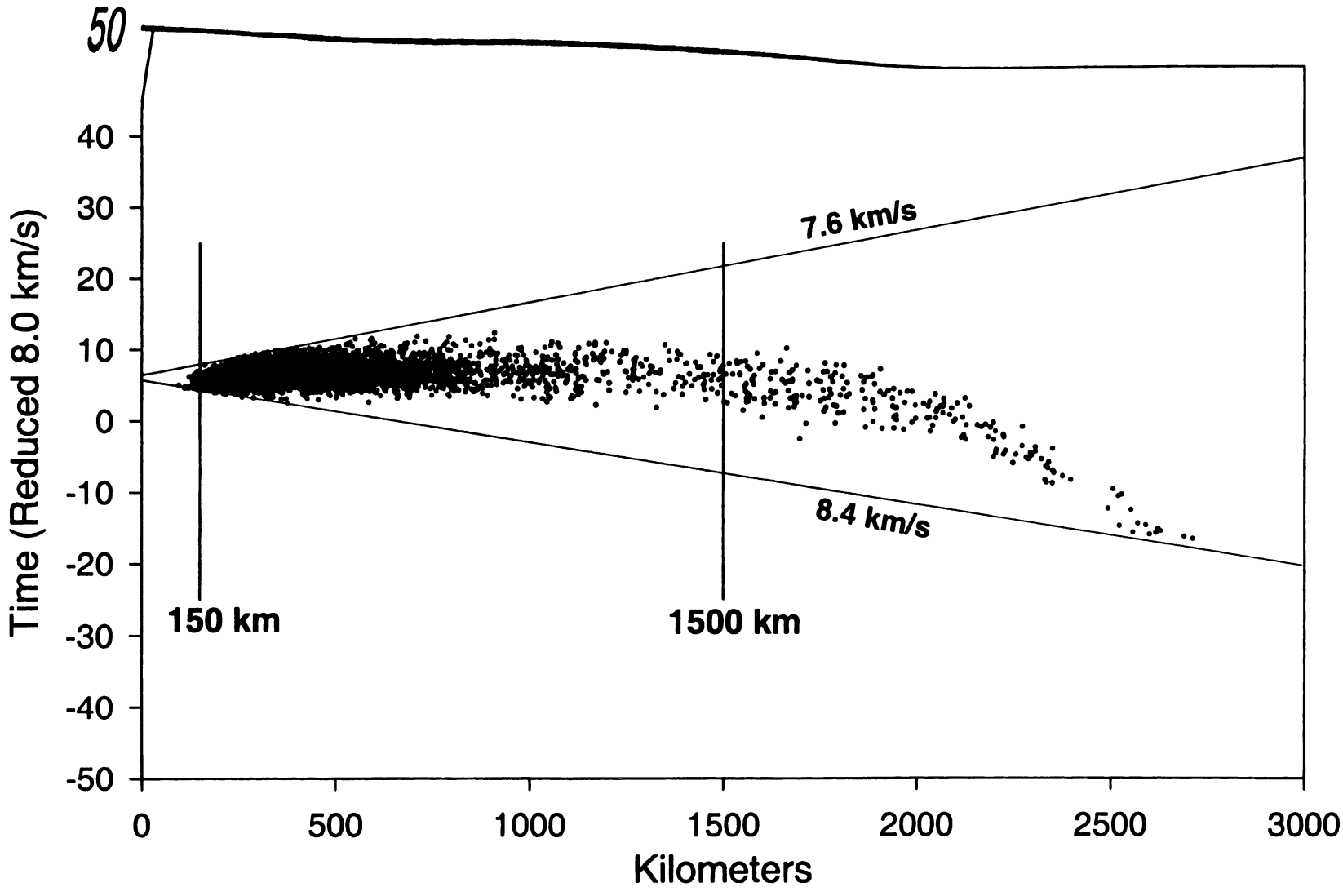

Figure 4-8. Pn arrivals based on relocated hypocenters. All points shown fall between the 7.4 km/s and 8.6 km/s velocity criteria. Vertical lines denote the accepted distance range of values used.

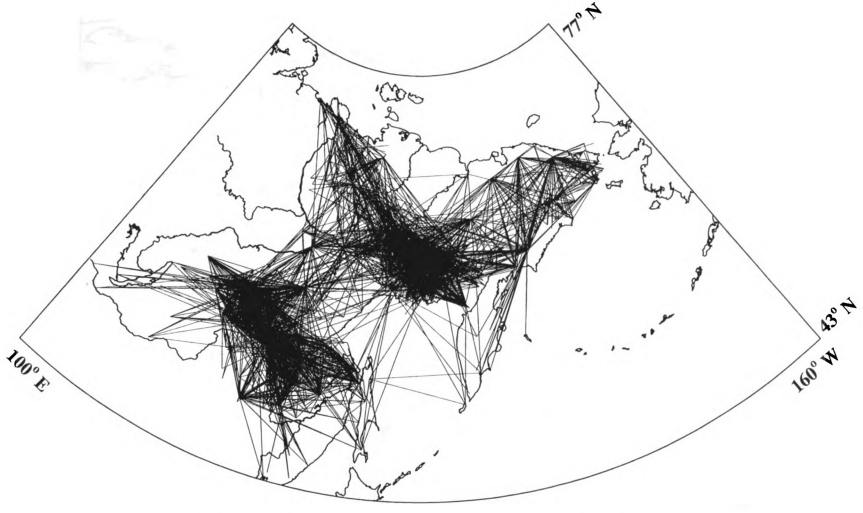

Figure 4-9. Raypath coverage for the tomography model using relocated hypocenters.

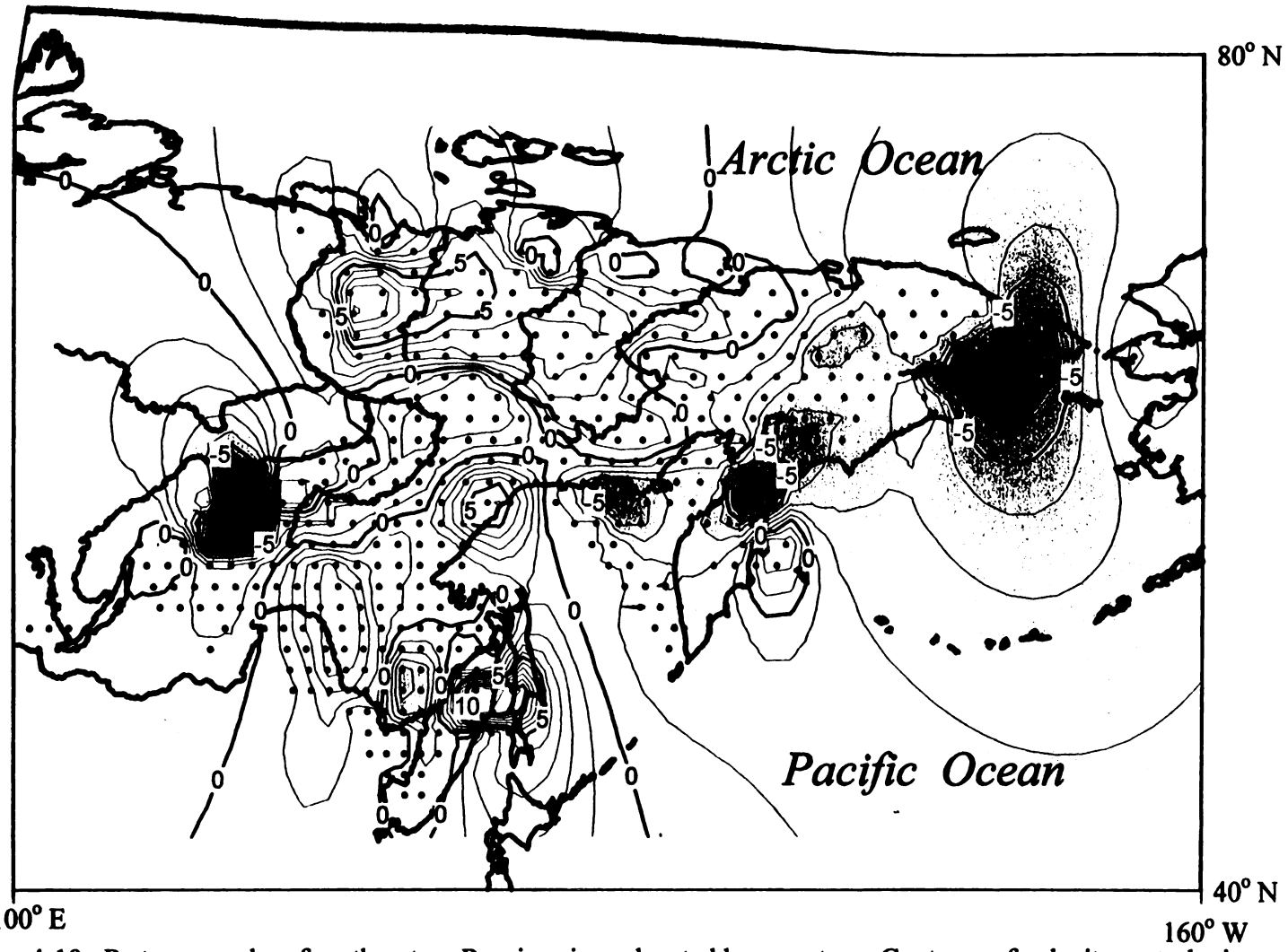

Figure 4-10. Pn tomography of northeastern Russia using relocated hypocenters. Contours of velocity perturbations are in percent deviation from 8.0 km/s. Points represent cell locations where perturbations were calculated.

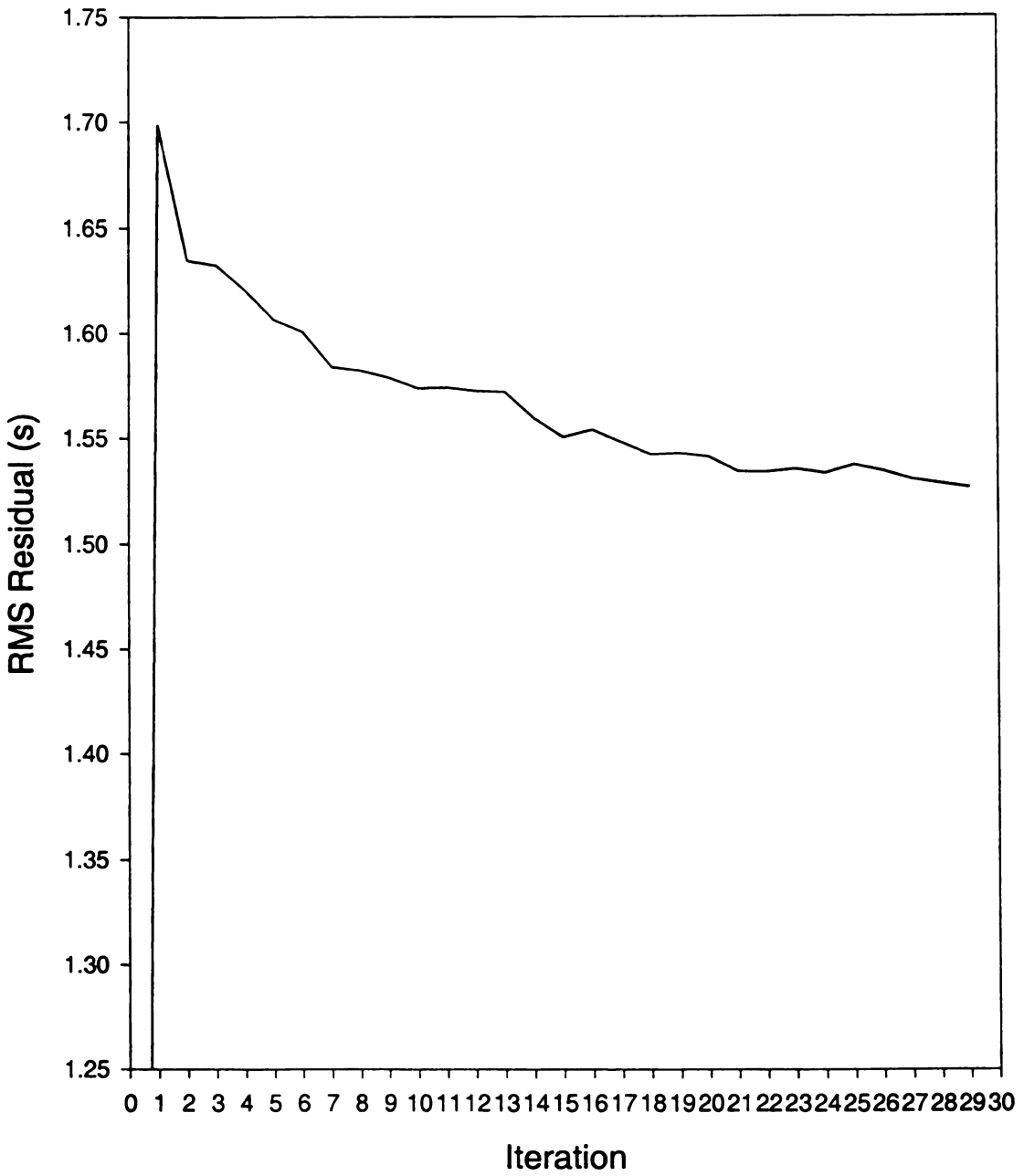

Figure 4-11. RMS residual vs. Iteration for tomography based on data from relocated hypocenters.

inconsistent with the known geology and tectonics. Many attempts were made to isolate the problem with the runaway static corrections, velocity perturbations, and higher than expected RMS residuals, including:

- Varying the range of acceptable velocities for data selection
- Changing the distance range for acceptable data
- Changing the number of smoothing passes between each iteration
- Changing the minimum number of Pn phases per event or station for usable data
- Varying the cell size used in the model
- Removal of some receiving stations
- Varying the assumed average crustal thickness
- Varying the assumed average Moho velocity

Variation of the above parameters yielded no improvements in the model. It is suspected that an odd distribution of events and several outlying stations results in a trade off between the event and station static corrections. The distribution of events and stations are such that the code is unable to solve for Moho velocities as static corrections applied are unreasonably large. Instead of the static corrections being reduced from iteration to iteration with more of the "time" going to perturb the Moho velocities, static corrections simply increase out of control. In one small experiment with the tomography code, several raypaths traversing an otherwise unsampled region of the Siberian Craton were intentionally added into the database. These arrivals all had known large negative residuals, which should map the area which the rays traveled through as having a higher velocity. This was essentially an attempt to force a solution in the areas sampled only by the added raypaths. The resulting model showed no high velocity perturbation where expected. The large negative residuals associated with these paths was apparently absorbed into the static corrections of the events and/or station.

Local Magadan Model

In an attempt to overcome the problem with many receiving stations lying on the edges of the raypath coverage and the associated trade off between station and event static corrections, a smaller region encompassing only events and stations in the western Magadan and central Yakutsk regions was studied. This model showed no drop in RMS residuals (Figure 4-12), and source static corrections varied tens of seconds, even on the first iteration. Receiver static corrections were of a reasonable magnitude, with most being less than an absolute value of 1.0 second.

CONCLUSIONS

The seismic phase data for northeastern has proven to be very difficult to use for the development of tomographic models with this code. In a general sense, the original Russian hypocenter locations seem to produce the most believable results, although significant problems remain. It is unclear why improved relocated hypocenters produce such poor tomographic models. It is possible that this tomography code has difficulty handling such a large area with such nonuniform event and station distributions, or raypaths at high latitudes.

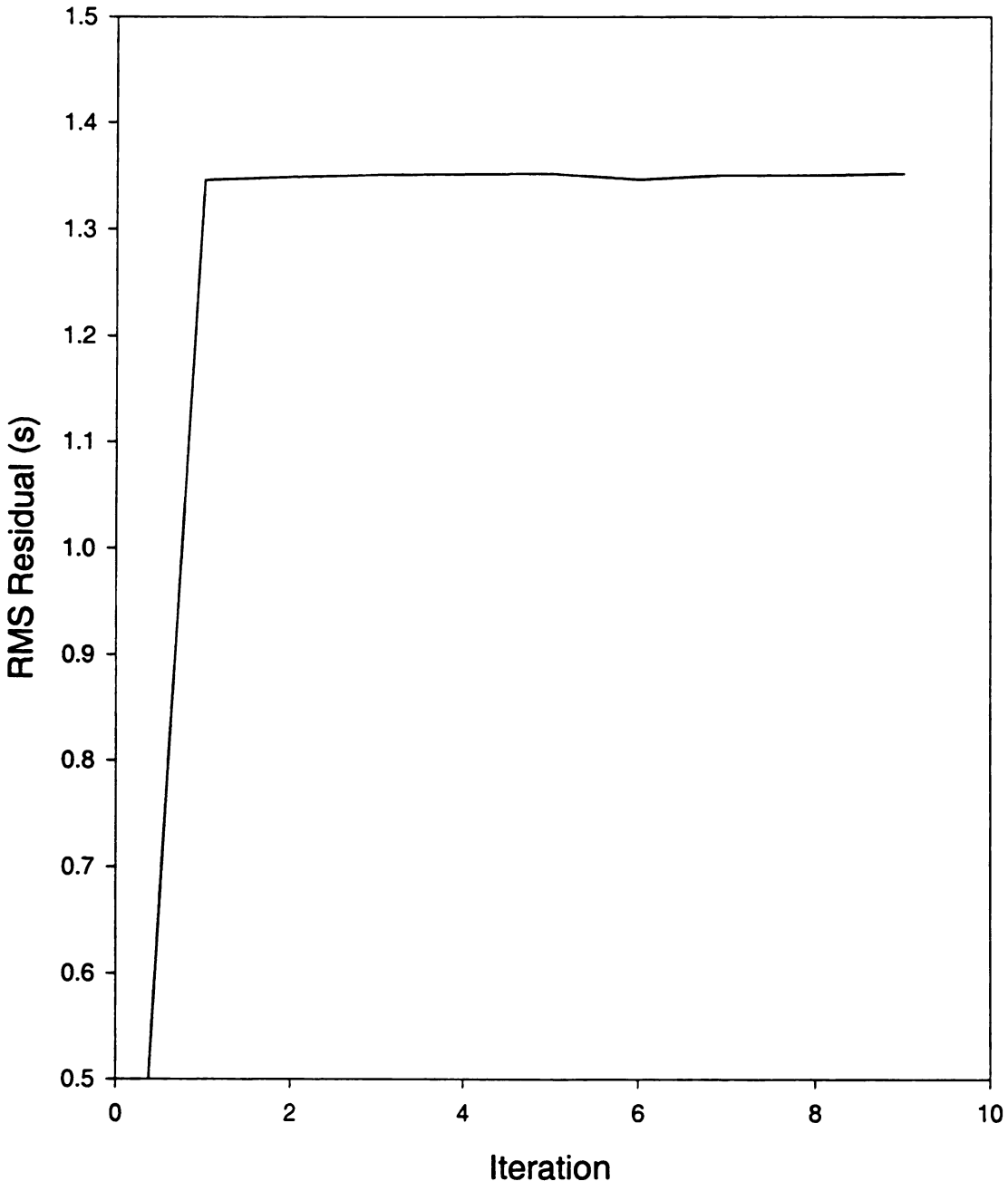

Figure 4-12. RMS residual vs. Iteration for tomography based on data from relocated hypocenters in the Magadan region.

REFERENCES

Cook, D.B., Fujita, K., and McMullen, C.A., 1986, Present-day plate interactions in northeast Asia: North American, Eurasian and Okhotsk plates: *Journal of Geodynamics*, v. 6, p. 33-51.

Hearn, T.M., 1984, Pn travel times in southern California: *Journal of Geopyhsical Research*, v. 89, p. 1843-1855.

Hearn, T.M., Beghoul, N., and Barazangi, M., 1991, Tomography of the western United States from regional arrival times: *Journal of Geopyhsical Research*, v. 96, p. 16,369-16,381.

Mackey, K.G., 1996, *Crustal thickness of Northeast Russia*: M.S. Thesis, Michigan State University, East Lansing, ix + 102 pp.

Mackey, K.G., Fujita, K., and Ruff, L.J., 1998, Crustal thickness of northeast Russia: *Tectonophysics*, v. 284, p. 283-297.

McNamara, D.E., 1995, *Lithospheric structure of the Tibetan Plateau*: PhD. Dissertation, University of South Carolina, x + 259 pp.

McNamara, D.E., Walter, W.R., Owens, T.J., and Ammon, C.J., 1997, Upper mantle velocity beneath the Tibetan Plateau from Pn travel time tomography: *Journal of Geopyhsical Research*, v. 102, p. 493-505.

Suvorov, V.D., and Kornilova, Z.A., 1986, Thickness of the earth's crust in the southeastern Verkhoyana-Kolyma fold system (according to near earthquakes): *Tikhookeanskaya Geologiya*, n. 4, p. 32-36 (in Russian).

Suvorov, V.D., and Kornilova, Z.A., 1985, Deep structure of the Aldan Shield according to near earthquake data: *Geology and Geophysics*, v. 26 (2), p. 79-84.

Wallace, T.C., and Tinker, M.A., 1998, Seismic characterization of Siberia: in *Proceedings of 20th annual symposium on monitoring a comprehensive test ban treaty (CTBT)*, Santa Fe, New Mexico, p. 536-541.

CHAPTER 5

Seismicity of the Bering Strait Region: Evidence for an Independent Bering Sea Plate

INTRODUCTION

Within North America, the Bering Strait region is one of the most poorly studied regions with a moderate to high level of seismic activity. Between 155° W and 180° W, and north of 64° N, at least one magnitude 7, eight magnitude 6, and tens of magnitude 5 events have occurred this century. For a comparable time period, the seismicity is more than an order of magnitude greater than the New Madrid zone. Prior to the political opening of the eastern Soviet Union, the international boundary between Alaska and Chukotka was closed to seismological data exchanges, thus seismicity maps of either side of the Bering Strait were incomplete because only Soviet or western data were used. New cooperation has allowed data sets to be combined, and the region to be viewed as a whole to better understand the regional seismicity and tectonic framework (Figures 5-1 and 5-2). Compilation of the existing data sets (Chapter 1) produces a seismicity map which outlines a proposed Bering plate. Focal mechanism data indicate that there is northeast-southwest extension in the Bering strait, right-lateral strike-slip motion in western Chukotka and the Gulf of Anadyr', and northwest directed thrusting in the Koryak Highlands. These motions, along with geological evidence presented below, support the existence of a Bering Plate rotating clockwise about an Euler pole in western Chukotka (Figure 5-3).

The existence of a Bering plate has been proposed previously by several workers. Ever since the first global plate motion inversion (Minster et al., 1974), there have been

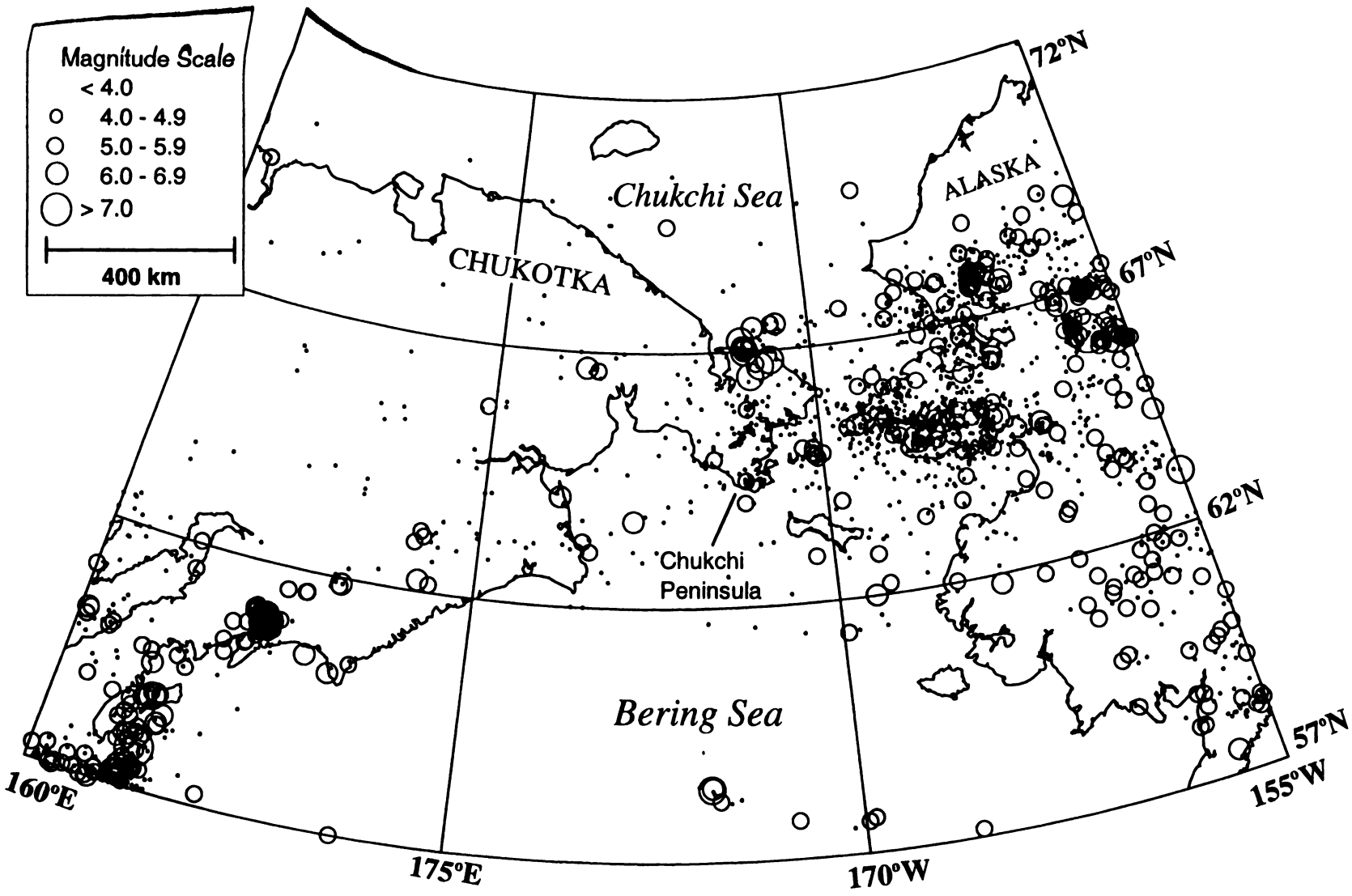

Figure 5-1. Seismicity map of the Bering Strait region.

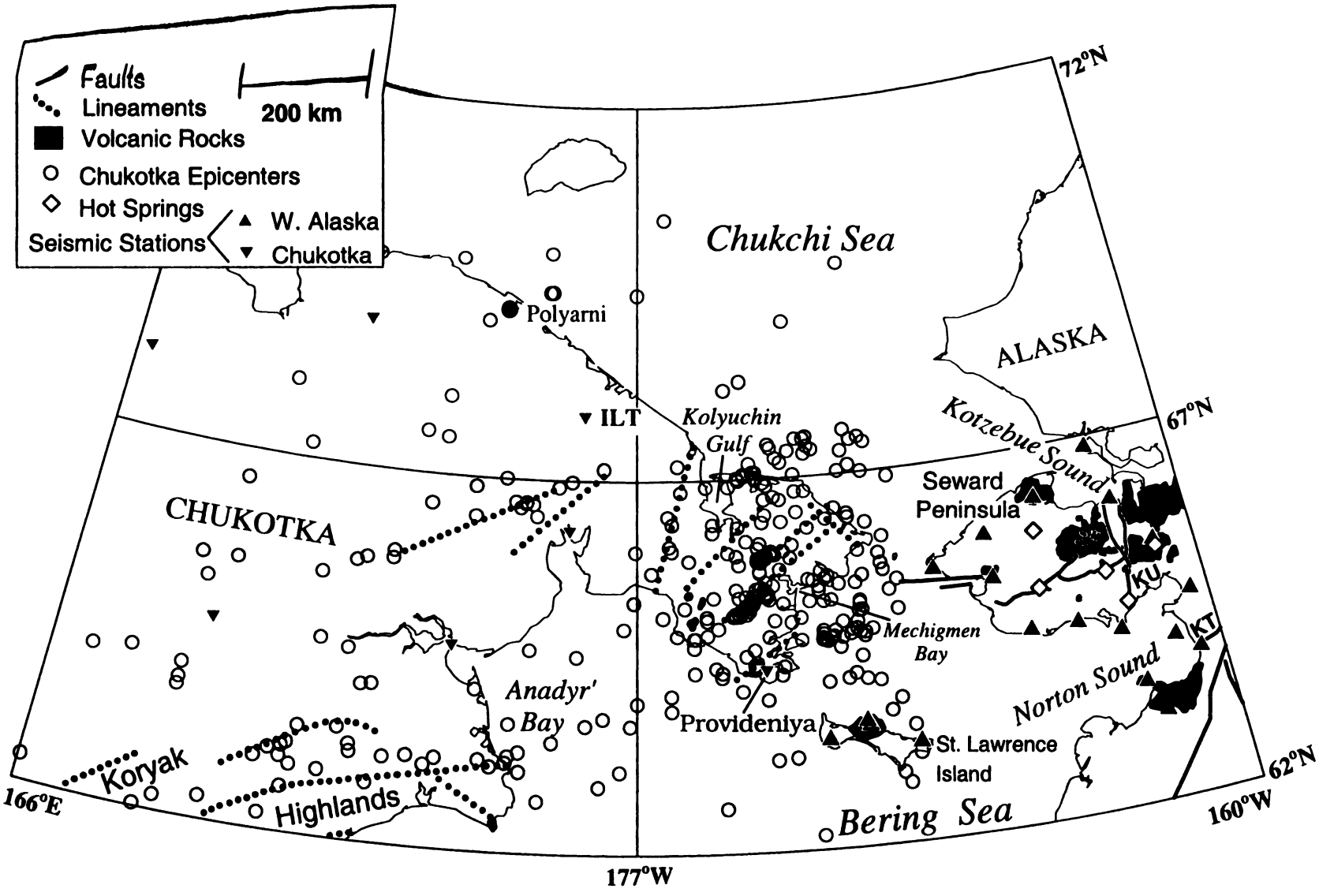

Figure 5-2. Neotectonic and index map of the Bering Strait region. Labeled faults are Kaltag (KT) and Kugruk (KU).

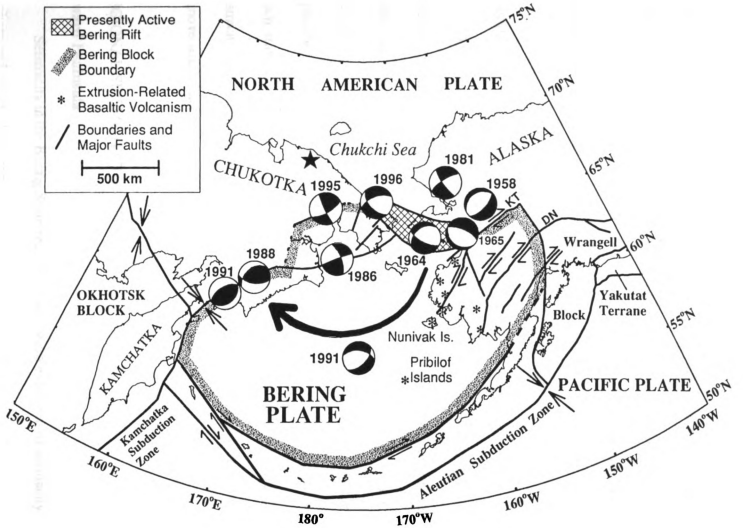

Figure 5-3. Regional tectonics of the Bering Plate, with representative focal mechanisms. Star denotes Euler pole.

various suggestions of a Bering plate. Although the reason that required Minster et al. (1974) to introduce a Bering plate (misfit of slip-vectors on the Aleutian Trench) has been shown to be erroneous (Engdahl et al., 1977), the seismicity of interior Alaska has allowed this proposal to continue (e.g., Stone, 1983). A Bering plate, nearly identical in regional extent to that proposed here, was also proposed recently by Lander et al. (1996) to explain the seismicity of the Koryak Highlands. However, no other supporting evidence was provided and it was not placed in a regional tectonic context.

SEISMICITY MAP

The Bering Strait seismicity map (Figure 5-1) is a compilation of epicenters, some relocated, from earthquakes recorded teleseismically and by regional networks in eastern Russia and western Alaska. A detailed discussion of the data used is given in Chapter 1. Relocations were performed for some of the larger historic earthquakes. For the event of September 7, 1933, the relocated epicenter varied nearly 1000 kilometers depending on which stations were used in the location process. This event was excluded from the seismicity map (Figure 5-1). A few other events originally located in this region were found to move south into the Aleutian subduction zone.

REGIONAL SEISMOTECTONICS AND GEOLOGY

Seward Peninsula

Seismicity in the Bering Strait region is a westward extension of seismicity from the northern end of the Alaska subduction zone (Figure 5-1). In western Alaska there are a few areas where the seismicity concentrates along specific lineaments, but in general the

seismicity tends to form diffuse zones. The heaviest concentration of seismicity in western Alaska is in the southern half of the Seward Peninsula. To the east of the Seward Peninsula, seismicity appears to extend almost to the Kaltag fault at the Yukon River, although there is a decrease in seismicity at the Kugruk fault zone. This does not seem to be due to station distribution, as several Western Alaska network stations operated in the immediate vicinity. North of the Seward Peninsula, seismicity occurs primarily in Kotzebue Sound. The apparent lack of seismicity in the eastern Chukchi Sea may be an artifact of seismic station distribution in the Western Alaska network. To the south of the Seward Peninsula is Norton Sound. Norton Sound is relatively free of seismicity compared to the southern half of the Seward Peninsula. Several seismic stations of the Western Alaska network were deployed in the vicinity of Norton Sound, thus the lower levels of microseismicity are likely real.

In the Seward Peninsula, focal mechanisms indicate that the region is under northeast-southwest extension (Biswas et al., 1983, 1986; Liu and Kanamori, 1980; Figure 5-3; Table 5-1). Focal mechanisms east of the Seward Peninsula show a mix of normal faults of various orientations indicating generally north-south extension and right-lateral strike-slip faulting (Figure 5-3; Estabrook et al., 1988). Focal mechanism solutions for the magnitude 7.3 Huslia event of 1958, the largest event in the region, indicate normal faulting, generally with northwest to southeast tension (Ritsema, 1962; Biswas, 1983; Wickens and Hodgson, 1967, and others; Table 5-1; Figure 5-3), although the nodal planes vary significantly among the different solutions.

An east-west striking rift across the southern Seward Peninsula was proposed by Turner and Swanson (1981), and is consistent with the north-south extension indicated by these focal mechanisms (Biswas el al., 1983). There is considerable evidence for the

Table 5-1. Focal mechanisms for western Alaska and Chukotka. Mechanisms are listed from west to east. Those followed by an asterisk are plotted on Figure 5-3.

Date	Lat.	Long.	Mag	Plane 1	Plane 2	Method	Reference	
85 09 10	60.43	168.86	5.6	072 46 136	196 60 53	CMT	HRV	
91 04 27	60.78	166.87	5.4	258 49 148	011 66 45	CMT	HRV	
91 03 08	60.86	167.02	6.7	037 34 84	224 56 94	CMT	HRV	*
92 07 17	60.86	167.32	5.3	333 47 18	230 77 136	CMT	HRV	
97 01 03	61.07	167.40	5.7	358 16 149	119 82 77	CMT	USGS	
88 10 13	61.85	169.65	5.7	070 53 164	170 77 39	CMT	HRV	*
				086 58 130	217 42 48	P	MSU	
95 10 02	66.69	179.14	5.1	055 71 170	148 81 19	CMT	HRV	*
86 10 19	63.90	-178.69	5.3	336 68 4	245 86 158	CMT	HRV	
				323 50 28	216 69 137	P	MSU	*
91 02 21	58.43	-175.45	6.6	276 52 -52	045 52 -128	CMT	USGS	*
71 10 05	67.38	-172.57	5.2	267 55 -145	142 50 -40	SYN	MSU	
96 10 24	67.13	-172.84	6.0	251 60 -138	136 54 -38	CMT	HRV	*
COMPOSITE	65.9	-166.2		319 50 -52	088 54 -126	P	BIW	
64 12 13	64.88	-165.75	5.3	240 36 -143	124 69 -58	P	BIW	*
66 08 26	66.71	-162.7	5.0	280 84 -170	190 80 -5	P	COL	
COMPOSITE	65.0	-162.0		102 16 -150	330 80 -11	P	BIW	
81 07 12	67.71	-161.20	6.2	154 79 -17	247 73 -168	CMT	HRV	*
				096 21 -108	296 70 -84	P	BIW	
65 04 16	64.69	-160.23	5.8	305 66 -93	137 25 -82	SYN	LIU	*
73 04 11	64.61	-160.04	4.2	250 70 -60	010 35 -144	P	COO	
58 04 13	65.82	-155.65		341 79 -65	095 29 -154	P	BAL	
58 04 07	66.03	-156.59	7.3	058 64 -95	250 26 -80	PS	RIT	*
				072 66 -78	222 27 -116	P	WIC	
80 10 14	66.93	-155.17	4.3	124 66 178	214 88 24	P	GED	
80 10 06	66.97	-155.15	4.6	243 81 169	335 79 9	P	EST	
80 10 06	66.86	-155.05	4.2	124 85 -163	031 73 -5	P	GED	

References are: BIW- Biswas, 1983; COL - Coley, 1983; HRV - Harvard Moment Tensor; USGS - USGS Moment Tensor; LIU; Liu and Kanamori, 1980; COO, Cook, 1988; WIC - Wickens and Hodgson, 1967; EST - Estabrook, 1988; GED - Gedney and Marshall, 1981; BAL - Balakina, 1962; RIT, Ritsema, 1962; MSU - Fujita (pers. comm.).

existence of this rift. There is a series of generally east-west striking Quaternary normal faults offset by short north-south striking strike-slip faults, which is similar to basin and range type extension (Plafker et al., 1993). In addition, sediment filled grabens as much as 1.2 km deep, hot springs (Turner and Swanson, 1981; Till and Dumoulin, 1994), and Quaternary and older late Cenozoic basaltic volcanism have been mapped (generally < 5.8 Ma; e.g., Moll-Stalcup, 1994). South of the Seward Peninsula, east-striking faults of Pleistocene age have been identified in central Norton sound (Plafker et al., 1993) and young (1.5-0.2 Ma) cinder cones on St. Lawrence Island also form an east trend (Moll-Stalcup, 1994) indicating north-south tension. Northeast-southwest extension is also in agreement with the predicted orientation of the T-axis as obtained from geologic indicators in the region (Nakamura et al., 1980; Estabrook and Jacob, 1991). North of the Seward Peninsula, sedimentary basins underlie Kotzebue Sound and the eastern Chukchi Sea where late Cenozoic normal faults abound (Tolson, 1987). Refraction profiles conducted in 1994 through the Bering strait by the R/V Ewing show a slightly elevated Moho, at a depth of 30-35 km, through the Bering Strait (Allen et al., 1995). This elevated Moho is also consistent with crustal gravity modeling of the Bering Strait (McCaleb et al., 1998). Thus, throughout the Seward Peninsula region, there is widespread evidence for young (<6 Ma) crustal extension. The extension in the Bering Strait-Seward Peninsula region may have originated with the post-orogenic collapse of the crust in the mid-Cretaceous and the formation of gneiss domes in the Seward Peninsula (Miller and Hudson, 1991; Dumitru et al., 1995) and reactivated at ca. 6-10 Ma. To the east, the presently active right-lateral Kobuk fault (Estabrook et al., 1988) may link with the Seward rift system.

Chukchi Peninsula

From the Seward Peninsula, seismicity continues further west across the Bering Strait and into and off the north coast of the Chukchi Peninsula. Four large earthquakes with magnitudes of 6.2 - 6.9 occurred near Kolyuchin Gulf (Figure 5-2) in 1928. The most recent large event in this region was a magnitude 6.0 in October, 1996. The Harvard centroid moment tensor (CMT) for this event indicates normal faulting with northeast to southwest extension (Figure 5-3), assuming the preferred fault plane is parallel to the edge of Hope basin. A magnitude 5.5 event occurred in this region in 1971, for which Fujita and Koz'min (1994), and Biswas et al. (1986) proposed a focal mechanism with fault plane solutions nearly perpendicular to those of the 1990 event. These mechanisms were constrained by Alaskan network first motion data, which are emergent and could be erroneous. The event is poorly recorded, however, short-period synthetic seismograms calculated using the method of Kroeger (1978) for several stations are consistent with a mechanism nearly identical to the 1996 event (R. McCaleb, pers. comm.; Figure 5-4; Table 5-1). An additional event occurred in the region in 1962. Because the teleseismic P-wave first motion data and waveform characteristics are similar between the 1971 and 1962 events (Fujita and Koz'min, 1994) it is likely that the 1962 event has a similar transtensional mechanism.

The geology of Chukotka is less well known. Russian geophysical data suggest a fault bounded trough just offshore of Kolyuchin Gulf (Aksenov et al., 1987), which may be a portion of a much larger Cenozoic rift system that covered the southern Chukchi Sea (Shipilov et al., 1989). The rift system terminates roughly at the meridian of Kolyuchin Gulf and there is no indication in the published Russian literature that these grabens extend further to the west. Since there is also no seismicity west of the gulf, it appears either that the rift

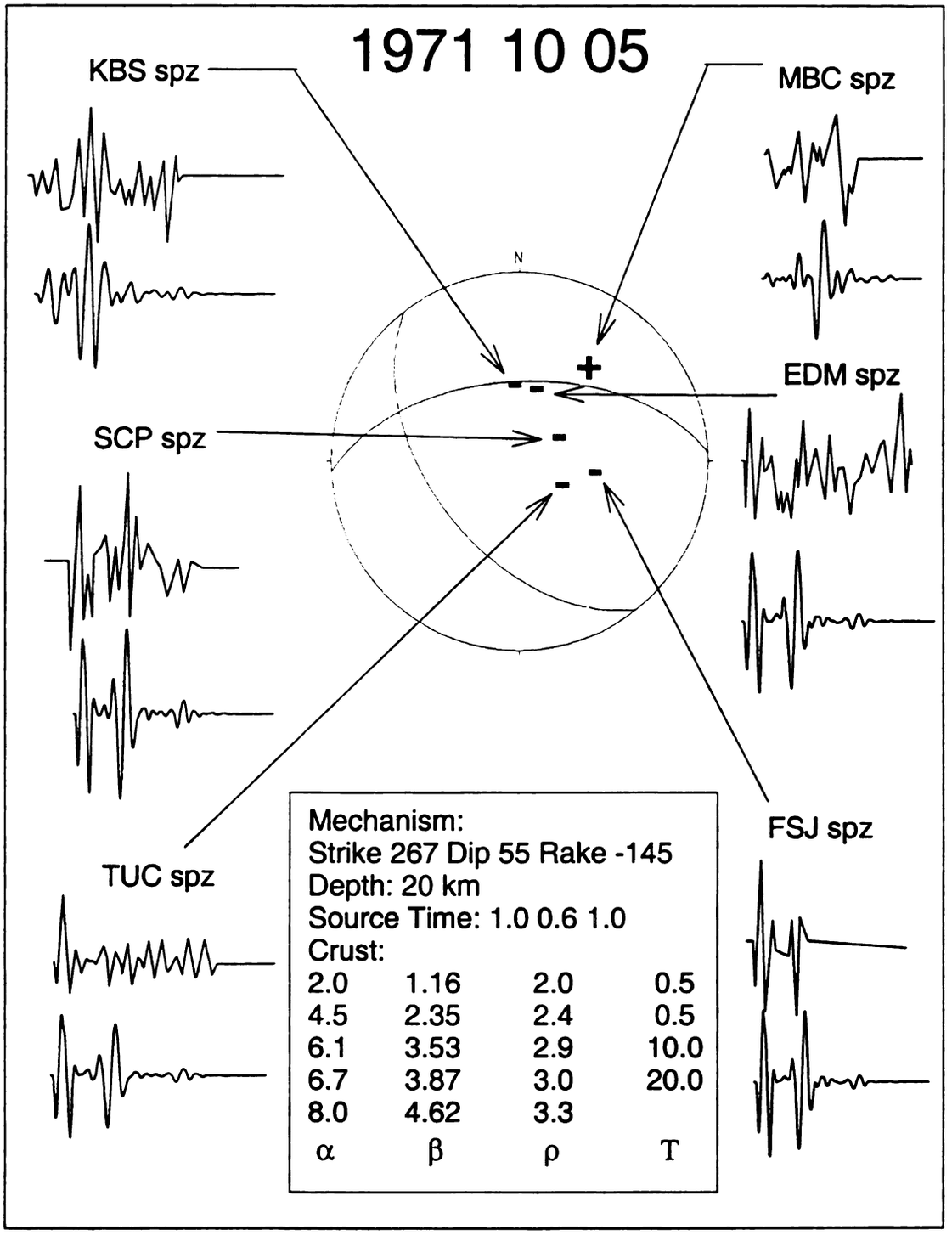

Figure 5-4. Focal mechanism and synthetic seismograms from the October 10, 1971 Chukchi earthquake (R. McCaleb, pers. comm.). Top traces show actual digitized records, while bottom traces show synthetics. All digitized records are short-period vertical components from the stations indicated.

system ends at the gulf or that any segment west of the gulf is now inactive. A fault-bounded topographic lowland termed the Kolyuchin-Mechigmen graben (Pol'kin, 1984) extends from the southern end of Kolyuchin Gulf, east through the Chukchi Peninsula, to Mechigmen Bay. The graben is asymmetric with a steeper and higher northern side, and the faults are expressed in geophysical fields (Pol'kin, 1984). The southeastern end may be offset further to the south but there is no clear topographic basin. It is possible that the upper Ioniveem valley and the lowlands north of Yanrakinot represent an incipient rift.

Russian geophysical investigations using both seismic reflection and potential fields have identified additional faults off the north coast of Chukotka and in the Bering Strait region (Aksenov et al., 1987; Shipilov et al., 1989). Those of northwest and northeast strike, i.e., parallel to the northern and Bering Strait coasts of the Chukchi Peninsula, are thought to be normal faults (Aksenov et al., 1987). Re-leveling studies (Zolotarskaya et al., 1987) suggest that most of the north coast of the Chukchi Peninsula is undergoing weak uplift (0.6 – 2.3 mm/yr), Diomede Island, in the Bering Strait, is subsiding (-2.1 mm/yr), and the entire south coast of Chukchi Peninsula is subsiding (-2 to -4 mm/yr), which may indicate post-rifting-related subsidence on the southern side of the Chukchi Peninsula. The region of the most intense seismicity lies near the mouth of Kolyuchin Gulf where northwest-striking normal-fault-bounded basins filled with Neogene to Quaternary sediments are also found. Northeast to southwest lineaments in the seismicity extend parallel to the direction of extension of the northern coast of the Chukchi and Seward Peninsulas, and may represent transform faults offsetting rift segments (Figure 5-2). Natal'in et al. (1996) mapped a northeast-southwest trending fault with possible right lateral strike-slip offsets along the Chegitun river on the Chukchi Peninsula which corresponds with one of the linear trends of

seismicity (Figure 5-2). This linear trend is parallel to another seismicity trend just to the north. Both lineaments also parallel the regional seismicity trends extending from the Bering strait region towards the Koryak Highlands (Figure 5-2). Late Cenozoic basaltic volcanism (K-Ar dated at 10.7-3.9 Ma) has also been identified along the southern coast of the Chukchi Peninsula (Belyi, 1970; Akinin and Apt, 1994). Imaev et al. (1998) cite the existence of multiple hot springs in the eastern portion of the Chukchi Peninsula, also consistent with an extensional regime. Based on the evidence, it is suggested that the Seward Peninsula rift extends into the northern Chukchi Peninsula. Perhaps the rift was once to the south, along the southern edge of the Chukchi Peninsula, which is now cooling and subsiding.

Koryak Highlands

The Koryak Highlands are located to the southwest of the Chukchi Peninsula. Seismicity trends enter the Koryak Highlands from the Chukchi Peninsula along two somewhat linear trends. The more southerly of the two trends, which crosses the Gulf of Anadyr', is the better defined (Figure 5-2). The largest recent event along this trend was the magnitude 5.3 Gulf of Anadyr' event of 1986. The Harvard CMT for this event indicates right-lateral transpressional motion with one nodal plane parallel to the seismic trend, although first motion data are more consistent with a greater thrust component (Figure 5-3; Table 5-1). The northern trend is weakly defined, primarily by teleseisms, the largest of which was a magnitude 5.1 event in 1995. The Harvard CMT for this event indicates right-lateral strike-slip motion with a nodal plane parallel to the trend (Figure 5-3; Table 5-1). The exact southwestern extent of the northern trend is difficult to define, although it probably connects with the southern trend in the northern Koryak Highlands.

In the Koryak Highlands there are abundant northeast-southwest trending lineaments visible on Landsat images and 1:200,000 topographic maps, many of which have been mapped as Cenozoic thrust faults (Kovaleva et al., 1983; Figure 5-2). Present day seismicity crosses the Gulf of Anadyr' and enters the northern Koryak Highlands where it follows a series of faults between 63° N and 63.3° N. These faults are superposed on, and cut across, a curved series of faults which follow the regional large scale structural trend. The seismicity and faults enter a large Quaternary sedimentary basin near 175° E. From this area, the seismicity trends to the southwest, where thrust faults and lineaments are also coincident with the present day seismicity, thus the thrust faults may be undergoing reactivation. In addition, recent tomographic studies have imaged imaged a deep northward dipping high velocity planar structure under the southern Koryak Highlands, which is suggested to represent localized subduction (Bijwaard et al., 1998). The location and focal mechanisms of recent seismicity are consistent with the suggested localized subduction, although there is a clear absence of deep events.

The largest event recorded in the Koryaks was a magnitude 6.7 in 1991, which was followed by an extensive aftershock sequence. CMTs from the 1991 event and its aftershocks, as well as other events in 1985 and 1988, indicate thrusting with southeast to northwest compression (Figure 5-3; Table 5-1). As most of the Koryak Highlands are more than 600 km from at least four seismic stations, the mapped level of microseismicity in the Koryaks is artificially low when compared to that of western Alaska.

The neotectonics of the Koryak Highlands have not been extensively studied. Examination of presumed peneplanation surfaces and river terraces have been used by Russian authors to suggest recent uplift of 500 to 1000 m in the seismically active region of

the Koryak Highlands (Smirnov, 1995), although such surfaces may simply represent equilibrium surfaces (Keller and Pinter, 1996). Based on re-leveling surveys, the Anadyr' lowlands to the north of the active seismogenic zone are subsiding at a rate of around 5-7 mm/yr, while the coastline south is subsiding at about 2 mm/yr (Zolotarskaya et al., 1987). Portions of the Koryak range itself appear to be undergoing uplift between 2 and 5 mm/yr (Smirnov, pers. comm.). Terraces along river valleys show uplift rates of about 1 mm/yr (Glushkova et al., 1987). These values are consistent with thrusting of the southern side over the Anadyr' lowlands, as indicated by the region's focal mechanisms (Figure 5-3; Table 5-1).

The seismic trend continues southwest through the Koryak Highlands and into northern Kamchatka (Figures 5-1 and 5-2) where it borders a small region of the Okhotsk plate to the west (Riegel et al., 1993), and connects to the western end of the Aleutian arc.

Aleutian Arc

The Aleutian arc, under which the Pacific plate is subducting, is located along the southern and southwestern boundary of the Bering plate. Right-lateral strike-slip faulting occurs at and immediately behind the volcanoes of the Aleutian Arc (Figure 5-3; Ekstrom and Engdahl, 1989; Taber et al., 1991; Ave Lallemant, 1996). The strike-slip faulting here is a result of transpressional fault motion partitioning along the subduction zone. Individual portions of the western Aleutian Arc are found to invrease velocity and rotate clockwise as they move westward (Geist et al., 1988). The increase in velocity and rotation of the Aleutian Islands occurs as faulting along the Aleutian Islands changes from subduction in the east to strike-slip in the west where a greater degree of coupling may exist. North of the Aleutian Arc, the Bering Sea forms a rigid core and is generally aseismic, with the exception

of the magnitude 6.6 1991 Zemchug Canyon normal-faulting event with north-south extension.

DISCUSSION

Many authors (e.g., Dumitru et al., 1995; Whitney and Wallace, 1995) have proposed that southwestern Alaska is being extruded westward along a series of right-lateral strike-slip faults, including the Kaltag and Denali (Figure 5-3), resulting from north-south compression in south-central Alaska. Present day compression results from the ongoing accretion of the greater Yakutat (Brocher et al., 1991) and other terranes in south-central Alaska (Estabrook et al., 1988) and subduction of the Pacific plate, driving the Wrangell block to the northwest (Perez and Jacob, 1980; Nakamura et al., 1980; Lahr and Plafker, 1980). The overall stress pattern through central Alaska is consistent with the Wrangell block acting as an indenter in southern Alaska (Estabrook and Jacob, 1991; Nakamura et al., 1980). This, in conjunction with Pacific plate subduction, is the driving force for the motion of the Bering plate. Activity along the Kaltag, Denali, and associated faults drastically decreases once they extend onto the Bering shelf. Dumitru et al. (1995) predicts north-south extension in the shelf, perpendicular to the direction of extrusion, along the western extent of the faults, resulting in basin formation on the Bering Shelf, as documented by Worrall (1991). This is also consistent with the CMT for the 1991 Zemchug Canyon event (Figure 5-2). Several of the young (<6 Ma) basaltic volcanic fields and basins in western Alaska and the Bering Sea coincide with normal or strike-slip faults (Moll-Stalcup, 1994; Worrall, 1991). The volcanic field near St. Michael Island likely falls along a splay of the Kaltag fault (Moll-Stalcup, 1994). In the Yukon delta, many of the volcanic fields follow the trace of the Anvik fault

(Moll-Stalcup, 1994). A focal mechanism from the April 1973 event which may be associated with the Kaltag fault indicates northwest-southeast normal faulting (Cook, 1988; Table 5-1). On St. Lawrence Island, Nunivak Island, and the Pribilof Islands, young volcanic cones are aligned approximately east-west along apparent faults or fractures (Moll-Stalcup, 1994).

The westward motion and rotation of the western Aleutian islands implies that motion of the Pacific directly assists the motion and rotation of the Bering plate. The right lateral strike-slip faulting behind the Aleutian arc is also supportive of the extrusion along right-lateral strike slip faults in southern Alaska and the clockwise rotation of the Bering Plate. The strike-slip faulting here has two implications for the Bering plate. First, it defines the southern boundary of the Bering plate proper (Figure 5-3). Second, given the westward motion and clockwise rotation of the Aleutian Arc, it is not unreasonable that some degree of coupling exists with the Bering plate, which assists the motion of the plate as a whole.

Experimental work also supports development of an extensional regime oriented perpendicular to the direction of extrusion as one travels away from the region of compression driving the system (Peltzer and Tapponnier, 1988). The same work also indicates that very complex motions and fault patterns can develop in regions under extrusion, which may explain the seemingly random distribution of earthquakes (Figure 5-1) and historic difficulty in explaining the tectonics of central and western Alaska. The exact position of the Bering plate boundary in southern Alaska is probably diffuse, with motion taken up along many faults, thus it is not easy to locate the boundary. However, as southwestern Alaska is extruding westward with respect to North America, it is most consistent to assign portions of Alaska west of the Wrangell block to the Bering plate, with

the boundary on the western side of the Wrangell block following Lahr and Plafker (1980) until it intersects the right-lateral faulting associated with Aleutian Arc (Figure 5-3). Although south-central and south-western Alaska are clearly seismically active, historically it has been unclear as to whether the large right-lateral strike-slip faults are presently active. Plafker et al. (1993) map much of the Denali fault as active in the Holocene, although not within historic times. However, compilation of continental microseismicity in central Alaska clearly shows activity on the central segment of the Denali fault (Figure 5-5).

This tectonic setting is not unique to the Bering strait region. As noted by Whitney and Wallace (1995), a nearly identical, although latitudinally a mirror image, tectonic situation exists with the southeastward extrusion of southeast Asia resulting from the collision of India with Eurasia (Figure 5-6; Peltzer and Tapponnier, 1988; Tapponnier and Peltzer, 1982; compare with Figure 5-3). This is comparable to the westward extrusion of portions of Alaska due to terrane accretion (Perez and Jacob, 1980). In both cases, compression to the north of accreting continental material results in horizontal extrusion along a series of strike-slip faults (left-lateral in southeast Asia and right-lateral in southwest Alaska) that splay into normal-fault systems without reaching a plate boundary (Peltzer and Tapponnier, 1988; Tapponnier and Peltzer, 1982; Dumitru et al., 1995; Worrall, 1991). In southeast Asia, extrusion to the southeast is possible because the Sunda arc offers little resistance to the movement, basically being a free boundary (Peltzer and Tapponnier, 1988). Similarly, the Aleutian arc may act as a free boundary to the westward extrusion of portions of Alaska (Dumitru et al., 1995). The geometries of extrusion in Southeast Asia and southwest Alaska are similar (Figures 5-3 and 5-6). Extension in the South China Sea (Peltzer and Tapponnier, 1988; Tapponnier and Peltzer, 1982) and Bering strait are both due

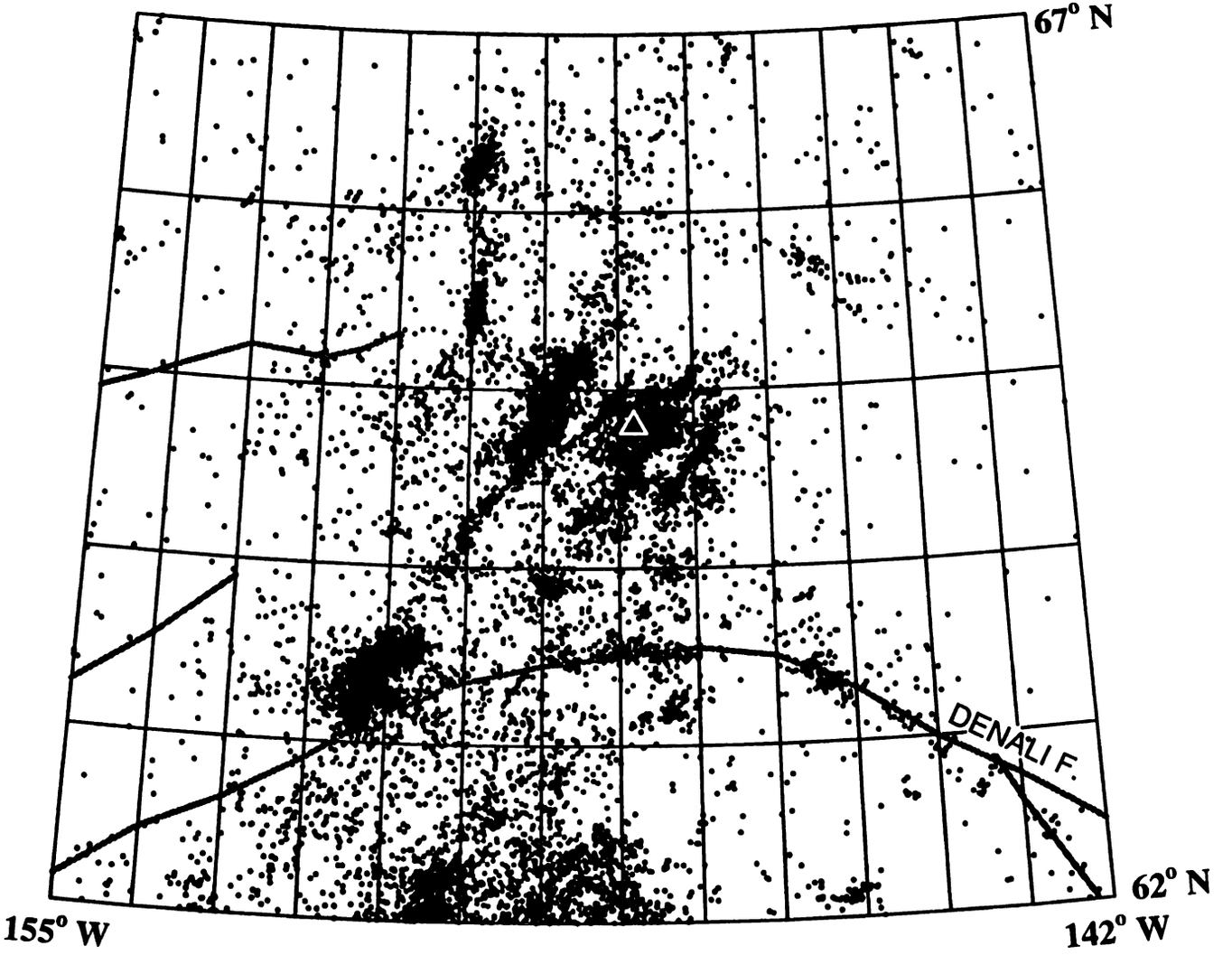

Figure 5-5. Crustal seismicity of interior Alaska showing activity on the Denali fault. Data compliments of the Alaska Earthquake Information Center (AEIC), Geophysical Institute, University of Alaska, Fairbanks. Triangle denotes Fairbanks.

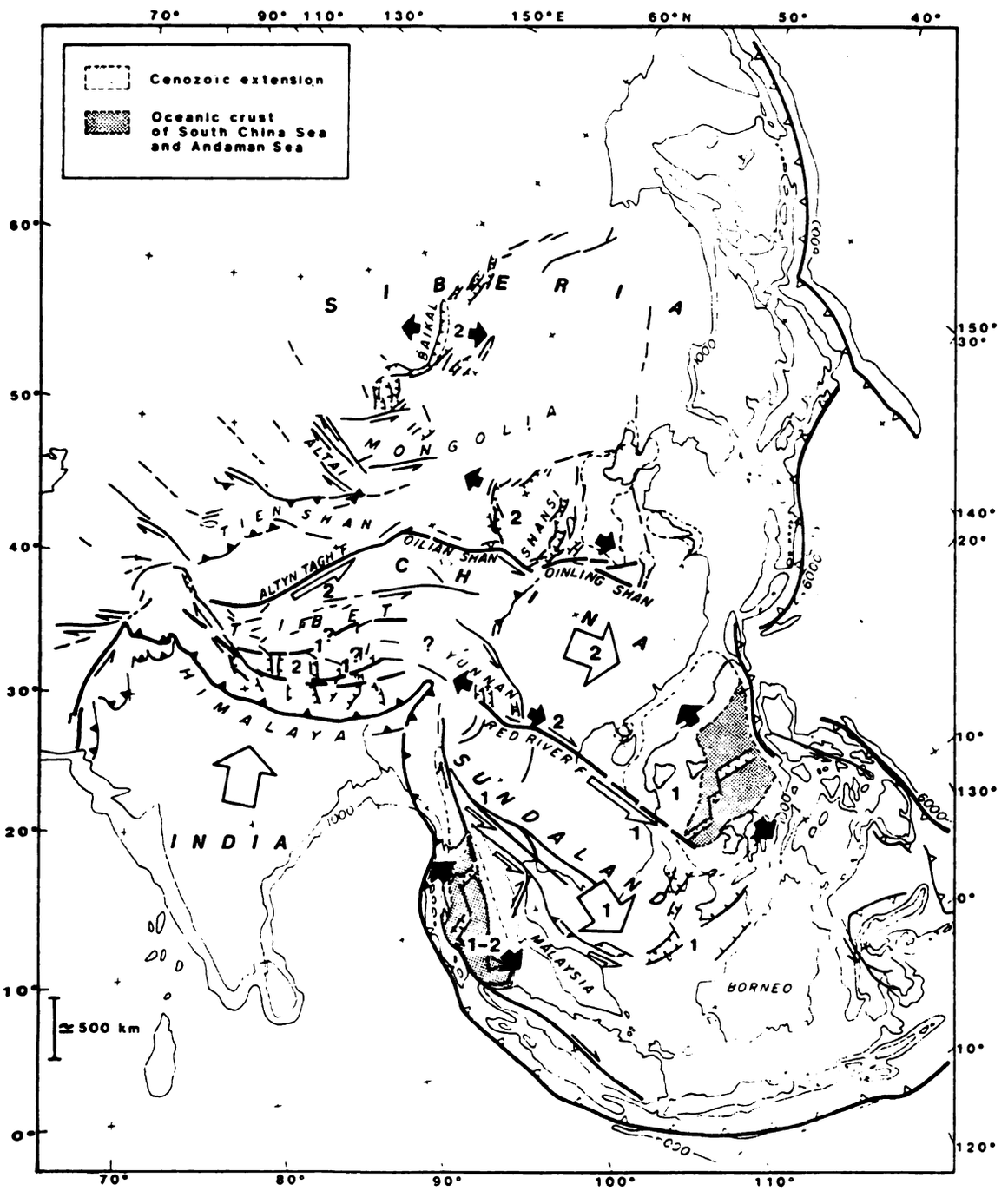

Figure 5-6. Extrusion tectonics of southeast Asia (Peltzer and Tapponnier, 1988). Note similarity to Alaska and the Bering Plate in relative locations of indentor, rift zones, and faults.

to the lateral extrusion of material along strike-slip faults (left-lateral faults in southeast Asia and right-lateral faults in western Alaska). In addition, the orientation of extension in the two cases, relative to the indenter and strike-slip faults, is similar. The similarities between the two regions may illustrate a fundamental tectonic situation which develops when terrane accretion occurs adjacent to a free edge boundary.

CONCLUSIONS

The merging of multiple data sets of seismicity for the Bering strait region clarifies seismic trends from western Alaska to the Koryak highlands of Chukotka, that, when combined with regional geology, supports the existence of an independent Bering Plate slowly rotating clockwise as a result of terrane accretion in southern Alaska. Ages of volcanic rocks suggest that the current tectonic setting had developed at least by 6 Ma. Additional data, especially in Chukotka, will contribute to a better understanding of the tectonics of this region and of continental deformation in general.

REFERENCES

Allen, R.M., Brocher, T.M., Klemperer, S.L., and Galloway, B.K., 1995, Analysis of offshore-onshore wide-angle seismic recordings from western Alaska, Bering-Chukchi Sea: *Eos* (Transactions, American Geophysical Union), v. 76, no. 46, p. 590.

Akinin, V.V., and Apt, Y.E., 1994, *Enmelen volcanoes (Chukchi Peninsula): Petrology of Alkaline Lavas and Deep-Seated Inclusions*: SVKNII, Magadan, 97 pp. (in Russian).

Aksenov, A.A., Dunaev, N.N., Ionin, A.S., Kalinenko, V.V., Medvedev, V.S., Pavlidis, Y.A., and Yurkevich, M.G., 1987, *The Arctic shelf of Eurasia in Late Quaternary time*: Nauka, Moscow, 275 pp. (in Russian).

Ave Lallemant, H.G., 1996, Displacement partitioning and arc-parallel extension in the Aleutian volcanic island arc: *Tectonophysics*, v. 256, p. 279-293.

Balakina, L.M., 1962, General regularities in the directions of the principal stresses effective in the earthquake foci of the seismic belt of the Pacific Ocean: *Izvestia, Bulletin, Geophysics Series*, p. 918-926.

Baranov, B.V., Seliverstov, N.I., Murav'ev, A.V., and Muzurov, E.L., 1991, The Komandorsky Basin as a Product of Spreading Behind a Transform Plate Boundary: *Tectonophysics*, v. 199, p. 237-269.

Belyi, V.F., 1970, Okhotsk-Chukotka volcanogenic belt, Cenozoic volcanism, Magmatism: *in* Drabkin, I.E., ed., *Northeast USSR, Geology of the USSR*, v. 30, part 2, p. 225-226 (in Russian).

Bijwaard, H., Spakman, W., and Engdahl, E.R., 1998, Closing the gap between regional and global travel time tomography: *Journal of Geophysical Research*, v. 103 (12), p. 30,055-30,078.

Biswas, N.N., Pujol, J., Tytgat, G., and Dean, K., 1983. *Synthesis of seismicity studies for western Alaska, Final report for contract NA81-RAC00112*: Geophysical Institute, University of Alaska, Fairbanks, 74 pp.

Biswas, N.N., Pujol, J., Tytgat, G., and Dean, K., 1986, Synthesis of seismicity studies for western Alaska: *Tectonophysics*, v. 131, p. 369-392.

Brocher, T.M., Moses, M.J., Fisher, M.A., Stephens, C.D., and Geist, E.L., 1991, Images of the plate boundary beneath southern Alaska, *in* Meissner, R., Brown, L., Durbaum, H.-J., Franke, W., Fuchs, K., and Seifert, F., eds., Continental lithosphere: *Deep seismic reflections: American Geophysical Union Geodynamics Series 22*, p. 241-246.

...ley, M.J.,
Michi

...ck, D.B.,
northe
Lansi

...mmu, T.A
and G
Alask

...ssom, G.,
in the
Geopi

...ddell, E.R.
zones

...brook, C.
Journa

...brook, C.
Englis
Ameri
1, p. 3

..., K., an
relatio
Proce
Service

..., L., a
northw
1587-1

..., E.L., C
Aleutia
p. 327-

...ova, O.
feature
Highla
Magada

Coley, M.J., 1983, *Intraplate seismicity in central Alaska and Chukotka*: M.S. Thesis, Michigan State University, East Lansing, 97 pp.

Cook, D.B., 1988, *Seismology and tectonics of the North American Plate in the arctic: northeast Siberia and Alaska*: Ph. D. Dissertation, Michigan State University, East Lansing, 250 pp.

Dumitru, T.A., Miller, E.L., O'Sullivan, P.B., Amato, J.M., Hannula, K.A., Calvert, A.T., and Gans, P.B., 1995, Cretaceous to Recent Extension in the Bering Strait Region, Alaska: *Tectonics*, v. 13, p. 549-563.

Ekstrom, G., and Engdahl, E.R., 1989, Earthquake source parameters and stress distribution in the Adak Island region of the central Aleutian Islands, Alaska: *Journal of Geophysical Research*, v. 94, p. 15,499-15,519.

Engdahl, E.R., Sleep, N.H., and Lin, M.-T., 1977, Plate effects in North Pacific subduction zones: *Tectonophysics*, v. 37, p. 95-116.

Estabrook, C.H., Stone, D.B., and Davies, J.N., 1988, Seismotectonics of northern Alaska: *Journal of Geophysical Research*, v. 93, p. 12026-12040.

Estabrook, C.H., and Jacob, K.H., 1991, Stress indicators in Alaska, *in* Slemmons, D.B., Engdahl, E.R., Zoback, M.D., and Blackwell, D.D., eds., *Neotectonics of North America*: Boulder, Colorado, Geological Society of America, Decade Map Volume 1, p. 387-399.

Fujita, K., and Koz'min, B.M., 1994, Seismicity of the Amerasian Arctic shelf and its relationship to tectonic features, *in* Thurston, D. K., and Fujita, K., eds., *1992 Proceedings International Conference on Arctic Margins*: US Mineral Management Service, OCS Study MMS 94-0040, p. 307-312.

Gedney, L., and Marshall, D., 1981, A rare earthquake sequence in the Kobuk Trench, northwestern Alaska: *Bulletin of the Seismological Society of America*, v. 71 (5), p. 1587-1592.

Geist, E.L., Childs, J.R., and Scholl, D.W., 1988, The origin of summit basins of the Aleutian Ridge: Implications for block rotation of an arc massif: *Tectonics*, v. 7(2), p. 327-341.

Glushkova, O.Y., Degtyarenko, Y.P., and Prokhorova, T.P., 1987, Pleistocene freezing and features of sedimentation and reconstruction of the hydrologic network in the Koryak Highlands, *in The Quaternary Period in Northeast Asia*: NEISRI FESC AS USSR, Magadan, p. 33-54 (in Russian).

Imaev, V.S., Imaeva, L.P., Koz'min, B.M., Mackey, K., and Fujita, K., 1998, Seismotectonic processes along the boundary of lithospheric plates of Northeast Asia and Alaska: *Pacific Geology*, v. 17, no. 2, p. 3-17 (in Russian).

Keller, E.A., and Pinter, N., 1996, *Active tectonics, earthquakes, uplift, and landscape*: Prentice Hall, Upper Saddle River, NJ, 338 pp.

Kovaleva, V.V., Smelovskaya, M.M., Poleshchuk, M.I., Rozenkrants, A.A., Klimov, V.N., and Kotova, N.N., 1986, *Geologic Map of the USSR (New Series), Map of Pre-Quaternary Deposits, Quadrangle P-58,59 (Kamenskoe; dated 1983)*: VSEGEI, Leningrad, scale 1:1,000,000.

Kroeger, G.C., 1978, *Synthesis and analysis of teleseismic body wave seismograms*: Ph.D. Dissertation, Stanford University, Palo Alto, 135 pp.

Lahr, J.C., and Plafker, G., 1980, Holocene Pacific-North American plate interaction in southern Alaska: Implications for the Yakataga seismic gap: *Geology*, v. 8, p. 483-486.

Lander, A.V., Bukchin, B.G., Droznin, D.V., and Kiryushin, A.V., 1996, The tectonic environment and source parameters of the Khailino, Koryakia earthquake of March 8, 1991: Does a Beringia plate exist?: *Computational Seismology and Geodynamics*, v. 3, p. 80-96.

Liu, H.L., and Kanamori, H., 1980, Determination of source parameters of mid-plate earthquakes from the waveforms of body waves: *Bulletin of the Seismological Society of America*, v. 70, p. 1989-2004.

McCaleb, R.C., Fujita, K., and Wolf, L.W., 1998, Crustal models of the Hope Basin, Chukchi Sea, Alaska, from gravity data: Transactions, American Geophysical Union (EOS), 1998 Fall Meeting, v. 79, # 45 (Supplement), p. 808.

Miller, E.L., and Hudson, T.L., 1991, Mid-Cretaceous extensional fragmentation of a Jurassic-Early Cretaceous compressional orogen, Alaska: *Tectonics*, v. 10, p. 781-796.

Minster, J.B., Jordan, T.H., Molnar, P., and Haines, E., 1974, Numerical modelling of instantaneous plate tectonics, *Geophysical Journal of the Royal Astronomical Society*, v. 36, p. 541-576.

Moll-Stalcup, E. J., 1994, Latest Cretaceous and Cenozoic magmatism in mainland Alaska, *in* Plafker, G., and Berg, H.C., eds. *The Geology of Alaska*: Geological society of America, The Geology of North America, v. G-1, Boulder, p. 589-620.

Yamamura, K., P
map of
Earthqua

Yan'in, B.A., T
NW M
Geophy

Yeats, G., and
and Bas
Geophy

Yeats, O.J., an
Gulf o
7132-7

Yeh, Y.L.,
Structu
9. Sea

Yeltsov, G., C
and B
Geolo

Yegel, S.A.,
tecton
p 60

Yemets, A.R
Type

Yemets, E.V
Chuk

Yemets, V.
Arch
pp.

Yerk, D.B.,
Alas

Yerkes, J.L.,
Stem
Neot
U.S.

Nakamura, K., Plafker, G., Jacob, K.H., and Davies, J.N., 1980, A tectonic stress trajectory map of Alaska using information from volcanoes and faults: *Bulletin of the Earthquake Research Institute*, v. 55, p. 89-100.

Natal'in, B.A., Toro, J., and Amato, J., 1996, Strike-Slip Faulting Along the Chegitun River, NW Margin of the Koolen Dome, Chukotka: *Eos* (Transactions, American Geophysical Union), v. 77(46), p. 642.

Peltzer, G., and Tapponnier, P., 1988, Formation and Evolution of Strike-Slip Faults, Rifts, and Basins During the India-Asia Collision: An Experimental Approach: *Journal of Geophysical Research*, v. 93, p. 15,085-15,117.

Perez, O.J., and Jacob, K.H., 1980, Tectonic Model and Seismic Potential of the Eastern Gulf of Alaska and Yakataga: *Journal of Geophysical Research*, v. 85, p. 7132-7150.

Pol'kin, Y.I., 1984, Chukchi Sea, *in* Gramberg, I.S., and Pogrebitsky, Y.E., eds., *Geologic Structure of the USSR and Regularities in the Distribution of Mineral Resources, v. 9, Seas of the Soviet Arctic*: Nedra, Leningrad, p. 67-79 (in Russian).

Plafker, G., Gilpin, L.M., and Lahr, J.C., 1993, Neotectonic map of Alaska, *in* Plafker, G., and Berg, H. C., eds., *The geology of Alaska*: Geological Society of America, Geology of North America, Boulder, v. G-1, scale 1:2,500,000.

Riegel, S.A., Fujita, K., Koz'min, B.M., Imaev, V.S., and Cook, D.B., 1993, Extrusion tectonics of the Okhotsk plate, Northeast Asia: *Geophysical Research Letters*, v. 20, p. 607-610.

Ritsema, A.R., 1962, P and S Amplitudes of Two Earthquakes of the Single Force Couple Type: *Bulletin of the Seismological Society of America*, v.52, p. 723-746.

Shipilov, E.V., Senin, B.V., and Yunov, A.Y., 1989, Sedimentary cover and basement of the Chukchi Sea from seismic data: *Geotectonics*, v. 23, p. 456-463.

Smirnov, V.N., 1995, *Morphotectonics of mountain-building regions of northeast Asia*: Author's summary of Doctoral dissertation, Moscow State University, Moscow, 40 pp. (in Russian).

Stone, D.B., 1983, Present day plate boundaries in Alaska and the Arctic: *Journal of the Alaska Geological Society*, v. 3, p. 1-14.

Taber, J.J., Billington, S., and Engdahl, E.R., 1991, Seismicity of the Aleutian Arc, *in* Slemmons, D.B., Engdahl, E.R., Zoback, M.D., and Blackwell, D.D., eds., *Neotectonics of North America*: Geological Society of America, Decade Map Volume 1, Boulder, p. 29-46.

[illegible], P., P
extrusion
Geology,

[illegible] A.B., and D
Island, *in*
North Am

[illegible]ska, R.B., 19
Alaska, *i*
Potentia
Basins -
Mineral

[illegible]ner, D.L., a
central
Recon
Alaska

[illegible]ney, J.W.
Alaska

[illegible]kens, A.J.
soluti
1, 560

[illegible]mill, D.N
Strike
257,

[illegible]manskaya
move
ed., *I*
121 (

Tapponnier, P., Peltzer, G., Le Dain, AY., Armijo, R., and Cobbold, P., 1982, Propagating extrusion tectonics is Asia: new insights from simple experiments with plasticine: *Geology*, v. 10, p. 611-616.

Till, A.B., and Dumoulin, J.A., 1994, Geology of Seward Peninsula and Saint Lawrence Island, *in* Plafker, G., and Berg, H.C., eds., *The Geology of Alaska*: The Geology of North America, v. G-1, Geological Society of America, Boulder, p. 141-152.

Tolson, R.B., 1987, Structure and stratigraphy of the Hope Basin, southern Chukchi Sea, Alaska, *in* Scholl, D.W., Grantz, A., and Vedder, J.G., editors, *Geology and Resource Potential of the Continental Margin of Western North America and Adjacent Ocean Basins -- Beaufort Sea to Baja California*: Circum-Pacific Council for Energy and Mineral Resources, Earth Science Series, v. 6, Houston, p. 59-71.

Turner, D.L., and Swanson, S.E., 1981, Continental rifting -- a new tectonic model for the central Seward Peninsula, *in* Wescott, E., and Turner, D., eds., *Geothermal Reconnaissance Survey of the Central Seward Peninsula, Alaska*: University of Alaska, Geophysical Institute Report UAG R-284, p. 7-36.

Whitney, J.W., and Wallace, K., 1995, Plate tectonic model for the neotectonics of northern Alaska: *Geological Society of America Abstracts with Programs*, v. 27, no. 5, p. 84.

Wickens, A.J., and Hodgson, J.H., 1967, *Computer re-evaluation of earthquake mechanism solutions, 1922-1962*: Publications of the Dominion Observatory, Ottawa, v. 33, no. 1, 560 p.

Worrall, D.M., 1991, *Tectonic History of the Bering Sea and the Evolution of Tertiary Strike-Slip Basins of the Bering Shelf*: Geological Society of America Special Paper, 257, 120 p.

Zolotarskaya, S.B., Nikitenko, Y.P., and Ufimtsev, G.F., 1987, Contemporary vertical movements of the Earth's crust, Eastern Siberia and the Far East, *in* Logachev, N.A., ed., *Processes in the formation of the relief of Siberia*: Nauka, Novosibirsk, p. 116-121 (in Russian).

CONCLUSIONS

A seismicity catalog, including phase data, was assembled for northeastern Russia. This catalog was found to be heavily contaminated with anthropogenic sources in some areas. However, this problem can be overcome by plotting only nighttime events, which is representative of the region's tectonic activity. The resulting plot shows several trends of seismicity that are found to correlate with known faults (Figure C-1). In general, it is still difficult to trace individual active faults throughout the study area and precisely locate the regions plate boundaries. In addition, a large percentage of seismicity occurs in poorly defined, diffuse regions not presently associated with specific faults. This indicates in a broad sense the diffuse and complex nature of continental plate boundaries. Although focal mechanism studies have given us the broad tectonic plate motions for northeastern Russia, the microseismicity indicate that the boundary regions between the major plates are comprised of many small blocks and slivers that interact in a complex fashion. Considerable additional work remains to be done to fully understand these small scale plate interactions.

Careful analysis of the assembled database resulted in the development of a new tectonic model for the Bering Sea region. This model proposes an independent Bering Plate which is driven by westward extrusion of south-central Alaska as a result of terrane accretion. The similarity of this model to the extrusion of southeast Asia from the India-Eurasia collision illustrates the occurrence and importance of lateral extrusion as a means of continental deformation.

The assembled seismic phase data allowed the relocation of over 1,100 earthquakes while simultaneously determining the first crustal velocity model for the region. Although

the method employed to develop the velocity model was simple, it was clearly able to discriminate velocity differences among different geologic/tectonic settings. Because of the method's simplicity and positive results, it may be useful for other regions where regional crustal velocities are poorly known.

This study has greatly improved our understanding of the tectonics and crustal structure of northeastern Russia, a region of interaction between several major and minor lithospheric plates and blocks. However, considerable work remains bevore we understand the activity and behavior of plate boundaries in this region. The combined data set of hypocenters and earthquake phase data for northeastern Russia assembled in this study will provide a base for future studies..

Future work in northeast Russia will include the deployment of digital acquisition seismic stations, which will be useful for seismic wave attenuation studies, better velocity models, explosion discrimination, etc. Future work in the region will also hopefully include comprehensive GPS studies to map the complexities of the regions small-scale tectonic interactions, which will reflect on the fundamental character of continental deformation.

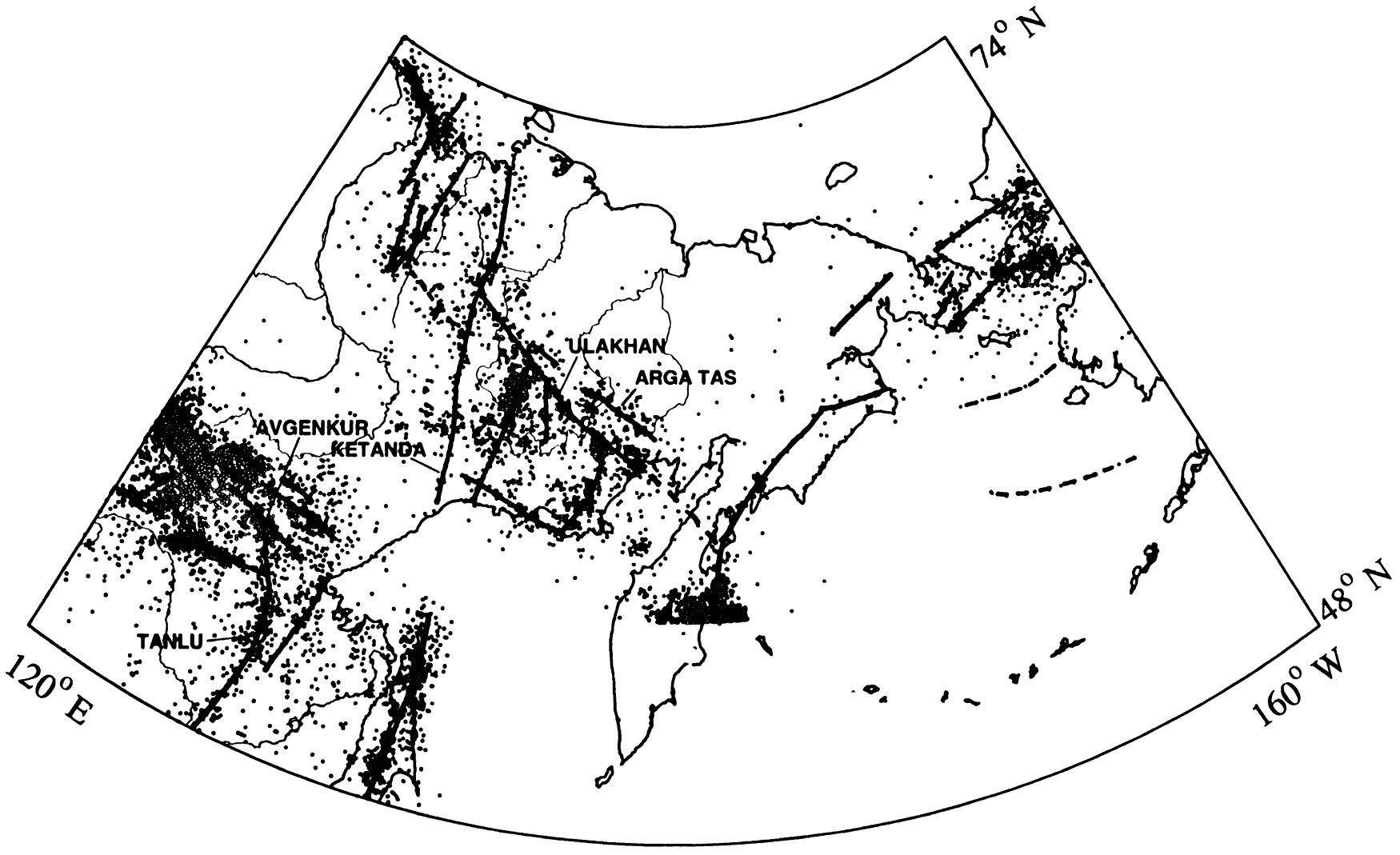

Figure C-1. Nighttime seismicity and active faults of northeastern Russia. Major faults are labeled and other faults are located based on interpretation of seismicity lineations.

APPENDICES

APPENDIX A

Alphabetized list of northeastern Russia seismic stations.

APPENDIX A

Alphabetized list of northeastern Russia seismic stations.

Station Name	Engl. Code	Russian Code	Lat. (°N)	Long. (°E)	Elev. (m)	Date Open	Date Close	Qual.
Aku			56.46	120.91	700	--/68	--/68	1
Alla	ALL	АЛ	54.688	110.82	550	10/63	5/70	1
Alygdzher	ALY		53.633	98.218	920	1/66	1/67	1
Amedichi	ACHS	АМД	57.03	122.85	930	05/89	08/89	1
Amguema	AMG	АМГ	67.05	178.88W	150	11/65	4/66	2
Ammonl'naya	MMS		64.55	143.18	540	--/61	--/62	1
Anadyr	ANYS	АНД	64.734	177.496	55	4/89	7/93	1
						9/96	OPEN	
Anadyr-1	ANSS	АНД	64.77	177.57	40	11/80	1/89	3
Angarakan	AGK		56.348	113.67	1430	11/76	8/81	1
Anyuisk	ANC	АНС	68.34	161.56	10	6/64	3/65	1
Apacha	APC		52.925	157.131		2/90	OPEN	1
Apakhonchich	APN	АПХ	56.00	160.84	700	–/64	–/80	1
Arshan	ARS	АРШ	51.908	102.433	840	–/58		1
Artyk	AYKS	АР	64.18	145.13	700	06/71	--/71	1
						—/88	---	1
Avacha - old	AVH	АВЧ	53.07	158.5	---	–/63	10/76	-
Avacha - new	AVH	АВЧ	53.265	158.738	900	7.76	OPEN	1
Babushkin	BAU		51.717	105.867	470	6/66	9/66	1
Baikal'sk	BKK		51.522	104.133	460	1/64	2/66	1
Balygychan	BLG	БЛГ	63.91	154.09	139	7/63	6/64	1
Barluk	BRUS		54.533	101.717	525	11.60		1
Batagai	BTGS	БТГ	67.653	134.630	127	--/75	OPEN	1
Bazovskii			56.53	123.42	1080	--/70	--/70	1
Berezovaya	BER	БРЗ	52.27	158.433		–/81	–/94	1
Bering	BKI	БРН	55.195	165.99	400	–/62	OPEN	-
(Nikol'skoe)		БРГ						
Bilibino GSN	BILL	BILL	68.065	166.452	299	8/95	OPEN	1
Bilibino	BILS	БЛБ	68.059	166.449	283	8/81	4/92	1
		БЛН						
Bilibino-1	BL1	БЛБ	68.04	166.44	260	8/64	1/65	1
Bodaibo	BOD	БДБ	57.807	114.03	245	11/60	---	1
Bodon	BDN	БОД	53.713	110.1	540	11/69	--/83	1
		БДН						
Bogachevka	BGC		54.850	160.900		–/64	–/65	1
Bomnak	BMKS	БМН	54.705	128.847	325	3/74	---	1
Bykov			47.317	142.567	40	6/68	10/68	-
Chagda	CGD	ЧГД	58.75	130.60	185	--/68	---	1
Chara	CRS	ЧР	56.9	118.267	710	11/61	---	1

Ebeniki
Ebeyibi
Ecra
Ecuburd
Ecuchor
Edikman
Edikman
Dzedza
Dekin
Dzmoe
Dzoochaz
Dzuu
Dyganu
Fyedzino
Ekimchar
Emgoach
Enso
Enzoru
Ugle
Eretsk
Fusovo
Gazali
Garmash
Gorely
Gornoz
Gornovo
Gornozav
Gornyi
Gusinoo
Ilanei
Imagra
Imagra
Inzutu
Vulk
Irkana
Irkutsk
Ishim
Kabakt
Kabans
Kalgan
Kamen
Kamen
Kamen
Karam
Karym

Cherskii	CES	ЧРС	68.75	161.33	10	--/79	--/88	1
Chil'chi			56.06	122.33	500	--/70	--/70	1
Chita	CIT	ЧТ	52.033	113.55	790	6/70		1
Chochurdakh			72.83	116.25		08/13/75	09/26/75	-
Chokchoi	CKHS	ЧКЧ	57.65	121.72	240	--/89	--/89	1
Chul'man-1	CL1S	ЧЛМ	56.85	124.90	650	--/62	--/86	1
Chul'man-2	CLNS	ЧЛМ	56.84	124.90	760	--/86	---	1
Davsha	DAS		54.538	109.503	460	1/64	6/65	1
Debin	DBI	ДБН	62.339	150.751	332	–/74	–/92	G
Dimnoe			73.233	142.400		3/74	4/74	-
Dovochan	DOV		56.462	117.533	1094	7/62	9/63	1
Dunai	DUYS	ДН	73.92	124.49	5	11/89	---	1
Dyrynmakit			56.60	121.13	460	--/67	--/67	1
Egvekinot	EGVS	ЭГВ	66.323	179.127W	18	–/90	–/94	1
Ekimchan	EKI	ЕКМ	53.067	132.945	485	11/79	---	1
Emegachi	EMG		56.567	118.158	960	9/62	4/63	1
Esso	ESO	ЭСС	55.925	158.700	490	–/65	OPEN	1
Esutoru (Uglegorsk)	ESU		49.083	142.033	100	12/39	--/45	-
Evensk	EVES	ЭВН	61.92	159.23	22	–/80	7/93	1
Firsovo			47.65	142.567	20	8/79	11/79	-
Ganali	GNL	ГНЛ	53.942	157.620	1200	1/88	OPEN	1
Garmanda	GRM	ГРМ	62.18	159.08	140	12/66	5/67	1
Gorely	GRL	ГРЛ	52.552	158.080	1250	7/80	OPEN	1
Gornotaezhnoe	GRZ GRT	ГРТ	43.70	132.15	220	7/90	---	3
Gornovodnoe	GRD GRV	ГРВ	43.70	134.733	270	7/88	---	1
Gornozavodsk			46.567	141.85	50	12/71	6/72	-
Gornyi	GNY	ГРН	50.762	136.455	500	12/78	---	2
Gusinoozersk	GOO	ГСН	51.283	106,517	600	11/71	2/72	1
Ilirnei	ILR	ИЛР	67.26	167.96	350	10/64	10/65	1
Imangra-1			56.75	121.24	395	07/67	08/67	1
Imangra-2	IMNS	ИМГ	56.62	120.71	540	--/75	--/79	1
Institut Vulkanologii	INS		53.066	158.605	175	11/81	OPEN	1
Irkana	IKN		55.867	111.253	480	1/64	3/66	1
Irkutsk	IRK	ИРК	52.272	104.31	467	12/01	OPEN	1
Iul'tin	ILT	ИЛТ	67.87	178.74W	235	3/66	7/93	1
Kabaktan	KBKS	КБК КБТ	56.68	122.42	1010	05/89	08/89	1
Kabansk	KAB	КБ	52.05	106.658	465	1/51		1
Kalgannakh			71.83	114.33		07/21/75	08/10/75	-
Kamenistyi	UL2S	КМН	65.41	144.83	670	--/88	--/88	1
Kamenistaya	KMN		55.76	160.240	1100	10/90	OPEN	1
Kamenskoe	KAM		62.456	166.210		–/94	OPEN	1
Karam	KRMS		55.133	107.583	600	1/66	3/66	1
Karymski - old	KII	КРМ? КАР?	54.030	159.480	790	7/74	–/86	1

Krymski -
Krum
Kundyga
Kuni

Kupchera
Kupstyr

Kurgansk

Kuybyshe
Kovalski
Kyrsha

Kuski
Kuskol sha
Kusto
Kusnakov
Kuzyak
Kuzmy
Kukavo
Kuvshin
Kuznetsky
Kuzyevsk
Kuzy
Kustanay
Kustovsk
Kvasky
Kvitneg

Kyzyl-
Kyz

Kyzyla
Kyzyl-Ja
Kyzyla
Kyzyl-Ja
Kyzyr
Kyzyrbe
Kyz
Kyzyl
Kyzyl-Ja
Kyzyl-Ku
Kyzyl-Ta
Kyzyl-Ta

Karymski - new	KRY		54.036	159.449	900	9/89	OPEN	1
Khaim	KAIS	ХМ	52.602	108.085	480	10/69	5/70	1
Khandyga	KHG	ХНД	62.65	135.56	125	--/69	--/94	1
Khani	KHNS	ХН	57.04	121.01	390	--/67	--/67	1
						--/75?	--/76?	
Khapcheranga	KPC	КПЧ	49.707	112.392	950	12/68		1
Khatystyr	KHY	ХТС	55.71	121.57	475	--/68	--/68	1
						--/75	--/82?	
Khingansk	KNN	ХНГ	49.122	131.192	520	7/80	4/84	1
	KNG							
Kigilyakh			73.367	139.867		6/73	9/73	-
Kirovskii	KIRS	КРС	54.428	126.983	440	4/74	---	1
Klyuchi	KLY	КЛЧ	56.313	160.852	80	–/48	---	1
						2/89	OPEN	
Kobdi	AY1S		64.20	145.51	800	06/71	--/71	1
Kolokol'chik						–/67	–/67	
Korito	KRT		55.966	160.222	1000	10/97	OPEN	1
Korsakov						--/51	1/52	-
Koryak	KRK	КРК	53.292	158.636	1050	7.75	OPEN	1
Kotelnyi			75.767	137.60		8/72	9/72	-
Kotikovo			49.133	144.25	10	7/69	9/70	-
Kovokta	KVO	КВК	56.133	113.05	1180	--/81	---	1
Kozelskaya	KZL	КЗЛ	53.201	158.894	950	–/76	–/84	1
Kozyrevsk	KOZ	КЗР	56.05	159.87	40	–/62	–/89	1
Kozyr	KZY		56.070	159.900	450	11/89	OPEN	1
Krestovaya	KTB		52.665	106.395	560	7/71	9/71	1
Krestovskii	KRS		56.214	160.558	1200	7/87	OPEN	1
Kronoki	KRI	КРН	54.596	161.134	5	8/66	OPEN	1
Krutoberegovo	KBG	КБГ	56.255	162.705	10	–/68	OPEN	1
		КБ						
		КРБ						
Kul'dur	KLDS	КЛД	49.205	131.642	425	—	---	1
Kulu	KU-S	КЛ	61.889	147.431	655	1/80	10/92	G
		КЛУ						
Kumora	KMO	КМР	55.883	111.208	475	9/66	---	1
Kurbulik	KBK		53.708	109.038	460	1/64	9/65	1
Kurul'ta			56.90	121.11	495	--/68	--/68	1
Kyakhta	KYA	КХТ	50.35	106.45	760	3.52	5/70	1
Kyubyme			63.38	140.95	950	--/74	--/74	2
Kyusyur	KYUS	КСР	70.68	127.37	20	--/85	08/89	1
Lamutskoe	LMT	ЛМТ	65.54	168.85	178	4/65	10/65	1
Lapri			55.69	124.91	640	--/72	--/73	1
Lazarev	LZR	ЛЗР	52.2	141.493	120	12/80	---	2
Lesogorsk			49.442	142.2	40	7/69	10/69	-
Lopatino			46.6	141.825	40	4/69	10/69	-
Lurbun	LRB		56.63	117.883	780	8/62	9/63	1
						5/67	9.68	1
Magadan	MAG	МГД	59.560	150.805	78	1/52	1/92	1
Magadan-GSN	MA2	МА2	59.575	150.768	339	9/93	OPEN	1

Maiskii	MKI	МАЙ	68.97	173.71	261	8/82	6/94	1
Mal. Ipelka	MIP		52.276	156.758	370	8/97	OPEN	1
Maritui	MRU		51.783	104.217	520	–/08	–/18	1
Markovo	MKVS MKN	МРК	64.68	170.41	25	10/86	4/92	1
Mednyi	MED	МДН	54.786	167.556		–/73	–/75	1
Milkovo	MLK	МЛК	54.70	158.63	155	–/62	–/63	1
						10/89	–.93	
Moma-Khonuu	MKUS	МОМА	66.47	143.22	192	--/83	---	1
Moneron			46.258	141.25	40	9/71	5/72	-
Mondy	MOY	МНД	51.673	100.993	1300	–/58		1
Murino	MUO		51.475	104.408	470	8/66	9/66	1
Myakit	MYAS	МКТ	61.407	152.093	670	--/83	--/88	G
Mys Khvoinova			74.267	140.883		4/76	6/76	-
Mys Nerpichii			75.833	143.333		4/76	6/76	-
Mys Diring-Ayan			75.950	139.917		5/76	6/76	-
Mys Shmidta	SMT	ШМТ	68.88	179.38W	5	4/65	1/66	1
Nagornyi Sta		НГР	55.92	124.97	920	--/77	--/77	1
Nagornyi			55.95	124.92	840	--/69	--/69	1
Naiba	NAYS	НБ	70.85	130.73	5	--/85	---	1
Nalychevo	NLC	НЛЧ	53.171	159.345	5	–/67	–/67	-
						3/69	12/69	-
						3/84	—	1
Naminga	NMG		56.60	118.517	1380	5/67	4/69	1
Naminga-1	NMG1		56.70	118.583	1160	--/63	--/63	1
Nel'koba	NKBS	НЛБ	61.34	148.81	531	9/83	6/97	1
Nel'koba	NK1	НЛБ	61.34	148.81	531	6/63	1/64	1
			61.338	148.813	531	6/97	9/99	G
Nelyaty	NLY	НЛТ	56.492	115.7	470	1/61	---	1
Nesterikha	NSR	НСТ	53.647	109.708	480	7/70	9/70	1
Neryungri	NYGS	НРГ	56.68	124.66	760	--/77	--/78	1
						--/80	--/82	
Nezhdaninsk	NZDS	НЖД	62.50	139.06	603	--/80	---	1
Nikola	NKO		51.893	104.827	460	7.71	9.71	1
Nikolaevsk-Amur	NKL	НКЛ	53.142	140.783	25	9/70	---	1
Nizhnii Angarsk	NIZ	N-A	55.766	109.55	487	10/61		1
Nizhnii Armudan			50.817	142.533	150	9/66	4/69	-
Nogliki		НКЛ	51.817	143.15	25	10/64	12/64	-
						--/88	---	-
Novaya Sibir			75.050	147.000		4/75	6/75	-
Nyvrovo	NVV	НВР	54.317	142.617	5	11/81	---	-
O. Vrangelya	VRN	ВРН	70.94	179.62W	10	2/66	4/66	3
Obo	OBO		61.80	149.77	440	--/77	—/77	1
Ogon'ki			46.775	142.383	70	6/68	9/68	-
Oimur	OIM		53.333	106.833	460	10/59	–/60	1
Okha (New)						--/65	---	-
Okha	OKH	ОХА	53.55	142.933	24	12/58	--/65	-

Ol'khon	OLK		53.20	107.342	490	7/69	9.69	1
Omchak	OMCH	ОМЧ	61.67	147.87	820	9/99	OPEN	1
Omolon	OMOS	ОМЛ	65.23	160.54	260	6/82	7/93	1
Omolon-1	OL1	ОМЛ	65.25	160.52	260	12/63	1/65	1
Omsukchan	OS1	ОМС	62.52	155.77	527	1/63	1/64	1
Omsukchan	OMS	ОМС	62.52	155.77	527	12/67	OPEN	1
Onguren	ONR	ОНГ	53.233	107.592	500	–/88		2
Ootomari (Korsakov)	OOT		46.65	142.767	36	--/09	--/45	-
Oran	ORA	ОРН	55.933	113.667	705	9/79	---	1
Orlik	ORA	ОРЛ	56.295	113.983	620	9/78		1
Orotukan	ORT		62.26	151.34	470	--/77	--/77	1
Ossora	OSS	ОСС	59.25	163.065	10	–/73	OPEN	1
Ostrov Mednyi	MED	МДН	54.786	167.566	---	–/73	–/75	-
Otiai (Bykov?)	OTI		47.325	142.783	20	2/34	--/45	-
Ozernaya	OZE	ОЗН	56.295	113.983	620	9/78	---	1
Ozernaya	AY2S	ОЗР	63.75	146.11	875	06/71	--/71	2
Ozero	OZR	ОЗР	54.692	160.392	---	10/66	–/77	1
Ozhidaevo			47.033	142.392	220	--/76	--/77	-
Pakhach	PCH		60.558	169.125		–/92	–/94	1
Palana	PAL		59.093	159.963		–/94	–/96	1
Pauzhetka	PAU	ПЖТ	51.467	156.810	110	11/61	OPEN	1
Petropavlovsk	PET	ПТР	53.024	158.650	150	–/51	OPEN	1
Pevek	PVK	ПВК	69.70	170.27	20	5/65	11/65	1
Podkova	PDK	ПДК	56.140	160.780	800	–/83?	OPEN	1
Polovinka	PLK		51.798	104.35	470	8/66	9/66	1
Pravda			46.942	142.008	40	9/71	11/71	-
Provideniya	PVD	ПРВ	64.424	173.226W	25	9/80	12/93	1
Provideniya-1	PV1	ПРВ	64.45	173.18W	20	1/65	6/66	2
Romny	RMNS	РМН	50.855	129.4	210	10/78	–/87	2
Russkaya	RUS	РУС	52.432	158.507	75	12/87	OPEN	1
Saidy	SAYS	СД	68.70	134.45	88	--/80	---	1
Sasyr	SSYS	ССР	65.16	147.08	580	--/86	---	1
Savino	SOV		52.543	102.15	720	9/68	8/69	1
Sedlovina	SDL		53.278	158.884	1235	9/91	OPEN	1
Seimchan	SEY	СМЧ	62.93	152.38	211	4/69	---	1
Semlyachik	SEL	СМЛ	54.12	159.98	---	11/61	7/74	1
Severo Baikalsk	SVBS	С-Б	55.64	109.35	505	–/78	–/89	1
Severo Muisk	SVK	С-М	56.183	113.533	850	11/76	---	2
Shamanka	SHMS		53.125	105.6	700	8/59	2/63	1
Shara-Tagot	SRTS		53.005	106.717	500	10/59	–/60	1
Shebunino			46.433	141.858	40	9/71	11/71	-
Shikka (Shikuka; Poronaisk)	SKK		49.233	143.117	2	--/28	--/45	-
Shimki	SMKS		51.675	102.012	765	11/66	11/67	1
Shipunski	SPN	ШПН	53.107	160.011	170	–/62	OPEN	1
Sinegor'e	SNES	СНГ	62.09	150.52	400	--/76	--/88	1
Slyuda			56.33	124.12	1080	--/73	--/73	2
Solontsovaya	SOL	СЛЦ	54.17	108.35	458	–/79	–/87	1

Jovetskaya
Jrednekolym
Jrednii Kala
Jrednii Sake
Jrkolnyy
Jrkolnyy

Jrsk
Jrsuman

Jsam
Jsvo
Jsyakh
Jsyl'kan
Jtrakhkit

Jtsyl'yr

Jtkhoyan
Jtkaya

Jtkaya
Jtkhuryakh
Jtkhuryakh
Jtrakh
Jtrmen
Jtrskiki
Jtkhmenskoye
Jtsa
JTU
Jtsarskaya
Jtskoi
Jtsmel'nyy
Jtsoloyo

Jtsokara
Jtsykan
Jtsykuch
Jtsyrcha-
Jtsyrcha-
Jtsyrskiy
Jtyk
Jtyn
Jtykan
Jtyrskoe

Ju

Sovetskaya Gavan			48.967	140.283	50	6/69	11/70	-
Srednekolymsk	S-K	С-К	67.46	158.71	30	4/64	12/64	1
Srednii Kalar	SRK	КЛР	55.86	117.38	716	–/61	---	1
Srednii Sakutan	SDK		56.898	118.095	750	2/63	10/63	1
Stekol'nyi	STK	СТК	60.046	150.730	221	7/64	5/66	1
Stekol'nyi	MGD	МА1	60.046	150.730	221	3/71	–/94	1
		МГД-1 СТК	(60.046)	(150.730)		–/94	OPEN	1
Stolb	SOTS	СТБ	72.40	126.82	10	--/85	---	1
Susuman	SUU	СМН	62.78	148.15	640	8/69	--/95	1
		ССМ	(62.78)	(148.15)	—	--/95	--/98	1
			62.779	148.163	---	--/98	OPEN	G
Sutam			55.96	127.59	700	--/69	--/69	1
Suvo	SUVS	СУВ	63.655	110.008	1000	–/84	---	1
Syllakh	SYLS	СЛХ	57.12	121.86	600	--/89	--/89	1
Syul'ban	SYB		56.065	117.222	1000	6/62	9/63	1
Tabalakh	TBKS	ТБЛ ТБ	67.54	136.52	200	--/80	---	1
Taimylyr	TMLS	ТМЛ ТМР	72.61	121.92	60	--/86	---	1
Takhtoyamsk	TTYS	ТХТ	60.20	154.68	11	9/87	---	1
Talaya	TL-	ТЛА ТЛ	61.134	152.398	730	1/89	OPEN	G
Talaya	TAL	ТАЛ	51.681	103.644	579	11/82	OPEN	1
TasYuryakh-1			56.64	121.33	395	02/67	03/67	1
TasYuryakh-2			56.62	121.41	415	07/67	08/67	1
Tenkeli	TLIS	ТНК	70.18	140.78	110	--/84	--/93	1
Ternei	TEI	ТРН	45.067	136.6	30	7/82	---	2
Tilichiki	TIL		60.433	166.075		–/94	–/96	1
Tikhmenevo			49.2	142.9	150	6/69	10/69	-
Tiksi	TIK	ТКС	71.632	128.863	38	3/56	--/93	1
TIXI	Tiksi-GSN		71.64	128.87	30	--/95	OPEN	1
Tokarikan			56.10	126.42	800	--/72	--/73	3
Tokhoi	TKH	ТХ	51.361	106.608	640	11/71	4/73	1
Tonnel'nyi	TNL	ТНЛ	56.283	113.35	820	11/76	---	1
Topolovo	TOP	ТОП ТПЛ	53.230	158.041	155	11/61	–/93	1
Toyohara (Yuzhno)						--/43	--/45	-
Tsipikan	ZIP	ЦРК	54.917	113.35	1110	–/75	2/86	1
Tsiveluch	SVL	ШВЛ	56.583	161.225	900	10/80	OPEN	1
Tungurcha-1	TUG1		57.33	121.48	440	--/70	--/70	1
Tungurcha-2	TUG	ТНГ	57.27	121.48	315	--/78	---	1
Tungusskii	AY3S		64.20	146.38	1080	--/71	--/71	1
Tupik	TUP	ТПК	54.425	119.933	630	11/61	---	1
Turan	TRNS		51.633	101.666	870	12/66	11/68	1
Turikan	TNKS	ТНК	56.383	113.108	695	8/81	---	1
Tymovskoe	TYV TMSS	ТМС	50.85	142.65	100	4/69	---	-
Tynda	TYD	ТНД	55.133	123.717	610	7/70	1/72	2

Tyrgan	TRG	ТРГ	52.758	106.342	600	1/60		1
Tyubelyakh	UL1S	ТЕБ	65.37	143.15	380	--/88	--/88	3
Uakit	UKT	УКТ	55.495	113.62	1140	12/62	–/75	2
Udokan	UDK		56.75	118.305	810	4/67	4/69	1
Udzha			71.25	117.17		08/27/75	09/19/75	-
Uelen			66.16	169.84W	5	--/81	–/82	1
Uglegorsk	UGL	УГЛ	49.083	142.083	20	-/51	---	-
Ulyukchikan	UCK	УЛК	53.87	109.598	490	7/70	9/70	1
Ulyunkhan	ULNS	ОЛЯ	54.867	111.07	560	7/89	---	2
Unknown	UNYS	УНЮ						
Uoyan	YOA	УН	56.13	111.77	520	–/79	---	1
Ust' Nera-1	UNR1	У-НР	64.566	143.230	485	--/62	--/92	1
Ust' Nera-2	UNR	У-Н	64.565	143.242	485	--/92	OPEN	G
Ust' Nyukzha	USZ	У-Н	56.56	121.59	415	--/64	---	1
Ust' Urkima	UURS	УРК	56.31	123.16	540	--/81	---	1
Ust' Bolsheretsk	UBL		52.842	156.308	20	11/61	–/64	1
Ust' Belaya	U-B	У-Б	65.51	173.28	20	11/66	5/67	1
Ust' Srednikan	SRD	СРД	62.44	152.32	580	12/62	11/63	1
Ust' Omchug	USO	У-ОМ	61.13	149.63	580	--/68	--/83	1
Utesnoe			46.6	143.075	20	7/73	9/79	-
Vankarem	VNK	ВНК	67.84	175.85W	10	3/66	6/66	1
Verkhene Kamchatsk	VKM		54.627	158.473	170	10/66	–/75?П	1
Vladivostok	VLA	ВЛД	43.12	131.893	75	–/29	–/31	-
Vodopadnii	VDP	ВДР	55.770	160.220	1060	–/77	–/91	1
Vzmor'e			48.85	142.517	20	7/82	12/82	-
Yablochnyi			47.167	142.067	20	6/68	9/68	-
Yagodnoe	YAG		62.53	149.62	480	--/77	--/77	1
Yakutsk-1	YAK1		62.015	129.722	90	10/57	--/62	1
Yakutsk-2	YAK	ЯК	62.030	129.677	91	--/62	OPEN	1
Yaruga	YRGS	ЯРГ	57.49	123.07	780	--/89	--/89	2
Yasnyi	YASS	ЯСН	53.29	127.983	310	1/75	--	1
Yubileniya	YUBS	ЮБЛ ЮБТ	70.74	136.10	10	--/86	--/93	1
Yuzhno Sakhalinsk	YSS	ЮСХ	46.958	142.762	100	--/57	OPEN	1
Yuzhno Sakhalinsk (Novo Aleks-androvsk)	YSS1		47.02	142.717	40	10/47	--/57	-
Zakamensk	ZAK	ЗКМ	50.383	103.292	1125	12/60	---	1
Zapadnyi	ZAP		56.613	118.433	1600	4/67	8/67	1
Zarech'e	ZARS		52.550	107.15	460	7/59 7/69	–/60 9/69	1
Zarya	ZRY		57.24	118.917	655	10/59	9/68	2
Zemlya Bunge			74.833	142.583		4/75	6/75	-
Zeya	ZEA	ЗЕЯ	53.755	127.293	270	6.76	--	1
Zhigalovo	ZGL		54.808	105.15	625	12/67	2/67	1
Zhuravlikha	ZRV	ЖРВ	53.517	109.375	475	7/70	9/70	1
Zimniki	ZMN	ЗМН	45.475	134.258	150	7/88	--	2

Zyryanka	ZYRS	3PH	65.72	149.82	120	--/82	--/90	1
Zyryanka-1	ZY1	3PH	65.74	150.89	37	1/64	10/64	1

APPENDIX B

Annual plots of seismicity in northeast Russia. Original Russian epicenters are used.

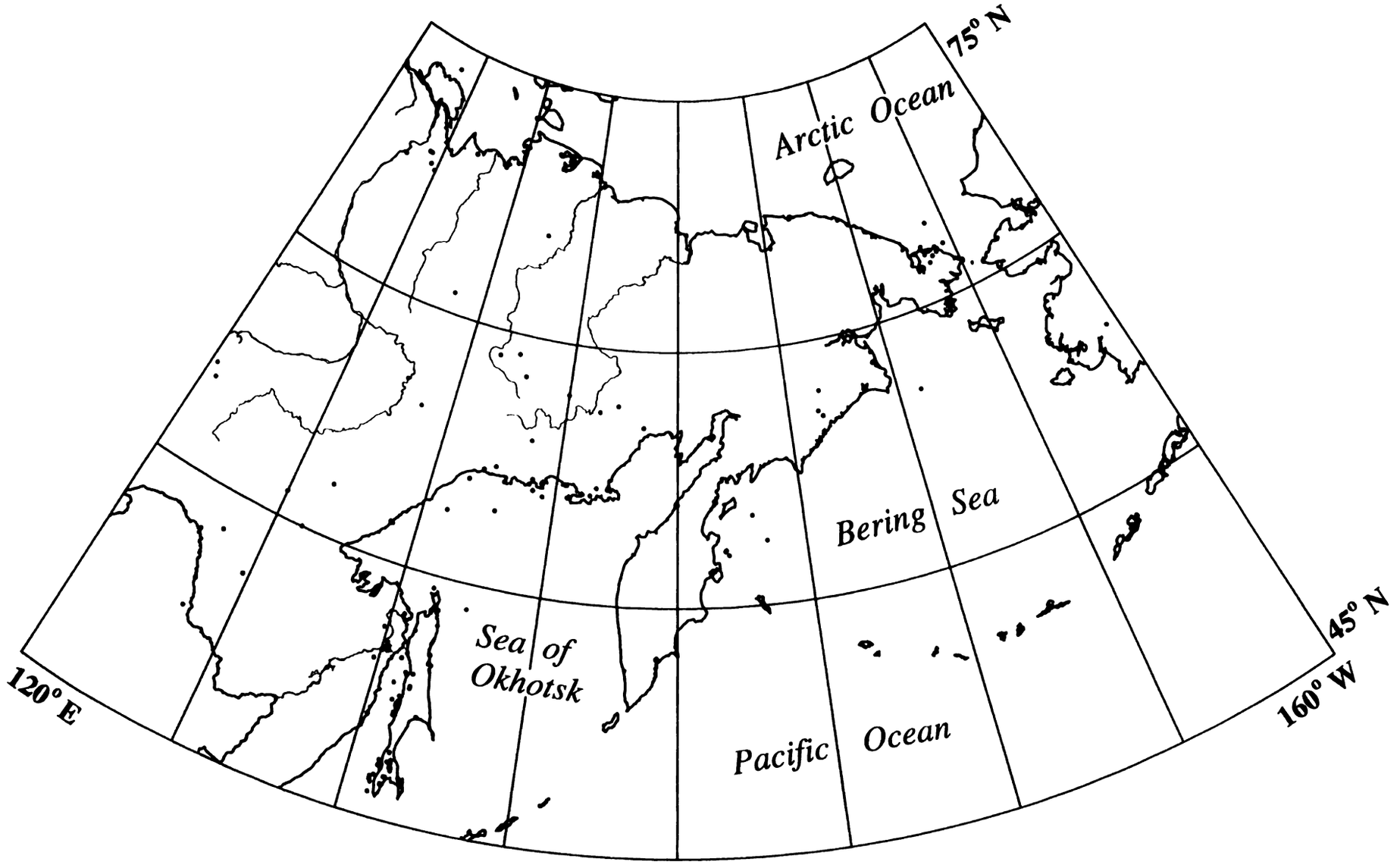

Figure B-1. Historic seismicity of northeastern Russia (pre 1950).

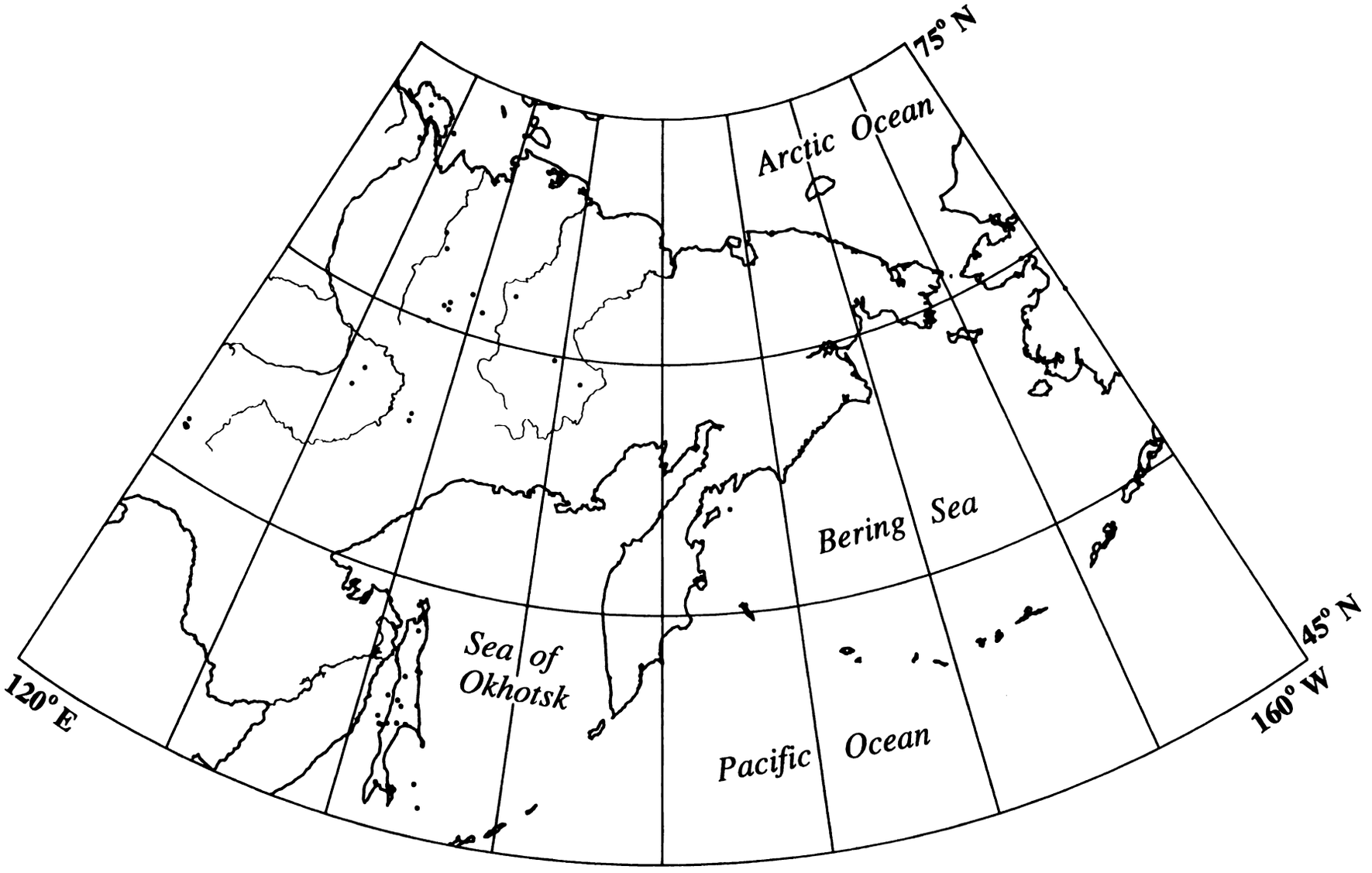

Figure B-2. Seismicity of northeastern Russia in 1950-1959.

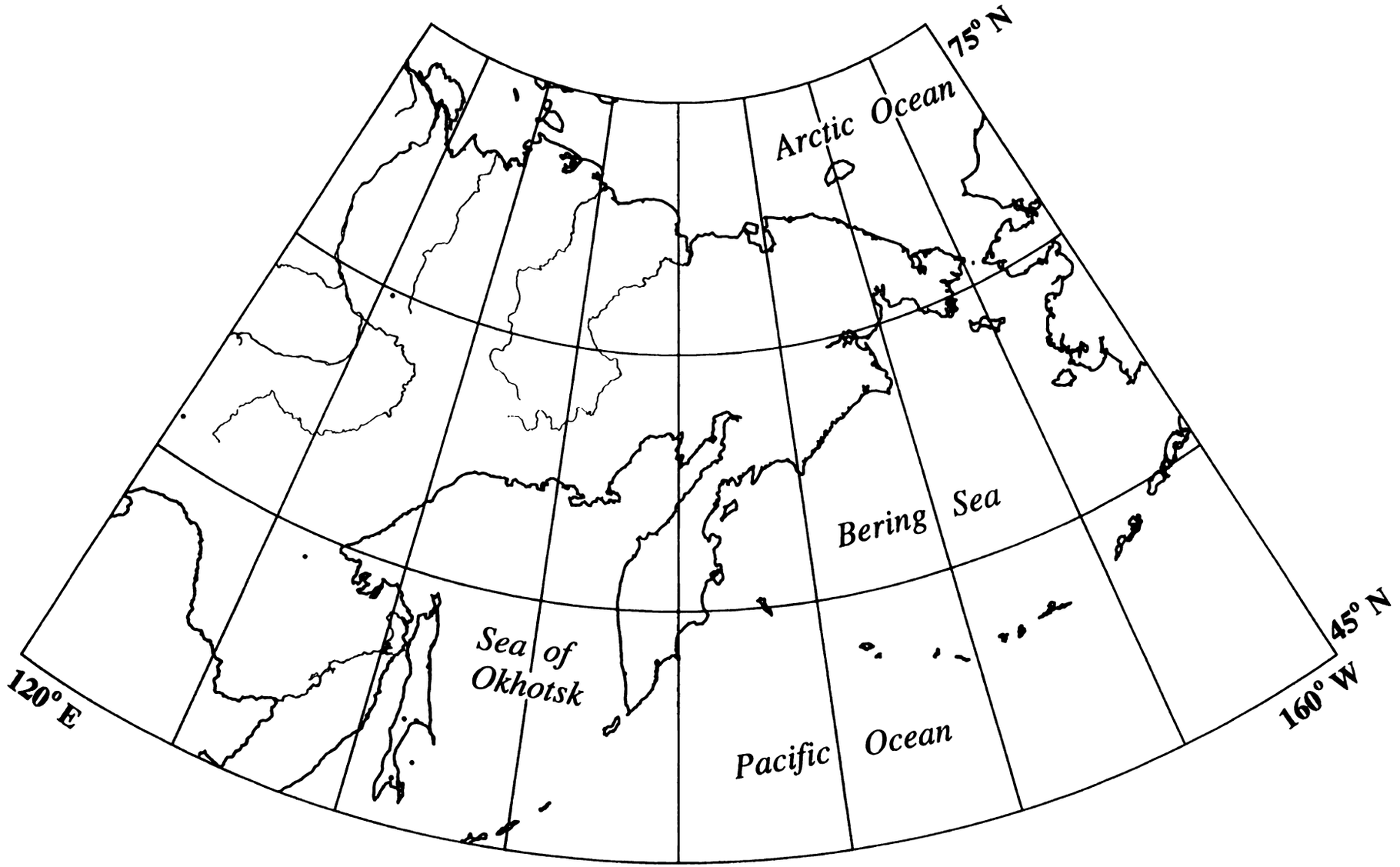

Figure B-3. Seismicity of northeastern Russia in 1960.

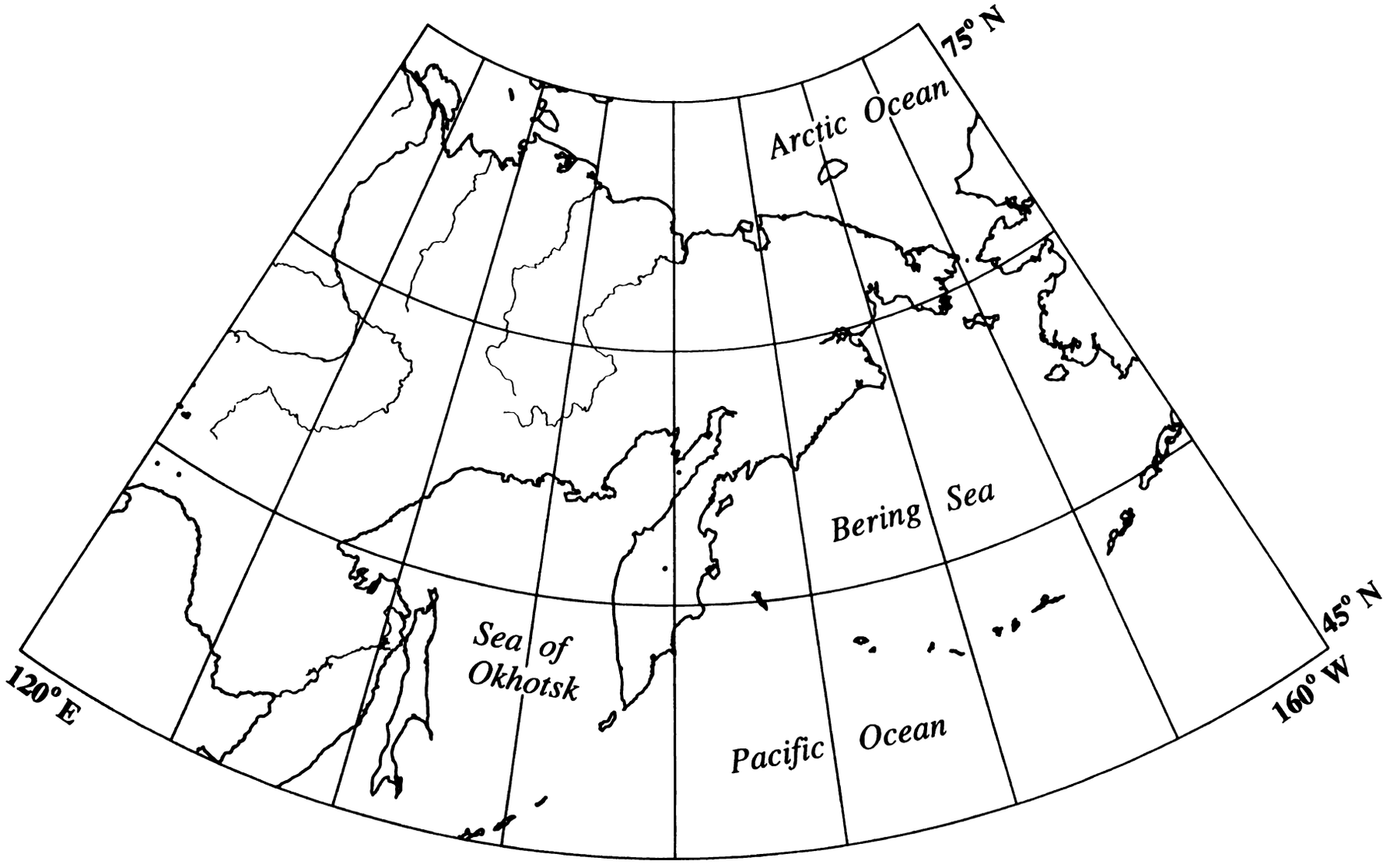

Figure B-4. Seismicity of northeastern Russia in 1961.

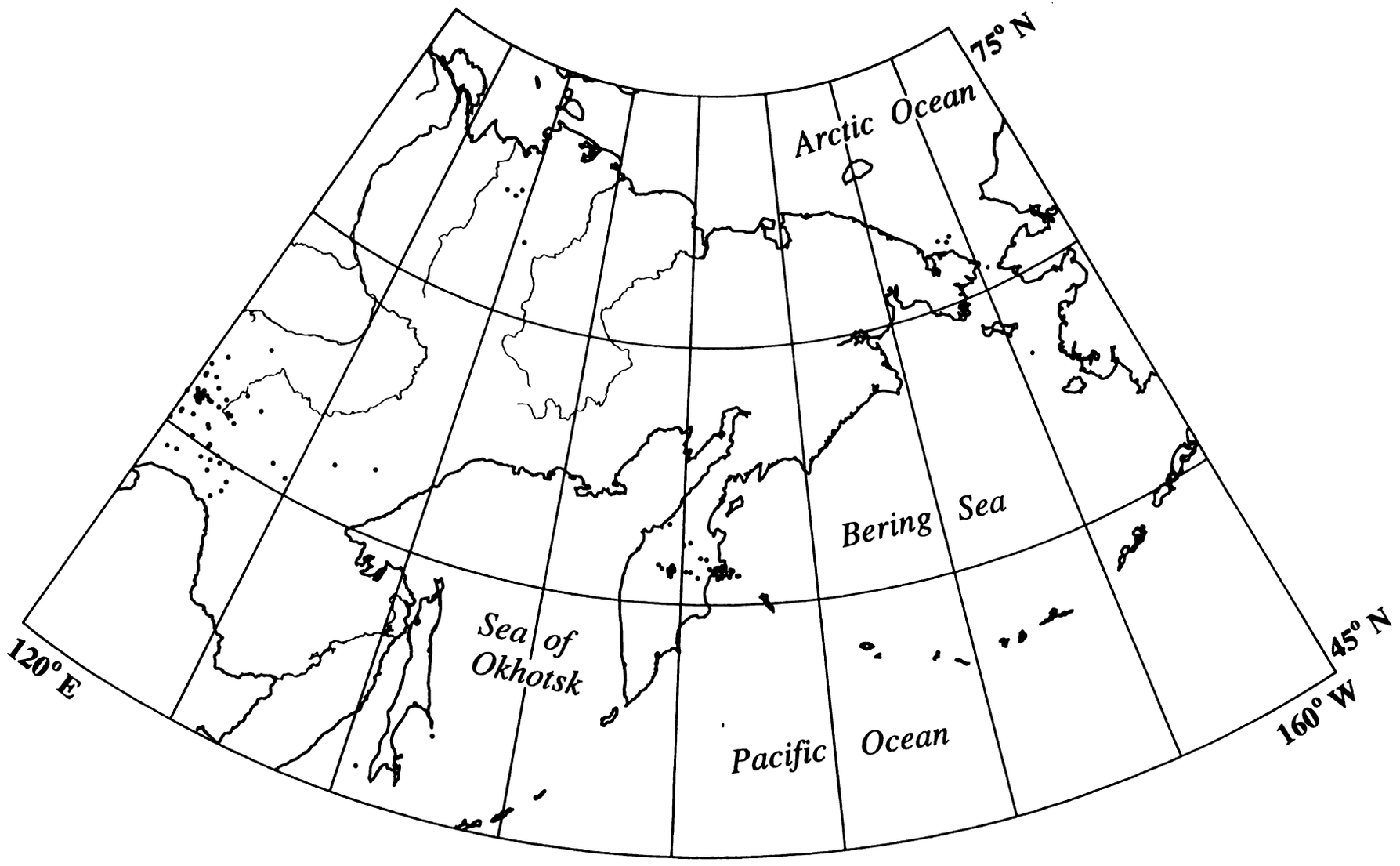

Figure B-5. Seismicity of northeastern Russia in 1962.

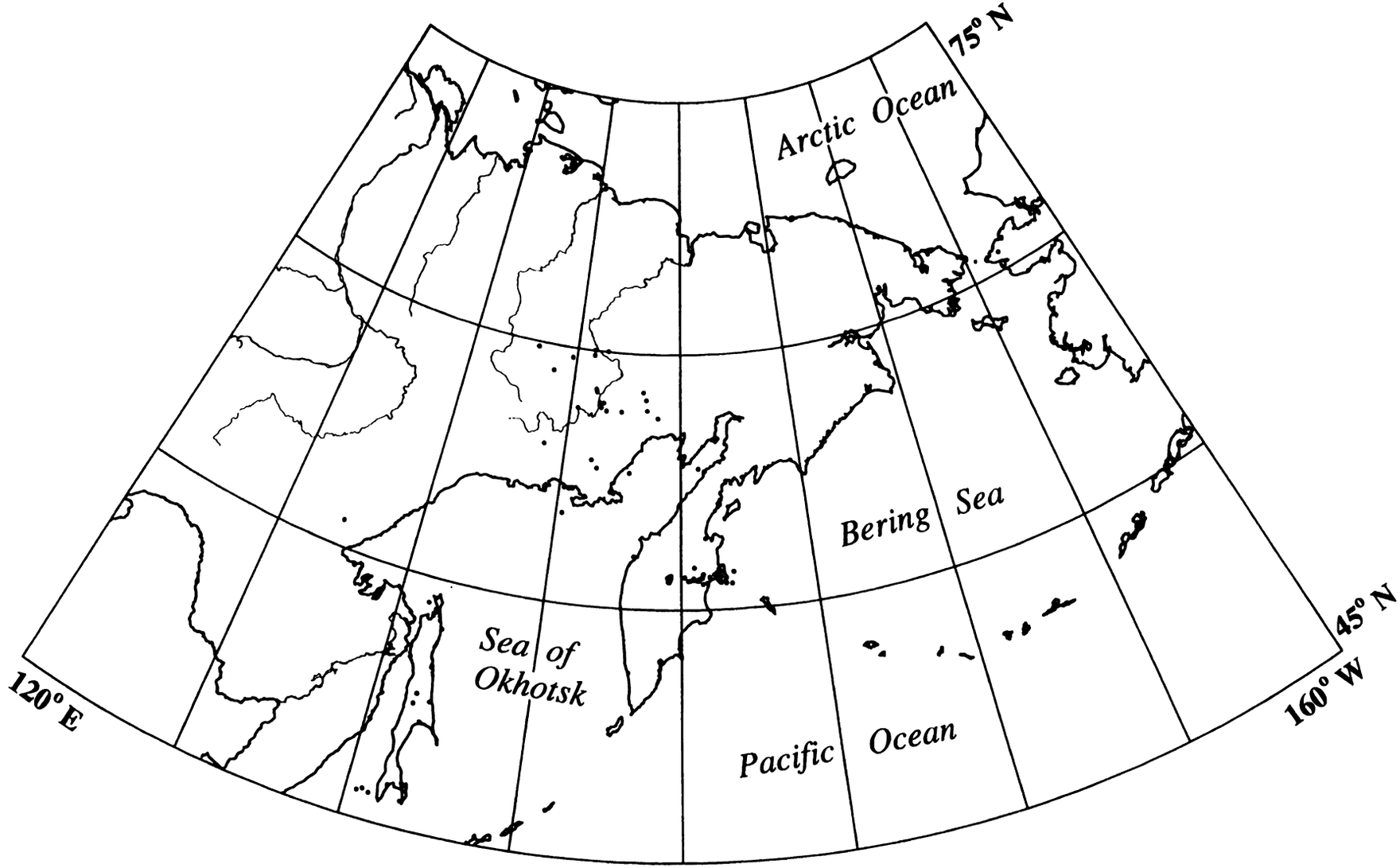

Figure B-6. Seismicity of northeastern Russia in 1963.

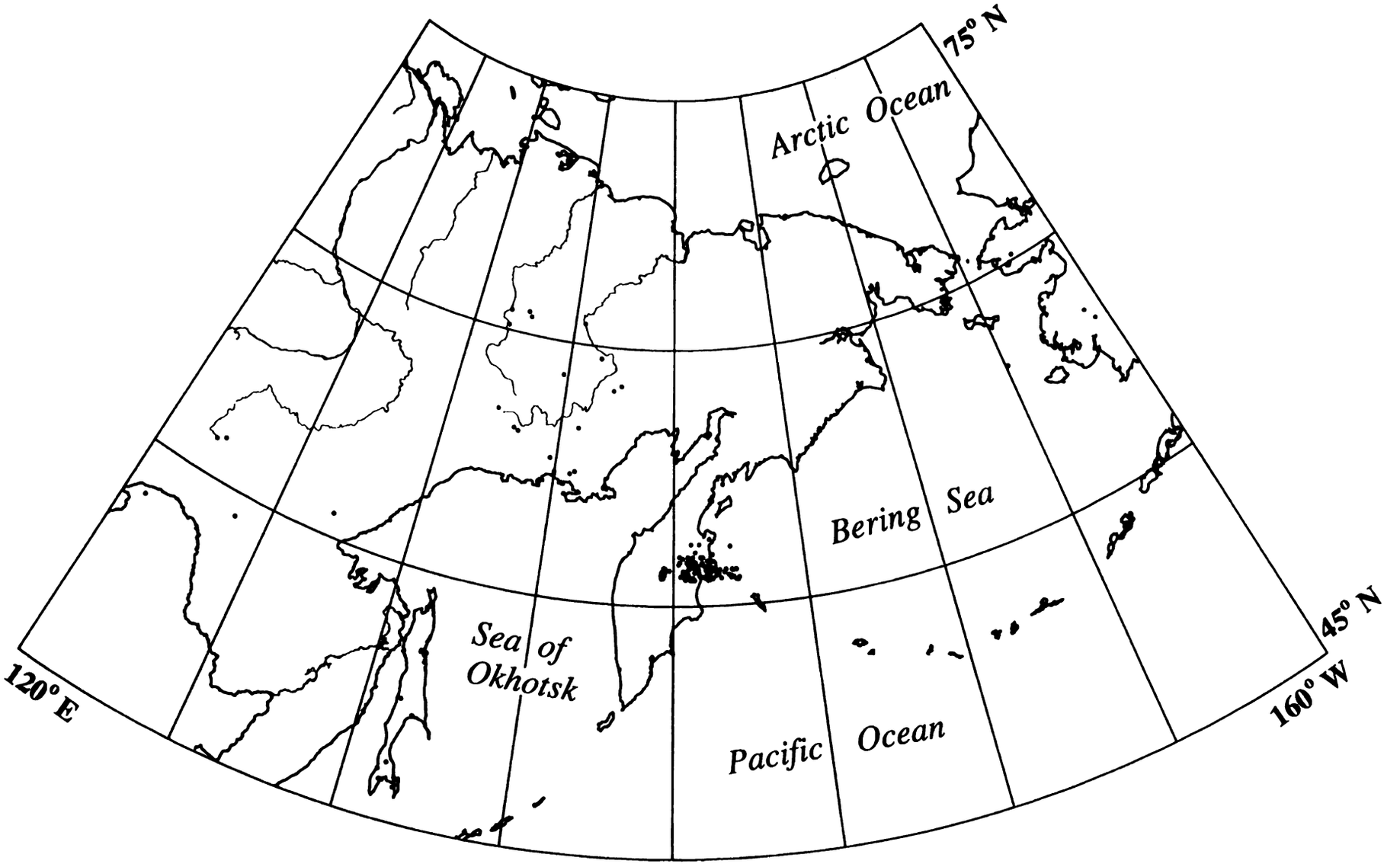

Figure B-7. Seismicity of northeastern Russia in 1964.

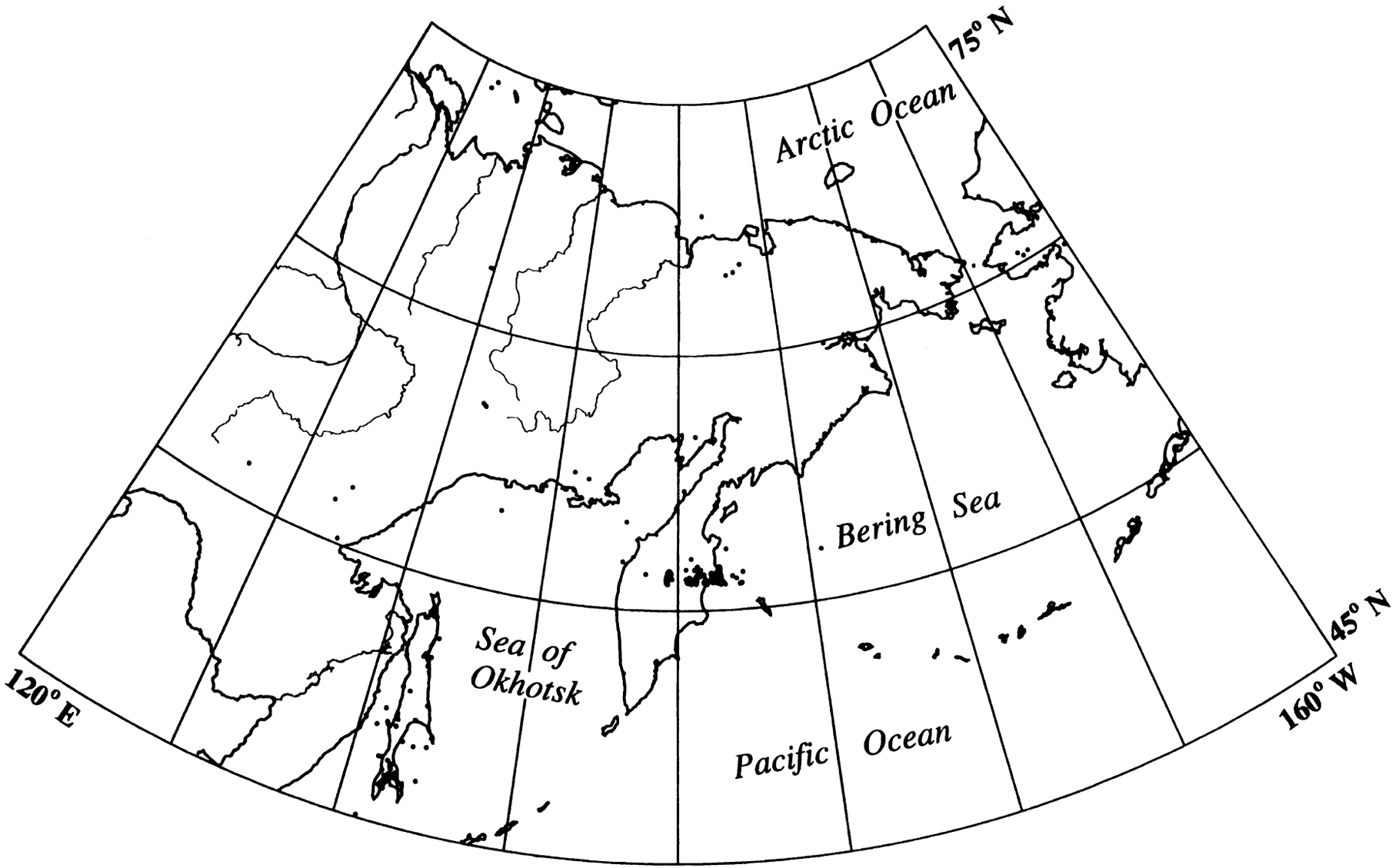

Figure B-8. Seismicity of northeastern Russia in 1965.

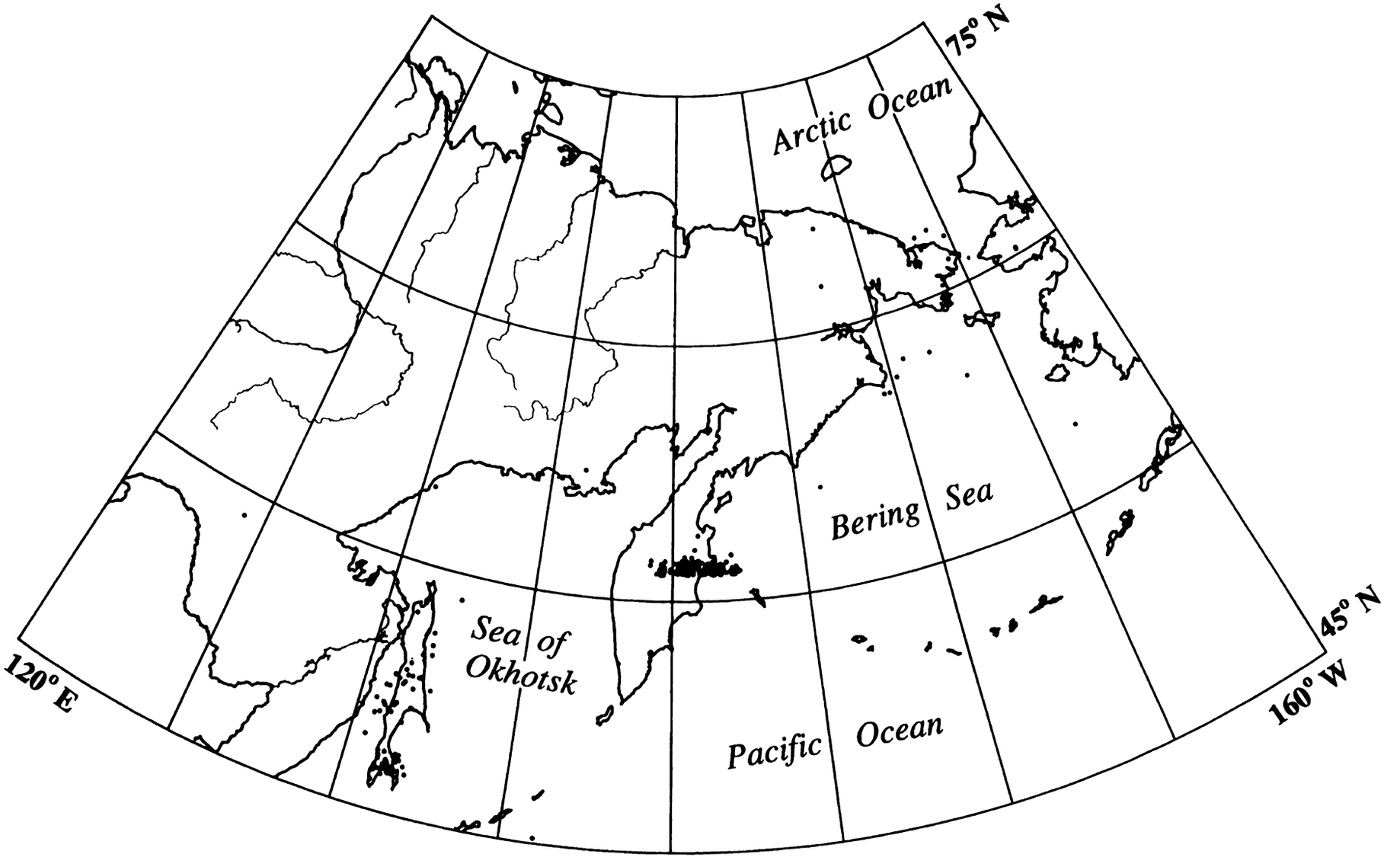

Figure B-9. Seismicity of northeastern Russia in 1966.

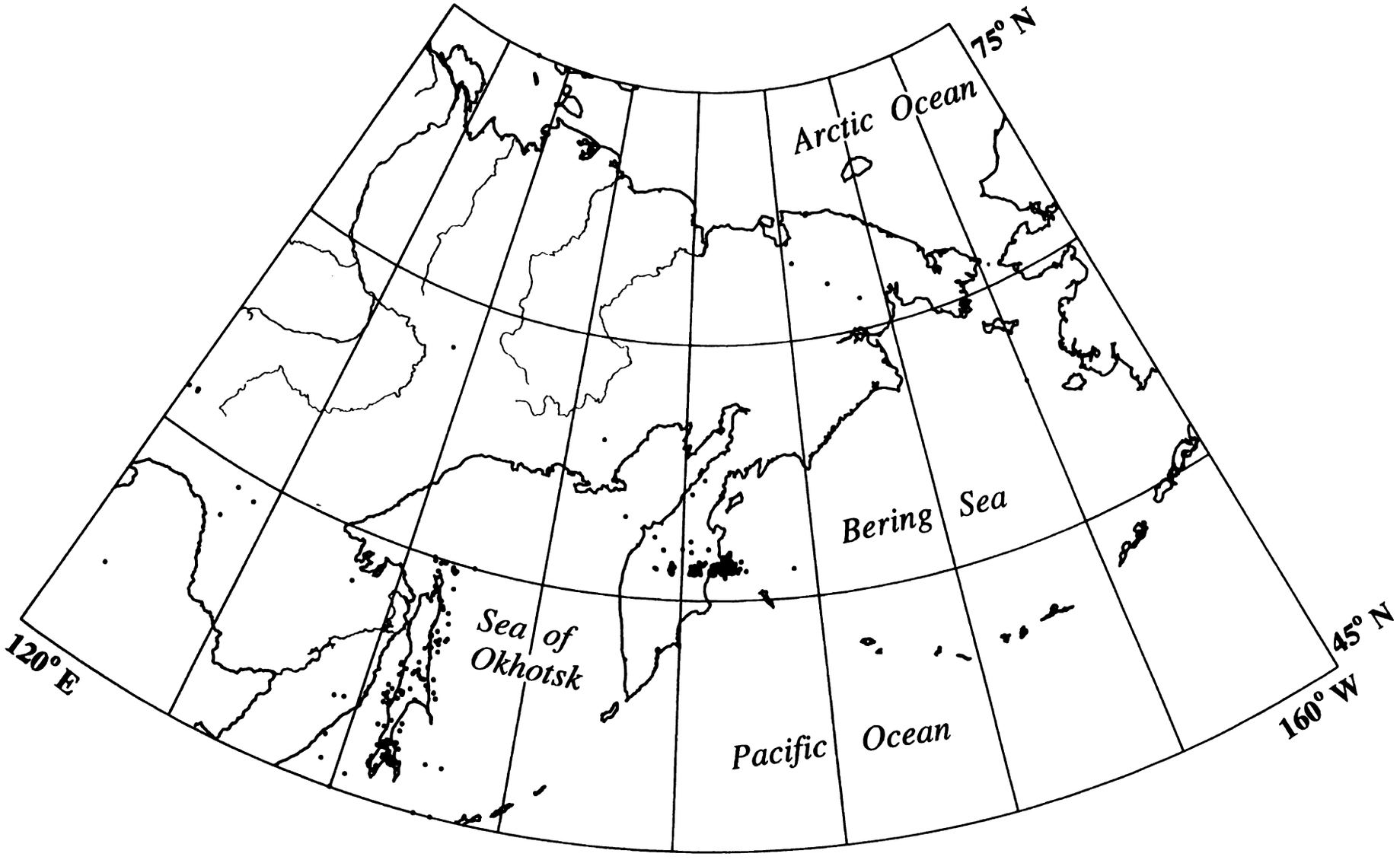

Figure B-10. Seismicity of northeastern Russia in 1967.

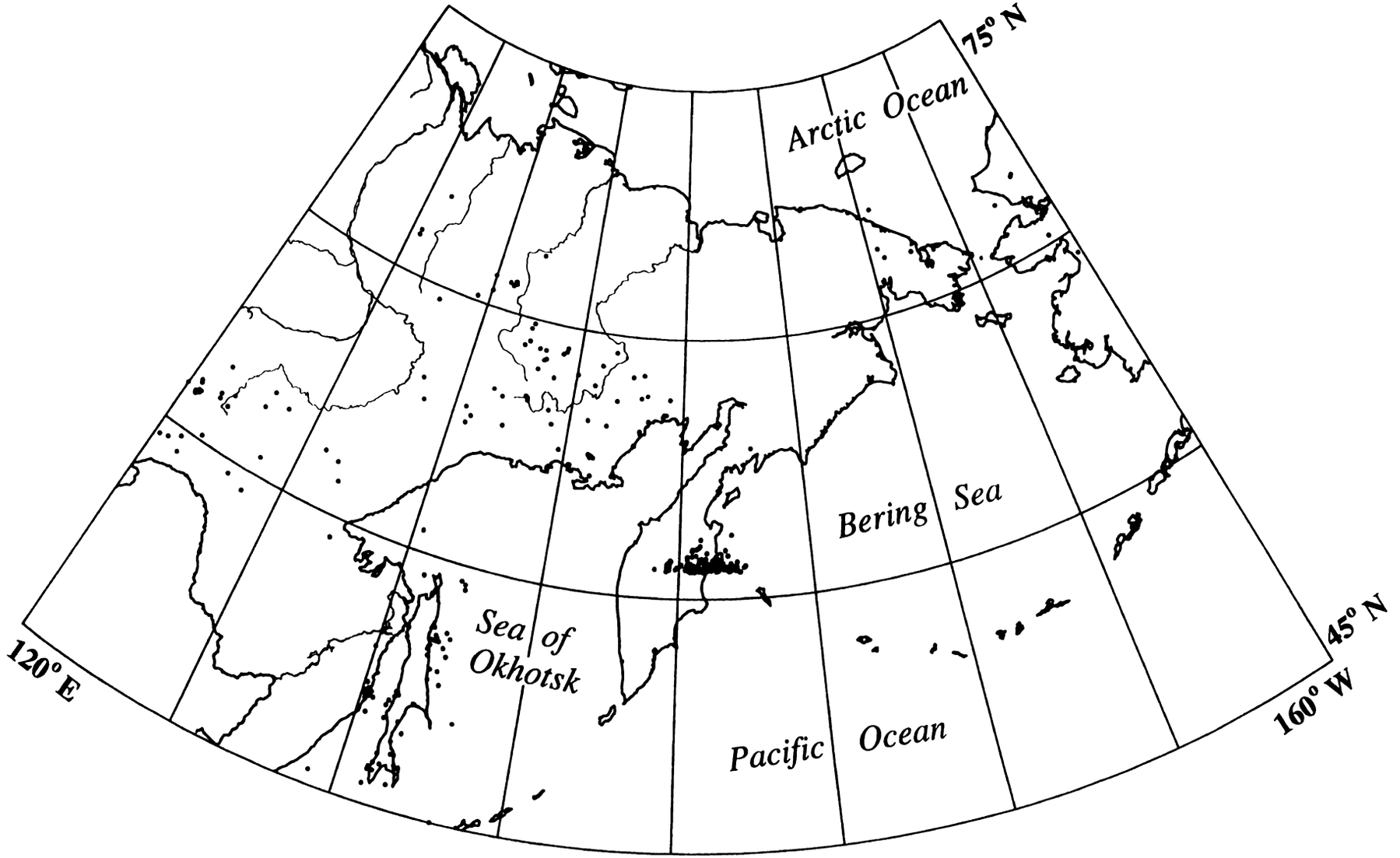

Figure B-11. Seismicity of northeastern Russia in 1968.

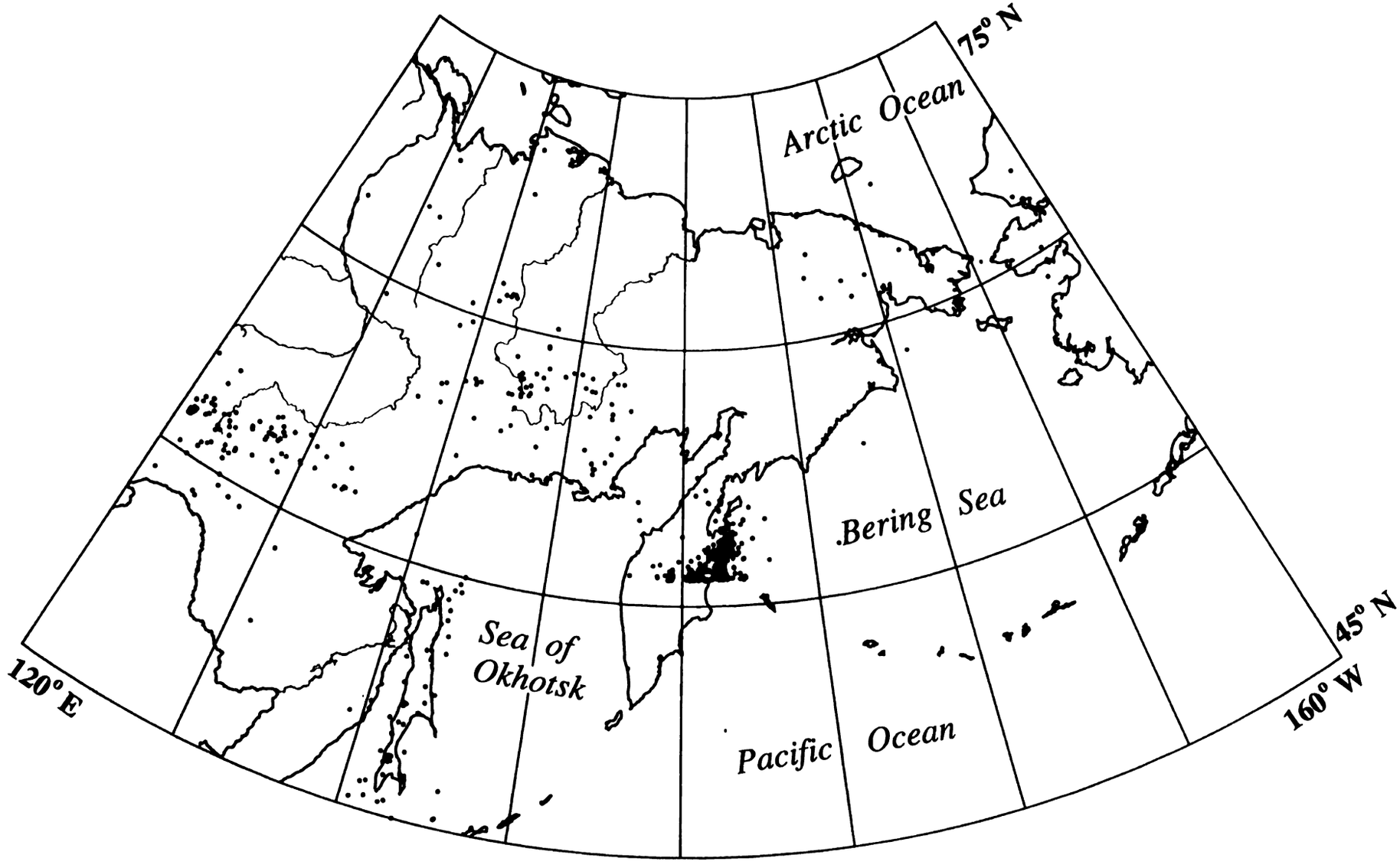

Figure B-12. Seismicity of northeastern Russia in 1969.

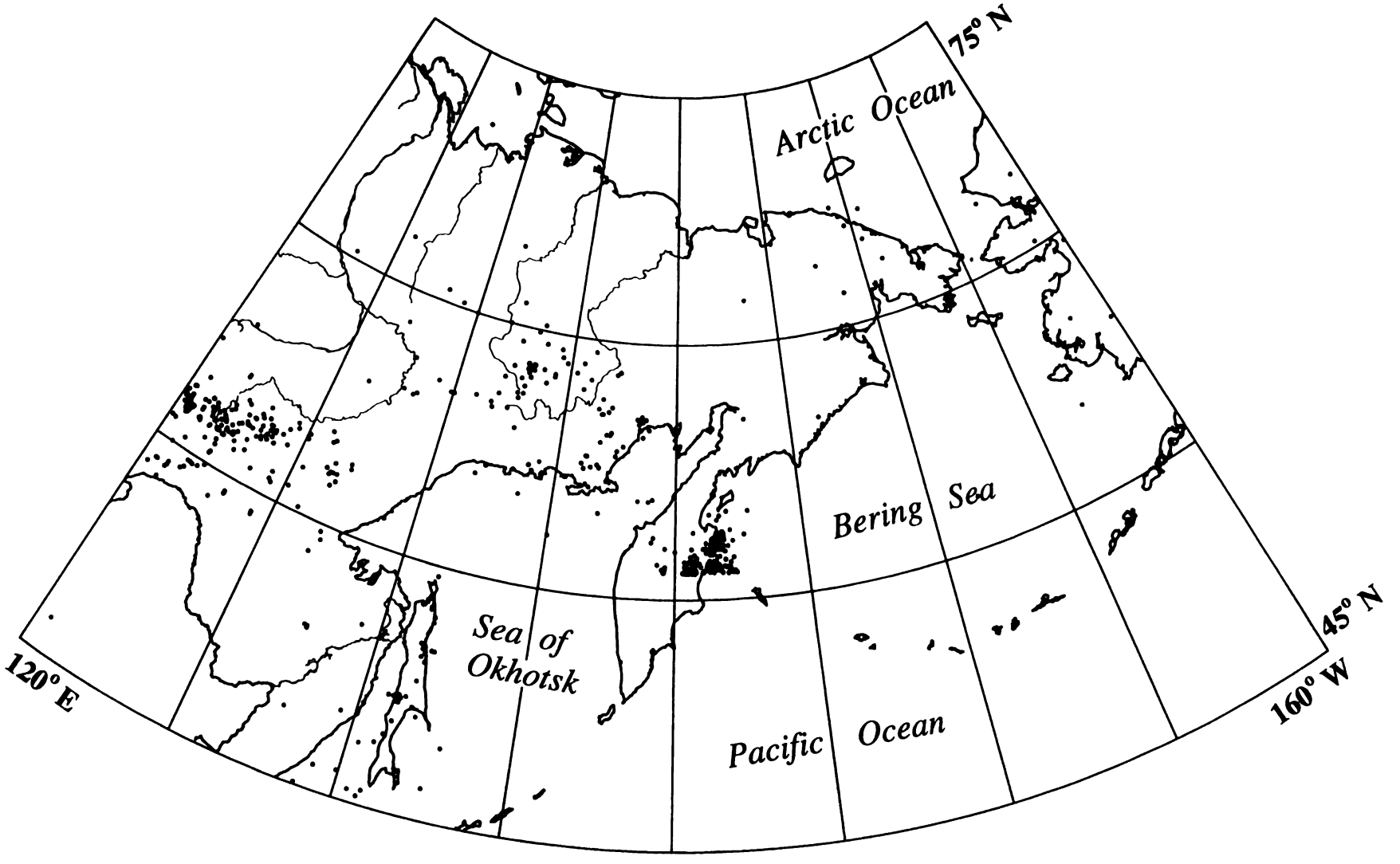

Figure B-13. Seismicity of northeastern Russia in 1970.

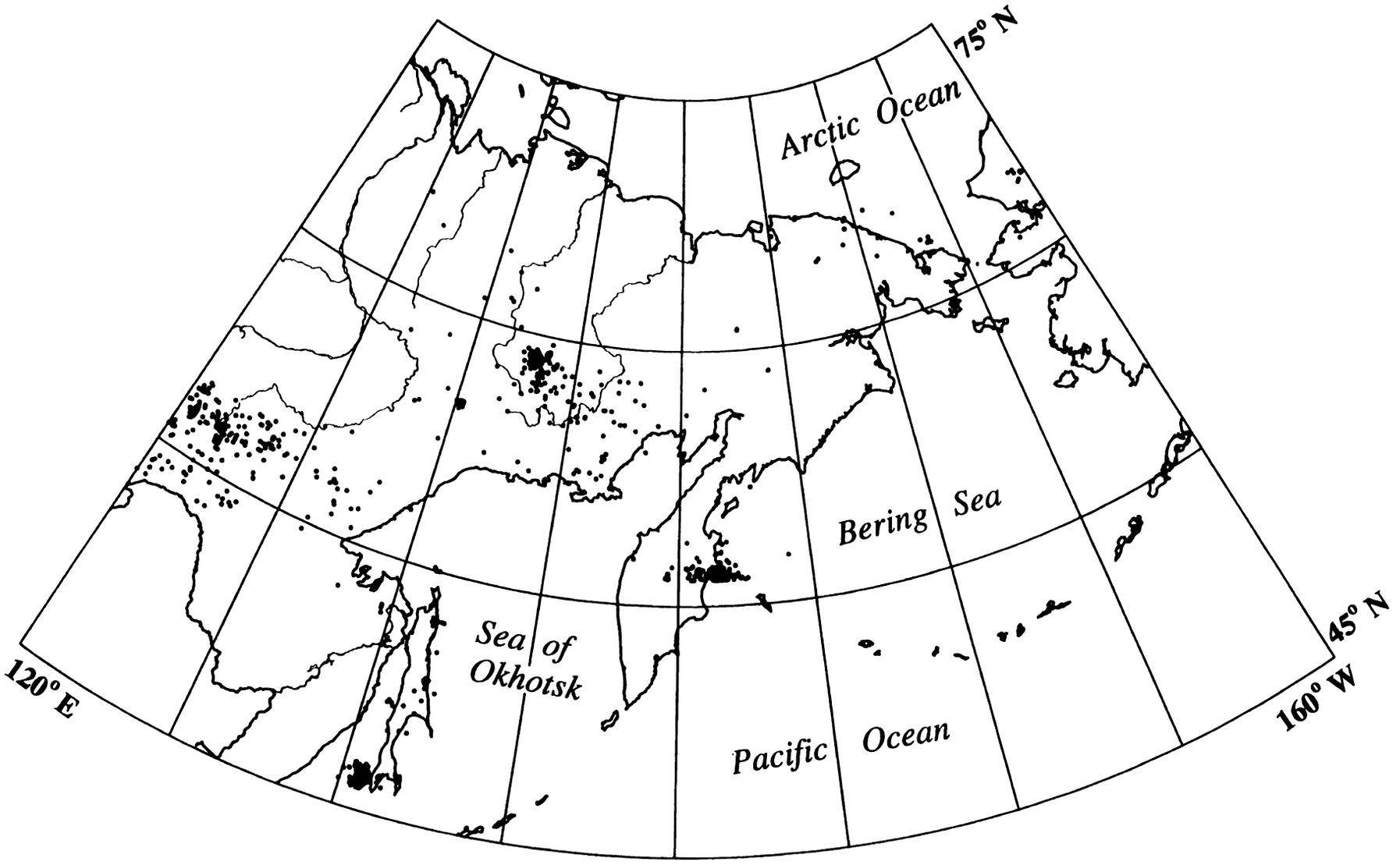

Figure B-14. Seismicity of northeastern Russia in 1971.

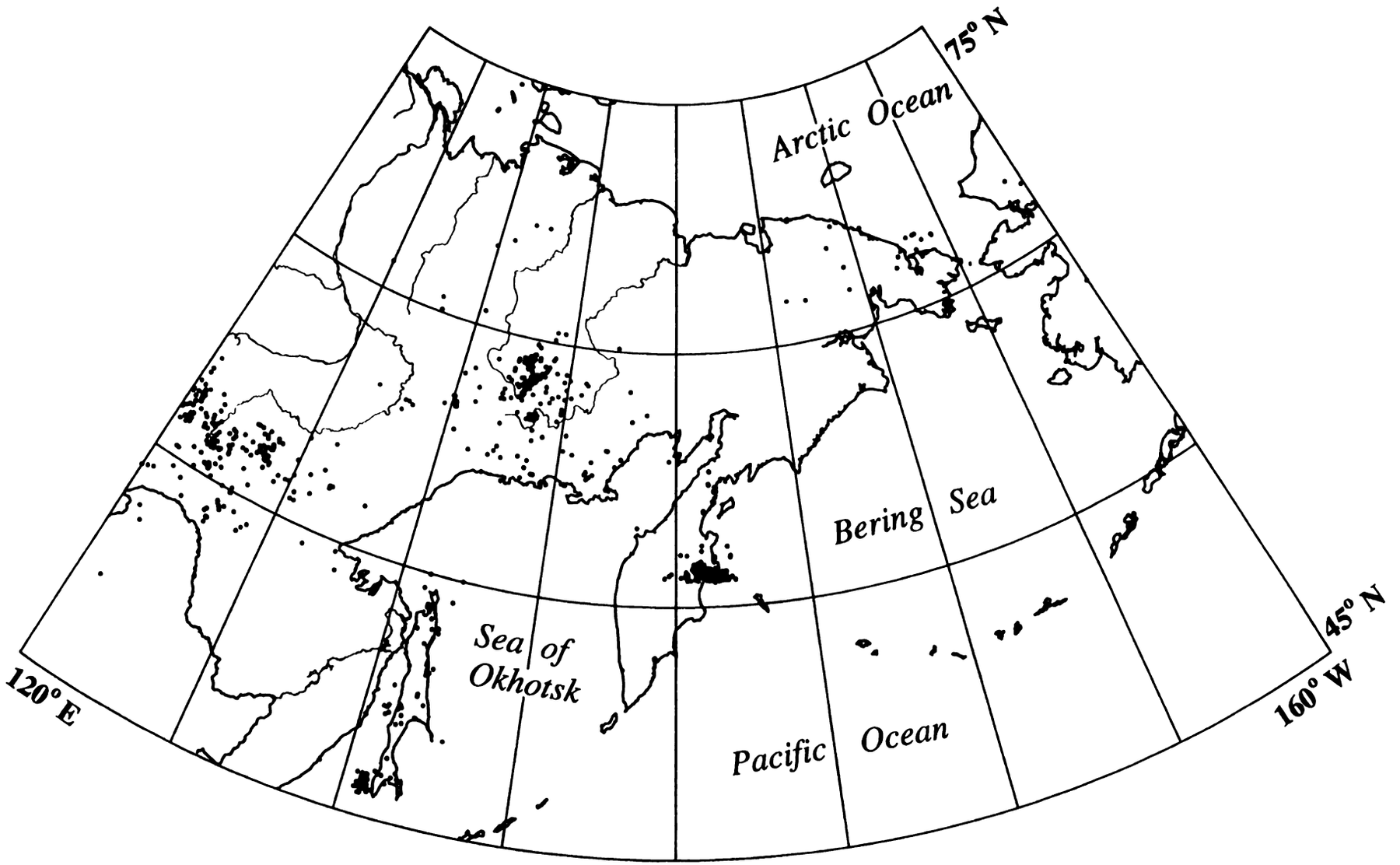

Figure B-15. Seismicity of northeastern Russia in 1972.

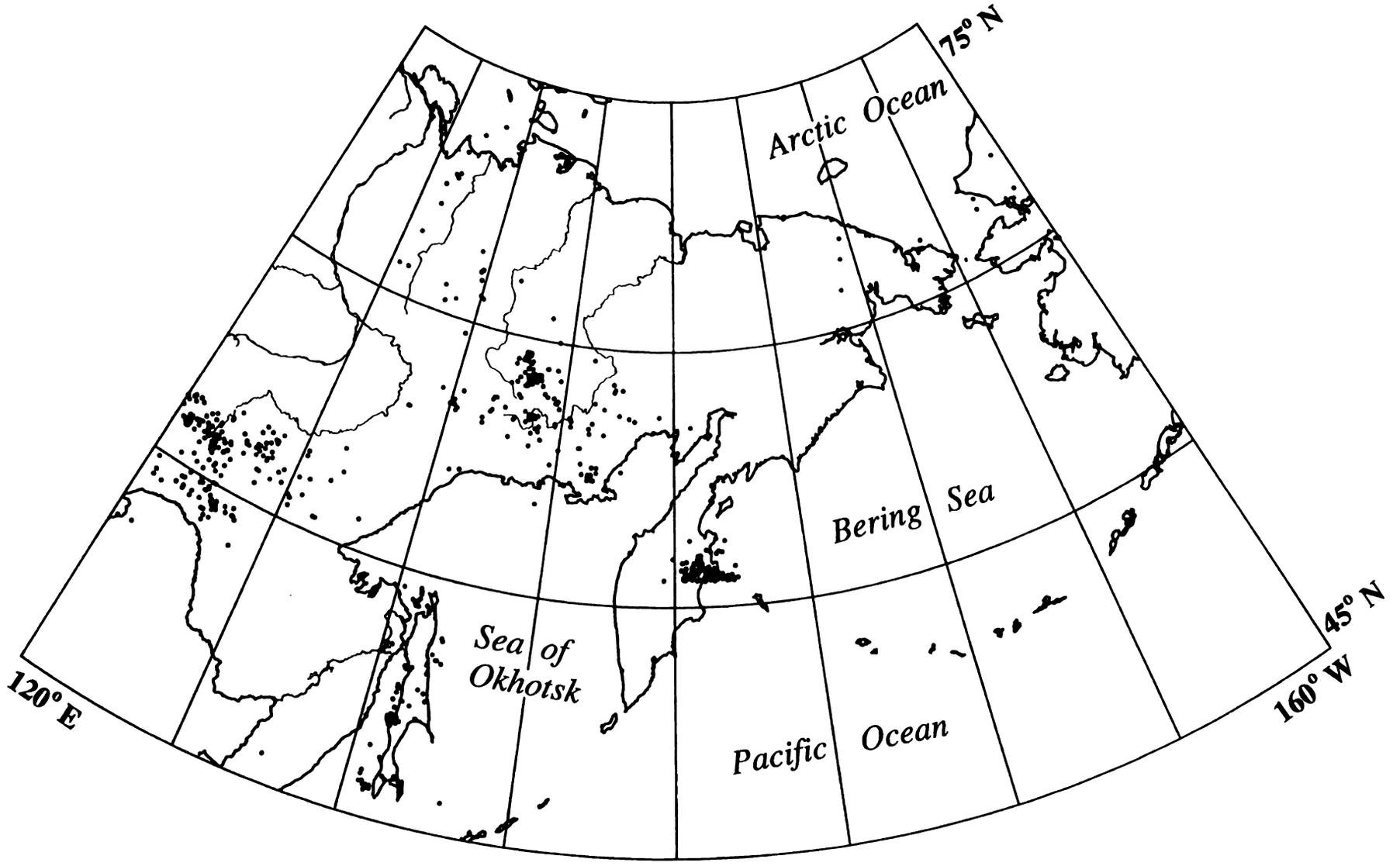

Figure B-16. Seismicity of northeastern Russia in 1973.

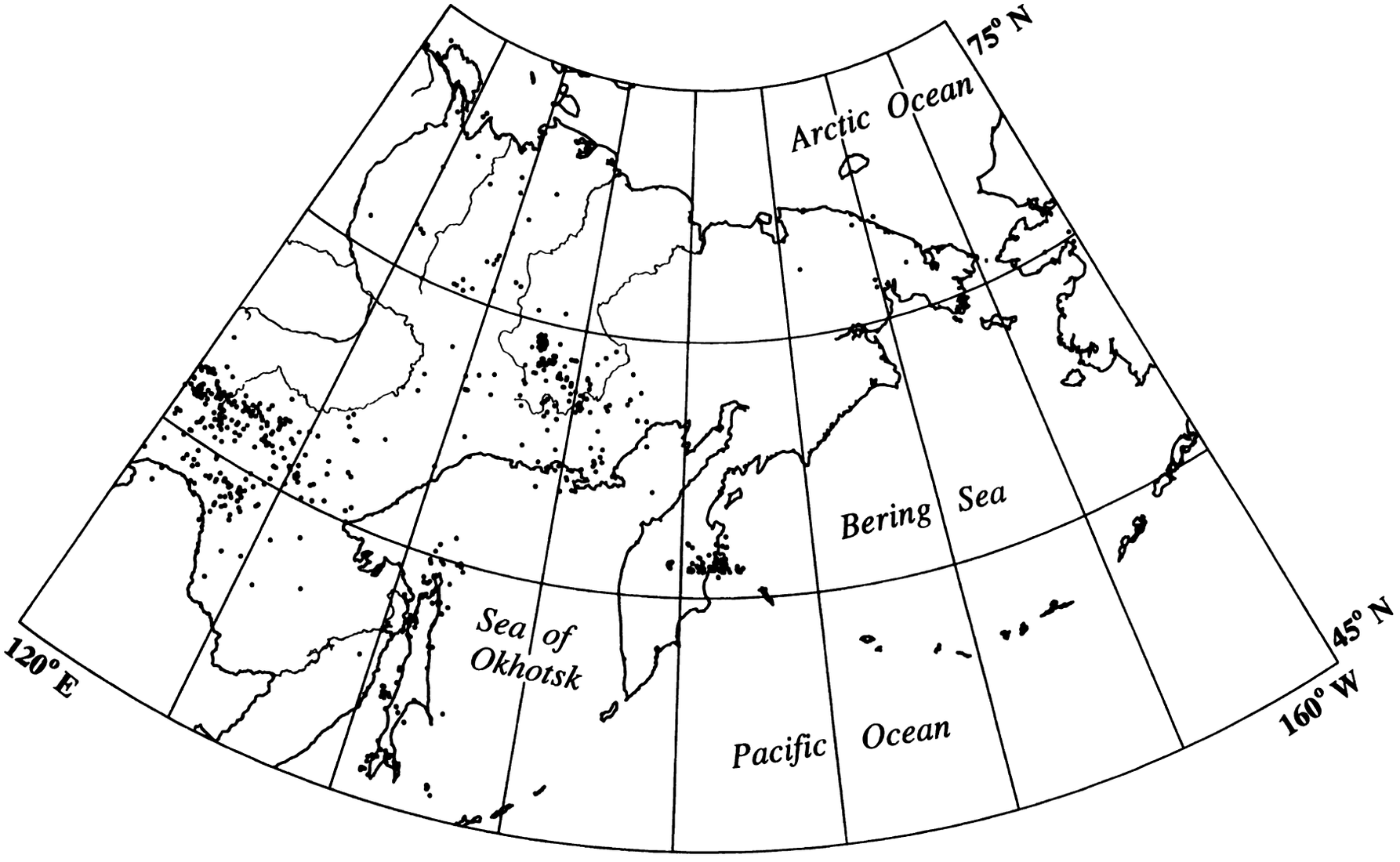

Figure B-17. Seismicity of northeastern Russia in 1974.

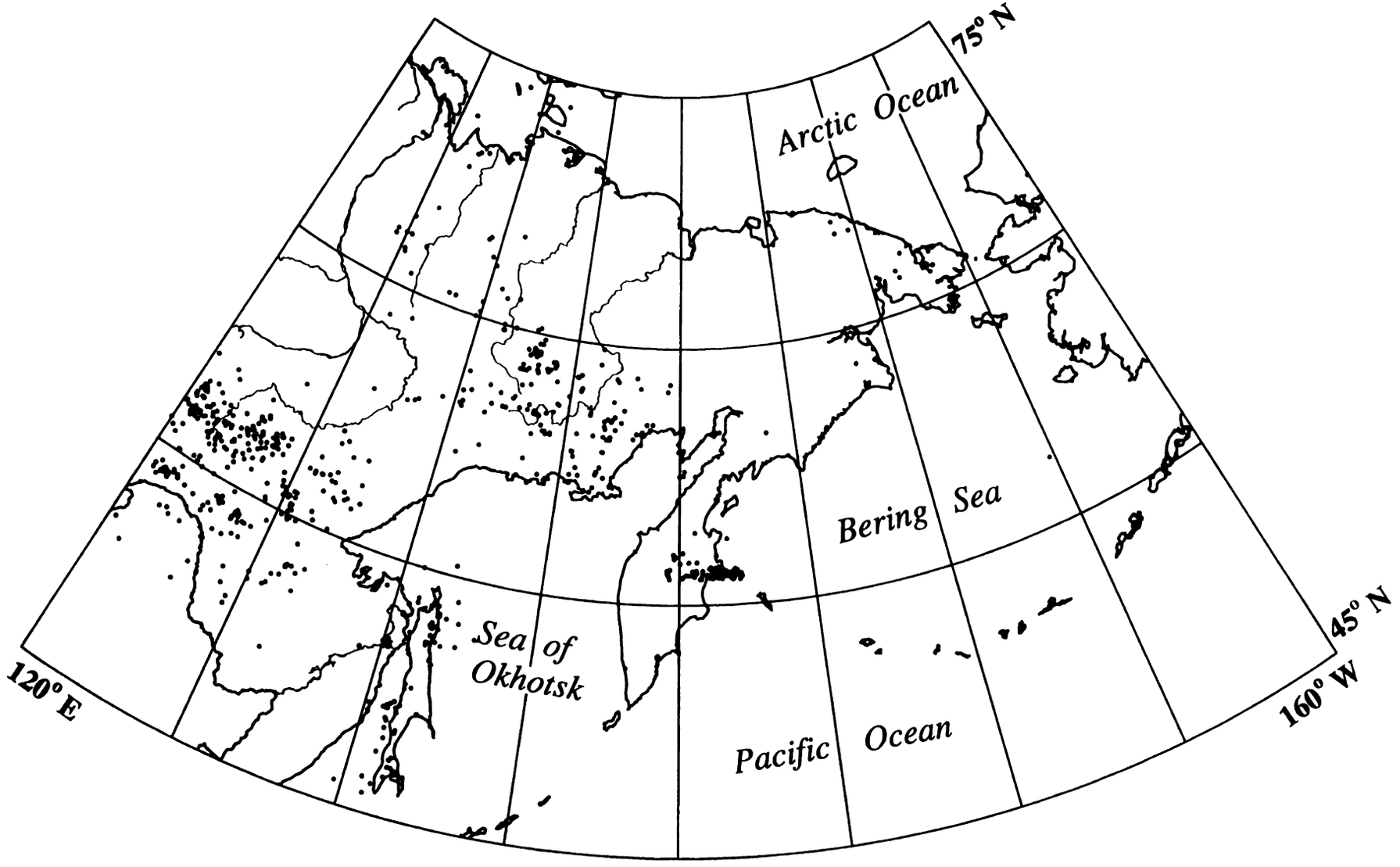

Figure B-18. Seismicity of northeastern Russia in 1975.

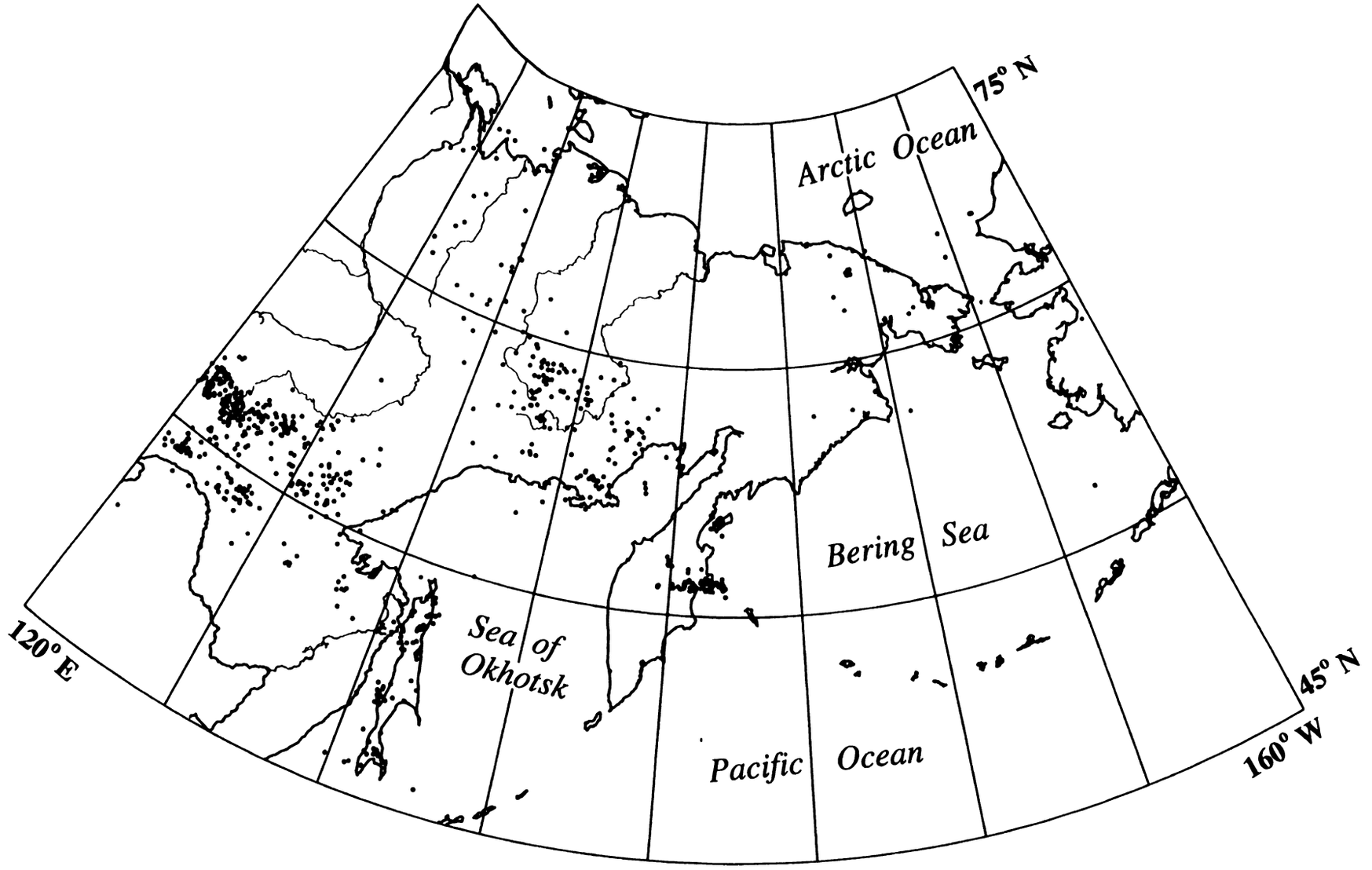

Figure B-19. Seismicity of northeastern Russia in 1976.

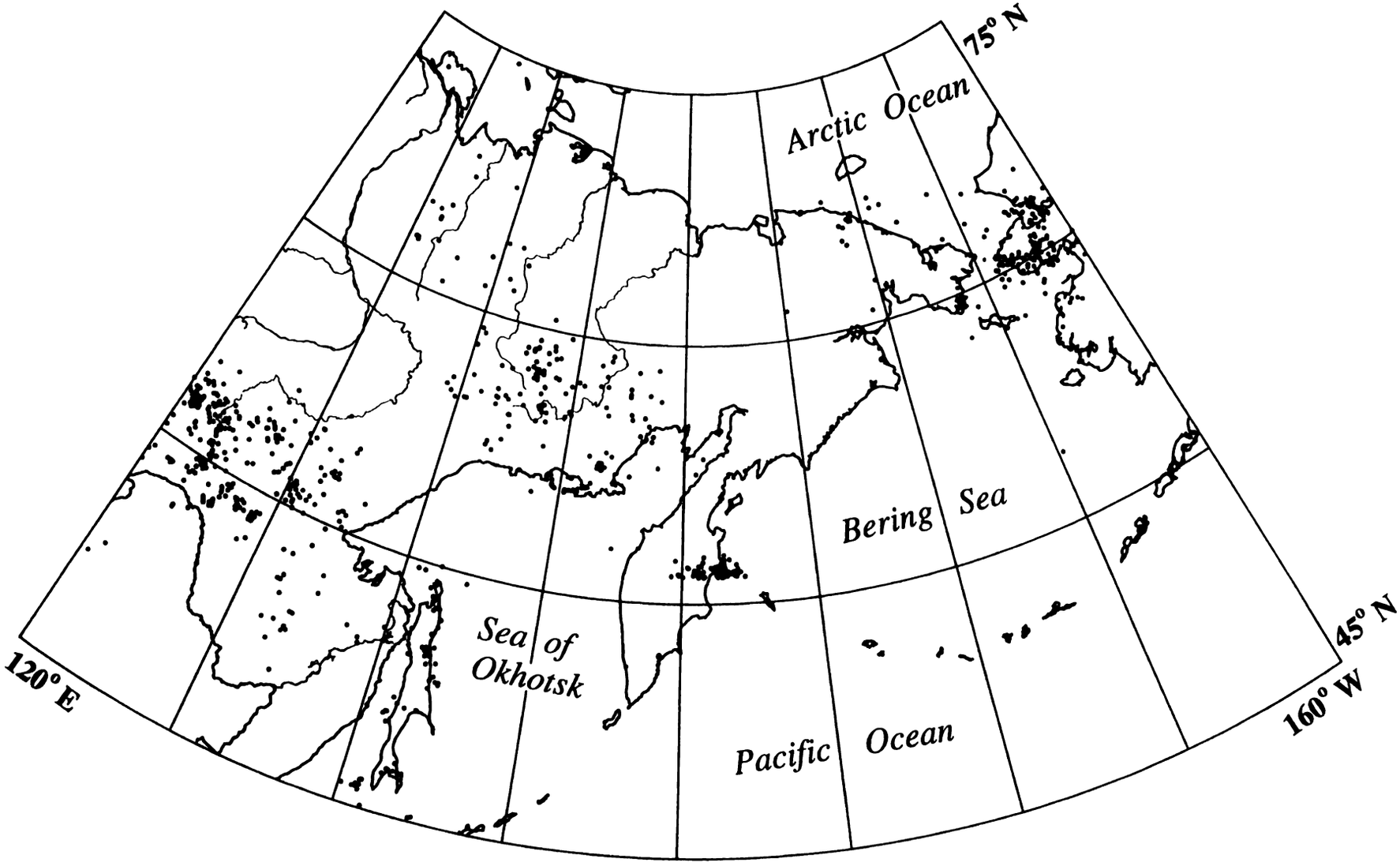

Figure B-20. Seismicity of northeastern Russia in 1977.

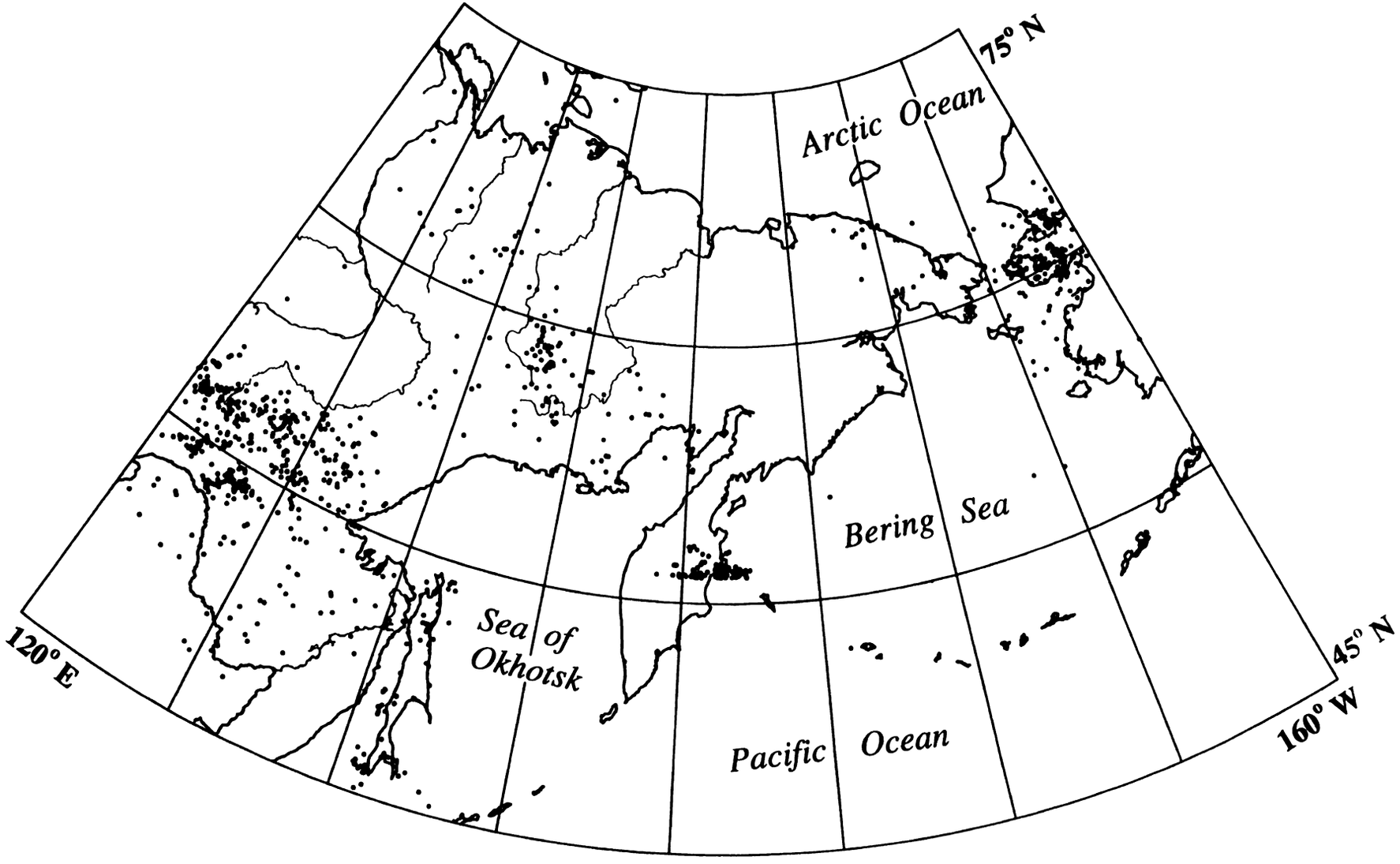

Figure B-21. Seismicity of northeastern Russia in 1978.

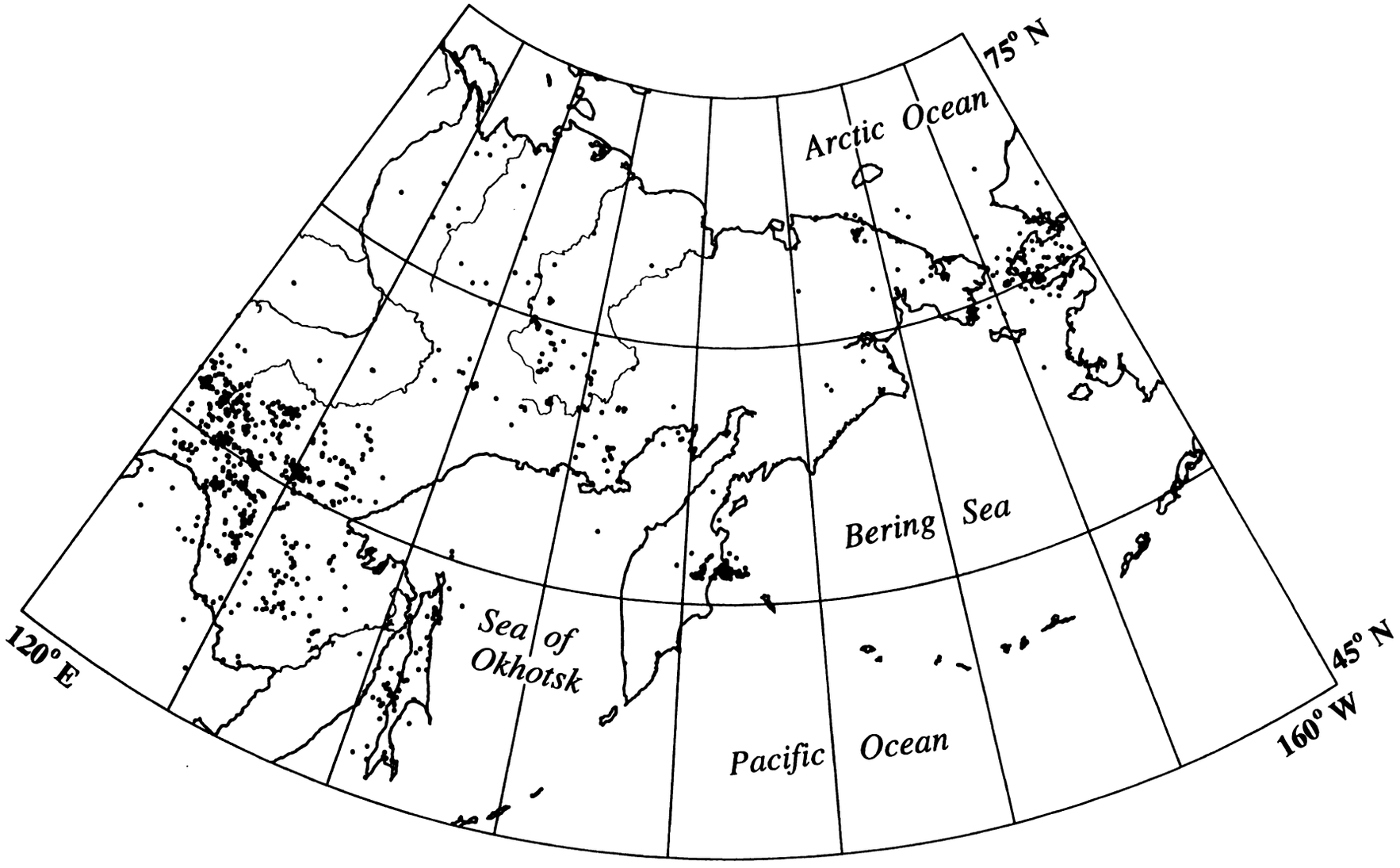

Figure B-22. Seismicity of northeastern Russia in 1979.

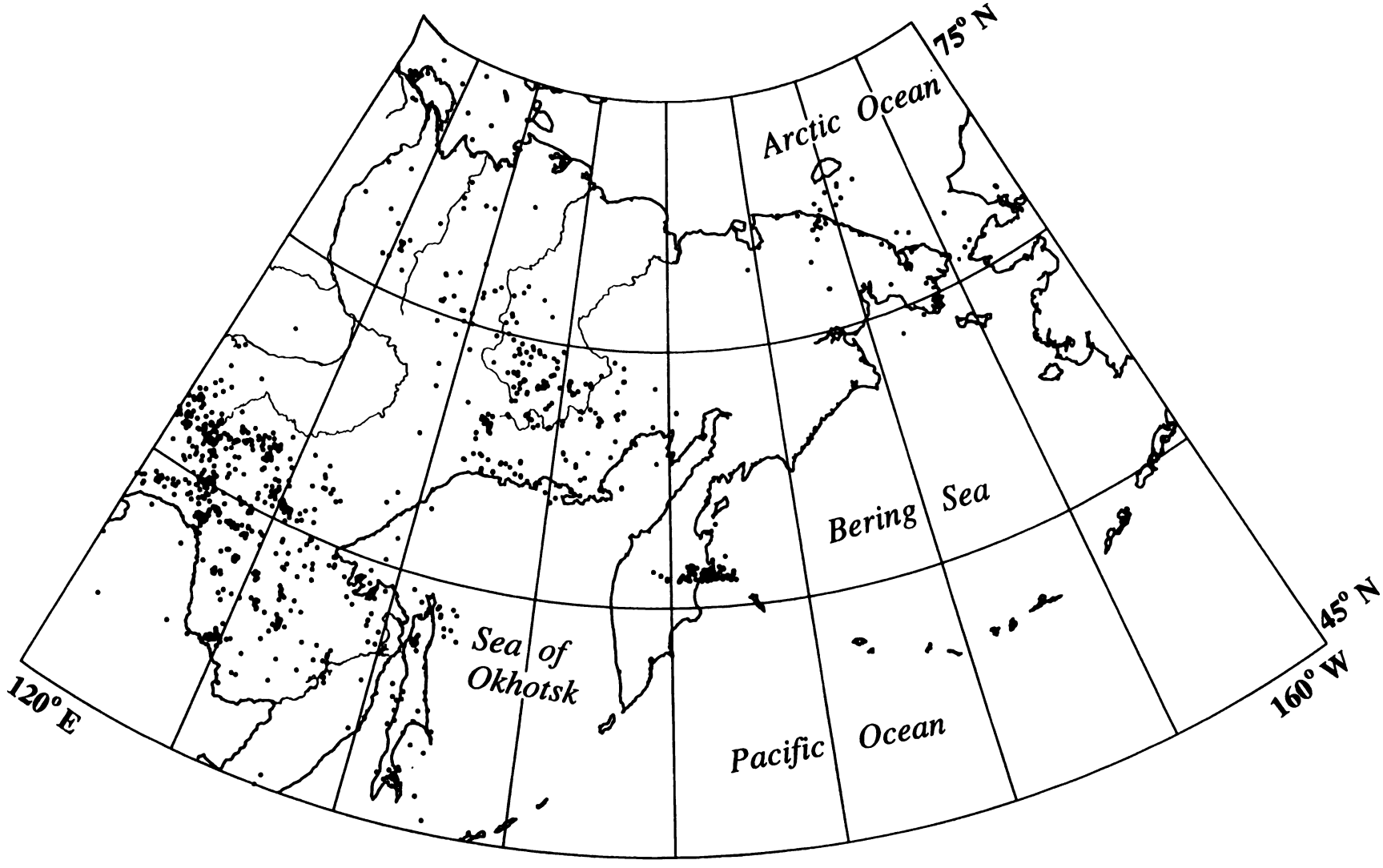

Figure B-23. Seismicity of northeastern Russia in 1980.

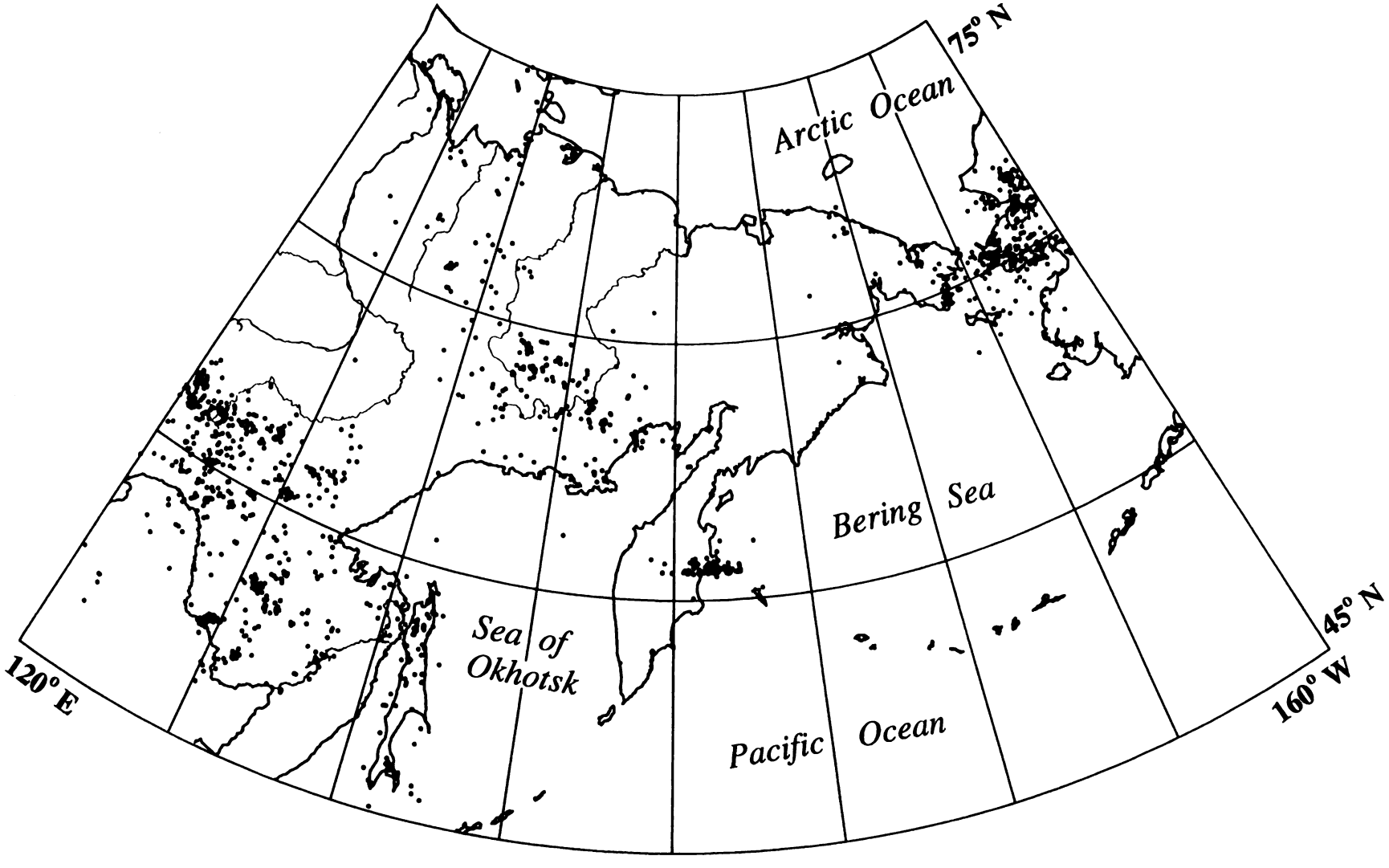

Figure B-24. Seismicity of northeastern Russia in 1981.

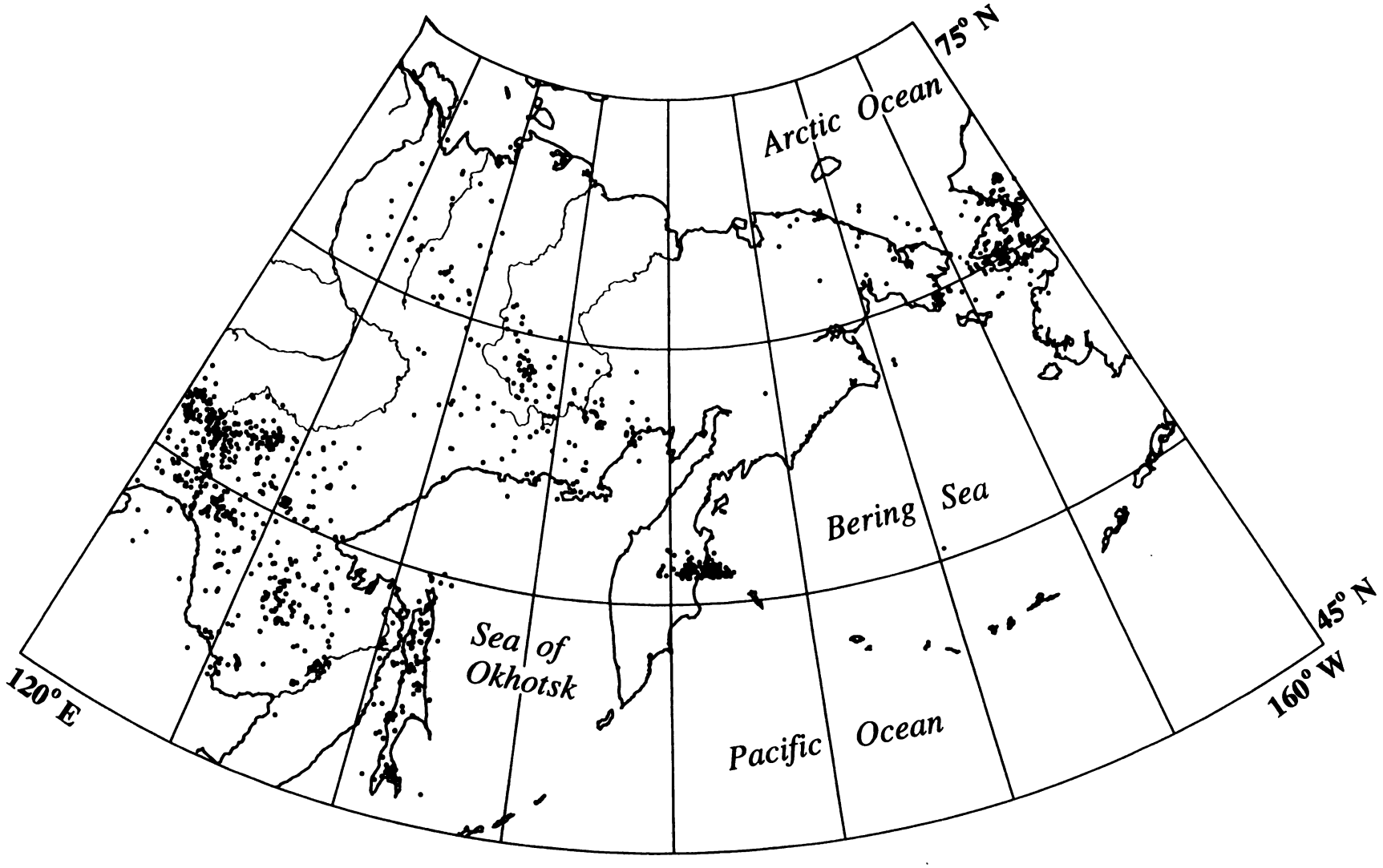

Figure B-25. Seismicity of northeastern Russia in 1982.

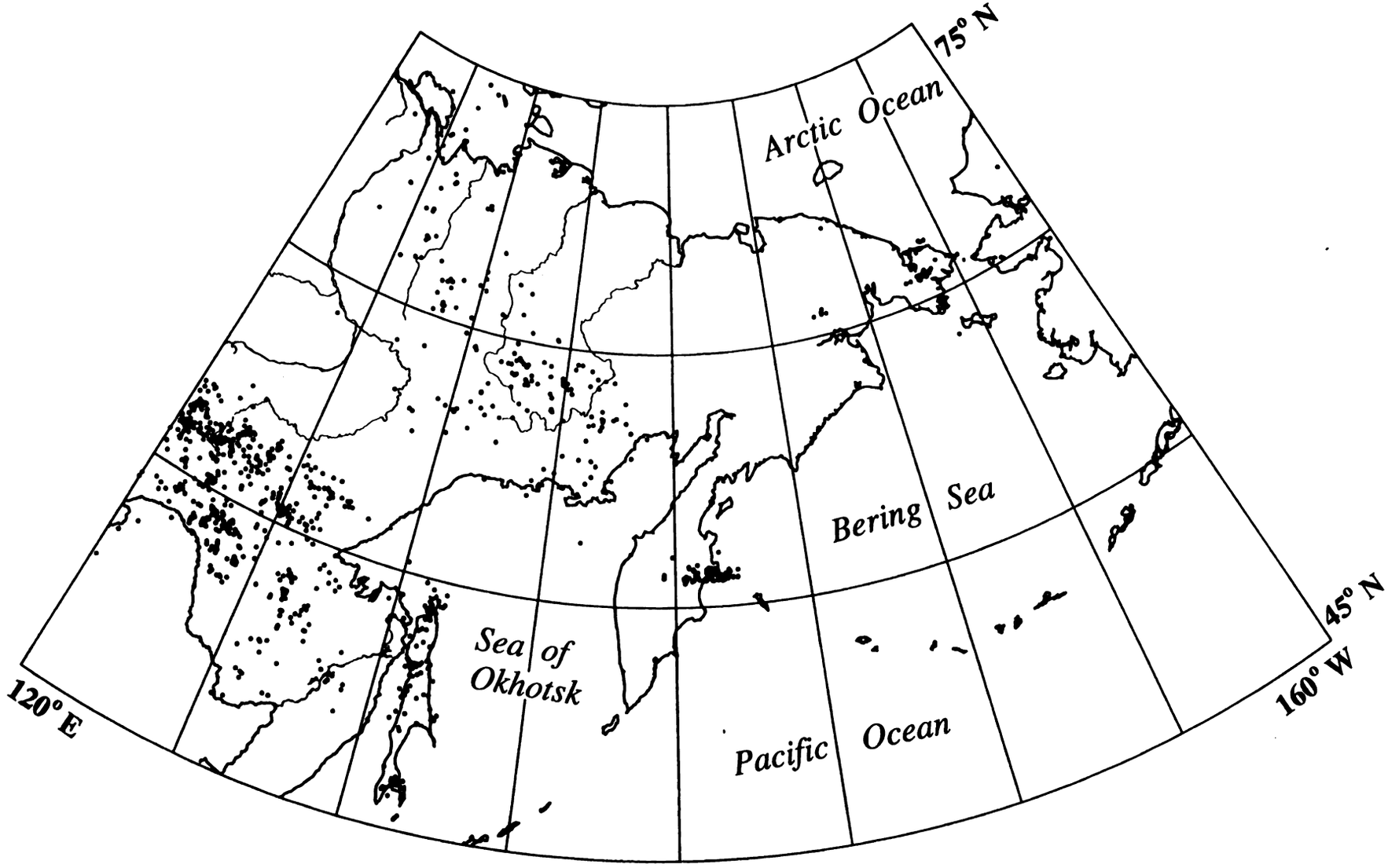

Figure B-26. Seismicity of northeastern Russia in 1983.

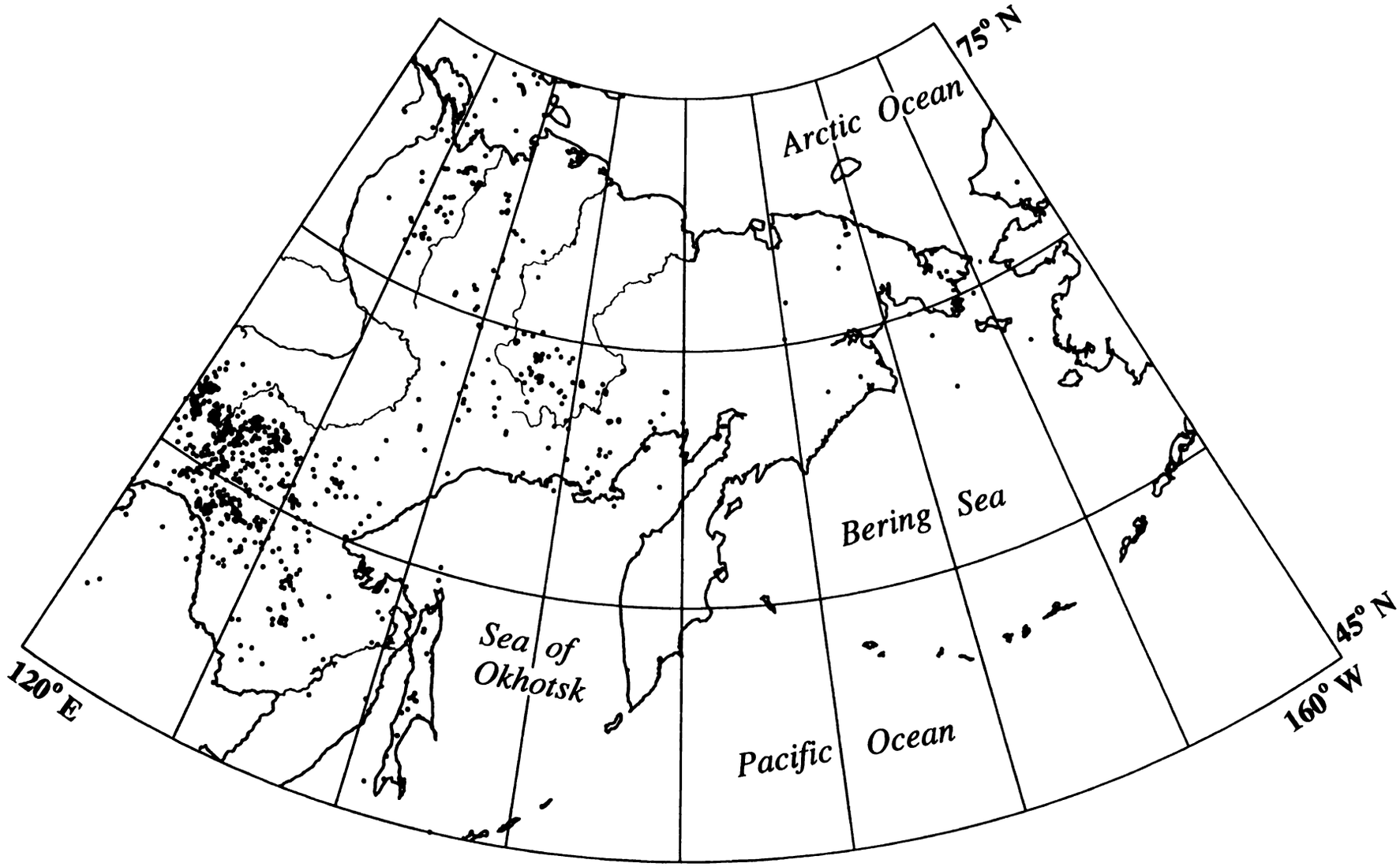

Figure B-27. Seismicity of northeastern Russia in 1984.

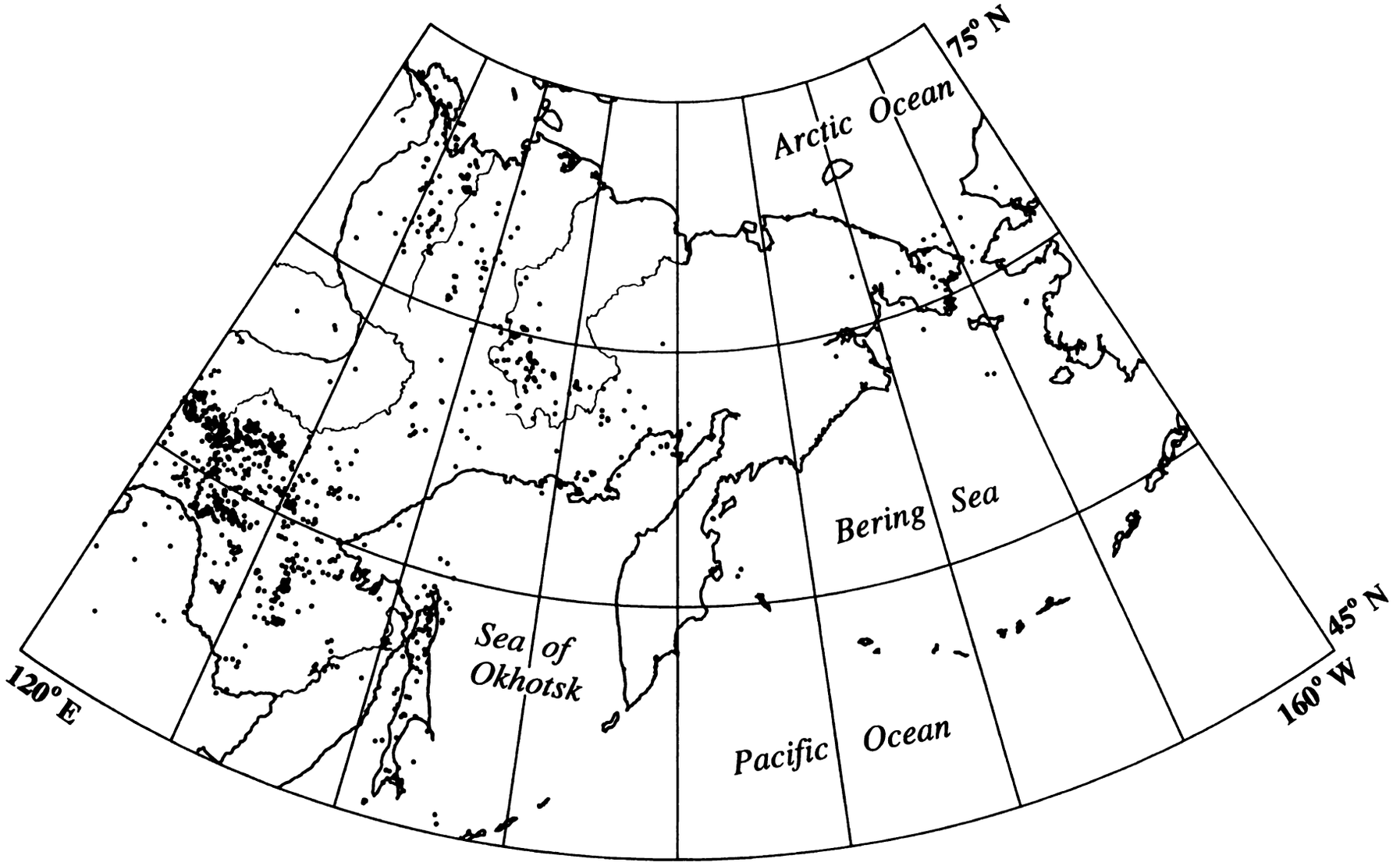

Figure B-28. Seismicity of northeastern Russia in 1985.

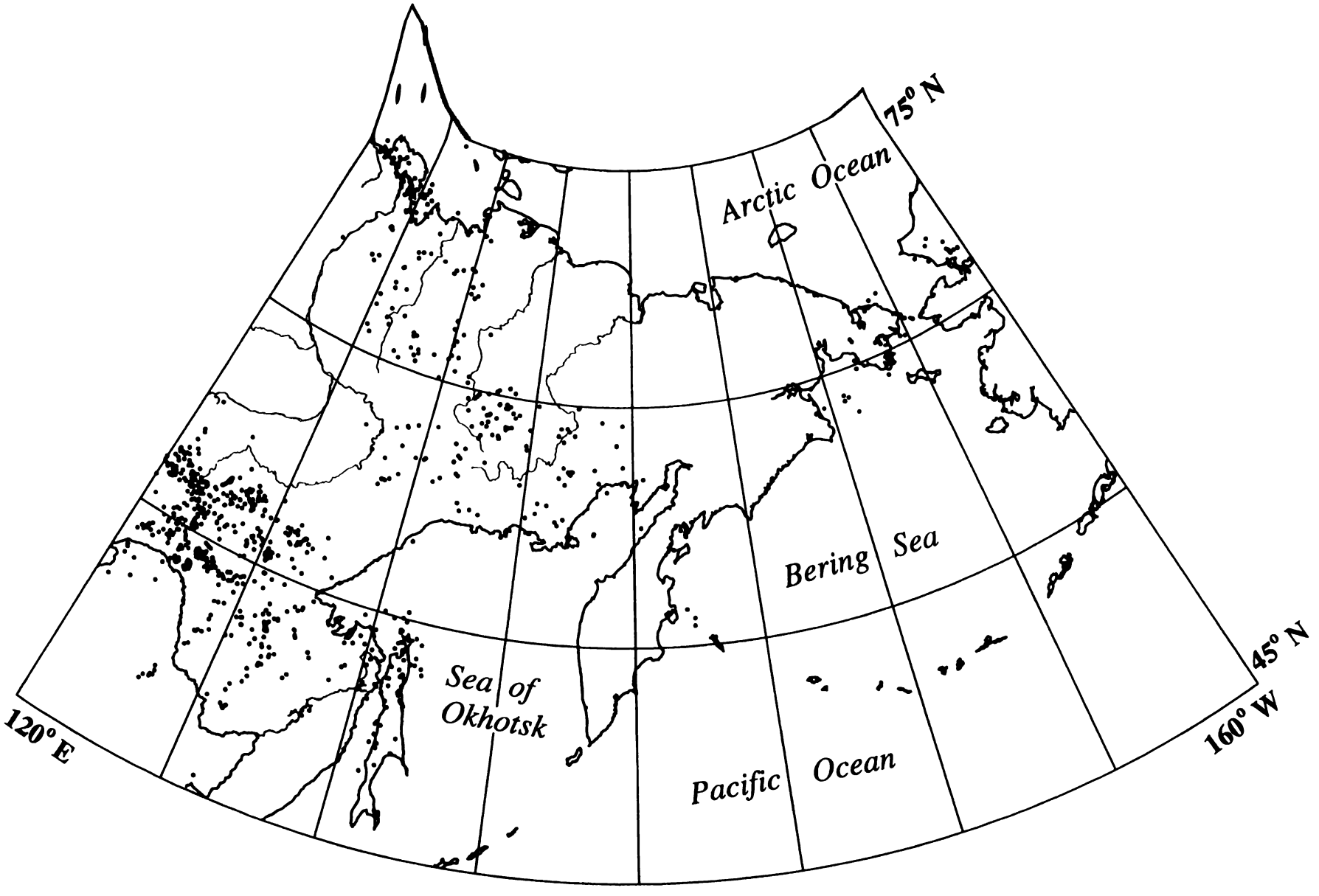

Figure B-29. Seismicity of northeastern Russia in 1986.

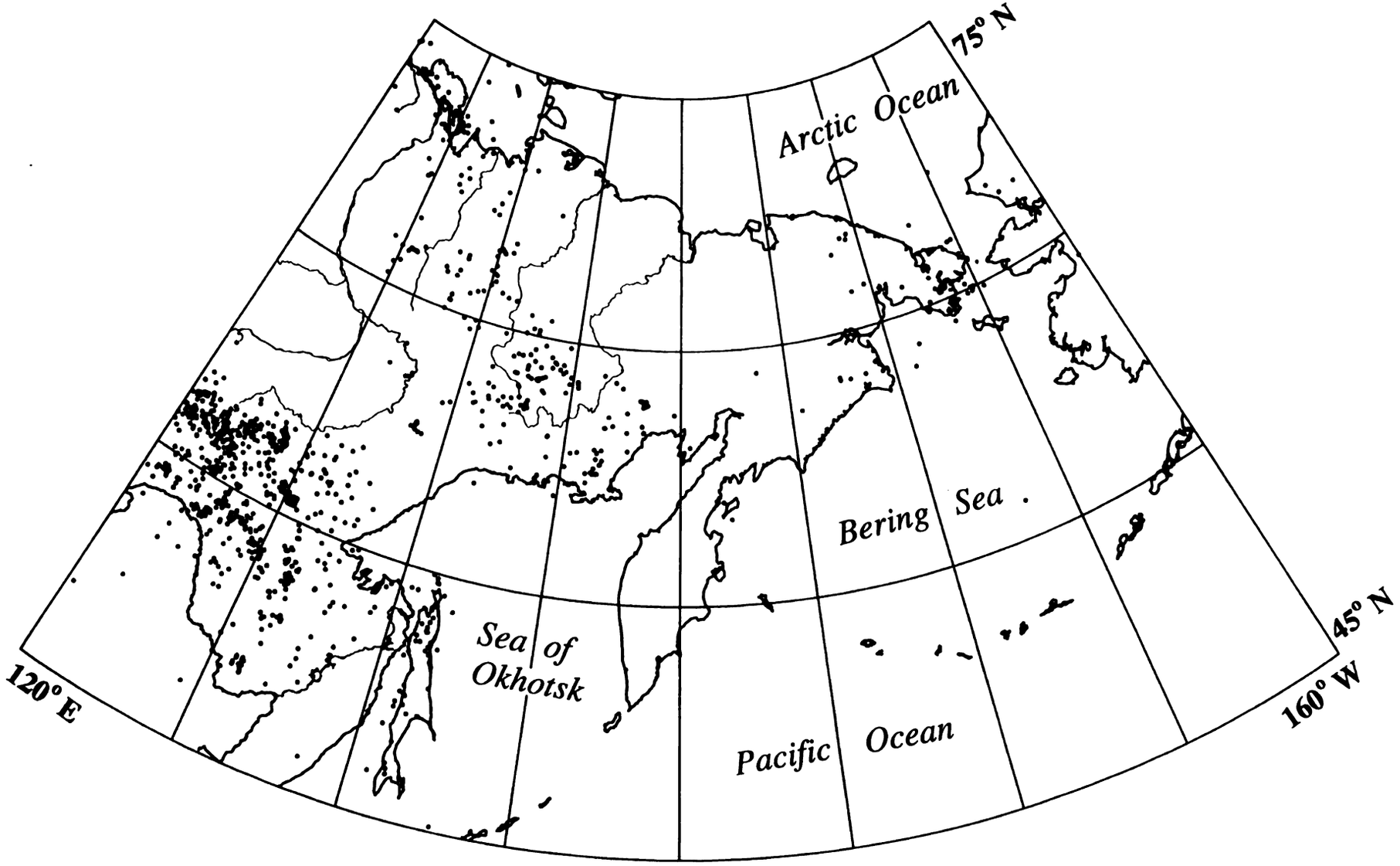

Figure B-30. Seismicity of northeastern Russia in 1987.

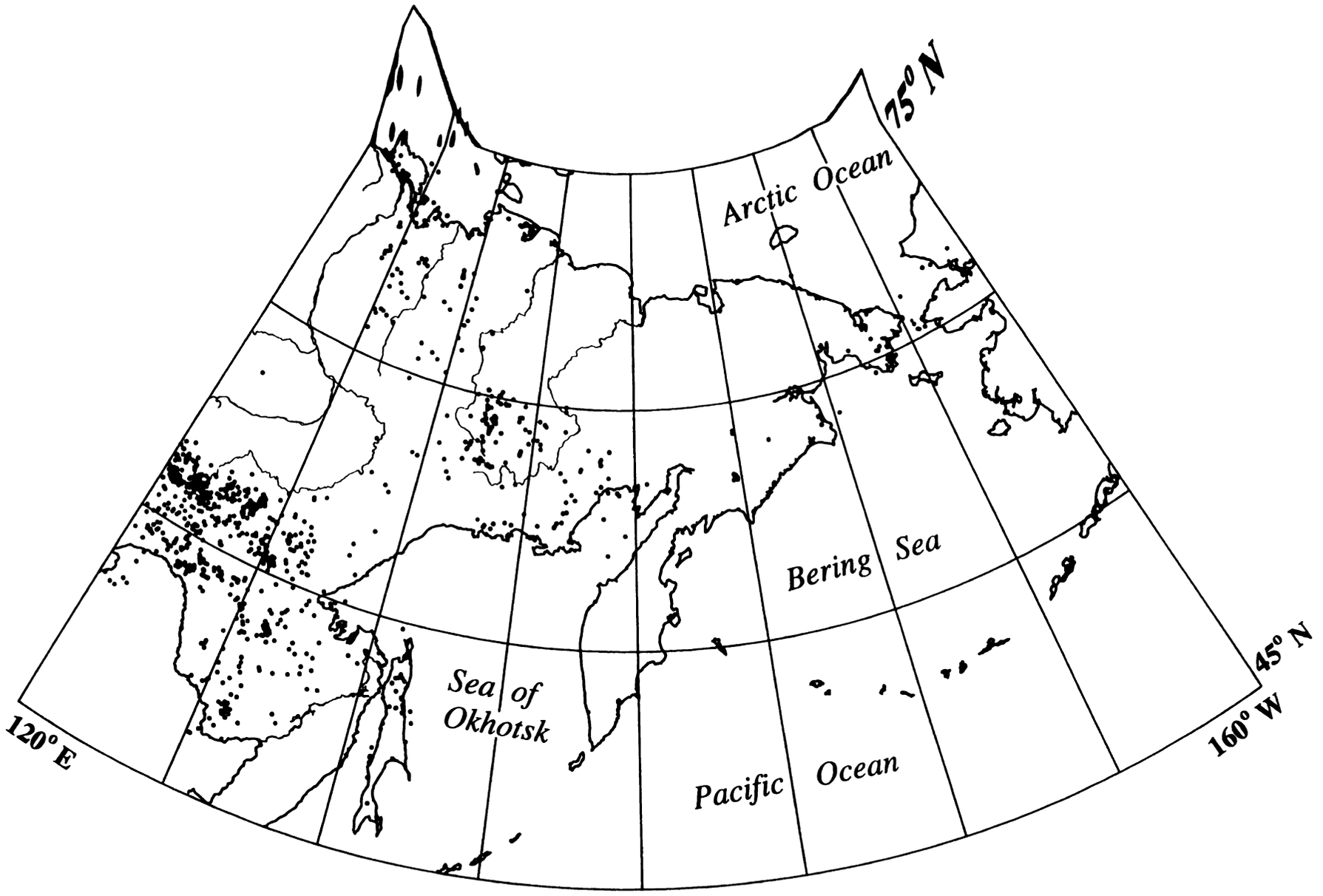

Figure B-31. Seismicity of northeastern Russia in 1988.

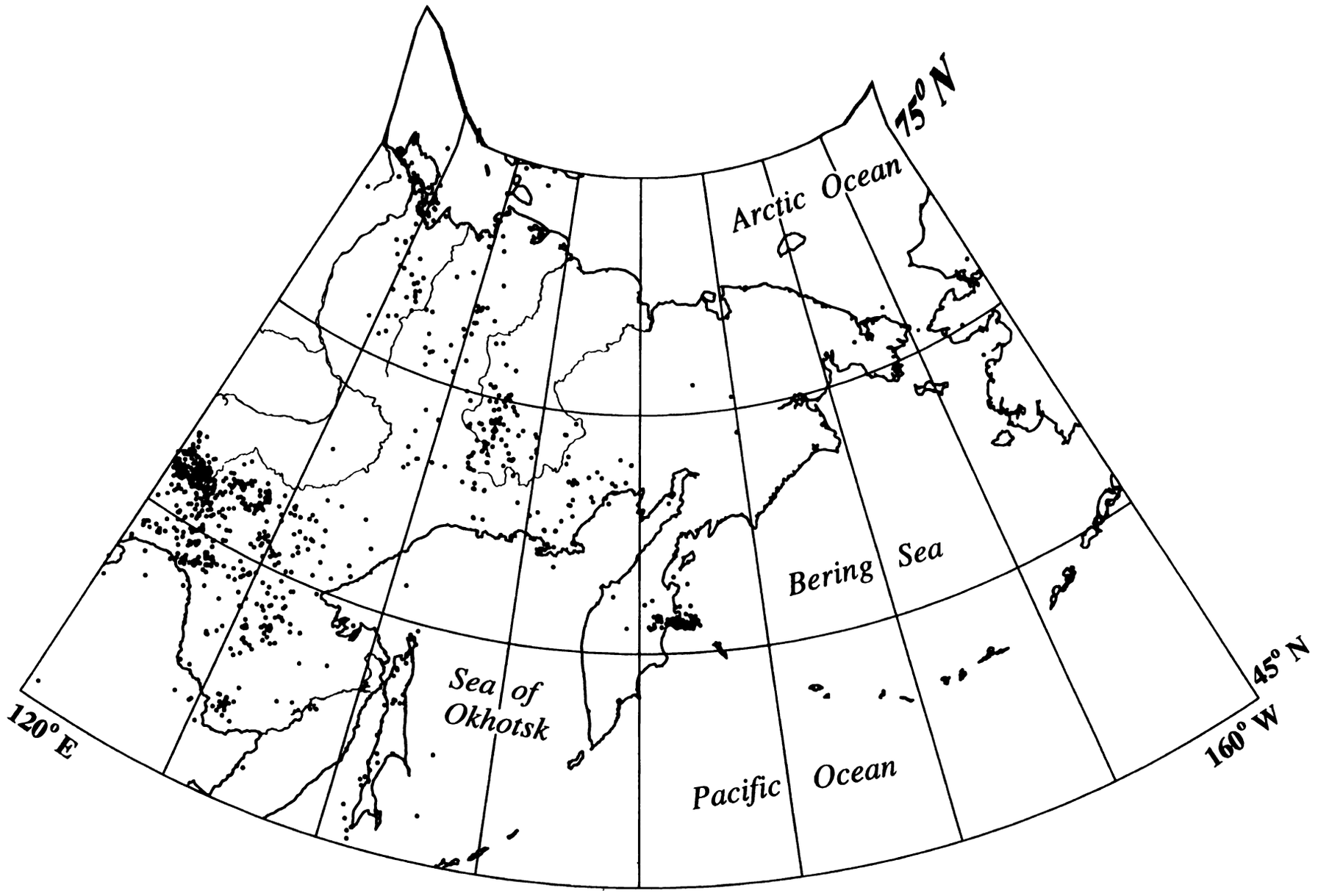

Figure B-32. Seismicity of northeastern Russia in 1989.

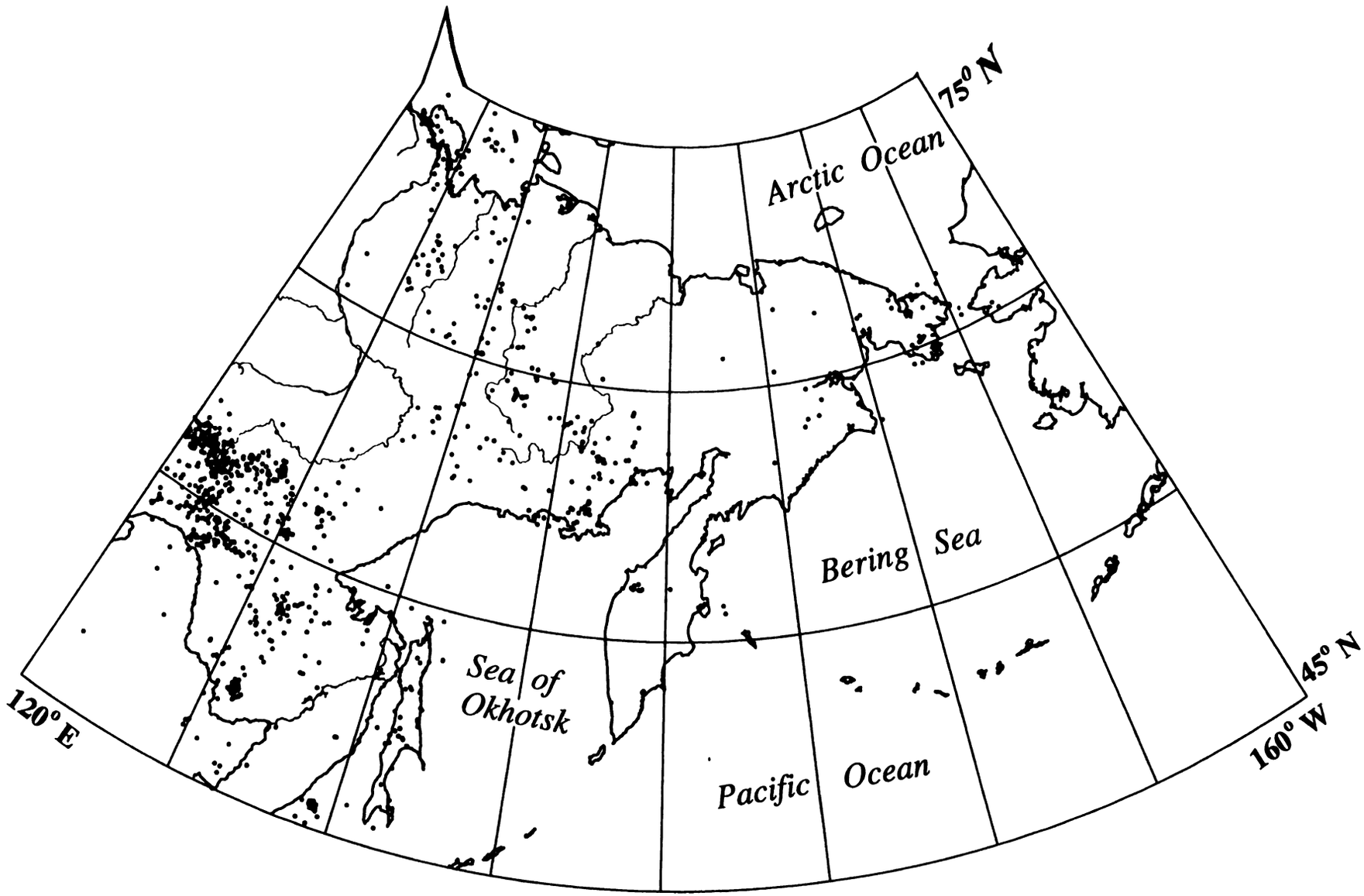

Figure B-33. Seismicity of northeastern Russia in 1990.

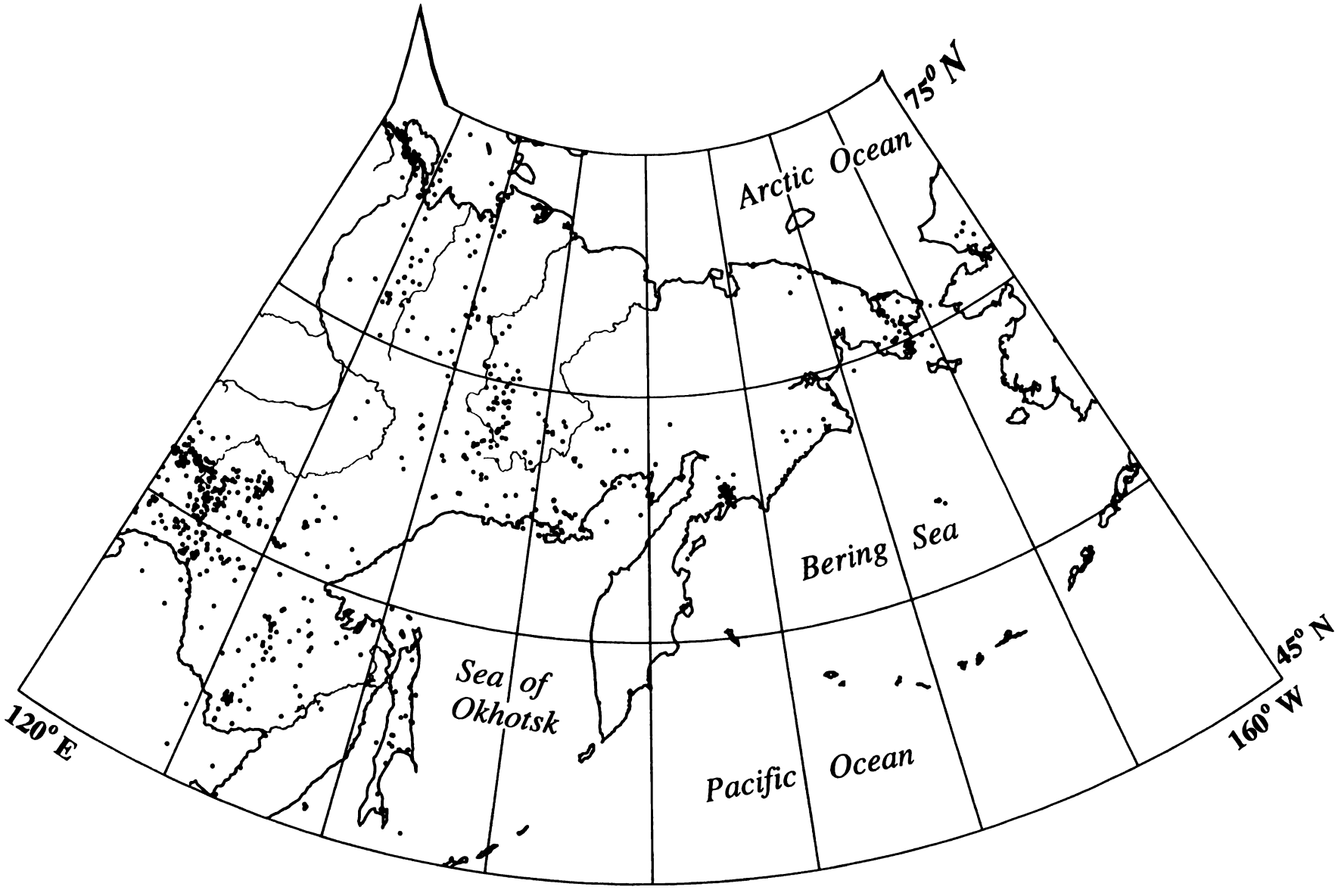

Figure B-34. Seismicity of northeastern Russia in 1991.

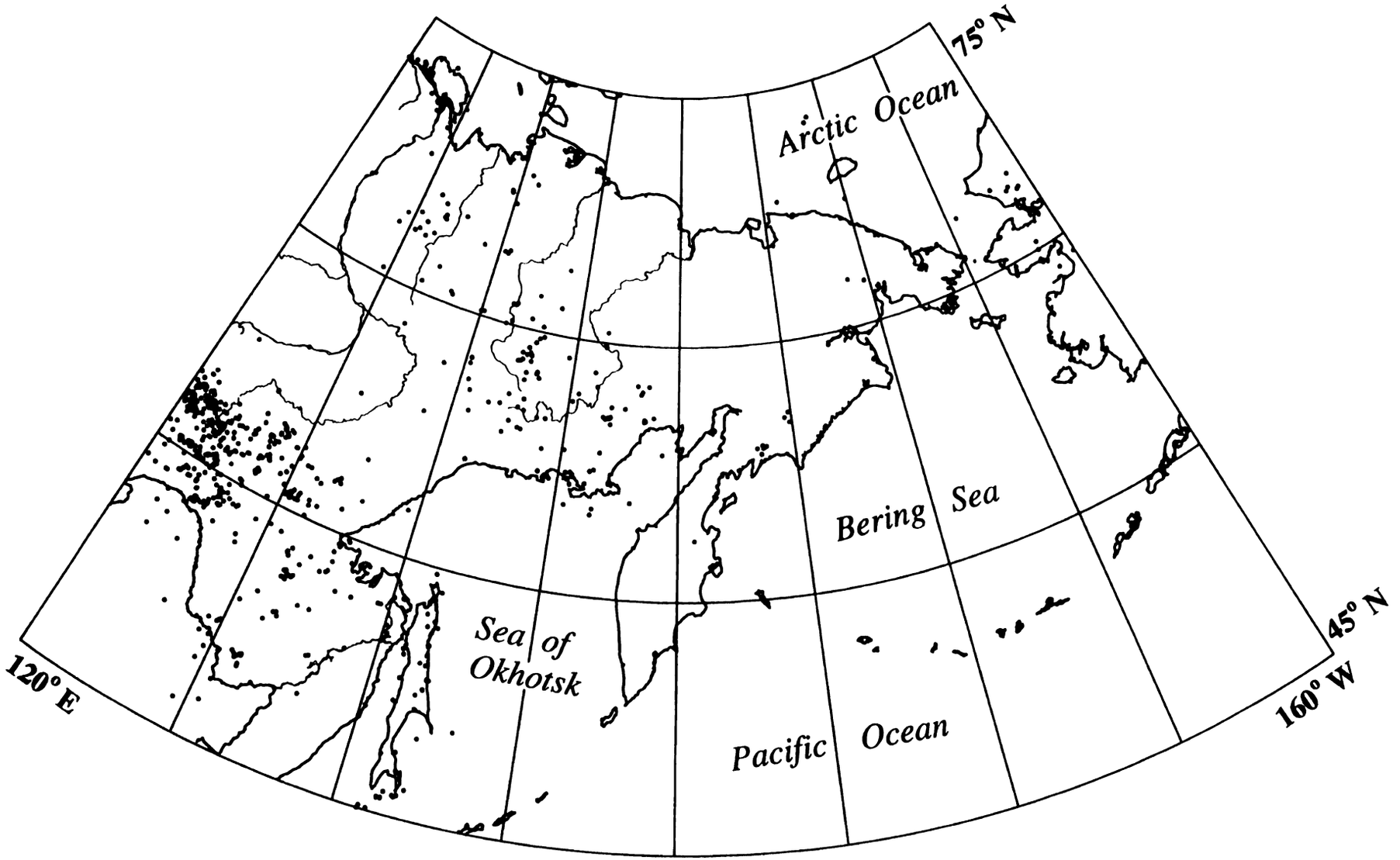

Figure B-35. Seismicity of northeastern Russia in 1992.

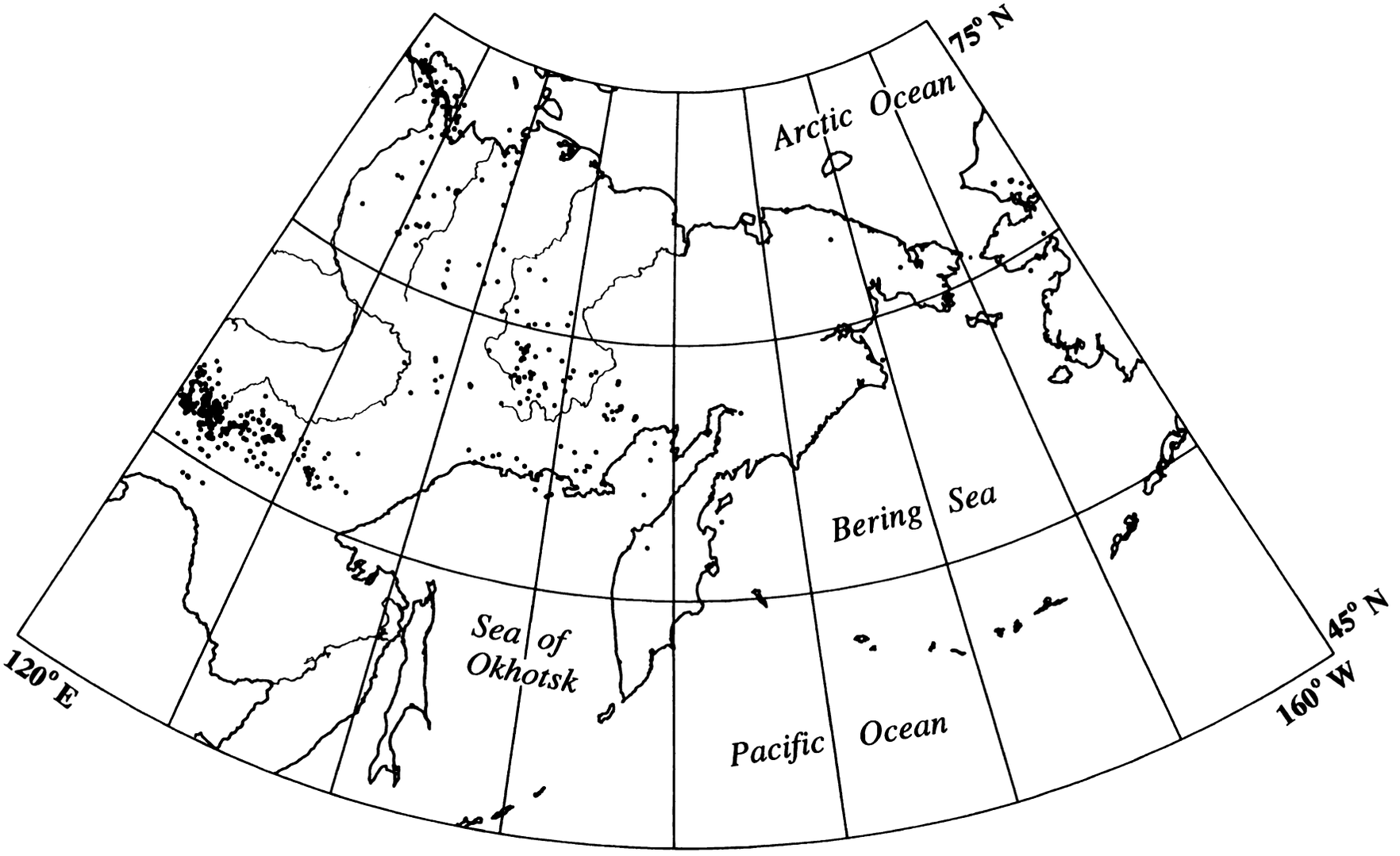

Figure B-36. Seismicity of northeastern Russia in 1993.

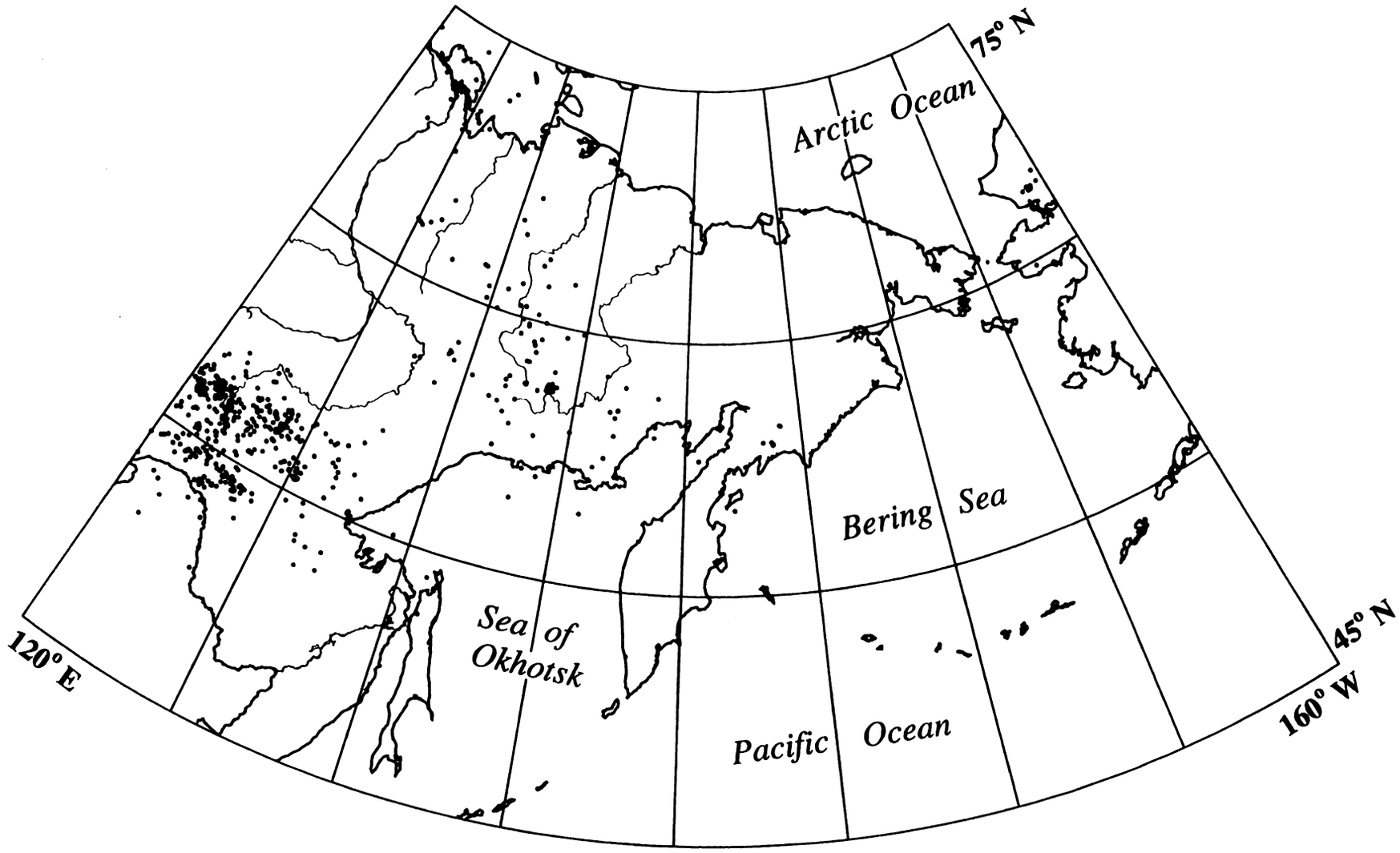

Figure B-37. Seismicity of northeastern Russia in 1994.

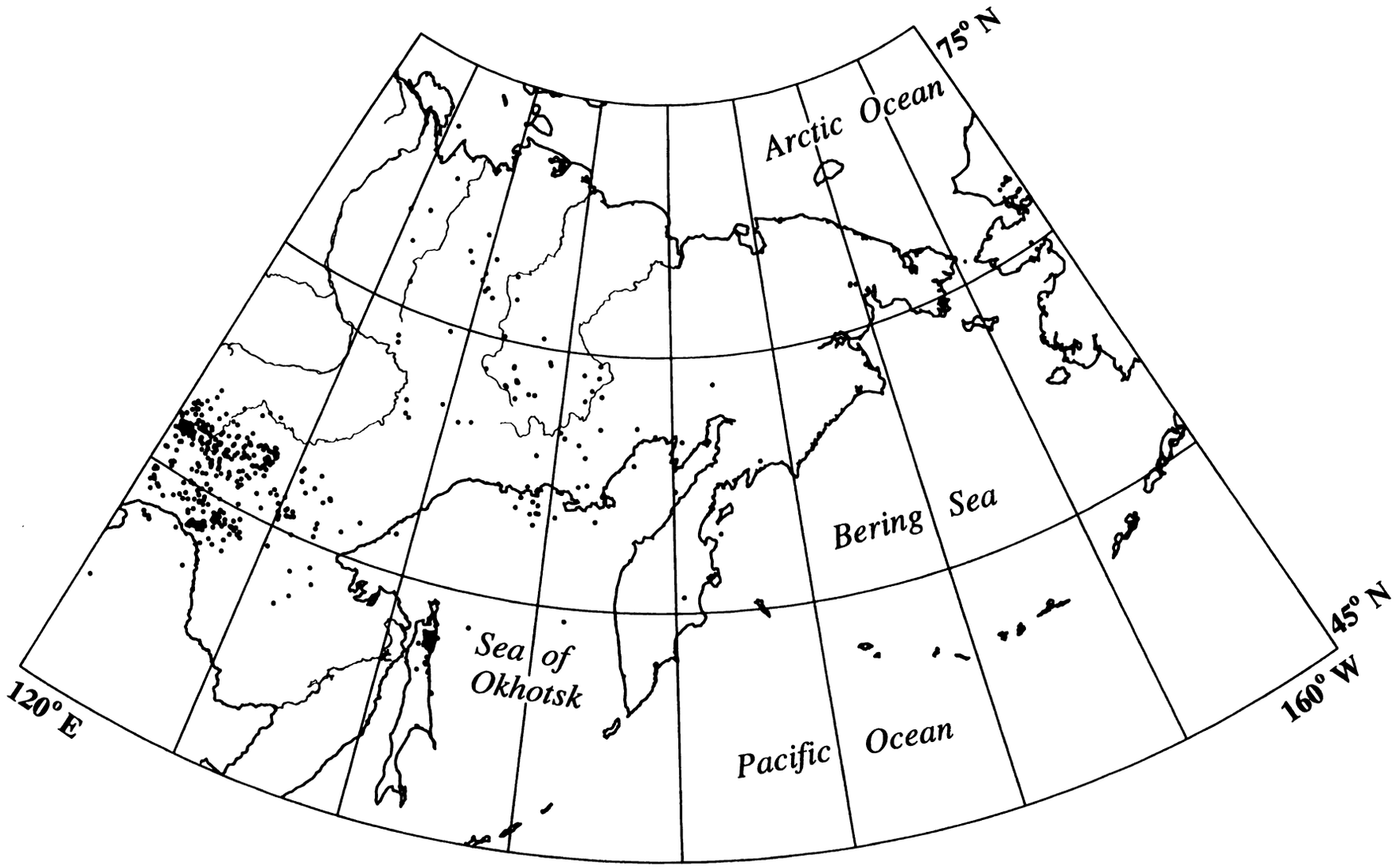

Figure B-38. Seismicity of northeastern Russia in 1995.

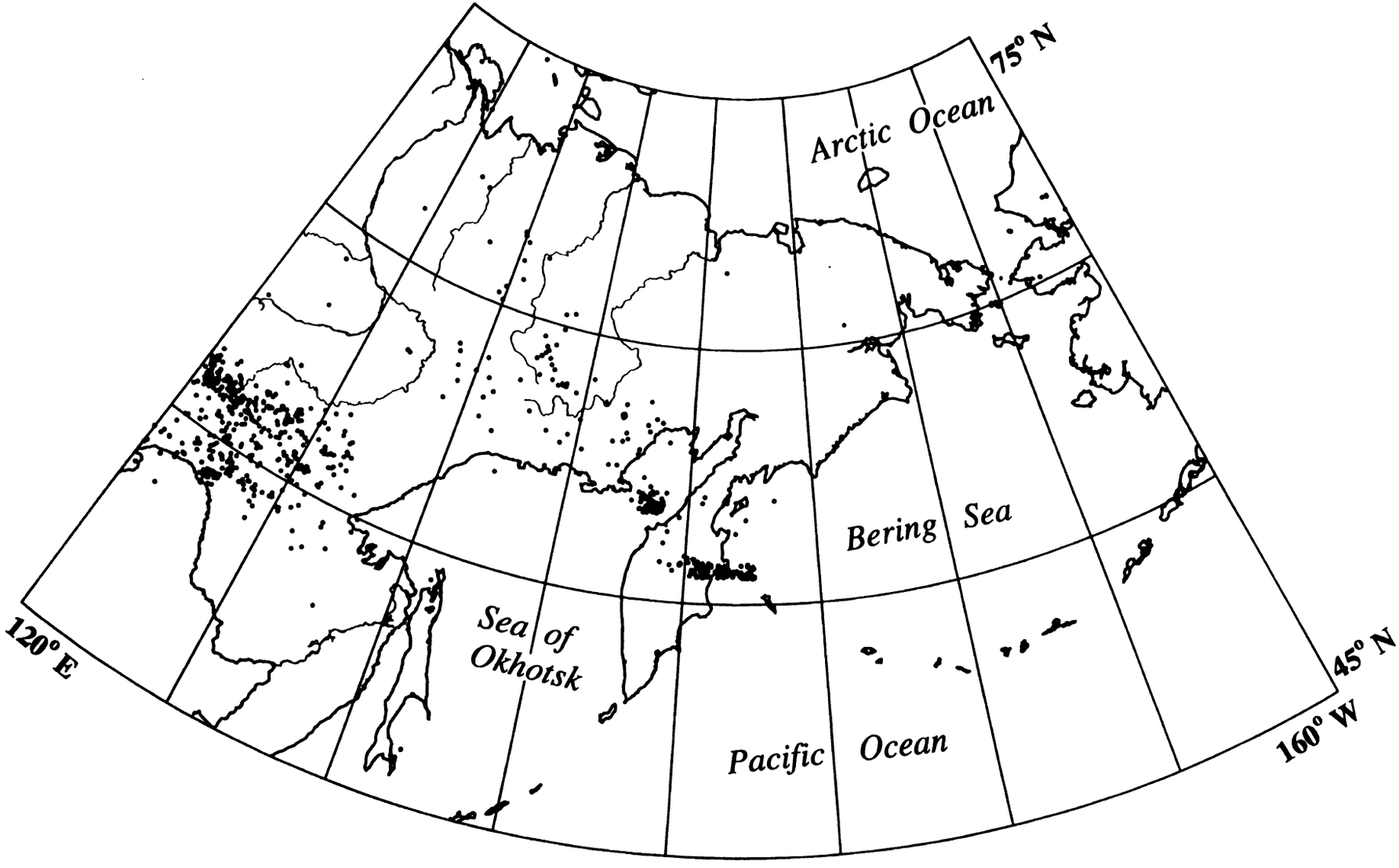

Figure B-39. Seismicity of northeastern Russia in 1996.

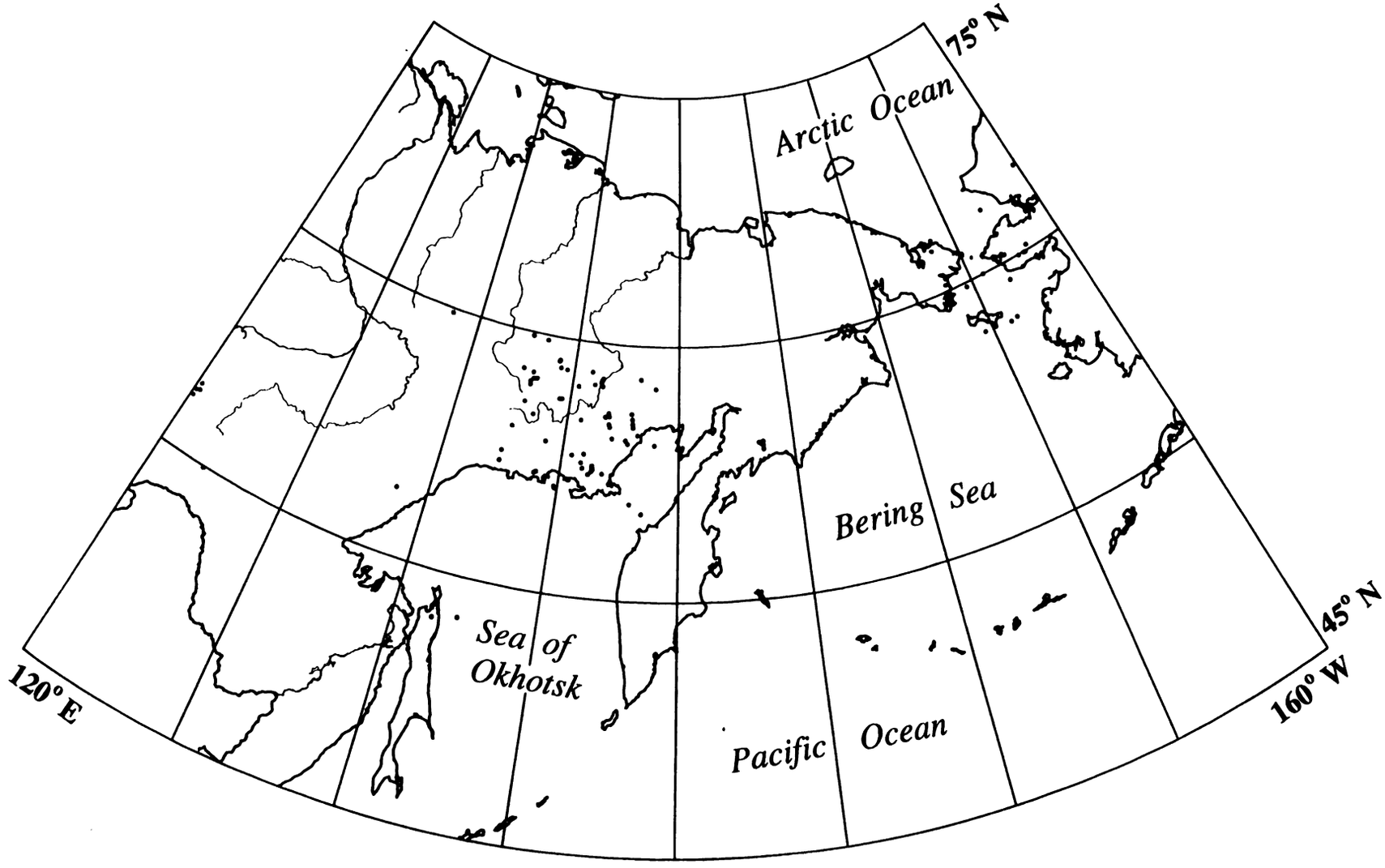

Figure B-40. Seismicity of northeastern Russia in 1997.

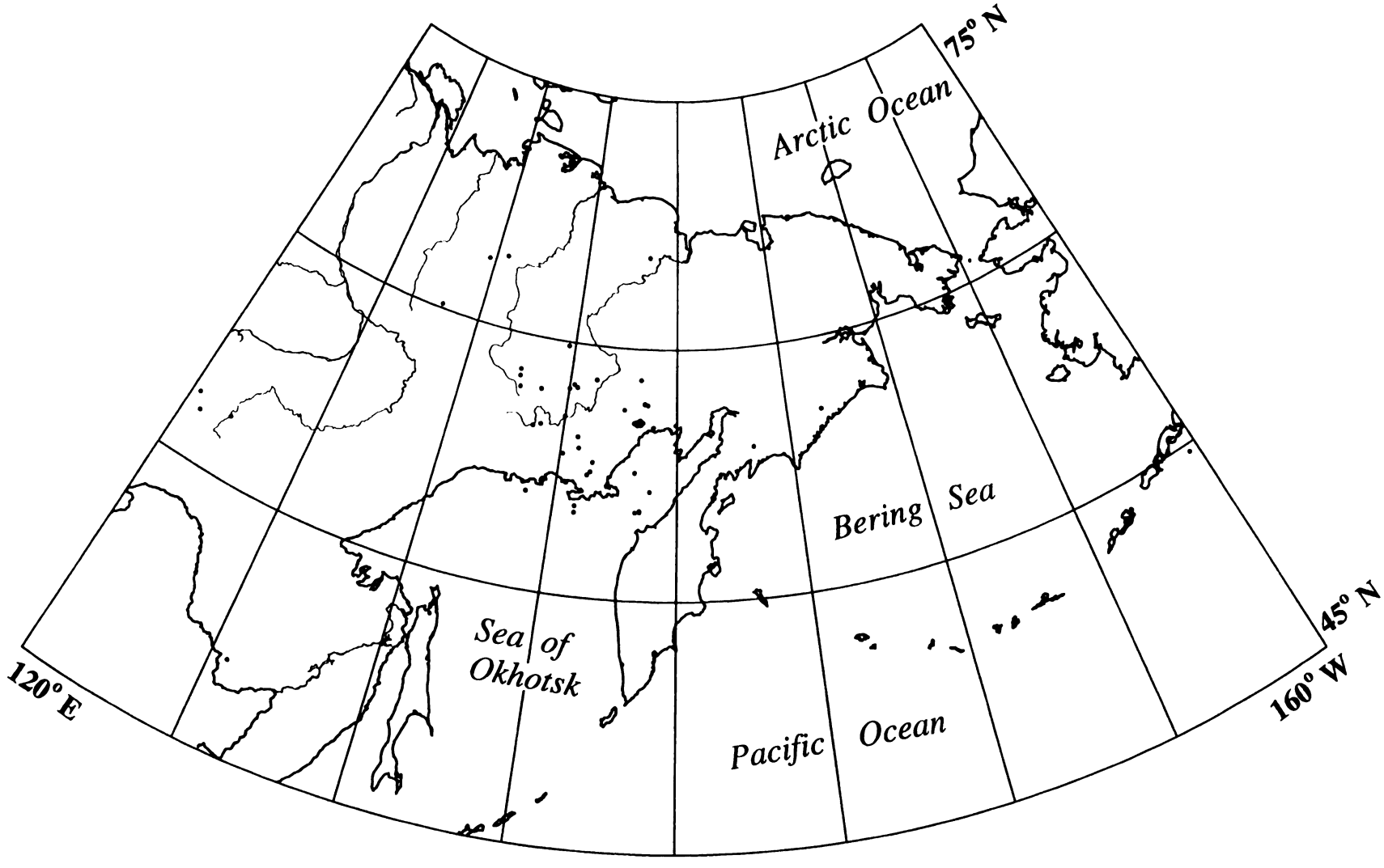

Figure B-41. Seismicity of northeastern Russia in 1998.

APPENDIX C

1999 Digital station deployments and observations

APPENDIX C

1999 Digital station deployments and observations

Overview

In the summer of 1999, the author traveled to Magadan to upgrade existing photo paper seismic stations to digital acquisition. This work was performed in conjunction with the Magadan Experimental Methodological Seismological Division (MEMSD), from Magadan, Russia.

A total of six digital acquisition systems were purchased and imported into Russia for deployment. The digital acquisition systems were manufactured by PC System Design, Palo Alto CA, and use 8 channel, 24 bit A/D cards with GPS timing. Data are recorded on PC computers, which were purchased in Russia. At all stations, except as noted, the seismometers (3 components) recorded are Russian (Soviet) SM3-KV short period instruments, with the free period set at 1.5 seconds. Seismometer output is amplified 1000 times, and a 10hz cutoff low pass filter is used. The amplifier/filter was designed and manufactured by MEMSD. Digitization of time and all seismometer components is 30 s.p.s.

During the travel period, four stations (Susuman, Talaya, Nelkoba, and Ust'Nera) were deployed in permanent locations, upgrading existing photo paper stations, and two stations were deployed temporarily (Stokolviya and Matrosova) during fieldwork. Coordinates for all stations were determined with a Magellan handheld GPS unit. Location of stations deployed are shown in Figure C-1. A brief description of each station follows.

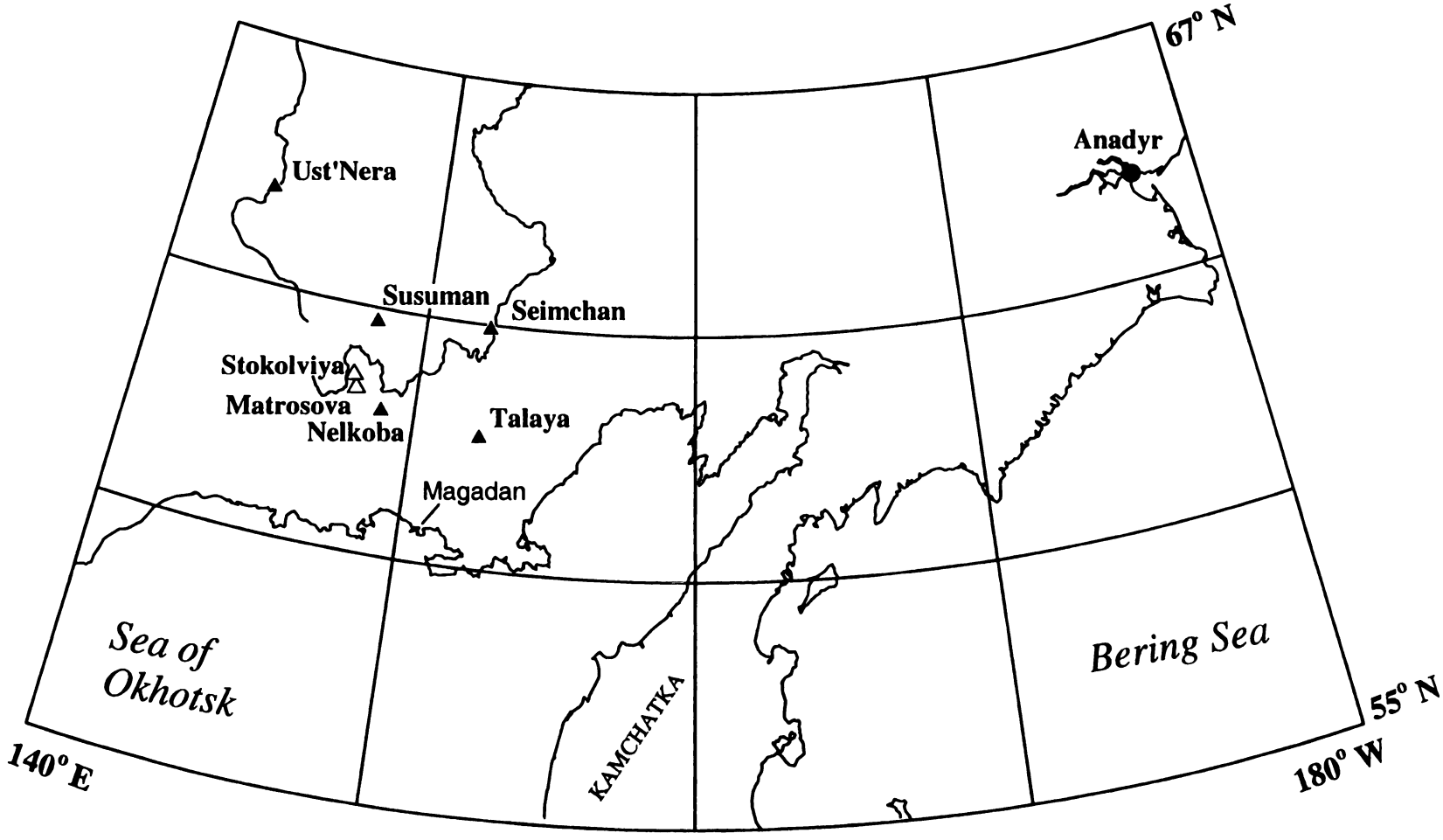

Figure C-1. Map of the Magadan region showing locations of seismic stations deployed in 1999. Permanent stations (closed triangles), temporary stations (open triangles), and near future station (circles).

Permanent Stations

SUSUMAN (62.7792° N, 148.1633° E) Susuman is a town of approximately 5,000 people and is the center of placer gold production in the Magadan region. The seismic station is operated by MEMSD and is located at the meteorological station just west of the main town. The station is sufficiently far from the town that cultural noise should be minimal. The seismic vault in Susuman consists of a large concrete block set approximately 1.5 m into a permafrost foundation.

TALAYA (61.1337° N, 152.3980° E) Talaya is a resort town of approximately 500 people; the main attraction is a large resort with natural hot springs. The seismic station is operated by MEMSD. The seismic vault in Talaya consists of a concrete pad set into volcanic bedrock on the side of a hill. The seismic station is located on the east side of town next to the now abandoned cinema theater.

NELKOBA (61.3383° N, 148.8128° E) Nelkoba is a small town whose primary function was a regional supply and repair center for support of the gold mining industry in the region. The seismic vault in Nelkoba consists of a concrete pad measuring approximately 1 m x 1 m set into permafrost. The concrete pad is housed in a small wooden shed on the grounds of the Nelkoba kindergarten, on the west side of town. The current station site was constructed in the summer of 1997 and is approximately 200 m north of the previous site. At some time in the past, SKM instruments were operated at the old station site. The town of Nelkoba was permanently abandoned in late September, 1999. The station was moved into an abandoned mine near the Matrosova temporary station deployment site (see below).

UST' NERA (64.565° N, 143.242° E) The seismic station in Ust'Nera is operated by the Yakutsk seismic network. The station in Ust'Nera has occupied its present site since 1992. The seismic vault consists of a large concrete block set into a permafrost foundation. The vault is located between two large apartment buildings, thus cultural noise can be high at times due to passing cars and children playing on top of the vault. Seismometers recorded here are Russian (Soviet) SKM short period instruments. Seismometer output is amplified 60 db and a 30hz cutoff low pass filter is applied. The amplifier used in Ust' Nera is a USGS Prototype Series Seismic Amplifier. The amplifier was originally part of an IASPEI system installed by the author in Ust'Nera in 1997.

Temporary Stations

MATROSOVA (61.6432° N, 147.8205° E) Matrosova is a small town with an operating gold mine. Seismometers were located on the concrete foundation of a building used for ore transfer. The foundation of the building was set into bedrock consisting of black shale. In Matrosova, digitization of time and all seismometer components was 120 s.p.s. The station was operated for only a few hours, to record blasting from the mine. Two large blasts of 1,300 and 1,500 kg of Ammonite were recorded, among several much smaller explosions. Several abandoned mine adits are also in and near Matrosova, which may be good sites for future permanent stations.

In late September, 1999, equipment from the closed station in Nelkoba was moved to a site a few kilometers northeast of Matrosova and a new permanent station was constructed (Omchak, 61.67° N, 147.87° E, h = 820 m). The station was constructed in an abandoned mine adit.

STOKOLVIYA (61.8475° N, 147.6598° E) Stokolviya is a hydrological research station in a remote, unpopulated region. The seismic vault consisted of a one meter pit dug into the side of a hill. Ground material consisted primarily of angular cobble sized rocks of volcanic origin. The material was consistent with the bedrock surface being close. When installing the station, it was intended that Stokolviya would be a permanent site. All permissions were obtained, and the hydrologic research station agreed to operate it prior to installation. However, the individual workers at the station were unfamiliar with computers and refused to consider operating the station. This was unfortunate, as the site is quiet. Also at Stokolviya are several boreholes, some of which exceed 200 m depth. These boreholes are not is use, thus may be ideal for borehole instrument installation.

Results of Station Deployments and Future Research

One objective of the station deployment was to try to record regional mine blasts to get ground truth seismic velocities and seismic waveform signatures. Two blasts (1,300 and 1,500 kg) from the Matrosova mine were recorded at the mine and at the station in Stokolviya (Figure C-2). The explosions were not large enough to be recorded at the other deployed digital stations.

Equipment from the temporary stations deployed in Matrosova and Stokolviya is being redeployed. One station has been installed in Seimchan. The GEOSCOPE station in Seimchan has not operated for several years due to a failed tape drive used to log data. Based on conversations between MEMSD, who operate the station, and the French who installed the station, there is little hope of repair in the near future. Therefore, the output of the existing Streckeisen seismometer is being recorded at 30 s.p.s. on one of the ViSeis PC based

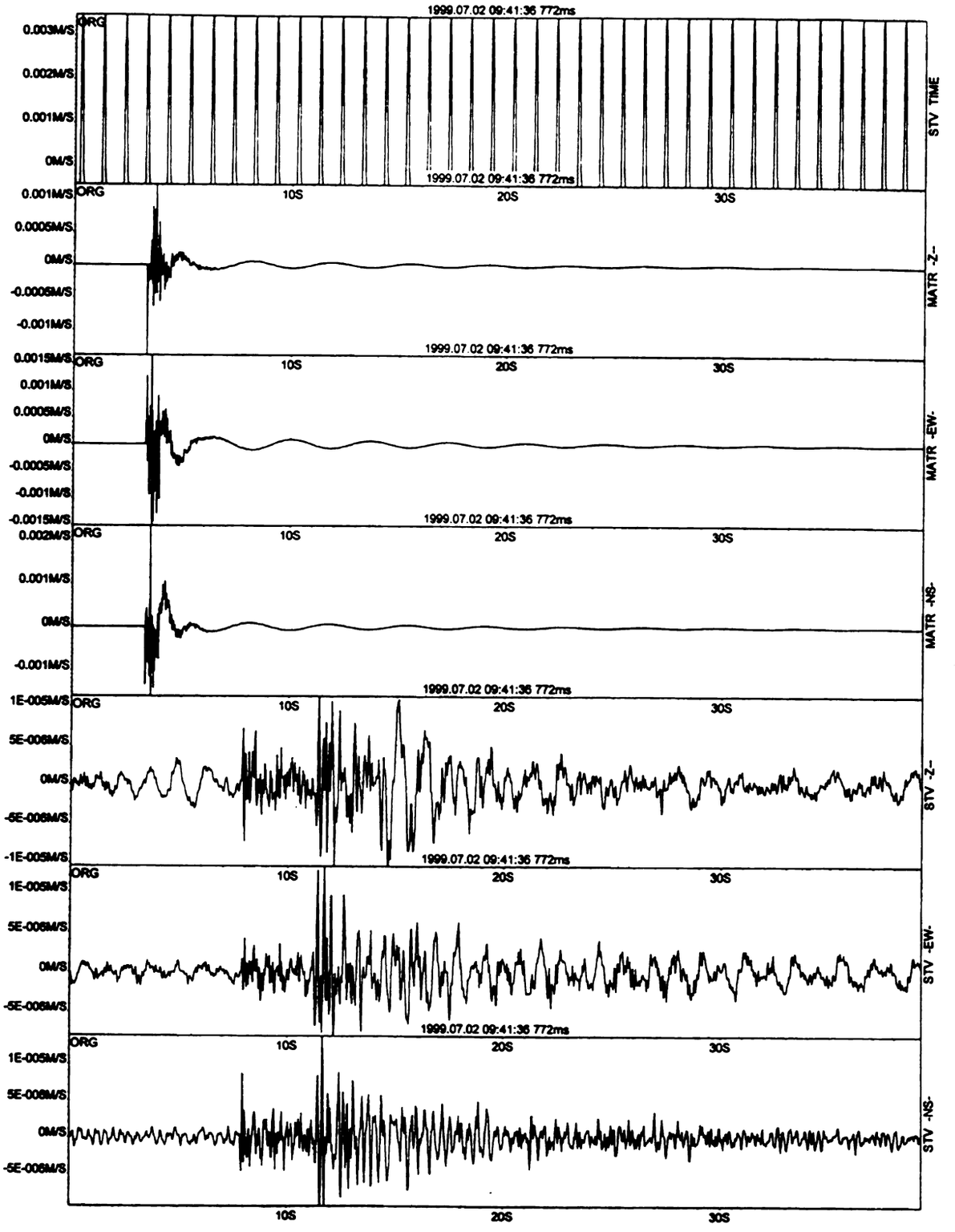

Figure C-2. Recording of 1,500 kg blast from the Matrosova gold mine. Trace 1 - time, traces 2,3,4 - from Matrosova mine (250 m from blast), traces 5,6,7 - station at Stokolviya (25 km north of Matrosova).

systems. Data acquisition began in early October, 1999. The remaining station and a Guralp CMG-40T seismometer will be moved to a permanent location in Anadyr in late 1999, travel permitting.

Figures C-3 through C-5 are sample seismograms recorded at the deployed stations. All seismograms are raw data.

It is hoped that additional larger explosions can be recorded in the future to use as ground truth events to develop seismic discriminants between explosions and tectonic events and to improve location capabilities. This deployment of digital stations is the first step in developing a digital seismic network in the region. The digital stations will allow much easier analysis of the data, as well as greatly increase the portability of the data. The next proposed station deployment will be Okhotsk, in the summer of 2000. Okhotsk is on the north shore of the Sea of Okhotsk, about 400 km west of Magadan. A station here would provide data in the "hole" of seismicity north of Sakhalin Island that occurs near the juncture of several of the northeastern Russia seismic network boundaries. Microseismicity levels have never been studied in this region, although it is speculated that the boundary between the Eurasian plate and Okhotsk plate is in this vicinity.

Other Stations Visited

In the course of fieldwork associated with this dissertation, several other seismic station sites have been visited in the Magadan and Yakutsk region. A brief description of station sites is given below. Coordinates listed below were obtained on-site with a GPS unit.

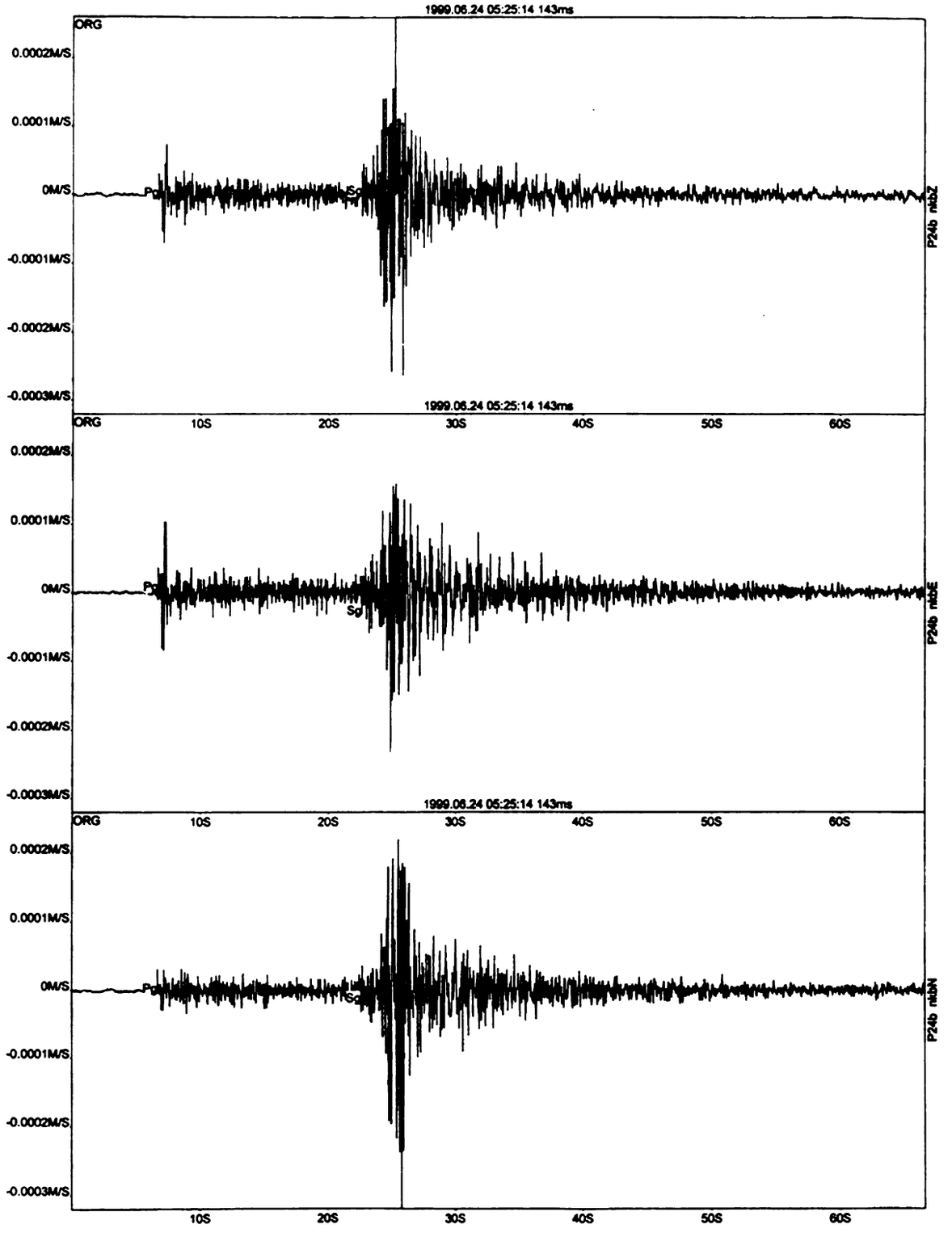

Figure C-3. Local event recorded at Susuman on June 24, 1999. Epicenter unknown.

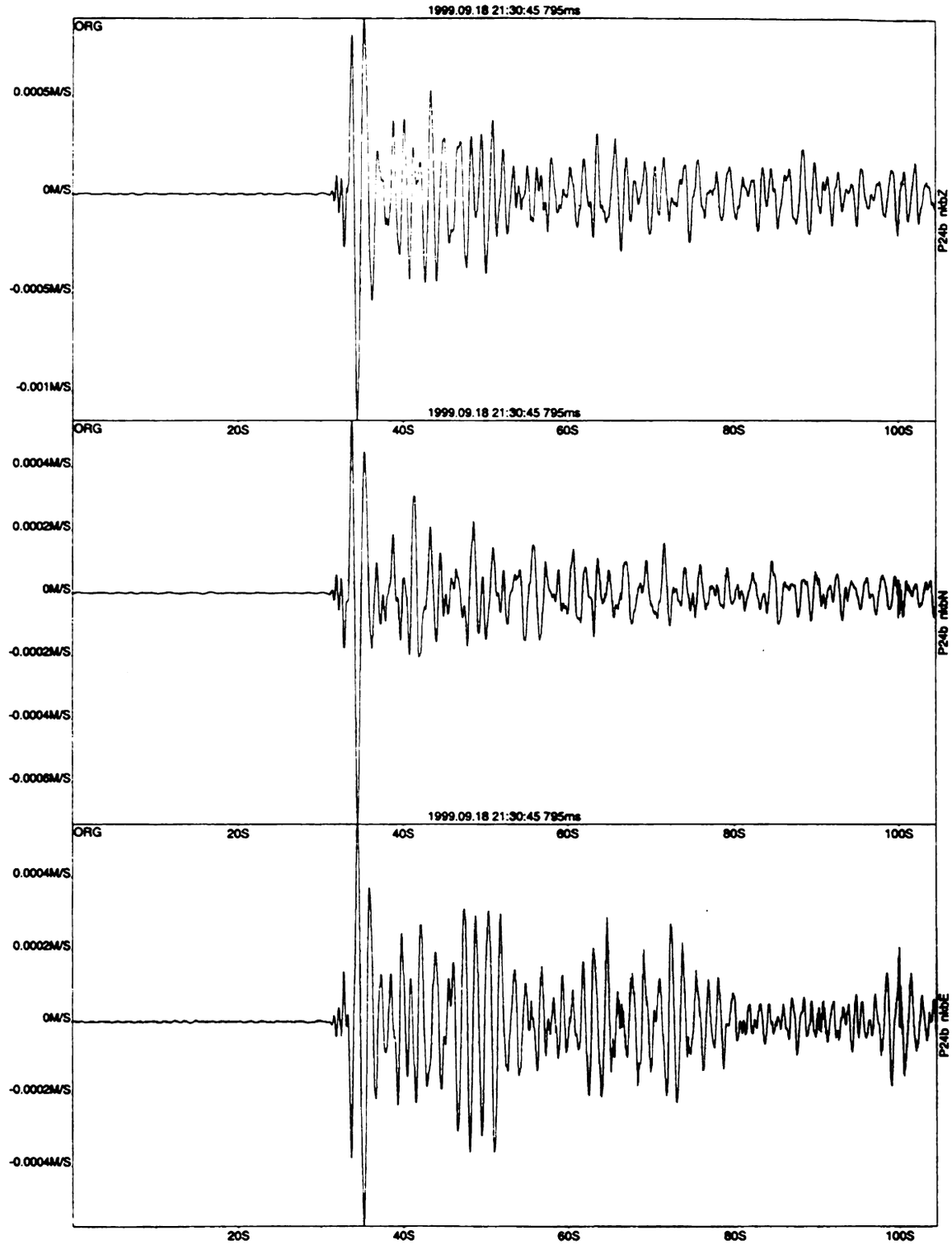

Figure C-4. Regional distance recording from Nelkoba of M_b 6.2 Kurile Island event of September 18, 1999.

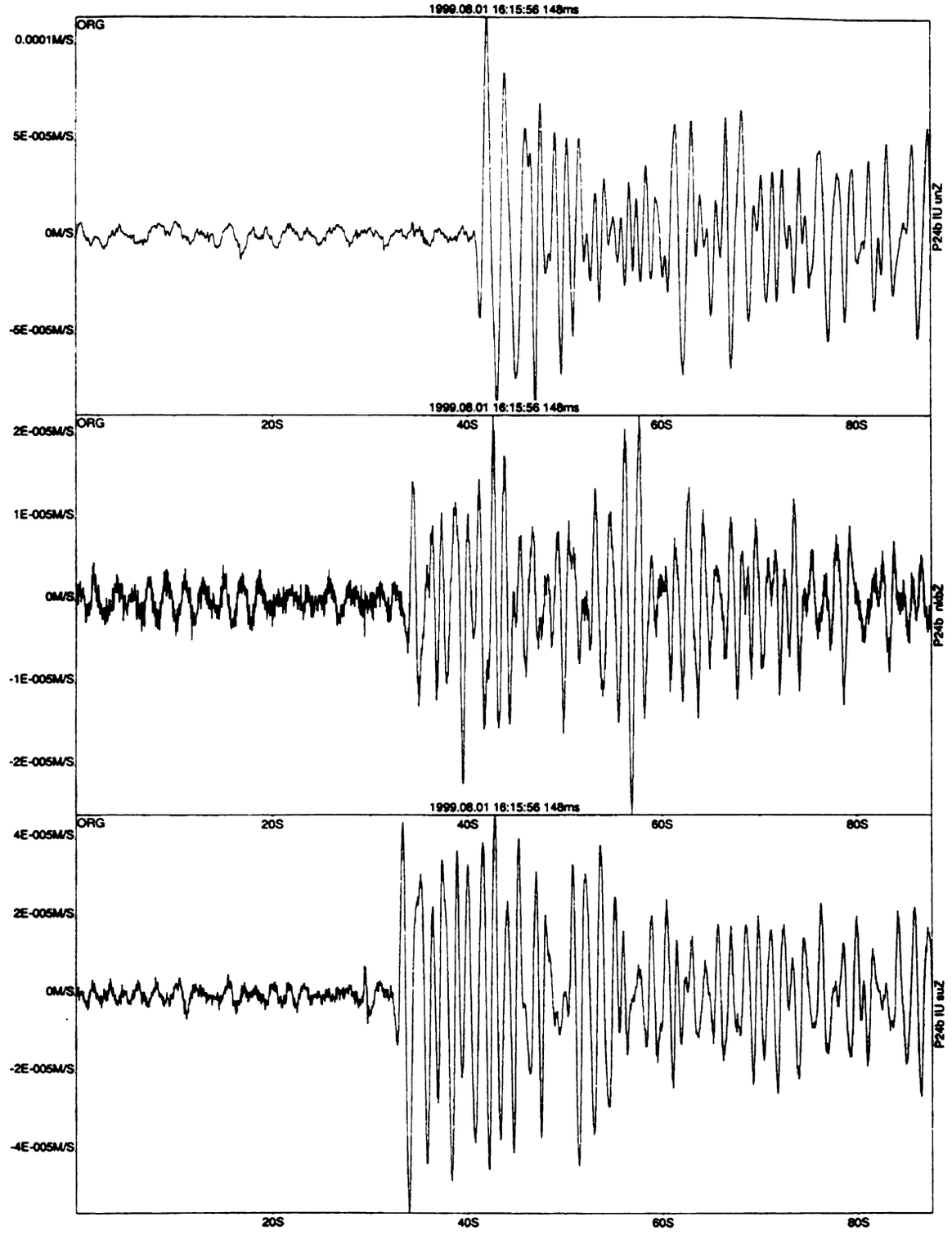

Figure C-5. Teleseismic vertical component recordings of the M_b 5.8 California-Nevada border region event of August 1, 1999. Stations are, from top to bottom, Ust'Nera, Nelkoba, and Susuman.

KULU. (61.889° N, 147.431° E) The town of Kulu is an agricultural town of about 200 people. The station was located in a house approximately 1 km north of the center of town, which is outside of town. The vault, located in a wooden outbuilding, consists of a large concrete pad set into permafrost. The town of Kulu is presently about 50% abandoned.

DEBIN. (62.339° N, 150.751° E) The town of Debin is located along the Kolyma River. The seismic station was located in the southwest portion of the town, about 100 m north of the Kolyma highway. The station was in a house which is now destroyed. Based on station location, it is assumed that the vault consisted of a concrete pad set into permafrost.

MYAKIT. (61.407° N, 152.093° E) The station in Myakit was located near the center of town. Within the town, the station was in a house just in front of the of the blue wooden schoolhouse, and about 30 m off the east side of the Kolyma Highway. The vault in Myakit consisted of a small concrete block (about 0.7 m on a side) set into permafrost ground. The town of Myakit is now entirely abandoned, with the schoolhouse one of only a few buildings remaining intact. The house containing the station has been burned.

PROVIDENIYA. (64.424° N, 173.226° W) The station in Provideniya was located in a large apartment building just west of the center of town. The site is located at the base of a mountain consisting of volcanics. Although the exact vault was not inspected, ground material around the site consists of rock rubble and dirt matrix.

MAGADAN. Two station sites have been visited in Magadan. The original Magadan station, and headquarters of the Magadan network, is located in a residential part of the city about 1 km south and a little west from the center of town. The station consists of a single story moderately sized wooden office building. The seismic vault is located under the station in a cellar about 5 m below the ground surface. The vault contains a large concrete pad measuring about 2 m per side mounted in a rocky soil. This old station site in Magadan had considerable noise due to vault conditions and cultural noise. The vault is no longer used except for instrument testing purposes.

The new GSN station Magadan (MA2) is recorded at the old Magadan station site. The vault of the new Magadan GSN station is located on top of a mountain about 2.5 km to the northwest of the old station. The vault consists of a bunker set into bedrock of granitic composition.

YAKUTSK. The seismic station at Yakutsk is the headquarters of the Yakutsk network, and is the site of the GSN station Yakutsk (YAK). Located about 2 km southwest of the center of town in a residential/light industrial area, the station property contains two buildings. The main station building consists of a single story moderately sized wooden office building. The second building is a two story concrete building used for storage and engineering work. The seismic vault contains a large concrete pad and is located at the bottom of a 15 m vertical shaft below the concrete building. The entire shaft is in permafrost. Coordinates for the station in Yakutsk (see Table 1-1 or A-1) were taken from 1:200,000 scale Russian military topographic maps.

BATAGAI. The town of Batagai, in northern Yakutia, is a regional headquarters for geological expeditions. The seismic station here is located about 1 km west of the center of town in a wooden house. The vault is in a room attached to the side of the house and consists of a dirt pad on permafrost ground. A PC based IASPEI digital acquisition system recording a three component set of Kinemetrics Ranger seismometers was installed in Batagai in 1993 by S. Crumley of the Geophysical Institute, University of Alaska. The seismometers failed within weeks due to leveling problems with the dirt pad. The Rangers were removed in 1995, with the IASPEI system remaining in place and recording the Russian seismometers. The station was rebuilt in 1996 or 1997 and a concrete pad may have been installed.

IRKUTSK. The station in Irkutsk is at the Institute of the Earth's Crust. The institute is located approximately 3.5 kilometers south and a bit west of downtown Irkutsk, across the Angara River. The vault is located in the basement at the rear of the main building on the institute grounds. It is unclear whether the concrete pad in the vault is isolated from the building foundation. Judging from the surrounding area, the vault is located in soil as opposed to permafrost or bedrock.

APPENDIX D

Output of event relocations for comparison with Iul'tin and Western Alaska network hypocenter determinations

APPENDIX D

Output of event relocations for comparison with Iul'tin and Western Alaska network hypocenter determinations

EVENT OF 1981 4 6 MAGNITUDE = 2.1
STATIONS USED = 5

DEPTH FREE, ORIGIN TIME FREE, HYPOCENTER FREE, NO CORRS USED NO CORRS WRITTEN

N RES	ORIGIN TIME	DOT	LAT.	DLAT(KM)	LONG.	DLON(KM)	DEPTH.	DH(KM)	RMS
0	23 33 6.50+	0.00	66.3100+	0.0000	190.1300+	0.0000	1.00		
1	23 33 57.28+	13.31	67.1480+	63.1547	-171.8160+	42.8311	61.12+	56.58	*****
2	23 33 45.45+	7.10	67.5654+	53.5936	-172.8196+	38.4771	33.32+	0.17	2.87
3	23 33 48.43+	3.55	67.3707+	30.7685	-172.4739+	25.0753	33.08+	0.20	0.89
4	23 33 48.42+	3.54	67.3693+	30.0916	-172.4793+	23.7306	33.08+	0.20	0.89
5	23 33 48.42+	3.54	67.3694+	30.0869	-172.4791+	23.7267	33.08+	0.20	0.89

			DIST.	AZ.	RES.	SCOR.	WT.
TCY	EP	23 34 26.9	2.57	132.89	-1.59	0.00	1.0
EAM	EP	23 34 34.1	2.88	117.46	1.05	0.00	1.0
KKL	EP	23 34 48.0	3.90	165.98	0.53	0.00	1.0
ANV	PG	23 35 4.0	4.05	130.77	-0.13	0.00	1.0
ANV	SG	23 35 59.8	4.05	130.77	0.27	0.00	0.5

EVENT OF 1981 4 6 MAGNITUDE = 2.4
STATIONS USED = 8

DEPTH FREE, ORIGIN TIME FREE, HYPOCENTER FREE, NO CORRS USED NO CORRS WRITTEN

N RES	ORIGIN TIME	DOT	LAT.	DLAT(KM)	LONG.	DLON(KM)	DEPTH.	DH(KM)	RMS
0	23 45 23.90+	0.00	64.0900+	0.0000	191.9800+	0.0000	41.00		
1	23 46 22.88+	6.94	65.8519+	64.8174	-170.3192+	47.5447	34.70+	0.76	17.99
2	23 45 49.63+	2.75	67.1554+	23.4334	-172.6012+	17.5379	33.35+	0.19	3.18
3	23 45 44.91+	1.63	67.4155+	15.1923	-172.5616+	10.0253	33.12+	0.10	0.80
4	23 45 44.97+	1.69	67.4040+	15.9232	-172.5512+	10.6205	33.11+	0.10	0.79
5	23 45 44.97+	1.69	67.4042+	15.9031	-172.5506+	10.5977	33.11+	0.10	0.79

			DIST.	AZ.	RES.	SCOR.	WT.
TCY	EP	23 46 24.1	2.61	132.97	-1.57	0.00	1.0
TCY	PG	23 46 34.9	2.61	132.97	-0.13	0.00	1.0
TCY	SG	23 47 10.3	2.61	132.97	-0.66	0.00	0.5
EAM	EP	23 46 31.1	2.92	117.75	0.92	0.00	1.0
KKL	EP	23 46 45.4	3.94	165.65	0.80	0.00	1.0
ANV	EP	23 46 46.5	4.09	130.82	-0.21	0.00	1.0
CDY	SG	23 48 29.6	5.05	122.97	1.01	0.00	0.5

EVENT OF 1981 4 7 MAGNITUDE = 2.7
STATIONS USED = 27

DEPTH FREE, ORIGIN TIME FREE, HYPOCENTER FREE, NO CORRS USED NO CORRS WRITTEN

N	ORIGIN TIME	DOT	LAT.	DLAT(KM)	LONG.	DLON(KM)	DEPTH.	DH(KM)	RMS RES
0	7 8 35.80+	0.00	66.8100+	0.0000	186.0100+	0.0000	0.00		
1	7 8 38.21+	0.89	66.6907+	4.5902	-174.1667+	4.2795	32.03+	3.68	0.92
2	7 8 38.25+	0.90	66.6788+	4.6537	-174.1380+	4.4234	39.77+	5.32	63.38
3	7 8 37.57+	0.67	66.6878+	4.9677	-174.1543+	4.6419	33.04+	0.03	0.76
4	7 8 37.61+	0.62	66.6818+	4.5795	-174.1517+	4.1393	33.04+	0.03	0.76
5	7 8 37.61+	0.62	66.6817+	4.5771	-174.1517+	4.1389	33.04+	0.03	0.76

			DIST.	AZ.	RES.	SCOR.	WT.
TCY	EP	7 9 20.9	2.76	111.20	0.45	0.00	1.0
TCY	PG	7 9 30.3	2.76	111.20	1.03	0.00	1.0
TCY	SG	7 10 6.3	2.76	111.20	-0.99	0.00	0.5
EAM	EP	7 9 27.8	3.29	99.82	-0.21	0.00	1.0
EAM	PG	7 9 38.7	3.29	99.82	-0.19	0.00	1.0
EAM	SG	7 10 23.9	3.29	99.82	-0.16	0.00	0.5
KKL	EP	7 9 32.2	3.49	151.03	1.28	0.00	1.0
KKL	PG	7 9 42.1	3.49	151.03	-0.56	0.00	1.0
DMA	EP	7 9 36.0	3.88	91.24	-0.35	0.00	1.0
DMA	PG	7 9 49.7	3.88	91.24	-0.03	0.00	1.0
DMA	SG	7 10 44.2	3.88	91.24	1.32	0.00	0.5
AVN	EP	7 9 41.8	4.21	116.21	0.70	0.00	1.0
AVN	PG	7 9 55.9	4.21	116.21	0.05	0.00	1.0
AVN	SG	7 10 52.5	4.21	116.21	-1.09	0.00	0.5
KTA	EP	7 9 46.0	4.58	82.71	-0.31	0.00	1.0
KTA	PG	7 10 2.0	4.58	82.71	-0.56	0.00	1.0
ACK	EP	7 9 49.6	4.86	92.48	-0.74	0.00	1.0
ACK	PG	7 10 8.3	4.86	92.48	0.56	0.00	1.0
ACK	SG	7 11 17.0	4.86	92.48	2.60	0.00	0.5
CDY	EP	7 9 56.7	5.28	111.17	0.56	0.00	1.0
CDY	PG	7 10 14.4	5.28	111.17	-0.94	0.00	1.0
CDY	SG	7 11 26.3	5.28	111.17	-1.31	0.00	0.5
CDY	PG	7 10 15.8	5.28	111.17	0.46	0.00	1.0
CRK	EP	7 10 3.9	5.98	103.41	-2.09	0.00	1.0
KGR	EP	7 10 10.3	6.24	118.85	0.69	0.00	1.0

EVENT OF 1981 4 7 MAGNITUDE = 0.0
STATIONS USED = 21

DEPTH FREE, ORIGIN TIME FREE, HYPOCENTER FREE, NO CORRS USED NO CORRS WRITTEN

N	ORIGIN TIME	DOT	LAT.	DLAT(KM)	LONG.	DLON(KM)	DEPTH.	DH(KM)	RMS RES
0	7 15 52.00+	0.00	67.1000+	0.0000	186.0000+	0.0000	0.00		
1	7 16 3.73+	1.31	66.6497+	5.8440	-174.1484+	5.7484	32.49+	5.82	1.15
2	7 16 3.67+	1.23	66.6461+	5.4446	-174.0632+	5.6965	39.59+	7.77	57.88
3	7 16 2.98+	0.87	66.6503+	5.7422	-174.0857+	5.9149	33.04+	0.04	0.84
4	7 16 3.04+	0.80	66.6486+	5.2718	-174.0751+	5.2892	33.04+	0.05	0.84
5	7 16 3.04+	0.80	66.6486+	5.2690	-174.0750+	5.2876	33.04+	0.05	0.84

			DIST.	AZ.	RES.	SCOR.	WT.
TCY	EP	7 16 46.0	2.72	110.85	0.69	0.00	1.0
TCY	PG	7 16 54.3	2.72	110.85	0.33	0.00	1.0
TCY	SG	7 17 31.7	2.72	110.85	0.27	0.00	0.5
EAM	IP	7 16 52.7	3.25	99.40	-0.24	0.00	1.0
EAM	PG	7 17 3.8	3.25	99.40	0.13	0.00	1.0
EAM	SG	7 17 47.1	3.25	99.40	-1.27	0.00	0.5
KKL	EP	7 16 54.0	3.45	151.28	-1.73	0.00	1.0
KKL	PG	7 17 6.9	3.45	151.28	-0.39	0.00	1.0
KKL	SG	7 17 56.8	3.45	151.28	2.18	0.00	0.5

DMA	EP	7 17 0.9	3.85	90.83	-0.44	0.00	1.0
DMA	PG	7 17 14.5	3.85	90.83	-0.10	0.00	1.0
DMA	SG	7 18 10.4	3.85	90.83	3.08	0.00	0.5
ANV	IP	7 17 7.8	4.17	116.05	1.86	0.00	1.0
ANV	PG	7 17 21.0	4.17	116.05	0.48	0.00	1.0
ANV	SG	7 18 15.9	4.17	116.05	-1.78	0.00	0.5
KTA	IP	7 17 10.9	4.56	82.32	-0.48	0.00	1.0
ACK	EP	7 17 14.9	4.83	92.17	-0.42	0.00	1.0
CDY	PG	7 17 39.3	5.24	111.02	-0.73	0.00	1.0
CDY	SG	7 18 51.1	5.24	111.02	-0.65	0.00	0.5
KGR	EP	7 17 35.3	6.20	118.79	0.86	0.00	1.0
BBO	SG	7 19 11.7	5.91	109.49	-1.50	0.00	0.5

EVENT OF 1982 1 16 MAGNITUDE = 0.0
STATIONS USED = 21

DEPTH FREE, ORIGIN TIME FREE, HYPOCENTER FREE, NO CORRS USED NO CORRS WRITTEN

N	ORIGIN TIME	DOT	LAT.	DLAT(KM)	LONG.	DLON(KM)	DEPTH.	DH(KM)	RMS
RES									
0	12 35 8.00+	0.00	64.7700+	0.0000	188.6000+	0.0000	0.00		
1	12 35 10.16+	0.71	64.8141+	2.6128	-170.8251+	3.9558	13.61+	3.27	0.65
2	12 35 9.91+	0.64	64.8008+	2.7501	-170.8400+	3.7136	12.53+	3.11	0.62
3	12 35 9.91+	0.64	64.8006+	2.7400	-170.8397+	3.7257	12.53+	3.12	0.62
4	12 35 9.91+	0.64	64.8006+	2.7400	-170.8397+	3.7256	12.53+	3.12	0.62
5	12 35 9.91+	0.64	64.8006+	2.7400	-170.8397+	3.7256	12.53+	3.12	0.62

			DIST.	AZ.	RES.	SCOR.	WT.
SOV	PG	12 35 30.9	1.17	171.44	-0.62	0.00	1.0
SOV	SG	12 35 48.3	1.17	171.44	0.71	0.00	0.5
TLR	EP	12 35 44.0	2.03	73.03	-0.15	0.00	1.0
TLR	PG	12 35 47.5	2.03	73.03	0.17	0.00	1.0
TLR	SG	12 36 16.0	2.03	73.03	0.85	0.00	0.5
AVN	EP	12 35 49.7	2.36	93.26	0.75	0.00	1.0
AVN	PG	12 35 53.4	2.36	93.26	0.00	0.00	1.0
EAM	PG	12 35 51.2	2.23	57.68	0.15	0.00	1.0
TPK	EP	12 35 57.8	2.95	91.79	0.50	0.00	1.0
TPK	PG	12 36 3.7	2.95	91.79	-0.49	0.00	1.0
TPK	SG	12 36 44.3	2.95	91.79	-0.33	0.00	0.5
ACK	EP	12 36 8.8	3.81	67.57	-0.74	0.00	1.0
ACK	PG	12 36 21.8	3.81	67.57	1.77	0.00	1.0
ACK	SG	12 37 11.8	3.81	67.57	-0.40	0.00	0.5
CDY	PG	12 36 13.5	3.50	93.94	-0.86	0.00	1.0
CDY	SG	12 37 2.6	3.50	93.94	0.27	0.00	0.5
BBO	EP	12 36 14.5	4.19	95.06	-0.35	0.00	1.0
KTA	SG	12 37 15.6	3.96	55.20	-1.35	0.00	0.5

APPENDIX E

Event relocations for northeast Russia

APPENDIX E

Event relocations for northeast Russia

DATE	TIME h	m	s	LAT.	LONG	DEP. km	MAG.
700321	11	21	10.84	56.92N	133.18E	6.8	.
700919	08	53	32.16	57.38N	127.50E	10.3	.
701014	23	57	13.00	56.61N	124.78E	33.0	.
710126	09	08	35.28	58.00N	126.75E	9.1	.
710202	12	11	40.74	63.49N	146.12E	8.4	.
710220	14	05	13.95	56.41N	127.41E	0.	.
710318	20	08	41.2	55.77N	133.48E	3.4	.
710414	11	18	03.2	56.54N	121.07E	7.1	.
710518	22	44	41.90	64.05N	145.76E	33.1	7.1
710518	23	09	08.04	64.14N	146.05E	1.2	.
710519	00	33	04.31	64.07N	145.79E	4.2	.
710519	02	53	46.48	63.99N	145.84E	11.9	.
710519	16	35	16.69	64.08N	145.83E	0.	.
710529	09	19	15.99	64.12N	145.68E	1.2	.
710607	12	09	46.79	64.02N	145.61E	4.7	.
710614	13	48	52.9	56.25N	123.70E	18.3	.
710614	14	25	54.0	56.20N	123.67E	12.7	.
710707	21	50	43.65	64.02N	146.13E	1.4	.
710801	18	50	05.62	56.90N	127.63E	19.7	.
710809	11	51	53.7	56.22N	123.59E	18.8	.
710812	09	54	22.2	56.18N	123.85E	3.0	.
710812	11	44	06.66	66.05N	142.20E	14.1	.
710912	13	32	57.46	65.89N	142.34E	33.1	.
711001	15	13	13.56	63.35N	150.37E	5.9	.
711004	12	59	08.33	66.12N	142.11E	0.0	.
711008	03	27	30.6	56.26N	123.60E	16.5	.
720113	17	24	17.07	61.63N	147.11E	0.9	.
720113	22	20	12.45	61.86N	147.11E	9.0	.
720115	18	08	00.1	57.69N	121.10E	4.5	.
720117	09	22	49.64	61.91N	147.12E	7.9	.
720117	10	38	29.25	61.87N	147.17E	11.4	.
720120	15	38	38.88	54.25N	127.24E	17.9	.
720120	19	48	46.28	62.51N	145.01E	16.3	.
720214	22	35	35.9	57.28N	122.14E	16.9	.
720330	20	20	52.40	64.01N	145.97E	6.1	.
720401	10	00	26.5	56.52N	121.08E	14.1	.
720404	11	32	18.77	54.54N	134.83E	1.8	.
720421	10	41	42.75	63.69N	151.47E	13.8	.
720428	02	57	24.6	56.63N	121.18E	13.2	.
720504	14	20	02.20	61.84N	147.11E	4.7	.
720509	21	32	25.47	67.39N	139.31E	33.0	.
720513	16	17	50.5	55.42N	124.13E	10.4	.
720519	08	42	44.17	54.01N	128.64E	21.6	.
720602	08	32	52.28	64.02N	146.10E	11.2	.
720613	10	45	03.55	54.88N	126.46E	19.7	.
720620	09	18	25.57	57.34N	127.66E	9.7	.
720717	03	05	10.56	64.10N	145.79E	14.9	.
720809	20	51	46.90	56.88N	127.80E	12.2	.
720811	12	45	21.1	53.95N	128.19E	7.1	.
720831	13	43	17.2	56.07N	124.56E	7.2	.
720908	19	48	53.4	56.00N	130.60E	0.0	.
721221	02	12	57.58	62.82N	140.45E	4.0	.
730130	22	53	22.38	56.69N	128.83E	0.	.
730222	05	44	15.1	54.07N	123.91E	30.1	.
730429	06	18	50.6	54.58N	124.72E	9.5	.
730519	02	24	24.80	59.98N	152.87E	0.	.
730527	05	49	09.67	62.23N	161.72E	2.5	.
730608	11	43	47.07	63.82N	146.17E	26.1	.
730616	02	12	18.31	59.99N	152.63E	11.1	.
730618	13	59	47.7	56.84N	121.05E	9.2	.
730727	15	09	19.99	60.19N	153.55E	0.	.
730813	06	50	19.74	62.68N	145.62E	4.6	.
730820	21	03	41.27	60.92N	148.05E	12.9	.
730821	01	26	53.05	67.09N	139.59E	0.8	.
730915	07	15	05.94	63.24N	154.41E	13.7	.
731012	03	08	38.48	61.40N	142.99E	0.	.
731022	05	12	56.0	57.54N	121.05E	30.9	.
731026	11	26	57.1	56.23N	123.55E	13.3	.
731028	17	45	51.02	64.07N	145.76E	7.2	.
731102	07	31	28.68	54.10N	125.71E	0.	.
731102	12	14	45.89	54.26N	125.80E	12.8	.
731114	17	12	35.60	62.27N	143.25E	0.	.
740111	23	10	18.93	60.51N	153.11E	0.	.
740406	19	00	50.33	62.19N	153.23E	5.8	.
740411	20	32	36.14	61.71N	156.78E	10.0	.
740426	03	33	13.06	57.29N	127.79E	8.7	.
740516	09	05	19.6	56.16N	123.74E	7.2	.
740518	06	45	06.25	59.26N	148.66E	30.0	.
740619	03	09	36.78	63.26N	151.10E	30.0	.
740629	14	33	23.9	56.55N	121.05E	7.5	.
740702	09	19	19.70	66.85N	139.51E	20.0	.
740702	17	04	03.15	66.53N	138.27E	12.2	.
740727	12	19	51.68	54.52N	127.23E	25.4	.
740829	06	18	51.37	59.89N	152.49E	33.0	.
740829	13	54	21.96	57.25N	127.24E	0.	.
740928	15	01	25.31	67.00N	139.41E	33.0	.
741206	12	43	09.95	67.92N	140.21E	33.0	.
741217	07	11	03.74	66.15N	125.79E	0.	.
741217	16	40	13.77	60.23N	153.15E	15.6	.
741220	22	58	13.94	64.12N	145.89E	16.5	.
741223	04	20	10.71	59.09N	150.41E	5.4	.
750119	16	22	33.76	59.82N	161.23E	16.5	.
750227	02	09	11.90	66.86N	129.02E	1.0	.
750315	07	36	42.3	56.27N	122.96E	10.9	.
750317	12	14	12.62	63.31N	146.09E	18.2	.
750629	12	24	39.6	53.11N	132.13E	4.7	.
750812	15	00	00.6	70.76N	126.95E	0.5	5.1
750921	09	30	37.5	54.13N	122.26E	31.7	.
750921	10	03	29.3	54.20N	122.33E	24.6	.
750924	20	12	54.91	66.13N	143.43E	3.8	.
751103	12	06	58.01	57.70N	126.24E	0.	.
751104	12	41	06.83	59.81N	160.17E	10.3	.
751224	01	29	02.01	61.85N	144.28E	0.	.
751227	03	54	20.52	62.06N	154.92E	10.9	.
760121	06	01	48.46	67.69N	140.27E	22.7	5.3
760216	22	06	23.82	58.17N	131.02E	4.4	4.6
760226	17	23	03.3	56.53N	121.10E	12.8	.
760408	04	20	58.28	67.03N	139.69E	10.0	.
760426	20	12	21.41	61.77N	155.97E	13.5	.
760508	11	39	25.77	60.09N	152.72E	2.3	.
760520	16	53	29.2	56.36N	132.48E	0.0	.
760614	11	58	01.9	55.57N	130.72E	5.9	.
760624	17	58	01.07	59.94N	157.70E	33.2	.
760627	16	03	23.8	55.39N	131.22E	1.8	.
760704	23	23	31.80	65.60N	134.98E	25.7	.
760730	21	53	19.7	55.61N	132.87E	0.0	.
760803	16	21	29.55	60.26N	146.99E	19.7	.
760907	20	04	29.02	61.19N	156.07E	15.2	.
760930	21	05	38.48	57.96N	147.55E	26.2	.
761120	08	02	54.3	54.02N	122.20E	12.0	.
761121	15	51	55.5	54.15N	121.98E	22.9	.
761124	18	33	34.1	54.12N	122.25E	31.8	.
761203	01	50	34.7	54.13N	122.17E	25.6	.
761203	03	55	56.5	54.14N	122.01E	17.9	5.
770116	00	09	28.9	55.66N	130.54E	5.1	.
770124	15	19	56.83	58.99N	149.38E	28.6	.
770203	11	13	24.99	61.40N	156.81E	7.7	.
770215	06	58	07.97	62.47N	147.00E	7.8	.

770410	15	48	43.99	65.99N	142.04E	0.	.		800321	17	26	51.0	51.32N	133.26E	20.6	.
770422	18	29	12.41	54.48N	125.35E	13.9	.		800404	23	10	18.84	63.23N	148.07E	5.2	.
770502	06	50	14.1	56.64N	121.19E	8.5	.		800406	02	28	55.0	54.00N	127.93E	24.8	.
770503	11	40	26.00	60.70N	161.31E	33.1	.		800422	19	07	44.66	65.55N	136.65E	1.0	.
770504	03	18	29.9	57.68N	121.11E	17.2	.		800507	05	04	35.	60.25N	152.03E	23.	.
770514	21	18	57.11	58.96N	150.66E	18.5	.		800508	10	28	11.16	62.65N	155.32E	7.2	.
770611	19	28	33.3	52.75N	123.49E	33.0	.		800512	09	06	56.82	63.24N	147.70E	0.	.
770627	17	47	15.58	62.80N	146.19E	6.4	.		800512	09	09	13.57	63.15N	147.67E	4.0	.
770720	00	31	40.58	54.72N	126.43E	6.7	.		800512	19	30	13.46	63.14N	147.64E	5.2	.
770720	02	03	37.90	54.73N	126.40E	7.1	.		800514	08	24	07.0	49.66N	130.13E	22.8	.
770816	13	56	54.40	53.84N	128.86E	0.	.		800514	19	20	30.8	49.66N	130.15E	24.6	.
771101	03	54	22.5	55.56N	130.64E	3.8	.		800516	20	53	46.73	57.58N	128.06E	11.0	.
771106	04	31	20.26	59.20N	146.48E	24.5	.		800519	17	29	47.00	59.92N	144.24E	28.1	.
771118	21	55	36.23	60.14N	143.42E	9.1	4.7		800602	13	15	06.91	62.85N	145.86E	8.2	.
771210	11	42	23.79	54.11N	125.89E	3.8	.		800607	02	04	51.54	64.30N	145.41E	3.2	.
780103	03	17	39.05	67.81N	139.38E	0.	.		800616	01	52	29.36	58.85N	150.11E	7.4	.
780201	01	08	38.6	54.20N	123.00E	33.0	.		800622	00	07	48.34	59.76N	146.14E	1.8	.
780207	04	55	21.69	63.27N	146.33E	6.1	.		800701	03	57	15.52	56.32N	125.67E	19.3	.
780213	05	27	00.9	54.26N	122.97E	33.0	.		800706	22	02	07.74	56.77N	127.66E	5.5	.
780222	23	41	46.48	63.08N	146.13E	12.0	.		800714	10	20	17.22	64.16N	154.68E	11.7	.
780328	18	57	20.05	58.79N	151.04E	8.9	.		800719	17	21	11.52	56.99N	127.71E	13.2	.
780401	16	56	35.7	56.86N	120.75E	19.7	.		800720	03	19	07.92	59.47N	144.63E	10.3	.
780428	14	56	23.9	53.74N	124.99E	12.0	.		800723	11	51	13.23	62.57N	155.34E	12.2	.
780505	16	06	58.25	67.61N	139.25E	23.7	.		800808	16	36	33.95	59.43N	147.91E	7.8	.
780601	07	40	14.5	56.52N	121.20E	9.5	.		800829	16	31	55.01	56.14N	129.59E	19.4	.
780605	07	05	56.92	60.12N	160.06E	31.8	.		800916	11	17	51.81	61.52N	143.29E	14.4	.
780605	21	01	40.67	60.11N	159.72E	33.1	.		800919	18	28	49.57	63.23N	148.22E	10.4	.
780622	06	12	35.73	62.94N	145.34E	5.8	.		801015	02	52	49.8	54.73N	133.90E	12.6	.
780626	02	51	20.89	55.82N	126.31E	10.0	.		801021	18	06	19.7	58.56N	121.81E	29.0	.
780630	11	57	01.5	53.92N	125.71E	11.9	.		801103	06	31	10.23	63.35N	146.25E	7.8	.
780805	23	12	20.27	58.39N	134.48E	5.8	.		801127	14	26	00.38	57.51N	125.66E	11.0	.
780821	10	15	53.4	55.21N	124.81E	15.2	.		801203	17	58	15.05	63.65N	152.22E	8.7	.
780822	17	41	38.55	61.23N	144.48E	3.1	.		801208	05	27	22.59	58.79N	149.86E	14.4	.
780822	18	26	27.02	61.27N	159.97E	19.0	.		801217	08	59	42.56	67.11N	129.08E	11.3	.
781027	06	34	39.54	64.63N	145.36E	9.8	.		801223	01	38	02.8	53.47N	132.31E	16.2	.
781201	13	25	59.4	55.17N	124.03E	5.9	.		801229	20	19	07.83	69.73N	139.11E	4.0	.
781206	08	20	46.30	63.61N	144.27E	6.6	.		801231	05	00	17.98	63.92N	140.69E	23.9	.
781211	14	05	58.9	53.82N	125.65E	12.7	.		810202	19	15	15.92	62.36N	144.44E	14.4	.
790103	03	20	27.4	52.61N	127.48E	12.2	.		810217	12	15	13.34	64.12N	145.91E	11.5	.
790104	21	50	16.7	54.18N	122.96E	29.2	.		810222	23	06	20.73	63.15N	150.98E	3.9	.
790221	15	03	27.35	63.37N	146.28E	6.6	.		810301	18	39	33.88	62.14N	143.25E	7.3	.
790427	19	38	13.8	55.76N	130.47E	12.7	.		810304	10	43	02.8	57.78N	120.68E	10.6	.
790428	09	34	06.23	57.45N	126.92E	10.7	.		810313	12	49	58.16	63.79N	149.07E	12.0	.
790502	22	10	28.88	64.19N	149.21E	2.5	.		810315	03	50	34.85	69.63N	137.59E	24.7	.
790517	06	39	09.4	53.70N	126.09E	8.3	.		810324	17	06	38.46	64.75N	149.55E	2.7	.
790523	17	37	33.9	53.61N	126.09E	21.2	.		810404	11	49	19.38	62.41N	144.65E	21.4	.
790531	10	49	26.2	55.68N	130.26E	14.5	.		810406	08	34	37.05	63.38N	146.70E	4.2	.
790531	11	52	35.3	56.51N	124.88E	13.8	.		810429	02	35	28.81	59.62N	144.09E	0.	.
790616	20	41	48.41	64.89N	143.67E	26.7	.		810505	02	08	19.66	56.25N	125.86E	20.0	.
790618	22	09	57.41	57.50N	126.06E	5.3	.		810509	07	48	28.43	56.67N	127.48E	2.6	.
790623	08	22	37.82	58.14N	133.73E	4.9	.		810510	18	08	26.38	61.54N	157.26E	10.1	.
790627	17	45	11.6	53.18N	135.16E	0.0	.		810522	04	59	20.88	61.12N	156.72E	9.4	.
790713	15	12	46.9	62.29N	130.29E	18.1	.		810527	02	57	00.51	54.40N	125.55E	24.8	.
790727	04	28	47.64	63.08N	172.66E	11.3	4.4		810527	08	45	21.41	54.36N	125.52E	17.6	.
790818	19	31	47.9	60.60N	131.82E	29.3	.		810528	12	17	09.2	48.50N	130.71E	13.6	.
790819	07	10	00.09	61.28N	159.81E	7.0	.		810718	19	53	51.16	59.79N	153.93E	9.5	.
790827	02	55	01.00	62.97N	145.53E	11.0	.		810718	20	08	30.13	59.91N	153.89E	5.5	.
791007	01	29	26.10	64.99N	144.03E	13.0	.		810803	08	16	38.50	70.43N	130.49E	25.9	.
791026	00	26	26.24	62.19N	153.87E	13.4	.		810809	19	13	39.23	63.36N	146.36E	6.9	.
791111	19	27	35.91	62.27N	153.75E	12.2	.		810809	19	17	02.62	63.27N	146.12E	30.0	.
791116	07	24	05.1	56.45N	124.26E	11.0	.		810817	06	58	08.16	63.11N	147.99E	1.3	.
791118	08	59	15.84	62.24N	153.80E	11.9	.		810819	19	17	29.66	67.56N	140.25E	9.1	.
791229	04	22	16.69	61.45N	142.68E	9.5	.		810820	14	14	38.3	57.66N	121.08E	13.1	.
800102	00	42	39.20	59.68N	156.07E	9.1	.		810826	10	45	04.91	58.46N	140.97E	7.2	.
800110	20	57	35.50	64.14N	148.58E	10.9	.		810905	01	52	59.2	51.17N	132.33E	12.4	.
800125	18	45	46.77	64.07N	146.00E	18.2	.		810905	13	01	33.50	59.75N	146.71E	1.5	.
800127	18	55	40.06	63.36N	150.50E	5.1	.		811006	23	32	06.91	63.17N	150.96E	9.1	.
800128	05	11	57.58	63.42N	150.57E	12.1	.		811021	05	16	42.79	63.40N	146.21E	6.2	.
800129	08	55	17.59	64.07N	149.02E	11.0	.		811022	12	45	40.9	53.13N	134.55E	21.9	.
800129	17	35	52.83	61.01N	155.80E	5.4	.		811028	11	38	05.58	60.81N	142.80E	15.0	.
800201	17	30	17.83	73.27N	119.98E	15.4	5.7		811103	03	43	01.29	70.28N	141.03E	7.9	.
800205	11	10	32.8	66.79N	146.58E	0.0	.		811105	06	15	33.38	62.06N	150.39E	15.0	.
800205	13	14	04.8	55.95N	122.59E	28.1	.		811108	21	56	09.35	61.82N	153.64E	21.9	.
800214	04	09	46.0	52.24N	126.67E	23.4	.		811109	00	33	20.34	61.83N	153.67E	12.1	.
800225	23	50	02.67	54.91N	125.21E	31.5	.		811109	05	23	40.20	61.80N	153.71E	13.0	.
800307	03	15	14.22	62.01N	150.50E	15.0	.		811110	10	07	51.78	63.97N	148.67E	5.2	.
800311	18	11	21.46	56.99N	127.72E	2.6	.		811110	10	54	15.80	63.92N	148.71E	10.7	.
800321	15	03	55.7	51.46N	133.19E	22.6	.		811111	14	22	18.67	61.85N	153.62E	14.9	.

811111	15	29	48.07	61.79N	153.68E	5.1	.		830530	07	04	18.66	65.94N	173.05W	5.0	.	
811120	18	06	37.5	56.68N	122.59E	12.5	.		830608	18	29	43.26	59.40N	148.07E	7.9	.	
811122	21	44	48.9	51.85N	122.59E	14.8	.		830626	05	43	56.98	71.26N	129.65E	28.0	.	
811203	14	41	25.70	63.93N	148.55E	13.4	.		830629	13	42	55.77	61.98N	152.56E	10.5	.	
811205	01	49	09.0	57.00N	123.15E	18.0	.		830706	18	49	44.70	58.61N	147.65E	12.9	.	
811208	02	17	05.93	59.88N	153.82E	7.8	.		830710	14	40	45.9	48.51N	134.03E	12.5	.	
811208	10	57	21.18	61.83N	153.67E	15.8	.		830730	15	42	09.4	53.30N	132.48E	13.2	4.8	
811212	01	05	58.29	59.60N	148.10E	33.0	.		831012	16	07	25.11	60.04N	149.98E	8.0	.	
811215	19	19	13.75	61.82N	153.63E	5.6	.		831025	19	44	59.98	60.03N	153.04E	9.9	.	
811221	04	58	05.42	62.43N	150.13E	16.6	.		831107	14	20	58.82	65.43N	136.53E	17.7	.	
811229	05	10	34.93	61.99N	149.83E	8.8	.		831112	01	17	41.12	57.64N	125.43E	2.3	.	
820120	03	12	45.08	61.20N	156.99E	2.4	.		831124	15	17	31.39	62.91N	145.46E	2.1	.	
820123	04	15	49.58	62.73N	179.68E	11.6	.		831125	11	22	43.6	51.05N	132.87E	10.0	.	
820123	16	19	36.27	64.00N	154.30E	6.4	.		831201	15	48	43.45	63.62N	142.82E	8.8	.	
820123	19	55	36.54	63.03N	144.75E	11.3	.		831211	11	01	15.96	59.60N	147.18E	5.8	.	
820123	21	38	24.81	63.00N	144.79E	5.6	.		840108	23	18	37.35	54.47N	125.09E	24.2	.	
820124	17	02	37.01	62.66N	179.81E	31.7	.		840203	18	35	55.8	49.38N	128.26E	26.4	.	
820214	10	12	52.59	58.87N	155.13E	8.6	.		840217	20	34	18.89	59.76N	152.45E	10.3	.	
820223	17	29	56.14	63.26N	146.14E	13.3	.		840307	12	24	10.23	54.45N	136.98E	11.9	.	
820307	01	21	31.56	63.88N	148.62E	9.9	.		840324	01	03	19.16	54.50N	136.96E	12.9	.	
820316	19	23	28.2	53.02N	134.86E	14.0	.		840324	02	23	40.11	54.57N	137.04E	8.4	.	
820325	10	52	35.4	51.43N	131.94E	9.5	.		840401	22	43	47.84	59.42N	146.56E	5.4	.	
820404	11	45	28.18	66.04N	143.11E	33.	.		840403	02	53	24.94	57.54N	125.53E	0.	.	
820406	14	41	13.75	61.79N	153.61E	3.2	.		840405	10	35	22.25	58.66N	148.70E	2.9	.	
820407	07	22	01.3	55.58N	130.50E	2.0	.		840411	20	50	38.97	59.29N	147.99E	6.0	.	
820416	08	11	13.9	51.12N	132.39E	7.4	.		840524	20	55	36.98	63.69N	145.58E	0.2	.	
820427	19	40	54.4	51.33N	136.85E	33.0	.		840529	06	20	22.54	63.29N	146.60E	0.	.	
820502	03	28	35.6	52.59N	136.21E	10.9	.		840625	08	13	17.87	62.10N	157.05E	2.2	.	
820504	23	35	10.82	66.01N	172.91E	23.2	.		840707	08	06	53.55	59.81N	152.62E	0.	.	
820623	08	04	28.92	60.50N	137.85E	0.	.		840716	18	26	43.59	66.58N	170.47E	0.	.	
820626	18	47	11.32	63.33N	178.55E	14.1	.		840802	21	25	39.50	60.89N	144.59E	23.3	.	
820706	06	16	39.01	65.43N	136.47E	4.0	.		840808	22	33	46.33	63.29N	152.78E	15.9	.	
820707	01	40	12.00	55.78N	125.57E	18.6	.		840812	14	45	31.8	49.05N	131.42E	17.4	.	
820724	08	39	02.38	63.58N	146.24E	3.8	.		840821	17	41	02.66	60.92N	153.85E	06.7	.	
820725	14	29	38.52	59.85N	145.78E	12.5	.		840912	20	10	41.05	59.37N	138.57E	8.8	.	
820730	01	51	46.2	56.60N	121.07E	13.9	.		840915	13	52	08.39	54.30N	126.37E	23.6	.	
820803	05	41	52.19	64.17N	148.95E	14.2	.		840919	11	36	33.01	63.44N	145.63E	17.9	.	
820804	20	17	03.66	62.39N	146.95E	5.9	.		840926	19	01	08.5	57.60N	120.91E	7.2	.	
820806	19	06	42.31	54.00N	139.66E	22.0	.		841003	13	11	04.74	63.22N	176.81E	9.2	.	
820903	07	29	26.80	66.99N	133.53E	26.1	.		841019	20	26	26.4	57.04N	120.68E	13.0	.	
821005	01	52	27.36	54.37N	126.08E	23.6	.		841020	08	41	36.21	54.23N	126.24E	22.2	.	
821011	02	10	28.85	54.57N	126.27E	10.5	.		841029	14	06	14.17	62.13N	163.77E	19.9	.	
821217	16	42	35.96	59.64N	144.15E	20.2	.		841101	21	49	03.4	52.86N	138.86E	11.4	.	
821221	16	01	47.80	54.37N	126.08E	21.8	.		841103	18	48	55.0	49.19N	139.91E	8.2	.	
821222	12	10	02.78	64.04N	156.70E	12.4	.		841117	22	40	15.8	52.71N	135.62E	11.0	.	
821222	15	47	03.61	59.18N	152.70E	7.6	.		841121	07	31	36.2	56.84N	121.09E	18.1	.	
830104	07	17	14.13	62.14N	143.68E	4.2	.		841122	13	52	57.27	68.47N	140.84E	21.8	.	
830114	01	57	13.11	67.29N	172.44W	5.4	.		841129	21	03	33.2	50.66N	132.60E	21.2	.	
830122	05	20	29.4	53.66N	135.97E	14.8	.		841202	08	35	44.98	63.39N	150.50E	20.6	.	
830123	23	24	25.79	65.99N	172.89W	6.3	.		841202	12	32	02.58	63.38N	150.50E	0.	.	
830130	08	44	30.40	65.98N	172.90W	8.5	.		850103	12	47	13.82	55.81N	129.36E	18.1	.	
830205	09	21	42.2	53.05N	127.18E	20.3	.		850104	09	08	57.02	65.87N	173.16W	14.4	.	
830207	15	34	27.0	53.53N	128.51E	31.8	.		850105	12	58	48.0	50.30N	139.40E	11.2	.	
830214	15	21	05.47	62.46N	145.83E	3.7	.		850108	09	20	16.14	67.02N	169.39W	0.0	.	
830307	18	42	19.9	56.73N	134.47E	7.0	.		850117	01	05	26.5	52.53N	133.05E	11.0	.	
830312	11	55	12.43	64.23N	140.96E	14.1	.		850121	18	03	51.11	60.81N	155.28E	7.7	.	
830315	22	10	24.4	51.50N	134.89E	0.0	.		850121	23	53	55.5	51.40N	130.09E	11.2	.	
830323	14	45	06.73	62.96N	155.66E	10.7	.		850124	20	26	34.02	66.92N	132.96E	16.7	.	
830325	10	36	56.02	63.54N	149.93E	8.1	.		850129	00	36	06.03	64.17N	145.84E	6.0	4.6	
830404	14	37	35.26	66.97N	140.09E	13.6	.		850129	09	45	51.84	64.15N	145.75E	8.4	.	
830409	19	57	18.73	69.26N	178.36E	16.5	.		850130	05	12	49.8	51.18N	133.14E	9.1	.	
830427	00	30	36.7	50.49N	132.23E	11.2	.		850131	20	02	05.2	53.65N	124.86E	11.4	.	
830504	06	52	56.55	57.54N	125.38E	17.1	.		850201	08	31	45.9	62.91N	127.20E	20.5	4.9	
830509	16	48	05.84	63.27N	146.26E	8.9	.		850201	10	20	50.6	62.72N	127.55E	17.7	.	
830510	05	27	24.32	64.21N	150.95E	5.0	.		850201	21	53	18.04	64.17N	145.77E	3.4	.	
830514	08	09	13.46	65.85N	174.82E	0.	.		850202	11	28	41.67	65.86N	137.04E	33.3	.	
830515	04	53	38.49	65.90N	173.19W	11.5	.		850205	08	07	04.9	53.58N	124.68E	8.7	.	
830515	04	57	19.77	65.96N	173.03W	0.9	.		850205	15	30	22.9	53.16N	134.44E	0.0	.	
830515	05	05	43.42	65.96N	173.07W	4.8	.		850213	06	05	22.3	51.16N	133.03E	10.3	.	
830515	06	00	36.69	65.86N	173.24W	2.9	.		850218	12	51	31.60	65.58N	136.40E	4.5	.	
830515	06	22	47.62	65.96N	173.04W	8.1	.		850218	14	22	33.0	55.35N	123.34E	24.7	.	
830515	06	37	06.34	65.89N	173.09W	6.0	.		850222	07	06	21.86	63.24N	146.00E	10.2	.	
830516	03	28	29.67	65.93N	173.13W	6.8	.		850224	19	59	23.3	55.63N	130.55E	0.0	.	
830516	06	33	56.24	65.92N	173.13W	11.2	.		850301	09	19	18.60	57.55N	125.49E	8.6	4.5	
830516	18	41	00.86	65.94N	173.02W	15.6	.		850306	10	06	57.70	54.34N	135.09E	6.9	.	
830517	04	14	02.01	65.95N	173.03W	0.	.		850308	22	24	38.14	59.35N	152.10E	19.4	.	
830518	12	07	58.96	65.94N	173.12W	6.9	.		850311	21	12	07.08	53.92N	128.47E	27.3	.	
830528	02	57	57.57	61.98N	150.43E	6.0	.		850318	23	09	15.4	53.72N	125.51E	24.7	.	

850321	19	26	55.49	63.59N	148.48E	9.7	.		860124	13	25	22.91	60.56N	138.72E	0.	.	
850330	04	51	39.5	51.18N	133.04E	33.0	.		860201	02	29	57.33	54.78N	139.27E	22.8	.	
850331	06	13	01.6	53.40N	132.91E	12.6	.		860206	04	36	10.52	63.56N	179.79E	0.	.	
850402	15	50	16.7	50.98N	132.08E	12.1	.		860209	12	42	53.5	48.69N	126.41E	26.1	5.1	
850406	22	01	56.0	53.62N	125.50E	24.0	.		860211	18	44	57.0	54.72N	131.67E	17.3	.	
850410	11	27	44.55	70.43N	141.27E	20.1	.		860212	03	46	43.88	68.86N	128.23E	9.2	.	
850410	13	50	51.70	54.48N	125.58E	15.6	.		860215	20	30	26.41	63.98N	153.10E	3.5	.	
850417	01	27	19.16	54.51N	135.37E	5.9	.		860216	06	21	49.7	48.31N	126.25E	33.0	.	
850417	20	37	20.14	65.37N	142.78E	16.0	.		860228	17	07	24.6	48.61N	126.39E	19.1	.	
850420	09	22	31.6	50.86N	131.56E	33.0	.		860304	08	15	21.73	64.81N	144.02E	16.2	.	
850420	22	29	16.83	59.22N	141.85E	10.9	.		860307	23	28	08.21	64.11N	153.46E	15.4	.	
850424	06	11	40.9	53.62N	124.71E	16.1	.		860311	12	33	14.38	64.47N	172.58W	5.7	.	
850426	03	19	53.82	59.79N	152.40E	0.	.		860313	11	17	58.5	54.00N	136.79E	19.1	.	
850429	20	36	31.09	62.81N	146.19E	15.9	.		860314	03	09	56.31	60.26N	161.04E	10.5	.	
850502	04	41	22.96	64.38N	175.65W	33.0	.		860315	04	01	54.67	59.82N	144.98E	17.9	.	
850506	06	02	57.4	52.04N	122.37E	21.3	.		860318	19	36	33.41	63.66N	152.66E	11.1	.	
850506	12	17	30.34	65.51N	171.16W	29.7	.		860327	09	44	44.3	49.87N	131.67E	16.1	.	
850506	12	48	42.16	65.52N	171.66W	33.0	.		860330	11	46	32.5	52.86N	134.74E	17.1	.	
850506	15	20	35.70	54.86N	126.11E	13.4	.		860402	20	06	19.3	53.96N	128.26E	15.8	.	
850507	19	47	09.88	60.20N	143.22E	33.1	.		860403	15	38	15.94	59.12N	154.48E	15.4	.	
850508	12	57	00.8	54.33N	122.90E	20.6	.		860406	01	27	20.73	70.72N	130.29E	10.5	.	
850516	02	52	04.88	60.03N	151.71E	10.8	.		860407	09	08	07.71	64.07N	145.25E	6.5	.	
850524	06	22	43.67	54.19N	125.90E	12.9	.		860407	12	19	30.1	49.40N	131.77E	6.0	.	
850525	21	32	05.7	54.42N	123.23E	10.4	.		860413	21	47	48.87	59.75N	145.79E	14.1	.	
850527	19	54	59.0	55.09N	131.46E	0.0	.		860428	09	39	02.3	54.97N	135.38E	5.2	.	
850529	19	04	60.0	55.58N	133.00E	12.0	.		860504	03	13	22.19	57.40N	126.38E	30.3	.	
850602	04	08	09.40	64.85N	144.06E	7.0	.		860508	18	21	03.4	55.30N	123.55E	30.9	.	
850609	15	16	15.6	55.14N	123.97E	22.4	.		860515	21	22	49.8	51.81N	131.93E	5.2	.	
850611	10	15	24.52	65.23N	144.70E	8.7	.		860601	15	34	00.31	64.86N	144.05E	16.0	.	
850612	04	04	33.7	52.50N	132.82E	11.1	5.2		860602	07	43	26.3	55.45N	124.44E	23.8	.	
850620	12	10	07.5	53.62N	135.19E	4.2	.		860603	12	49	40.8	55.89N	124.30E	24.1	.	
850622	15	38	04.24	64.85N	144.06E	12.0	.		860605	06	00	25.9	53.55N	124.74E	4.6	.	
850624	03	54	34.50	65.25N	144.63E	14.9	.		860605	09	46	52.00	64.08N	145.25E	9.8	.	
850627	00	37	55.0	54.04N	127.86E	10.6	.		860606	19	42	13.34	66.96N	130.34E	23.4	.	
850630	13	30	05.86	54.19N	125.91E	14.6	.		860615	06	55	38.09	72.81N	126.31E	25.3	.	
850701	11	07	44.91	67.41N	171.10W	27.7	.		860615	11	46	38.3	51.56N	138.09E	5.3	.	
850701	18	35	16.51	69.80N	133.63E	10.7	.		860616	19	40	25.45	59.89N	156.86E	7.9	.	
850704	05	12	40.1	53.68N	125.49E	14.2	.		860701	20	04	16.9	54.80N	131.08E	14.7	.	
850704	09	42	08.33	69.84N	176.30E	32.5	.		860703	22	41	06.3	49.03N	131.63E	24.0	5.2	
850707	12	15	49.76	55.91N	126.87E	20.9	.		860704	15	01	55.7	50.08N	132.36E	15.7	.	
850708	16	27	39.95	54.85N	126.10E	14.4	.		860707	16	26	06.41	72.87N	121.69E	16.8	.	
850712	16	03	53.8	55.61N	130.89E	0.0	.		860709	22	14	58.30	54.71N	126.49E	11.2	.	
850721	22	34	18.2	48.97N	126.48E	20.8	5.5		860712	09	52	09.1	49.58N	123.45E	33.0	.	
850812	15	19	56.8	49.80N	131.96E	10.2	.		860714	14	39	09.98	65.11N	176.28W	2.7	.	
850820	03	41	38.80	62.23N	145.58E	5.5	.		860716	14	04	59.0	52.15N	126.32E	20.0	.	
850901	19	03	47.38	58.92N	149.02E	16.8	.		860720	21	38	07.9	53.61N	125.47E	6.7	.	
850904	21	03	05.7	53.71N	135.99E	4.0	.		860726	20	58	04.5	56.50N	121.03E	9.0	.	
850910	10	52	56.34	62.22N	143.37E	27.1	.		860727	11	25	40.82	64.60N	147.10E	17.0	.	
850915	03	44	10.2	53.43N	125.01E	0.0	.		860729	20	41	17.2	53.87N	123.79E	27.0	.	
850921	19	28	20.2	55.95N	130.53E	0.0	.		860730	20	41	18.1	53.91N	123.51E	33.0	.	
850922	01	09	29.8	54.25N	123.64E	27.4	.		860809	02	24	44.7	55.07N	123.42E	33.0	.	
850928	05	12	59.0	49.71N	127.55E	22.4	.		860810	11	11	59.55	63.55N	147.80E	5.6	.	
851001	18	59	11.8	53.75N	125.54E	15.7	.		860814	22	36	00.84	63.40N	143.98E	22.8	.	
851005	22	32	35.95	59.43N	150.25E	17.5	.		860815	17	53	09.3	48.70N	126.61E	29.3	.	
851022	02	26	11.6	54.11N	128.94E	0.0	.		860815	20	20	34.0	48.75N	126.36E	15.9	6.5	
851025	07	06	08.3	53.58N	125.46E	1.5	.		860825	17	00	44.0	52.98N	132.58E	17.9	.	
851029	10	54	06.3	55.41N	132.19E	0.0	.		860826	04	45	21.73	56.01N	125.99E	20.1	.	
851030	03	34	09.9	54.74N	134.06E	0.0	.		860826	13	09	14.6	52.34N	138.55E	13.9	.	
851106	07	17	51.08	63.28N	146.65E	4.9	.		860909	12	15	52.21	69.75N	140.40E	5.2	.	
851108	03	53	47.27	65.67N	172.20W	5.6	.		860909	22	21	39.8	52.41N	131.71E	17.8	.	
851109	04	09	19.0	53.98N	136.80E	29.6	.		860915	16	23	09.01	57.63N	125.52E	12.4	.	
851110	16	47	51.8	50.30N	122.95E	8.1	.		860916	14	30	32.4	51.96N	122.37E	5.5	.	
851122	00	53	39.7	53.73N	125.52E	16.4	.		860918	08	40	47.1	55.60N	120.76E	25.8	.	
851122	02	37	32.10	60.63N	149.71E	0.	.		860919	05	45	32.5	52.17N	136.17E	4.6	.	
851123	23	00	00.45	64.30N	175.42E	29.5	.		860919	07	47	43.7	53.60N	132.07E	13.4	5.0	
851128	08	38	22.15	64.89N	144.25E	16.6	.		860925	21	52	07.0	54.01N	134.37E	8.5	.	
851128	20	13	49.02	57.29N	127.52E	18.5	.		861003	18	14	46.39	65.47N	173.10W	7.3	.	
851129	16	57	09.6	53.62N	125.47E	21.9	.		861007	01	01	15.90	55.65N	126.50E	21.7	.	
851204	05	42	03.86	55.86N	125.87E	16.2	.		861007	01	15	05.48	55.65N	126.49E	11.1	.	
851208	08	28	32.69	54.35N	135.38E	1.9	.		861010	20	52	31.9	53.69N	125.51E	11.4	.	
851210	12	27	14.34	55.16N	128.47E	15.1	.		861013	20	01	59.41	65.29N	170.33W	33.0	.	
851217	16	43	11.3	52.91N	128.94E	11.2	.		861019	18	30	58.46	63.88N	178.48W	16.6	5.1	
851221	05	42	49.0	51.26N	133.07E	22.4	.		861023	10	50	02.6	51.62N	130.11E	12.5	.	
860105	00	35	22.80	70.20N	128.53E	2.6	.		861030	10	15	06.28	65.37N	173.06W	24.3	.	
860106	05	27	24.5	53.08N	134.52E	28.8	5.4		861102	08	50	08.6	53.73N	125.53E	13.8	.	
860108	07	25	18.8	52.35N	132.69E	0.0	.		861103	09	16	26.1	55.77N	130.58E	5.7	.	
860110	02	30	38.70	64.70N	142.05E	6.8	.		861103	21	54	38.20	54.21N	126.06E	19.5	.	
860118	13	13	22.73	60.21N	153.71E	4.3	.		861111	17	58	06.89	63.78N	145.72E	12.2	.	

861129	20	04	59.9	54.26N	131.37E	21.8	.		870603	11	36	36.4	52.57N	135.99E	8.2	.	
861130	03	17	12.70	64.94N	154.54E	13.9	.		870606	14	14	49.6	50.92N	135.51E	4.3	.	
861202	11	06	20.00	54.32N	126.12E	17.4	.		870610	02	12	14.0	53.71N	124.81E	10.2	.	
861203	19	32	37.5	53.66N	125.50E	19.9	.		870623	23	07	24.83	53.99N	127.92E	9.9	.	
861209	22	54	21.44	64.13N	148.42E	12.9	.		870701	11	52	32.3	52.03N	132.91E	13.7	.	
861218	09	26	40.43	67.49N	171.24W	10.8	.		870703	13	23	08.19	59.31N	148.65E	4.1	.	
861218	12	11	14.4	51.85N	133.69E	19.9	.		870704	18	30	29.2	54.31N	134.62E	11.4	.	
861218	18	04	12.03	61.20N	143.73E	22.7	.		870705	00	08	55.24	61.26N	144.60E	6.6	.	
861221	04	28	23.9	49.19N	130.83E	18.2	.		870711	03	15	14.3	49.11N	135.59E	0.8	.	
861225	19	12	29.45	62.36N	156.41E	5.7	.		870721	05	02	28.63	58.64N	149.64E	5.9	.	
861226	03	21	04.97	61.37N	149.44E	14.6	.		870725	15	49	25.25	62.86N	156.78E	7.2	.	
861229	17	16	49.6	55.04N	122.76E	33.0	.		870731	06	40	41.0	53.15N	127.76E	12.1	.	
861231	07	21	58.3	56.59N	121.11E	14.4	.		870731	12	55	25.4	48.73N	131.97E	23.7	.	
870109	04	29	45.00	60.04N	153.01E	2.4	.		870804	21	31	53.0	48.74N	132.02E	19.1	.	
870109	13	14	17.46	67.18N	140.08E	10.5	.		870806	14	50	07.50	56.16N	125.07E	22.4	.	
870110	19	33	25.18	65.44N	172.92W	32.3	.		870808	00	09	56.4	51.07N	131.87E	28.6	5.4	
870110	19	34	39.53	65.35N	173.38W	33.0	.		870808	03	37	36.6	51.09N	131.89E	25.7	.	
870116	23	53	18.12	58.57N	125.11E	10.3	.		870815	18	16	00.50	63.16N	175.90E	12.8	.	
870120	07	42	18.1	50.28N	134.78E	15.6	.		870821	07	07	07.9	53.39N	132.07E	16.8	4.4	
870122	19	01	23.4	55.71N	130.74E	3.0	.		870821	17	58	50.6	53.40N	132.05E	11.9	.	
870131	03	55	08.0	56.67N	124.78E	20.9	.		870825	11	31	22.6	55.43N	131.20E	5.6	.	
870203	17	16	45.7	55.54N	130.63E	9.0	.		870909	04	43	22.95	60.15N	150.41E	7.6	.	
870204	01	43	46.3	52.90N	132.72E	17.7	.		870909	19	10	41.9	51.81N	123.58E	20.9	.	
870204	05	58	31.62	64.53N	144.63E	17.0	.		870922	23	20	52.4	54.40N	132.19E	10.7	.	
870205	09	30	41.1	57.52N	120.85E	24.6	.		870923	17	43	01.0	53.01N	138.76E	14.6	.	
870208	19	57	21.8	49.15N	131.48E	14.1	.		870927	13	16	35.82	61.16N	160.97E	4.5	.	
870209	23	00	01.30	65.44N	172.78W	14.4	.		871007	16	21	48.8	52.82N	138.64E	7.7	.	
870210	12	34	42.73	65.47N	172.65W	22.8	.		871015	03	09	50.85	57.61N	125.45E	4.2	.	
870211	00	58	20.93	62.87N	156.84E	5.6	4.8		871030	21	42	48.1	48.89N	130.00E	33.0	.	
870211	01	03	09.55	62.77N	156.88E	14.8	.		871102	03	20	42.69	57.54N	128.20E	5.3	.	
870211	01	09	51.56	62.84N	156.78E	9.0	.		871102	23	21	05.41	55.05N	136.60E	2.9	.	
870211	01	22	23.15	62.89N	156.87E	5.1	.		871108	06	44	07.2	52.33N	132.66E	15.1	.	
870211	05	52	49.59	62.88N	156.78E	10.0	.		871115	07	07	47.87	63.18N	177.27E	15.2	.	
870211	06	19	16.38	62.85N	156.77E	8.1	.		871115	19	51	21.9	51.54N	138.19E	21.3	.	
870211	07	28	18.00	62.84N	156.91E	11.6	.		871116	07	41	47.06	57.61N	125.35E	13.5	.	
870211	07	28	59.72	62.89N	156.85E	5.6	.		871121	18	15	18.79	62.22N	170.88E	7.5	.	
870211	07	47	11.44	62.87N	156.86E	2.6	.		871125	00	43	07.41	62.91N	144.94E	12.6	.	
870211	08	42	45.18	62.86N	156.86E	8.3	.		871203	07	34	51.17	59.32N	147.87E	10.6	.	
870211	11	36	16.41	62.86N	156.86E	6.0	.		871205	21	16	21.07	71.18N	141.69E	20.8	.	
870211	17	32	23.70	62.88N	156.85E	10.7	.		871206	10	54	26.59	63.32N	144.60E	1.6	.	
870212	02	10	47.0	49.62N	134.74E	2.2	.		871207	10	50	58.61	63.68N	145.56E	10.3	.	
870212	02	12	21.01	62.81N	156.80E	8.9	.		871212	07	51	06.44	57.37N	127.40E	12.7	.	
870214	07	16	29.76	59.44N	148.03E	0.	.		871215	06	56	02.0	56.73N	123.01E	9.6	.	
870218	21	53	15.3	50.35N	132.28E	6.1	.		871222	22	04	33.79	62.95N	145.04E	4.0	.	
870221	19	33	14.6	53.49N	132.13E	26.7	4.8		871226	18	02	32.62	58.94N	147.76E	0.	.	
870222	16	12	04.33	62.90N	156.83E	7.2	.		880101	14	36	12.94	74.59N	130.81E	33.0	.	
870225	03	03	38.29	63.02N	179.04E	17.7	.		880114	14	35	33.3	52.60N	132.43E	22.8	.	
870303	04	52	02.51	65.40N	136.29E	12.1	.		880119	10	35	32.19	63.71N	145.68E	7.4	.	
870304	00	09	28.42	61.15N	148.42E	10.5	.		880122	12	51	56.52	62.20N	146.03E	6.2	.	
870308	06	47	26.71	62.06N	143.57E	11.7	.		880208	20	47	57.88	64.01N	146.03E	9.5	.	
870308	13	52	12.05	59.77N	145.49E	5.2	.		880212	09	19	25.2	56.61N	121.08E	9.9	.	
870310	06	00	02.0	50.41N	143.54E	2.1	.		880217	23	00	43.88	64.10N	145.62E	3.6	.	
870316	20	58	53.45	64.08N	167.31E	0.	.		880219	00	04	04.40	64.33N	148.58E	9.7	.	
870322	00	19	50.43	65.40N	172.98W	17.4	.		880219	20	41	05.2	53.04N	138.61E	9.3	.	
870324	02	39	54.16	65.41N	173.05W	13.2	.		880219	23	50	25.40	64.19N	145.81E	12.3	.	
870326	00	45	57.33	65.43N	173.00W	14.5	.		880221	23	10	04.9	56.58N	121.11E	12.2	.	
870329	20	16	36.8	52.46N	142.08E	12.6	3.4		880227	02	07	29.6	54.36N	124.27E	24.5	.	
870403	13	06	12.1	52.88N	134.63E	9.1	.		880309	20	18	01.55	68.04N	130.71E	14.9	.	
870405	10	00	15.49	63.11N	174.89E	12.1	.		880314	18	33	53.91	61.37N	154.22E	1.5	.	
870405	11	36	36.46	63.18N	174.81E	9.0	.		880315	19	10	31.9	52.72N	134.66E	28.8	.	
870412	02	31	18.5	53.61N	125.69E	11.3	.		880321	11	29	06.6	51.29N	131.43E	0.0	.	
870415	23	09	21.1	58.56N	121.59E	33.0	.		880325	06	30	09.24	64.51N	144.68E	9.7	.	
870421	12	39	48.43	64.92N	170.43W	12.6	.		880403	02	01	29.00	69.46N	138.77E	22.1	.	
870421	13	21	00.30	64.82N	170.86W	30.1	.		880503	00	39	00.74	65.38N	173.40W	5.8	.	
870421	18	20	46.72	64.90N	170.47W	18.9	.		880519	11	53	20.52	55.91N	128.82E	20.3	.	
870422	03	38	20.69	72.18N	129.73E	11.9	.		880525	16	55	43.86	64.21N	150.95E	9.0	.	
870430	03	57	45.88	69.34N	178.23E	14.2	.		880605	14	51	43.41	56.23N	128.67E	2.4	.	
870430	05	41	35.5	54.74N	123.28E	23.3	.		880609	13	37	33.18	63.27N	157.59E	8.1	.	
870430	20	04	20.34	62.87N	156.86E	1.5	.		880609	20	12	08.25	63.13N	173.04E	9.6	.	
870505	22	29	03.2	56.80N	122.95E	22.3	.		880614	14	44	44.27	63.37N	149.50E	10.3	.	
870510	12	11	04.73	64.46N	172.64W	9.3	.		880619	11	53	19.99	55.92N	128.87E	14.6	.	
870512	09	41	25.8	51.85N	132.60E	12.5	.		880620	18	30	53.9	65.49N	131.08E	11.1	.	
870516	09	29	41.1	48.44N	130.95E	27.1	.		880621	18	33	34.90	54.73N	135.58E	5.7	.	
870524	16	15	47.7	54.38N	121.75E	33.0	.		880621	22	50	18.1	57.86N	124.86E	14.1	.	
870525	00	58	03.0	53.26N	133.05E	13.2	.		880623	17	59	05.91	63.79N	169.87E	8.8	.	
870526	13	59	12.68	65.38N	173.27W	33.0	.		880701	21	37	33.73	64.72N	145.93E	19.1	.	
870528	14	46	55.68	66.96N	172.17W	27.4	.		880707	17	43	35.54	63.08N	144.69E	0.7	.	
870602	16	40	20.06	62.74N	156.73E	6.6	.		880717	23	08	00.41	63.43N	145.47E	2.8	.	

```
880728 15 30 47.34 57.12N 129.47E 13.7  .
880804 06 07 15.39 56.01N 129.85E  1.4  .
880818 08 00 43.08 59.69N 145.67E  0.   .
880825 05 03 27.58 56.87N 127.15E  5.6  .
880825 07 17 24.40 56.86N 127.17E  7.8  .
880830 12 58 55.7  54.00N 137.68E 18.6  .
880902 09 35 32.4  54.16N 122.71E 33.0  .
880922 11 25 41.9  57.41N 122.68E 19.2  .
880922 22 58 11.30 61.89N 160.48E 17.6  .
880923 08 32 14.25 55.45N 137.21E 33.0  .
880926 08 59 49.57 67.53N 143.86E  5.8  .
880930 03 09 09.3  54.15N 137.75E 10.4  .
881007 00 56 29.24 57.57N 125.12E 17.6  .
881013 00 32 09.10 61.71N 169.78E  8.7 5.9
881013 00 49 26.91 61.81N 169.63E 33.0  .
881013 03 24 33.51 61.95N 169.62E 24.0  .
881015 07 05 37.98 61.89N 169.57E 25.4  .
881017 00 27 59.09 62.85N 148.80E  6.7  .
881020 04 17 55.42 56.77N 127.11E  6.1  .
881024 07 15 32.1  54.80N 133.02E 17.2  .
881025 10 12 52.89 62.87N 148.85E  8.5  .
881101 21 37 31.2  56.85N 123.93E 14.0  .
881102 23 32 55.4  53.86N 126.39E  6.0  .
881109 13 07 58.6  57.90N 120.57E 22.5  .
881112 10 27 10.91 57.77N 126.45E 15.2  .
881118 11 29 32.4  57.86N 121.19E 26.0  .
881118 22 22 05.1  56.67N 121.68E  7.6  .
881203 15 29 49.50 56.06N 126.35E 11.5  .
881207 16 50 30.55 65.23N 144.66E  0.   .
881207 18 23 22.27 65.29N 144.71E  0.4  .
881222 20 10 11.1  52.46N 134.43E 28.5  .
881224 02 43 21.51 64.10N 148.74E  8.9  .
881226 13 29 00.65 61.63N 168.93E 10.9  .
881230 07 16 43.30 61.12N 153.70E  1.7  .
890113 12 52 11.1  49.01N 131.59E 22.1  .
890113 16 21 59.87 64.59N 147.17E 10.4  .
890114 04 53 36.49 61.89N 143.74E  9.5  .
890115 17 17 30.78 58.69N 151.20E  6.1  .
890115 22 13 26.8  57.08N 121.61E 32.5  .
890124 16 50 14.54 65.41N 144.43E 19.0  .
890129 23 23 01.67 62.86N 144.88E 12.7  .
890202 07 18 12.67 57.59N 128.30E 13.1  .
890205 16 26 59.20 54.21N 126.66E 25.7  .
890212 03 54 21.16 59.20N 147.66E  5.7  .
890213 09 35 29.09 66.17N 172.58E 11.8  .
890215 18 46 19.32 58.07N 129.42E 17.3  .
890217 02 57 48.16 63.37N 146.19E  6.9  .
890217 19 10 15.20 69.80N 129.14E 20.4  .
890218 05 47 41.5  48.52N 131.47E  2.5  .
890219 18 00 30.11 65.18N 146.22E  5.7  .
890224 11 44 19.57 61.25N 162.91E  9.8  .
890225 04 56 17.06 61.73N 157.71E  8.6  .
890321 10 53 05.21 64.91N 145.19E  9.3  .
890329 01 10 46.0  56.79N 123.52E 15.5  .
890331 12 47 12.06 69.73N 128.96E 17.0  .
890404 07 30 24.43 62.09N 157.49E 20.3  .
890409 04 16 24.70 59.80N 145.14E 33.0 5.0
890410 09 12 58.94 66.75N 174.60W 33.0  .
890412 00 45 33.7  56.72N 120.37E 22.2  .
890420 22 56 00.2  57.13N 122.23E 31.8  .
890420 22 59 52.3  57.34N 122.11E 16.3 6.6
890421 00 04 44.9  57.04N 122.18E 23.4  .
890421 00 16 00.7  57.08N 122.20E 18.8  .
890421 00 52 30.7  57.04N 122.18E 22.3  .
890421 00 57 54.6  57.01N 122.17E 19.2  .
890421 01 04 20.1  57.10N 122.06E 31.5  .
890421 01 44 00.1  57.01N 122.19E 17.7  .
890421 03 12 05.8  57.07N 122.14E 23.9  .
890421 08 10 05.7  57.05N 122.20E 22.7  .
890421 08 29 29.5  57.06N 122.16E 27.7  .
890421 08 30 08.2  57.10N 122.16E 25.7  .
890421 08 51 39.0  57.04N 122.18E 28.6  .
890421 15 22 01.0  57.04N 122.22E 27.6  .
890421 15 49 35.7  57.05N 122.21E 25.7  .
890421 19 08 37.4  57.07N 122.27E 33.0 4.9
890421 19 29 28.5  57.06N 122.25E 30.8  .
890421 20 09 42.2  57.07N 122.22E 30.8  .
890421 22 30 36.0  57.05N 122.18E 25.6  .

890423 02 45 40.1  57.08N 122.17E 24.1  .
890423 03 44 27.9  57.06N 122.18E 25.1  .
890423 17 58 28.7  57.09N 122.22E 29.3  .
890424 01 33 59.8  57.11N 122.27E 24.4 5.0
890424 04 45 38.19 58.95N 151.87E 10.0  .
890424 08 18 37.1  57.09N 122.18E 26.7  .
890428 15 20 53.0  57.07N 122.21E 33.0  .
890429 00 05 07.9  57.18N 122.20E 33.0  .
890429 01 27 13.8  57.09N 122.22E 30.6  .
890429 06 25 38.9  57.15N 122.24E 33.0 5.6
890429 07 05 24.2  57.14N 122.25E 28.2  .
890429 08 40 01.6  57.08N 122.30E  0.0  .
890429 10 33 56.1  57.05N 122.29E  0.0  .
890429 17 35 30.1  57.05N 122.25E  0.3  .
890429 21 00 46.4  57.08N 122.25E 24.4  .
890503 23 53 38.4  57.03N 122.17E 23.2  .
890504 14 10 28.4  56.57N 121.15E 14.8  .
890504 14 10 28.4  56.57N 121.15E 14.8  .
890506 06 54 38.5  57.13N 122.02E 26.8  .
890507 16 28 05.9  57.08N 122.22E 33.0 5.1
890508 11 49 47.0  57.05N 122.21E 27.8  .
890511 14 37 43.2  57.07N 122.20E 29.4  .
890514 16 21 51.7  57.14N 122.19E 27.0  .
890517 05 04 35.8  57.05N 122.24E 32.0 5.8
890517 07 25 49.0  57.05N 122.25E 30.7  .
890517 07 40 39.1  57.00N 122.13E 23.5  .
890517 10 21 02.1  57.06N 122.14E 19.9  .
890517 15 55 22.9  57.06N 122.24E 32.1  .
890518 10 06 01.1  57.02N 122.21E 29.8  .
890519 15 39 08.1  57.06N 122.22E 26.3  .
890519 19 29 23.96 62.42N 155.21E  3.3  .
890519 22 06 27.6  57.07N 122.20E 27.9  .
890523 08 12 12.2  57.00N 122.18E 29.2  .
890524 09 38 02.21 61.31N 144.72E 11.2  .
890524 19 42 32.5  57.07N 122.23E 30.5  .
890525 11 48 06.2  57.06N 122.23E 33.0  .
890601 08 17 10.5  57.07N 122.20E 29.9  .
890601 16 41 42.51 63.47N 139.82E  0.   .
890601 16 41 42.51 63.47N 139.82E  0.   .
890601 19 25 46.7  57.07N 122.29E 28.4  .
890601 22 38 53.0  56.99N 122.16E 28.5  .
890603 08 57 17.1  54.51N 123.23E 23.5  .
890604 04 17 01.52 68.12N 132.54E 30.9  .
890604 21 49 34.7  57.08N 122.14E 27.6  .
890605 00 13 20.7  57.02N 122.22E 30.3  .
890608 22 41 20.2  57.10N 122.25E 24.4  .
890610 05 09 43.96 71.31N 129.13E  2.9  .
890615 16 24 12.2  57.03N 122.23E 30.2  .
890616 07 36 08.68 63.57N 142.74E  9.0  .
890616 19 40 45.76 61.02N 145.44E 14.6  .
890617 13 37 27.02 67.24N 143.75E  8.5  .
890619 15 48 34.3  57.13N 122.27E 30.3  .
890622 20 52 20.7  57.10N 122.28E 23.5  .
890627 10 38 36.3  57.15N 122.30E 27.3  .
890628 20 16 28.1  57.05N 122.14E 26.5  .
890630 20 00 00.25 59.25N 152.73E  2.2  .
890701 14 14 40.42 57.21N 137.80E 33.   .
890702 22 58 49.62 59.61N 150.01E  4.2  .
890706 04 08 09.4  57.09N 122.22E 33.0  .
890707 10 51 43.57 64.99N 141.66E 14.4  .
890709 18 11 49.32 59.91N 152.71E  8.8  .
890709 20 07 46.3  57.09N 122.32E 33.0 4.2
890709 21 04 27.2  57.06N 122.24E 33.0  .
890710 07 19 33.9  57.05N 122.20E 33.0  .
890713 19 13 54.00 62.57N 143.88E  0.   .
890716 16 32 31.2  57.07N 122.21E 30.4  .
890718 03 02 54.7  57.07N 122.22E 33.0  .
890719 00 24 03.7  57.08N 122.17E 26.8  .
890720 02 53 38.2  57.05N 122.17E 30.1  .
890720 03 16 21.8  57.05N 122.18E 31.5  .
890720 23 26 43.7  57.09N 122.15E  9.7  .
890721 01 40 08.2  57.10N 122.16E 10.3  .
890721 01 46 35.0  57.04N 122.16E 26.6  .
890721 07 43 50.5  57.08N 122.20E 10.5  .
890722 02 36 12.6  57.09N 122.15E  7.5  .
890722 10 01 40.8  57.07N 122.22E 27.7  .
890723 12 01 31.2  54.54N 124.92E 27.0  .
890723 14 33 00.4  54.55N 124.97E 18.8  .
```

890723	14	33	01.4	54.61N	124.94E	21.2	.		900502	10	12	58.04	57.77N	128.21E	3.3	.	
890723	22	35	55.3	57.12N	122.24E	31.4	.		900504	18	13	17.11	66.28N	172.56W	13.8	.	
890724	01	35	24.2	54.54N	124.93E	18.4	.		900505	03	28	08.24	59.34N	149.48E	0.	.	
890725	00	58	37.6	51.53N	132.00E	8.2	.		900517	18	37	36.4	56.52N	121.19E	18.4	.	
890731	00	27	03.6	54.47N	122.99E	.	.		900524	02	44	24.0	57.10N	122.22E	31.6	.	
890801	00	03	03.4	57.09N	122.17E	14.7	.		900528	23	47	38.3	57.11N	122.99E	20.4	.	
890801	17	05	23.61	59.89N	151.65E	20.3	.		900530	11	56	45.68	62.91N	144.88E	6.0	.	
890803	21	46	19.90	54.14N	136.77E	25.8	.		900530	14	06	04.06	62.90N	144.92E	9.2	.	
890804	11	35	25.1	57.08N	122.16E	10.8	.		900602	17	11	19.7	55.65N	130.66E	10.9	.	
890804	11	48	30.8	57.10N	122.11E	13.0	.		900614	19	39	35.66	64.08N	156.62E	5.3	.	
890804	13	47	50.1	57.08N	122.13E	4.8	.		900618	13	22	59.88	64.03N	175.02E	5.1	.	
890804	21	39	26.0	57.11N	122.12E	8.7	.		900624	10	15	33.2	53.99N	122.29E	17.3	.	
890806	00	59	48.3	56.99N	122.22E	2.9	.		900625	07	33	54.07	66.81N	130.68E	18.8	.	
890906	15	20	32.20	61.73N	144.18E	6.9	.		900625	13	12	48.23	66.88N	130.45E	8.1	.	
890910	05	16	37.9	57.06N	122.20E	27.0	.		900629	12	30	10.1	56.72N	124.04E	22.9	.	
890918	11	47	43.84	72.18N	128.86E	0.2	.		900701	17	03	53.76	61.94N	154.22E	7.9	.	
890919	22	44	26.29	54.43N	129.57E	23.1	.		900704	12	11	28.25	59.31N	126.38E	0.	.	
890924	10	18	10.38	65.47N	169.97E	21.5	.		900705	15	32	55.46	62.88N	153.26E	0.	.	
890924	16	35	43.98	63.97N	169.72E	1.6	.		900706	03	16	04.3	56.82N	124.39E	33.0	.	
890926	06	41	32.9	57.06N	122.10E	13.7	.		900706	16	09	08.59	67.17N	144.67E	0.0	.	
890927	15	42	43.4	57.11N	122.08E	14.1	.		900712	02	22	50.75	62.07N	153.82E	7.5	.	
891004	20	56	47.62	64.70N	146.83E	11.0	.		900717	03	37	25.0	48.70N	132.00E	19.2	.	
891017	03	47	41.7	57.08N	122.18E	26.6	.		900717	04	01	11.3	48.71N	132.05E	17.3	.	
891018	18	49	22.58	68.76N	133.09E	19.7	.		900717	05	15	32.2	57.01N	124.63E	25.5	.	
891027	01	18	42.1	55.36N	120.45E	23.8	.		900724	15	17	19.86	60.25N	142.65E	0.	.	
891028	16	41	50.18	57.57N	125.38E	10.0	.		900726	17	34	20.1	57.10N	122.25E	20.5	.	
891030	01	03	39.4	48.48N	129.62E	33.0	.		900729	13	17	25.96	63.55N	174.40E	15.1	.	
891030	03	38	25.9	57.09N	122.14E	33.0	.		900731	05	50	45.1	53.67N	124.78E	15.2	.	
891106	10	01	11.57	54.40N	129.58E	12.6	.		900802	03	22	15.90	54.27N	126.45E	19.5	.	
891109	09	57	37.20	68.46N	132.58E	33.0	.		900803	05	06	52.46	65.49N	136.68E	17.5	.	
891109	20	57	54.53	66.16N	165.74E	11.1	.		900803	14	02	08.49	57.54N	127.81E	19.0	.	
891110	08	55	55.7	48.88N	131.55E	17.1	.		900812	20	51	01.20	65.28N	173.49W	9.8	.	
891113	18	15	40.26	62.28N	143.54E	15.1	.		900816	19	52	33.63	69.92N	139.29E	18.6	.	
891118	05	22	38.1	57.01N	122.20E	18.0	.		900819	19	45	35.00	72.98N	122.75E	16.4	.	
891202	16	21	59.0	57.15N	122.25E	29.7	.		900820	23	48	16.3	54.34N	123.57E	6.1	.	
891207	21	33	54.5	57.00N	122.18E	21.3	.		900824	01	04	44.73	63.04N	151.18E	9.6	.	
891208	01	36	10.07	64.93N	145.90E	10.7	.		900825	03	17	34.67	60.12N	165.48E	33.0	.	
891208	09	57	25.9	54.95N	134.96E	3.1	.		900827	01	31	06.1	56.55N	121.08E	12.0	.	
891212	15	19	04.4	57.06N	122.13E	25.0	.		900901	21	56	05.51	54.23N	125.97E	20.2	.	
891213	21	39	09.3	57.03N	122.21E	31.7	.		900906	17	41	18.23	63.05N	172.92E	14.2	.	
891222	12	46	34.70	65.48N	136.71E	10.8	.		900907	07	15	16.50	65.19N	148.22E	12.6	.	
891223	01	24	26.1	54.12N	122.00E	24.9	.		900928	11	47	56.7	57.02N	122.16E	30.8	.	
900108	06	18	52.0	57.64N	121.13E	17.4	.		901006	00	17	17.2	55.31N	121.84E	26.6	.	
900109	01	44	43.62	57.57N	125.39E	3.1	.		901008	22	58	13.28	57.02N	129.48E	33.0	.	
900110	16	29	04.0	57.02N	122.22E	26.5	.		901015	15	27	17.61	65.36N	173.01W	26.6	.	
900114	16	07	31.1	50.20N	125.48E	23.8	.		901016	10	03	30.31	65.35N	173.16W	1.1	.	
900121	14	37	11.80	63.10N	151.95E	6.4	.		901016	12	04	26.5	49.84N	129.54E	18.8	.	
900202	06	02	55.8	56.94N	132.17E	8.9	.		901018	23	27	40.84	55.26N	139.01E	7.9	.	
900206	03	40	46.6	57.06N	122.06E	9.2	.		901025	15	36	41.1	56.82N	121.07E	18.6	.	
900208	09	19	35.9	57.15N	122.08E	33.0	.		901029	10	21	07.95	54.70N	136.54E	11.6	.	
900208	20	22	30.5	57.12N	122.15E	16.9	.		901031	21	04	25.9	57.05N	122.20E	22.3	.	
900216	12	59	41.3	57.10N	122.16E	32.4	.		901101	04	58	32.57	57.59N	125.47E	13.1	.	
900224	16	29	24.42	57.08N	125.75E	9.6	.		901101	13	42	05.88	61.29N	156.90E	6.6	.	
900225	21	17	23.1	54.35N	122.85E	28.6	.		901102	21	54	02.28	64.81N	146.61E	3.9	4.2	
900227	13	04	13.5	57.06N	122.25E	26.3	.		901109	17	16	48.69	68.84N	131.89E	11.1	.	
900303	22	24	15.91	57.01N	125.66E	19.2	.		901111	17	47	35.51	59.33N	152.22E	3.4	.	
900305	15	40	16.20	54.60N	125.00E	18.8	.		901116	13	39	26.03	69.44N	129.71E	10.1	.	
900306	07	18	08.99	67.05N	125.24E	26.7	.		901117	11	11	09.4	57.71N	121.50E	18.4	.	
900312	03	26	58.1	52.75N	138.63E	19.2	.		901117	14	14	26.82	57.25N	125.46E	20.5	.	
900313	00	33	01.59	73.30N	134.76E	32.8	.		901121	01	12	19.11	59.84N	153.46E	2.9	.	
900314	01	12	22.02	73.32N	134.34E	11.6	.		901121	04	04	03.61	61.73N	142.87E	11.4	.	
900318	02	22	49.1	57.03N	122.31E	20.6	.		901122	19	36	25.37	62.78N	156.82E	7.0	.	
900319	14	34	18.4	53.14N	131.66E	16.6	.		901203	04	33	44.7	57.15N	122.23E	23.1	.	
900321	04	31	25.21	73.30N	133.99E	33.0	.		901204	08	46	20.24	61.78N	169.79E	18.0	.	
900329	20	47	29.87	64.02N	145.04E	6.8	.		901208	08	23	30.66	59.42N	152.52E	4.9	.	
900330	10	16	45.2	54.96N	123.89E	26.8	.		901213	21	34	39.60	64.46N	140.51E	11.2	.	
900330	15	15	38.63	64.04N	145.07E	7.2	.		910102	04	19	22.94	61.77N	145.69E	0.	.	
900330	22	46	11.4	57.02N	122.18E	27.3	.		910109	08	15	37.4	56.88N	120.39E	20.0	.	
900402	15	32	46.87	62.12N	138.02E	15.4	.		910201	08	09	25.81	65.68N	145.97E	0.	.	
900408	10	58	40.6	57.03N	122.19E	20.7	.		910210	18	16	31.98	62.94N	145.58E	12.5	.	
900411	16	09	43.42	61.96N	154.26E	6.4	.		910211	10	58	26.96	72.60N	125.08E	16.3	.	
900412	19	10	48.37	62.40N	138.12E	0.	.		910213	09	46	15.45	62.21N	160.73E	10.0	.	
900419	09	00	39.81	72.95N	123.81E	0.	.		910217	20	15	00.74	60.68N	167.35E	0.	.	
900421	02	15	30.68	65.48N	170.68E	17.2	.		910217	20	47	09.33	60.81N	167.04E	1.1	.	
900424	08	24	09.6	57.95N	120.95E	16.7	.		910217	23	41	23.6	56.80N	132.02E	1.2	.	
900426	23	19	05.09	70.57N	137.26E	25.2	.		910218	11	13	49.00	60.88N	167.01E	15.8	.	
900427	10	12	27.0	50.66N	132.62E	0.0	.		910220	04	46	32.45	60.84N	167.09E	0.	.	
900501	13	27	29.40	56.86N	132.09E	13.6	.		910301	18	14	14.03	60.02N	152.79E	3.9	.	

910303	01	57	04.56	72.17N	126.74E	26.5	5.0		930210	14	09	48.95	59.42N	147.42E	10.4	.	
910307	16	20	43.04	61.28N	157.00E	5.8	.		930221	09	37	53.1	57.96N	120.71E	28.1	.	
910308	09	02	21.93	60.86N	167.03E	33.0	.		930224	17	45	25.24	69.59N	128.82E	0.	.	
910309	01	49	34.4	57.39N	120.87E	33.0	.		930305	01	43	43.31	62.95N	145.59E	7.9	.	
910314	02	20	42.8	54.76N	120.88E	19.6	.		930305	04	21	03.78	63.73N	145.65E	8.1	.	
910316	11	02	10.12	62.39N	153.10E	13.3	.		930313	03	26	28.31	63.77N	142.40E	22.2	.	
910322	16	00	22.89	62.35N	148.41E	8.4	.		930322	18	14	04.48	62.91N	145.56E	7.4	.	
910330	01	52	52.22	57.12N	132.96E	8.5	.		930324	16	19	06.11	65.38N	142.64E	11.9	.	
910330	17	06	23.65	66.64N	126.07E	14.0	.		930324	22	43	29.02	71.68N	130.34E	12.8	4.5	
910331	15	39	45.44	58.93N	149.12E	0.	.		930413	02	36	25.63	62.52N	155.34E	10.7	.	
910401	07	21	57.27	71.36N	130.02E	8.4	.		930429	12	21	31.23	69.21N	139.91E	25.8	.	
910420	11	48	29.64	56.90N	127.14E	7.9	.		930519	08	32	06.79	57.97N	140.63E	0.	.	
910505	16	17	47.70	54.68N	125.40E	11.4	.		930615	11	51	14.06	62.33N	141.50E	1.9	.	
910518	08	49	28.0	57.44N	120.92E	33.0	.		930618	19	16	14.33	62.05N	146.22E	12.0	.	
910527	08	55	35.2	57.07N	122.20E	30.7	.		930701	03	52	03.21	63.26N	146.72E	11.1	.	
910621	11	04	24.3	55.85N	124.50E	25.4	.		930705	05	44	53.91	63.28N	179.51E	13.7	.	
910701	20	41	59.50	63.82N	156.12E	11.5	.		930820	21	26	20.20	57.52N	126.62E	9.4	.	
910711	23	23	07.30	62.73N	175.42E	0.	.		930825	11	50	10.7	56.86N	124.64E	10.8	.	
910722	12	05	27.3	55.79N	131.11E	32.3	.		930830	07	56	35.44	64.07N	145.84E	5.5	.	
910723	10	28	19.41	59.74N	156.45E	11.9	.		930926	10	58	20.86	59.66N	145.14E	29.7	.	
910724	02	26	03.08	62.25N	143.64E	3.7	.		931019	07	02	40.2	56.69N	124.60E	23.9	.	
910728	01	37	01.15	59.88N	153.36E	0.6	.		931028	09	40	51.87	59.28N	148.04E	25.6	.	
910731	01	44	03.82	72.08N	127.59E	11.5	.		931220	03	42	07.66	63.48N	150.51E	6.5	.	
910804	19	08	06.08	65.49N	143.24E	25.1	.		940104	20	00	24.5	53.53N	132.24E	22.6	.	
910804	19	14	40.50	65.48N	143.25E	10.5	.		940105	12	29	31.7	57.45N	122.49E	17.5	.	
910811	18	50	48.20	59.97N	150.19E	5.0	.		940116	14	51	07.5	57.42N	122.50E	23.5	.	
910825	13	51	02.79	70.64N	140.99E	11.8	.		940128	01	05	12.10	55.06N	135.29E	6.6	5.0	
910826	09	35	49.41	63.33N	146.31E	1.0	.		940130	08	18	38.9	57.53N	122.37E	33.0	.	
910915	10	56	22.12	63.82N	151.66E	6.7	.		940204	17	10	10.46	59.66N	143.93E	10.1	.	
911013	00	36	28.86	60.87N	144.94E	13.7	3.5		940215	17	40	57.09	57.86N	128.57E	8.2	.	
911016	05	04	25.7	54.58N	120.80E	27.6	.		940216	12	43	17.5	56.96N	123.51E	23.8	.	
911105	10	16	38.60	59.01N	150.60E	6.0	.		940223	17	56	12.2	57.30N	123.25E	17.4	.	
911106	19	14	17.47	63.66N	155.03E	3.6	.		940301	17	48	03.00	55.13N	138.47E	0.	.	
911114	01	01	50.65	62.38N	153.14E	6.0	.		940317	13	55	31.6	57.06N	121.57E	26.5	.	
911201	17	13	50.30	59.41N	147.66E	0.	.		940328	00	57	32.40	62.49N	147.57E	8.9	3.6	
911216	07	34	56.14	62.76N	146.03E	7.9	.		940331	15	14	18.06	72.07N	127.78E	2.4	.	
911223	06	04	15.31	62.45N	140.86E	33.0	.		940331	22	28	42.96	71.77N	128.31E	33.0	.	
920112	11	21	48.48	64.51N	174.36W	11.8	.		940402	11	30	00.2	66.70N	148.33E	14.0	.	
920121	18	07	36.05	61.79N	169.77E	14.6	4.6		940409	08	36	19.6	56.15N	124.06E	16.1	.	
920122	06	29	16.56	65.86N	143.27E	11.2	.		940419	21	16	54.9	54.88N	124.10E	33.0	.	
920128	00	07	26.80	68.17N	133.13E	19.5	.		940421	15	15	47.75	56.52N	127.71E	7.6	.	
920212	17	14	52.51	64.89N	153.01E	7.3	.		940426	09	55	39.00	57.02N	127.82E	4.1	.	
920222	17	55	21.52	70.09N	139.44E	7.0	.		940426	14	58	45.4	54.75N	122.02E	13.1	.	
920223	08	21	41.66	70.05N	139.45E	9.9	.		940504	00	36	22.57	58.83N	146.40E	14.7	.	
920301	18	04	13.7	57.01N	120.79E	26.9	.		940510	13	39	10.4	54.27N	122.96E	25.2	.	
920307	06	07	14.46	66.85N	177.89E	7.1	.		940522	11	35	12.6	54.63N	123.39E	33.0	.	
920322	12	35	00.41	60.84N	166.87E	33.0	.		940523	07	22	47.8	57.04N	122.20E	33.0	.	
920323	15	37	22.29	60.54N	167.14E	7.1	.		940609	02	27	17.94	62.51N	147.59E	8.4	.	
920324	03	58	42.27	62.07N	169.60E	12.7	.		940616	17	53	18.18	62.46N	147.58E	12.8	3.8	
920405	17	55	25.64	59.33N	152.39E	0.	.		940619	19	03	27.16	62.43N	147.50E	5.6	.	
920413	22	47	21.2	56.59N	121.13E	15.1	.		940621	14	52	00.5	57.08N	122.22E	20.9	.	
920507	23	22	54.7	63.65N	133.51E	33.0	.		940703	08	41	29.3	56.70N	122.48E	19.6	.	
920628	23	53	17.73	63.74N	145.70E	5.6	.		940705	13	32	04.0	54.27N	122.86E	26.1	.	
920709	09	57	15.79	63.14N	156.74E	11.9	.		940708	13	40	29.5	56.66N	132.92E	6.2	.	
920826	11	02	16.12	71.60N	133.23E	1.7	.		940710	22	30	06.1	55.75N	122.92E	25.6	.	
920828	14	27	05.12	58.94N	149.22E	22.4	3.8		940711	02	39	36.48	62.49N	147.59E	10.9	3.5	
920909	00	14	31.84	71.42N	132.83E	9.9	.		940711	11	33	04.04	62.13N	143.57E	6.2	.	
920913	21	42	56.22	62.07N	153.79E	9.7	4.9		940711	16	48	02.43	62.53N	147.59E	7.4	.	
920913	22	05	31.34	62.04N	153.78E	4.3	.		940715	00	20	42.86	66.90N	130.08E	31.9	.	
920928	08	05	55.06	64.66N	173.41W	10.7	.		940718	15	43	04.16	62.02N	153.64E	13.8	.	
921009	21	43	39.25	68.57N	140.84E	4.9	.		940722	18	39	09.0	54.73N	131.83E	0.0	.	
921010	17	47	51.42	62.49N	154.05E	7.0	.		940727	00	17	04.9	57.00N	122.36E	28.6	.	
921011	21	40	09.21	62.05N	153.61E	11.1	.		940731	04	45	38.32	73.03N	123.50E	7.1	.	
921030	14	20	30.07	72.75N	123.74E	27.1	.		940802	02	30	44.77	57.28N	125.54E	8.8	.	
921114	20	43	15.37	73.01N	123.21E	21.7	.		940803	18	51	44.0	57.38N	122.17E	15.7	.	
921117	07	55	14.2	67.20N	128.59E	24.2	.		940811	22	44	12.8	57.09N	122.19E	21.5	.	
921121	06	09	38.38	65.60N	170.41W	33.0	.		940828	10	11	28.2	55.45N	122.50E	20.3	.	
921206	08	39	43.42	62.06N	157.13E	4.0	.		940918	16	17	49.07	62.42N	147.64E	18.2	.	
921214	16	46	32.61	65.28N	171.31W	4.3	.		940928	10	38	08.4	52.73N	122.26E	29.2	.	
921218	13	28	08.81	63.39N	156.39E	13.5	.		941001	08	52	54.27	72.26N	127.24E	11.9	.	
921220	10	20	23.65	62.06N	157.00E	7.2	.		941003	23	12	59.06	72.41N	127.50E	4.4	.	
921221	07	40	14.63	64.37N	173.30W	15.6	.		941007	12	58	52.2	54.31N	124.57E	18.1	.	
921222	08	54	39.43	63.26N	152.37E	8.2	.		941026	07	53	18.76	57.22N	125.81E	13.9	.	
921223	12	48	25.10	62.04N	157.01E	10.2	.		941105	06	42	09.12	71.79N	130.98E	14.3	.	
930121	05	08	56.12	63.13N	146.43E	17.4	.		941207	19	52	17.4	56.12N	124.15E	11.4	.	
930124	20	10	28.6	56.78N	131.52E	7.9	.		941228	06	23	27.98	57.55N	132.08E	33.0	.	
930124	20	45	17.2	57.23N	123.29E	22.8	.		950106	13	05	14.96	58.59N	148.46E	5.8	2.6	
930206	22	05	37.23	62.22N	156.78E	2.4	.		950115	00	54	27.77	60.77N	148.39E	5.7	.	

950131	12	43	43.36	72.73N	131.66E	33.0	.	
950201	07	57	35.2	56.64N	121.86E	14.4	.	
950209	16	53	19.1	63.64N	133.92E	26.5	.	
950301	17	29	29.7	51.83N	125.51E	33.0	.	
950327	21	20	00.18	54.22N	126.78E	29.5	.	
950504	13	53	37.0	57.24N	122.22E	16.6	.	
950527	13	03	52.7	52.63N	142.83E	.	.	
950616	11	34	53.4	57.11N	124.90E	14.5	.	
950806	08	30	43.7	56.99N	122.00E	14.0	.	
950815	01	53	25.23	58.12N	148.90E	14.1	.	
960128	01	10	18.76	59.30N	147.66E	9.5	.	
960212	18	56	59.9	57.53N	120.77E	26.2	.	
960212	18	57	01.2	57.51N	120.90E	21.9	.	
960220	23	32	54.09	61.23N	158.42E	25.4	.	
960303	10	53	57.77	58.26N	158.17E	4.4	.	
960303	11	54	41.62	58.26N	158.04E	33.0	.	
960318	20	15	14.89	58.35N	143.97E	30.6	.	
960403	23	39	29.97	62.85N	147.32E	6.1	.	
960406	00	20	39.37	62.83N	147.63E	11.6	.	
960606	21	53	42.36	63.02N	144.73E	6.0	.	
960612	17	08	01.2	56.84N	121.24E	24.9	.	
960707	10	50	00.61	58.58N	157.54E	12.2	5.8	
960707	14	19	52.14	58.63N	157.34E	6.3	.	
960707	14	29	03.55	58.56N	157.50E	12.0	.	
960707	15	39	03.11	58.28N	157.42E	31.6	.	
960707	17	58	34.14	58.53N	157.49E	3.9	.	
960707	23	23	49.02	58.50N	157.32E	16.8	.	
960708	01	06	25.24	58.47N	157.28E	0.	.	
960708	13	29	51.71	58.59N	157.38E	15.1	.	
960709	04	07	41.83	58.43N	157.17E	8.4	.	
960709	10	07	05.5	56.61N	120.95E	7.4	.	
960709	11	52	51.98	58.33N	157.19E	0.	.	
960710	05	20	11.74	58.45N	157.70E	0.8	.	
960710	06	22	05.38	58.52N	157.34E	18.2	.	
960710	07	15	54.93	58.67N	157.45E	15.2	.	
960710	14	09	33.80	58.57N	157.64E	3.9	.	
960710	18	36	37.17	58.46N	157.30E	28.1	.	
960727	07	28	34.95	60.49N	148.66E	7.4	3.6	
960803	12	32	49.64	58.65N	157.21E	29.4	.	
960803	13	09	13.64	58.68N	157.08E	0.	.	
960807	18	51	14.48	58.58N	157.21E	7.6	.	
960808	17	09	40.38	58.75N	157.20E	22.2	.	
960824	07	29	41.80	60.05N	153.05E	17.7	.	
960902	23	37	54.6	56.60N	123.88E	19.4	.	
960904	12	56	31.38	57.55N	128.03E	15.1	.	
960913	15	45	07.54	58.70N	157.64E	6.5	.	
960914	05	29	59.84	58.65N	157.41E	9.8	.	
960914	05	41	45.02	58.73N	157.48E	8.3	.	
960914	09	57	57.82	58.74N	157.14E	0.	.	
960916	03	05	07.56	58.56N	157.35E	14.6	.	
960925	01	48	26.12	63.38N	150.43E	9.9	.	
961024	19	31	50.91	67.04N	173.08W	0.	6.0	
961024	21	57	36.71	67.08N	173.20W	14.1	.	
961126	20	18	18.31	58.66N	157.54E	5.8	.	
961207	10	38	20.98	62.12N	153.75E	10.6	.	
970129	15	51	38.11	58.81N	149.65E	5.4	.	
970304	21	49	26.30	62.07N	155.92E	10.0	.	
970607	11	59	41.19	64.19N	148.32E	0.	.	
970614	13	31	08.39	63.87N	148.57E	2.9	.	
970616	09	54	07.72	64.07N	148.43E	9.0	.	
970629	21	37	46.82	59.78N	152.40E	4.6	.	
970721	12	37	49.52	60.08N	144.68E	10.2	.	
970825	06	00	43.24	63.54N	144.91E	8.2	.	
970910	18	42	42.47	61.77N	156.15E	1.5	.	
970914	14	07	54.73	61.10N	145.23E	0.	.	
970915	05	48	00.77	59.95N	151.96E	0.	.	
971122	11	41	15.58	61.14N	155.44E	7.7	.	
971206	16	06	07.04	59.40N	147.91E	10.9	.	
980103	03	15	51.98	59.81N	152.50E	0.	.	
980130	23	11	39.97	63.48N	150.29E	20.1	.	
980201	02	33	13.50	63.24N	150.00E	2.4	.	
980215	04	35	42.38	61.49N	147.43E	0.	.	
980221	22	22	47.82	60.33N	152.86E	5.4	.	
980304	04	57	18.17	62.08N	156.99E	6.3	.	
980309	10	38	11.91	63.87N	156.95E	0.	.	
980311	23	46	07.01	58.46N	157.22E	0.	.	
980312	03	15	54.71	62.10N	157.03E	1.5	.	
980314	17	03	29.87	58.40N	157.41E	3.5	.	
980316	05	33	08.13	58.42N	157.30E	13.7	.	
980318	21	30	34.19	58.39N	156.98E	8.3	.	
980320	16	50	52.81	62.06N	157.06E	7.9	.	
980325	23	52	55.66	62.11N	156.94E	5.0	.	
980326	02	17	29.32	62.09N	157.05E	3.4	.	
980326	02	24	00.38	62.08N	156.93E	3.2	.	
980326	06	41	33.48	62.09N	156.73E	8.7	.	
980327	09	29	59.56	62.07N	156.87E	5.6	.	
980327	09	42	36.02	62.09N	156.95E	7.2	.	
980404	14	02	34.13	62.05N	156.76E	7.6	.	
980505	21	31	57.75	59.05N	147.14E	5.1	.	
980508	22	32	49.88	62.02N	157.03E	4.9	.	
980531	08	02	51.19	62.04N	156.54E	11.7	.	
980604	12	03	23.75	62.06N	157.18E	2.3	.	
980901	10	26	39.52	63.06N	147.28E	8.4	.	
980917	22	50	11.78	64.95N	149.24E	0.	.	
981106	03	48	20.34	63.40N	158.75E	12.6	.	
981218	14	03	48.02	63.23N	159.45E	4.2	.	

APPENDIX F

An alternate method of determining earthquake focal depths.

APPENDIX F

An alternate method of determining earthquake focal depths

As discussed in Chapter 3, the depths determined for the relocated earthquakes depend primarily on the Pn arrivals, but problems may arise if the Pn velocity used is incorrect. The discussion here outlines a procedure for determining depth of earthquakes from apparent Pn arrival residuals calculated from a location and origin time determined using the best-fit Pg and Sg velocities.

The depth determination dependence on the Pn arrivals can be illustrated by locating a set of earthquakes using only the best-fit Pg and Sg travel time curves, allowing the depth to range between 0 and 15 km. Because there are few close stations, the Pg and Sg arrivals cannot constrain the depth, which tends go either above the surface or below the 15 km boundary. In general, events constrained to the surface are too shallow, which results in a raypath for the Pn phase that is too long. Thus when we observe the residuals associated with the Pn arrivals, they should be negative. Likewise, events constrained too deep shorten the Pn raypath, which will result in positive residuals. This is observed in a test area from the Magadan region (60-63 N x 150-155 E); the same test area and events are used throughout the remainder of this discussion. Here, we see Pn residuals for events constrained at the surface generally being negative, at around -2.0 seconds, and Pn residuals for events constrained at 15 km generally being positive, at about 1.0 second (Figure F-1). If the Pn phase arrivals were used in these hypocenter determination, these residuals would be essentially nulled out in the depth determination. Therefore, we can use these residuals to

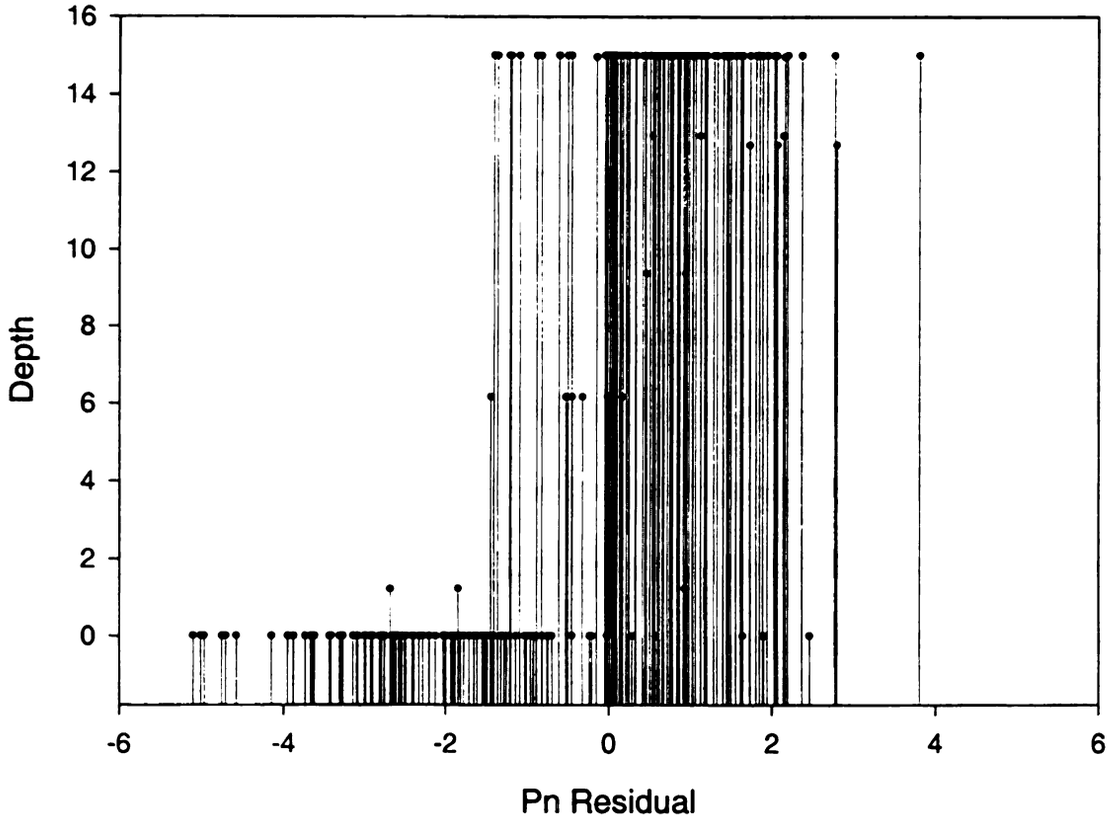

Figure F-1. Illustration showing that Pn residuals are low when depth is 0, and high when depth is 15 km. Events here were located by Pg and Sg arrivals with the best fitting velocities. The Pg and Sg arrivals are generally unable to constrain the depth which was allowed to vary from a minimum of 0.0 km to a maximum of 15 km. Events used here are from the Magadan test region.

calculate depths when the actual Pn velocity is unknown, or differs from the available travel time curve.

First, an assumption is made that for continental seismicity, the average depth of earthquakes is 10 km. Of course, this can be changed, but 10 km is probably reasonable. In this procedure, a set of earthquakes is located with the Pg and Sg phases only, using the best-fit velocities determined by the trial method outlined in Chapter 3. However, the depth here is constrained to 10 km in the location procedure. For each event, the Pn residuals are summed and the average residual is determined. Because we make the assumption that the average depth is 10 km, we would expect that half of the events would have positive residuals, and half would have negative, and that the sum of all the average residuals would be zero. Of course, this would actually only be true if the Pn travel time curve were correct. If the Pn travel time curve were too fast, we would expect the sum of all residuals to be positive, and negative if the travel time curve were too slow. Correcting for this will be discussed below.

A table can be constructed by using the Pythagorean Theorem to determine the differences in travel time for depths above or below the assumed 10 km average. An average crust with a Pg velocity of 6.0 km/sec and 35 km thickness overlying an 8.0 km/sec mantle is used here. Although the actual thickness and velocities may vary somewhat, the effect of this on the travel times is negligible, as we are only worrying about changes in the initial short downgoing segment. Figure F-2 illustrates the simplified crustal model, with three different initial earthquake depths of 0, 10, and 35 km. In the case of the 10 km depth, the assumed earthquake average, it will take the downgoing P wave 7.72 seconds to reach point A (the critical angle here is 41.4°, thus the wave travels 37.8 km in the crust and 11.4 km

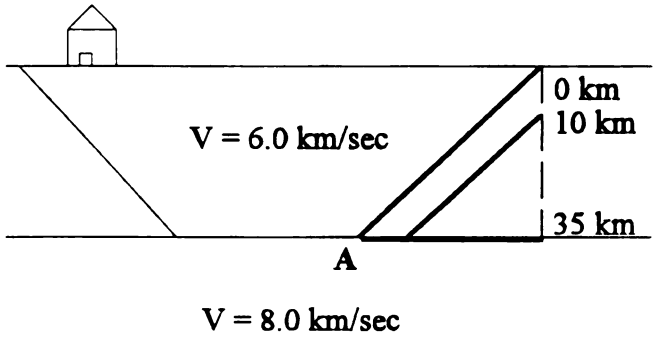

Figure F-2. Simplified crustal model and diagram used to calculate differences in Pn travel time from hypocenters of varying depth to point A. Path length from point A to the seismic station is the same for all depths.

along the Moho). For the event at 0 km depth, the P wave takes 8.82 seconds to reach point A, traveling 52.9 km through the crust. The path beginning at a 35 km depth travels 39.7 km along the Moho boundary, taking 4.96 seconds to reach point A. Thus, relative to the event occurring at 10 km, the difference in travel time for the 0 km event is 1.1 seconds, and the difference for the deeper event is -2.76 seconds. Column 2 in Table F-1 lists the theoretical Pn travel time differences relative to a depth of 10 km for events up to a depth of 25 km.

It is also necessary to adjust our table here to account for a shift in the origin time determined with the Pg - Sg best fit travel time curves as the depth is increased or decreased from the 10 km average. It would be difficult to theoretically calculate the effect of changing the depth on origin time because this is related to the distances and distribution of stations relative to the epicenter, which are different for every earthquake. Therefore, an empirical relationship is developed using the events in the Magadan region test area. In doing this, the events are first located, constraining the depths to 10 km, and the calculated origin time is noted. The same events are then located again, constraining the depths at 0, 5, 15, 20, etc. km, and the shift in origin time from the 10 km depth determination is noted for each event at the various depths. It should be noted that changing the constraining depth of the earthquakes between 0 and 25 km has essentially no effect on epicenter coordinates, which generally vary less than 0.003°. Figure F-3 shows the resulting shift in origin times of the Magadan test area events from different constrained depths, with a second order regression fitting the data. Column 3 on Table F-1 gives the result of this regression. At this point, you are probably wondering where the heck I am going with all this gibberish. Because the shift in origin time is depth-dependent and not event-dependent, the origin time-depth correction can be added onto the Pn time difference in column two (Table F-1) to get column four

Table F-1. Depth determination table based on Pn residuals.

Depth h (km)	Pn Time Diff. from h of 10 km (sec)	Depth-O.T. Correction (sec)	Pn Residual Shift (sec)
0	1.103	0.078	1.181
			1.124
1	0.9927	0.0752	1.068
			1.011
2	0.8824	0.0716	0.9540
			0.8966
3	0.7721	0.0671	0.8392
			0.7813
4	0.6618	0.0615	0.7233
			0.6648
5	0.5515	0.0548	0.6063
			0.5474
6	0.4412	0.0472	0.4884
			0.4289
7	0.3309	0.0385	0.3694
			0.3094
8	0.2206	0.0289	0.2495
			0.1890
9	0.1103	0.0182	0.1285
			0.0642
10	0.0	0.0	0.0
			-0.0585
11	-0.1103	-0.0063	-0.1169
			-0.1788
12	-0.2206	-0.0201	-0.2407
			-0.3033
13	-0.3309	-0.0349	-0.3658
			-0.4289
14	-0.4412	-0.0507	-0.4919
			-0.5555
15	-0.5515	-0.0675	-0.6190
			-0.6830
16	-0.6618	-0.0853	-0.7471
			-0.8117
17	-0.7721	-0.1042	-0.8763
			-0.9414
18	-0.8824	-0.1241	-1.0065
			-1.0721
19	-0.9927	-0.1450	-1.1377
			-1.2038
20	-1.103	-0.1670	-1.2700
			-1.3366
21	-1.2133	-0.1899	-1.4032
			-1.4704
22	-1.3236	-0.2139	-1.5375
			-1.6052
23	-1.4339	-0.2389	-1.6728
			-1.7410
24	-1.5442	-0.2649	-1.8091
			-1.8778
25	-1.6545	-0.2920	-1.9465

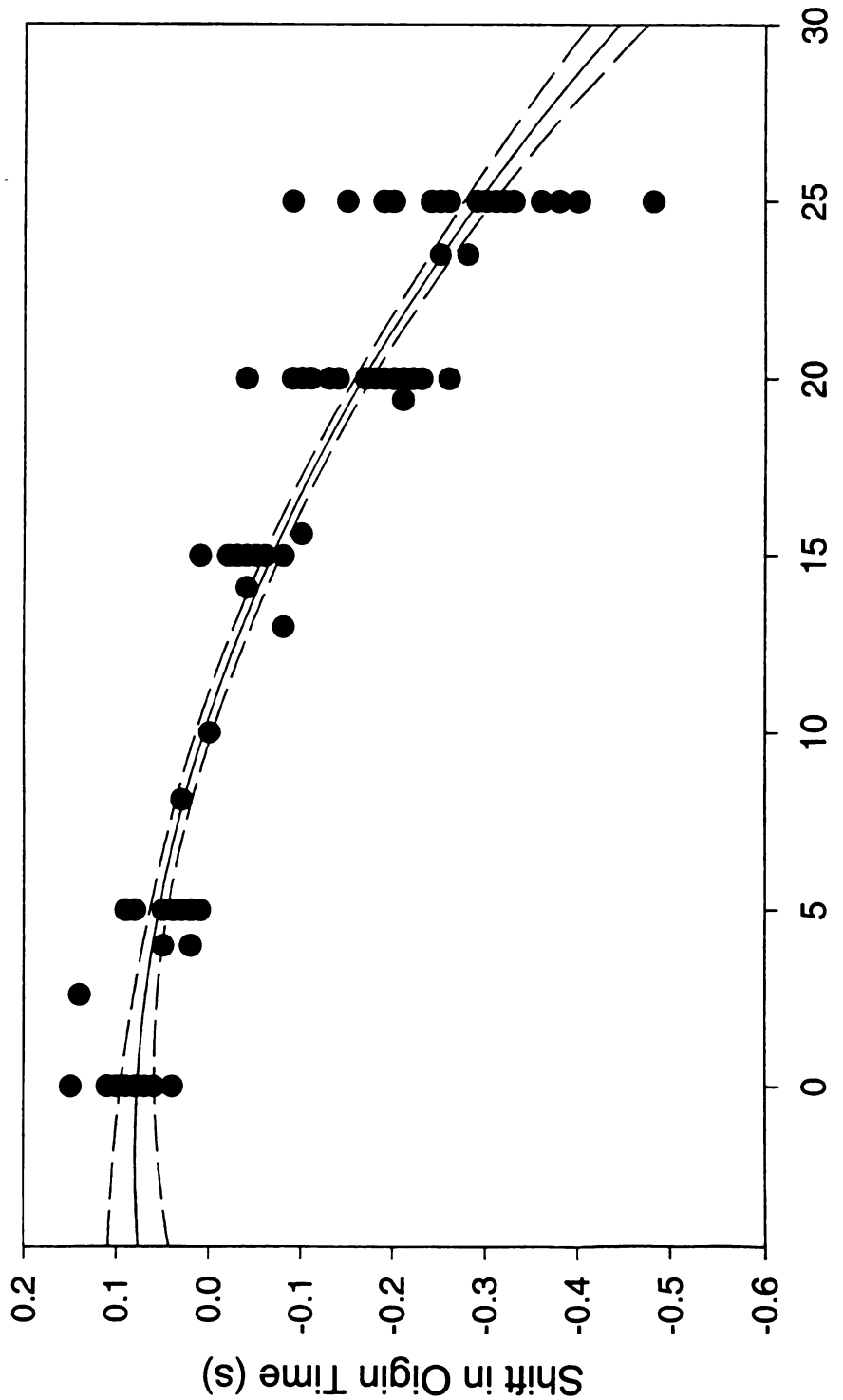

Figure F-3. Empirical relationship between change in depth from 10 km and associated shift on origin time. Data are fit with a second order regression (solid line) with 95% confidence intervals (dashed lines).

(Table F-1), which is the expected Pn residual shift from a 10 km focal depth. This column is now used to determine the depths of the earthquakes, matching the average Pn residual for an event, and reading off the depth. The origin time correction should also be used to adjust the origin time of the earthquake after the final depth is determined.

As noted above, if the Pn velocity in the travel time curve used to compute the residuals is too high or low, the average of all the residuals will be nonzero when depth is held at 10 km. In this case, we can assume the calculated average is simply an offset due to an incorrect Pn velocity (it could also be true that the offset is due to the average depth being other than 10 km, although it probably does not vary greatly). This correction will be termed the residual offset correction. The offset can simply be defined as the new residual zero point, and the Pn residual can be recalculated from this for each event. The new average Pn residual can then be used to determine hypocenter depths from Table F-1.

The depth determination method is tested here with events from the Magadan test area. Table F-2 lists the Pn residuals for the events, which were constrained at 10 km, as well as the depths determined using Table F-1. The Pn arrivals here were not used in the locations, but the residuals were calculated using the Jeffreys-Bullin P wave travel time curve. The depths calculated in the normal location procedure, which used the Pn phase, are also given for comparison. However, in this case, the average Pn residual (sum of column four divided by 46 events) is 0.34 seconds, which indicates that the Pn velocity used to determine the residuals is a bit off, with a resulting average depth of about 7 km. This is corrected by subtracting 0.34 from the average Pn residual and using the resulting value to determine the final Pn residual calculated depth (column 7, Table F-2). On average, this

Table F-2. Depth determinations from the Magadan test area. All depths (h) are in kilometers.

EVENT NUMBER	SUM OF RES-IDUALS (s)	NUMBER OF Pn PHASES	AVERAGE Pn RESIDUAL	h FROM Pn RES.	ORIG. DEPTH	Pn OFFSET CORRECTED h
1	3.375	2	1.688	0	0	0
2	5.303	3	1.768	0	0	0
3	1.940	3	0.647	5	5	7
4	-1.299	3	-0.433	14	15	16
5	-0.011	2	-0.005	10	10	13
6	3.213	3	1.071	1	2	4
7	-1.495	5	-0.299	12	12	15
8	-0.538	2	-0.269	12	12	15
9	-0.710	4	-0.177	11	11	14
10	-2.381	2	-1.191	19	15	22
11	-22.797	21	-1.086	19	20	21
12	-2.050	7	-0.293	12	12	15
13	-0.664	2	-0.332	13	13	15
14	-6.010	7	-0.859	17	15	19
15	1.815	2	0.908	2	5	5
16	-0.744	4	-0.186	12	15	15
17	1.919	3	0.640	5	5	7
18	-1.664	2	-0.832	17	17	19
19	4.749	4	1.187	0	2	3
20	1.821	3	0.607	5	6	8
21	-0.475	5	-0.095	11	11	13
22	2.305	5	0.461	6	8	9
23	0.597	6	0.099	9	9	12
24	4.676	8	0.584	5	6	8
25	4.983	6	0.831	3	4	6
26	2.198	2	1.099	1	2	3
27	2.284	6	0.381	7	7	9
28	2.330	2	1.165	0	1	3
29	3.556	3	1.185	0	1	3
30	1.693	3	0.564	5	6	8
31	0.760	2	0.380	7	8	9
32	6.353	3	2.118	0	0	0
33	1.399	4	0.350	7	7	10
34	1.922	2	0.961	2	4	5
35	-2.097	6	-0.349	13	13	16
36	1.822	2	0.911	2	5	5
37	1.895	3	0.632	5	6	7
38	0.445	26	0.017	10	10	12
39	2.819	4	0.705	4	6	7
40	3.294	3	1.098	1	6	3
41	0.037	8	0.005	10	10	13
42	-1.700	2	-0.850	17	14	19
43	-2.614	2	-1.307	20	20	23
44	0.152	4	0.038	10	11	12
45	2.916	2	1.458	0	1	0
46	1.430	2	0.715	4	5	7

residual offset correction results in a 3 km increase in the depth of each earthquake for the test region, with the resulting average then being 10.0 km.

The depths determined by both the original location, which used Pn arrivals, and the method derived here correlate extremely well. Figure F-4 compares the depth results determined from both methods. Open circles depict comparison of the original location depths with depths determined using this method, prior to inclusion of the residual offset correction (Table F-2, column 4). Here, there is a near 1:1 correlation, with differences in most cases being 1 km or less. The maximum observed difference is 5 km, in event number 40. Closed circles depict comparison of the original location depths with depths determined in this study using the residual offset correction.

Although this method was not used for depth determination throughout northeast Russia, it illustrates an alternate method of depth determination using Pn residuals when the actual Pn velocity is unknown. It also illustrates the dependence of depth on Pn arrivals when the crust is assumed to be one layer with one velocity for crustal Pg and Sg arrivals.

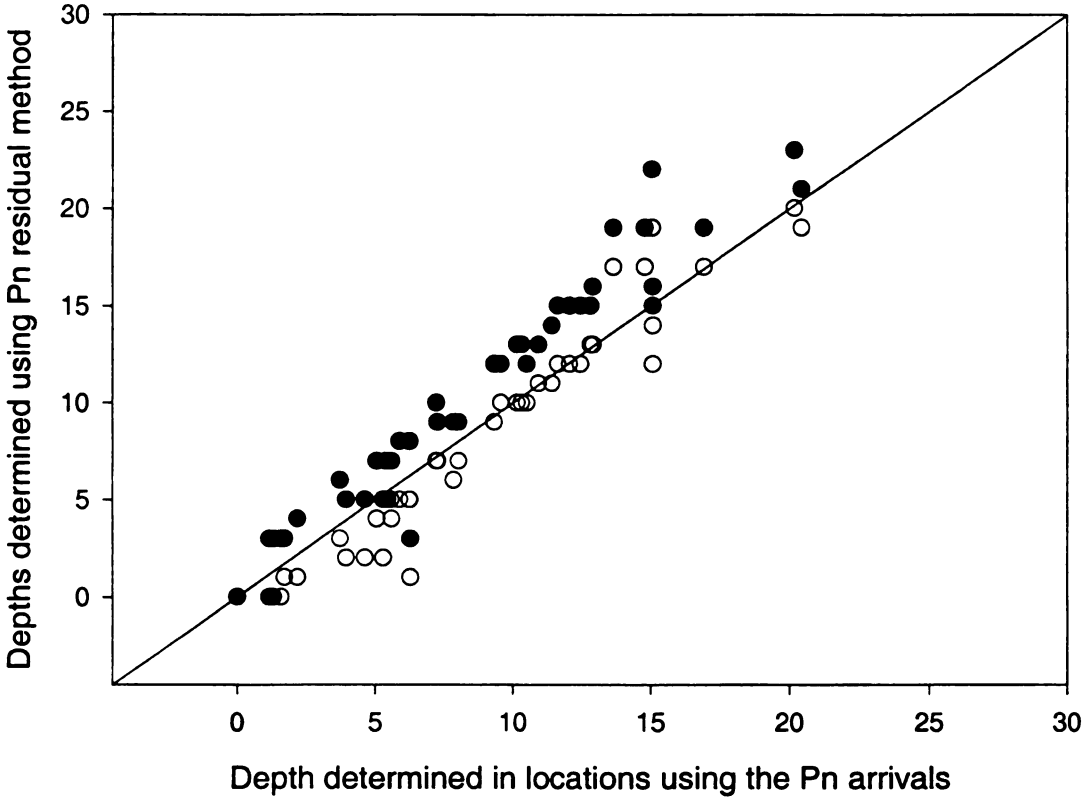

Figure F-4. Comparison of depths determined in the normal location routine with depths determined by the Pn residual method described here. Note the near 1:1 correlation. Open circles without residual offset correction. Closed circles with residual offset correction.